JAERI-M
85-037

BWR RECIRCULATION LOOP DISCHARGE LINE BREAK LOCA TESTS WITH BREAK AREAS OF 50 AND 100% ASSUMING HPCS FAILURE AT ROSA-III FACILITY

March 1985

Mitsuhiro SUZUKI, Kanji TASAKA,
Taisuke YONOMOTO, Yoshinari ANODA,
Hiroshige KUMAMARU, Hideo NAKAMURA,
Hideo MURATA, Masanori IRIKO
and Masayoshi SHIBA

日本原子力研究所
Japan Atomic Energy Research Institute

JAERI-Mレポートは，日本原子力研究所が不定期に公刊している研究報告書です。
入手の問合わせは，日本原子力研究所技術情報部情報資料課（〒319－11茨城県那珂郡東海村）あて，お申しこしください。なお，このほかに財団法人原子力弘済会資料センター（〒319-11茨城県那珂郡東海村日本原子力研究所内）で複写による実費頒布をおこなっております。

JAERI-M reports are issued irregularly.
Inquiries about availability of the reports should be addressed to Information Division, Department of Technical Information, Japan Atomic Energy Research Institute, Tokai-mura, Naka-gun, Ibaraki-ken 319-11, Japan.

編集兼発行　日本原子力研究所
印　　刷　日立高速印刷株式会社

JAERI-M 85-037

BWR RECIRCULATION LOOP DISCHARGE LINE BREAK LOCA TESTS WITH BREAK AREAS OF 50 AND 100% ASSUMING HPCS FAILURE AT ROSA-III TEST FACILITY

Mitsuhiro SUZUKI, Kanji TASAKA, Taisuke YONOMOTO, Yoshinari ANODA, Hiroshige KUMAMARU, Hideo NAKAMURA, Hideo MURATA, Masanori IRIKO* and Masayoshi SHIBA

Department of Nuclear Safety Research,
Tokai Research Establishment, JAERI

(received January 31, 1985)

This report presents the experimental results of RUN 962 and RUN 963 in ROSA-III program, which are 50 and 100% break LOCA tests at the BWR recirculation pump discharge line, respectively. The ROSA-III test facility simulates a volumetrically scaled (1/424) BWR system and has four half-length electrically heated fuel bundles, two active recirculation loops, three types of ECCSs and steam and feedwater systems.

The experimental data of RUN 962 and RUN 963 were compared with those of RUN 961, a 200% discharge line break test to study the break area effects on the transient thermal hydraulic phenomena. The least flow areas at the jet pump drive nozzles and recirculation pump discharge nozzle in the broken recirculation loop limitted the discharge flows from the pressure vessel and the depressurization rate in the 100 and 200% break tests, whereas the least flow area at break nozzle limitted the depressurization rate in the 50% break test. The highest PCT was observed in the 50% break test among the three tests.

Keywords: BWR, LOCA, ECCS, Integral Test, ROSA-III Program, Large Break, Recirculation Pump Discharge Line Break, Break Area, Data Report

---

* Computer Service Co. (CSK)

ＲＯＳＡ－Ⅲにおける ＨＰＣＳ故障下のＢＷＲ再循環ポンプ吐出側配管50％および100％破断ＬＯＣＡ実験

日本原子力研究所東海研究所安全工学部
鈴木　光弘・田坂　完二・与能本泰介・安濃田良成
熊丸　博滋・中村　秀夫・村田　秀男・入子　真規*
斯波　正誼

（１９８５年１月31日受理）

本報告は，ＲＯＳＡ－Ⅲ試験装置を用いて行なわれたＢＷＲ再循環ポンプ吐出側配管の50％および100％破断ＬＯＣＡ実験であるＲＵＮ962とＲＵＮ963の実験結果をまとめたものである。ＲＯＳＡ－Ⅲ試験装置は，ＢＷＲ体系を１／424に体積縮小したシステムであり，電気加熱の１／２長さの燃料バンドル４体と２つの再循環ループ，３種類のＥＣＣＳ，および蒸気・給水系を備えている。

ＲＵＮ962とＲＵＮ963の実験結果は，過渡的熱水力現象に及ぼす破断口面積の影響を調べる観点から，同じ吐出側配管における200％破断実験であるＲＵＮ961の結果と比較した。再循環ループの破断径路におけるジェットポンプ駆動ノズルと再循環ポンプ出口ノズルにおける最小流路面積が，100％および200％破断実験においては圧力容器からの流出流量に，従って減圧にも支配的影響を及ぼし，50％破断実験においては破断口面積が減圧を支配した。これら３実験における最高燃料被ふく管温度（ＰＣＴ）は50％破断実験において見られたが，この傾向はＲＯＳＡ－Ⅲ計画における再循環ループ吸込側配管破断シリーズの結果と同じであった。

＊コンピューターサービス株式会社（ＣＳＫ）

Contents

目　　次

List of Tables for RUNs 962 and 963

List of Figures for RUNs 962 and 963

List of Figures of Experiment Data for RUN 962

List of Figures of Experiment Data for RUN 963

List of Figures for RUNs 962 and 963

ABBREVIATIONS

ADS	Automatic Depressurization System
AT	Air Tank
AV	Air Actuation Valve
(2)B	(2) inches Pipe of Schedule 80
BN	Boron Nitride
BWR	Boiling Water Reactor
CA	Chromel-Alumel
CCFL	Counter Current Flow Limiting
CHV	Check Valve
CP	Conductivity Prove
CV	Control Valve
CWT	Cooling Water Tank
D	Differential Pressure
d	Diameter
DF	Density of Fluid
DL(+100)	Elevation (+100 mm) from the Bottom of PV
ECCS	Emergency Core Cooling System
ESF	Engineered Safety Features
EX	Heat Exchanger
F	Flow Rate
Fig.	Figure
FS	Full Scale
FW	Feedwater
FWLF	Feedwater Line Flashing
FWP	Feedwater Pump
FWT	Feedwater Tank
HPCS	High Pressure Core Spray
HPCSP	High Pressure Core Spray Pump
HPCST	High Pressure Core Spary Tank

MW	Megawatt
N	Rotation Speed
OR	Orifice
P	Pressure
	Power
PCT	Peak Cladding Temperature
PV	Pressure Vessel
PWT	Pure Water Tank
QOBV	Quick Opening Blowdown Valve
QSV	Quick Shut-off Valve
RCN	Rapid Condencer
ROSA	Rig of Safety Assessment
rpm	Revolution per Minute
S	Signal
s	Second
Sch	Schedule
SUS	Stainless Steel
T	Temperature
T/C	Thermocouple
TC	Temperature of Fluid
TF	Temperature of Fuel
TS	Temperature of Structure Material
UTP	Upper Tie Plate
V	Valve
VF	Void Fraction
W	Watt
WL	Water Level
WSP	Water Supply Pump

HPWP	High Pressure Water Pump
ID	Inner diameter
INC 600	Inconel 600
JP	Jet Pump
K	Kelvin
kg	Kilogram
kPa	Kilopascal
kW	Kilowatt
L	Liter
LB	Liquid Level in Channel Box
LBWR	Large Boiling Water Reactor
LL	Liquid Level
LOCA	Loss-of-Coolant Accident
LOCE	Loss-of-Coolant Experiment
LP	Lower Plenum
LPCI	Low Pressure Coolant Injection
LPCIP	Low Pressure Coolant Injection Pump
LPCIT	Low Pressure Coolant Injection Tank
LPCS	Low Pressure Core Spray
LPCSP	Low Pressure Core Spary Pump
LPCST	Low Pressure Core Spary Tank
LPF	Lower Plenum Flashing
LTP	Lower Tie Plate
M	Momentum Flux
m	Meter
mm	Milimeter
MLHR	Maximum Linear Heat Rate
MPa	Megapascal
MRP	Main Recirculation Pump
MSIV	Main Steam Isolation Valve
MSL	Main Steam Line

1. Introduction

The Rig of Safety Assessment (ROSA)-III program[1] was initiated in 1976 to study the thermal hydraulic behavior of a Boiling Water Reactor (BWR) during a postulated Loss-of-Coolant Accident (LOCA) with the Emergency Core Cooling System (ECCS) actuation and to provide the data base to evaluate the predictability of computer codes developed for reactor safety analysis. The ROSA-III test facility[2] fabricated in 1978 consists of a volumetrically scaled (1/424) primary system of a 3800 MW BWR/6(251-848)[3] with the electrically heated core, the break simulator and the scaled ECCS. Special emphasis of the ROSA-III test program is made on the following objectives, as

(1) To provide the system data required to improve and evaluate the analytical codes currently used to predict the LOCA transients of large BWRs. The performances of the ECCSs are of primary interest.

(2) To identify and investigate any unexpected event(s) or threshold(s) in the response of the plant and to develop analytical techniques that adequately account for such unexpected behavior.

To meet these objectives various kinds of ROSA-III tests have been performed and those results have been published[4]-[30].

Up to the present time, similar experimental studies on the BWR/LOCA phenomena have been performed with respect to some test parameters in TLTA[31], FIST[32] and TBL.[33] The recirculation pump discharge line break tests, however, have not been conducted in those test programs. Three recirculation pump discharge line break tests were conducted in the ROSA-III facility, ie., RUN 961[24], a 200% break test, and RUN 962 (50% break) and RUN 963 (100% break) shown below.

RUNs 962 and 963, conducted on April 20 and 27 in 1982, respectively, have the objectives to study (1) the effects of break area on the recirculation pump discharge line break LOCA and (2) the similarity or difference of the fundamental phenomena between the discharge line break and the suction line break tests performed previously in the ROSA-III program. RUN 962 is a 50% discharge line break test with an assumption of HPCS failure and RUN 963 is a similar test with break area of 100% with HPCS failure. The effects of break areas are described in the present report.

2. ROSA-III Test Facility

The ROSA-III test facility is a volumetrically scaled (1/424) BWR system with an electrically heated core designed to study the response of the primary system, the core and the ECCS during the postulated LOCA. The test facility is instrumented such that various thermal-hydraulic parameters are measured and recorded during the test. Details of the test facility can be refered to the reference (2).

The test facility consists of four subsystems. These subsystems are : (a) the pressure vessel, (b) the steam line and the feedwater line, (c) the recirculation loops and (d) the ECCS. Figures 2.1, 2.2 and 2.3 illustrate configuration of the test facility, the pressure vessel internals and the piping schematics, respectively. Table 2.1 compares the major dimensions of the ROSA-III test facility to the corresponding dimensions of the reference BWR system.

The ROSA-III pressure vessel includes various components in it simulating the internal structures of the reactor vessel in the BWR system as shown in Fig. 2.4. The interior of the vessel is divided into the core, the lower plenum, the upper plenum, the downcomer annulus, the steam separator, the steam dome and the steam dryer. The core is consisted of four simulated fuel assemblies of half length and a control rod simulator. Each fuel assembly contains 62 heater rods (Fig. 2.5) and 2 water rods spaced in a 8 x 8 square array and supported by spacers and upper and lower tie plates. The heater rod is heated electrically with chopped cosine power distribution along the axis as shown in Fig. 2.6. The effective heated length is 1880 mm, one half of the active length of a BWR fuel rod. The high power with radial peaking factor of 1.4 was supplied to the fuel assembly "A" and average power was supplied to the other three bundles "B", "C" and "D" with radial peaking factor of 1.0. The heater rods in each assembly are divided into three groups with respect to heat generation rate as shown in Fig. 2.7. The total electric power is limitted as 4.24 MW by limitation of the power supply system. The relative power generation rate of a heater rod in each group is 1.1, 1.0 and 0.875 respectively. The orifice plate with 44 mm I.D. in one assembly is inserted at at each core inlet to control the core inlet flow.

The steam line is connected to the steam dome of the pressure vessel. A control valve is installed in the steam line to control the steam dome pressure in steady state before the initiation of the tests. The steam line

has a branch in which the automatic depressurization system (ADS) is installed. The operation of valves in the steam line is described in Chap.4. The feedwater is supplied from the feedwater tank (FWT) through the feedwater line (Fig. 2.8) and the feedwater sparger (Fig.2.9) below the steam separator.

Figure 2.10 shows the recirculation lines consisted of two loops. Each loop is furnished with a recirculation pump and two jet pumps. The jet pumps are installed outside the pressure vessel to simulte the relative volume and the relative height to the core. Two break simulators and a quick shut-off valves (QSV) are installed in the broken loop. In RUNs 962 and 963, break B unit located at the discharge line of the recirculation pump (MRP2) is used to simulate a large split break. The break simulator consists of an nozzle to determine the break size and a quick opening blowdown valve (QOBV) to initiate the test. The break mode (double-ended or split), the break size and the break location can be changed as test parameters. The inner diameters of the nozzle used in RUNs 962 and 963 are 18.5 mm (Area: $A=2.69\times10^{-4}$ m^2) and 26.2 mm ($A=5.39\times10^{-4}$ m^2), respectively. Figure 2.10 shows the QOBV, a QSV and flow nozzle installed upstream of the QOBV.

The ROSA-III test facility is furnished with all kinds of the ECCS available in the BWR system, i.e., the High Pressure Core Spray (HPCS), the Low Pressure Core Spray (LPCS), the Low Pressure Coolant Injection (LPCI), and the ADS. The HPCS and the LPCS spray the cooling water on the top of the core. The LPCI injects the cooling water into the core bypass. Each ECCS consists of a pump, a tank, piping, and a control system. In both tests RUNs 962 and 963, a single failure of HPCS diesel generator is assumed and therefore LPCS, 3LPCI and ADS are prepared.

The water level in the upper downcomer, which has influencial contribution in the small break LOCA test, is measured and used for trip signals of MSIV closure and ECCS actuation as follows.

MSIV Closure = L1 + 3s
LPCS Actuation = (L1 + 40s) + (P less than 1.86 MPa)
LPCI Actuation = (L1 + 40s) + (P less than 1.57 MPa)
ADS Actuation = L1 + 120s
Scram Level = L3 (Initial Level)

where, L1, L2 and L3 are the water level trip points in the upper downcomer as shown in Table 4.1.

3. Instrumentation

The instrumentation of the ROSA-III is designed to obtain thermal-hydraulic data during the simulated BWR LOCA. The data obtained from the experiments will contribute to assess the analytical computer codes for LOCA analyses and to investigate the transient fluid and fuel responses during the simulated LOCA. Table 3.1 summarizes the No.4 instrumentation list used in RUNs 962 and 963.

Tables 3.2 and 3.3 show the measurement list and the core instrumentation list for RUN 962, respectively. These are common for RUN 963. The figure numbers of corresponding measurements for RUN 963 are described in the chapter 5. Instrumentation locations are shown in Fig. 3.1 through Fig. 3.6.

Typical measured parameters in the ROSA-III are pressure, differential pressure, flow rate, electric power, pump speed, fluid and metal temperatures, collapsed liquid level, two-phase mixture level, fluid density, trip signals and so on.

Pressure and differential pressure transducers are two-wire, direct-current type which convert diaphragm displacement to electric capacitance. The pressure lead pipes are either the standard single, cylindrical pipes used in conjunction with condensate pots, or dual concentric cylinders capable of the circulation of cooling water to prevent flashing of the fluid.

The flow rate is measured by four types of instrumentations, i.e., turbine flow meter, orifice type flow meter, Venturi type flow meter and momentum flux measurement equipment depending on the fluid condition and measuring location. The turbine flow meter is used for subcooled water flow such as ECCS injection flow and feedwater flow. The orifice type flow meter is used for both flows, one is steam line flow including ADS flow and another one is jet pump discharge flow in the intact loop. The Venturi flow meters used for recirculation flows in both loops and jet pump discharge flow in the intact loop. The momentum flux measurement using drag-disk is shown later.

The temperatures of the fluid, structural material and fuel rod cladding are measured with chromel-alumel thermocouples (CA T/C) of 1.6 or 1.0 mmφ. The thermocouples for fuel rod cladding temperatures are imbedded at the surface of the cladding as shown in Fig. 2.5. There are seven (max.) thermocouples for one fuel rod along the axial direction and total measuring

points of rod cladding temperatures for A, B, C and D channels are 65, 22, 35 and 18, respectively.

Liquid levels are measured by either differential pressure transducers, described above or needle type electrical conductivity probes (CP) developed in the ROSA-III program. The probes are distributed along the vessel height to detect the existence of water or vapor at different levels.

The electric power supplied to the simulated fuel rods is controlled to follow the predetermined power curve with function of time and measured by a fast response electric power meter.

Pump speed is measured by a pulse generator integral of the pump. Trip signals such as selected valve positions, decay heat and pump coastdown simulation initiations and so on are detected in order to record the exact actuation times of trip signals.

Fluid density in the pipe is measured by means of gamma densitometers. Preliminary studies indicate that a three-beam densitometer should be used to determine the flow regime. Figures 3.7 and 3.8 show the beam directions of the three-beam and two-beam gamma densitometesr. The gamma-ray source is ^{137}Cs and the detector is a water cooled NaI(Tl) scintillation counter.

Momentum flux is measured by a drag disk as shown in Fig. 3.9. The combination of signals from a drag disk and a gamma densitometer is used to determine the two-phase flow rate as shown in Fig. 3.10.

The data acquisition system (DATAC 2000B, Iwasaki Tsushinki Co.) scans all of signals with the frequency up to 30 Hz. The data recorded on magnetic tape are processed by the FACOM M200 system computer at JAERI by off-line control. After evaluation, for example by comparing the initial and final pressure values with standard values, the data is reprocessed using the correct conversion factors as determined from the consistency examination.

More detailed information on the data processing procedure are available in reference (34).

4. Test Conditions and Procedure

4.1 RUN 962, A 50% Break Test

The test conditions of RUN 962 are summarized in Table 4.1. RUN 962 simulated a 50% split break at the recirculation pump discharge line. The break was simulated by the nozzle shown in Fig. 4.1. Blowdown was initiated by opening the quick opening blowdown valves at the immediate downstream of the break nozzle (18.5 mm ID). The break nozzle area is 50% of the 1/424 scaled recirculation line pipe flow area of the reference BWR. The major test sequences and events observed in RUN 962 are summarized in Table 4.2.

Water level signal in the downcomer was used to close the MSIV (main steam isolation valve) and initiate ECCS actuation in the test. The initial water level in the downcomer was 5.00 m since the liquid volume below 5.00 m in ROSA-III, including the volume of the jet pump suction pipings, corresponded to the volume below the scram level (L3) in a BWR/6 . The L2 and L1 water levels in the downcomer of ROSA-III were 4.76 m and 4.25 m, respectively. MSIV closure was initiated by the L2 level signal with the time delay of 3s, and LPCS, LPCI and ADS actuations were initiated by the L1 level signal with time delay of 40s, 40s and 120s, respectively. These time delays are used in the safety analysis of a BWR.[3] LPCS and LPCI injections were also specified to initiate at system pressures below 2.16 MPa and 1.57 MPa, respectively.

The measured primary initial test conditions were as follows. The steam dome pressure was 7.35 MPa and the corresponding saturation temperature was 562.3 K. The core inlet flow rate was 16.1 kg/s and the upper plenum quality was estimated to be 13.2% by assuming 9.5% core bypass flow rate.

Experiment procedure of RUN 962 was as follows. The steady state power supply to the simulated fuel assembly was 3972 kW which corresponds to 44% of the BWR steady power. The MLHR (maximum linear heat rate) was 16.72 kW/m. The power supply to the core was switched to the transient power at the break initiation in order to simulate the heat transfer of the BWR core[35] neglecting the stored heat of ROSA-III heater rods (see Fig. 4.2).

The feedwater line (see Fig. 4.3) supplied hot feedwater (489 K) into the downcomer by the feedwater pump (FWP) in the initial state. Some amount of steam discharge flow which passed through the heat exchangers (EX1 and EX2) contributed to heat up the feedwater. At the time of break, the steam flow passed through the heat exchangers was terminated by closing quickly

the control valves (CV1 and CV2). And the feedwater flow was terminated at 1.7 s after break and completed at 3.8 s after break.

The main steam line (see Fig. 4.4) has three branches. The transient line was not used in RUN 962. The steady line acted as steam discharge line in the initial state and as pressure regulator to maintain the system pressure at 6.67 MPa automatically after break. Closure of MSIV was simulated by closing manually the CV-130 in the steady steam line. However, the MSIV was closed before the system pressure dropped below 6.67 MPa in RUN 962. The MSIV closure was initiated at 12 s by the L2 level signal with the time delay of 3 s and completed at 15 s. The characteristics of the steam discharge line valves and control sequences for them in RUN 962 are shown in Tables 4.3 and 4.4, respectively. Then CV-130 was set to simulate SRV (safety relief valve) maintaining the system prssure below 8.14 MPa automatically. However, the system pressure did not reach to 8.14 MPa in RUN 962, therefore the safety valve simulator was not used.

LPCS started to spray coolant into the upper plenum at the system pressure 2.17 MPa at 167 s after break. The water injection from LPCI into the core bypass was initiated at the system pressure 1.58 MPa at 200 s after break.

The ADS valve was opened at 139 s after break. The orifice with a diameter of 15.5 mm was set in ADS line to simulate the typical ADS line steam flow in a BWR.

The data aquisition was initiated 121 s prior to the break initiation and terminated at 812 s after break. The specified time to close the feedwater line valve is based on the evaluation guide for the BWR safety analysis.[36] The specified system pressure for actuating LPCS and LPCI were decided from LPCS and LPCI pump characteristics used in the safety analysis of BWR[31]. The specified flow rates of LPCS and LPCI were also decided from these pump characteristics.

4.2 RUN 963, A 100% Break Test

The test conditions of RUN 963 shown in Table 4.5 are similar to those of RUN 962 except for the break area. The break nozzle of 26.2 mm I.D. was used to determine the break flow area. The initial test conditions, such as pressure, core power, core flow rate and water level and the transient trip logics including MSIV and ECCS of RUN 963 were the same as those of RUN 962.

The major test sequences and events observed in RUN 963 are summarized in Table 4.6. The experiment procedure of RUN 963 was as follows. Blowdown was initiated by opening the QOBV at break B unit. The QSV installed between the breakA and break B units was kept opened. The main recirculation pumps initiated to coast down immediately after break. The feedwater flow stopped at 2.1 s after break and completed at 4.3 s after break. The MSIV closure was initiated at 9.5 s by the L2 trip water level with time delay of 1.3 s. The transient power turned to decrease at 8.8 s after break and followed along the power curve simulating the BWR core heat transfer rate.

The LPCS and LPCI were actuated at the designed pressure at 2.12 MPa and 1.46 MPa, respectively. The ADS was actuated at 135 s after break by the L1 trip water level with time delay of 121 s. The data aquisition system in RUN 963 was initiated 125 s prior to break initiation and terminated at 886 s after break.

RUN 963 was conducted successfully and most of the instrumentations functioned normally.

5. Data Processing

In RUNs 962 and 963, the data acquisition frequency was 10 Hz. The test data was processed and reduced to 1000 data points for computer plotting. The time span and frequency of the reduced data for plotting were 1000 s and 1 Hz, respectively.

The test data of RUN 962 are shown in Figs. 5.1 through 5.164. In these figures, the measured quantity is identified by the channel number and the alphabetic characters (ref. Table 3.2). The test data of RUN 963 are shown in Figs. 5.165 through 5.335, which are described after description of the test data of RUN 962.

At first the test data of RUN 962 are described below. Figures 5.1 through 5.5 show the pressure data in the pressure vessel and recirculation loop. Figures 5.6 through 5.35 show differential pressure data between various positions in the pressure vessel and the recirculation loop. Figures 5.36 and 5.37 show the liquid levels in the ECCS tanks and downcomer. Figures 5.38 through 5.44 show the flow rates. Figure 5.45 shows the power supplied to the core with the maximum capacities of 2100 and 3150 kW. The pump speeds of the recirculation pumps are shown in Fig. 5.46. The trip signals such as the break initiation signal and the valve positioning signals are shown in Figs. 5.47 through 5.49. Figures 5.50 through 5.59 show the fluid densities measured by the gamma densitometer. Figures 5.60 through 5.64 show momentum fluxes measured by drag disks. Figures 5.65 through 5.74 show the fluid temperatures at various positions in the system. The fuel rod cladding temperature and the surface temperatures of the water rods and the channel boxes measured at positions 1 through 7 are given in Figs. 5.75 through 5.94. Figures 5.95 through 5.118 show the fuel rod cladding temperatures in a different manner. Figures 5.119 through 5.131 show the fluid temperatures at the inlet and outlet of the channel box. The outer surface temperatures of the channel box are shown in Fig. 5.132. The fluid temperature in the lower plenum was measured as shown in Fig. 5.133. The liquid level signals in the core, the upper and lower plena, the guide tube and the downcomer are shown in Figs. 5.134 through 5.141. The peak cladding temperature (PCT) distribution in the core is given in Table 5.1.

Quantities obtained from reduction of the test data are shown in Fig. 5.142 through 5.164.

Figures 5.142 and 5.143 show the estimated liquid levels in the core and the pressure vessel obtained by reducing the conductivity probe signals previously shown in Figs. 5.134 through 5.141. Figure 5.144 shows transients of the dryout and quenching times of the representative fuel rods in the core. Figures 5.145 through 5.148 show the average fluid density calculated from the data shown in Fig. 5.50 throughFig. 5.59. The average density is calculated as an arithmetic mean of the densities in multi-directions with the weight of each cord length.

For the three beam densitometer at the jet pump outlet spool,

$$\rho_{av} = 0.3221\rho_A + 0.43\rho_B + 0.2479\rho_C \tag{5.1}$$

where,

ρ_{av}: average density obtained from the three-beam gamma densitometer,
ρ_A : density measured by beam A (bottom),
ρ_B : density measured by beam B (middle).
ρ_C : density measured by beam C (top).

For the two-beam densitometer at the break spool piece,

$$\rho_{av} = 0.5863\rho_A + 0.4137\rho_B \tag{5.2}$$

where,

ρ_{av}: average density obtained from the two-beam gamma densitometer,
ρ_A : density measured by beam A (bottom),
ρ_B : density measured by beam B (top).

Figures 5.149 through 5.152 show the flow rates at upstream sides of the break in the recirculation loop. The flow rate is computed from the drag disk data and the gamma densitometer data using the following equation,

$$G = C_D \cdot A \cdot \sqrt{\rho_{av} \cdot \rho v^2} \tag{5.3}$$

where,

G : mass flow rate,
C_D : drag coefficient (= 1.13),
A : flow area (= 1.923×10^{-3} m^2),

ρ_{av}: average density from gamma densitometer,
ρv^2: momentum flux from drag disk.

The break flow is derived from the flow rate in the recirculation loop as follows,

$$G_B = G_P - G_V \tag{5.4}$$

where,

G_B : break flow,
G_P : flow rate at the pump side of the break,
G_V : flow rate st the vessel side of the break,

Figures 5.153 through 5.162 show the fluid flow rates at the channel inlet orifices, the bypass hole and the jet pump outlets. The fluid flow rates are calculated from the test data which are the pressure drop across the orifices or venturi flow meters and the liquid density obtained from the temperature and the pressure condition. The equation used for the calculation is as follows :

$$G = C_D \cdot A \cdot \sqrt{2g \cdot \rho_l \cdot \Delta P} \tag{5.5}$$

where,

G : flow rate,
ΔP : pressure drop across the orifice,
C_D : discharge coefficient,
= 0.6552 (the orifice to measure the steam discharge flow rate)
= 0.4761 (the channel inlet orifice)
= 0.8032 (the bypass hole)
= 0.7383 (the orifice to measure the jet pump outlet flow rate)
= 1.1260 (the venturi tube to measure the jet pump outlet flow rate)

A : flow area (m^2)
= 2.875×10^{-3} (the orifice to measure the steam discharge flow rate)
= 1.521×10^{-3} (the channel inlet orifice)

$= 1.758 \times 10^{-4}$ (the bypass hole)

$= 1.133 \times 10^{-3}$ (the orifice to measure the jet pump outlet flow rate)

$= 9.095 \times 10^{-4}$ (the venturi tube to measure the jet pump outlet flow rate)

g : gravitational acceleration (= 9.807 m/s^2),

ρ_l : density of the single-phase liquid (kg/m^3),

This calculation method is not applicable for two-phase flow condition after the LPF initiation at the channel inlet orifice, the bypass hole and the jet pump outlet. The calculated value shows only a trend in two-phase flow condition. Total channel inlet flow rate presents the sum of four channel inlet flow rates.

Figure 5.163 shows the collapsed water level inside the core shroud. The level is obtained from corresponding differential pressure. The differential pressure may include the flow resistance effect, however, the flow resistance becomes negligible after completion of the recirculation pump coastdown.

Figure 5.164 shows the fluid mass inventory inside core shroud. The fluid mass inventory is determined from the density and configurational data inside and outside the core shroud,

$$M = \rho_l \cdot Q \tag{5.6}$$

where,

M : fluid inventory,

ρ_l : liquid density estimated from the satulation temperature and/or pressure,

Q : liquid volume calculated from the liquid level.

The volume Q (m^3) inside the shroud is also given as a function of collapsed water level inside core shroud (L),

$Q = 0.0$ ($L \leqq 0.0$)

$Q = 0.2350L$ ($0.0 < L \leqq 0.497$)

$Q = 0.1245L + 0.0549$ ($0.497 < L \leqq 1.354$)

$Q = 0.0698L + 0.1290$ ($1.354 < L \leqq 3.589$)

$Q = 0.1648L - 0.2120$ ($3.589 < L \leqq 3.744$)

$$
\begin{aligned}
Q &= 0.1963L - 0.3299 \quad (3.744 < L \leqq 4.243) \\
Q &= 0.0196L + 0.4199 \quad (4.243 < L \leqq 4.578) \\
Q &= 0.0186L + 0.4244 \quad (4.578 < L \leqq 4.654) \\
Q &= 0.0410L + 0.3201 \quad (4.654 < L \leqq 5.099) \\
Q &= 0.0196L + 0.4292 \quad (5.099 < L \leqq 5.365) \\
Q &= 0.5344 \quad (5.365 < L)
\end{aligned} \tag{5.7}
$$

Next, the test data of RUN 963 are described below.

The data of RUN 963 are presented in the same order as those of RUN 962 and also the data aquisition frequency was 10 Hz. The test data processed in the same method as in the data processing of RUN 962. Therefore, only the figure numbers and the measured data are described below for the test results of RUN 963. The mass inventory in the downcomer was calculated in RUN 963 (see Fig. 5.328). And the total mass in PV, mass balance, discharged mass and discharge mass flow rate were calculated (see Fig. 5.332 through 5.335).

The test data of RUN 963 are shown in Figs. 5.165 through 5.335. In these figures, the measured quantity is identified by the channel number and the alphabetic characters (ref. Table 3.3).

Figures 5.165 through 5.169 show the pressure data in the pressure vessel and recirculation loop. Figures 5.170 through 5.199 show differential pressure data between various positions in the pressure vessel and recirculation loops. Figures 5.200 and 5.201 show the liquid levels in the ECCS tanks and downcomer. Figures 5.202 through 5.208 show the flow rates. Figure 5.209 shows the power supplied to the core with the maximum capacities of 2100 and 3150 kW. The pump speeds of the recirculation pumps are shown in Fig. 5.210. The trip signals such as the break initiation signal and the valve positioning signals are shown in Fig. 5.211 through 5.213. Figures 5.214 through 5.223 show the fluid densities measured by the gamma densitometers. Figures 5.224 through 5.228 show momentum fluxes measured by the drag-disks. Figures 5.229 through 5.238 show the fluid temperatures at various positions in the system. The fuel rod cladding temperatures and the surface temperatures of the water rods and the channel boxes are given in the Figs. 5.239 through 5.258. Figures 5.259 through 5.282 show the fuel rod cladding temperatures in a different manner. Figures 5.283 through

5.295 show the fluid temperatures at the inlet and outlet of the channel boxes. The outer surface temperatures of the channel box are shown in Fig. 5.296. The fluid temperatures in the lower plenum was measured as shown in Fig. 5.297. The liquid level signals in the core, the upper and lower plena, the guide tube and the downcomer are shown in Figs. 5.298 through 5.306. The peak cladding temperature (PCT) distribution in the core is given in Table 5.2.

Quantities obtained from reduction of the test data are shown in Figs. 5.307 through 5.335.

Figure 5.307 shows the estimated liquid levels in the core and the pressure vessel obtained by reducing the conductivity probe signals previously shown in Figs. 5.298 through 5.306. Figures 5.308 and 5.309 show transients of the dryout and quenching times of the representative fuel rod in the high and average power bundles. Figures 5.310 through 5.313 show the average fluid density calculated from the data shown in Figs. 5.214 through 5.223. Figures 5.314 through 5.316 show the mass flow rates at upstream side of the break in the recirculation loop. Figures 5.317 through 5.327 show the fluid flow rates at the channel inlet orifices, the bypass holes and the jet pump outlets. The fluid flow rates are calculated like as the calculation of the data of RUN 962 from the test data which are the pressure drop across the orifices or Venturi flow meters and the liquid density obtained from the temperature and pressure condition. This calculation method, however, is not applicable for two-phase flow condition after the lower plenum flashing at the channel inlet orifices, the bypass holes and the jet pump outlets. The calculated value shows only a trend in the two-phase flow condition. Total channel inlet flow rate presents the sum of four channel inlet flow rates.

Figures 5.328 and 5.329 show the collapsed water levels outside and inside of the core shroud. The level is obtained from corresponding differential pressure. The differential pressure may include the flow resistance effect, however, the flow resistance becomes negligible after completion of coast down of the recirculation flow.

Figures 5.330 through 5.332 show the fluid mass inventories in the pressure vessel. The fluid mass inventory was determined from the fluid density and configurational data inside and outside of the core shroud,

$$M = \rho_l \cdot Q \tag{5.8}$$

where,

M : fluid inventory,

ρ_l : liquid density estimated from the saturation temperature and/or pressure,

Q : liquid volume calculated from the liquid level.

The volume Q (m^3) outside the shroud is given below as a function of collapsed water level (L),

$$
\begin{aligned}
Q &= 0.0 && (\ L \leqq 0.494\ ) \\
Q &= 0.0225L - 0.0111 && (\ 0.494 < L \leqq 1.384\ ) \\
Q &= 0.0697L - 0.0769 && (\ 1.384 < L \leqq 1.519\ ) \\
Q &= 0.0225L - 0.0048 && (\ 1.519 < L \leqq 3.355\ ) \\
Q &= 0.0801L - 0.1980 && (\ 3.355 < L \leqq 4.250\ ) \\
Q &= 0.2443L - 0.8959 && (\ 4.250 < L \leqq 4.413\ ) \\
Q &= 0.2611L - 0.9700 && (\ 4.413 < L \leqq 4.578\ ) \\
Q &= 0.2504L - 0.9211 && (\ 4.578 < L \leqq 4.654\ ) \\
Q &= 0.2375L - 0.8610 && (\ 4.654 < L \leqq 4.815\ ) \\
Q &= 0.2866L - 1.0974 && (\ 4.815 < L \leqq 4.915\ ) \\
Q &= 0.3396L - 1.3580 && (\ 4.915 < L \leqq 5.143\ ) \\
Q &= 0.3607L - 1.4665 && (\ 5.143 < L \leqq 5.365\ ) \\
Q &= 0.3848L - 1.5960 && (\ 5.365 < L \leqq 5.955\ ) \\
Q &= 0.7111 && (\ 5.955 < L\ )
\end{aligned}
\tag{5.9}
$$

The volume Q (m^3) inside the shroud is also given as a function of collapsed water level inside core shroud (L),

$$
\begin{aligned}
Q &= 0.0 && (\ L \leqq 0.0\ ) \\
Q &= 0.2350L && (\ 0.0 < L \leqq 0.497\ ) \\
Q &= 0.1245L + 0.0549 && (\ 0.497 < L \leqq 1.354\ ) \\
Q &= 0.0698L + 0.1290 && (\ 1.354 < L \leqq 3.589\ ) \\
Q &= 0.1648L - 0.2120 && (\ 3.589 < L \leqq 3.744\ ) \\
Q &= 0.1963L - 0.3299 && (\ 3.744 < L \leqq 4.243\ ) \\
Q &= 0.0196L + 0.4199 && (\ 4.243 < L \leqq 4.578\ ) \\
Q &= 0.0186L + 0.4244 && (\ 4.578 < L \leqq 4.654\ ) \\
Q &= 0.0410L + 0.3201 && (\ 4.654 < L \leqq 5.099\ ) \\
Q &= 0.0196L + 0.4292 && (\ 5.099 < L \leqq 5.365\ ) \\
Q &= 0.5344 && (\ 5.365 < L\ )
\end{aligned}
\tag{5.10}
$$

The total fluid mass inventory in the pressure vessel (see Fig. 5.330) is obtained as the summation of the mass inventory outside and inside the shroud. However, it should be noted that the estimated mass inventories contain a certain amount of ambiguity due to the unknown void distribution over the wide regions with various flow areas. The initial mass inventory before the break initiation is estimated as 640 kg.

Figure 5.333 shows the mass decrease by the fluid discharge from the break and the fluid mass recovery by the ECCS water and the feedwater injections. The variation of fluid mass inventory with time is calculated by the following equation,

$$M = \int_0^t \{ G + \rho_1 \cdot (W_H + W_L + W_I) + \rho_2 \cdot W_F \} dt \qquad (5.11)$$

where,

M : mass accumulation,
G : steam discharge flow rate,
ρ_1 : density of satulated liquid at 315 K,
ρ_2 : density of satulated liquid at 489 K,
W_H : volumetric flow rate of the HPCS,
W_L : volumetric flow rate of the LPCS,
W_I : volumetric flow rate of the LPCI,
W_F : volumetric flow rate of the feedwater.

Figure 5.334 shows the fluid mass discharged from the break. The fluid mass discharge M_B is calculated as follows neglecting the change of the fluid mass inventory in the loops,

$$M_B = (M_P)_i - M_P + M_F \qquad (5.12)$$

where,

M_B : fluid mass discharged from the break,
$(M_P)_i$: fluid mass inventory in the pressure vessel (= 640 kg),
M_P : fluid mass inventory in the pressure vessel,
M_F : net fluid mass increase by the ECCS, the feedwater flow and the steam discharge flow.

Figure 5.335 shows the break flow calculated from the fluid mass inven-

tory in the pressure vessel. The break flow is estimated from the mass inventory as follows,

$$G_B = \frac{d}{dt} M_B \tag{5.13}$$

where,

G_B : break flow,

M_B : fluid mass discharged from the break.

6. Test Results

Brief interpretations for the test results of RUN 962 and RUN 963 are presentd in the sections of 6.1 and 6.2, respectively. The effects of break area on the transient thermal hydraulic phenomena in the recirculation loop discharge line breaks are presented in the section of 6.3 by comparing the test results of 100 and 50% break tests with those of 200% break test (RUN 961 [24]).

6.1 Major Events of 50% Break Test (RUN 962)

(1) Pressure Response and Major Events

The pressure in PV (see Fig. 1) showed decrease after break initiation until the MSIV closure at 12 s after break. The pressure control system, which was available in the test, was not actuated because the MSIV was tripped prior to the actuation of the pressure control system. At the break time, the main recirculation pumps (MRP1 and MRP2) tripped and began to coast down (see Fig. 5.46). The feedwater supply was tripped at 1.7 s after break (see Fig. 5.40). After MSIV closure, the pressure in PV turned to increase rapidly and showed maximum value at 24 s after break, when the jet pump suction line was uncovered by the water level in the downcomer. The recirculation loop nozzle in the downcomer was uncovered at 32 s after break and resulted in the rapid depressurization. The initiation of lower plenum flashing followed the recirculation loop nozzle uncovery and slowered the depressurization rate at 50 s after break. The feedwater remained in the feedwater line piping began to flash at the saturation pressure of 2.2 MPa and delayed the depressurization. The ADS was opened at 139 s after break. The LPCS and 3 LPCI were injected at 167 s and 200 s after break, respectively (see Fig. 5.39). The times of major events are shown in Table 4.2.

The pressure in the broken recirculation loop (see Figs. 5.2 through 5.5) show pressure distribution or the major flow restriction along the break flow paths. Pressure differences across the jet pump (JP3,4) drive nozzles (see Fig. 5.13) and main recirculation pump (MRP) (see Fig. 5.14) were very small compared with that across the break nozzle shown in Fig. 5.5. These pressure differences indicate choking occurrence only at the break nozzle.

(2) Break Flow Rates

The fluid in the PV discharged through two break flow paths i.e., through the jet pump drive nozzles and the MRP2, and finally flowed out together through one break nozzle (Break B).

Fluid densities at the break units are detected by the gamma densitometes as shown in Figs. 5.56, 5.57 and 5.147 for the JP-side break flow and Figs. 5.58, 5.59 and 5.148 for the MRP-side break flow. These fluid densities show abrupt decreases due to steam discharge at 29 s and 35 s after break at the break A and break B, respectively. The decrease of fluid density at break A occurred 5 s after the jet pump suction uncovery (JPSU, 24 s after break) and that at break B occurred 3 s after the recirculation line uncovery (RLU, 32 s after break). These time differences are caused by the limitted fluid velocities in the recirculation line pipings as shown below.

The pipe length (L) from the recirculation line outlet nozzle to the break B unit through the MRP2 and that from the JP-3 drive nozzle to the break A unit are 19 m and 9.2 m, respectively. The flow area of 2B pipe of the recirculation line is 1.92×10^{-3} m^2. Average fluid density in the recirculation line during the short time period after break is 750 kg/m^3. By using the average mass flow rates shown below, the average fluid velocities (V) in the MRP-side and PV-side flow paths are calculated as V = 5.3 m/s and V = 1.7 m/s, respectively, and therefore, the arrival times of steam from the downcomer to the break units are 3.6 s and 5.5 s respectively. These times agree with the time differences shown above.

The mass flow rate through the jet pump drive nozzles (see Fig. 5.150) was lower than that through the MRP2 (see Fig. 5.151). The average mass flow rate through the JP-3,4 drive nozzles in the first 29 s was about 2.4 kg/s (24% of the total flow), while that through the MRP2 in 35 s was 7.6 kg/s (76% of the total flow). The total mass flow rate through the break nozzle shown in Fig. 5.152 decreased abruptly at 35 s after break due to steam discharge and thereafter decreased gradually. Increase of discharge flow was observed at 205 s after break due to ECCS water discharge. The discharged mass during the first 35 s is calculated by integrating the total break flow rate as about 340 kg, which corresponds to a half of the initial mass inventory in the system including the recirculation loops.

(3) Level Measurement in Pressure Vessel

The mixture levels were detected by the conduction probes installed on the inner surfaces of pressure vessel wall and channel box wall as shown in Fig. 5.142. The mixture level fall in the lower downcomer agreed well with the collapsed level fall shown in Fig. 5.37. The L2 level (4.76 m from PV bottom) was tripped at 9 s after break following the MSIV closure at 12 s after break. From 250 s after break (50 s after LPCI actuation), the mixture level in the downcomer recovered rapidly, while the collapsed level in the downcomer showed comparatively slower recovery indicating high level swell due to high void fraction.

The mixture level in fuel bundles fell later and recovered earlier than the downcomer mixture level (Fig. 5.142). Due to the level fall in fuel bundles, bottom of the core dried out at 116 s after break. The mixture level recovery began at 210 s after break (10 s after LPCI actuation) and proceeded rapidly. A little differences were observed between the high power and average power bundles, i.e., a little earlier mixture level fall and a little delayed recovery in the average power bundles.

After initiation of lower plenum flashing, a mixture level was formed in the lower plenum until 258 s after break. The mixture level formation in the lower plenum indicates CCFL occurrence at the core inlet orifices. A mixture level was also detected in the guide tube between 120 s and 208 s after break. After LPCS actuation, mixture level was detected above the upper tie plate indicating CCFL at the tie plate.

(4) Fuel Rod Temperature Responses

Figures 5.143 and 5.144 show the dryout and quench fronts of fuel rods in the high and average power bundles. Following facts have been observed. (1) The dryout and quench behaviors in the high power bundle agreed well with those in the average power bundles. (2) The dryout fronts showed little scattering and agreed well with the mixture level fall in each bundle. (3) The quench fronts, however, distributed widely in the upper core because of top-down and bottom-up coolings. The quench times distributed between the LPCS actuation time and the arrival time of bottom-up collapsed level. The final quench was accomplished by the bottom-up quench.

By investigating all the test results of fuel rod surface temperatures shown in Fig. 5.75 through 5.118, following facts have been obtained. (1) The peak cladding temperature (PCT) was detected as 933 K at 208 s after

break (41 s after LPCS actuation or 8 s after LPCI actuation) at the mid-plane of A82 rod in the high power bundle. (2) Dryout of fuel rods occurred twice after break. The first dryout occurred only at the upper part (Positions 1 and 2) of the core at 36 s after break and diminished by the initiation of lower plenum flashing. The second dryout occurred after termination of the lower plenum flashing from the top of core (62 s) to the bottom of core (116 s) after break. (3) The fuel rods in the high power bundle (radial peaking factor of 1.4) showed temperature increasing rate after dryout higher than those of average power bundles (radial peaking factor of 1.0) and caused the PCT. (4) The LPCS actuation contributed to slower fuel rod temperature increase (middle part of core) and quench of fuel rods (top and bottom of core). The 3 LPCI actuation resulted in turnaround of fuel temperature responses and completed the quench process. The final quench was completed at 272 s after break (72 s after LPCI actuation) at the positions 1 and 2.

6.2 Major Events of 100% Break Test (RUN 963)

(1) Pressure Response and Major Events

The pressures in the pressure vessel shown in Fig. 5.165 began to decrease after break and turned to increase by MSIV closure at 9.5 s after break. The L2 and L1 level signals were sent at 8.2 s and 14 s after break, respectively. The suction lines of jet pumps and main recirculation pump were uncovered at 19 s and 25.0 s, respectively. After jet pump suction uncovery, the pressure turned to decrease and the depressurization was promoted rapidly by the recirculation pump suction line uncovery. The lower plenum flashing (at 35 s after break) followed the recirculation line uncovery and contributed to slower the depressurization. The feedwater flashing began at 111 s after break and delayed the depressurization. The LPCS and 3 LPCI were injected at 126 s and 155 s, respectively. The ADS was actuated at 135 s after break.

The pressure at the upstream of break nozzle showed fairly lower value than those in the pressure vessel. The differential pressure across the jet pump drive nozzles (see Fig. 5.177) and the main recirculation pump (see Fig. 5.178) in the broken loop were the same because the pressures at the upstream and downstream of the jet pump drive nozzle were common to those of

the main recirculation pump. After the recirculation pump suction line uncovery, the differential pressure increased abruptly and showed maximum value of 1.8 MPa.

(2) Break Flow Rate

The fluid in the pressure vessel discharged through two break flow paths, i.e., through the jet pump drive nozzles and the recirculation pump, and finally flowed out together through one break nozzle (Break B). The fluid densities at the break A and break B showed decrease twice after break. The second decreases correspond to the jet pump suction uncovery (JPSU, 19 s after break) and the recirculation line uncovery (RLU, 25 s after break).

The mass flow rate through the jet pump drive nozzle (see Fig. 5.315) was lower than that through the main recirculation pump (see Fig. 5.316). The average mass flow rate through the jet pump drive nozzle during the first 22 s was 3.5 kg/s (24% of the total flow rate shown in Fig. 5.317) and that through the recirculation pump during the first 25 s was 11.2 kg/s (76% of the total flow rate). The total mass flow rate through the break nozzle showed abrupt decrease at 25 s after break and thereafter decreased gradually. The discharged mass during the first 25 s was calculated by integrating the flow rate as about 360 kg, which corresponds to about a half of the initial mass inventory in the system including the recirculation loops.

(3) Level Measurement in Pressure Vessel

Figure 5.308 shows the mixture level transients detected by the conduction probes in PV. The mixture level in the lower downcomer decreased rapidly and agreed with the response of the collapsed water level in the downcomer shown in Fig. 5.201. The mixture level recovery, however, was not so evident as the level fall. During 200 s and 240 s, the mixture level recovered in the lower downcomer. The collapsed water level in the lower and upper downcomers shown in Fig. 5.201 indicate that some amount of voids existed in the recovery process.

The mixture level in the fuel bundles fell later and recovered earlier than the mixture level in the downcomer. A temporary level fall was observed during 23 s and 39 s after break and diminished by initiation of the lower plenum flashing. The second level fall began at 50 s after break

in the average power bundles and at 60 s after break in the high power bundle. The bottom of the core was uncovered at 89 s after break. The mixture level was recovered at 162 s after break (7 s after LPCI actuation) from bottom of the core. It is shown that the mixture level in the average power bundle was lower than that in the high power bundle above the midplane of the core.

The mixture level was formed in the lower plenum after initiation of lower plenum flasing. Similar level was formed in the guide tube.

(4) Fuel Rod Temperature Responses

Figure 5.309 shows the dryout and quench fronts of fuel rods in the high and average power bundles, respectively. These figures indicate the followings. (1) The dryout front of rods agreed well with the transient mixture level fall in each bundle. (2) The dryouts of fuel rods occurred simultaneously in the same horizontal plane. (3) The quench fronts, however, distributed widely in both bundles between the time of LPCS actuation and the arrival time of the bottom-up collapsed level. (4) The final quench was completed by the bottom-up quench. (5) Earlier dryout and later quench were observed in the average power bundles than those of the high power bundle.

By investigating all the test results of fuel rods surface temperatures shown in Figs. 5.239 through 5.282, following foundings were obtained. (1) The PCT was detected as 915 K at 167 s after break (41 s after LPCS actuation or 12 s after LPCI actuation) at the midplane of the peak power rod A82 in the high power bundle. (2) Dryout of fuel rods was observed twice at the upper part (Positions 1 and 2) of core. The second dryout occurred from the top of core at 50 s after break in the average power bundles and 61 s after break in the high power bundle. Bottom of core was uncovered at 89 s after break in both bundles. (3) The effect of radial peaking factor (1.4 for the high power bundle and 1.0 for the average power bundles) appeared on the temperature increasing rate after dryout. The higher heat flux in the high power bundle caused the PCT. (4) The actuation of LPCS contributed to better heat transfer in the steam flow cooling phase and the actuation of 3 LPCI resulted in completion of quench process. The final quench of fuel rods was completed at positions 1 and 2 of D22 rod in the average power bundle at 233 s after break (78 s after LPCI actuation).

6.3 Effects of Break Area on Major Events of RUNs 961, 962 and 963

The effects of break area on the following items are studied below by comparing the test results of 200% (RUN 961), 100% (RUN 963) and 50% (RUN 962) i.e., (1) pressure response and major events, (2) level measurement and mass inventory, (3) break flows and pressure distribution along the two break flow paths, (4) core cooling behavior. The test conditions and procedures of RUN 961 were the same as those of RUN 962 and 963 except for the break area.

(1) Effects of Break Area on Pressure Response and Major Events

Figure 6.1 shows the lower plenum pressures of the three tests. It is shown in the figure that the pressure responses of RUNs 961 and 963 agree well within a small time difference and that they are clearly different from that of RUN 962. The agreement of pressure response between RUNs 961 and 963 means agreement of total break flow rates because the other transient test conditions are the same in these two tests.

Table 6.1 compares the major events of the three tests. After break initiation, the main recirculation pump was tripped and decreased the core flow rate in each test. The feedwater supply was terminated similarly in each test. The MSIV closure times of RUNs 961, 963 and 962 are 8.5 s, 9.5 s and 12 s, respectively. The initiaions of the lower plenum flashing of RUNs 961, 963 and 962 are 30 s, 35 s and 50 s, respectively. The initiations of feedwater flashing at 2.2 MPa in RUNs 961, 963 and 962 are 105 s, 111 s and 154 s after break, respectively.

The depressurization rates of RUNs 961, 963 and 962 between 6.4 and 2.2 MPa are obtained as 0.056, 0.055 and 0.040 MPa/s, respectively. The depressurization rate of RUN 963 agreed well with that of RUN 961, while the depressurization rate of RUN 962 is 71% of that of RUN 961. Thus, the break mass flow in RUN 962 must be fairly different from those of RUNs 961 and 963.

The LPCS of RUN 963 was actuated at a little lower pressure than that of RUN 961, and therefore, actuated 21 s after that of RUN 961. The times of major events of RUN 963 agreed well with those of RUN 961 within 21 s as shown in Table 6.1. On the other hand, the times of major events of RUN 962 delayed further than those of RUN 961 as the system pressure went down.

(2) Effects of Break Area on Water Level and Mass Inventory

The collapsed water levels in the downcomer in the three tests are compared in Fig. 6.5. The upper downcomer collapsed level in RUN 962 was not measured. The times of recirculation pump suction line uncovery in RUNs 961, 963 and 962 are 22 s, 25 s and 32 s, respectively, which are dependent mainly on the mass discharge flow rate from the downcomer to the break nozzles after break. A little time difference exists between the level falls in RUNs 961 and 963 due to the difference of mass flow rates through the breaks in the early blowdown phase (see Fig. 6. 12). The times of L1 level in RUNs 961, 963 and 962 are 12 s, 14 s and 19 s after break, respectively. As there is a little time difference among the L1 level times of the three tests, the ADS actuated in the similar times as shown in Table 6.1.

Figure 6.6 shows the differential pressure data measured between the elevations of the jet pump suction line (EL 2.814 m) and top of the steam dome (EL 5.910 m), and it contributed to understand the mass inventory transient in the upper downcomer. The downcomer mass inventories of the three tests showed similar trend with some time difference. Figures 6.7 and 6.8 show the differential pressures between the lower plenum and upper plenum and between the lower plenum and steam dome, respectively. Figure 6.9 shows the mass inventory inside the core shroud. These figures suggest that the transients of mass inventory inside core shroud occurred similarly with some time differences among the three tests. The time period between the decrease and recovery of mass inventory corresponds the dryout time of fuel rods.

(3) Effects of Break Area on Break Flows and Pressure Distribution along the Break Flow Paths

Figures 6.10, 6.11 and 6.12 compare the break mass flow rates through the jet pump (JP-3,4) drive nozzles, the main recirculation pump (MRP2) discharge nozzle and the break nozzle of three tests, respectively. The total break flow rate is a sum of the two break mass flow rates through JP-3,4 and MRP2.

All the break flow data show the same tendancies, such as abrupt increase after break, high mass flow rate until steam discharge and rapid decrease due to steam discharge after the recirculation line uncovery. The

changes of depressurization rate after MSIV closure mentioned in the section 6.3 (1) correspond to the times of steam discharge shown in the figures.

Table 6.2 compares the discharge mass flow rates of RUNs 961, 963 and 962 in a short time periods after break until the recirculation line uncoveries. Followings are found from these figures and table.

(a) The discharge mass flow rates in RUN 963 (100% break) agree well with those of RUN 961 (200% break) in all test period in spite of the different break conditions. This fact confirms the same choking conditions along the two break flow paths in both tests. A very small difference is observed in RUN 963 in a short time period after break, which caused a little delay of downcomer level fall and recirculation line uncovery time in RUN 963 compared with those of RUN 961.

(b) The discharge mass flow rates in RUN 962 (50% break) are similar but fairly smaller compared with those in RUNs 961 and 963. The total break mass flow rate during the high mass flow rate phase after break in RUN 962 is about 60% of that in RUN 961. This ratio of 60% is small compared with the ratio of choking flow areas between RUNs 962 and 961 (70%). In RUN 962, the break mass flow rate is determined by the choking flow at the break nozzle as mentioned previously. However, the pressure at the upstream of break nozzle is lower than that in the downcomer due to a pressure loss at the JP-3,4 drive nozzles (see Fig. 6.17, pressure difference across the nozzle is 0.5 MPa at 50 s after break in RUN 962), while the pressure at the upstream of the choked JP-3,4 drive nozzles in RUN 961 are nearly equal to the pressure in the downcomer. And the pressure at the upstream of the MRP2 drive nozzle, where choking occurred in RUN 961, is also nearly equal to the pressure in the downcomer. Therefore, the pressure at the upstream of choking location in RUN 962 is a little lower than those in RUN 961 and this is a reason why the ratio of total break mass flow rates between RUN 962 and RUN 961 in the short time period after break is smaller than a ratio of the least choking flow areas between RUN 962 ($A = 50\%$) and RUN 961 ($A_j + A_p = 72\%$), i.e., $50/72 = 0.7$.

(c) It is concluded that the discharge mass flow from the pressure vessel and therefore the depressurization rate in the pressure vessel are controlled by a sum of the least choking flow areas along the break flow paths. It is also concluded that the depressurization rate is affected a little by the flow resistances at the upstream of the least choking

flow areas. The sum of the least choking flow areas is named here an effective choking flow area in each break test. Namely, the effective choking flow area is 72% for the 200 and 100% discharge line break tests and 50% for the 50% discharge line break test in the ROSA-III tests as shown in Table 6.3.

(d) The ratio of JP-side discharge mass flow rate and MRP-side flow rate in the short time period after break is equal to 1 : 3 for the three tests. This ratio is deviated from the flow area ratio between A_j and A_p, i.e., $A_j : A_p = 1 : 2.2$, due to a large energy loss at the inlet region of the JP-3,4 drive nozzles.

In general, the effective choking flow area of the recirculation pump discharge line break LOCAs is $(A_j + A_p)$ for the breaks with larger break areas than $(A_j + A_p)$ and is A (=break area) for the breaks with smaller break areas than $(A_j + A_p)$. In a BWR/6 system, A_j is 21% of the recirculation line flow area, while A_p varies from 30 to 100% depending on the reactor.

Figures 6.13 and 6.14 show the average fluid densities at the upstreams of break nozzle. The fluid densities of RUN 962 show no vapor formation at the upstreams of the break nozzle in the time period after break until the recirculation line uncoveries. The fluid densities in the region during the short time period after break in RUN 963 are higher than those of RUN 961 because of the higher pressure and lower void fraction in RUN 963.

Pressures at the upstream of break nozzle in RUNs 961, 963 and 962 are compared in Figs. 6.15 and 6.16. In spite of the similar trends of pressures in PV in RUNs 961 and 963, the pressures at the upstreams of break nozzle in RUN 963 are fairly higher than those in RUN 961. The difference was created immediately after break, when larger mass flowed out through the larger break nozzle area (A = 200%) in RUN 961 and the pressure at the upstream of break nozzle decreased rapidly. The larger deprrssurization in RUN 961 resulted in higher void fraction in the upstreams of the break nozzles. However, this difference of fluid conditions in the region between RUNs 963 and 961 does not affect the choking flows at the nozzles of JP-3,4 and MRP2. Thus, the pressure response in PV is controlled by the least choking flow areas along the break flow paths mentioned above. Figure 6.17 shows the differential pressures across the JP-3 drive nozzle in the three tests.

(4) Comparison of Fluid Temperatures in the System

Figures 6.18 through 6.21 compare the fluid temperatures in the lower plenum, upper plenum, steam dome and bottom of the downcomer in the three tests. These figures show good agreements between the responses of fluid temperatures in RUN 963 and RUN 961 and show a similar but delayed response of RUN 962 compared with those of RUN 961. These tendancies among the fluid temperatures of three tests correspond well to the tendancies of pressure responses shown before. The lower plenum temperature in each test was close to each saturation temperature except for the time periods before the lower plenum flashing and in the later reflooding phase when the subcooling temperatures were detected. The steam dome temperature showed super-heated steam temperature at 90 s through 125 s after break in three tests. The fluid temperatures in the upper plenum and downcomer showed intermediate trends between the former two.

(5) Effects of Break Area on Core Cooling Phenomena

Figures 6.22 through 6.24 show the representative surface temperatures at the top (position 1), middle (position 4) and bottom (position 7) of the core in the three tests. The fuel rod A11 has the highest local peaking factor of 1.13 in the high power bundle A (radial peaking factor of 1.4). It is found from these figures that (a) the major dryout of fuel rod appeared at the midplane (axial peaking factor of 1.4) of the fuel rod in the three tests and (b) the temperature responses of three tests were similar in all the test periods. The dryout and quench processes of RUNs 962 and 963 (see the section 6.1 and 6.2) were similar with some time differences.

Figure 6.25 shows the surface temperature responses at the midplane of C11 rod, which has the local peaking factor of 1.13 in the average power bundle C with the radial peaking factor of 1.0. The dryout of fuel rod C11 occurred a little earlier and the quench occurred a little later than those of A11 rod. The maximum surface temperature of C11 rod, however, is lower than that of A11 rod due to the smaller temperature increasing rate after dryout caused by the smaller heat flux. Therefore, the peak cladding temperature (PCT) was observed at the midplane of the high power bundle A. And the PCT occurred immediately after the LPCI actuation. These trends are common in the three tests. The PCT of the three discharge line break tests

are listed in Table 6.4 by comparing with those of corresponding suction line break tests. It is shown that the highest PCT was observed in the 50% break test among the discharge and suction line break tests.

The actuation times of LPCI (see Table 6.1) of three tests are 144 s after break in RUN 961, 155 s after break in RUN 963 and 200 s after break in RUN 962. On the other hand, the dryout times of the PCT rods (see Fig. 6.26) in the three tests are 63 s, 68 s and 81 s after break in RUNs 961, 963 and 962, respectively. The time periods between the initiation of dryout and LPCI actuation in the three tests are derived as 81 s, 87 s and 119 s in RUNs 961, 963 and 962, respectively. Thus, the longer time period of dryout resulted in the higher PCT among the three tests.

Figure 6.27 shows a relation of the PCT and the break area ratio among the recirculation loop break tests with HPCS failure in the ROSA-III program. The PCT values of 200 and 100% discharge line break tests are fairly higher than those of 200 and 100% suction line break tests. However, the PCT value of 200 and 100% discharge line break tests are rather close to the PCT value of the 75% suction line break test shown in Table 6.4.

7. Conclusions

Two recirculation pump discharge line break tests with break areas of 100% (RUN 963) and 50% (RUN 962) were performed at the ROSA-III test facility. These test results were compared with those of a 200% discharge line break test (RUN 961[24]) to clarify the effects of break area on the fundamental thermal hydraulic phenomena. Following conclusions have been obtained.

(1) An effective choking flow area, which is a sum of the least choking flow areas in the two break flow paths limits the depressurization rate after break and controls the major events in the recirculation line break LOCA, such as downcomer level fall, lower plenum flahing, ECCSs actuation and the core cooling phenomena. The effective choking for the depressurization occurs at the jet pump drive nozzle (area : A_j) and the main recirculation pump discharge nozzle (area : A_p) or the break nozzle (area : A) in the recirculation line.

(2) In the 200 and 100% discharge line break tests at ROSA-III facility, the effective choking flow area is $A_j + A_p$ (= 72%), where A_j = 21% and A_p = 51% of 1/424 scaled BWR recirculation line flow area. Therefore, the fundamental phenomena in the 100% break test are similar to those of the 200% break test within a small time difference. On the other hand, the effective choking flow in the 50% break test occurrs at the break nozzle (A = 50%). The ratio of depressurization rate after lower plenum flashing between the 50 and 200% break tests agrees well to the ratio of the effective choking flow areas between them.

(3) In general, the maximum effective choking flow area is $A_j + A_p$ for recirculation pump discharge line break LOCAs. Similaly the maximum effective choking flow area is A_j + 100% for recirculation pump suction line break LOCAs. These conclusions can be applied to the BWR LOCAs. The A_j for the BWR/6 is 21%, whereas the A_p varies from 30 to 100% in reactors.

(4) The peak cladding temperatures (PCT) are 933 K, 915 K and 894 K in the 50, 100 and 200% break tests, respectively. The highest PCT is observed in the 50% break test and this tendancy is the same as the recirculation pump suction line break tests with HPCS failure in the ROSA-III program.

Acknowledgment

The authors are grateful to M. OKAZAKI of Institute of Nuclear Safety, Japan, Y. KOIZUMI of Reactor Safety Lab.1 in JAERI for their planning and conducting the ROSA-III program, H. ASAHI, T. ODAIRA, T. TAKAYASU, S. SEKIGUCHI, Y. KITANO and T. NUMATA of Nuclear Engineering Corporation for their assistance in conducting the experiment and H. GOTOH of Information System Laboratory Corpolation for preparing the data plots. The authors are also grateful to M. SOBAJIMA of Reactor Safety Lab.2 in JAERI for his useful comments.

References

(1) K.TASAKA, et al., "Study on the Similarity between ROSA-III Experiment and BWR LOCA", JAERI-M 6703 (1976) (in Japanese).
(2) Y.ANODA, et. al.,"ROSA-III System Description for Fuel Assembly No. 4", JAERI-M 9363 (1981) (in Japanese).
(3) General Electric Company, "General Electric Standard Safety Analysis Report, BWR/6", DOCKET-STN-50477 (1978).
(4) M.SHIBA, et. al.,"Small Break LOCA Experiment in ROSA-III", IAEA-CN-39/69 (1981).
(5) M.SHIBA, et. al.,"Break Area Test Series of ROSA-III for BWR LOCA/ECCS Test", 9th Water Reactor Safety Research Information Meeting (1981).
(6) K.TASAKA, et. al.,"BWR LOCA/ECCS Integral Test at ROSA-III, (Recirculation Pump Discharge Line and Steam Line Breaks)", 10th Water Reactor Safety Research Information Meeting (1982).
(7) K.TASAKA, et. al.,"The LOCA/ECCS System Effect Tests at ROSA-III Changing the Break Area as Test Parameter", Int. Meeting on Ther. Nucl. Reactor Safety (Chicago, 1982).
(8) K.SODA et al.,"Boiling Water Reactor Loss of Coolant Tests (Single Failure Tests with ROSA-III)", J. Nucl. Sci. Tech. (20) (1983).
(9) K.TASAKA, et. al.,"Simulation Experiment of Five Percent Small Break LOCA of BWR", J. Nucl. Sci. Tech. (20) (1983).
(10) K.TASAKA et. al.,"ROSA-III Base Test Series for a Large Break Loss of Coolant Accident in a Boiling Water Reactor", Nucl. Techn. (57)(1982)
(11) K.TASAKA et. al.,"Steam Line Break, Jet Pump Drive Line Break and Natural Circulation Tests in ROSA-III Program for BWR LOCA/ECCS Integ-

Acknowledgment

The authors are grateful to M. OKAZAKI of Institute of Nuclear Safety, Japan, Y. KOIZUMI of Reactor Safety Lab.1 in JAERI for their planning and conducting the ROSA-III program, H. ASAHI, T. ODAIRA, T. TAKAYASU, S. SEKIGUCHI, Y. KITANO and T. NUMATA of Nuclear Engineering Corporation for their assistance in conducting the experiment and H. GOTOH of Information System Laboratory Corpolation for preparing the data plots. The authors are also grateful to M. SOBAJIMA of Reactor Safety Lab.2 in JAERI for his useful comments.

References

(1) K.TASAKA, et al., "Study on the Similarity between ROSA-III Experiment and BWR LOCA", JAERI-M 6703 (1976) (in Japanese).

(2) Y.ANODA, et. al.,"ROSA-III System Description for Fuel Assembly No. 4", JAERI-M 9363 (1981) (in Japanese).

(3) General Electric Company, "General Electric Standard Safety Analysis Report, BWR/6", DOCKET-STN-50477 (1978).

(4) M.SHIBA, et. al.,"Small Break LOCA Experiment in ROSA-III", IAEA-CN-39/69 (1981).

(5) M.SHIBA, et. al.,"Break Area Test Series of ROSA-III for BWR LOCA/ECCS Test", 9th Water Reactor Safety Research Information Meeting (1981).

(6) K.TASAKA, et. al.,"BWR LOCA/ECCS Integral Test at ROSA-III, (Recirculation Pump Discharge Line and Steam Line Breaks)", 10th Water Reactor Safety Research Information Meeting (1982).

(7) K.TASAKA, et. al.,"The LOCA/ECCS System Effect Tests at ROSA-III Changing the Break Area as Test Parameter", Int. Meeting on Ther. Nucl. Reactor Safety (Chicago, 1982).

(8) K.SODA et al.,"Boiling Water Reactor Loss of Coolant Tests (Single Failure Tests with ROSA-III)", J. Nucl. Sci. Tech. (20) (1983).

(9) K.TASAKA, et. al.,"Simulation Experiment of Five Percent Small Break LOCA of BWR", J. Nucl. Sci. Tech. (20) (1983).

(10) K.TASAKA et. al.,"ROSA-III Base Test Series for a Large Break Loss of Coolant Accident in a Boiling Water Reactor", Nucl. Techn. (57)(1982)

(11) K.TASAKA et. al.,"Steam Line Break, Jet Pump Drive Line Break and Natural Circulation Tests in ROSA-III Program for BWR LOCA/ECCS Integ-

ral Tests", 11th Water Reactor Safety Research Inform. Meeting (1983).
(12) K.TASAKA, et. al.,"ROSA-III Double-Ended Break Test Series for a Loss-of-Coolant Accident in a Boiling Water Reactor", Nucl. Techn. (68) (1985).
(13) M.SUZUKI, et. al.,"Recirculation Pump Discharge Line Break Tests at ROSA-III for a Boiling Water Reactor", Nucl. Techn. to be published.
(14) M.SOBAJIMA, et. al.,"Experiment Test Data of ROSA-III Test RUN 701 (Decay Heat Simulation Test with ECCS Actuation)", JAERI-M 8604 (1979).
(15) Y.ANODA et. al.,"Experiment Data of ROSA-III Test RUN 703 (Split Break Simulation Test with ECCS Actuation)", JAERI-M 8967 (1980).
(16) Y.ANODA et. al.,"Experiment Data of ROSA-III Test RUN 704 (Standard Test with ECCS Actuation)", JAERI-M 8968 (1980).
(17) M.OKAZAKI et. al.,"Experimet Test Data of ROSA-III Integral Test RUN 705 (Isothermal Blowdown Test without ECCS Actuation)", JAERI-M 8723 (1980).
(18) M.SUZUKI et. al.,"Experiment Data of ROSA-III Integral Test, RUN 706", JAERI-M 8737 (1980).
(19) M.OKAZAKI et. al.,"Experiment Data of ROSA-III Integral Test RUN 708 (Standard Test without ECCS Actuation)", JAERI-M 8738 (1980).
(20) Y.KOIZUMI et. al.,"Experiment Data of ROSA-III Integral Test, RUN 710", JAERI-M 9249 (1981).
(21) Y.ANODA et. al.,"Experimet Data of ROSA-III Integral Test RUN912 (5% Split Break Test without HPCS Actuation)", JAERI-M 82-010.
(22) H.NAKAMURA et. al.,"Experiment Data of ROSA-III Integral Test RUN 901 (200% Double-Ended Break with Full ECCS Actuation)", JAERI-M 84-007.
(23) H.NAKAMURA et. al.,"Experiment Data of ROSA-III Integral Test RUN 926 (200% Double-Ended Break with HPCS Failure)", JAERI-M 84-008.
(24) M.SUZUKI et. al.,"Experiment Data of 200% Recirculation Pump Discharge Line Break Integral Test RUN 961 with HPCS Failure at ROSA-III and Comparison with Results of Suction Line Break Tests", JAERI-M 84-045, (1984).
(25) M.SUZUKI, et. al.,"Recirculation Pump Suction Line 2.8% Break Integral Test at ROSA-III with HPCS Failure, RUN 984", JAERI-M 84-100, (1984).
(26) M.SUZUKI, et. al.,"Recirculation Pump Suction Line 200% Break Integral Test at ROSA-III with Two LPCI Failures, RUN 983", JAERI-M 84-135, (1984).
(27) M.KAWAJI et. al.,"A Main Steam Line Break Experiment at ROSA-III RUN 952 (Standard Run with Full ECCS", JAERI-M 84-229, (1984).

(28) M.SUZUKI et. al.,"Heat Loss and Fluid Leakage Tests of the ROSA-III Facility", JAERI-M 9834 (1981).

(29) M.SUZUKI, et. al.,"Characteristics of the ROSA-III Test Facility (Characteristics Test of the Jet Pumps in Normal and Reverse Flow)", JAERI-M 8670, (1980) (in Japanese).

(30) M.SUZUKI, et. al.,"Evaluation of a Jet Pump Model for RELAP5 Code", JAERI-M 84-245, (1985) (in Japanese).

(31) W. J. Letzring, et. al.,"BWR Blowdown/ECC Program Preliminary Facility Description Report for the BD/ECC1a Test Phase", GEAP-23592.

(32) GE, EPRI and NRC,"Full Integral Simulation Test (FIST) Program Test Plan", EPRI NP-2313, GEAP 22053, (1981).

(33) M.MURASE et. al.,"BWR Loss-of-Coolant Integral Test -- Parallel Channel Effect", NUREG/CP-0027-Vol.3, (1982).

(34) M.SOBAJIMA et. al.,"Instrumentation and Data Processing Method of the ROSA-III Test", JAERI-M 8499 (1979) (in Japanese).

(35) N.ABE et. al.,"Electric Power Tansient Curve for ROSA-III Tests", JAERI-M 8728 (1980).

(36) GE Company, "General Electric Standard Safety Analysis Report, BWR/6", DOCKET-STN-50531-22.

Table 2.1 Primary chracteristics of ROSA-III and BWR/6

	BWR-6	ROSA-III	BWR/ROSA
No. of Recirc. Loops	2	2	1
No. of Jet Pumps	24	4	6
No. of Separators	251	1	251
No. of Fuel Assemblies	848	4	212
Active Fuel Length (m)	3.76	1.88	2
Total Volume (m^3)	621	1.42	437
Power (MW)	3800	4.40	864
Pressure (MPa)	7.23	7.23	1
Core Flow (kg/s)	1.54×10^4	36.4	424
Recirculation Flow (l/s)	2970	7.01	424
Feedwater Flow (kg/s)	2060	4.86	424
Feedwater Temp (K)	489	489	1

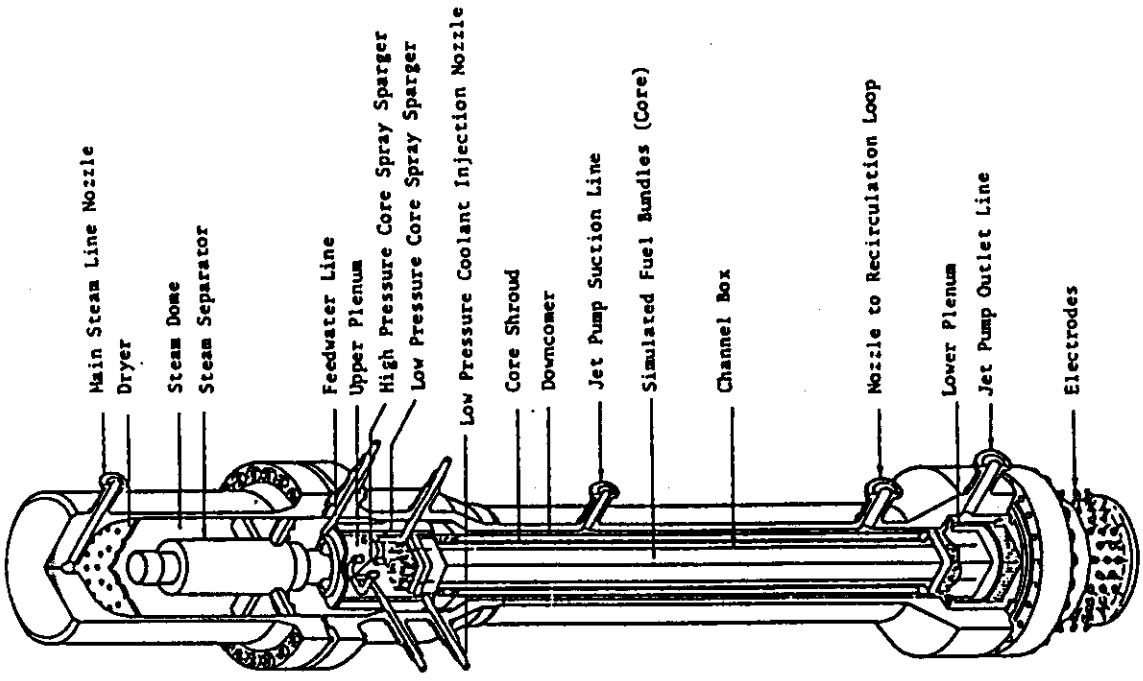

Fig.2.2 Internal structure of the pressure vessel of ROSA-III

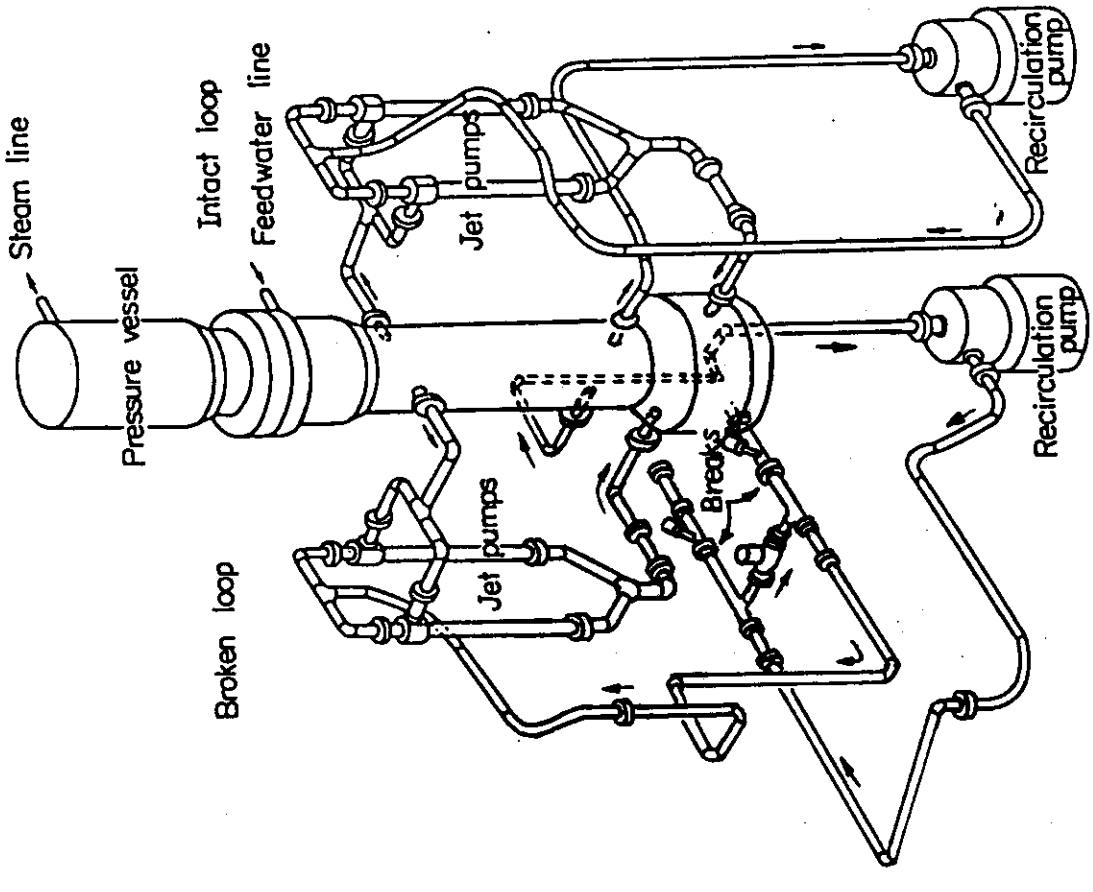

Fig.2.1 Schematic diagram of the ROSA-III Test Facility

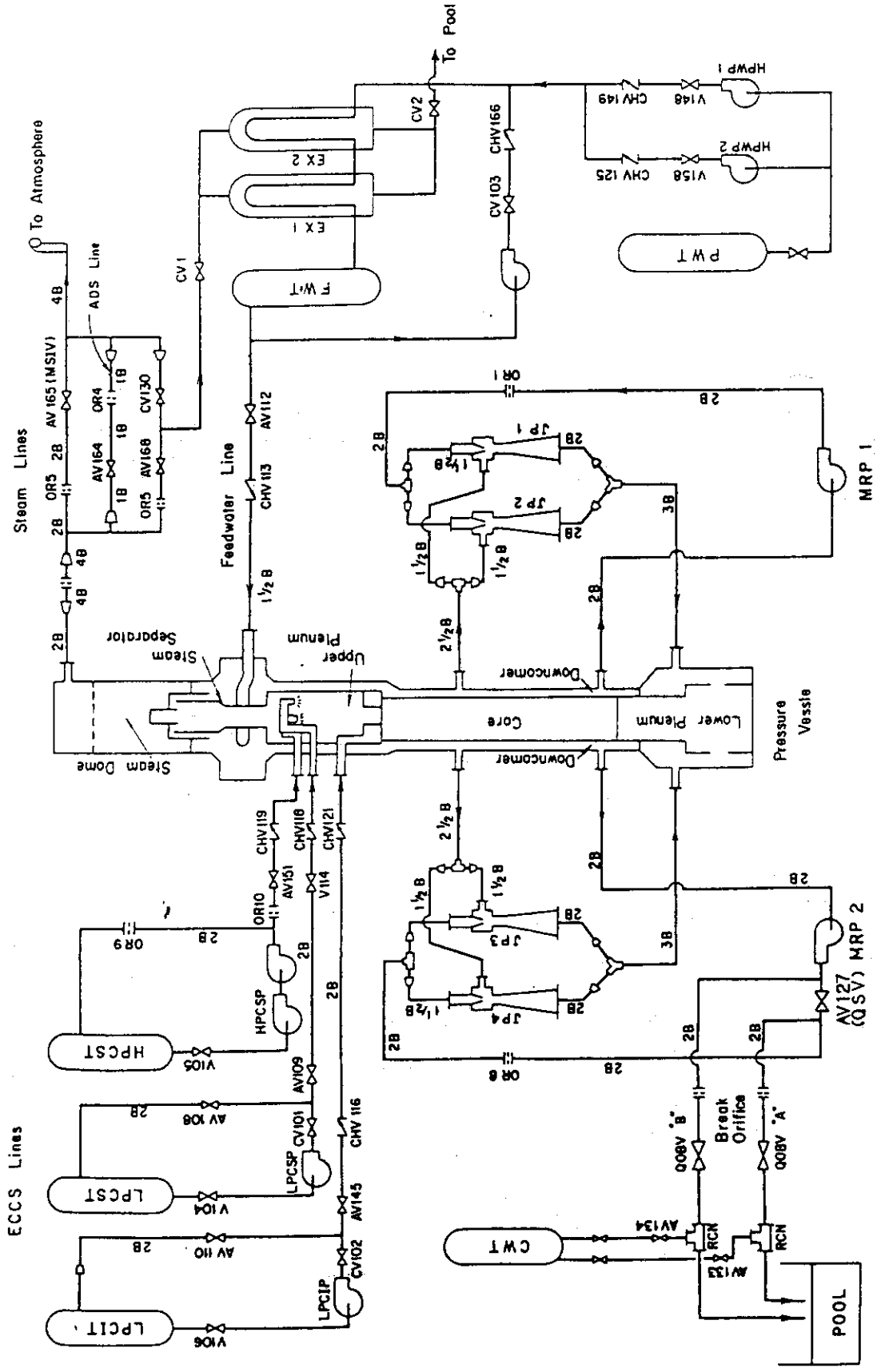

Fig.2.3 ROSA-III piping schematic

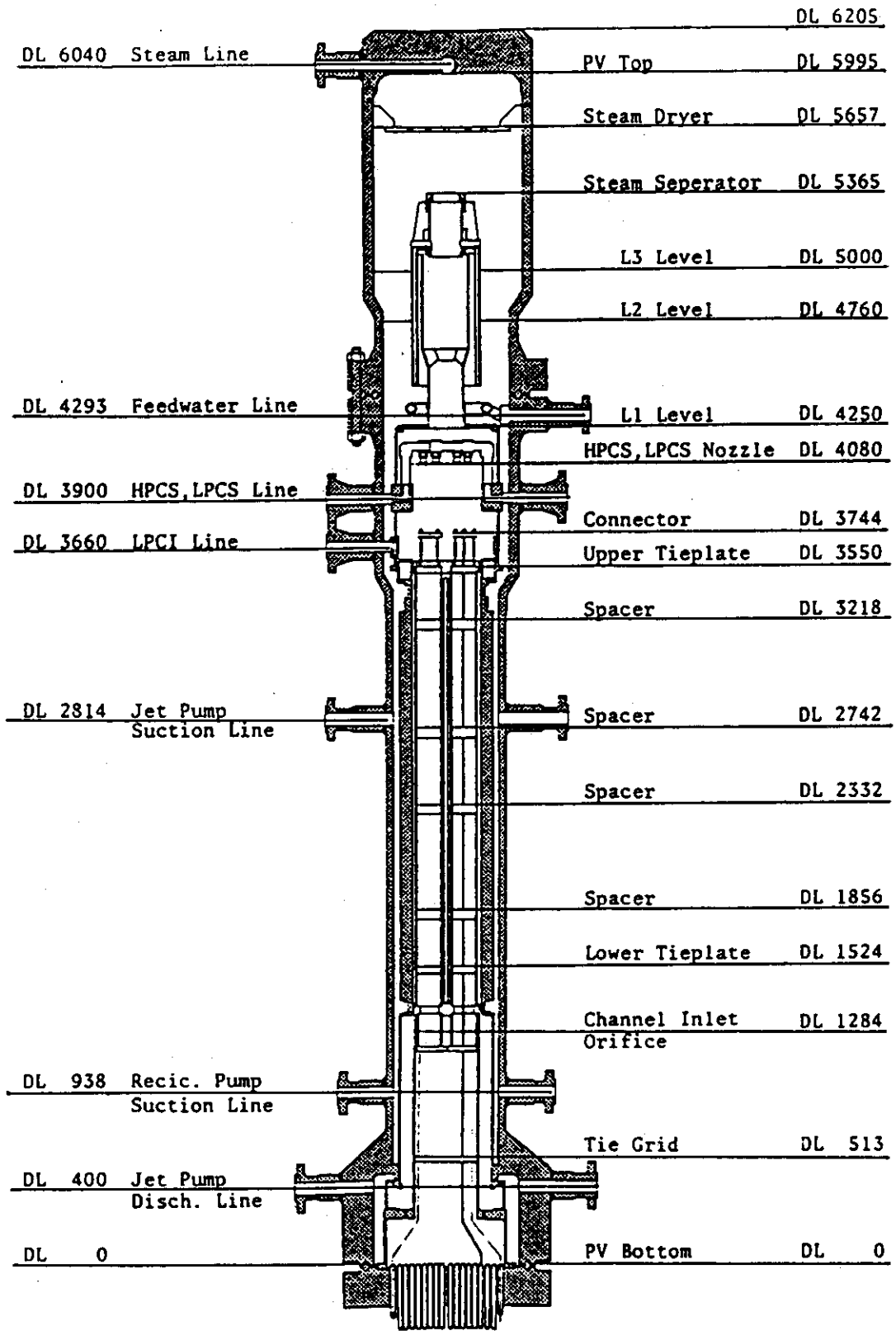

Fig. 2.4 Pressure vessel internals arrangement

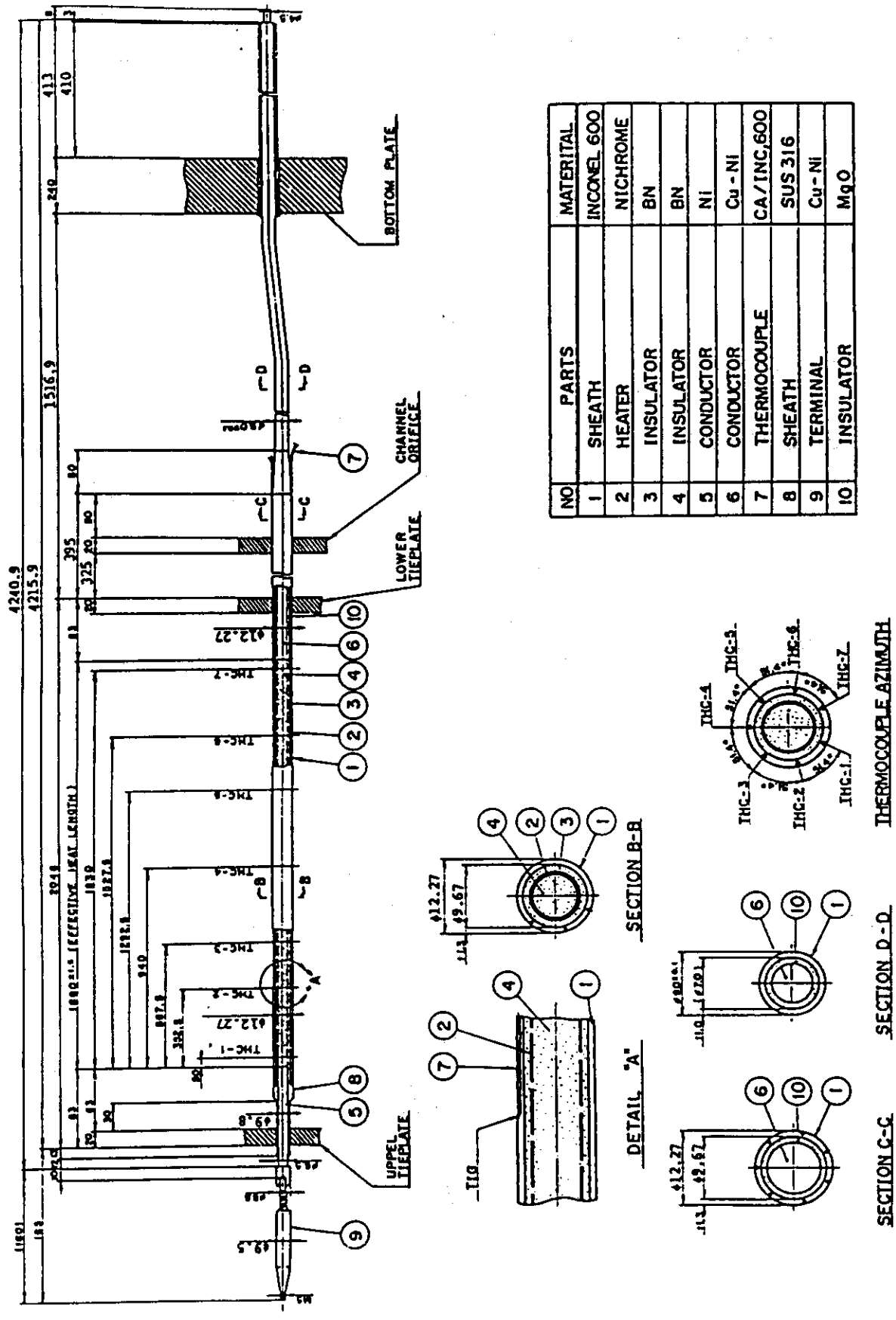

NO	PARTS	MATERITAL
1	SHEATH	INCONEL 600
2	HEATER	NICHROME
3	INSULATOR	BN
4	INSULATOR	BN
5	CONDUCTOR	Ni
6	CONDUCTOR	Cu - Ni
7	THERMOCOUPLE	CA/INC,600
8	SHEATH	SUS 316
9	TERMINAL	Cu - Ni
10	INSULATOR	MgO

Fig. 2.5 Simulated fuel rod of ROSA-III

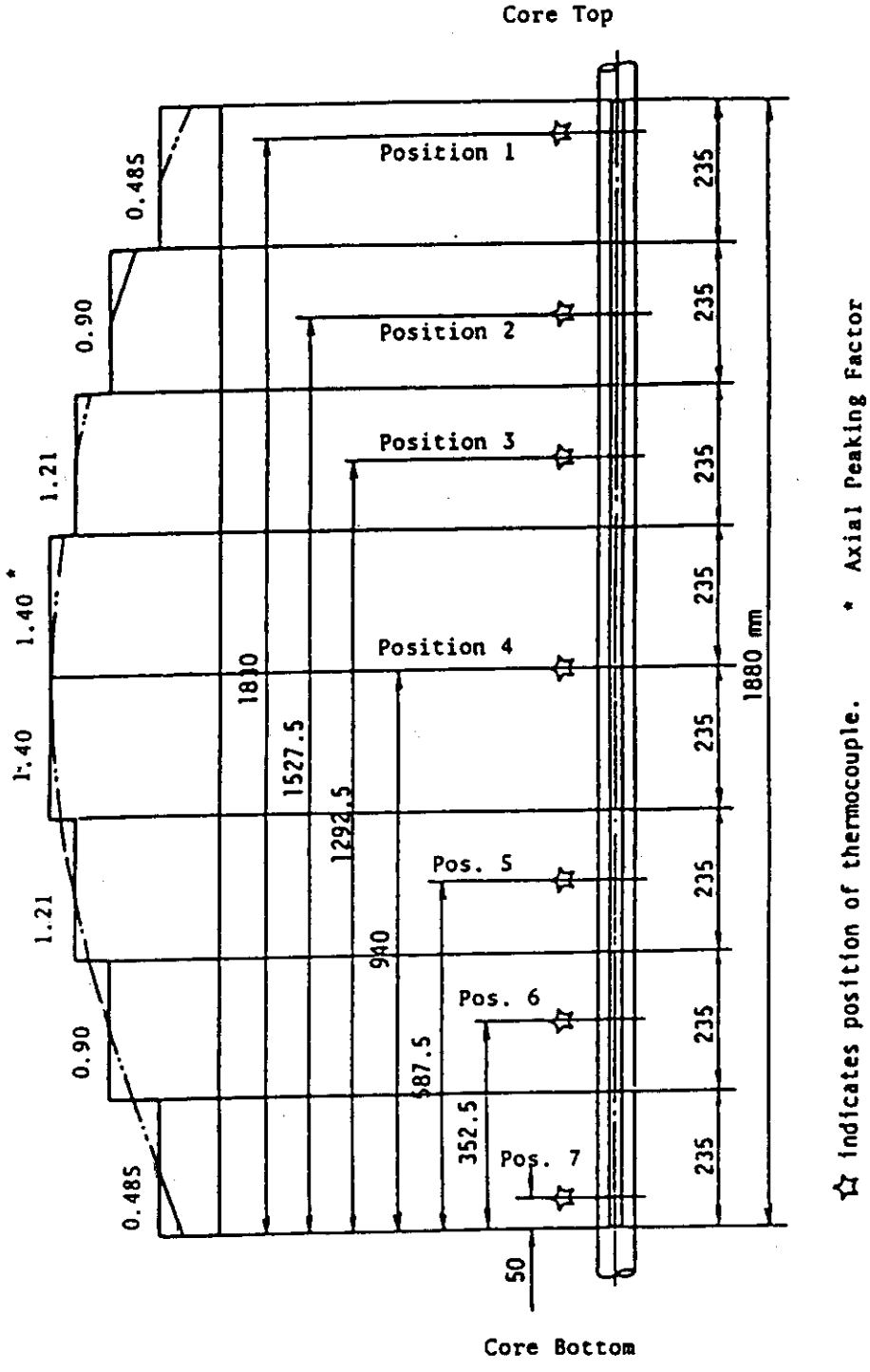

Fig. 2.6 Axial power distribution of heater rod

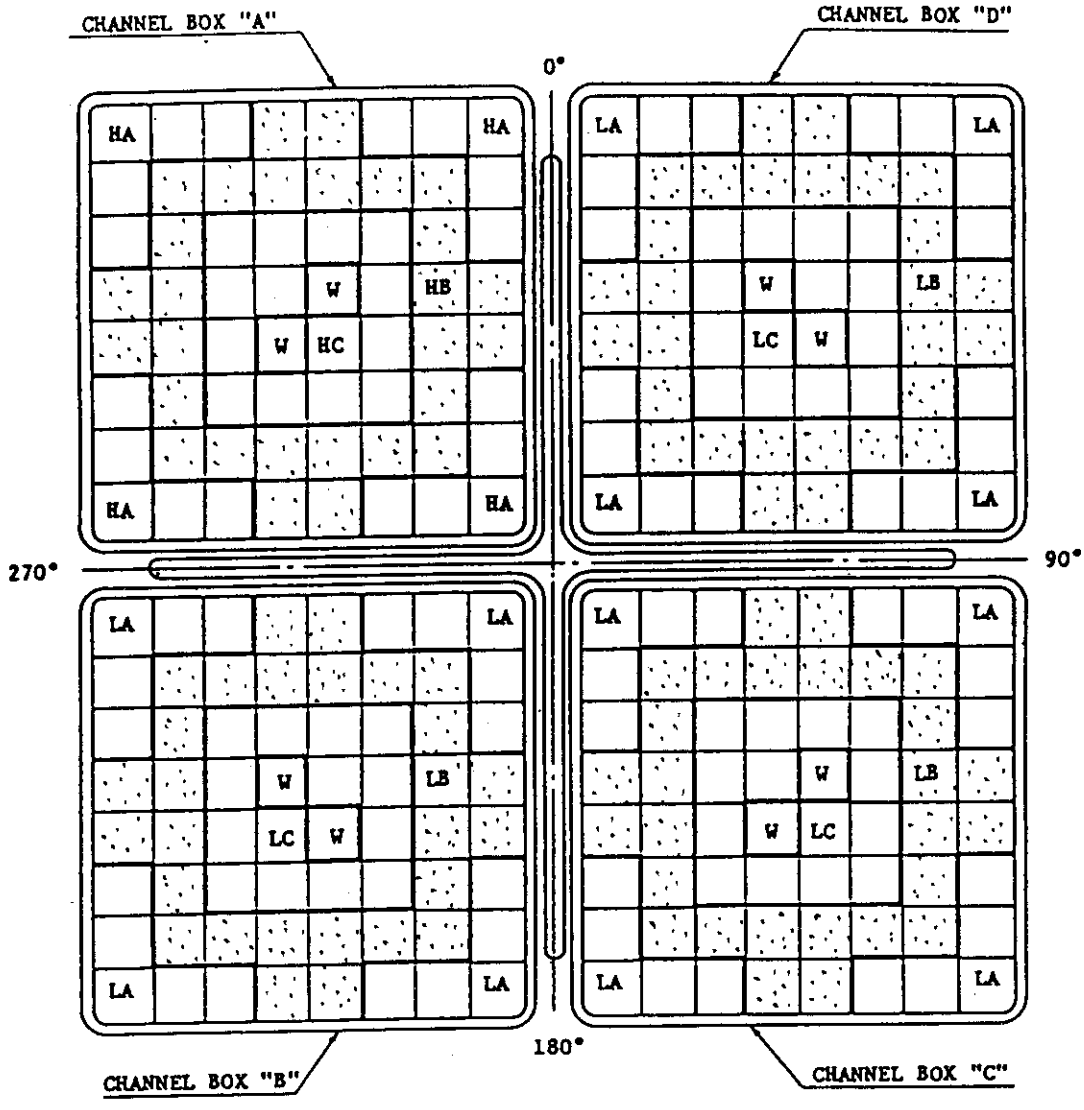

Region	HA	HB	HC	LA	LB	LC	W
Lenear Heat Rate (kW/m)	18.5	16.81	14.41	13.21	12.01	10.29	0.0
Local peaking factor	1.1	1.0	0.875	1.1	1.0	0.875	0.0
No. of Rods	20	28	14	60	84	42	8

* note : Radial peaking factor is 1.4

Fig. 2.7 Radial power distribution of core

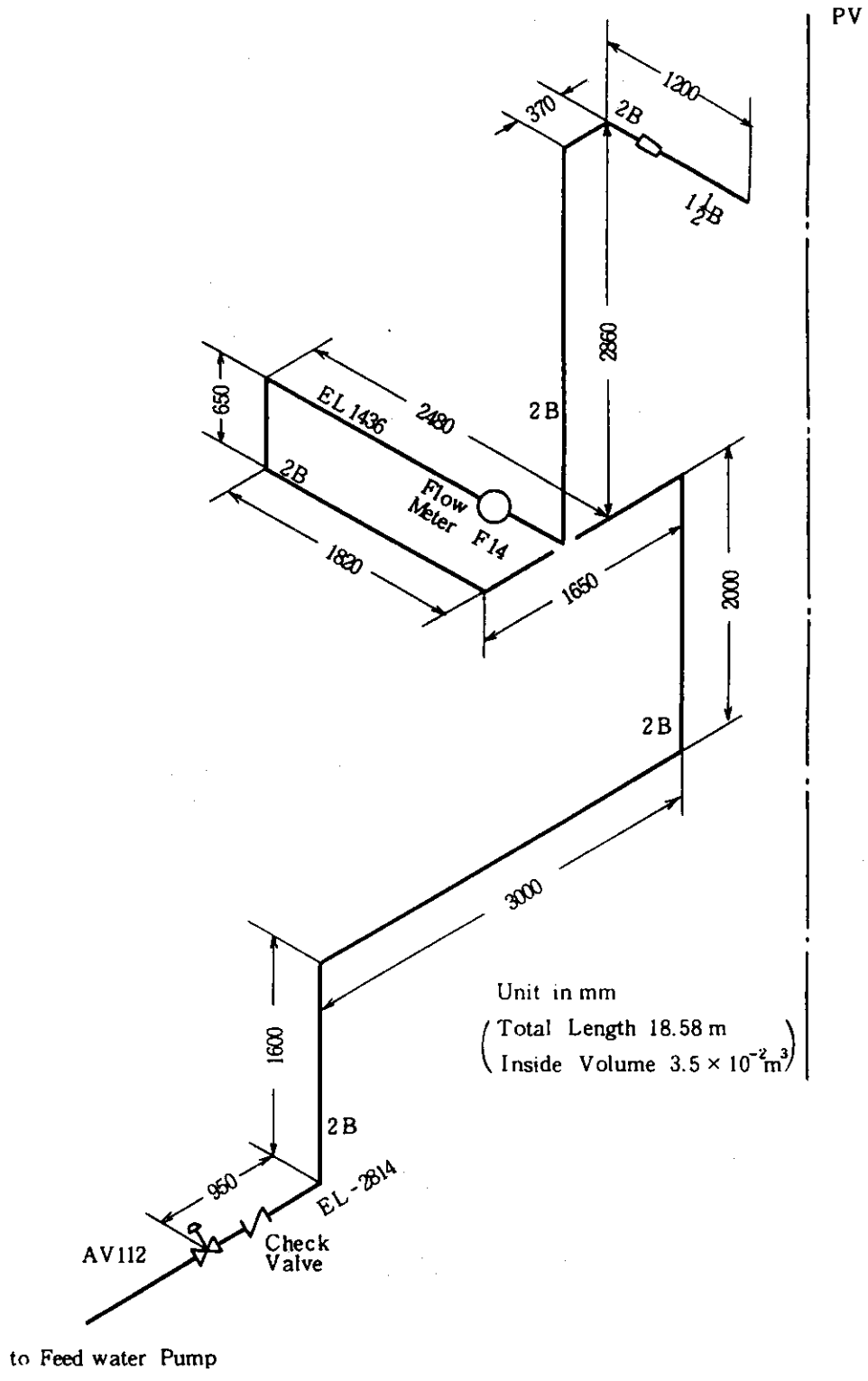

Fig. 2.8 Feedwater line between PV and AV-112

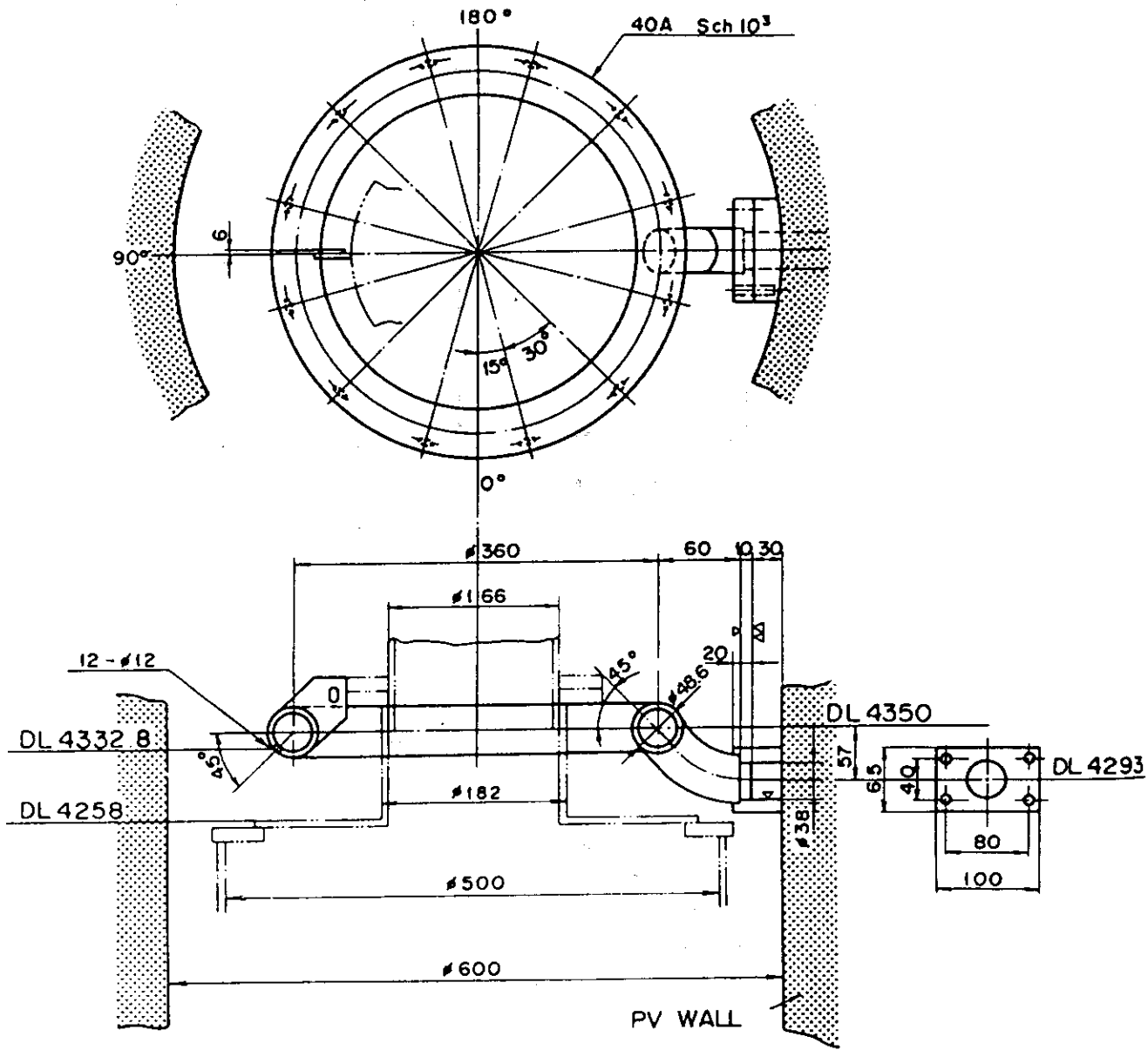

Fig. 2.9 Feedwater sparger configuration

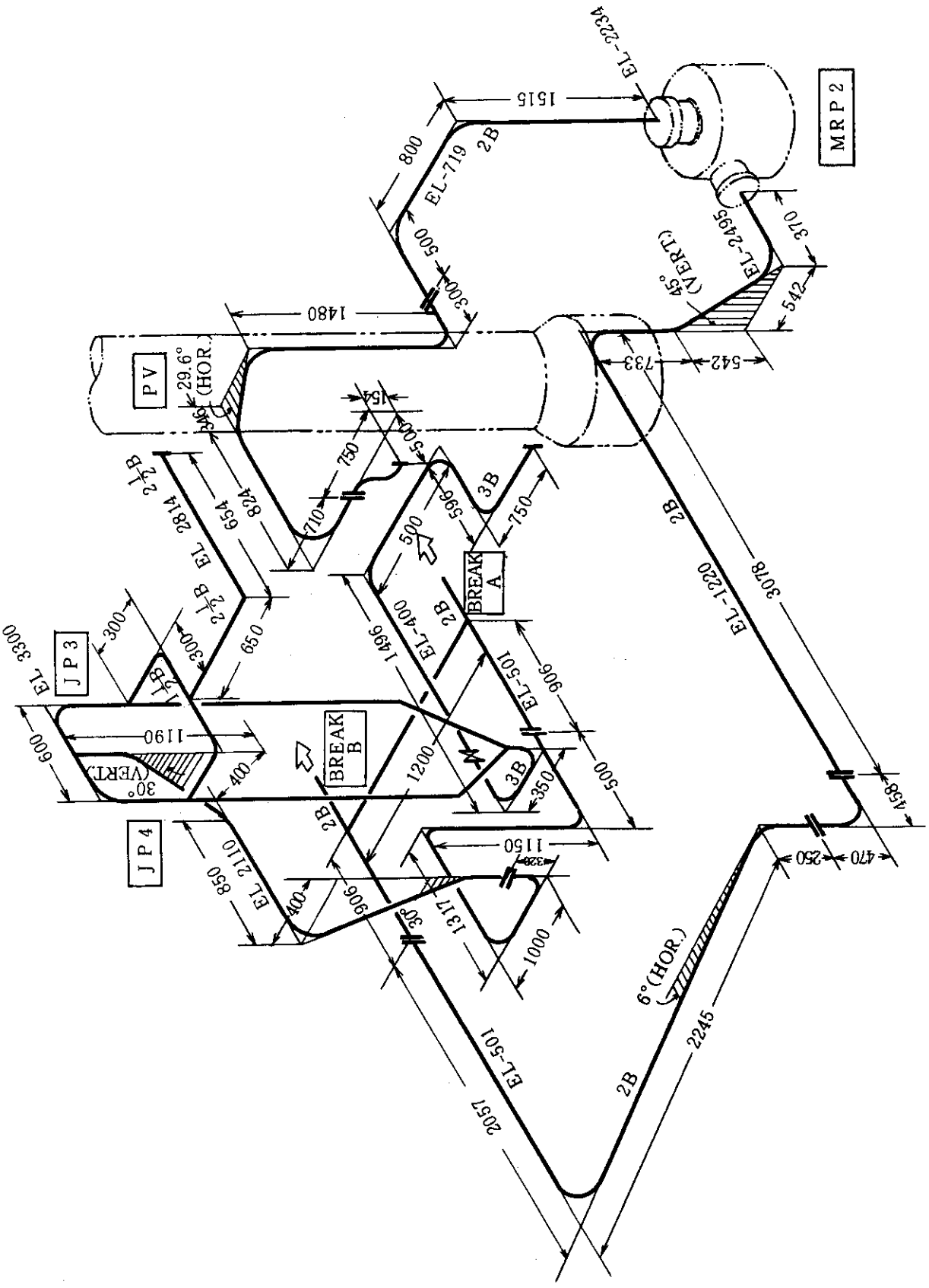

Fig. 2.10 Piping layout of recirculation loops and jet pumps

Table 3.1 ROSA-III instrumentation summary list

TYPE	SENSOR	NUMBER	NOTE	
PRESSURE	PRESSURE TRANSDUCER	20		
DIFFERENTIAL PRESSURE	DP CELL	60	PV AND LOOP LEVEL MEASUREMENT FLOW METER	44 5 11
FLUID TEMPERATURE	CA THERMOCOUPLE	129	PRIMARY LOOP DTT TIE ROD UPPER PLENUM LOWER PLENUM TIE PLATE BY PASS	23 4 28 10 10 40 14
FUEL ROD TEMPERATURE	CA THERMOCOUPLE	213		
SLAB SURFACE TEMPERATURE	CA THERMOCOUPLE	70	CORE BARREL PRESSURE VESSEL CHANNEL BOX SHROUD SUPPORT	24 3 35 8
SLAB INNER TEMPERATURE	CA THERMOCOUPLE	9	JP DIFFUSER PV WALL	4 5
VOLUMETRIC FLOW RATE	TURBINE METER VENTURI METER ORIFICE METER	3 4 6	ECCS LOOP PRIMARY LOOP	3 10
MASS FLOW RATE	TURBINE METER ORIFICE METER	4 3	RECIC. LOOP STEAM LINE	4 3
LIQUID LEVEL	CONDUCTIVITY PROBE CAPACITANCE PROBE	138 2		
DENSITY	GAMMA DENSITOMETER	10	2 BEAM GD 3 BEAM GD	2 2
MOMENTUMR FLUX	DRAG DISK	7		
SIGNAL	ON/OFF SWITCH	14		
PUMP SPEED	REVOLUTION COUNTER	2		
ELECTRIC POWER	VA METER	2		
TOTAL		696		

Table 3.2 Measurement List for RUN 962

1Ch.- 50Ch.

Ch.	Item	Symbol	ID.		Location	Fig.No.	Range			Unit	Accuracy
1	Press.	P- 1	PA	1	Lower Plenum	Fig.5. 1	0.100	-	10.0	MPa	1.08%FS
2	Press.	P- 2	PA	2	Upper Plenum	Fig.5. 1	0.100	-	10.0	MPa	1.08%FS
3	Press.	P- 3	PA	3	Steam Dome	Fig.5. 1	0.100	-	10.0	MPa	1.08%FS
4	Press.	P- 4	PA	4	Downcomer Bottom	Fig.5. 1	0.100	-	10.0	MPa	1.08%FS
5	Press.	P- 5	PA	5	JP-3 Drive	Fig.5. 2	0.100	-	10.0	MPa	1.08%FS
6	Press.	P- 6	PA	6	JP-4 Drive	Fig.5. 2	0.100	-	10.0	MPa	1.08%FS
7	Press.	P- 7	PA	7	JP-3 Suction	Fig.5. 2	0.100	-	10.0	MPa	1.08%FS
8	Press.	P- 8	PA	8	JP-4 Suction	Fig.5. 2	0.100	-	10.0	MPa	1.08%FS
9	Press.	P- 9	PA	9	MRP-1 Suction	Fig.5. 3	0.100	-	10.0	MPa	1.08%FS
10	Press.	P-10	PA	10	MRP-2 Suction	Fig.5. 3	0.100	-	10.0	MPa	1.08%FS
11	Press.	P-11	PA	11	MRP-2 Delivery	Fig.5. 3	0.100	-	10.0	MPa	1.08%FS
12	Press.	P-12	PA	12	Break A Upstream		0.100	-	10.0	MPa	1.08%FS
13	Press.	P-13	PA	13	Break A Downstream		0.100	-	10.0	MPa	1.08%FS
14	Press.	P-14	PA	14	Break B Upstream	Fig.5. 5	0.100	-	10.0	MPa	1.08%FS
15	Press.	P-15	PA	15	Break B Downstream	Fig.5. 5	0.100	-	10.0	MPa	1.08%FS
16	Press.	P-16	PA	16	Steam Line		0.100	-	10.0	MPa	1.08%FS
17	Press.	P-17	PA	17	JP-1,2 Outlet Spool		0.100	-	10.0	MPa	1.08%FS
18	Press.	P-18	PA	18	JP-3,4 Outlet Spool		0.100	-	10.0	MPa	1.08%FS
19	Press.	P-19	PA	19	Break A Spool Piece	Fig.5. 4	0.100	-	10.0	MPa	1.08%FS
20	Press.	P-30	PA	20	Break B Spool Piece	Fig.5. 5	0.100	-	10.0	MPa	1.08%FS
21	Diff.P.	D- 1	PD	21	Lower Pl.-Upper Pl.	Fig.5. 6	-50.0	-	350.	kPa	0.63%FS
22	Diff.P.	D- 2	PD	22	Upper Pl.-Steam Dome	Fig.5. 7	-10.0	-	90.0	kPa	0.63%FS
23	Diff.P.	D- 3	PD	23	Lower Plenum Head	Not Measured					
24	Diff.P.	D- 4	PD	24	Downcomer Head	Fig.5. 8	0.0	-	100.	kPa	0.63%FS
25	Diff.P.	D- 5	PD	25	PV Bottom-Top	Fig.5. 9	-100.	-	900.	kPa	0.63%FS
26	Diff.P.	D- 6	PD	26	JP-1 Disch.-Suction	Fig.5.10	-100.	-	300.	kPa	0.63%FS
27	Diff.P.	D- 7	PD	27	JP-1 Drive -Suction	Fig.5.11	0.0	-	2.50	MPa	0.63%FS
28	Diff.P.	D- 8	PD	28	JP-2 Disch.-Suction	Fig.5.10	-100.	-	300.	kPa	0.63%FS
29	Diff.P.	D- 9	PD	29	JP-2 Drive -Suction	Fig.5.11	0.0	-	2.50	MPa	0.63%FS
30	Diff.P.	D-10	PD	30	JP-3 Disch.-Suction	Fig.5.12	-100.	-	300.	kPa	0.63%FS
31	Diff.P.	D-11	PD	31	JP-3 Drive -Suction	Fig.5.13	-4.00	-	2.00	MPa	0.63%FS
32	Diff.P.	D-12	PD	32	JP-4 Disch.-Suction	Fig.5.12	-100.	-	300.	kPa	0.63%FS
33	Diff.P.	D-13	PD	33	JP-4 Drive -Suction	Fig.5.13	-4.00	-	2.00	MPa	0.63%FS
34	Diff.P.	D-14	PD	34	MRP-1 Deliv.-Suction	Fig.5.14	-0.100	-	2.50	MPa	0.63%FS
35	Diff.P.	D-15	PD	35	MRP-2 Deliv.-Suction	Fig.5.14	-0.100	-	2.50	MPa	0.63%FS
36	Diff.P.	D-16	PD	36	DC Bottom- MRP-1 Suc.	Fig.5.15	-50.0	-	50.0	kPa	0.63%FS
37	Diff.P.	D-17	PD	37	MRP1 Deliv.-JP1 Drive	Fig.5.16	0.0	-	250.	kPa	0.63%FS
38	Diff.P.	D-18	PD	38	MRP1 Deliv.-JP2 Drive	Fig.5.16	0.0	-	250.	kPa	0.63%FS
39	Diff.P.	D-19	PD	39	DC Middle-JP1 Suction	Fig.5.17	0.0	-	250.	kPa	0.63%FS
40	Diff.P.	D-20	PD	40	DC Middle-JP2 Suction	Fig.5.17	0.0	-	250.	kPa	0.63%FS
41	Diff.P.	D-21	PD	41	JP1 Disch.-Lower Pl.	Fig.5.18	-100.	-	100.	kPa	0.63%FS
42	Diff.P.	D-22	PD	42	JP2 Disch.-Lower Pl.	Fig.5.18	-100.	-	100.	kPa	0.63%FS
43	Diff.P.	D-23	PD	43	DC Bottom- Break B	Fig.5.19	-60.0	-	540.	kPa	0.63%FS
44	Diff.P.	D-24	PD	44	Break B- Break A	Fig.5.20	0.0	-	100.	kPa	0.63%FS
45	Diff.P.	D-25	PD	45	Break A- MRP2 Suction	Fig.5.21	-500.	-	100.	kPa	0.63%FS
46	Diff.P.	D-26	PD	46	MRP2 Deliv.-JP3 Drive	Fig.5.22	-500.	-	500.	kPa	0.63%FS
47	Diff.P.	D-27	PD	47	MRP2 Deliv.-JP4 Drive	Fig.5.22	-500.	-	500.	kPa	0.63%FS
48	Diff.P.	D-28	PD	48	DC Middle-JP3 Suction	Fig.5.23	-250.	-	250.	kPa	0.63%FS
49	Diff.P.	D-29	PD	49	DC Middle-JP4 Suction	Fig.5.23	-250.	-	250.	kPa	0.63%FS
50	Diff.P.	D-30	PD	50	JP3 Disch.-Confluence	Fig.5.24	-100.	-	100.	kPa	0.63%FS

Table 3.2 Measurement List for RUN 962 (Continued)

51Ch.- 100Ch.

Ch.	Item	Symbol	ID.		Location	Fig.No.	Range			Unit	Accuracy
51	Diff.P.	D-31	PD	51	JP4 Disch.-Confluence	Fig.5.24	-100.	-	100.	kPa	0.63%FS
52	Diff.P.	D-32	PD	52	Confluence -Lower Pl.	Fig.5.25	-50.0	-	50.0	kPa	0.63%FS
53	Diff.P.	D-33	PD	53	Lower Pl.-DC Middle	Fig.5.26	-250.	-	250.	kPa	0.63%FS
54	Diff.P.	D-34	PD	54	Lower Pl.-DC Bottom	Fig.5.27	-250.	-	250.	kPa	0.63%FS
55	Diff.P.	D-35	PD	55	DC Bottom-DC Middle	Fig.5.28	-50.0	-	50.0	kPa	0.63%FS
56	Diff.P.	D-36	PD	56	DC Middle-Steam Dome	Fig.5.29	-50.0	-	50.0	kPa	0.63%FS
57	Diff.P.	D-37	PD	57	Lower Pl.Mid-Upper PL	Not Measured					
58	Diff.P.	D-38	PD	58	Lower Pl.Bottom-Mid.	Fig.5.30	0.0	-	50.0	kPa	0.63%FS
59	Diff.P.	D-39	PD	59	Upper Pl.-DC High	Not Used	-20.0	-	100.	kPa	0.63%FS
60	Diff.P.	D-40	PD	60	Channel Orifice A	Fig.5.31	-50.0	-	50.0	kPa	0.63%FS
61	Diff.P.	D-41	PD	61	Channel Orifice B	Fig.5.32	-50.0	-	50.0	kPa	0.63%FS
62	Diff.P.	D-42	PD	62	Channel Orifice C	Fig.5.33	-25.0	-	75.0	kPa	0.63%FS
63	Diff.P.	D-43	PD	63	Channel Orifice D	Fig.5.34	-50.0	-	50.0	kPa	0.63%FS
64	Diff.P.	D-44	PD	64	Lower Plenum Head	Fig.5.35	-100.	-	100.	kPa	0.63%FS
65	Level	WL- 1	LM	65	HPCS Tank	Not Used	0.0	-	2.30	m	1.00%FS
66	Level	WL- 2	LM	66	LPCS Tank	Fig.5.36	0.0	-	2.30	m	1.00%FS
67	Level	WL- 3	LM	67	LPCI Tank	Fig.5.36	0.0	-	4.25	m	1.00%FS
68	Level	WL- 4	LM	68	Upper Downcomer		3.90	-	6.04	m	1.00%FS
69	Level	WL- 5	LM	69	Lower Downcomer	Fig.5.37	0.938	-	3.90	m	1.00%FS
70	Mass.F.	F- 1	FM	70	Steam Line (Low Range)	Fig.5.38	0.0	-	1.13	kg/s	0.92%FS
71	Mass.F.	F- 2	FM	71	Steam Line(High Range)	Fig.5.38	0.0	-	3.00	kg/s	0.92%FS
72	Mass.F.	F- 3	FM	72	Steam Line (Mid Range)	Fig.5.38	0.0	-	1.94	kg/s	1.40%FS
73	Vol.F.	F- 7	FV	73	HPCS (Upper Plenum)	Not Used	0.0	-	0.250E-02	m3/s	0.79%FS
74	Vol.F.	F- 9	FV	74	LPCS (Upper Plenum)	Fig.5.39	0.0	-	0.250E-02	m3/s	0.79%FS
75	Vol.F.	F-11	FV	75	LPCI (Core Bypass)	Fig.5.39	0.0	-	0.830E-02	m3/s	0.79%FS
76	Vol.F.	F-15	FV	76	Feedwater	Fig.5.40	0.0	-	0.100E-01	m3/s	0.79%FS
77	Vol.F.	F-16	FV	77	PWT Flow	Not Used	0.0	-	0.420E-02	m3/s	0.79%FS
78	Vol.F.	F-17	FV	78	JP1 Discharge	Fig.5.41	0.0	-	0.170E-01	m3/s	0.88%FS
79	Vol.F.	F-18	FV	79	JP2 Discharge	Fig.5.41	0.0	-	0.170E-01	m3/s	0.88%FS
80	Vol.F.	F-19	FV	80	JP3 Disch. Positive	Fig.5.42	0.0	-	0.170E-01	m3/s	0.92%FS
81	Vol.F.	F-20	FV	81	JP3 Disch. Negative	Fig.5.43	0.0	-	0.500E-02	m3/s	0.92%FS
82	Vol.F.	F-21	FV	82	JP4 Disch. Positive	Fig.5.42	0.0	-	0.170E-01	m3/s	0.92%FS
83	Vol.F.	F-22	FV	83	JP4 Disch. Negative	Fig.5.43	0.0	-	0.500E-02	m3/s	0.92%FS
84	Mass.F.	F-23	FM	84	JP1,2 Outlet Spool	Not Measured	0.0	-	30.0	kg/s	1.40%FS
85	Mass.F.	F-24	FM	85	JP3,4 Outlet Spool	Not Measured	0.0	-	30.0	kg/s	1.40%FS
86	Mass.F.	F-25	FM	86	Break A Spool Piece	Not Measured	0.0	-	30.0	kg/s	1.40%FS
87	Mass.F.	F-26	FM	87	Break B Spool Piece	Not Measured	0.0	-	30.0	kg/s	1.40%FS
88	Vol.F.	F-27	FV	88	MRP-1	Fig.5.44	0.0	-	0.120E-01	m3/s	0.88%FS
89	Vol.F.	F-28	FV	89	MRP-2	Fig.5.44	0.0	-	0.120E-01	m3/s	0.63%FS
90	Diff.P.	D-F1	PD	90	F1 Orifice		0.0	-	4.90	kPa	0.63%FS
91	Diff.P.	D-F2	PD	91	F2 Orifice		0.0	-	34.9	kPa	0.63%FS
92	Diff.P.	D-F3	PD	92	F3 Orifice		0.0	-	14.6	kPa	0.63%FS
93	Diff.P.	D-F17	PD	93	F17 Venturi		0.0	-	98.1	kPa	0.63%FS
94	Diff.P.	D-F18	PD	94	F18 Venturi		0.0	-	98.1	kPa	0.63%FS
95	Diff.P.	D-F19	PD	95	F19 Orifice		0.0	-	147.	kPa	0.63%FS
96	Diff.P.	D-F20	PD	96	F20 Orifice		0.0	-	13.2	kPa	0.63%FS
97	Diff.P.	D-F21	PD	97	F21 Orifice		0.0	-	147.	kPa	0.63%FS
98	Diff.P.	D-F22	PD	98	F22 Orifice		0.0	-	13.2	kPa	0.63%FS
99	Diff.P.	D-F27	PD	99	F27 Venturi		0.0	-	200.	kPa	0.63%FS
100	Diff.P.	D-F28	PD	100	F28 Venturi		0.0	-	200.	kPa	0.63%FS

Table 3.2 Measurement List for RUN 962 (Continued)

101Ch.- 150Ch.

Ch.	Item	Symbol	ID.		Location	Fig.No.	Range			Unit	Accuracy
101	Power	W- 1	WE	101	2100 kW Power Supplier	Fig.5.45	0.0	-	0.210E+04	kW	1.00%FS
102	Power	W- 2	WE	102	3150 kW Power Supplier	Fig.5.45	0.0	-	0.315E+04	kW	1.00%FS
103											
104	Rev.	N- 1	SR	104	MRP-1 Revolution	Fig.5.46	0.0	-	0.500E+04	RPM	1.08%FS
105	Rev.	N- 2	SR	105	MRP-2 Revolution	Fig.5.46	0.0	-	0.500E+04	RPM	1.08%FS
106	Signal	S- 1	EV	106	Break Signal A	Fig.5.47					
107	Signal	S- 2	EV	107	Break Signal B	Fig.5.47					
108	Signal	S- 3	EV	108	QSV Signal	Fig.5.47					
109	Signal	S- 6	EV	109	HPCS Valve	Fig.5.48					
110	Signal	S- 7	EV	110	LPCS Valve	Fig.5.48					
111	Signal	S- 8	EV	111	LPCI Valve	Fig.5.48					
112	Signal	S- 9	EV	112	Feedwater Control	Fig.5.47					
113	Signal	S-10	EV	113	MSIV Signal	Fig.5.47					
114	Signal	S-11	EV	114	Steam Line Valve	Fig.5.47					
115	Signal	S-12	EV	115	ADS Valve	Fig.5.48					
116	Signal	S-13	EV	116	MRP-1 Power OFF	Fig.5.49					
117	Signal	S-14	EV	117	MRP-2 Power OFF	Fig.5.49					
118	Signal	RD- 1	EV	118	MRP-1 Rev. Direction	Not Used					
119	Signal	RD- 2	EV	119	MRP-2 Rev. Direction	Not Used					
120	Density	DF- 1	DE	120	JP1,2 Outlet Beam A	Fig.5.50	0.0	-	0.100E+04	kg/m3	1.00%FS
121	Density	DF- 2	DE	121	JP1,2 Outlet Beam B	Fig.5.51	0.0	-	0.100E+04	kg/m3	1.00%FS
122	Density	DF- 3	DE	122	JP1,2 Outlet Beam C	Fig.5.52	0.0	-	0.100E+04	kg/m3	1.00%FS
123	Density	DF- 4	DE	123	JP3,4 Outlet Beam A	Fig.5.53	0.0	-	0.100E+04	kg/m3	1.00%FS
124	Density	DF- 5	DE	124	JP3,4 Outlet Beam B	Fig.5.54	0.0	-	0.100E+04	kg/m3	1.00%FS
125	Density	DF- 6	DE	125	JP3,4 Outlet Beam C	Fig.5.55	0.0	-	0.100E+04	kg/m3	1.00%FS
126	Density	DF- 7	DE	126	Break A Beam A	Fig.5.56	0.0	-	0.100E+04	kg/m3	1.00%FS
127	Density	DF- 8	DE	127	Break A Beam B	Fig.5.57	0.0	-	0.100E+04	kg/m3	1.00%FS
128	Density	DF- 9	DE	128	Break B Beam A	Fig.5.58	0.0	-	0.100E+04	kg/m3	1.00%FS
129	Density	DF-10	DE	129	Break B Beam B	Fig.5.59	0.0	-	0.100E+04	kg/m3	1.00%FS
130	Mo.Flux	M- 1	MF	130	JP1,2 Outlet Spool	Fig.5.60	0.0	-	0.220E+05	kg/ms2	1.00%FS
131	Mo.Flux	M- 2	MF	131	JP3,4 Outlet Spool	Fig.5.61	0.0	-	0.220E+05	kg/ms2	1.00%FS
132	Mo.Flux	M- 3	MF	132	Break A (Low Range)	Fig.5.62	0.0	-	0.220E+05	kg/ms2	1.00%FS
133	Mo.Flux	M- 4	MF	133	Break B (Low Range)	Failure	0.0	-	0.220E+05	kg/ms2	1.00%FS
134	Mo.Flux	M- 5	MF	134	Break A (High Range)	Fig.5.63	0.0	-	0.220E+06	kg/ms2	1.00%FS
135	Mo.Flux	M- 6	MF	135	Break B (High Range)	Fig.5.64	0.0	-	0.220E+06	kg/ms2	1.00%FS
136	Mo.Flux	M- 7	MF	136	Break Orifice	Not Measured	0.0	-	0.220E+05	kg/ms2	1.00%FS
137											
138	Fluid T.	T- 1	TE	138	Lower Plenum	Fig.5.65	273.	-	673.	K	0.64%FS
139	Fluid T.	T- 2	TE	139	Upper Plenum	Fig.5.65	273.	-	673.	K	0.64%FS
140	Fluid T.	T- 3	TE	140	Steam Dome	Fig.5.66	273.	-	673.	K	0.64%FS
141	Fluid T.	T- 4	TE	141	Upper Downcomer	Fig.5.67	273.	-	673.	K	0.64%FS
142	Fluid T.	T- 5	TE	142	Lower Downcomer	Fig.5.67	273.	-	673.	K	0.64%FS
143	Fluid T.	T- 6	TE	143	JP-1 Drive	Fig.5.68	273.	-	673.	K	0.64%FS
144	Fluid T.	T- 7	TE	144	JP-2 Drive	Fig.5.68	273.	-	673.	K	0.64%FS
145	Fluid T.	T- 8	TE	145	JP-3 Drive	Fig.5.69	273.	-	673.	K	0.64%FS
146	Fluid T.	T- 9	TE	146	JP-4 Drive	Fig.5.69	273.	-	673.	K	0.64%FS
147	Fluid T.	T-10	TE	147	JP-1 Discharge	Fig.5.70	273.	-	673.	K	0.64%FS
148	Fluid T.	T-11	TE	148	JP-2 Discharge	Fig.5.70	273.	-	673.	K	0.64%FS
149	Fluid T.	T-12	TE	149	JP-3 Discharge	Fig.5.71	273.	-	673.	K	0.64%FS
150	Fluid T.	T-13	TE	150	JP-4 Discharge	Fig.5.71	273.	-	673.	K	0.64%FS

Table 3.2 Measurement List for RUN 962 (Continued)

151Ch.- 200Ch.

Ch.	Item	Symbol	ID.		Location	Fig.No.	Range			Unit	Accuracy
151	Fluid T.	T-14	TE	151	MRP-1 Suction	Fig.5.68	273.	-	673.	K	0.64%FS
152	Fluid T.	T-15	TE	152	MRP-1 Delivery	Fig.5.68	273.	-	673.	K	0.64%FS
153	Fluid T.	T-16	TE	153	MRP-2 Suction	Fig.5.69	273.	-	673.	K	0.64%FS
154	Fluid T.	T-17	TE	154	MRP-2 Delivery	Fig.5.69	273.	-	673.	K	0.64%FS
155	Fluid T.	T-18	TE	155	Break A Upstream	Fig.5.72	273.	-	673.	K	0.64%FS
156	Fluid T.	T-19	TE	156	Break B Upstream	Fig.5.72	273.	-	673.	K	0.64%FS
157	Fluid T.	T-20	TE	157	RCN A Condenced Water	Not Used	273.	-	698.	K	0.64%FS
158	Fluid T.	T-21	TE	158	RCN B Condenced Water	Not Used	273.	-	698.	K	0.64%FS
159	Fluid T.	T-22	TE	159	Discharged Steam	Fig.5.66	273.	-	673.	K	0.64%FS
160	Fluid T.	T-24	TE	160	JP-1,2 Outlet Spool	Fig.5.70	273.	-	763.	K	0.64%FS
161	Fluid T.	T-25	TE	161	JP-3,4 Outlet Spool	Fig.5.71	273.	-	763.	K	0.64%FS
162	Fluid T.	T-26	TE	162	Break A Spool Piece	Fig.5.72	273.	-	763.	K	0.64%FS
163	Fluid T.	T-27	TE	163	Break B Spool Piece	Fig.5.72	273.	-	763.	K	0.64%FS
164	Fluid T.	T-28	TE	164	Feedwater	Fig.5.73	273.	-	673.	K	0.64%FS
165	Fluid T.	T-29	TE	165	Break Orifice 1	Not Measured	273.	-	673.	K	0.64%FS
166	Fluid T.	T-30	TE	166	Break Orifice 2	Not Measured	273.	-	673.	K	0.64%FS
167	Fluid T.	T-31	TE	167	Break A Down DD(Low)	Not Measured	273.	-	673.	K	0.64%FS
168	Fluid T.	T-32	TE	168	Break B Down DD(Low)	Not Measured	273.	-	673.	K	0.64%FS
169	Fluid T.	T-33	TE	169	Break A Up. DD(High)		273.	-	673.	K	0.64%FS
170	Fluid T.	T-34	TE	170	Break B Up. DD(High)		273.	-	673.	K	0.64%FS
171	Fluid T.	T-F17	TE	171	JP1 Fluid D. Correc.	Fig.5.74	273.	-	673.	K	0.64%FS
172	Fluid T.	T-F18	TE	172	JP2 Fluid D. Correc.	Fig.5.74	273.	-	673.	K	0.64%FS
173	Fluid T.	T-F19	TE	173	JP3 Fluid D. Correc.	Fig.5.74	273.	-	673.	K	0.64%FS
174	Fluid T.	T-F21	TE	174	JP4 Fluid D. Correc.	Fig.5.74	273.	-	673.	K	0.64%FS
175	Slab T.	TS-11	TE	175	Core Barrel A Pos.5	Not Measured	273.	-	673.	K	0.64%FS
176	Slab T.	TS-12	TE	176	Core Barrel A Pos.6	Not Measured	273.	-	673.	K	0.64%FS
177	Slab T.	TS-13	TE	177	Filler Block C Pos.1	Not Measured	273.	-	673.	K	0.64%FS
178	Slab T.	TS-14	TE	178	Filler Block C Pos.2	Not Measured	273.	-	673.	K	0.64%FS
179	Slab T.	TS-15	TE	179	Filler Block C Pos.3	Not Measured	273.	-	673.	K	0.64%FS
180	Slab T.	TS-16	TE	180	Filler Block C Pos.4	Not Measured	273.	-	673.	K	0.64%FS
181	Slab T.	TS-17	TE	181	Filler Block C Pos.5	Not Measured	273.	-	673.	K	0.64%FS
182	Slab T.	TS-18	TE	182	Filler Block C Pos.6	Not Measured	273.	-	673.	K	0.64%FS
183	Slab T.	TS-19	TE	183	Filler Block A Pos.1	Not Measured	273.	-	673.	K	0.64%FS
184	Slab T.	TS-20	TE	184	Filler Block A Pos.2	Not Measured	273.	-	673.	K	0.64%FS
185	Slab T.	TS-21	TE	185	Filler Block A Pos.3	Not Measured	273.	-	673.	K	0.64%FS
186	Slab T.	TS-22	TE	186	Filler Block A Pos.4	Not Measured	273.	-	673.	K	0.64%FS
187	Slab T.	TS-23	TE	187	Filler Block A Pos.5	Not Measured	273.	-	673.	K	0.64%FS
188	Slab T.	TS-24	TE	188	Filler Block A Pos.6	Not Measured	273.	-	673.	K	0.64%FS
189	Slab T.	TS-25	TE	189	JP-1 Diffuser Wall	Not Measured	273.	-	673.	K	0.64%FS
190	Slab T.	TS-26	TE	190	JP-2 Diffuser Wall	Not Measured	273.	-	673.	K	0.64%FS
191	Slab T.	TS-27	TE	191	JP-3 Diffuser Wall	Not Measured	273.	-	673.	K	0.64%FS
192	Slab T.	TS-28	TE	192	JP-4 Diffuser Wall	Not Measured	273.	-	673.	K	0.64%FS
193	Slab T.	TS-29	TE	193	PV Wall Inside 1-1	Not Measured	273.	-	673.	K	0.64%FS
194	Slab T.	TS-30	TE	194	PV Inner Surface 1-2	Not Measured	273.	-	673.	K	0.64%FS
195	Slab T.	TS-31	TE	195	PV Inner Surface 1-3	Not Measured	273.	-	673.	K	0.64%FS
196	Slab T.	TS-32	TE	196	PV Wall Inside 2	Not Measured	273.	-	673.	K	0.64%FS
197	Slab T.	TS-33	TE	197	PV Wall Inside 3	Not Measured	273.	-	673.	K	0.64%FS
198	Slab T.	TS-34	TE	198	PV Wall Inside 4	Not Measured	273.	-	673.	K	0.64%FS
199	Slab T.	TS-35	TE	199	L.P. Inner Surface	Not Measured	273.	-	673.	K	0.64%FS
200	Slab T.	TS-36	TE	200	L.P. Wall Inside	Not Measured	273.	-	673.	K	0.64%FS

Table 3.2 Measurement List for RUN 962 (Continued)

201Ch.- 250Ch.

Ch.	Item	Symbol	ID.	Location	Fig.No.	Range	Unit	Accuracy
201	Temp.	TF- 1	TE 201	A11 Fuel Rod Pos.1	Fig.5.75, 98	273. - 0.147E+04	K	0.64%FS
202	Temp.	TF- 2	TE 202	A11 Fuel Rod Pos.2	Fig.5.75, 99	273. - 0.147E+04	K	0.64%FS
203	Temp.	TF- 3	TE 203	A11 Fuel Rod Pos.3	Fig.5.75, 100	273. - 0.147E+04	K	0.64%FS
204	Temp.	TF- 4	TE 204	A11 Fuel Rod Pos.4	Fig.5.75, 101	273. - 0.147E+04	K	0.64%FS
205	Temp.	TF- 5	TE 205	A11 Fuel Rod Pos.5	Fig.5.75, 102	273. - 0.147E+04	K	0.64%FS
206	Temp.	TF- 6	TE 206	A11 Fuel Rod Pos.6	Fig.5.75, 103	273. - 0.147E+04	K	0.64%FS
207	Temp.	TF- 7	TE 207	A11 Fuel Rod Pos.7	Fig.5.75, 104	273. - 0.147E+04	K	0.64%FS
208	Temp.	TF- 8	TE 208	A12 Fuel Rod Pos.1	Fig.5.76, 98	273. - 0.147E+04	K	0.64%FS
209	Temp.	TF- 9	TE 209	A12 Fuel Rod Pos.2	Fig.5.76, 99	273. - 0.147E+04	K	0.64%FS
210	Temp.	TF- 10	TE 210	A12 Fuel Rod Pos.3	Fig.5.76, 100	273. - 0.147E+04	K	0.64%FS
211	Temp.	TF- 11	TE 211	A12 Fuel Rod Pos.4	Fig.5.76, 101	273. - 0.147E+04	K	0.64%FS
212	Temp.	TF- 12	TE 212	A12 Fuel Rod Pos.5	Fig.5.76, 102	273. - 0.147E+04	K	0.64%FS
213	Temp.	TF- 13	TE 213	A12 Fuel Rod Pos.6	Fig.5.76, 103	273. - 0.147E+04	K	0.64%FS
214	Temp.	TF- 14	TE 214	A12 Fuel Rod Pos.7	Fig.5.76, 104	273. - 0.147E+04	K	0.64%FS
215	Temp.	TF- 15	TE 215	A13 Fuel Rod Pos.1	Fig.5.77, 98	273. - 0.147E+04	K	0.64%FS
216	Temp.	TF- 16	TE 216	A13 Fuel Rod Pos.2	Fig.5.77, 99	273. - 0.147E+04	K	0.64%FS
217	Temp.	TF- 17	TE 217	A13 Fuel Rod Pos.3	Fig.5.77, 100	273. - 0.147E+04	K	0.64%FS
218	Temp.	TF- 18	TE 218	A13 Fuel Rod Pos.4	Fig.5.77, 101	273. - 0.147E+04	K	0.64%FS
219	Temp.	TF- 19	TE 219	A13 Fuel Rod Pos.5	Fig.5.77, 102	273. - 0.147E+04	K	0.64%FS
220	Temp.	TF- 20	TE 220	A13 Fuel Rod Pos.6	Fig.5.77, 103	273. - 0.147E+04	K	0.64%FS
221	Temp.	TF- 21	TE 221	A13 Fuel Rod Pos.7	Fig.5.77, 104	273. - 0.147E+04	K	0.64%FS
222	Temp.	TF- 22	TE 222	A14 Fuel Rod Pos.1	Not Measured	273. - 0.147E+04	K	0.64%FS
223	Temp.	TF- 23	TE 223	A14 Fuel Rod Pos.2	Not Measured	273. - 0.147E+04	K	0.64%FS
224	Temp.	TF- 24	TE 224	A14 Fuel Rod Pos.3	Not Measured	273. - 0.147E+04	K	0.64%FS
225	Temp.	TF- 25	TE 225	A14 Fuel Rod Pos.4	Not Measured	273. - 0.147E+04	K	0.64%FS
226	Temp.	TF- 26	TE 226	A14 Fuel Rod Pos.5	Not Measured	273. - 0.147E+04	K	0.64%FS
227	Temp.	TF- 27	TE 227	A14 Fuel Rod Pos.6	Not Measured	273. - 0.147E+04	K	0.64%FS
228	Temp.	TF- 28	TE 228	A14 Fuel Rod Pos.7	Not Measured	273. - 0.147E+04	K	0.64%FS
229	Temp.	TF- 29	TE 229	A15 Fuel Rod Pos.1	Not Measured	273. - 0.147E+04	K	0.64%FS
230	Temp.	TF- 30	TE 230	A15 Fuel Rod Pos.4	Not Measured	273. - 0.147E+04	K	0.64%FS
231	Temp.	TF- 31	TE 231	A17 Fuel Rod Pos.1	Not Measured	273. - 0.147E+04	K	0.64%FS
232	Temp.	TF- 32	TE 232	A17 Fuel Rod Pos.4	Fig.5. 95	273. - 0.147E+04	K	0.64%FS
233	Temp.	TF- 33	TE 233	A22 Fuel Rod Pos.1	Fig.5.78, 105	273. - 0.147E+04	K	0.64%FS
234	Temp.	TF- 34	TE 234	A22 Fuel Rod Pos.2	Fig.5.78, 106	273. - 0.147E+04	K	0.64%FS
235	Temp.	TF- 35	TE 235	A22 Fuel Rod Pos.3	Fig.5.78, 107	273. - 0.147E+04	K	0.64%FS
236	Temp.	TF- 36	TE 236	A22 Fuel Rod Pos.4	Fig.5.78, 108	273. - 0.125E+04	K	0.64%FS
237	Temp.	TF- 37	TE 237	A22 Fuel Rod Pos.5	Fig.5.78, 109	273. - 0.125E+04	K	0.64%FS
238	Temp.	TF- 38	TE 238	A22 Fuel Rod Pos.6	Fig.5.78, 110	273. - 0.125E+04	K	0.64%FS
239	Temp.	TF- 39	TE 239	A22 Fuel Rod Pos.7	Fig.5.78, 111	273. - 0.125E+04	K	0.64%FS
240	Temp.	TF- 40	TE 240	A24 Fuel Rod Pos.1	Not Measured	273. - 0.125E+04	K	0.64%FS
241	Temp.	TF- 41	TE 241	A24 Fuel Rod Pos.2	Not Measured	273. - 0.125E+04	K	0.64%FS
242	Temp.	TF- 42	TE 242	A24 Fuel Rod Pos.3	Not Measured	273. - 0.125E+04	K	0.64%FS
243	Temp.	TF- 43	TE 243	A24 Fuel Rod Pos.4	Not Measured	273. - 0.125E+04	K	0.64%FS
244	Temp.	TF- 44	TE 244	A24 Fuel Rod Pos.5	Not Measured	273. - 0.125E+04	K	0.64%FS
245	Temp.	TF- 45	TE 245	A24 Fuel Rod Pos.6	Not Measured	273. - 0.125E+04	K	0.64%FS
246	Temp.	TF- 46	TE 246	A24 Fuel Rod Pos.7	Not Measured	273. - 0.125E+04	K	0.64%FS
247	Temp.	TF- 47	TE 247	A26 Fuel Rod Pos.1	Not Measured	273. - 0.125E+04	K	0.64%FS
248	Temp.	TF- 48	TE 248	A26 Fuel Rod Pos.2	Not Measured	273. - 0.125E+04	K	0.64%FS
249	Temp.	TF- 49	TE 249	A28 Fuel Rod Pos.1	Not Measured	273. - 0.125E+04	K	0.64%FS
250	Temp.	TF- 50	TE 250	A28 Fuel Rod Pos.4	Fig.5. 95	273. - 0.125E+04	K	0.64%FS

Table 3.2 Measurement List for RUN 962 (Continued)

251Ch.- 300Ch.

Ch.	Item	Symbol	ID.	Location	Fig.No.	Range	Unit	Accuracy
251	Temp.	TF- 51	TE 251	A31 Fuel Rod Pos.1		273. - 0.125E+04	K	0.64%FS
252	Temp.	TF- 52	TE 252	A31 Fuel Rod Pos.4	Fig.5. 95	273. - 0.125E+04	K	0.64%FS
253	Temp.	TF- 53	TE 253	A33 Fuel Rod Pos.1	FIG.5.79	273. - 0.125E+04	K	0.64%FS
254	Temp.	TF- 54	TE 254	A33 Fuel Rod Pos.2	FIG.5.79	273. - 0.125E+04	K	0.64%FS
255	Temp.	TF- 55	TE 255	A33 Fuel Rod Pos.3	FIG.5.79	273. - 0.125E+04	K	0.64%FS
256	Temp.	TF- 56	TE 256	A33 Fuel Rod Pos.4	FIG.5.79	273. - 0.125E+04	K	0.64%FS
257	Temp.	TF- 57	TE 257	A33 Fuel Rod Pos.5	FIG.5.79	273. - 0.125E+04	K	0.64%FS
258	Temp.	TF- 58	TE 258	A33 Fuel Rod Pos.6	FIG.5.79	273. - 0.125E+04	K	0.64%FS
259	Temp.	TF- 59	TE 259	A33 Fuel Rod Pos.7	FIG.5.79	273. - 0.125E+04	K	0.64%FS
260	Temp.	TF- 60	TE 260	A34 Fuel Rod Pos.1	Not Measured	273. - 0.125E+04	K	0.64%FS
261	Temp.	TF- 61	TE 261	A34 Fuel Rod Pos.2	Not Measured	273. - 0.125E+04	K	0.64%FS
262	Temp.	TF- 62	TE 262	A34 Fuel Rod Pos.3	Not Measured	273. - 0.125E+04	K	0.64%FS
263	Temp.	TF- 63	TE 263	A34 Fuel Rod Pos.4	Not Measured	273. - 0.125E+04	K	0.64%FS
264	Temp.	TF- 64	TE 264	A34 Fuel Rod Pos.5	Not Measured	273. - 0.125E+04	K	0.64%FS
265	Temp.	TF- 65	TE 265	A34 Fuel Rod Pos.6	Not Measured	273. - 0.125E+04	K	0.64%FS
266	Temp.	TF- 66	TE 266	A34 Fuel Rod Pos.7	Not Measured	273. - 0.125E+04	K	0.64%FS
267	Temp.	TF- 67	TE 267	A37 Fuel Rod Pos.1	Not Measured	273. - 0.125E+04	K	0.64%FS
268	Temp.	TF- 68	TE 268	A37 Fuel Rod Pos.4	Not Measured	273. - 0.125E+04	K	0.64%FS
269	Temp.	TF- 69	TE 269	A42 Fuel Rod Pos.1	Not Measured	273. - 0.125E+04	K	0.64%FS
270	Temp.	TF- 70	TE 270	A42 Fuel Rod Pos.4	Not Measured	273. - 0.125E+04	K	0.64%FS
271	Temp.	TF- 71	TE 271	A44 Fuel Rod Pos.1	Not Measured	273. - 0.125E+04	K	0.64%FS
272	Temp.	TF- 72	TE 272	A44 Fuel Rod Pos.2	Not Measured	273. - 0.125E+04	K	0.64%FS
273	Temp.	TF- 73	TE 273	A44 Fuel Rod Pos.3	Not Measured	273. - 0.125E+04	K	0.64%FS
274	Temp.	TF- 74	TE 274	A44 Fuel Rod Pos.4	Not Measured	273. - 0.125E+04	K	0.64%FS
275	Temp.	TF- 75	TE 275	A44 Fuel Rod Pos.5	Not Measured	273. - 0.125E+04	K	0.64%FS
276	Temp.	TF- 76	TE 276	A44 Fuel Rod Pos.6	Not Measured	273. - 0.125E+04	K	0.64%FS
277	Temp.	TF- 77	TE 277	A44 Fuel Rod Pos.7	Not Measured	273. - 0.125E+04	K	0.64%FS
278	Temp.	TF- 78	TE 278	A48 Fuel Rod Pos.1	Not Measured	273. - 0.125E+04	K	0.64%FS
279	Temp.	TF- 79	TE 279	A48 Fuel Rod Pos.4	Not Measured	273. - 0.125E+04	K	0.64%FS
280	Temp.	TF- 80	TE 280	A51 Fuel Rod Pos.1	Not Measured	273. - 0.125E+04	K	0.64%FS
281	Temp.	TF- 81	TE 281	A51 Fuel Rod Pos.4	Not Measured	273. - 0.125E+04	K	0.64%FS
282	Temp.	TF- 82	TE 282	A53 Fuel Rod Pos.1	Not Measured	273. - 0.125E+04	K	0.64%FS
283	Temp.	TF- 83	TE 283	A53 Fuel Rod Pos.4	Not Measured	273. - 0.125E+04	K	0.64%FS
284	Temp.	TF- 84	TE 284	A57 Fuel Rod Pos.1	Not Measured	273. - 0.125E+04	K	0.64%FS
285	Temp.	TF- 85	TE 285	A57 Fuel Rod Pos.4	Fig.5. 96	273. - 0.125E+04	K	0.64%FS
286	Temp.	TF- 86	TE 286	A62 Fuel Rod Pos.1	Not Measured	273. - 0.125E+04	K	0.64%FS
287	Temp.	TF- 87	TE 287	A62 Fuel Rod Pos.4	Not Measured	273. - 0.125E+04	K	0.64%FS
288	Temp.	TF- 88	TE 288	A66 Fuel Rod Pos.1	Not Measured	273. - 0.125E+04	K	0.64%FS
289	Temp.	TF- 89	TE 289	A66 Fuel Rod Pos.4	Not Measured	273. - 0.125E+04	K	0.64%FS
290	Temp.	TF- 90	TE 290	A68 Fuel Rod Pos.1	Not Measured	273. - 0.125E+04	K	0.64%FS
291	Temp.	TF- 91	TE 291	A68 Fuel Rod Pos.4	Fig.5. 95	273. - 0.125E+04	K	0.64%FS
292	Temp.	TF- 92	TE 292	A71 Fuel Rod Pos.1	Not Measured	273. - 0.125E+04	K	0.64%FS
293	Temp.	TF- 93	TE 293	A71 Fuel Rod Pos.4		273. - 0.125E+04	K	0.64%FS
294	Temp.	TF- 94	TE 294	A73 Fuel Rod Pos.1	Not Measured	273. - 0.125E+04	K	0.64%FS
295	Temp.	TF- 95	TE 295	A73 Fuel Rod Pos.4	Fig.5. 96	273. - 0.125E+04	K	0.64%FS
296	Temp.	TF- 96	TE 296	A75 Fuel Rod Pos.1	Not Measured	273. - 0.125E+04	K	0.64%FS
297	Temp.	TF- 97	TE 297	A75 Fuel Rod Pos.4	Not Measured	273. - 0.125E+04	K	0.64%FS
298	Temp.	TF- 98	TE 298	A77 Fuel Rod Pos.1	Fig.5.80, 112	273. - 0.125E+04	K	0.64%FS
299	Temp.	TF- 99	TE 299	A77 Fuel Rod Pos.2	Fig.5.80, 113	273. - 0.125E+04	K	0.64%FS
300	Temp.	TF-100	TE 300	A77 Fuel Rod Pos.3	Fig.5.80, 114	273. - 0.125E+04	K	0.64%FS

Table 3.2 Measurement List for RUN 962 (Continued)

301Ch.- 350Ch.

Ch.	Item	Symbol	ID.		Location	Fig.No.	Range			Unit	Accuracy
301	Temp.	TF-101	TE	301	A77 Fuel Rod Pos.4	Fig.5.80, 115	273.	-	0.125E+04	K	0.64%FS
302	Temp.	TF-102	TE	302	A77 Fuel Rod Pos.5	Fig.5.80, 116	273.	-	0.125E+04	K	0.64%FS
303	Temp.	TF-103	TE	303	A77 Fuel Rod Pos.6	Fig.5.80, 117	273.	-	0.125E+04	K	0.64%FS
304	Temp.	TF-104	TE	304	A77 Fuel Rod Pos.7	Failure	273.	-	0.125E+04	K	0.64%FS
305	Temp.	TF-105	TE	305	A82 Fuel Rod Pos.1		273.	-	0.125E+04	K	0.64%FS
306	Temp.	TF-106	TE	306	A82 Fuel Rod Pos.4	Not Used	273.	-	0.125E+04	K	0.64%FS
307	Temp.	TF-107	TE	307	A84 Fuel Rod Pos.1		273.	-	0.125E+04	K	0.64%FS
308	Temp.	TF-108	TE	308	A84 Fuel Rod Pos.4	Fig.5. 96	273.	-	0.125E+04	K	0.64%FS
309	Temp.	TF-109	TE	309	A85 Fuel Rod Pos.1	Not Measured	273.	-	0.125E+04	K	0.64%FS
310	Temp.	TF-110	TE	310	A85 Fuel Rod Pos.2	Not Measured	273.	-	0.125E+04	K	0.64%FS
311	Temp.	TF-111	TE	311	A85 Fuel Rod Pos.3	Not Measured	273.	-	0.125E+04	K	0.64%FS
312	Temp.	TF-112	TE	312	A85 Fuel Rod Pos.4	Not Measured	273.	-	0.125E+04	K	0.64%FS
313	Temp.	TF-113	TE	313	A85 Fuel Rod Pos.5	Not Measured	273.	-	0.125E+04	K	0.64%FS
314	Temp.	TF-114	TE	314	A85 Fuel Rod Pos.6	Not Measured	273.	-	0.125E+04	K	0.64%FS
315	Temp.	TF-115	TE	315	A85 Fuel Rod Pos.7	Not Measured	273.	-	0.125E+04	K	0.64%FS
316	Temp.	TF-116	TE	316	A87 Fuel Rod Pos.1	Fig.5.81, 98	273.	-	0.125E+04	K	0.64%FS
317	Temp.	TF-117	TE	317	A87 Fuel Rod Pos.2	Fig.5.81, 99	273.	-	0.125E+04	K	0.64%FS
318	Temp.	TF-118	TE	318	A87 Fuel Rod Pos.3	Fig.5.81, 100	273.	-	0.125E+04	K	0.64%FS
319	Temp.	TF-119	TE	319	A87 Fuel Rod Pos.4	Fig.5.81, 101	273.	-	0.125E+04	K	0.64%FS
320	Temp.	TF-120	TE	320	A87 Fuel Rod Pos.5	Fig.5.81, 101	273.	-	0.125E+04	K	0.64%FS
321	Temp.	TF-121	TE	321	A87 Fuel Rod Pos.6	Fig.5.81, 103	273.	-	0.125E+04	K	0.64%FS
322	Temp.	TF-122	TE	322	A87 Fuel Rod Pos.7	Fig.5.81, 104	273.	-	0.125E+04	K	0.64%FS
323	Temp.	TF-123	TE	323	A88 Fuel Rod Pos.1	Fig.5.82, 98	273.	-	0.125E+04	K	0.64%FS
324	Temp.	TF-124	TE	324	A88 Fuel Rod Pos.2	Fig.5.82, 99	273.	-	0.125E+04	K	0.64%FS
325	Temp.	TF-125	TE	325	A88 Fuel Rod Pos.3	Fig.5.82, 100	273.	-	0.125E+04	K	0.64%FS
326	Temp.	TF-126	TE	326	A88 Fuel Rod Pos.4	Fig.5.82, 101	273.	-	0.125E+04	K	0.64%FS
327	Temp.	TF-127	TE	327	A88 Fuel Rod Pos.5	Fig.5.82, 102	273.	-	0.125E+04	K	0.64%FS
328	Temp.	TF-128	TE	328	A88 Fuel Rod Pos.6	Fig.5.82, 103	273.	-	0.125E+04	K	0.64%FS
329	Temp.	TF-129	TE	329	A88 Fuel Rod Pos.7	Fig.5.82, 104	273.	-	0.125E+04	K	0.64%FS
330	Temp.	TF-130	TE	330	B11 Fuel Rod Pos.1	Fig.5.83	273.	-	0.125E+04	K	0.64%FS
331	Temp.	TF-131	TE	331	B11 Fuel Rod Pos.2	Fig.5.83	273.	-	0.125E+04	K	0.64%FS
332	Temp.	TF-132	TE	332	B11 Fuel Rod Pos.3	Fig.5.83	273.	-	0.125E+04	K	0.64%FS
333	Temp.	TF-133	TE	333	B11 Fuel Rod Pos.4	Fig.5.83	273.	-	0.125E+04	K	0.64%FS
334	Temp.	TF-134	TE	334	B11 Fuel Rod Pos.5	Fig.5.83	273.	-	0.125E+04	K	0.64%FS
335	Temp.	TF-135	TE	335	B11 Fuel Rod Pos.6	Fig.5.83	273.	-	0.125E+04	K	0.64%FS
336	Temp.	TF-136	TE	336	B11 Fuel Rod Pos.7	Failure	273.	-	0.125E+04	K	0.64%FS
337	Temp.	TF-137	TE	337	B13 Fuel Rod Pos.4	Fig.5.97	273.	-	0.125E+04	K	0.64%FS
338	Temp.	TF-138	TE	338	B22 Fuel Rod Pos.1	Fig.5.84, 105	273.	-	0.125E+04	K	0.64%FS
339	Temp.	TF-139	TE	339	B22 Fuel Rod Pos.2	Fig.5.84, 106	273.	-	0.125E+04	K	0.64%FS
340	Temp.	TF-140	TE	340	B22 Fuel Rod Pos.3	Fig.5.84, 107	273.	-	0.125E+04	K	0.64%FS
341	Temp.	TF-141	TE	341	B22 Fuel Rod Pos.4	Fig.5.84, 108	273.	-	0.125E+04	K	0.64%FS
342	Temp.	TF-142	TE	342	B22 Fuel Rod Pos.5	Fig.5.84, 109	273.	-	0.125E+04	K	0.64%FS
343	Temp.	TF-143	TE	343	B22 Fuel Rod Pos.6	Fig.5.84, 110	273.	-	0.125E+04	K	0.64%FS
344	Temp.	TF-144	TE	344	B22 Fuel Rod Pos.7	Fig.5.84, 111	273.	-	0.125E+04	K	0.64%FS
345	Temp.	TF-145	TE	345	B31 Fuel Rod Pos.4	Not Measured	273.	-	0.125E+04	K	0.64%FS
346	Temp.	TF-146	TE	346	B33 Fuel Rod Pos.4	Not Measured	273.	-	0.125E+04	K	0.64%FS
347	Temp.	TF-147	TE	347	B51 Fuel Rod Pos.4	Not Measured	273.	-	0.125E+04	K	0.64%FS
348	Temp.	TF-148	TE	348	B53 Fuel Rod Pos.4	Not Measured	273.	-	0.125E+04	K	0.64%FS
349	Temp.	TF-149	TE	349	B66 Fuel Rod Pos.4	Not Measured	273.	-	0.125E+04	K	0.64%FS
350	Temp.	TF-150	TE	350	B77 Fuel Rod Pos.1	Fig.5.85, 112	273.	-	0.125E+04	K	0.64%FS

Table 3.2 Measurement List for RUN 962 (Continued)

351Ch.- 400Ch.

Ch.	Item	Symbol	ID.		Location	Fig.No.	Range			Unit	Accuracy
351	Temp.	TF-151	TE	351	B77 Fuel Rod Pos.2	Fig.5.85, 113	273.	-	0.125E+04	K	0.64%FS
352	Temp.	TF-152	TE	352	B77 Fuel Rod Pos.3	Fig.5.85, 114	273.	-	0.125E+04	K	0.64%FS
353	Temp.	TF-153	TE	353	B77 Fuel Rod Pos.4	Fig.5.85, 115	273.	-	0.125E+04	K	0.64%FS
354	Temp.	TF-154	TE	354	B77 Fuel Rod Pos.5	Fig.5.85, 116	273.	-	0.125E+04	K	0.64%FS
355	Temp.	TF-155	TE	355	B77 Fuel Rod Pos.6	Fig.5.85, 117	273.	-	0.125E+04	K	0.64%FS
356	Temp.	TF-156	TE	356	B77 Fuel Rod Pos.7	Fig.5.85, 118	273.	-	0.125E+04	K	0.64%FS
357	Temp.	TF-157	TE	357	B86 Fuel Rod Pos.4	Not Measured	273.	-	0.125E+04	K	0.64%FS
358	Temp.	TF-158	TE	358	C11 Fuel Rod Pos.1	Failure	273.	-	0.125E+04	K	0.64%FS
359	Temp.	TF-159	TE	359	C11 Fuel Rod Pos.2	Fig.5.86	273.	-	0.125E+04	K	0.64%FS
360	Temp.	TF-160	TE	360	C11 Fuel Rod Pos.3	Fig.5.86	273.	-	0.125E+04	K	0.64%FS
361	Temp.	TF-161	TE	361	C11 Fuel Rod Pos.4	Fig.5.86	273.	-	0.125E+04	K	0.64%FS
362	Temp.	TF-162	TE	362	C11 Fuel Rod Pos.5	Fig.5.86	273.	-	0.125E+04	K	0.64%FS
363	Temp.	TF-163	TE	363	C11 Fuel Rod Pos.6	Fig.5.86	273.	-	0.125E+04	K	0.64%FS
364	Temp.	TF-164	TE	364	C11 Fuel Rod Pos.7	Fig.5.86	273.	-	0.125E+04	K	0.64%FS
365	Temp.	TF-165	TE	365	C13 Fuel Rod Pos.1	Fig.5.87	273.	-	0.125E+04	K	0.64%FS
366	Temp.	TF-166	TE	366	C13 Fuel Rod Pos.2	Fig.5.87	273.	-	0.125E+04	K	0.64%FS
367	Temp.	TF-167	TE	367	C13 Fuel Rod Pos.3	Fig.5.87	273.	-	0.125E+04	K	0.64%FS
368	Temp.	TF-168	TE	368	C13 Fuel Rod Pos.4	Fig.5.87	273.	-	0.125E+04	K	0.64%FS
369	Temp.	TF-169	TE	369	C13 Fuel Rod Pos.5	Fig.5.87	273.	-	0.125E+04	K	0.64%FS
370	Temp.	TF-170	TE	370	C13 Fuel Rod Pos.6	Fig.5.87	273.	-	0.125E+04	K	0.64%FS
371	Temp.	TF-171	TE	371	C13 Fuel Rod Pos.7	Fig.5.87	273.	-	0.125E+04	K	0.64%FS
372	Temp.	TF-172	TE	372	C15 Fuel Rod Pos.4	Not Measured	273.	-	0.125E+04	K	0.64%FS
373	Temp.	TF-173	TE	373	C22 Fuel Rod Pos.1	Fig.5.88, 105	273.	-	0.125E+04	K	0.64%FS
374	Temp.	TF-174	TE	374	C22 Fuel Rod Pos.2	Fig.5.88, 106	273.	-	0.125E+04	K	0.64%FS
375	Temp.	TF-175	TE	375	C22 Fuel Rod Pos.3	Fig.5.88, 107	273.	-	0.125E+04	K	0.64%FS
376	Temp.	TF-176	TE	376	C22 Fuel Rod Pos.4	Fig.5.88, 108	273.	-	0.125E+04	K	0.64%FS
377	Temp.	TF-177	TE	377	C22 Fuel Rod Pos.5	Fig.5.88, 109	273.	-	0.125E+04	K	0.64%FS
378	Temp.	TF-178	TE	378	C22 Fuel Rod Pos.6	Fig.5.88, 110	273.	-	0.125E+04	K	0.64%FS
379	Temp.	TF-179	TE	379	C22 Fuel Rod Pos.7	Fig.5.88, 111	273.	-	0.125E+04	K	0.64%FS
380	Temp.	TF-180	TE	380	C31 Fuel Rod Pos.4	Not Measured	273.	-	0.125E+04	K	0.64%FS
381	Temp.	TF-181	TE	381	C33 Fuel Rod Pos.1	Fig.5.89	273.	-	0.125E+04	K	0.64%FS
382	Temp.	TF-182	TE	382	C33 Fuel Rod Pos.2	Fig.5.89	273.	-	0.125E+04	K	0.64%FS
383	Temp.	TF-183	TE	383	C33 Fuel Rod Pos.3	Fig.5.89	273.	-	0.125E+04	K	0.64%FS
384	Temp.	TF-184	TE	384	C33 Fuel Rod Pos.4	Fig.5.89	273.	-	0.125E+04	K	0.64%FS
385	Temp.	TF-185	TE	385	C33 Fuel Rod Pos.5	Fig.5.89	273.	-	0.125E+04	K	0.64%FS
386	Temp.	TF-186	TE	386	C33 Fuel Rod Pos.6	Fig.5.89	273.	-	0.125E+04	K	0.64%FS
387	Temp.	TF-187	TE	387	C33 Fuel Rod Pos.7	Fig.5.89	273.	-	0.125E+04	K	0.64%FS
388	Temp.	TF-188	TE	388	C35 Fuel Rod Pos.4	Not Measured	273.	-	0.125E+04	K	0.64%FS
389	Temp.	TF-189	TE	389	C66 Fuel Rod Pos.4	Not Measured	273.	-	0.125E+04	K	0.64%FS
390	Temp.	TF-190	TE	390	C68 Fuel Rod Pos.4	Not Measured	273.	-	0.125E+04	K	0.64%FS
391	Temp.	TF-191	TE	391	C77 Fuel Rod Pos.1	Fig.5.90, 112	273.	-	0.125E+04	K	0.64%FS
392	Temp.	TF-192	TE	392	C77 Fuel Rod Pos.2	Fig.5.90, 113	273.	-	0.125E+04	K	0.64%FS
393	Temp.	TF-193	TE	393	C77 Fuel Rod Pos.3	Fig.5.90, 114	273.	-	0.125E+04	K	0.64%FS
394	Temp.	TF-194	TE	394	C77 Fuel Rod Pos.4	Fig.5.90, 115	273.	-	0.125E+04	K	0.64%FS
395	Temp.	TF-195	TE	395	C77 Fuel Rod Pos.5	Fig.5.90, 116	273.	-	0.125E+04	K	0.64%FS
396	Temp.	TF-196	TE	396	C77 Fuel Rod Pos.6	Fig.5.90, 117	273.	-	0.125E+04	K	0.64%FS
397	Temp.	TF-197	TE	397	C77 Fuel Rod Pos.7	Fig.5.90, 118	273.	-	0.125E+04	K	0.64%FS
398	Temp.	TF-198	TE	398	D11 Fuel Rod Pos.4	Fig.5.97	273.	-	0.125E+04	K	0.64%FS
399	Temp.	TF-199	TE	399	D13 Fuel Rod Pos.4	Fig.5.97	273.	-	0.125E+04	K	0.64%FS
400	Temp.	TF-200	TE	400	D22 Fuel Rod Pos.1	Fig.5.91, 105	273.	-	0.125E+04	K	0.64%FS

Table 3.2 Measurement List for RUN 962 (Continued)

401Ch.- 450Ch.

Ch.	Item	Symbol	ID.		Location	Fig.No.	Range			Unit	Accuracy
401	Temp.	TF-201	TE	401	D22 Fuel Rod Pos.2	Fig.5.91, 106	273.	-	0.125E+04	K	0.64%FS
402	Temp.	TF-202	TE	402	D22 Fuel Rod Pos.3	Fig.5.91, 107	273.	-	0.125E+04	K	0.64%FS
403	Temp.	TF-203	TE	403	D22 Fuel Rod Pos.4	Fig.5.91, 108	273.	-	0.125E+04	K	0.64%FS
404	Temp.	TF-204	TE	404	D22 Fuel Rod Pos.5	Fig.5.91, 109	273.	-	0.125E+04	K	0.64%FS
405	Temp.	TF-205	TE	405	D22 Fuel Rod Pos.6	Fig.5.91, 110	273.	-	0.125E+04	K	0.64%FS
406	Temp.	TF-206	TE	406	D22 Fuel Rod Pos.7	Fig.5.91, 111	273.	-	0.125E+04	K	0.64%FS
407	Temp.	TF-207	TE	407	D31 Fuel Rod Pos.4	Not Measured	273.	-	0.125E+04	K	0.64%FS
408	Temp.	TF-208	TE	408	D33 Fuel Rod Pos.4	Not Measured	273.	-	0.125E+04	K	0.64%FS
409	Temp.	TF-209	TE	409	D51 Fuel Rod Pos.4	Not Measured	273.	-	0.125E+04	K	0.64%FS
410	Temp.	TF-210	TE	410	D53 Fuel Rod Pos.4	Not Measured	273.	-	0.125E+04	K	0.64%FS
411	Temp.	TF-211	TE	411	D66 Fuel Rod Pos.4	Not Measured	273.	-	0.125E+04	K	0.64%FS
412	Temp.	TF-212	TE	412	D77 Fuel Rod Pos.4		273.	-	0.125E+04	K	0.64%FS
413	Temp.	TF-213	TE	413	D86 Fuel Rod Pos.4	Fig.5.97	273.	-	0.125E+04	K	0.64%FS
414	Fluid T.	TW- 1	TE	414	A45 Tie Rod Pos.1	Fig.5.92	273.	-	0.125E+04	K	0.64%FS
415	Fluid T.	TW- 2	TE	415	A45 Tie Rod Pos.2	Fig.5.92	273.	-	0.125E+04	K	0.64%FS
416	Fluid T.	TW- 3	TE	416	A45 Tie Rod Pos.3	Fig.5.92	273.	-	0.125E+04	K	0.64%FS
417	Fluid T.	TW- 4	TE	417	A45 Tie Rod Pos.4	Fig.5.92	273.	-	0.125E+04	K	0.64%FS
418	Fluid T.	TW- 5	TE	418	A45 Tie Rod Pos.5	Fig.5.92	273.	-	0.125E+04	K	0.64%FS
419	Fluid T.	TW- 6	TE	419	A45 Tie Rod Pos.6	Fig.5.92	273.	-	0.125E+04	K	0.64%FS
420	Fluid T.	TW- 7	TE	420	A45 Tie Rod Pos.7	Fig.5.92	273.	-	0.125E+04	K	0.64%FS
421	Fluid T.	TW- 8	TE	421	B45 Tie Rod Pos.1	Not Measured	273.	-	0.125E+04	K	0.64%FS
422	Fluid T.	TW- 9	TE	422	B45 Tie Rod Pos.2	Not Measured	273.	-	0.125E+04	K	0.64%FS
423	Fluid T.	TW-10	TE	423	B45 Tie Rod Pos.3	Not Measured	273.	-	0.125E+04	K	0.64%FS
424	Fluid T.	TW-11	TE	424	B45 Tie Rod Pos.4	Not Measured	273.	-	0.125E+04	K	0.64%FS
425	Fluid T.	TW-12	TE	425	B45 Tie Rod Pos.5	Not Measured	273.	-	0.125E+04	K	0.64%FS
426	Fluid T.	TW-13	TE	426	B45 Tie Rod Pos.6	Not Measured	273.	-	0.125E+04	K	0.64%FS
427	Fluid T.	TW-14	TE	427	B45 Tie Rod Pos.7	Not Measured	273.	-	0.125E+04	K	0.64%FS
428	Fluid T.	TW-15	TE	428	C45 Tie Rod Pos.1	Fig.5.93	273.	-	0.125E+04	K	0.64%FS
429	Fluid T.	TW-16	TE	429	C45 Tie Rod Pos.2	Fig.5.93	273.	-	0.125E+04	K	0.64%FS
430	Fluid T.	TW-17	TE	430	C45 Tie Rod Pos.3	Fig.5.93	273.	-	0.125E+04	K	0.64%FS
431	Fluid T.	TW-18	TE	431	C45 Tie Rod Pos.4	Fig.5.93	273.	-	0.125E+04	K	0.64%FS
432	Fluid T.	TW-19	TE	432	C45 Tie Rod Pos.5	Fig.5.93	273.	-	0.125E+04	K	0.64%FS
433	Fluid T.	TW-20	TE	433	C45 Tie Rod Pos.6	Fig.5.93	273.	-	0.125E+04	K	0.64%FS
434	Fluid T.	TW-21	TE	434	C45 Tie Rod Pos.7	Fig.5.93	273.	-	0.125E+04	K	0.64%FS
435	Fluid T.	TW-22	TE	435	D45 Tie Rod Pos.1	Not Measured	273.	-	0.125E+04	K	0.64%FS
436	Fluid T.	TW-23	TE	436	D45 Tie Rod Pos.2	Not Measured	273.	-	0.125E+04	K	0.64%FS
437	Fluid T.	TW-24	TE	437	D45 Tie Rod Pos.3	Not Measured	273.	-	0.125E+04	K	0.64%FS
438	Fluid T.	TW-25	TE	438	D45 Tie Rod Pos.4	Not Measured	273.	-	0.125E+04	K	0.64%FS
439	Fluid T.	TW-26	TE	439	D45 Tie Rod Pos.5	Not Measured	273.	-	0.125E+04	K	0.64%FS
440	Fluid T.	TW-27	TE	440	D45 Tie Rod Pos.6	Not Measured	273.	-	0.125E+04	K	0.64%FS
441	Fluid T.	TW-28	TE	441	D45 Tie Rod Pos.7	Not Measured	273.	-	0.125E+04	K	0.64%FS
442	Fluid T.	TC- 1	TE	442	Channel Box A Inlet	Fig.5.119	273.	-	0.125E+04	K	0.64%FS
443	Fluid T.	TC- 2	TE	443	Channel Box B Inlet	Fig.5.119	273.	-	0.125E+04	K	0.64%FS
444	Fluid T.	TC- 3	TE	444	Channel Box C Inlet	Fig.5.119	273.	-	0.125E+04	K	0.64%FS
445	Fluid T.	TC- 4	TE	445	Channel Box D Inlet	Fig.5.119	273.	-	0.125E+04	K	0.64%FS
446	Fluid T.	TC- 5	TE	446	Channel Box Outlet A-1	Fig.5.120	273.	-	0.125E+04	K	0.64%FS
447	Fluid T.	TC- 6	TE	447	Channel Box Outlet A-2	Fig.5.120	273.	-	0.125E+04	K	0.64%FS
448	Fluid T.	TC- 7	TE	448	Channel Box Outlet A-3	Fig.5.120	273.	-	0.125E+04	K	0.64%FS
449	Fluid T.	TC- 8	TE	449	Channel Box Outlet A-4	Fig.5.120	273.	-	0.125E+04	K	0.64%FS
450	Fluid T.	TC- 9	TE	450	Channel Box Outlet A-6	Fig.5.120	273.	-	0.125E+04	K	0.64%FS

Table 3.2 Measurement List for RUN 962 (Continued)

451Ch.- 500Ch.

Ch.	Item	Symbol	ID.	Location	Fig.No.	Range	Unit	Accuracy
451	Fluid T.	TC-10	TE 451	Channel Box Outlet C-1	Fig.5.121	273. - 0.125E+04	K	0.64%FS
452	Fluid T.	TC-11	TE 452	Channel Box Outlet C-2	Fig.5.121	273. - 0.125E+04	K	0.64%FS
453	Fluid T.	TC-12	TE 453	Channel Box Outlet C-3	Fig.5.121	273. - 0.125E+04	K	0.64%FS
454	Fluid T.	TC-13	TE 454	Channel Box Outlet C-4	Fig.5.121	273. - 0.125E+04	K	0.64%FS
455	Fluid T.	TC-14	TE 455	Channel Box Outlet C-6	Fig.5.121	273. - 0.125E+04	K	0.64%FS
456	Fluid T.	TG- 1	TE 456	Upper Tieplate A Up.1	Fig.5.122, 126	273. - 0.125E+04	K	0.64%FS
457	Fluid T.	TG- 2	TE 457	Upper Tieplate A Up.2	Not Measured	273. - 0.125E+04	K	0.64%FS
458	Fluid T.	TG- 3	TE 458	Upper Tieplate A Up.3	Not Measured	273. - 0.125E+04	K	0.64%FS
459	Fluid T.	TG- 4	TE 459	Upper Tieplate A Up.4	Fig.5.122, 127	273. - 0.125E+04	K	0.64%FS
460	Fluid T.	TG- 5	TE 460	Upper Tieplate A Up.5	Not Measured	273. - 0.125E+04	K	0.64%FS
461	Fluid T.	TG- 6	TE 461	Upper Tieplate A Up.6	Not Measured	273. - 0.125E+04	K	0.64%FS
462	Fluid T.	TG- 7	TE 462	Upper Tieplate A Up.7	Not Measured	273. - 0.125E+04	K	0.64%FS
463	Fluid T.	TG- 8	TE 463	Upper Tieplate A Up.8	Not Measured	273. - 0.125E+04	K	0.64%FS
464	Fluid T.	TG- 9	TE 464	Upper Tieplate A Up.9	Not Measured	273. - 0.125E+04	K	0.64%FS
465	Fluid T.	TG-10	TE 465	Upper Tieplate A Up.10	Fig.5.123, 128	273. - 0.125E+04	K	0.64%FS
466	Fluid T.	TG-11	TE 466	Upper Tieplate A Lo.1	Fig.5.124, 126	273. - 0.125E+04	K	0.64%FS
467	Fluid T.	TG-12	TE 467	Upper Tieplate A Lo.2	Not Measured	273. - 0.125E+04	K	0.64%FS
468	Fluid T.	TG-13	TE 468	Upper Tieplate A Lo.3	Not Measured	273. - 0.125E+04	K	0.64%FS
469	Fluid T.	TG-14	TE 469	Upper Tieplate A Lo.4	Fig.5.124, 127	273. - 0.125E+04	K	0.64%FS
470	Fluid T.	TG-15	TE 470	Upper Tieplate A Lo.5	Not Measured	273. - 0.125E+04	K	0.64%FS
471	Fluid T.	TG-16	TE 471	Upper Tieplate A Lo.6	Not Measured	273. - 0.125E+04	K	0.64%FS
472	Fluid T.	TG-17	TE 472	Upper Tieplate A Lo.7	Not Measured	273. - 0.125E+04	K	0.64%FS
473	Fluid T.	TG-18	TE 473	Upper Tieplate A Lo.8	Not Measured	273. - 0.125E+04	K	0.64%FS
474	Fluid T.	TG-19	TE 474	Upper Tieplate A Lo.9	Not Measured	273. - 0.125E+04	K	0.64%FS
475	Fluid T.	TG-20	TE 475	Upper Tieplate A Lo.10	Fig.5.125, 128	273. - 0.125E+04	K	0.64%FS
476	Fluid T.	TG-21	TE 476	Upper Tieplate C Up.1	Fig.5.129, 133	273. - 0.125E+04	K	0.64%FS
477	Fluid T.	TG-22	TE 477	Upper Tieplate C Up.2	Not Measured	273. - 0.125E+04	K	0.64%FS
478	Fluid T.	TG-23	TE 478	Upper Tieplate C Up.3	Not Measured	273. - 0.125E+04	K	0.64%FS
479	Fluid T.	TG-24	TE 479	Upper Tieplate C Up.4	Fig.5.129, 134	273. - 0.125E+04	K	0.64%FS
480	Fluid T.	TG-25	TE 480	Upper Tieplate C Up.5	Not Measured	273. - 0.125E+04	K	0.64%FS
481	Fluid T.	TG-26	TE 481	Upper Tieplate C Up.6	Not Measured	273. - 0.125E+04	K	0.64%FS
482	Fluid T.	TG-27	TE 482	Upper Tieplate C Up.7	Not Measured	273. - 0.125E+04	K	0.64%FS
483	Fluid T.	TG-28	TE 483	Upper Tieplate C Up.8	Not Measured	273. - 0.125E+04	K	0.64%FS
484	Fluid T.	TG-29	TE 484	Upper Tieplate C Up.9	Not Measured	273. - 0.125E+04	K	0.64%FS
485	Fluid T.	TG-30	TE 485	Upper Tieplate C Up.10	Fig.5.130, 135	273. - 0.125E+04	K	0.64%FS
486	Fluid T.	TG-31	TE 486	Upper Tieplate C Lo.1	Fig.5.131, 133	273. - 0.125E+04	K	0.64%FS
487	Fluid T.	TG-32	TE 487	Upper Tieplate C Lo.2	Not Measured	273. - 0.125E+04	K	0.64%FS
488	Fluid T.	TG-33	TE 488	Upper Tieplate C Lo.3	Not Measured	273. - 0.125E+04	K	0.64%FS
489	Fluid T.	TG-34	TE 489	Upper Tieplate C Lo.4	Fig.5.131, 134	273. - 0.125E+04	K	0.64%FS
490	Fluid T.	TG-35	TE 490	Upper Tieplate C Lo.5	Not Measured	273. - 0.125E+04	K	0.64%FS
491	Fluid T.	TG-36	TE 491	Upper Tieplate C Lo.6	Not Measured	273. - 0.125E+04	K	0.64%FS
492	Fluid T.	TG-37	TE 492	Upper Tieplate C Lo.7	Not Measured	273. - 0.125E+04	K	0.64%FS
493	Fluid T.	TG-38	TE 493	Upper Tieplate C Lo.8	Not Measured	273. - 0.125E+04	K	0.64%FS
494	Fluid T.	TG-39	TE 494	Upper Tieplate C Lo.9	Not Measured	273. - 0.125E+04	K	0.64%FS
495	Fluid T.	TG-40	TE 495	Upper Tieplate C Lo.10	Fig.5.132, 135	273. - 0.125E+04	K	0.64%FS
496	Slab T.	TB- 1	TE 496	C.B. A1 Inner ,Pos.1	Not Measured	273. - 0.125E+04	K	0.64%FS
497	Slab T.	TB- 2	TE 497	C.B. A1 Inner ,Pos.2	Not Measured	273. - 0.125E+04	K	0.64%FS
498	Slab T.	TB- 3	TE 498	C.B. A1 Inner ,Pos.3	Not Measured	273. - 0.125E+04	K	0.64%FS
499	Slab T.	TB- 4	TE 499	C.B. A1 Inner ,Pos.4	Not Measured	273. - 0.125E+04	K	0.64%FS
500	Slab T.	TB- 5	TE 500	C.B. A1 Inner ,Pos.5	Not Measured	273. - 0.125E+04	K	0.64%FS

Table 3.2 Measurement List for RUN 962 (Continued)

501Ch.- 550Ch.

Ch.	Item	Symbol	ID.	Location	Fig.No.	Range	Unit	Accuracy
501	Slab T.	TB- 6	TE 501	C.B. A1 Inner ,Pos.6	Not Measured	273. - 0.125E+04	K	0.64%FS
502	Slab T.	TB- 7	TE 502	C.B. A1 Inner ,Pos.7	Not Measured	273. - 0.125E+04	K	0.64%FS
503	Slab T.	TB- 8	TE 503	C.B. A2 Inner ,Pos.1	Not Measured	273. - 0.125E+04	K	0.64%FS
504	Slab T.	TB- 9	TE 504	C.B. A2 Inner ,Pos.2	Not Measured	273. - 0.125E+04	K	0.64%FS
505	Slab T.	TB-10	TE 505	C.B. A2 Inner ,Pos.3	Not Measured	273. - 0.125E+04	K	0.64%FS
506	Slab T.	TB-11	TE 506	C.B. A2 Inner ,Pos.4	Not Measured	273. - 0.125E+04	K	0.64%FS
507	Slab T.	TB-12	TE 507	C.B. A2 Inner ,Pos.5	Not Measured	273. - 0.125E+04	K	0.64%FS
508	Slab T.	TB-13	TE 508	C.B. A2 Inner ,Pos.6	Not Measured	273. - 0.125E+04	K	0.64%FS
509	Slab T.	TB-14	TE 509	C.B. A2 Inner ,Pos.7	Not Measured	273. - 0.125E+04	K	0.64%FS
510	Slab T.	TB-15	TE 510	C.B. B Inner ,Pos.1	Not Measured	273. - 0.125E+04	K	0.64%FS
511	Slab T.	TB-16	TE 511	C.B. B Inner ,Pos.2	Not Measured	273. - 0.125E+04	K	0.64%FS
512	Slab T.	TB-17	TE 512	C.B. B Inner ,Pos.3	Not Measured	273. - 0.125E+04	K	0.64%FS
513	Slab T.	TB-18	TE 513	C.B. B Inner ,Pos.4	Not Measured	273. - 0.125E+04	K	0.64%FS
514	Slab T.	TB-19	TE 514	C.B. B Inner ,Pos.5	Not Measured	273. - 0.125E+04	K	0.64%FS
515	Slab T.	TB-20	TE 515	C.B. B Inner ,Pos.6	Not Measured	273. - 0.125E+04	K	0.64%FS
516	Slab T.	TB-21	TE 516	C.B. B Inner ,Pos.7	Not Measured	273. - 0.125E+04	K	0.64%FS
517	Slab T.	TB-22	TE 517	C.B. C Inner ,Pos.1	Not Measured	273. - 0.125E+04	K	0.64%FS
518	Slab T.	TB-23	TE 518	C.B. C Inner ,Pos.2	Not Measured	273. - 0.125E+04	K	0.64%FS
519	Slab T.	TB-24	TE 519	C.B. C Inner ,Pos.3	Not Measured	273. - 0.125E+04	K	0.64%FS
520	Slab T.	TB-25	TE 520	C.B. C Inner ,Pos.4	Not Measured	273. - 0.125E+04	K	0.64%FS
521	Slab T.	TB-26	TE 521	C.B. C Inner ,Pos.5	Not Measured	273. - 0.125E+04	K	0.64%FS
522	Slab T.	TB-27	TE 522	C.B. C Inner ,Pos.6	Not Measured	273. - 0.125E+04	K	0.64%FS
523	Slab T.	TB-28	TE 523	C.B. C Inner ,Pos.7	Not Measured	273. - 0.125E+04	K	0.64%FS
524	Slab T.	TB-29	TE 524	C.B. D Inner ,Pos.1	Not Measured	273. - 0.125E+04	K	0.64%FS
525	Slab T.	TB-30	TE 525	C.B. D Inner ,Pos.2	Not Measured	273. - 0.125E+04	K	0.64%FS
526	Slab T.	TB-31	TE 526	C.B. D Inner ,Pos.3	Not Measured	273. - 0.125E+04	K	0.64%FS
527	Slab T.	TB-32	TE 527	C.B. D Inner ,Pos.4	Not Measured	273. - 0.125E+04	K	0.64%FS
528	Slab T.	TB-33	TE 528	C.B. D Inner ,Pos.5	Not Measured	273. - 0.125E+04	K	0.64%FS
529	Slab T.	TB-34	TE 529	C.B. D Inner ,Pos.6	Not Measured	273. - 0.125E+04	K	0.64%FS
530	Slab T.	TB-35	TE 530	C.B. D Inner ,Pos.7	Not Measured	273. - 0.125E+04	K	0.64%FS
531	Fluid T.	TB-36	TE 531	C.B. A Outer ,Pos.1	Fig.5.94, 136	273. - 0.125E+04	K	0.64%FS
532	Fluid T.	TB-37	TE 532	C.B. A Outer ,Pos.2	Fig.5.94, 137	273. - 0.125E+04	K	0.64%FS
533	Fluid T.	TB-38	TE 533	C.B. A Outer ,Pos.3	Fig.5.94, 138	273. - 0.125E+04	K	0.64%FS
534	Fluid T.	TB-39	TE 534	C.B. A Outer ,Pos.4	Fig.5.94, 139	273. - 0.125E+04	K	0.64%FS
535	Fluid T.	TB-40	TE 535	C.B. A Outer ,Pos.5	Fig.5.94, 140	273. - 0.125E+04	K	0.64%FS
536	Fluid T.	TB-41	TE 536	C.B. A Outer ,Pos.6	Fig.5.94, 141	273. - 0.125E+04	K	0.64%FS
537	Fluid T.	TB-42	TE 537	C.B. A Outer ,Pos.7	Fig.5.94, 142	273. - 0.125E+04	K	0.64%FS
538	Fluid T.	TB-43	TE 538	C.B. C Outer ,Pos.1	Not Measured	273. - 0.125E+04	K	0.64%FS
539	Fluid T.	TB-44	TE 539	C.B. C Outer ,Pos.2	Not Measured	273. - 0.125E+04	K	0.64%FS
540	Fluid T.	TB-45	TE 540	C.B. C Outer ,Pos.3	Not Measured	273. - 0.125E+04	K	0.64%FS
541	Fluid T.	TB-46	TE 541	C.B. C Outer ,Pos.4	Not Measured	273. - 0.125E+04	K	0.64%FS
542	Fluid T.	TB-47	TE 542	C.B. C Outer ,Pos.5	Not Measured	273. - 0.125E+04	K	0.64%FS
543	Fluid T.	TB-48	TE 543	C.B. C Outer ,Pos.6	Not Measured	273. - 0.125E+04	K	0.64%FS
544	Fluid T.	TB-49	TE 544	C.B. C Outer ,Pos.7	Not Measured	273. - 0.125E+04	K	0.64%FS
545	Fluid T.	TP- 1	TE 545	Lower Pl. Center 1	Fig.5.143	273. - 0.125E+04	K	0.64%FS
546	Fluid T.	TP- 2	TE 546	Lower Pl. Center 2	Fig.5.143	273. - 0.125E+04	K	0.64%FS
547	Fluid T.	TP- 3	TE 547	Lower Pl. Center 3	Fig.5.143	273. - 0.125E+04	K	0.64%FS
548	Fluid T.	TP- 4	TE 548	Lower Pl. Center 4	Fig.5.143	273. - 0.125E+04	K	0.64%FS
549	Fluid T.	TP- 5	TE 549	Lower Pl. Center 5	Fig.5.143	273. - 0.125E+04	K	0.64%FS
550	Fluid T.	TP- 6	TE 550	Lower Pl. Center 7	Fig.5.143	273. - 0.125E+04	K	0.64%FS

Table 3.2 Measurement List for RUN 962 (Continued)

551Ch.- 600Ch.

Ch.	Item	Symbol	ID.		Location		Fig.No.	Range			Unit	Accuracy
551	Slab T.	TP- 7	TE	551	Lower Pl. North	1	Not Measured	273.	-	0.125E+04	K	0.64%FS
552	Slab T.	TP- 8	TE	552	Lower Pl. North	2	Not Measured	273.	-	673.	K	0.64%FS
553	Slab T.	TP- 9	TE	553	Lower Pl. North	4	Not Measured	273.	-	673.	K	0.64%FS
554	Slab T.	TP-10	TE	554	Lower Pl. North	6	Not Measured	273.	-	673.	K	0.64%FS
555	Slab T.	TP-11	TE	555	Lower Pl. South	1	Not Measured	273.	-	673.	K	0.64%FS
556	Slab T.	TP-12	TE	556	Lower Pl. South	2	Not Measured	273.	-	673.	K	0.64%FS
557	Slab T.	TP-13	TE	557	Lower Pl. South	4	Not Measured	273.	-	673.	K	0.64%FS
558	Slab T.	TP-14	TE	558	Lower Pl. South	6	Not Measured	273.	-	673.	K	0.64%FS
559	Level	LB- 1	LM	559	C.B.Liquid Level	A1-1	Not Measured					
560	Level	LB- 2	LM	560	C.B.Liquid Level	A1-2	Not Measured					
561	Level	LB- 3	LM	561	C.B.Liquid Level	A1-3	Not Measured					
562	Level	LB- 4	LM	562	C.B.Liquid Level	A1-4	Not Measured					
563	Level	LB- 5	LM	563	C.B.Liquid Level	A1-5	Not Measured					
564	Level	LB- 6	LM	564	C.B.Liquid Level	A1-6	Not Measured					
565	Level	LB- 7	LM	565	C.B.Liquid Level	A1-7	Not Measured					
566	Level	LB- 8	LM	566	C.B.Liquid Level	A2-1	Fig.5.144					
567	Level	LB- 9	LM	567	C.B.Liquid Level	A2-2	Fig.5.144					
568	Level	LB-10	LM	568	C.B.Liquid Level	A2-3	Fig.5.144					
569	Level	LB-11	LM	569	C.B.Liquid Level	A2-4	Fig.5.144					
570	Level	LB-12	LM	570	C.B.Liquid Level	A2-5	Failure					
571	Level	LB-13	LM	571	C.B.Liquid Level	A2-6	Fig.5.144					
572	Level	LB-14	LM	572	C.B.Liquid Level	A2-7	Fig.5.144					
573	Level	LB-15	LM	573	C.B.Liquid Level	B-1	Fig.5.145					
574	Level	LB-16	LM	574	C.B.Liquid Level	B-2	Fig.5.145					
575	Level	LB-17	LM	575	C.B.Liquid Level	B-3	Fig.5.145					
576	Level	LB-18	LM	576	C.B.Liquid Level	B-4	Fig.5.145					
577	Level	LB-19	LM	577	C.B.Liquid Level	B-5	Fig.5.145					
578	Level	LB-20	LM	578	C.B.Liquid Level	B-6	Fig.5.145					
579	Level	LB-21	LM	579	C.B.Liquid Level	B-7	Fig.5.145					
580	Level	LB-22	LM	580	C.B.Liquid Level	C-1	Fig.5.146					
581	Level	LB-23	LM	581	C.B.Liquid Level	C-2	Fig.5.146					
582	Level	LB-24	LM	582	C.B.Liquid Level	C-3	Fig.5.146					
583	Level	LB-25	LM	583	C.B.Liquid Level	C-4	Fig.5.146					
584	Level	LB-26	LM	584	C.B.Liquid Level	C-5	Fig.5.146					
585	Level	LB-27	LM	585	C.B.Liquid Level	C-6	Fig.5.146					
586	Level	LB-28	LM	586	C.B.Liquid Level	C-7	Fig.5.146					
587	Level	LB-29	LM	587	C.B.Liquid Level	D-1	Not Measured					
588	Level	LB-30	LM	588	C.B.Liquid Level	D-2	Not Measured					
589	Level	LB-31	LM	589	C.B.Liquid Level	D-3	Not Measured					
590	Level	LB-32	LM	590	C.B.Liquid Level	D-4	Not Measured					
591	Level	LB-33	LM	591	C.B.Liquid Level	D-5	Not Measured					
592	Level	LB-34	LM	592	C.B.Liquid Level	D-6	Not Measured					
593	Level	LB-35	LM	593	C.B.Liquid Level	D-7	Not Measured					
594	Level	LL- 1	LM	594	Ch.Box Outlet	A1-5	Not Measured					
595	Level	LL- 2	LM	595	Ch.Box Outlet	A1-6	Not Measured					
596	Level	LL- 3	LM	596	Ch.Box Outlet	A1-7	Failure					
597	Level	LL- 4	LM	597	Ch.Box Outlet	A2-5	Failure					
598	Level	LL- 5	LM	598	Ch.Box Outlet	A2-6						
599	Level	LL- 6	LM	599	Ch.Box Outlet	A2-7	Fig.5.147					
600	Level	LL- 7	LM	600	Ch.Box Outlet	A-1						

Table 3.2 Measurement List for RUN 962 (Continued)

601Ch.- 650Ch.

Ch.	Item	Symbol	ID.		Location	Fig.No.	Range	Unit	Accuracy
601	Level	LL- 8	LM	601	Ch.Box Outlet A-2	Failure			
602	Level	LL- 9	LM	602	Ch.Box Outlet A-3	Fig.5.148			
603	Level	LL-10	LM	603	Ch.Box Outlet A-4	Fig.5.148			
604	Level	LL-11	LM	604	Ch.Box Outlet A-6				
605	Level	LL-12	LM	605	Ch.Box Outlet C1-5				
606	Level	LL-13	LM	606	Ch.Box Outlet C1-6				
607	Level	LL-14	LM	607	Ch.Box Outlet C1-7				
608	Level	LL-15	LM	608	Ch.Box Outlet C2-5	Not Measured			
609	Level	LL-16	LM	609	Ch.Box Outlet C2-6	Not Measured			
610	Level	LL-17	LM	610	Ch.Box Outlet C2-7	Not Measured			
611	Level	LL-18	LM	611	Ch.Box Outlet C-1				
612	Level	LL-19	LM	612	Ch.Box Outlet C-2	Failure			
613	Level	LL-20	LM	613	Ch.Box Outlet C-3				
614	Level	LL-21	LM	614	Ch.Box Outlet C-4				
615	Level	LL-22	LM	615	Ch.Box Outlet C-6				
616	Level	LL-23	LM	616	Ch.Box Inlet A-1	Fig.5.149			
617	Level	LL-24	LM	617	Ch.Box Inlet A-2	Fig.5.149			
618	Level	LL-25	LM	618	Ch.Box Inlet B-1	Not Measured			
619	Level	LL-26	LM	619	Ch.Box Inlet B-2	Not Measured			
620	Level	LL-27	LM	620	Ch.Box Inlet C-1	Fig.5.150			
621	Level	LL-28	LM	621	Ch.Box Inlet C-2	Fig.5.150			
622	Level	LL-29	LM	622	Ch.Box Inlet D-1	Not Measured			
623	Level	LL-30	LM	623	Ch.Box Inlet D-2	Not Measured			
624	Level	LL-31	LM	624	Lower Pl. North 1	Fig.5.151			
625	Level	LL-32	LM	625	Lower Pl. North 2	Fig.5.151			
626	Level	LL-33	LM	626	Lower Pl. North 3				
627	Level	LL-34	LM	627	Lower Pl. North 4				
628	Level	LL-35	LM	628	Lower Pl. North 5				
629	Level	LL-36	LM	629	Lower Pl. North 6	Failure			
630	Level	LL-37	LM	630	Lower Pl. South 1	Not Measured			
631	Level	LL-38	LM	631	Lower Pl. South 2	Not Measured			
632	Level	LL-39	LM	632	Lower Pl. South 3	Not Measured			
633	Level	LL-40	LM	633	Lower Pl. South 4	Not Measured			
634	Level	LL-41	LM	634	Lower Pl. South 5	Not Measured			
635	Level	LL-42	LM	635	Lower Pl. South 6	Not Measured			
636	Level	LL-43	LM	636	Guide Tube North 0				
637	Level	LL-44	LM	637	Guide Tube North 1				
638	Level	LL-45	LM	638	Guide Tube North 3				
639	Level	LL-46	LM	639	Guide Tube North 6				
640	Level	LL-47	LM	640	Guide Tube South 0	Not Measured			
641	Level	LL-48	LM	641	Guide Tube South 1	Not Measured			
642	Level	LL-49	LM	642	Guide Tube South 3	Not Measured			
643	Level	LL-50	LM	643	Guide Tube South 6	Not Measured			
644	Level	L- 1	LM	644	Downcomer D-Side 1	Fig.5.152			
645	Level	L- 2	LM	645	Downcomer D-Side 2	Fig.5.152			
646	Level	L- 3	LM	646	Downcomer D-Side 3	Fig.5.152			
647	Level	L- 4	LM	647	Downcomer D-Side 4	Fig.5.152			
648	Level	L- 5	LM	648	Downcomer D-Side 5	Fig.5.152			
649	Level	L- 6	LM	649	Downcomer B-Side 1	Not Measured			
650	Level	L- 7	LM	650	Downcomer B-Side 2	Not Measured			

Table 3.2 Measurement List for RUN 962 (Continued)

651Ch.- 700Ch.

Ch.	Item	Symbol	ID.		Location	Fig.No.	Range			Unit	Accuracy
651	Level	L- 8	LM	651	Downcomer B-Side 3	Not Measured					
652	Level	L- 9	LM	652	Downcomer B-Side 4	Not Measured					
653	Level	L-10	LM	653	Downcomer B-Side 5	Failure					
654	Void	VF- 1	VD	654	A54 Tie Rod Pos.1	Not Measured	0.0	-	1.00		
655	Void	VF- 2	VD	655	A54 Tie Rod Pos.2	Not Measured	0.0	-	1.00		
656	Void	VF- 3	VD	656	A54 Tie Rod Pos.3	Not Measured	0.0	-	1.00		
657	Void	VF- 4	VD	657	A54 Tie Rod Pos.4	Not Measured	0.0	-	1.00		
658	Void	VF- 5	VD	658	A54 Tie Rod Pos.5	Not Measured	0.0	-	1.00		
659	Void	VF- 6	VD	659	A54 Tie Rod Pos.6	Not Measured	0.0	-	1.00		
660	Void	VF- 7	VD	660	A54 Tie Rod Pos.7	Not Measured	0.0	-	1.00		
661	Void	VF- 8	VD	661	B54 Tie Rod Pos.1	Not Measured	0.0	-	1.00		
662	Void	VF- 9	VD	662	B54 Tie Rod Pos.2	Not Measured	0.0	-	1.00		
663	Void	VF-10	VD	663	B54 Tie Rod Pos.3	Not Measured	0.0	-	1.00		
664	Void	VF-11	VD	664	B54 Tie Rod Pos.4	Not Measured	0.0	-	1.00		
665	Void	VF-12	VD	665	B54 Tie Rod Pos.5	Not Measured	0.0	-	1.00		
666	Void	VF-13	VD	666	B54 Tie Rod Pos.6	Not Measured	0.0	-	1.00		
667	Void	VF-14	VD	667	B54 Tie Rod Pos.7	Not Measured	0.0	-	1.00		
668	Void	VF-15	VD	668	C54 Tie Rod Pos.1	Not Measured	0.0	-	1.00		
669	Void	VF-16	VD	669	C54 Tie Rod Pos.2	Not Measured	0.0	-	1.00		
670	Void	VF-17	VD	670	C54 Tie Rod Pos.3	Not Measured	0.0	-	1.00		
671	Void	VF-18	VD	671	C54 Tie Rod Pos.4	Not Measured	0.0	-	1.00		
672	Void	VF-19	VD	672	C54 Tie Rod Pos.5	Not Measured	0.0	-	1.00		
673	Void	VF-20	VD	673	C54 Tie Rod Pos.6	Not Measured	0.0	-	1.00		
674	Void	VF-21	VD	674	C54 Tie Rod Pos.7	Not Measured	0.0	-	1.00		
675	Void	VF-22	VD	675	D54 Tie Rod Pos.7	Not Measured	0.0	-	1.00		
676	Void	VF-23	VD	676	D54 Tie Rod Pos.7	Not Measured	0.0	-	1.00		
677	Void	VF-24	VD	677	D54 Tie Rod Pos.7	Not Measured	0.0	-	1.00		
678	Void	VF-25	VD	678	D54 Tie Rod Pos.7	Not Measured	0.0	-	1.00		
679	Void	VF-26	VD	679	D54 Tie Rod Pos.7	Not Measured	0.0	-	1.00		
680	Void	VF-27	VD	680	D54 Tie Rod Pos.7	Not Measured	0.0	-	1.00		
681	Void	VF-28	VD	681	D54 Tie Rod Pos.7	Not Measured	0.0	-	1.00		
682	Void	VE- 1	VD	682	Channel A Outlet 1	Not Measured	0.0	-	1.00		
683	Void	VE- 2	VD	683	Channel A Outlet 2	Not Measured	0.0	-	1.00		
684	Void	VE- 3	VD	684	Channel A Outlet 3	Not Measured	0.0	-	1.00		
685	Void	VE- 4	VD	685	Channel B Outlet 1	Not Measured	0.0	-	1.00		
686	Void	VE- 5	VD	686	Channel B Outlet 2	Not Measured	0.0	-	1.00		
687	Void	VE- 6	VD	687	Channel B Outlet 3	Not Measured	0.0	-	1.00		
688	Void	VE- 7	VD	688	Channel C Outlet 1	Not Measured	0.0	-	1.00		
689	Void	VE- 8	VD	689	Channel C Outlet 2	Not Measured	0.0	-	1.00		
690	Void	VE- 9	VD	690	Channel C Outlet 3	Not Measured	0.0	-	1.00		
691	Void	VE-10	VD	691	Channel D Outlet 1	Not Measured	0.0	-	1.00		
692	Void	VE-11	VD	692	Channel D Outlet 2	Not Measured	0.0	-	1.00		
693	Void	VE-12	VD	693	Channel D Outlet 3	Not Measured	0.0	-	1.00		
694	Void	VE-13	VD	694	Lower Plenum Bottom 1	Not Measured	0.0	-	1.00		
695	Void	VE-14	VD	695	Lower Plenum Bottom 2	Not Measured	0.0	-	1.00		
696	Void	VE-15	VD	696	Lower Plenum Bottom 3	Not Measured	0.0	-	1.00		
697	Void	VP- 1	VD	697	Lower Plenum Inlet	Not Measured	0.0	-	1.00		
698	Void	VP- 2	VD	698	Lower Plenum Inlet	Not Measured	0.0	-	1.00		

Table 3.3 Core instrumentation map

Item	Pos. / DL / Rod NO.	Core Outlet	Pos.1	Pos.2	Pos.3	Pos.4	Pos.5	Pos.6	Pos.7	Core Inlet
		3660	3417	3114.5	2879.5	2527	2174.5	1939.5	1637	1454
Surface Temp.	A11		TF 1	TF 2	TF 3	TF 4	TF 5	TF 6	TF 7	
	A12		TF 8	TF 9	TF 10	TF 11	TF 12	TF 13	TF 14	
	A13		TF 15	TF 16	TF 17	TF 18	TF 19	TF 20	TF 21	
	A14		TF 22	TF 23	TF 24	TF 25	TF 26	TF 27	TF 28	
	A15		TF 29			TF 30				
	A17		TF 31			TF 32				
	A22		TF 33	TF 34	TF 35	TF 36	TF 37	TF 38	TF 39	
	A23		TF 40	TF 41	TF 42	TF 43	TF 44	TF 45	TF 46	
	A24		TF 47	TF 48	TF 49	TF 50	TF.51	TF 52	TF 53	
	A26		TF 54			TF 55				
	A28		TF 56			TF 57				
	A31		TF 58			TF 59				
	A33		TF 60	TF 61	TF 62	TF 63	TF 64	TF 65	TF 66	
	A34		TF 67	TF 68	TF 69	TF 70	TF 71	TF 72	TF 73	
	A35		TF 74			TF 75				
	A37		TF 76			TF 77				
	A42		TF 78			TF 79				
Fluid Temp.	A44	TC 1	TF180	TF181	TF182	TF183	TF184	TF185	TF186	TC 2
Surface Temp.	A45		TF 80			TF 81				
	A46		TF 82			TF 83				
	A48		TF 84			TF 85				
	A51		TF 86			TF 87				
	A53		TF 88			TF 89				
	A54		TF 90							
	A57		TF 91			TF 92				
	A62		TF 93			TF 94				
	A64		TF 95			TF 96				
	A66		TF 97			TF 98				
	A68		TF 99			TF100				
	A71		TF101			TF102				
	A73		TF103			TF104				
	A75		TF105			TF106				
	A77		TF107			TF108				

Table 3.3 Core instrumentation map (Continued)

Item	Pos. / Rod NO. / DL	Core Outlet	Pos.1	Pos.2	Pos.3	Pos.4	Pos.5	Pos.6	Pos.7	Core Inlet
		3660	3417	3114.5	2879.5	2527	2174.5	1939.5	1637	1454
Surface Temp.	A82		TF109			TF110				
	A84		TF111			TF112				
	A86		TF113			TF114				
	A88		TF115			TF116				
	B11					TF117				
	B13					TF118				
	B15		TF119	TF120	TF121	TF122	TF123	TF124	TF125	
	B31					TF126				
	B33					TF127				
	B35					TF128				
Fluid Temp.	B44	TC 3	TF187	TF188	TF189	TF190	TF191	TF192	TF193	TC 4
Surface Temp.	B51					TF129				
	B53					TF130				
	B85		TF131	TF132	TF133	TF134	TF135	TF136	TF137	
	C11					TF138				
	C13					TF139				
	C15					TF140				
	C31					TF141				
	C33		TF142	TF143	TF144	TF145	TF146	TF147	TF148	
	C35					TF149				
Fluid Temp.	C44	TC 5	TF194	TF195	TF196	TF197	TF198	TF199	TF200	TC 6
Surface Temp.	C51					TF150				
	C53					TF151				
	C77		TF152	TF153	TF154	TF155	TF156	TF157	TF158	
	D11					TF159				
	D13					TF160				
	D27		TF161	TF162	TF163	TF164	TF165	TF166	TF167	
	D31					TF168				
	D33					TF169				
	D35					TF170				
Fluid Temp.	D44	TC 7	TF201	TF202	TF203	TF204	TF205	TF206	TF207	TC 8
Surface Temp.	D51					TF171				
	D53					TF172				
	D88		TF173	TF174	TF175	TF176	TF177	TF178	TF179	

Table 3.3 Core instrumentation map (Continued)

Item	Pos. / Rod NO. / DL	Core Outlet	Pos.1	Pos.2	Pos.3	Pos.4	Pos.5	Pos.6	Pos.7	Core Inlet
		3660	3417	3114.5	2879.5	2527	2174.5	1939.5	1673	1454
Void	A55		VF 1	VF 2	VF 3	VF 4	VF 5	VF 6	VF 7	
	B55		VF 8	VF 9	VF 10	VF 11	VF 12	VF 13	VF 14	
	C55		VF 15	VF 16	VF 17	VF 18	VF 19	VF 20	VF 21	
	D55		VF 22	VF 23	VF 24	VF 25	VF 26	VF 27	VF 28	
Channel Box Surface Temp.	A1*		TB 1	TB 2	TB 3	TB 4	TB 5	TB 6	TB 7	
	A2*		TB 8	TB 9	TB 10	TB 11	TB 12	TB 13	TB 14	
	B*		TB 15	TB 16	TB 17	TB 18	TB 19	TB 20	TB 21	
	C*		TB 22	TB 23	TB 24	TB 25	TB 26	TB 27	TB 28	
	D*		TB 29	TB 30	TB 31	TB 32	TB 33	TB 34	TB 35	
Liquid Level in the Channel Box	A1*		LB 1	LB 2	LB 3	LB 4	LB 5	LB 6	LB 7	
	A2*		LB 8	LB 9	LB 10	LB 11	LB 12	LB 13	LB 14	
	B*		LB 15	LB 16	LB 17	LB 18	LB 19	LB 20	LB 21	
	C*		LB 22	LB 23	LB 24	LB 25	LB 26	LB 27	LB 28	
	D*		LB 29	LB 30	LB 31	LB 32	LB 33	LB 34	LB 35	

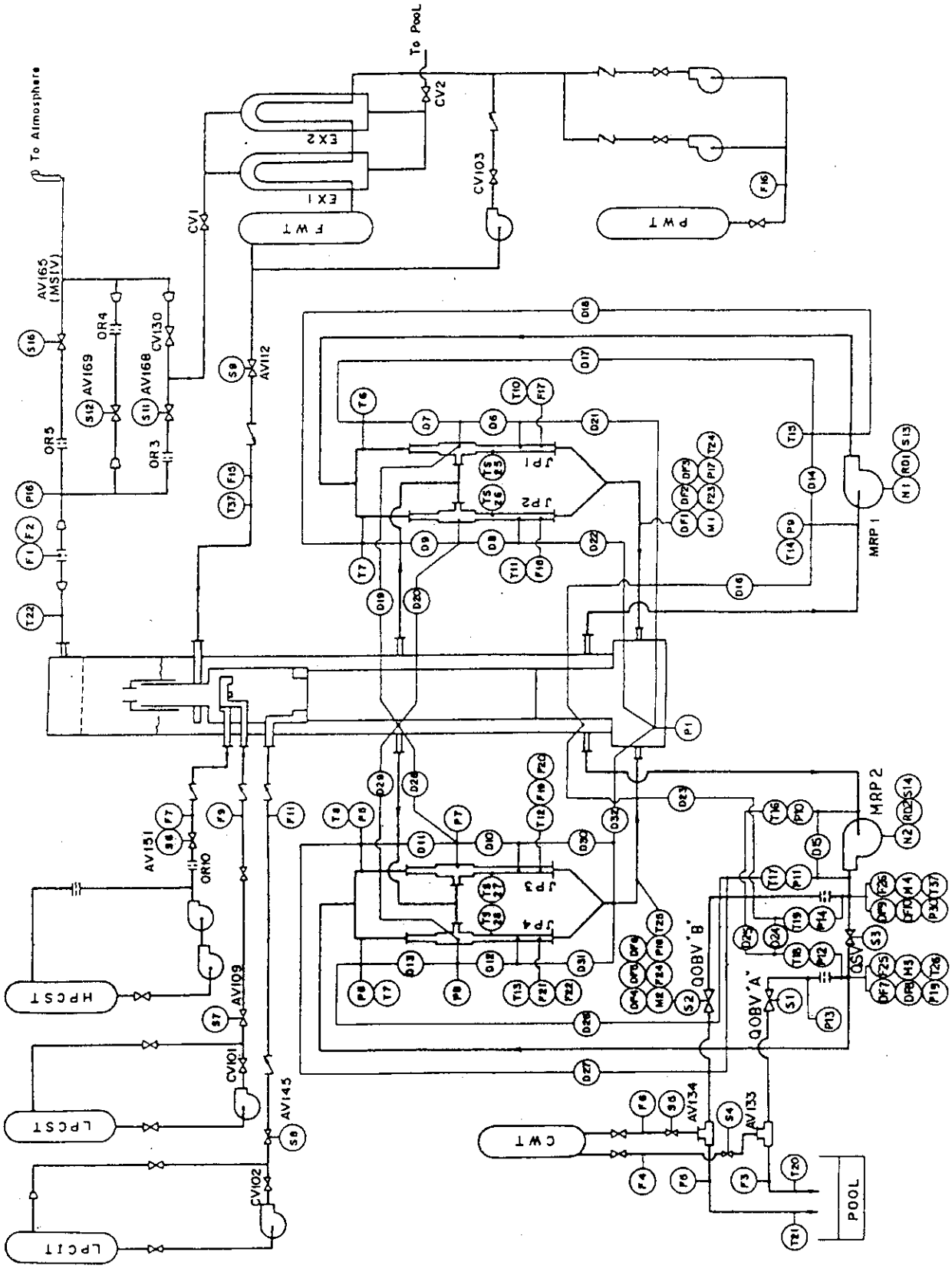

Fig. 3.1 Instrumentation location of ROSA-III test facility

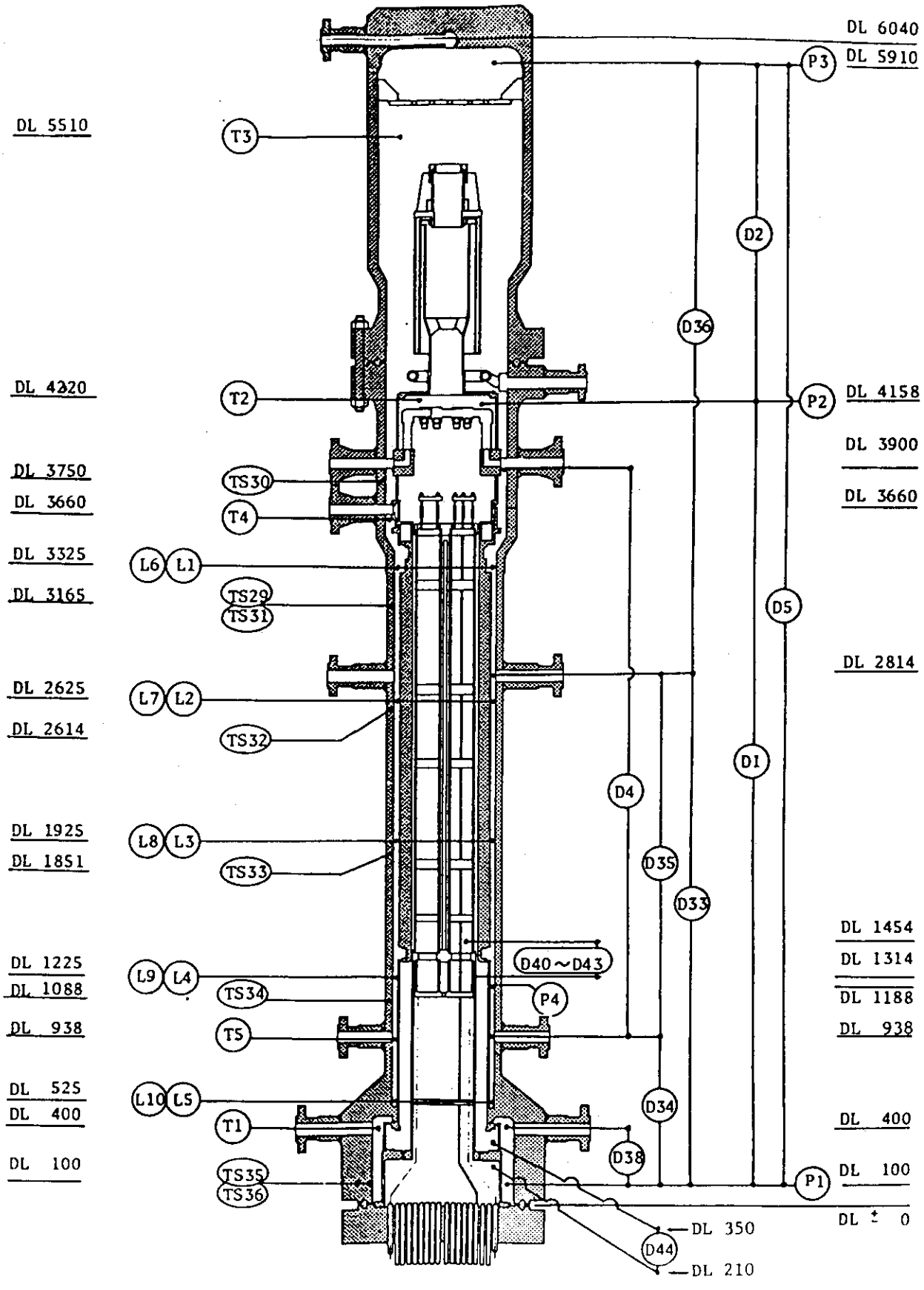

Fig. 3.2 Instrumentation location in pressure vessel

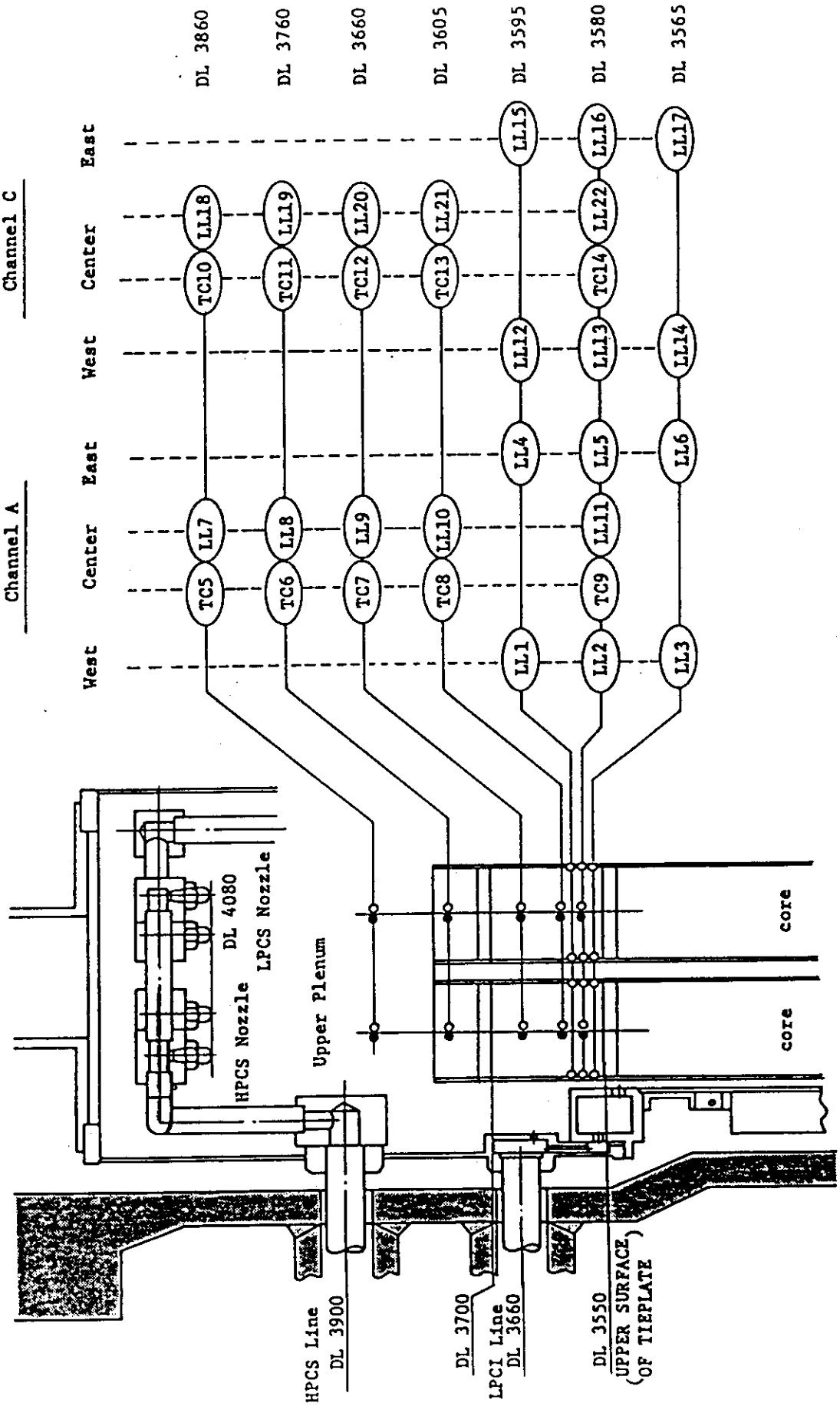

Fig. 3.3 Upper plenum instrumentation

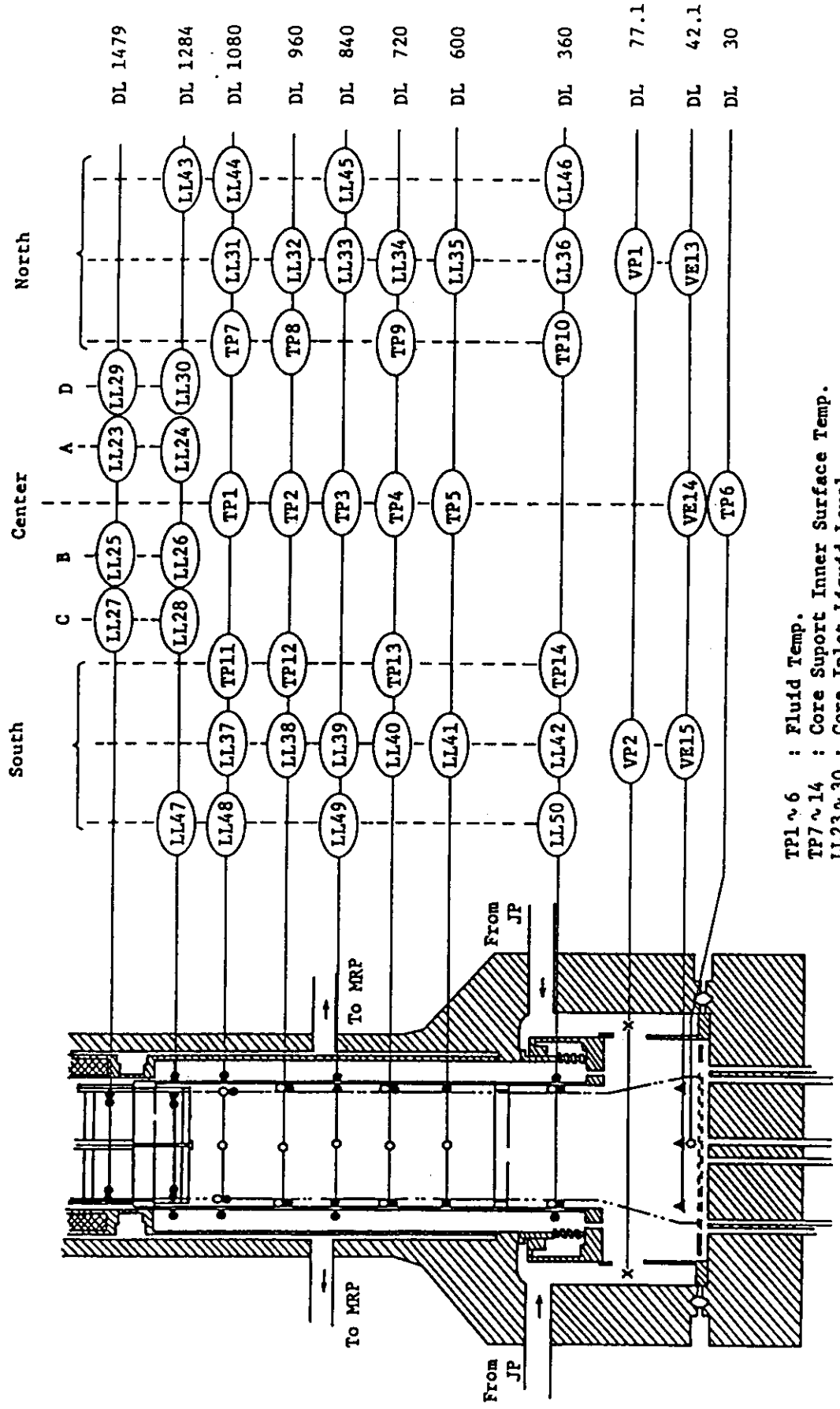

Fig. 3.4 Lower plenum instrumentation

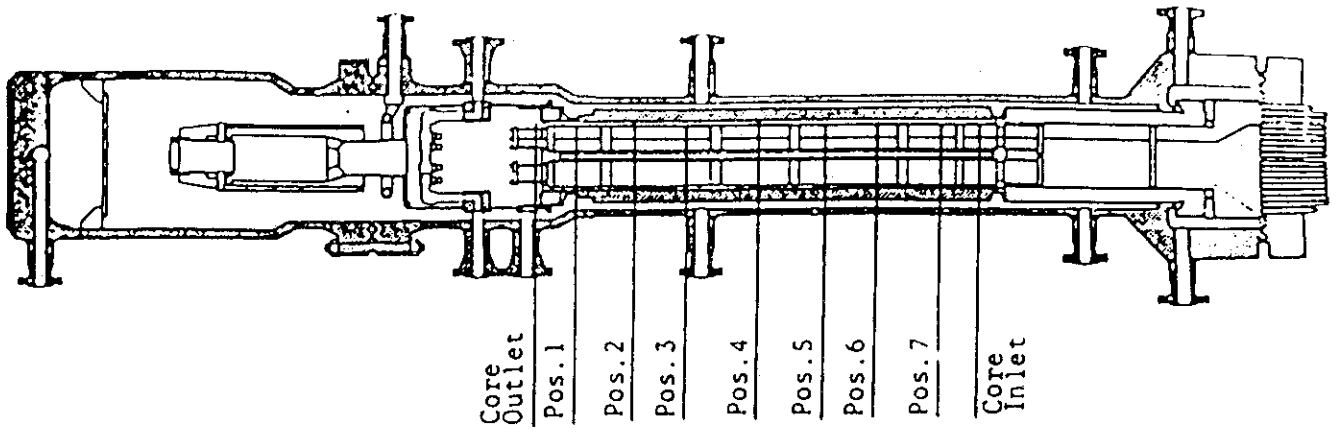

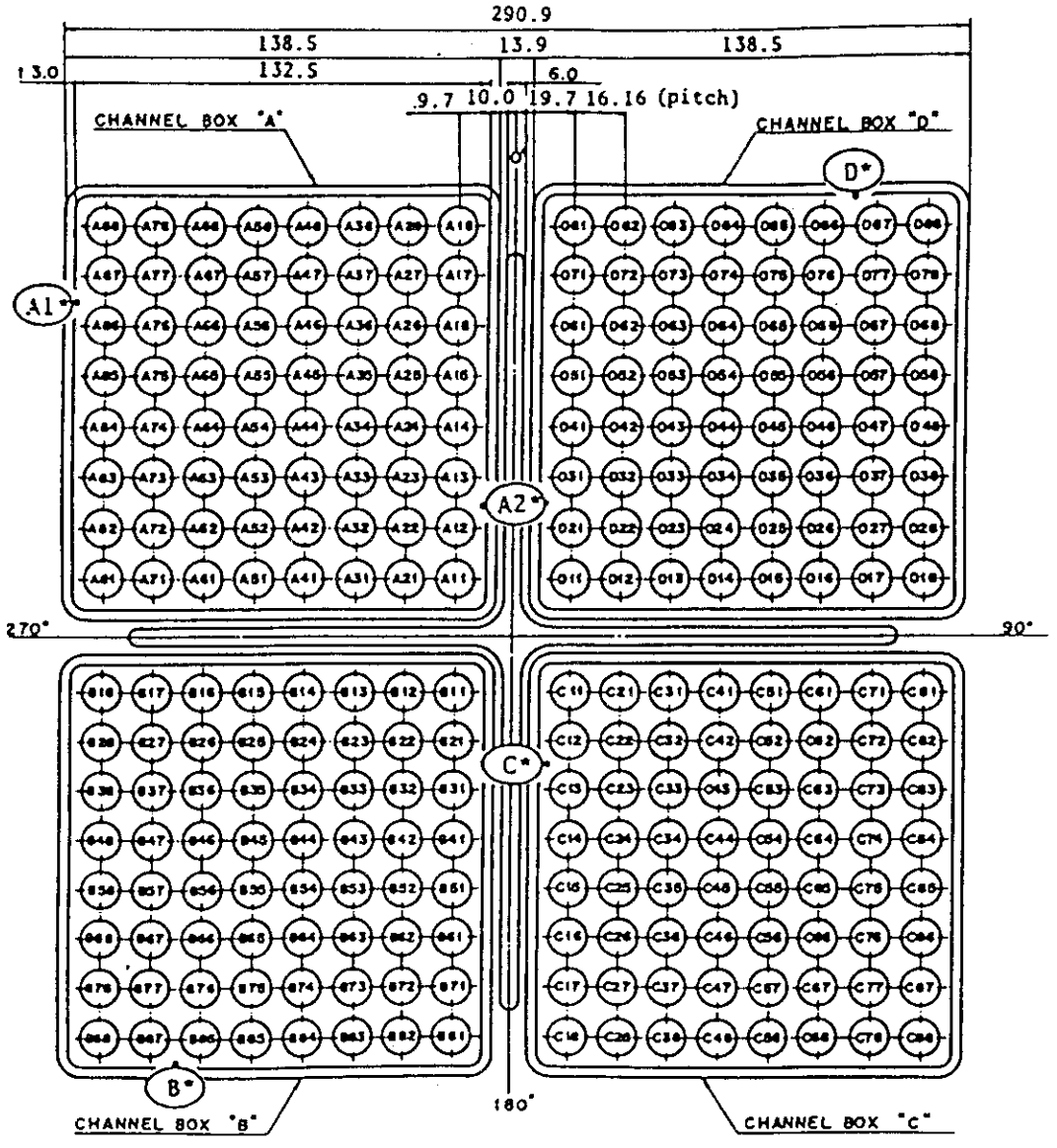

Heater rod O.D. is 12.27mm

A54,B54,C54 and D54 are water rod simulators with void probes, O.D.= 15.01mm

A45,B45,C45 and D45 are water rod simulators with thermocouples, O.D.= 15.01mm

Fig. 3.5 Core instrumentation (cf. Table 3.3)

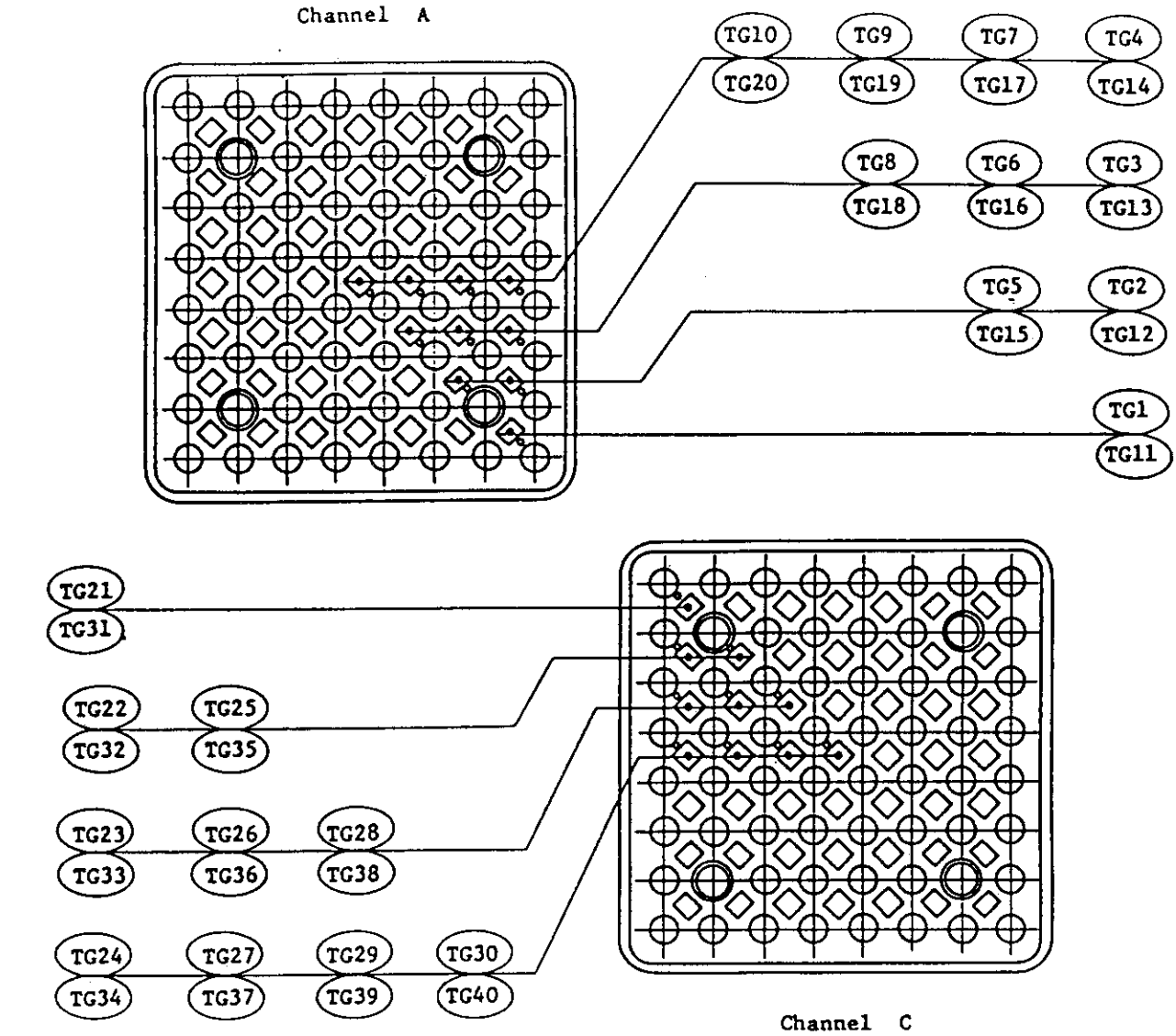

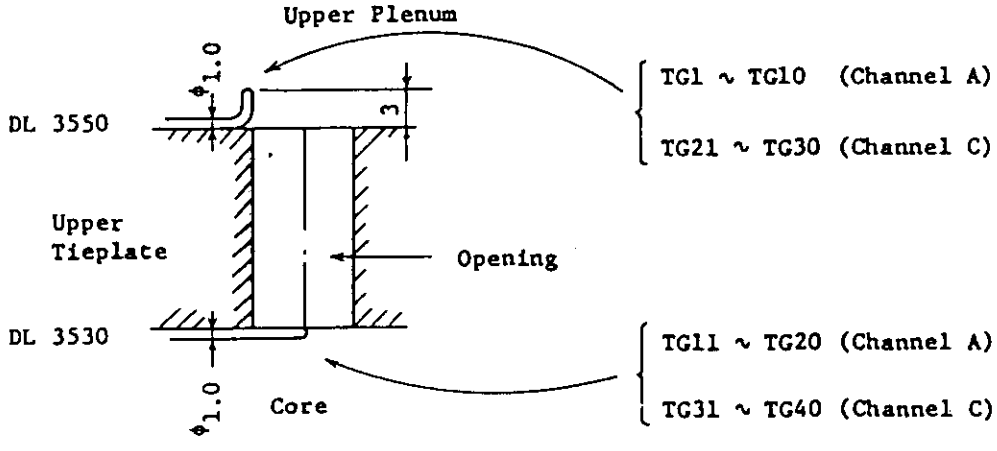

Fig. 3.6 Upper tieplate instrumentations

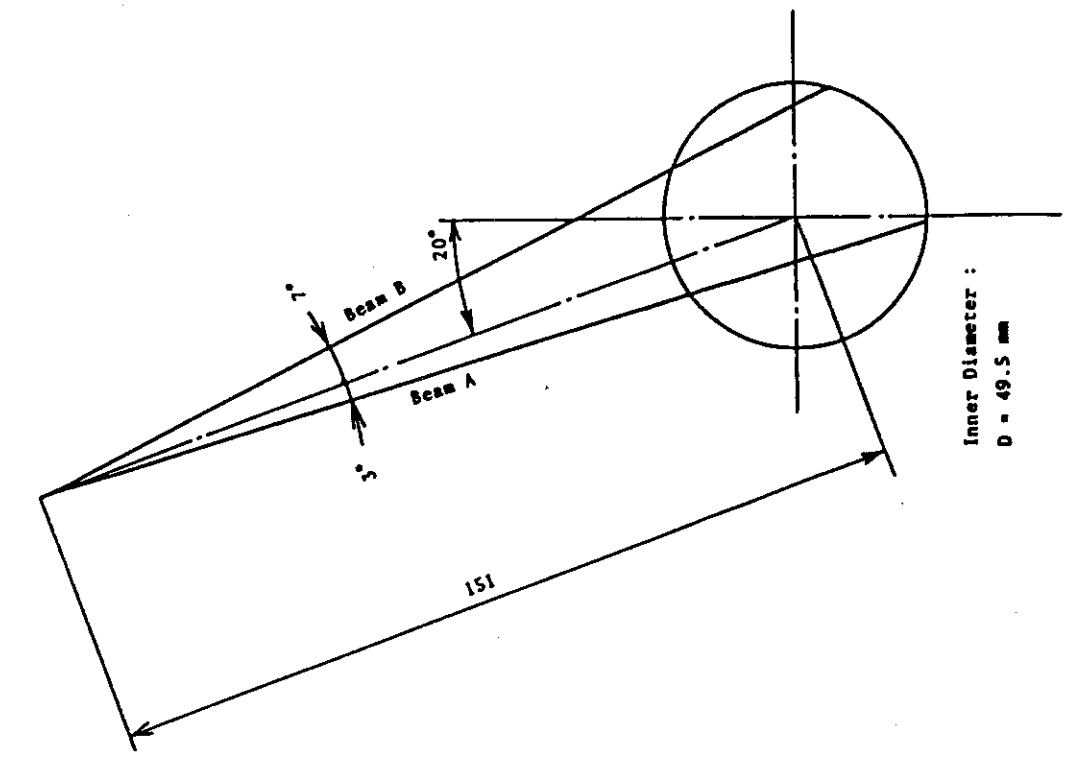

Fig. 3.8 Beam directions of two-beam gamma densitometer

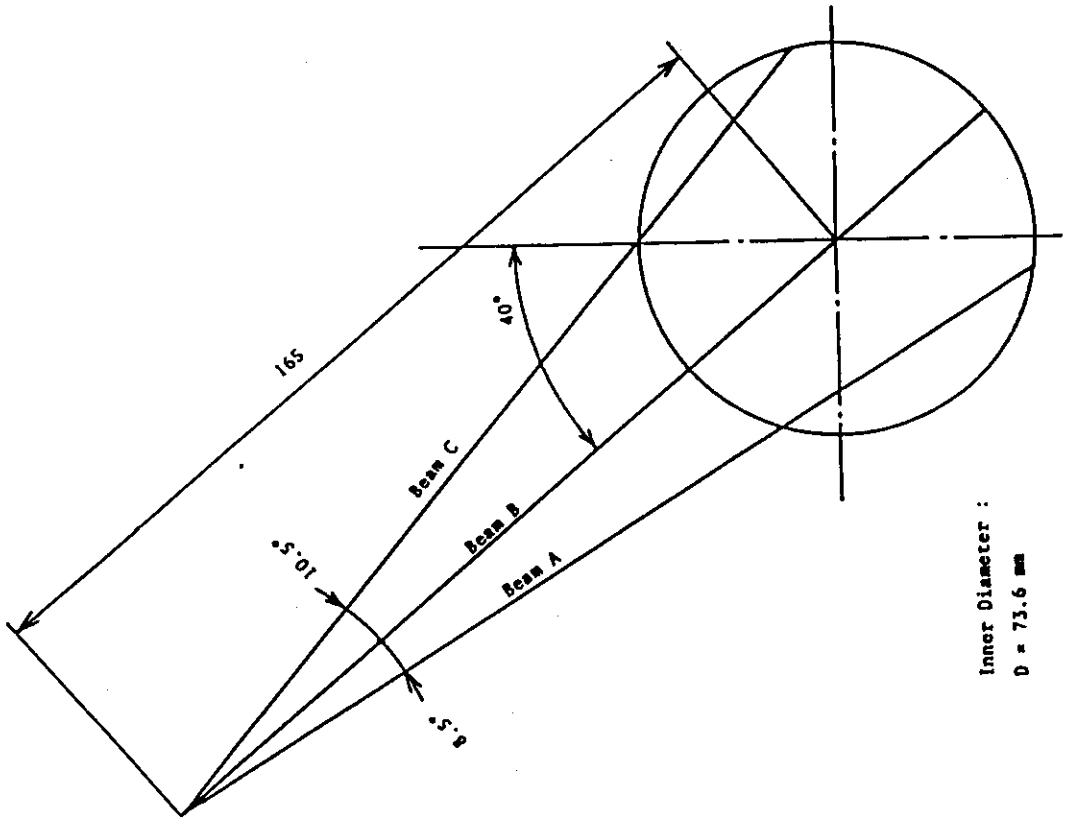

Fig. 3.7 Beam directions of three-beam gamma densitometer

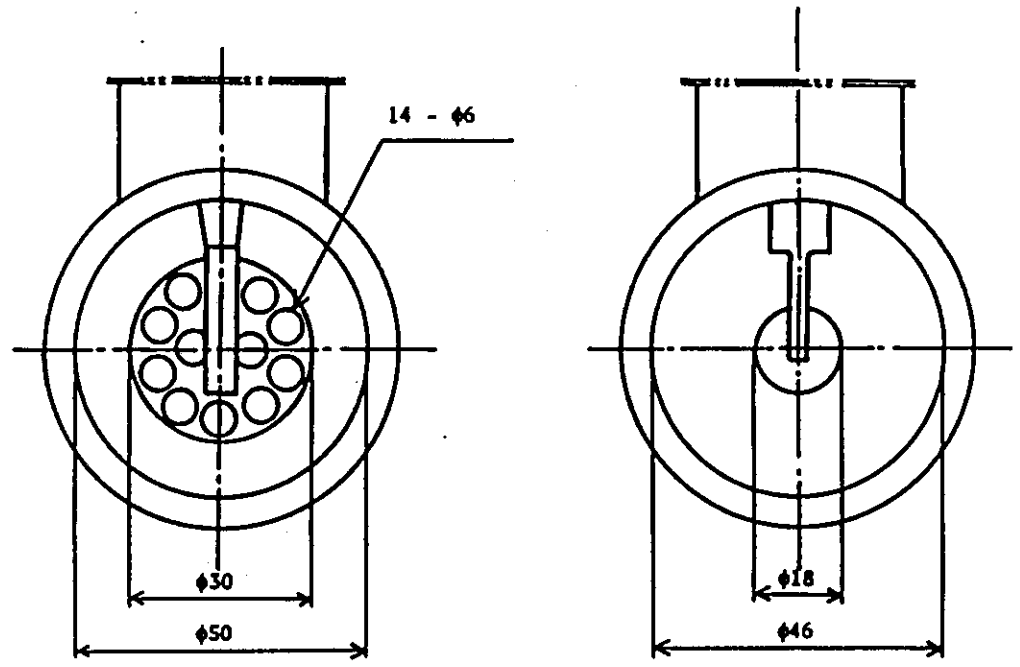

(a) High Range Drag Disc

(b) Low Range Drag Disc

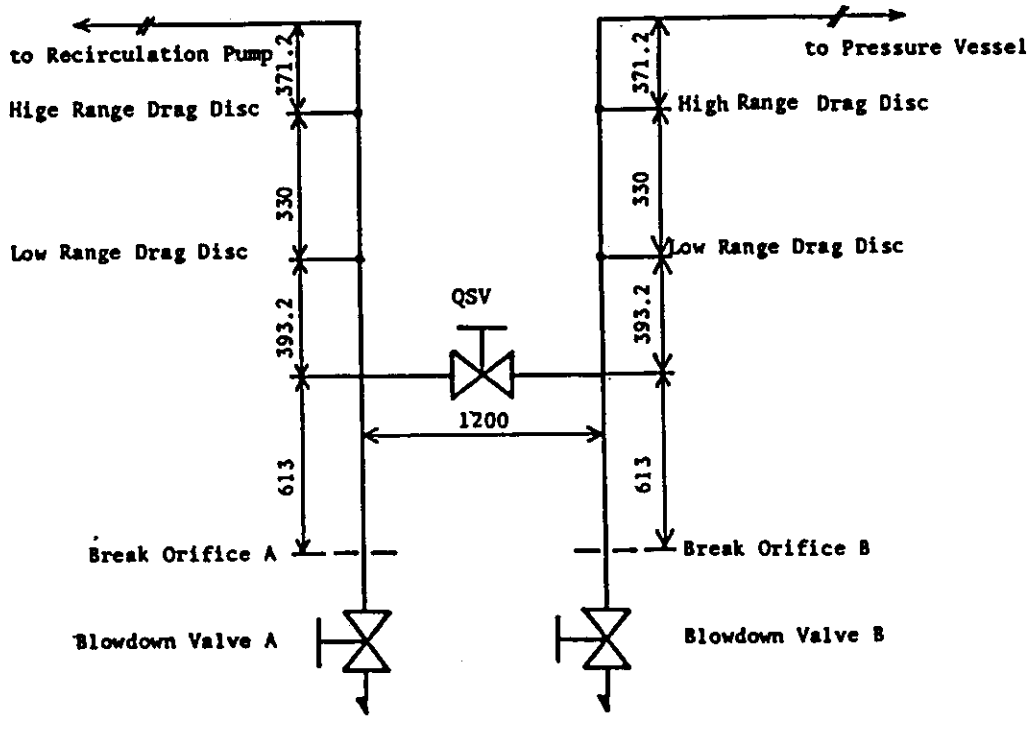

(c) Location of Drag Discs

Fig. 3.9 Arrangement and location of drag disks

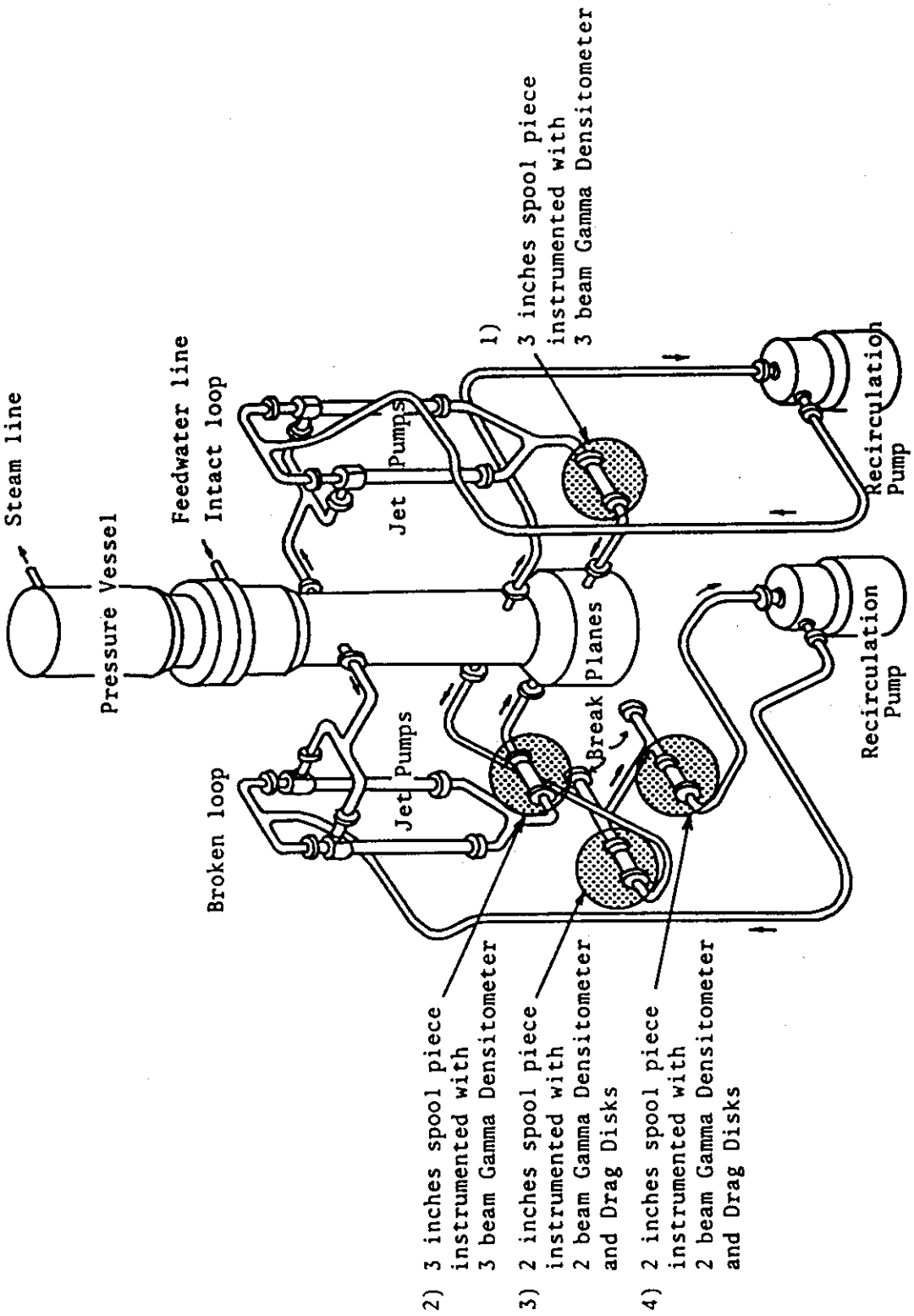

Fig. 3.10 Location of two-phase flow measurement spool pieces

This figure shows suction line break and break unit for discharge line break is removed between the recirculation pump and jet pumps in the broken loop. However, four two-phase instrumentation spool pieces are located similarly downstream the jet pumps and near the break units.

Table 4.1 Test conditions of RUN962

Items	Unit	Measured Value
Break Condition		
Location		MRP Discharge
Type		Split Break
Nozzle I. Diameter	mm	18.5
Initial System Condition		
Steam Dome Pressure	MPa	7.35
L. Plenum Temperature	K	552.2
L. Plenum Subcooling	K	10.9
Core Flow Rate*	kg/s	16.1
U. Plenum Quality	%	13.2
Core Power	KW	3972
Water Level in PV	m	5.0
Feedwater Temperature	K	490
Feedwater Flow Rate	kg/s	2.04
Steam Flow Rate	kg/s	2.05
Transient Condition		
MSIV Trip Time	s	L2**+ 3
Pressure Regulator	MPa	$P \geq 6.7$
SRV Actuation	MPa	$8.34 \geq P \geq 8.24$

Items	Unit	Measured Valve
ECCS Condition		
HPCS		not used
LPCS		
Injection Location		Up·Plenum
Initiation Condition	S	L1***+ 40
	MPa	$P \leq 2.17$
Coolant Temperature	K	314
LPCI		
Injection Location		Core Bypass
Initiation Condition	S	L1***+ 40
	MPa	$P \leq 1.58$
Coolant Temperature	K	314
ADS		
Initiation Condition	S	L1***+ 120
Orifice Diameter	mm	15.5
Trip Level		
** L2 from pV Bottom	m	4.76
***L1 from pV Bottom	m	4.25
* Include 9.5% of bypass flow		

Table 4.2 Major events and test procedure of RUN962

Time after break (s)	Events
0.0	· Break initiation
	· Recirculation pump trip
1.7	· Feedwater flow stop (completed at 3.8 s)
8.8	· Initiation of power decrease along power curve
12	· Initiation of MSIV closure (completed at 15 s)
24	· Jet pump suction line uncovery
32	· Recirculation pump suction line uncovery
36	· Initiation of top core uncovery (1st uncovery)
50	· Initiation of lower plenum flashing
62	· Initiation of top core uncovery (2nd uncovery)
116	· Bottom of core uncovered
139	· ADS valve opened
154	· Feedwater line flashing
167	· LPCS initiation
200	· LPCI initiation
208	· PCT at the midplane of A82 rod (933 K)
210	· Initiation of core reflooding
264	· Completion of core reflooding
272	· Completion of quench

Table 4.3 Characteristics of steam discharge line valves

Valve No.	Opening Time (s)	Closing Time (s)
AV 165	——	——
AV 168	——	0.1
AV 169	0.3	2.0

Orifice No.	Diameter (mm)	Area (mm^2)
OR 3	18.0	254.5
OR 4	15.5	188.7
OR 5	not used	——

Table 4.4 Control sequence for steam line valves in RUNs 962 and 963

Time	before break	break (t=0)	L2 + 3s	L1 + 120s
AV 168	Open	Open	Close	Close
CV 130	Control to maintain steady state pressure	Opened fully	Close	Close
AV 165	not used	not used	not used	not used
AV 169	Close	Close	Close	Open

AV ; Air Actuation Valve (Auto)

CV ; Control Valve (Manual)

Table 4.5 Test conditions of RUN963

Items	Unit	Measured Value
Break Condition		
Location		MRP Discharge
Type		Split Break
Nozzle I. Diameter	mm	26.2
Initial System Condition		
Steam Dome Pressure	MPa	7.35
L. Plenum Temperature	K	552.7
L. Plenum Subcooling	K	10.4
Core Flow Rate*	kg/s	16.2
U. Plenum Quality	%	13.1
Core Power	kW	3971
Water Level in PV	m	5.0
Feedwater Temperature	K	489
Feedwater Flow Rate	kg/s	2.03
Steam Flow Rate	kg/s	2.04
Transient Condition		
MSIV Trip Time	s	L2**+ 3s
Pressure Regurator	MPa	$P \geq 6.7$
SRV Actuation	MPa	$8.34 \geq P \geq 8.24$

Items	Unit	Measured Value
ECCS Condition		
HPCS		not used
LPCS		
Injection Location		Up·Plenum
Initiation Condition	s	L1***+ 40
	MPa	$P \leq 2.12$
Coolant Temperature	K	313
LPCI		
Injection Location		Core Bypass
Initiation Condition	s	L1***+ 40
	MPa	$P \leq 1.46$
Coolant Temperature	K	313
ADS		
Initiation Condition	s	L1***+ 120
Orifice Diameter	mm	15.5
Trip Level		
** L2 from PV bottom	m	4.76
*** L1 from PV bottom	m	4.25
* Include 9.5% of bypass flow		

Table 4.6 Major events and test procedure of RUN963

Time after break (s)	Events
0.0	· Break initiation
	· Recirculation pump trip
2.1	· Feedwater flow stop (completed at 4.3 s)
6.9	· Initiation of top core uncovery (1st uncovery)
8.2	· L2 level signal
8.8	· Initiation of power decrease along power curve
9.5	· Initiation of MSIV closure (completed at 15 s)
14	· L1 level signal
19	· Jet pump suction line uncovery (JPSU)
25	· Recirculation pump suction line uncovery (RLU)
35	· Initiation of lower plenum flashing
50	· Initiation of top core uncovery (2nd uncovery)
89	· Bottom of core uncovered
111	· Initiation of feedwater line flashing
126	· LPCS initiation
135	· ADS valve opened
155	· LPCI initiation
162	· Initiation of core reflooding
167	· PCT at the midplane of A82 rod (915 K)
233	· Completion of quench

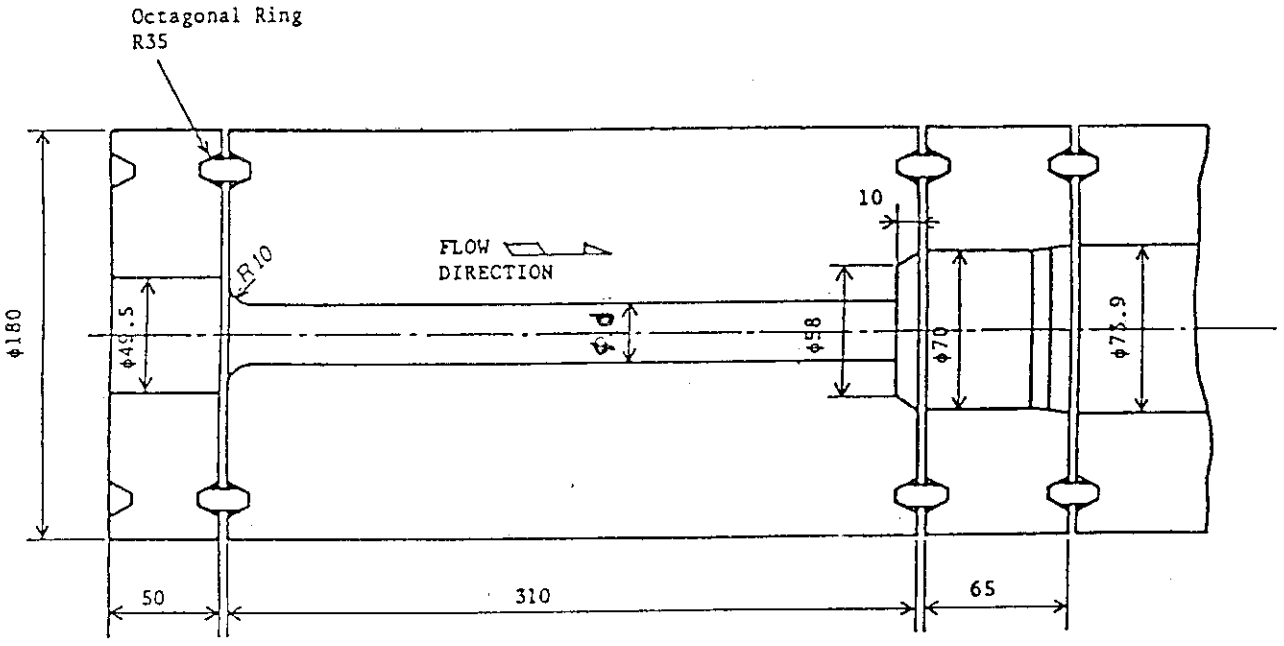

Material SUS304

Dimension in mm

Break area ratio (%)	d (mm)
100 , 50	26.2 , 18.5

Fig. 4.1 Break nozzle details

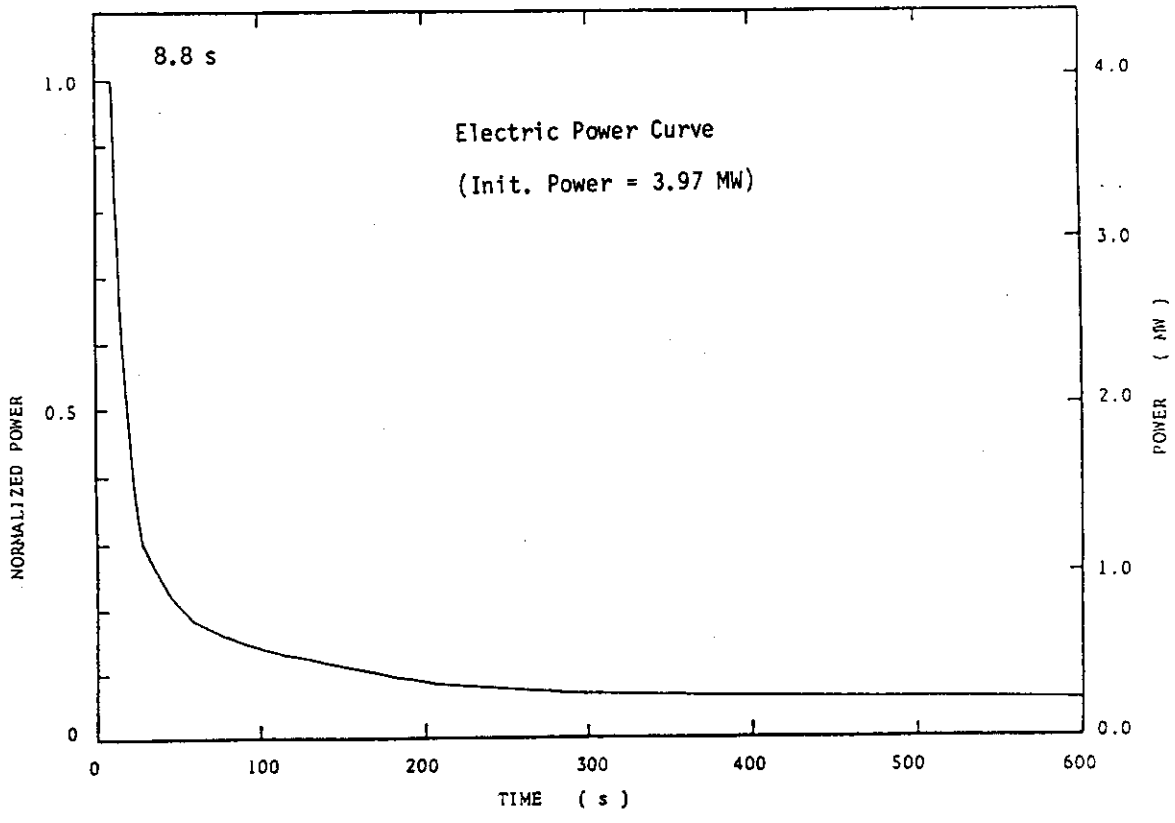

Fig. 4.2 Normalized power transient for ROSA-III test

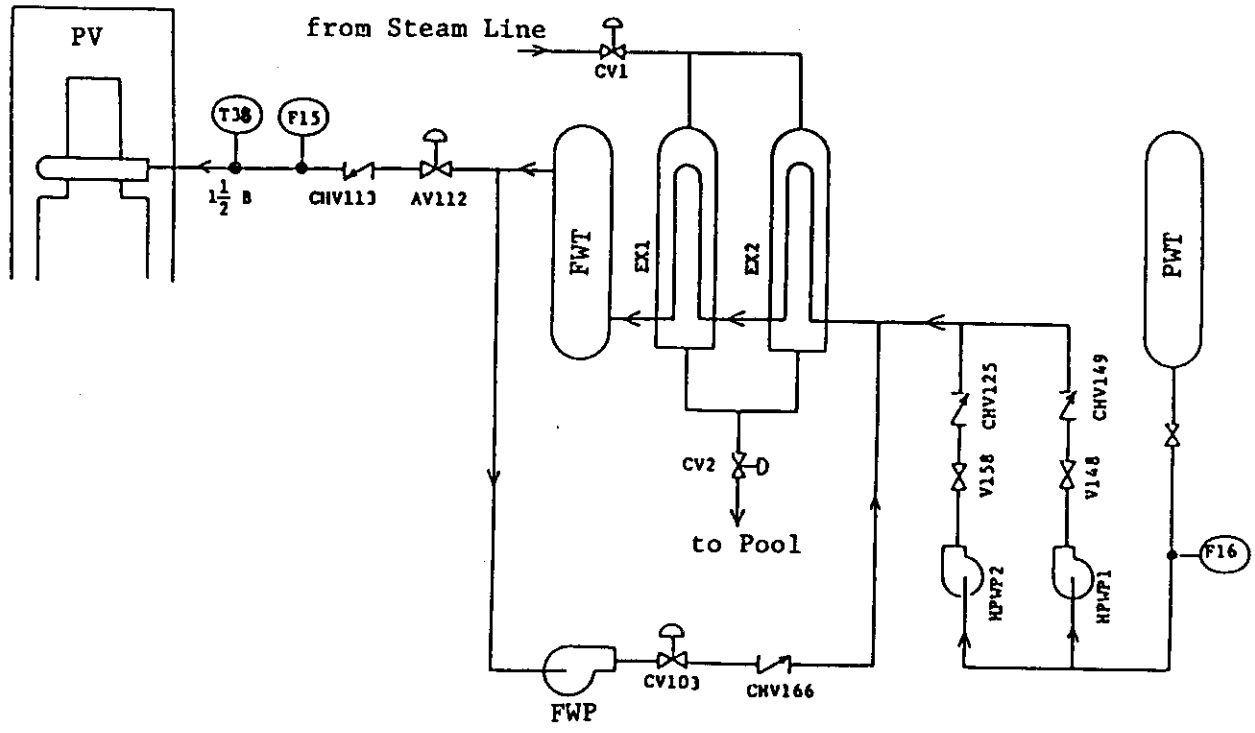

Fig. 4.3 Feedwater line schematic

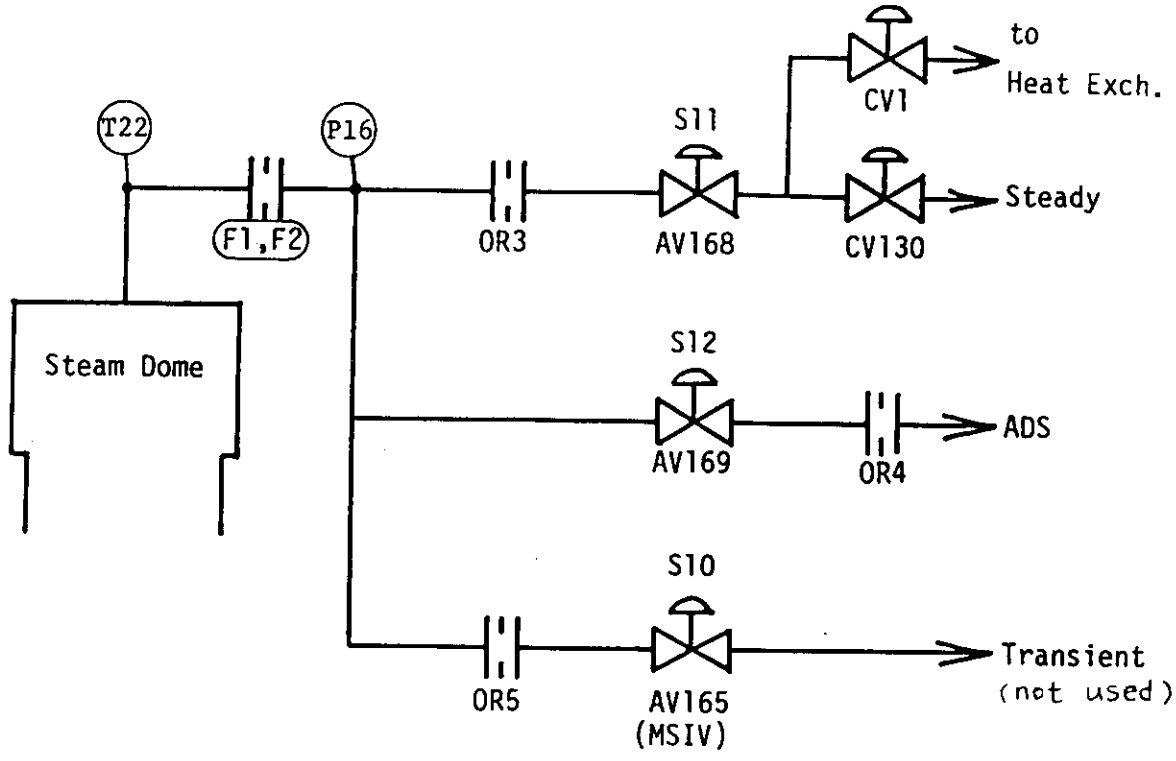

Fig. 4.4 Main steam line schematic

Table 5.1 Maximum Cladding Temperature Distribution in the Core of RUN962

	Pos.1	Pos.2	Pos.3	Pos.4	Pos.5	Pos.6	Pos.7
A-11 rod	TE 201	TE 202	TE 203	TE 204	TE 205	TE 206	TE 207
PCT (K)	604.3	742.3	889.9	911.5	847.9	735.1	594.7
Time (s)	103.8	229.8	207.6	207.6	209.4	203.4	185.4
A-12 rod	TE 208	TE 209	TE 210	TE 211	TE 212	TE 213	TE 214
PCT (K)	600.7	811.9	881.5	897.1	823.9	720.7	576.7
Time (s)	105.6	220.2	208.8	207.6	206.4	201.0	181.8
A-13 rod	TE 215	TE 216	TE 217	TE 218	TE 219	TE 220	TE 221
PCT (K)	606.7	792.7	863.5	883.9	816.7	718.3	579.1
Time (s)	106.2	176.4	211.2	208.8	207.0	201.0	176.4
A-14 rod	TE 222	TE 223	TE 224	TE 225	TE 226	TE 227	TE 228
PCT (K)	------	------	------	------	------	------	------
Time (s)	------	------	------	------	------	------	------
A-15 rod	TE 229			TE 230			
PCT (K)	------			------			
Time (s)	------			------			
A-17 rod	TE 231			TE 232			
PCT (K)	------			907.9			
Time (s)	------			207.6			
A-22 rod	TE 233	TE 234	TE 235	TE 236	TE 237	TE 238	TE 239
PCT (K)	671.5	809.5	880.3	894.7	826.6	724.3	569.0
Time (s)	219.6	220.8	210.6	207.6	208.2	207.0	175.2
A-24 rod	TE 240	TE 241	TE 242	TE 243	TE 244	TE 245	TE 246
PCT (K)	------	------	------	------	------	------	------
Time (s)	------	------	------	------	------	------	------

Table 5.1 Maximum Cladding Temperature Distribution in the Core (Continued)

	Pos.1	Pos.2	Pos.3	Pos.4	Pos.5	Pos.6	Pos.7
A-26 rod	TE 247			TE 248			
PCT (K)	------			------			
Time (s)	------			------			
A-28 rod	TE 249			TE 250			
PCT (K)	------			889.7			
Time (s)	------			208.2			
A-31 rod	TE 251			TE 252			
PCT (K)	------			892.0			
Time (s)	------			208.2			
A-33 rod	TE 253	TE 254	TE 255	TE 256	TE 257	TE 258	TE 259
PCT (K)	583.4	763.2	807.2	812.4	765.6	691.2	568.1
Time (s)	112.8	177.0	186.0	208.8	208.8	204.6	24.0
A-34 rod	TE 260	TE 261	TE 262	TE 263	TE 264	TE 265	TE 266
PCT (K)	------	------	------	------	------	------	------
Time (s)	------	------	------	------	------	------	------
A-37 rod	TE 267			TE 268			
PCT (K)	------			------			
Time (s)	------			------			
A-42 rod	TE 269			TE 270			
PCT (K)	------			------			
Time (s)	------			------			
A-44 rod	TE 271	TE 272	TE 273	TE 274	TE 275	TE 276	TE 277
PCT (K)	------	------	------	------	------	------	------
Time (s)	------	------	------	------	------	------	------

Table 5.1 Maximum Cladding Temperature Distribution in the Core (Continued)

	Pos.1	Pos.2	Pos.3	Pos.4	Pos.5	Pos.6	Pos.7
A-48 rod	TE 278			TE 279			
PCT (K)	------			------			
Time (s)	------			------			
A-51 rod	TE 280			TE 281			
PCT (K)	------			------			
Time (s)	------			------			
A-53 rod	TE 282			TE 283			
PCT (K)	------			------			
Time (s)	------			------			
A-57 rod	TE 284			TE 285			
PCT (K)	------			889.6			
Time (s)	------			208.8			
A-62 rod	TE 286			TE 287			
PCT (K)	------			------			
Time (s)	------			------			
A-66 rod	TE 288			TE 289			
PCT (K)	------			------			
Time (s)	------			------			
A-68 rod	TE 290			TE 291			
PCT (K)	412.8			895.2			
Time (s)	252.0			208.8			
A-71 rod	TE 292			TE 293			
PCT (K)	530.2			926.4			
Time (s)	251.4			207.0			

Table 5.1 Maximum Cladding Temperature Distribution in the Core (Continued)

	Pos.1	Pos.2	Pos.3	Pos.4	Pos.5	Pos.6	Pos.7
A-73 rod	TE 294			TE 295			
PCT (K)	521.4			907.5			
Time (s)	250.8			208.2			
A-75 rod	TE 296			TE 297			
PCT (K)	518.4			------			
Time (s)	250.8			------			
A-77 rod	TE 298	TE 299	TE 300	TE 301	TE 302	TE 303	TE 304
PCT (K)	731.8	843.5	883.0	880.2	810.7	700.7	555.6
Time (s)	217.2	217.8	212.4	208.8	207.6	204.6	5.4
A-82 rod	TE 305			TE 306			
PCT (K)	379.6			933.0			
Time (s)	242.4			207.6			
A-84 rod	TE 307			TE 308			
PCT (K)	442.7			901.8			
Time (s)	256.2			207.6			
A-85 rod	TE 309	TE 310	TE 311	TE 312	TE 313	TE 314	TE 315
PCT (K)	535.1	------	------	------	------	------	------
Time (s)	252.6	------	------	------	------	------	------
A-87 rod	TE 316	TE 317	TE 318	TE 319	TE 320	TE 321	TE 322
PCT (K)	708.2	820.1	877.3	889.6	824.7	718.6	578.8
Time (s)	179.4	214.8	209.4	207.6	208.2	204.6	178.2
A-88 rod	TE 323	TE 324	TE 325	TE 326	TE 327	TE 328	TE 329
PCT (K)	702.6	804.1	864.2	885.8	823.8	720.5	586.4
Time (s)	178.8	179.4	182.4	208.2	207.6	208.2	180.6

Table 5.1 Maximum Cladding Temperature Distribution in the Core (Continued)

	Pos.1	Pos.2	Pos.3	Pos.4	Pos.5	Pos.6	Pos.7
B-11 rod	TE 330	TE 331	TE 332	TE 333	TE 334	TE 335	TE 336
PCT (K)	597.0	741.2	806.0	803.2	752.5	671.4	440.7
Time (s)	105.0	174.6	183.6	193.2	208.2	205.2	212.4
B-13 rod				TE 337			
PCT (K)				800.4			
Time (s)				178.2			
B-22 rod	TE 338	TE 339	TE 340	TE 341	TE 342	TE 343	TE 344
PCT (K)	635.2	744.0	798.5	801.3	735.5	662.8	567.2
Time (s)	154.8	175.2	183.0	209.4	189.6	204.0	27.0
B-31 rod				TE 345			
PCT (K)				413.8			
Time (s)				223.8			
B-33 rod				TE 346			
PCT (K)				------			
Time (s)				------			
B-51 rod				TE 347			
PCT (K)				------			
Time (s)				------			
B-53 rod				TE 348			
PCT (K)				------			
Time (s)				------			
B-66 rod				TE 349			
PCT (K)				------			
Time (s)				------			

Table 5.1 Maximum Cladding Temperature Distribution in the Core (Continued)

	Pos.1	Pos.2	Pos.3	Pos.4	Pos.5	Pos.6	Pos.7
B-77 rod	TE 350	TE 351	TE 352	TE 353	TE 354	TE 355	TE 356
PCT (K)	723.3	800.4	832.3	827.6	756.2	660.0	567.2
Time (s)	215.4	213.6	207.0	211.2	204.6	190.8	20.4
B-86 rod				TE 357			
PCT (K)				425.7			
Time (s)				205.8			
C-11 rod	TE 358	TE 359	TE 360	TE 361	TE 362	TE 363	TE 364
PCT (K)	610.4	635.2	782.5	808.8	755.3	666.6	565.9
Time (s)	55.8	105.0	198.6	209.4	205.8	199.8	0.0
C-13 rod	TE 365	TE 366	TE 367	TE 368	TE 369	TE 370	TE 371
PCT (K)	594.1	660.0	789.1	807.9	753.4	662.8	567.2
Time (s)	54.6	122.4	200.4	208.8	199.2	195.0	22.8
C-15 rod				TE 372			
PCT (K)				461.7			
Time (s)				251.4			
C-22 rod	TE 373	TE 374	TE 375	TE 376	TE 377	TE 378	TE 379
PCT (K)	598.0	717.7	788.2	806.0	744.0	651.4	567.2
Time (s)	215.4	199.2	195.0	209.4	200.4	198.6	23.4
C-31 rod				TE 380			
PCT (K)				418.8			
Time (s)				198.0			
C-33 rod	TE 381	TE 382	TE 383	TE 384	TE 385	TE 386	TE 387
PCT (K)	584.5	655.2	751.5	768.5	712.0	626.7	566.2
Time (s)	54.0	131.4	182.4	205.8	202.8	183.6	24.0

Table 5.1 Maximum Cladding Temperature Distribution in the Core (Continued)

	Pos.1	Pos.2	Pos.3	Pos.4	Pos.5	Pos.6	Pos.7
C-35 rod				TE 388			
PCT (K)				448.7			
Time (s)				259.2			
C-66 rod				TE 389			
PCT (K)				------			
Time (s)				------			
C-68 rod				TE 390			
PCT (K)				------			
Time (s)				------			
C-77 rod	TE 391	TE 392	TE 393	TE 394	TE 395	TE 396	TE 397
PCT (K)	720.5	792.8	818.2	816.3	752.5	655.2	567.2
Time (s)	220.2	219.0	204.0	201.0	201.0	201.0	24.0
D-11 rod				TE 398			
PCT (K)				825.7			
Time (s)				226.8			
D-13 rod				TE 399			
PCT (K)				833.2			
Time (s)				229.8			
D-22 rod	TE 400	TE 401	TE 402	TE 403	TE 404	TE 405	TE 406
PCT (K)	620.9	753.4	804.1	822.9	755.3	665.7	567.2
Time (s)	247.8	232.8	223.8	229.8	203.4	199.8	25.2
D-31 rod				TE 407			
PCT (K)				487.7			
Time (s)				213.6			

Table 5.1 Maximum Cladding Temperature Distribution in the Core (Continued)

	Pos.1	Pos.2	Pos.3	Pos.4	Pos.5	Pos.6	Pos.7
D-33 rod				TE 408			
PCT (K)				------			
Time (s)				------			
D-51 rod				TE 409			
PCT (K)				------			
Time (s)				------			
D-53 rod				TE 410			
PCT (K)				------			
Time (s)				------			
D-66 rod				TE 411			
PCT (K)				------			
Time (s)				------			
D-77 rod				TE 412			
PCT (K)				------			
Time (s)				------			
D-86 rod				TE 413			
PCT (K)				817.2			
Time (s)				207.0			

Table 5.1 Maximum Cladding Temperature Distribution in the Core (Continued)

** Order of PCT **

No. 1	A-82 rod	Pos. 4	PCT = 933.0 (K)	Time = 207.6 (s)	
No. 2	A-71 rod	Pos. 4	PCT = 926.4 (K)	Time = 207.0 (s)	
No. 3	A-11 rod	Pos. 4	PCT = 911.5 (K)	Time = 207.6 (s)	
No. 4	A-17 rod	Pos. 4	PCT = 907.9 (K)	Time = 207.6 (s)	
No. 5	A-73 rod	Pos. 4	PCT = 907.5 (K)	Time = 208.2 (s)	
No. 6	A-84 rod	Pos. 4	PCT = 901.8 (K)	Time = 207.6 (s)	
No. 7	A-12 rod	Pos. 4	PCT = 897.1 (K)	Time = 207.6 (s)	
No. 8	A-68 rod	Pos. 4	PCT = 895.2 (K)	Time = 208.8 (s)	
No. 9	A-22 rod	Pos. 4	PCT = 894.7 (K)	Time = 207.6 (s)	
No.10	A-31 rod	Pos. 4	PCT = 892.0 (K)	Time = 208.2 (s)	

Table 5.2 Maximum Cladding Temperature Distribution in the Core for RUN963

	Pos.1	Pos.2	Pos.3	Pos.4	Pos.5	Pos.6	Pos.7
A-11 rod	TE 201	TE 202	TE 203	TE 204	TE 205	TE 206	TE 207
PCT (K)	617.5	773.5	857.5	886.3	832.3	730.3	605.5
Time (s)	13.3	141.4	171.5	165.2	163.8	163.8	161.7
A-12 rod	TE 208	TE 209	TE 210	TE 211	TE 212	TE 213	TE 214
PCT (K)	583.9	762.7	839.5	862.3	803.5	711.1	576.7
Time (s)	88.9	140.0	170.8	164.5	165.2	165.2	139.3
A-13 rod	TE 215	TE 216	TE 217	TE 218	TE 219	TE 220	TE 221
PCT (K)	640.3	755.5	833.5	856.3	802.3	706.3	580.3
Time (s)	128.1	139.3	169.4	165.9	164.5	162.4	140.7
A-14 rod	TE 222	TE 223	TE 224	TE 225	TE 226	TE 227	TE 228
PCT (K)	------	------	------	------	------	------	------
Time (s)	------	------	------	------	------	------	------
A-15 rod	TE 229			TE 230			
PCT (K)	------			------			
Time (s)	------			------			
A-17 rod	TE 231			TE 232			
PCT (K)	------			877.9			
Time (s)	------			166.6			
A-22 rod	TE 233	TE 234	TE 235	TE 236	TE 237	TE 238	TE 239
PCT (K)	658.3	771.1	853.9	864.6	816.3	711.6	577.7
Time (s)	174.3	173.6	174.3	170.8	164.5	163.8	144.9
A-24 rod	TE 240	TE 241	TE 242	TE 243	TE 244	TE 245	TE 246
PCT (K)	------	------	------	------	------	------	------
Time (s)	------	------	------	------	------	------	------

Table 5.2 Maximum Cladding Temperature Distribution in the Core (Continued)

	Pos.1	Pos.2	Pos.3	Pos.4	Pos.5	Pos.6	Pos.7
A-26 rod	TE 247			TE 248			
PCT (K)	------			------			
Time (s)	------			------			
A-28 rod	TE 249			TE 250			
PCT (K)	------			878.3			
Time (s)	------			168.0			
A-31 rod	TE 251			TE 252			
PCT (K)	------			892.2			
Time (s)	------			169.4			
A-33 rod	TE 253	TE 254	TE 255	TE 256	TE 257	TE 258	TE 259
PCT (K)	571.9	604.3	647.3	683.4	679.9	640.0	566.2
Time (s)	35.7	88.9	139.3	145.6	142.8	147.0	18.9
A-34 rod	TE 260	TE 261	TE 262	TE 263	TE 264	TE 265	TE 266
PCT (K)	------	------	------	------	------	------	------
Time (s)	------	------	------	------	------	------	------
A-37 rod	TE 267			TE 268			
PCT (K)	------			------			
Time (s)	------			------			
A-42 rod	TE 269			TE 270			
PCT (K)	------			------			
Time (s)	------			------			
A-44 rod	TE 271	TE 272	TE 273	TE 274	TE 275	TE 276	TE 277
PCT (K)	------	------	------	------	------	------	------
Time (s)	------	------	------	------	------	------	------

Table 5.2 Maximum Cladding Temperature Distribution in the Core (Continued)

	Pos.1	Pos.2	Pos.3	Pos.4	Pos.5	Pos.6	Pos.7
A-48 rod	TE 278			TE 279			
PCT (K)	------			------			
Time (s)	------			------			
A-51 rod	TE 280			TE 281			
PCT (K)	------			------			
Time (s)	------			------			
A-53 rod	TE 282			TE 283			
PCT (K)	------			------			
Time (s)	------			------			
A-57 rod	TE 284			TE 285			
PCT (K)	------			861.4			
Time (s)	------			169.4			
A-62 rod	TE 286			TE 287			
PCT (K)	------			------			
Time (s)	------			------			
A-66 rod	TE 288			TE 289			
PCT (K)	------			------			
Time (s)	------			------			
A-68 rod	TE 290			TE 291			
PCT (K)	388.3			877.3			
Time (s)	212.1			164.5			
A-71 rod	TE 292			TE 293			
PCT (K)	502.6			906.6			
Time (s)	211.4			170.8			

Table 5.2 Maximum Cladding Temperature Distribution in the Core (Continued)

	Pos.1	Pos.2	Pos.3	Pos.4	Pos.5	Pos.6	Pos.7
A-73 rod	TE 294			TE 295			
PCT (K)	494.7			885.8			
Time (s)	207.2			170.1			
A-75 rod	TE 296			TE 297			
PCT (K)	495.7			------			
Time (s)	207.9			------			
A-77 rod	TE 298	TE 299	TE 300	TE 301	TE 302	TE 303	TE 304
PCT (K)	723.3	818.2	856.7	854.8	793.8	692.2	548.8
Time (s)	177.8	175.0	174.3	170.1	165.9	163.1	162.4
A-82 rod	TE 305			TE 306			
PCT (K)	375.7			915.1			
Time (s)	188.3			166.6			
A-84 rod	TE 307			TE 308			
PCT (K)	420.7			882.0			
Time (s)	213.5			167.3			
A-85 rod	TE 309	TE 310	TE 311	TE 312	TE 313	TE 314	TE 315
PCT (K)	508.6	------	------	------	------	------	------
Time (s)	209.3	------	------	------	------	------	------
A-87 rod	TE 316	TE 317	TE 318	TE 319	TE 320	TE 321	TE 322
PCT (K)	585.5	807.9	862.3	877.3	811.6	713.0	583.6
Time (s)	140.0	173.6	169.4	163.8	163.8	163.8	154.7
A-88 rod	TE 323	TE 324	TE 325	TE 326	TE 327	TE 328	TE 329
PCT (K)	598.0	798.5	853.9	879.2	817.2	717.7	585.5
Time (s)	13.3	183.4	165.2	164.5	163.1	163.1	157.5

Table 5.2 Maximum Cladding Temperature Distribution in the Core (Continued)

	Pos.1	Pos.2	Pos.3	Pos.4	Pos.5	Pos.6	Pos.7
B-11 rod	TE 330	TE 331	TE 332	TE 333	TE 334	TE 335	TE 336
PCT (K)	582.6	658.1	753.4	813.5	747.8	657.1	425.7
Time (s)	37.1	88.9	137.2	167.3	163.1	159.6	176.4
B-13 rod				TE 337			
PCT (K)				811.6			
Time (s)				163.8			
B-22 rod	TE 338	TE 339	TE 340	TE 341	TE 342	TE 343	TE 344
PCT (K)	622.9	706.4	772.2	807.9	730.8	644.8	565.3
Time (s)	112.0	135.8	140.7	162.4	163.1	159.6	16.8
B-31 rod				TE 345			
PCT (K)				404.9			
Time (s)				221.9			
B-33 rod				TE 346			
PCT (K)				------			
Time (s)				------			
B-51 rod				TE 347			
PCT (K)				------			
Time (s)				------			
B-53 rod				TE 348			
PCT (K)				------			
Time (s)				------			
B-66 rod				TE 349			
PCT (K)				------			
Time (s)				------			

Table 5.2 Maximum Cladding Temperature Distribution in the Core (Continued)

	Pos.1	Pos.2	Pos.3	Pos.4	Pos.5	Pos.6	Pos.7
B-77 rod	TE 350	TE 351	TE 352	TE 353	TE 354	TE 355	TE 356
PCT (K)	713.0	794.7	827.6	824.7	745.0	651.4	567.2
Time (s)	179.2	173.6	169.4	162.4	163.1	158.2	23.1
B-86 rod				TE 357			
PCT (K)				414.8			
Time (s)				168.0			
C-11 rod	TE 358	TE 359	TE 360	TE 361	TE 362	TE 363	TE 364
PCT (K)	595.1	721.4	783.5	806.9	743.1	661.9	567.2
Time (s)	11.9	133.7	141.4	167.3	168.0	159.6	16.8
C-13 rod	TE 365	TE 366	TE 367	TE 368	TE 369	TE 370	TE 371
PCT (K)	587.4	729.9	781.6	804.1	744.0	659.0	567.2
Time (s)	37.1	137.2	156.1	163.8	167.3	158.2	19.6
C-15 rod				TE 372			
PCT (K)				444.7			
Time (s)				224.0			
C-22 rod	TE 373	TE 374	TE 375	TE 376	TE 377	TE 378	TE 379
PCT (K)	636.2	729.9	784.4	801.3	734.6	653.3	567.2
Time (s)	128.1	140.7	169.4	165.2	165.2	158.9	19.6
C-31 rod				TE 380			
PCT (K)				434.7			
Time (s)				216.3			
C-33 rod	TE 381	TE 382	TE 383	TE 384	TE 385	TE 386	TE 387
PCT (K)	588.4	697.9	760.9	760.9	696.9	622.9	565.3
Time (s)	36.4	137.2	170.1	164.5	163.1	158.9	17.5

Table 5.2 Maximum Cladding Temperature Distribution in the Core (Continued)

	Pos.1	Pos.2	Pos.3	Pos.4	Pos.5	Pos.6	Pos.7
C-35 rod				TE 388			
PCT (K)				422.7			
Time (s)				198.8			
C-66 rod				TE 389			
PCT (K)				------			
Time (s)				------			
C-68 rod				TE 390			
PCT (K)				------			
Time (s)				------			
C-77 rod	TE 391	TE 392	TE 393	TE 394	TE 395	TE 396	TE 397
PCT (K)	699.7	782.5	815.4	807.9	739.3	649.5	567.2
Time (s)	177.1	174.3	171.5	163.8	167.3	159.6	18.9
D-11 rod				TE 398			
PCT (K)				830.4			
Time (s)				186.2			
D-13 rod				TE 399			
PCT (K)				834.1			
Time (s)				162.4			
D-22 rod	TE 400	TE 401	TE 402	TE 403	TE 404	TE 405	TE 406
PCT (K)	645.7	797.5	829.4	826.6	744.0	653.3	567.2
Time (s)	130.2	197.4	193.9	190.4	161.7	161.0	20.3
D-31 rod				TE 407			
PCT (K)				------			
Time (s)				------			

Table 5.2 Maximum Cladding Temperature Distribution in the Core (Continued)

	Pos.1	Pos.2	Pos.3	Pos.4	Pos.5	Pos.6	Pos.7
D-33 rod				TE 408			
PCT (K)				------			
Time (s)				------			
D-51 rod				TE 409			
PCT (K)				------			
Time (s)				------			
D-53 rod				TE 410			
PCT (K)				------			
Time (s)				------			
D-66 rod				TE 411			
PCT (K)				------			
Time (s)				------			
D-77 rod				TE 412			
PCT (K)				------			
Time (s)				------			
D-86 rod				TE 413			
PCT (K)				816.3			
Time (s)				163.8			

Table 5.2 Maximum Cladding Temperature Distribution in the Core (Continued)

** Order of PCT **

No. 1	A-82 rod	Pos. 4	PCT =	915.1 (K)	Time =	166.6 (s)
No. 2	A-71 rod	Pos. 4	PCT =	906.6 (K)	Time =	170.8 (s)
No. 3	A-31 rod	Pos. 4	PCT =	892.2 (K)	Time =	169.4 (s)
No. 4	A-11 rod	Pos. 4	PCT =	886.3 (K)	Time =	165.2 (s)
No. 5	A-73 rod	Pos. 4	PCT =	885.8 (K)	Time =	170.1 (s)
No. 6	A-84 rod	Pos. 4	PCT =	882.0 (K)	Time =	167.3 (s)
No. 7	A-88 rod	Pos. 4	PCT =	879.2 (K)	Time =	164.5 (s)
No. 8	A-28 rod	Pos. 4	PCT =	878.3 (K)	Time =	168.0 (s)
No. 9	A-17 rod	Pos. 4	PCT =	877.9 (K)	Time =	166.6 (s)
No.10	A-68 rod	Pos. 4	PCT =	877.3 (K)	Time =	164.5 (s)

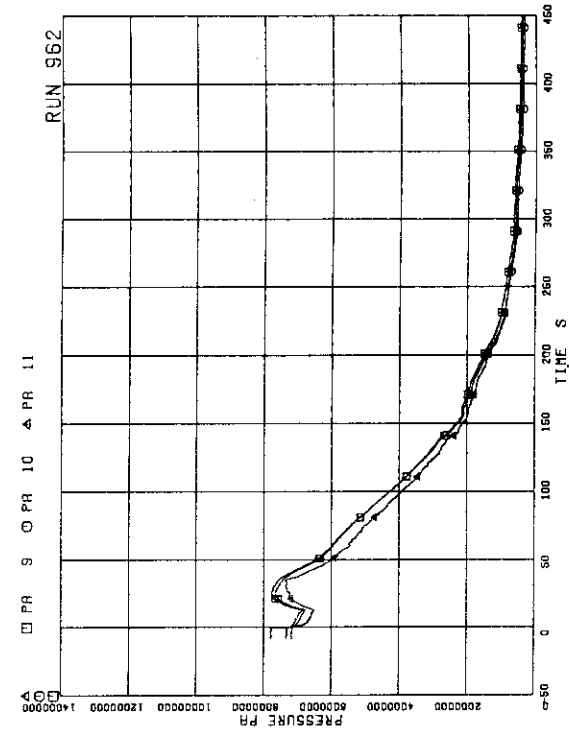

FIG.5. 3 PRESSURE NEAR MRP (MAIN RECIRCULATION PUMP)

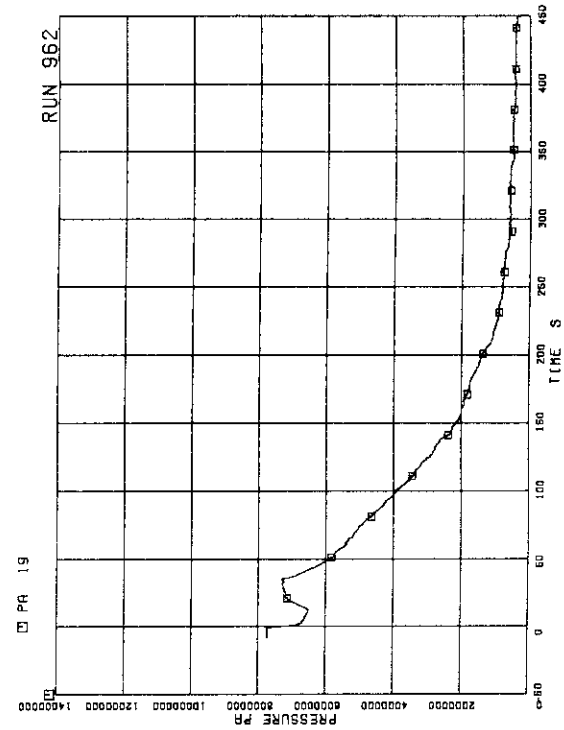

FIG.5. 4 PRESSURE AT BREAK A SPOOL

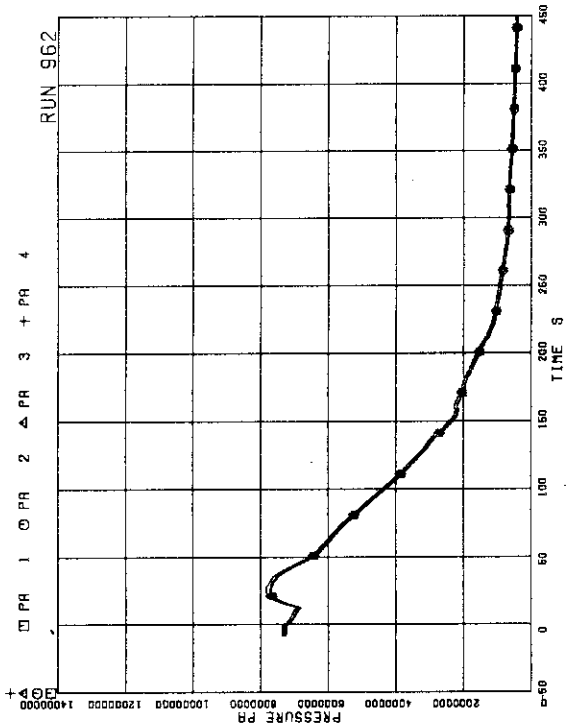

FIG.5. 1 PRESSURE IN PV (PRESSURE VESSEL)

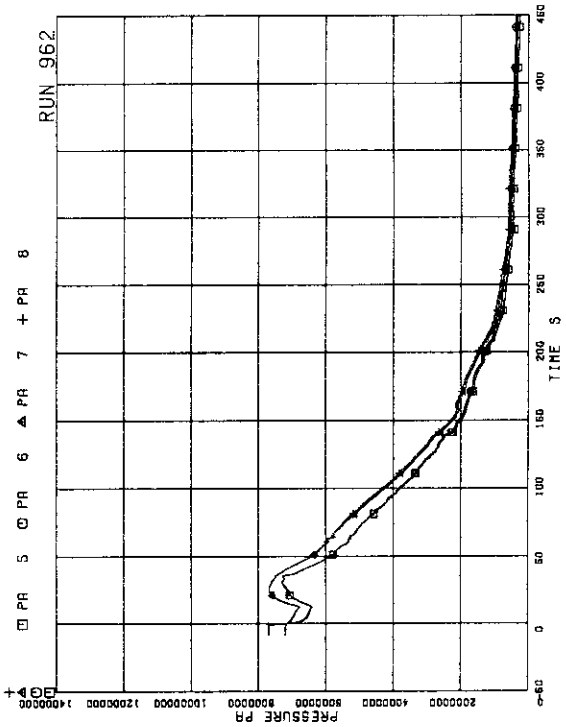

FIG.5. 2 PRESSURE IN BROKEN LOOP JP (JET PUMP)

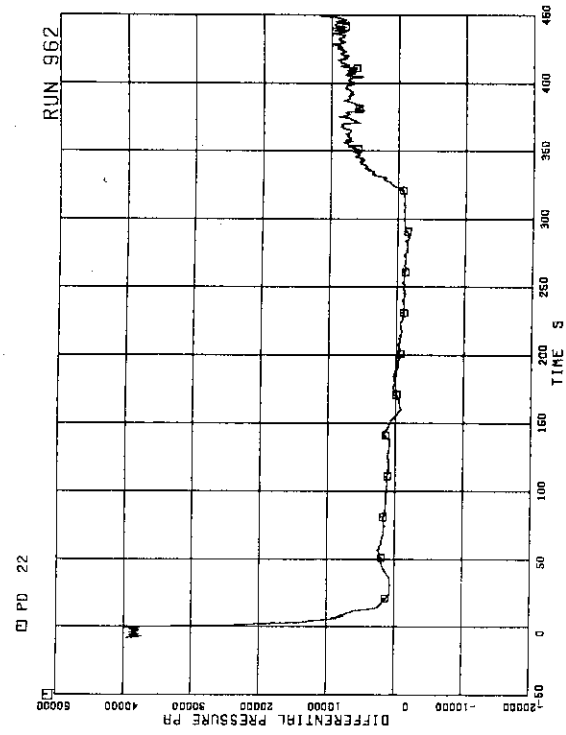

FIG.5. 7 DIFFERENTIAL PRESSURE BETWEEN UPPER PLENUM AND STEAM DOME

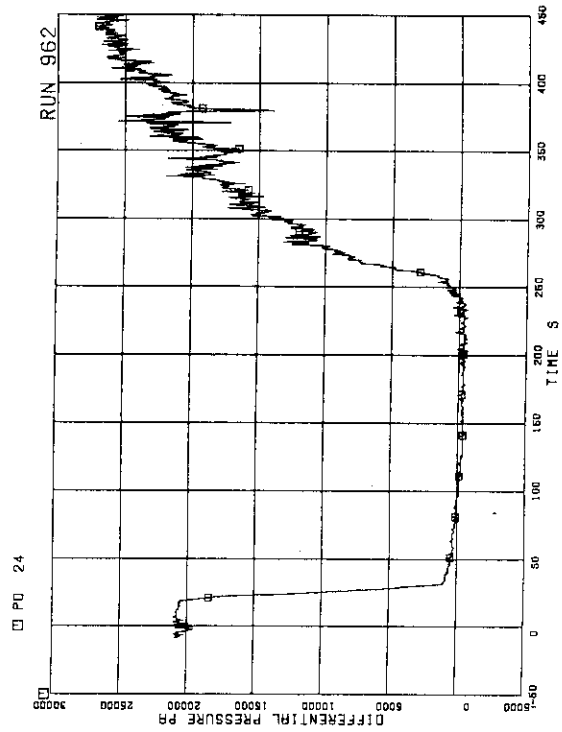

FIG.5. 8 DC (DOWNCOMER) HEAD

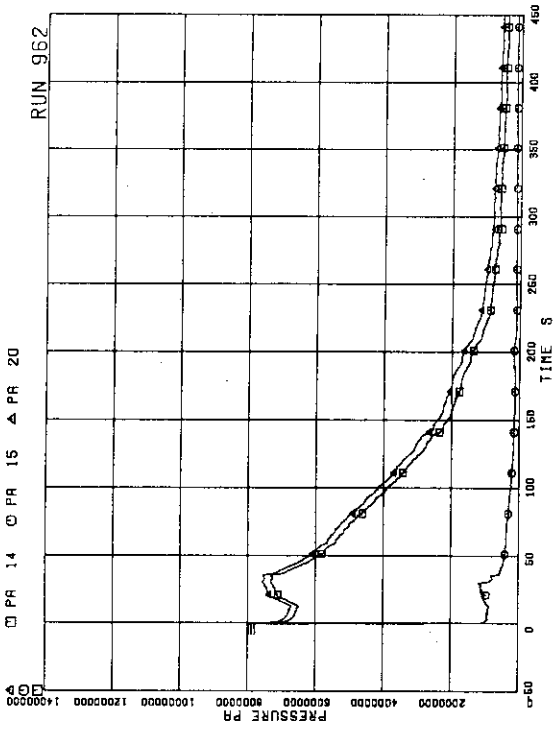

FIG.5. 5 PRESSURE AT PV SIDE OF BREAK

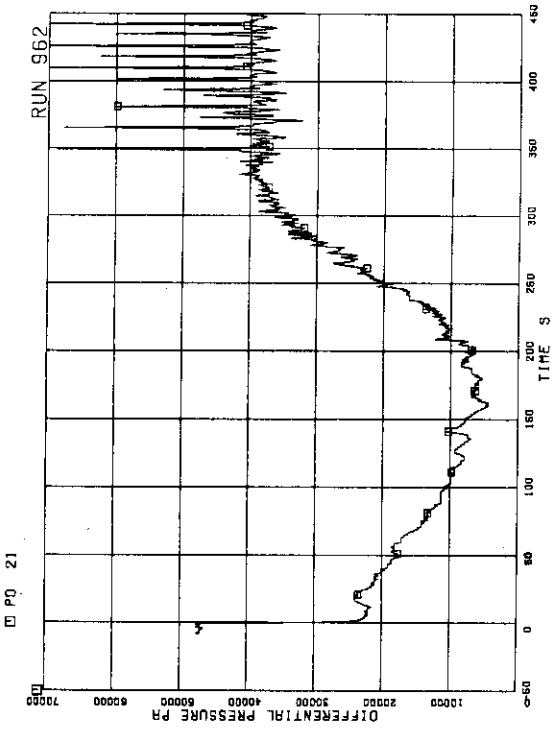

FIG.5. 6 DIFFERENTIAL PRESSURE BETWEEN LOWER PLENUM AND UPPER PLENUM

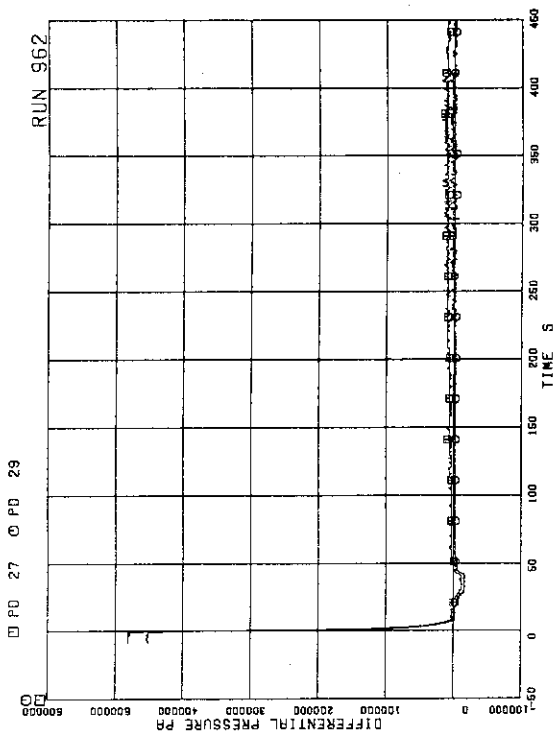

FIG.5. 11 DIFFERENTIAL PRESSURE BETWEEN JP-1,2 DRIVE AND SUCTION

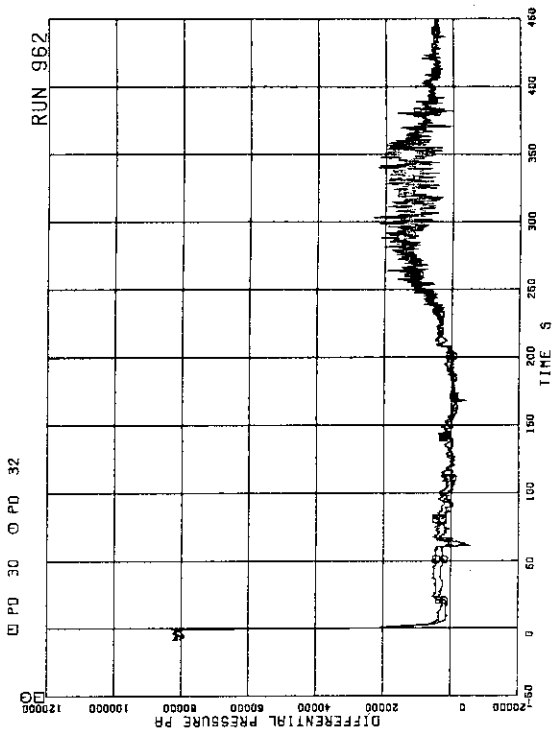

FIG.5. 12 DIFFERENTIAL PRESSURE BETWEEN JP-3,4 DISCHARGE AND SUCTION

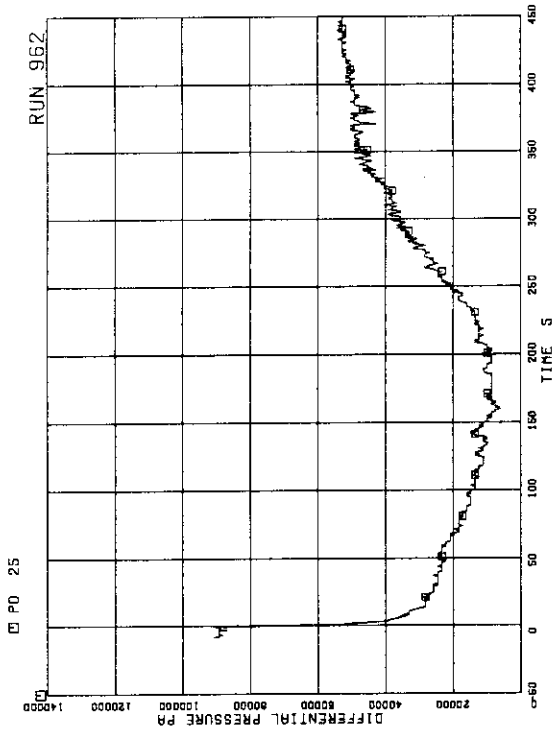

FIG.5. 9 DIFFERENTIAL PRESSURE BETWEEN PV BOTTOM AND TOP

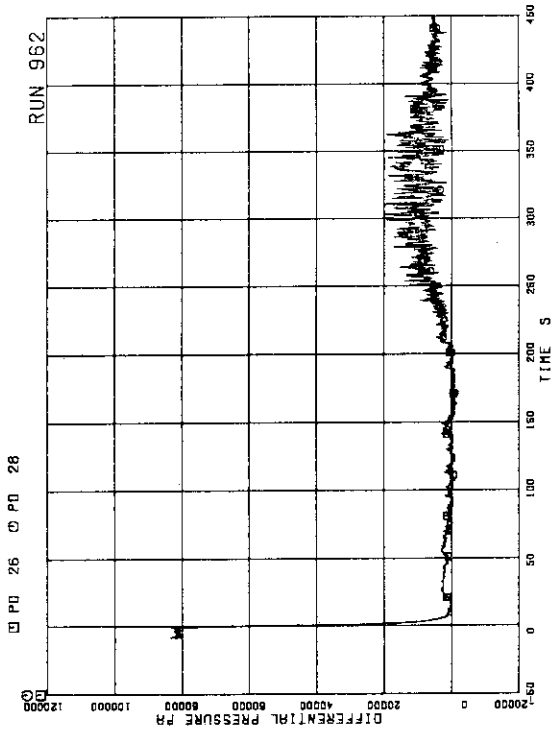

FIG.5. 10 DIFFERENTIAL PRESSURE BETWEEN JP-1,2 DISCHARGE AND SUCTION

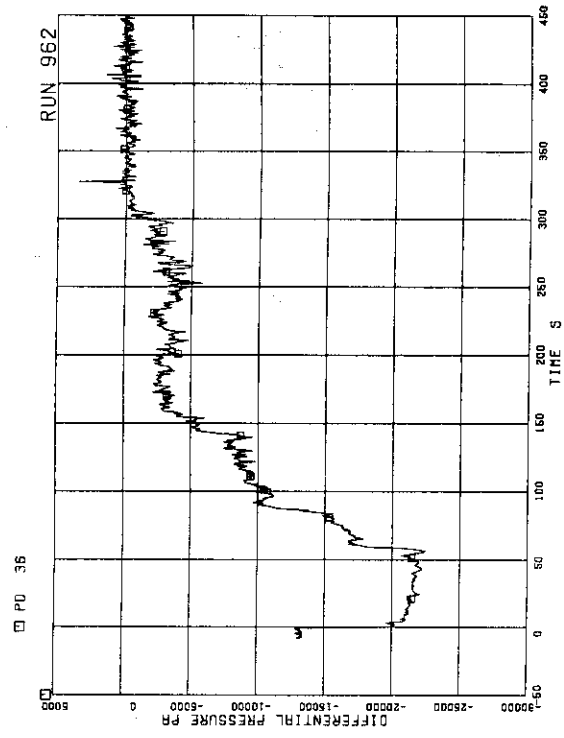

FIG.5. 15 DIFFERENTIAL PRESSURE BETWEEN DOWNCOMER BOTTOM AND MRP1 SUCTION

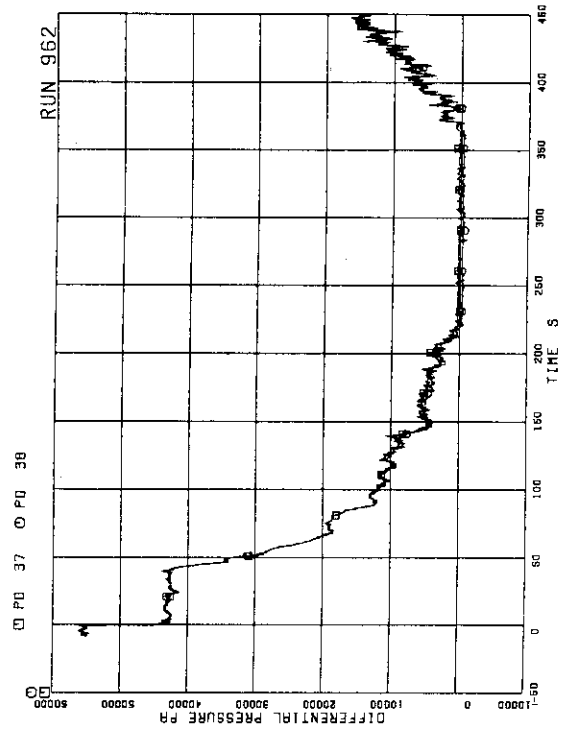

FIG.5. 16 DIFFERENTIAL PRESSURE BETWEEN MRP DELIVERY AND JP-1.2 DRIVE

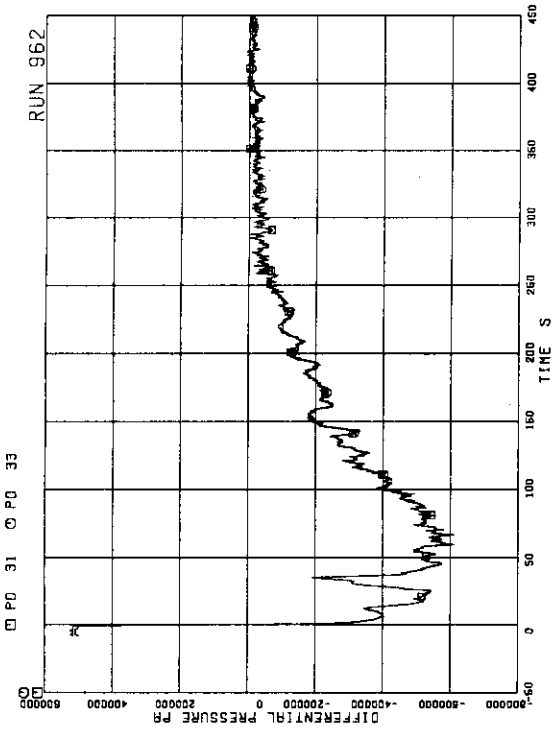

FIG.5. 13 DIFFERENTIAL PRESSURE BETWEEN JP-3.4 DRIVE AND SUCTION

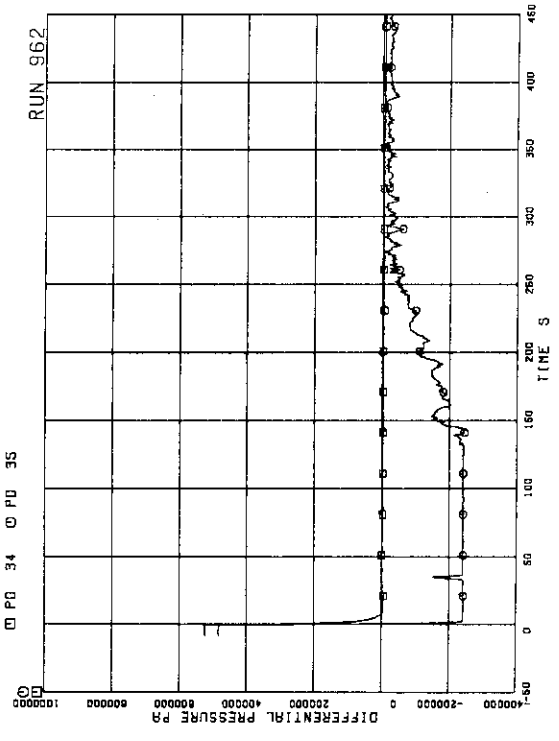

FIG.5. 14 DIFFERENTIAL PRESSURE BETWEEN MRP DELIVERY AND SUCTION

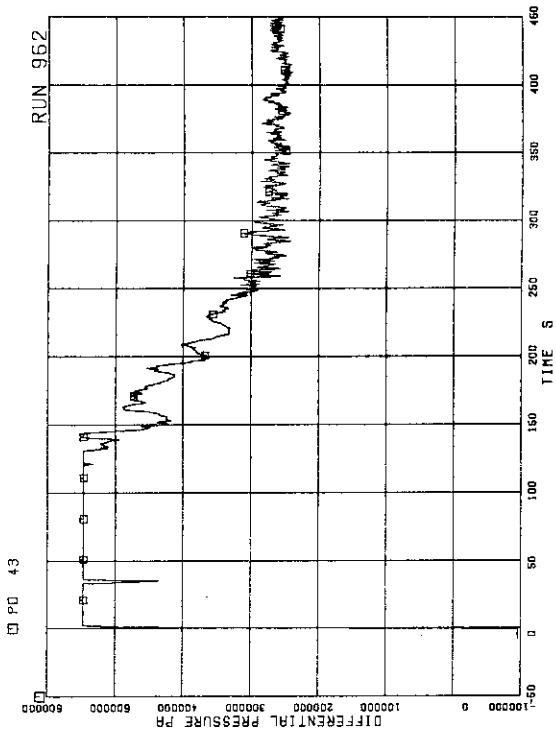

FIG.5. 19 DIFFERENTIAL PRESSURE BETWEEN DOWNCOMER BOTTOM AND BREAK B

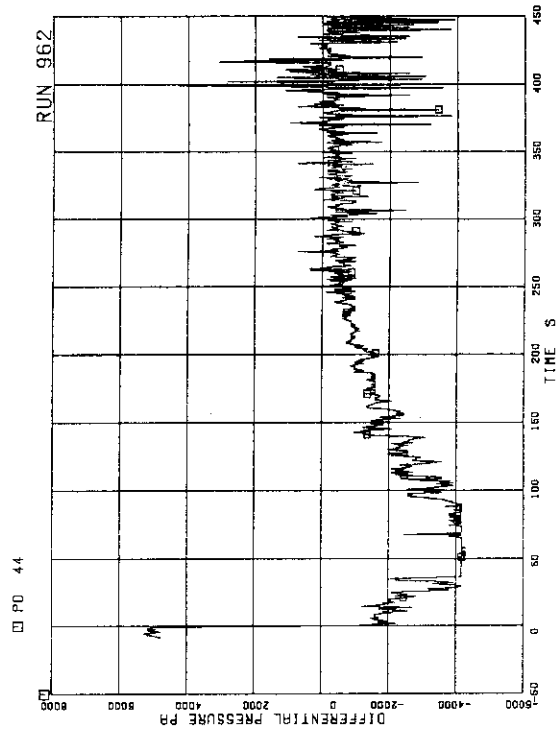

FIG.5. 20 DIFFERENTIAL PRESSURE BETWEEN BREAKS A AND B

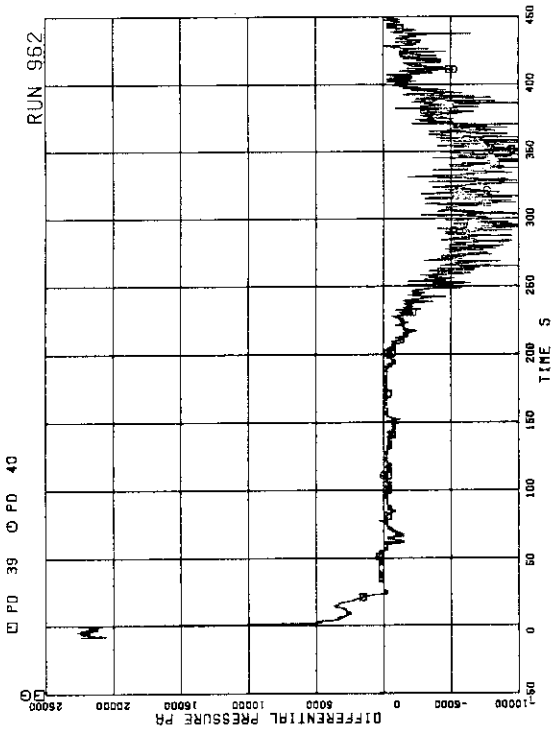

FIG.5. 17 DIFFERENTIAL PRESSURE BETWEEN DOWNCOMER MIDDLE AND JP-1.2 SUCTION

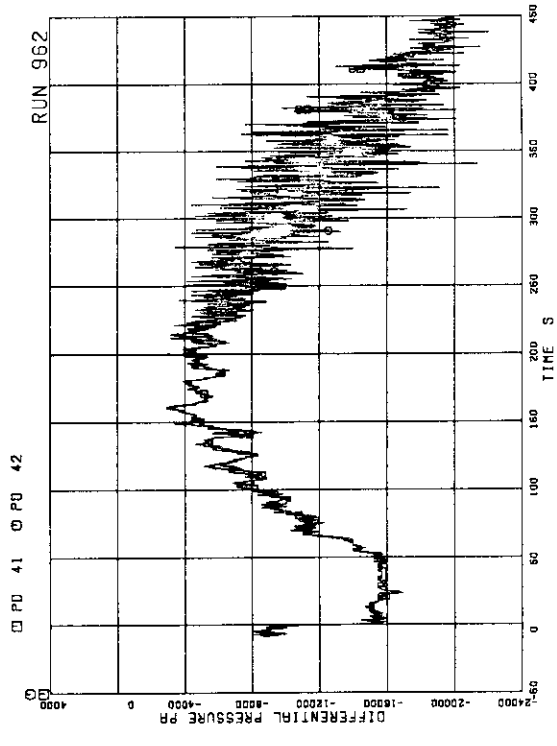

FIG.5. 18 DIFFERENTIAL PRESSURE BETWEEN JP-1.2 DISCHARGE AND LOWER PLENUM

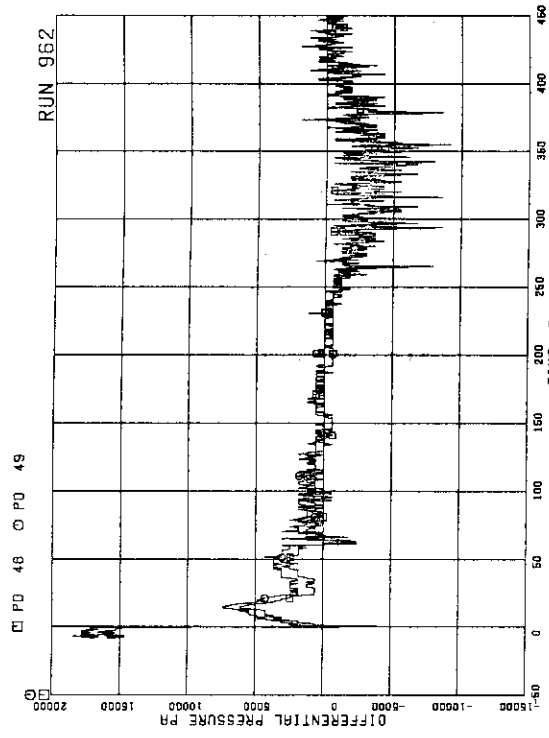

FIG.5. 23 DIFFERENTIAL PRESSURE BETWEEN DOWNCOMER MIDDLE AND JP-3,4 SUCTION

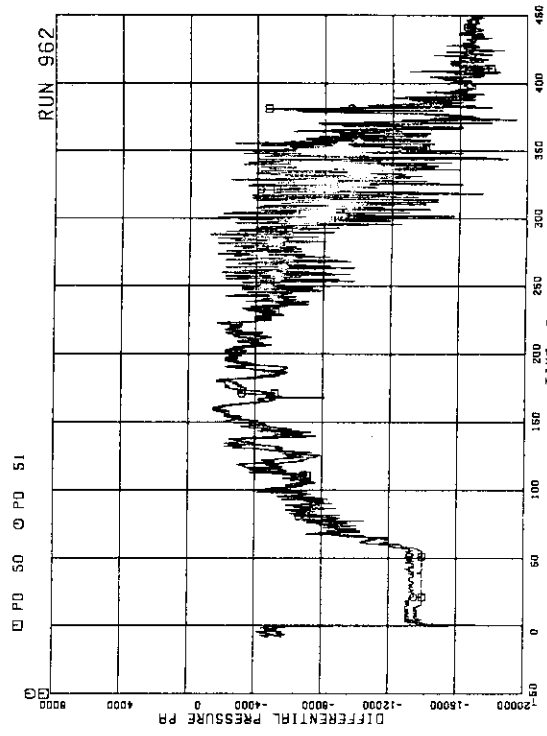

FIG.5. 24 DIFFERENTIAL PRESSURE BETWEEN JP-3,4 DISCHARGE AND CONFLURNCE

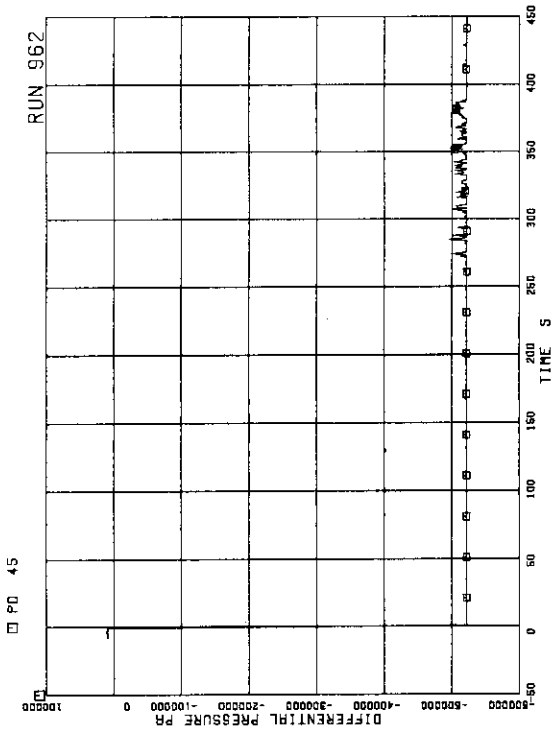

FIG.5. 21 DIFFERENTIAL PRESSURE BETWEEN BREAK A AND MRP2 SUCTION

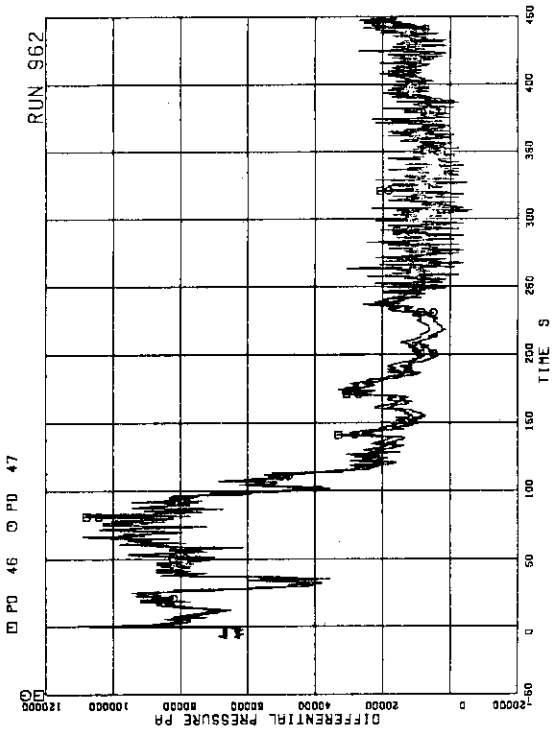

FIG.5. 22 DIFFERENTIAL PRESSURE BETWEEN MRP DELIVERY AND JP-3,4 DRIVE

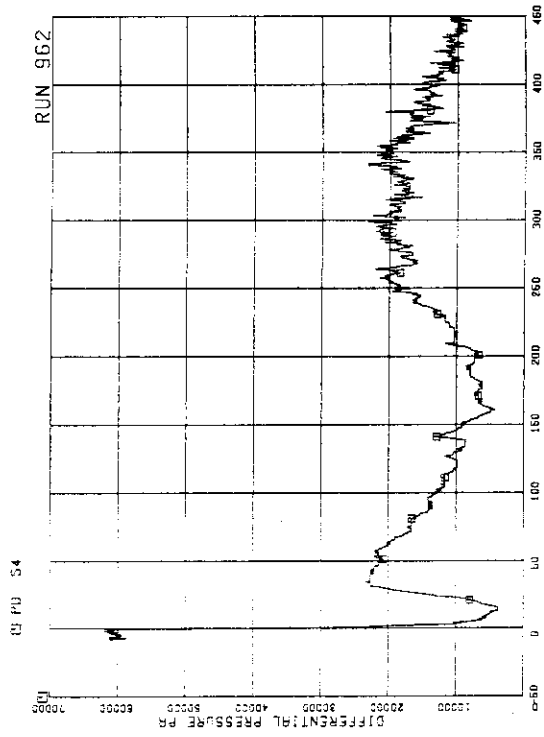

FIG.5. 27 DIFFERENTIAL PRESSURE BETWEEN LOWER PLENUM AND DOWNCOMER BOTTOM

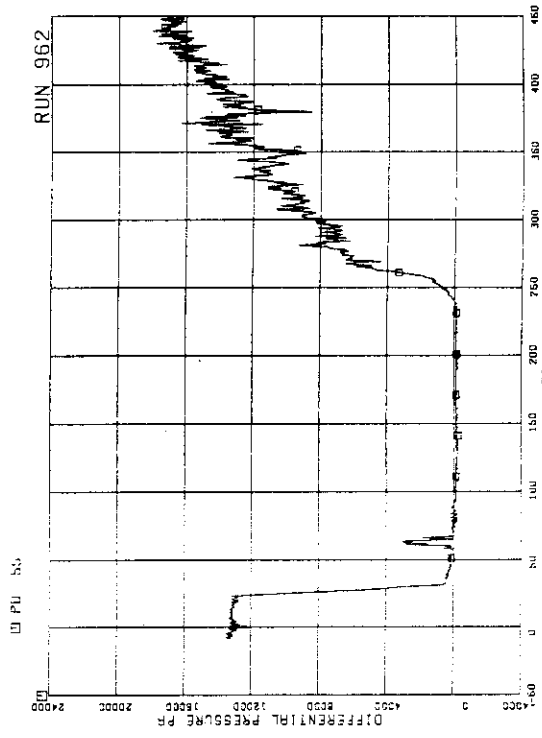

FIG.5. 28 DIFFERENTIAL PRESSURE BETWEEN DOWNCOMER BOTTOM AND DOWNCOMER MIDDLE

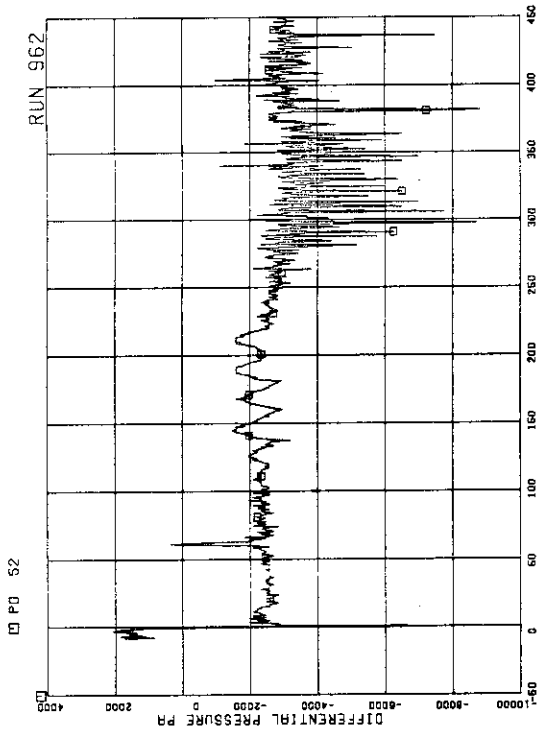

FIG.5. 25 DIFFERENTIAL PRESSURE BETWEEN JP-3.4 CONFLUENCE IN BROKEN LOOP AND LP

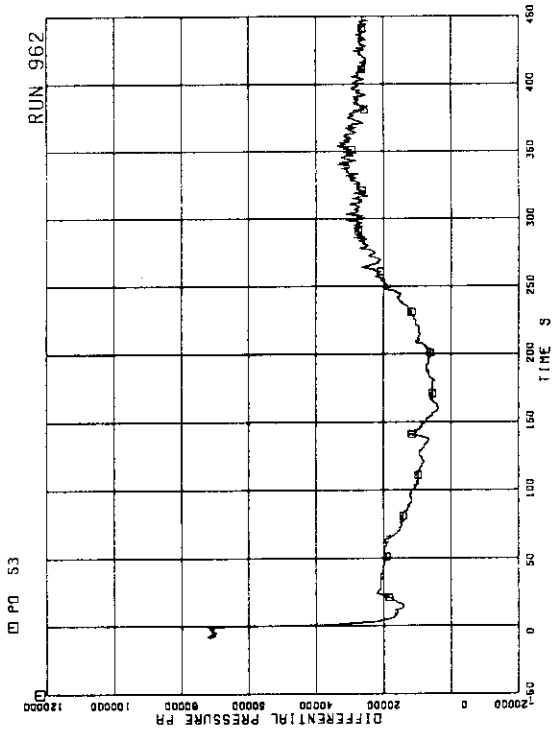

FIG.5. 26 DIFFERENTIAL PRESSURE BETWEEN LOWER PLENUM AND DOWNCOMER MIDDLE

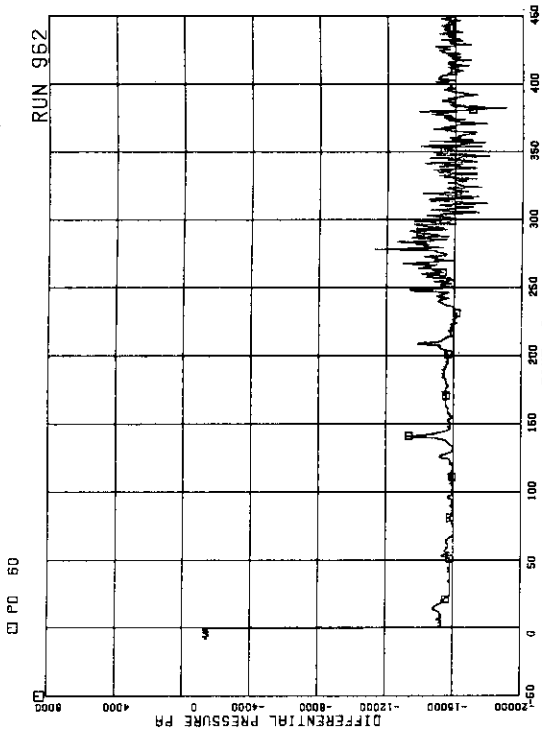

FIG.5. 31 DIFFERENTIAL PRESSURE ACROSS CHANNEL INLET ORIFICE A

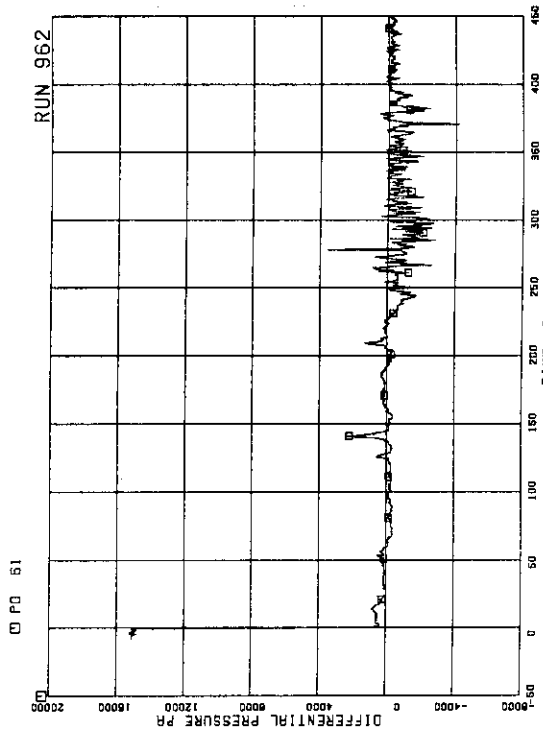

FIG.5. 32 DIFFERENTIAL PRESSURE ACROSS CHANNEL INLET ORIFICE B

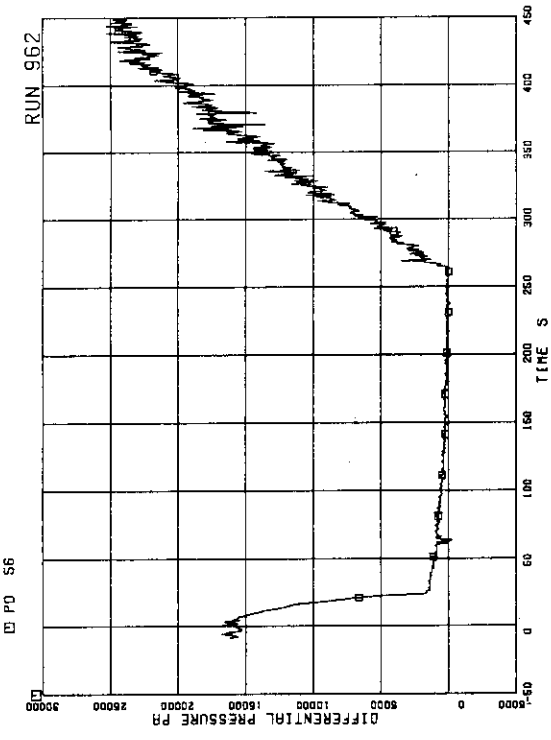

FIG.5. 29 DIFFERENTIAL PRESSURE BETWEEN DOWNCOMER MIDDLE AND STEAM DOME

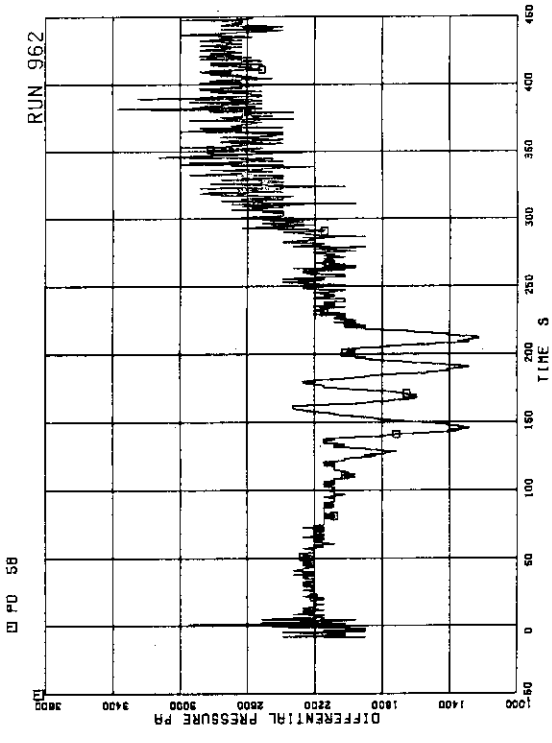

FIG.5. 30 DIFFERENTIAL PRESSURE BETWEEN LP BOTTOM AND LP MIDDLE

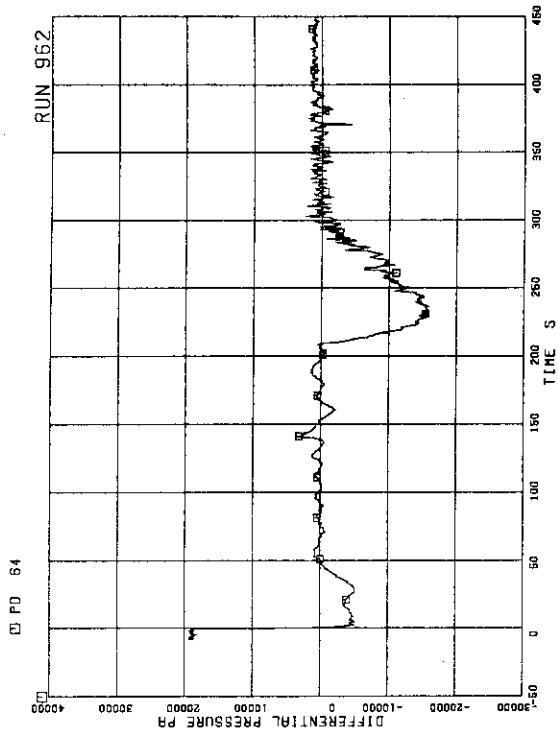

FIG.5. 35 DIFFERENTIAL PRESSURE ACROSS BYPASS HOLE

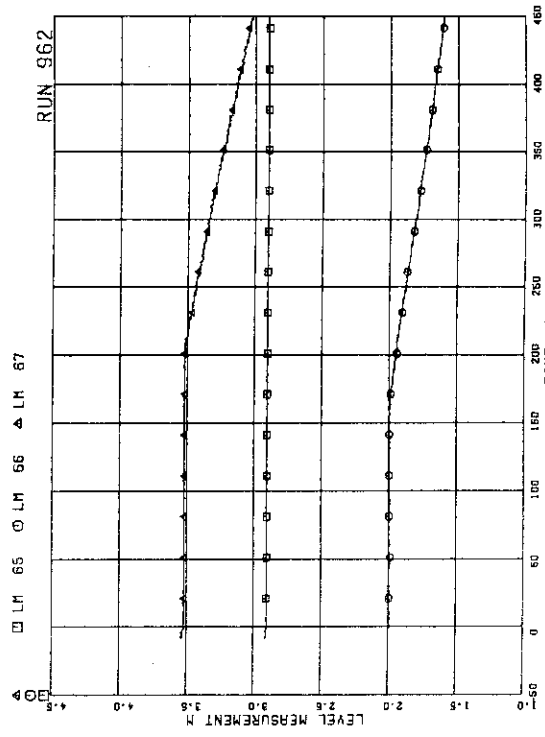

FIG.5. 36 LIQUID LEVELS IN ECCS TANKS

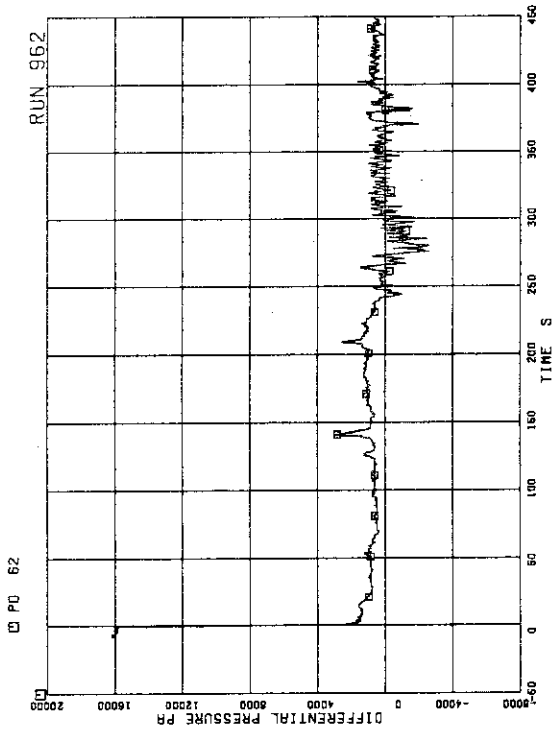

FIG.5. 33 DIFFERENTIAL PRESSURE ACROSS CHANNEL INLET ORIFICE C

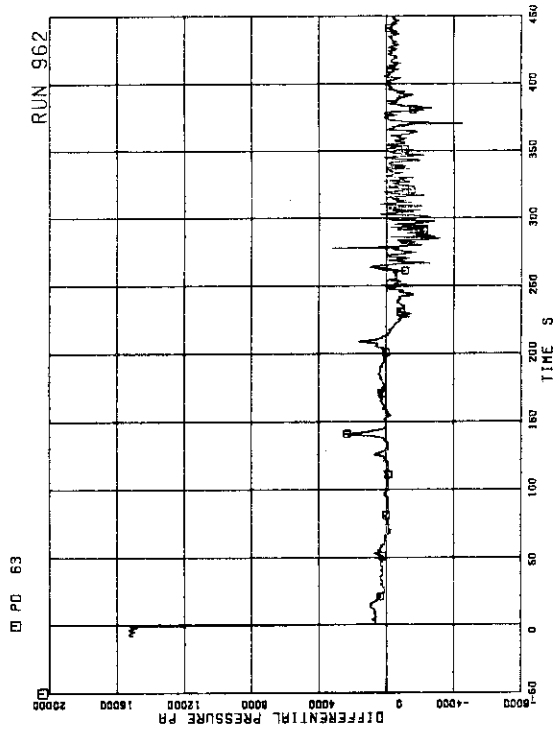

FIG.5. 34 DIFFERENTIAL PRESSURE ACROSS CHANNEL INLET ORIFICE D

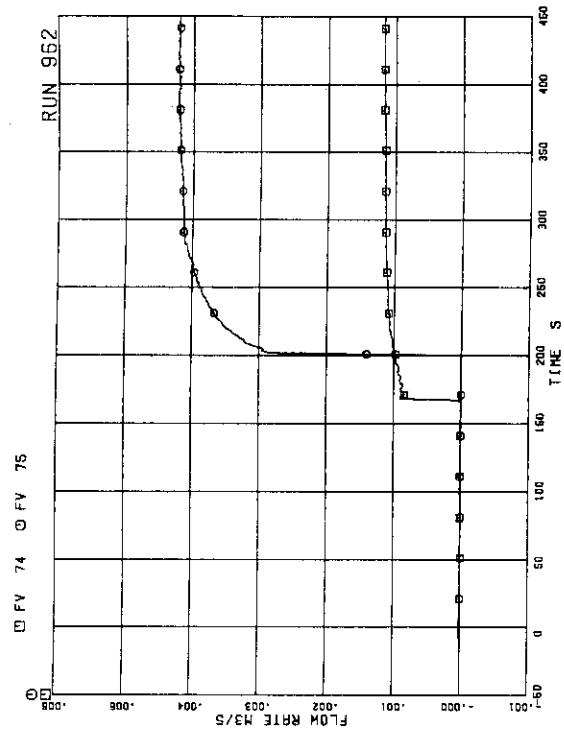

FIG.5. 39 ECC INJECTION FLOW RATES

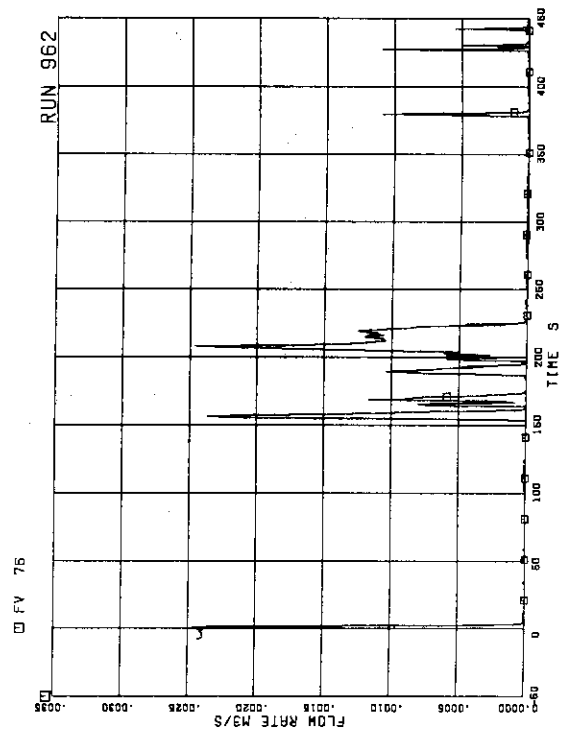

FIG.5. 40 FEEDWATER FLOW RATE

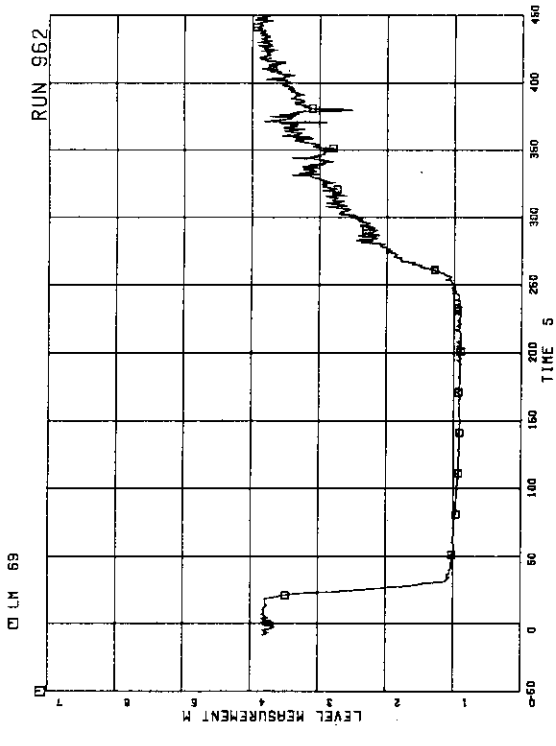

FIG.5. 37 LIQUID LEVEL IN LOWER DOWNCOMER

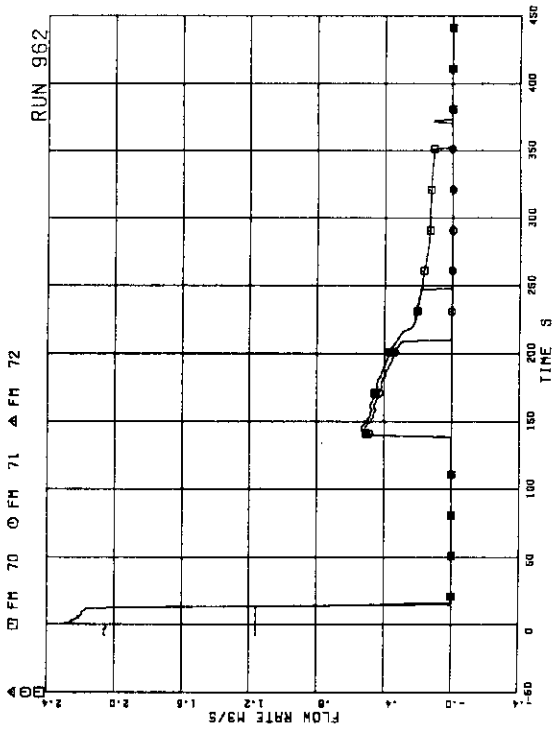

FIG.5. 38 MASS FLOW RATE IN MSL

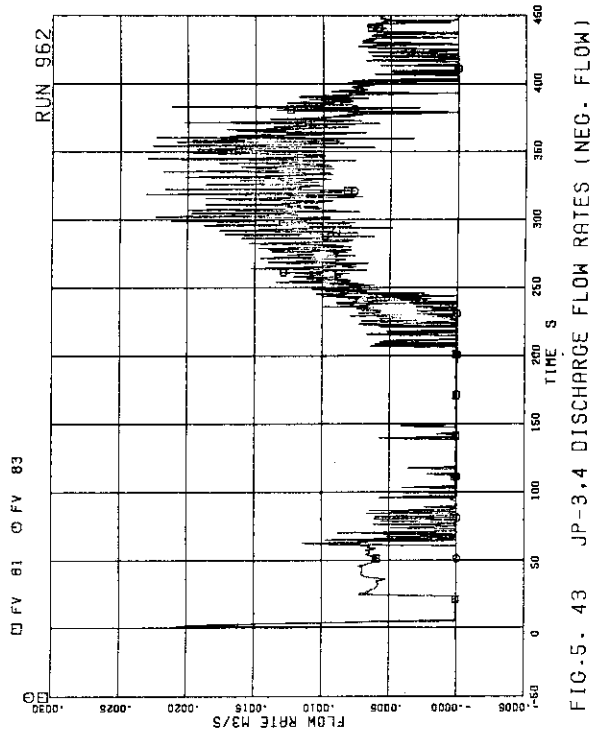

FIG.5. 43 JP-3,4 DISCHARGE FLOW RATES (NEG. FLOW)

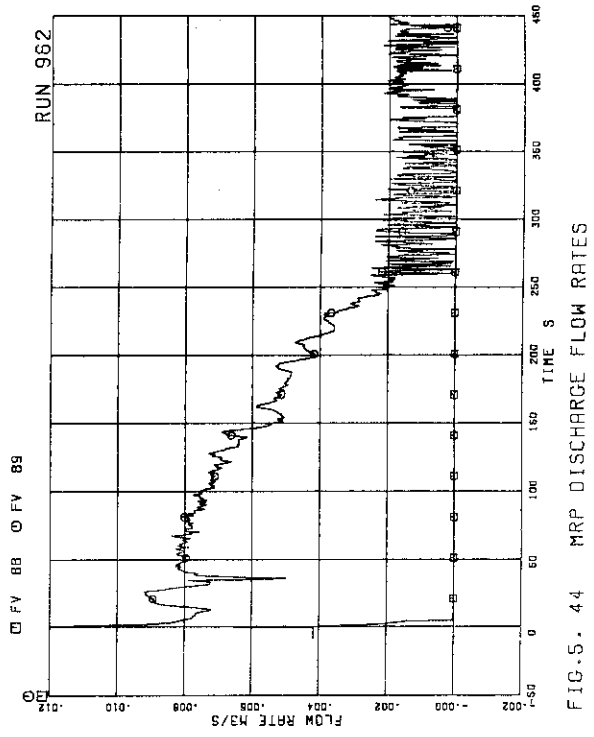

FIG.5. 44 MRP DISCHARGE FLOW RATES

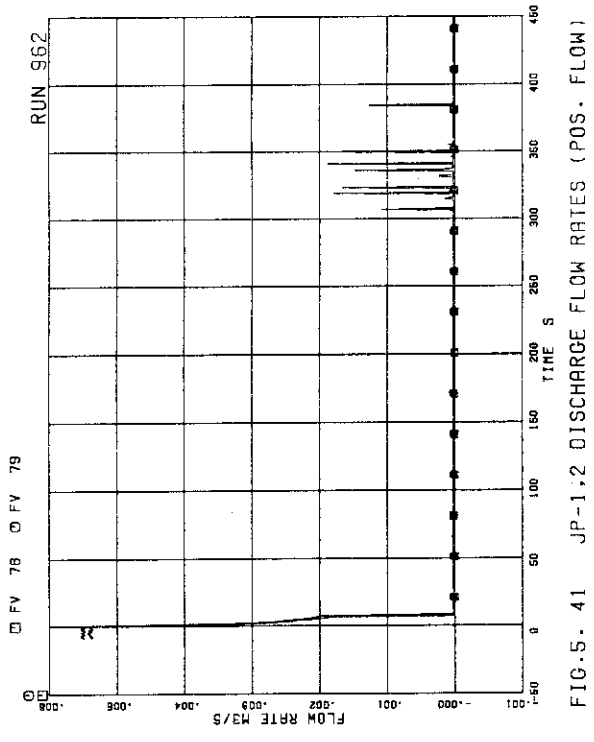

FIG.5. 41 JP-1,2 DISCHARGE FLOW RATES (POS. FLOW)

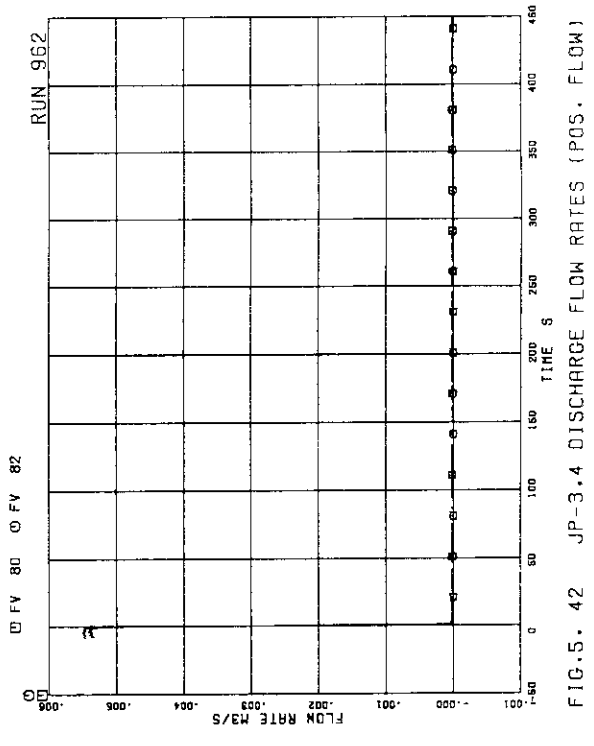

FIG.5. 42 JP-3.4 DISCHARGE FLOW RATES (POS. FLOW)

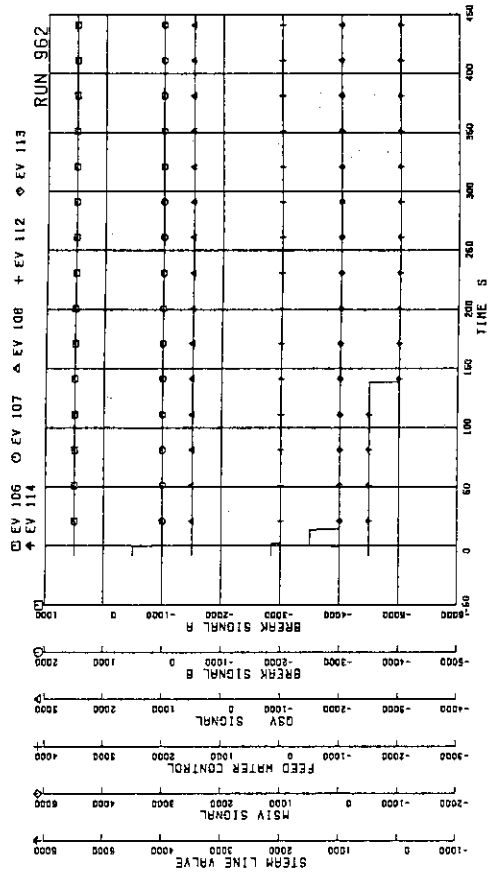

FIG.5. 47 VALVE OPERATION SIGNALS

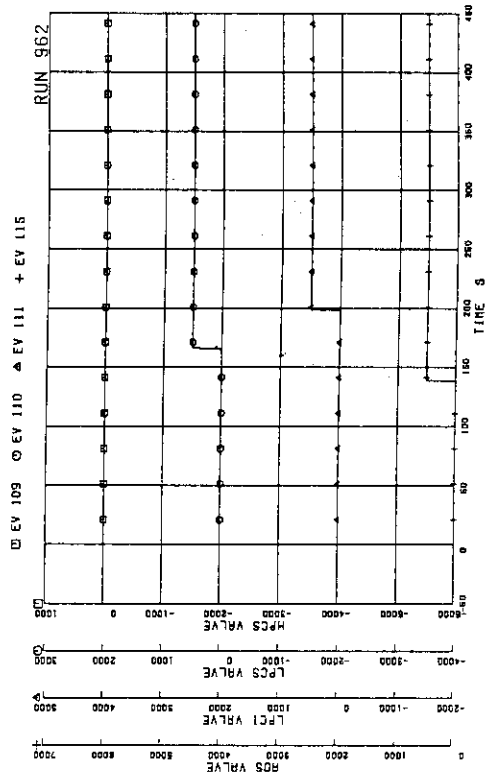

FIG.5. 48 ECCS OPERATION SIGNALS

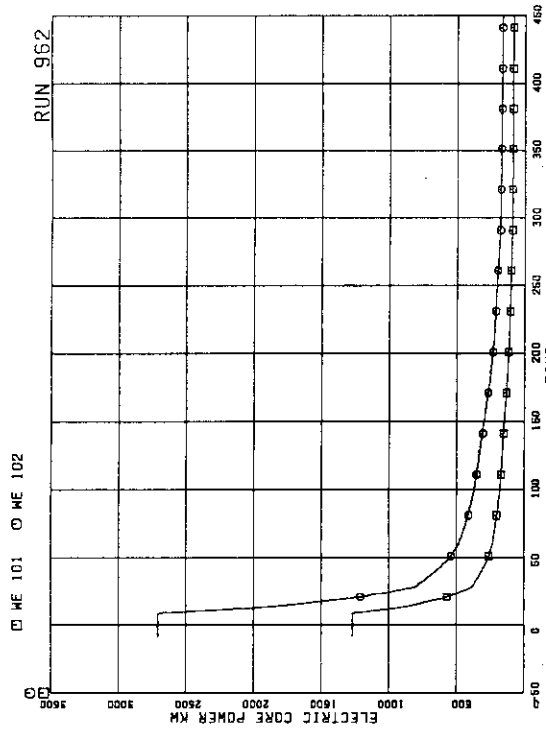

FIG.5. 45 ELECTRIC CORE POWER

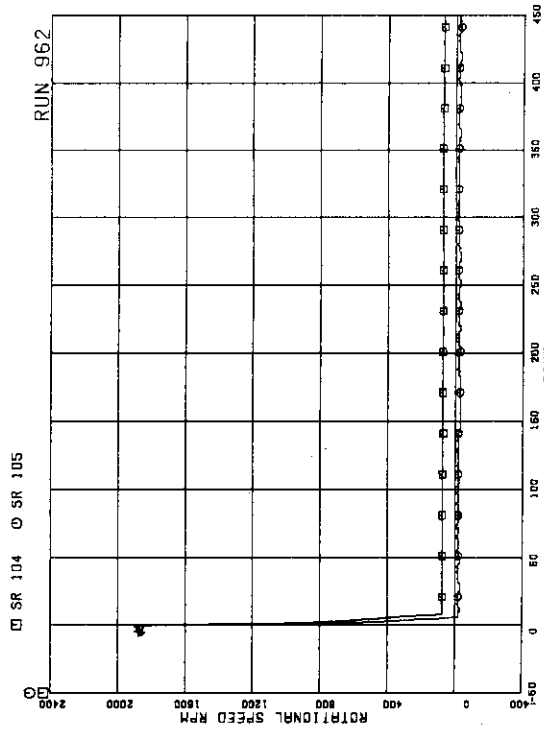

FIG.5. 46 MRP PUMP SPEED

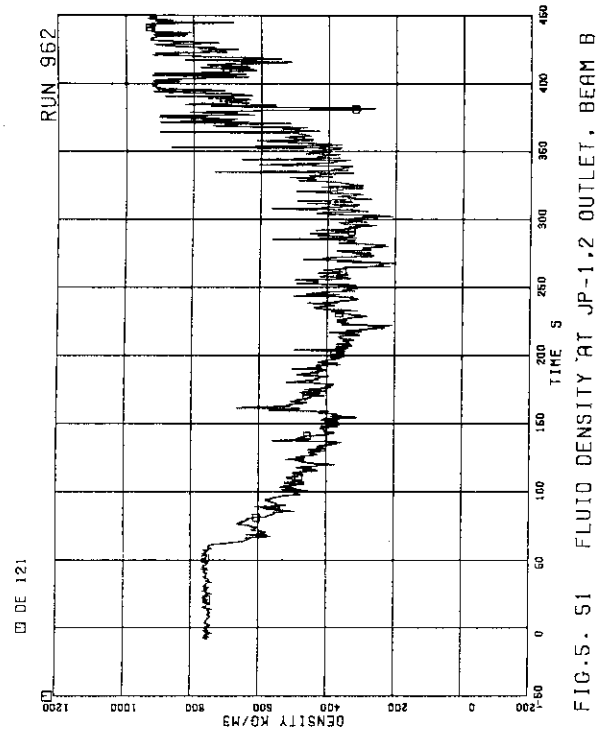

FIG.5. 51 FLUID DENSITY AT JP-1,2 OUTLET, BEAM B

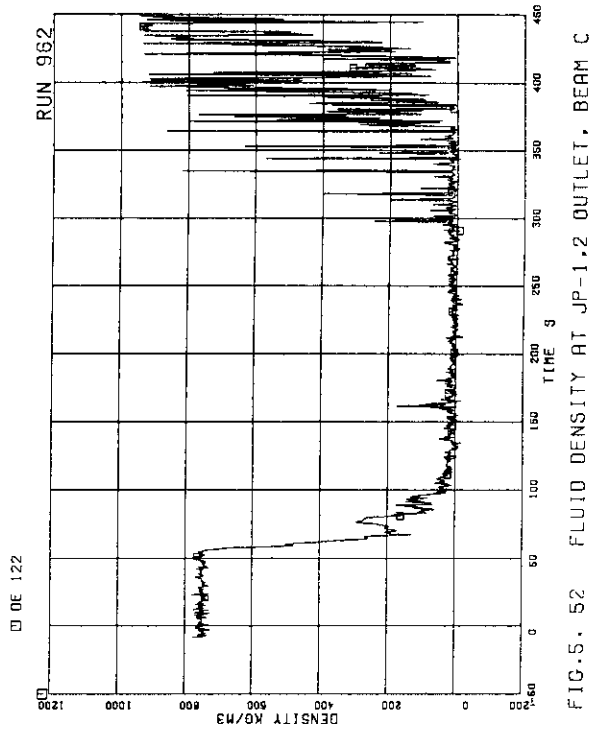

FIG.5. 52 FLUID DENSITY AT JP-1,2 OUTLET, BEAM C

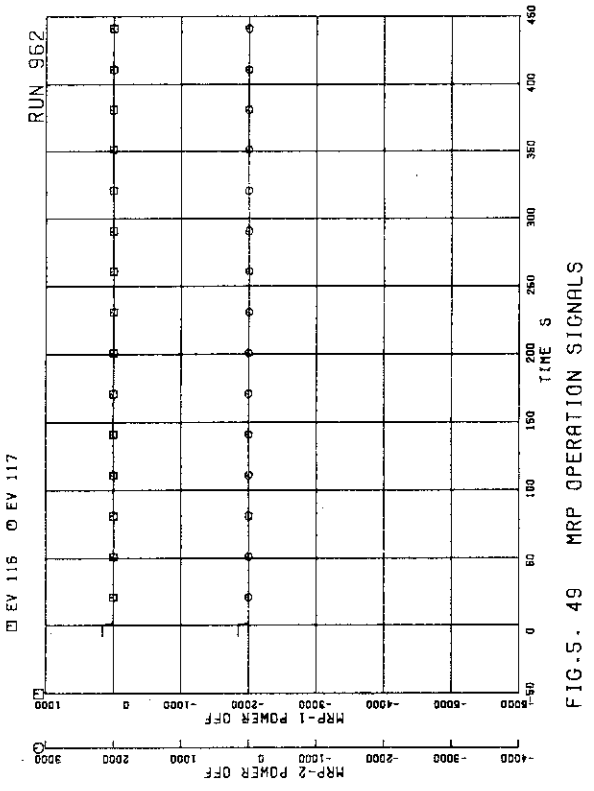

FIG.5. 49 MRP OPERATION SIGNALS

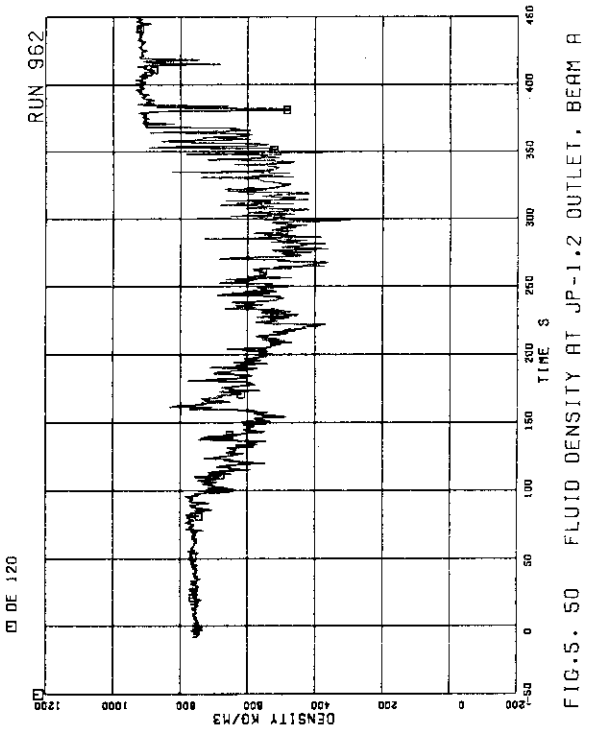

FIG.5. 50 FLUID DENSITY AT JP-1,2 OUTLET, BEAM A

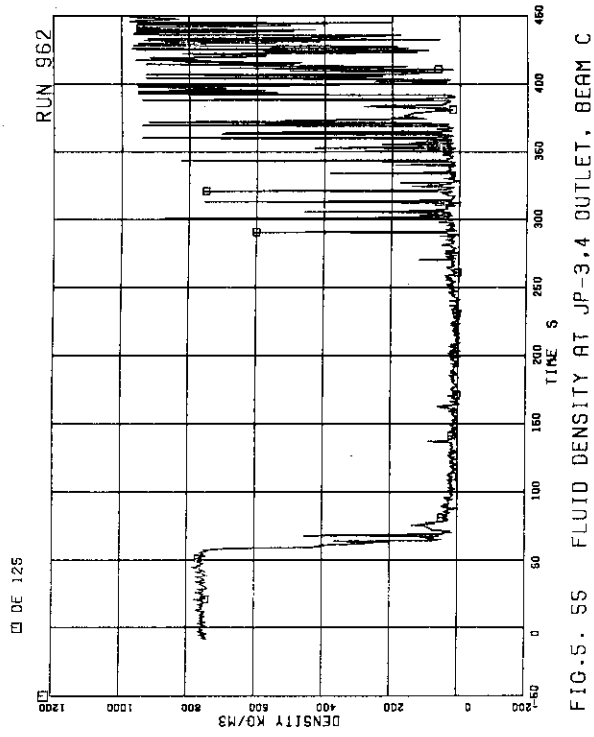

FIG.5. 55 FLUID DENSITY AT JP-3,4 OUTLET, BEAM C

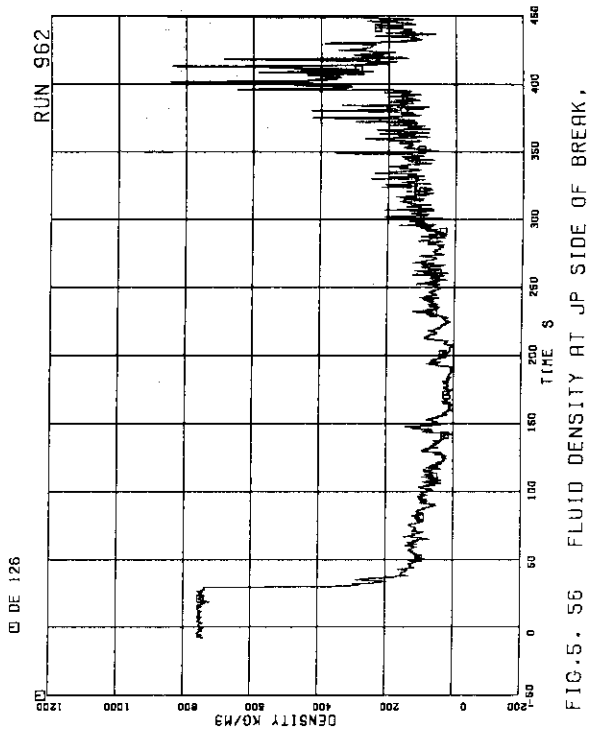

FIG.5. 56 FLUID DENSITY AT JP SIDE OF BREAK, BEAM A

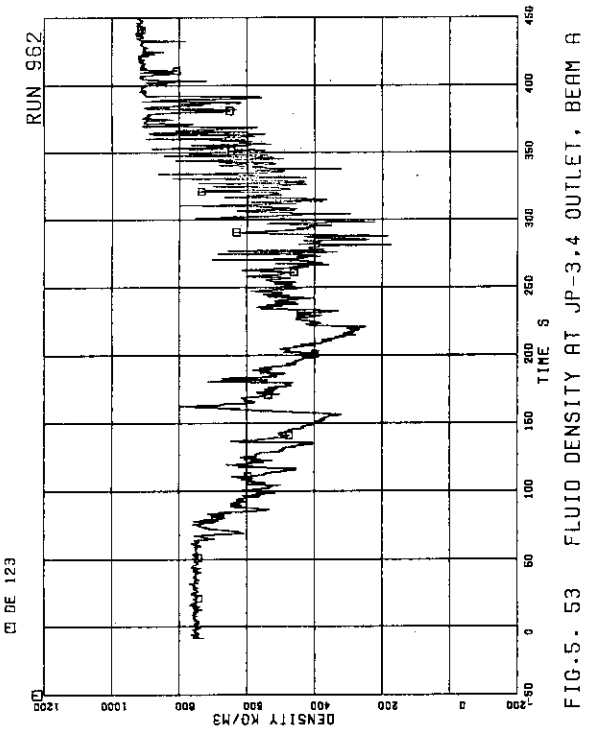

FIG.5. 53 FLUID DENSITY AT JP-3,4 OUTLET, BEAM A

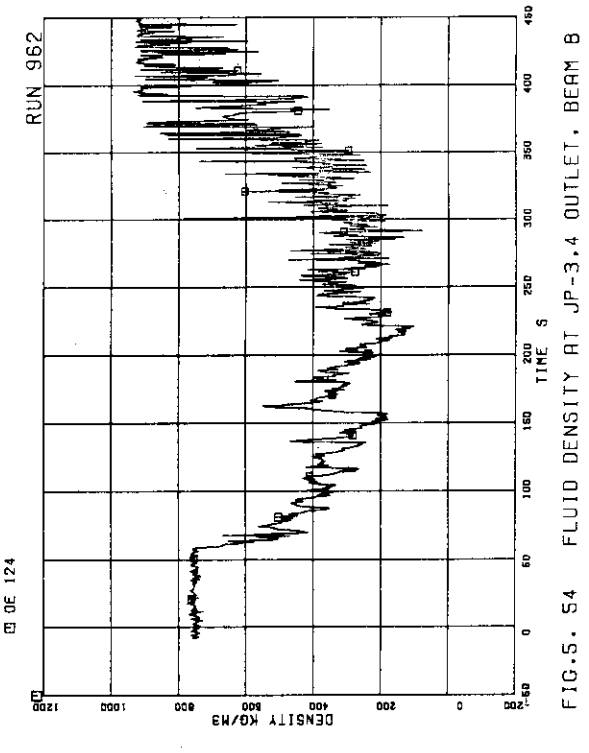

FIG.5. 54 FLUID DENSITY AT JP-3,4 OUTLET, BEAM B

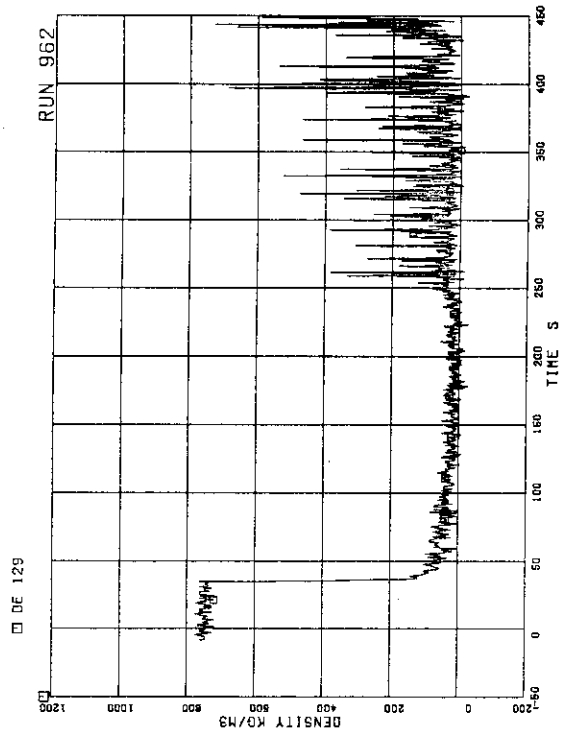

FIG.5. 59 FLUID DENSITY AT MRP SIDE OF BREAK, BEAM B

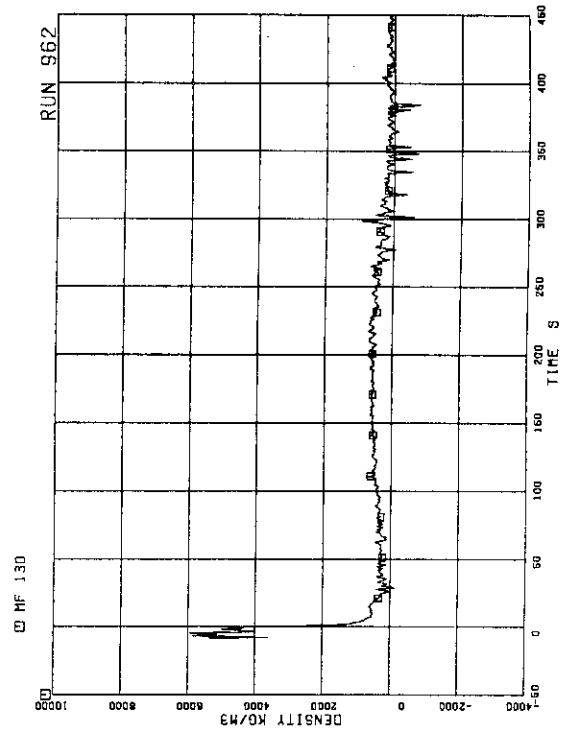

FIG.5. 60 MOMENTUM FLUX AT JP-1,2 OUTLET SPOOL

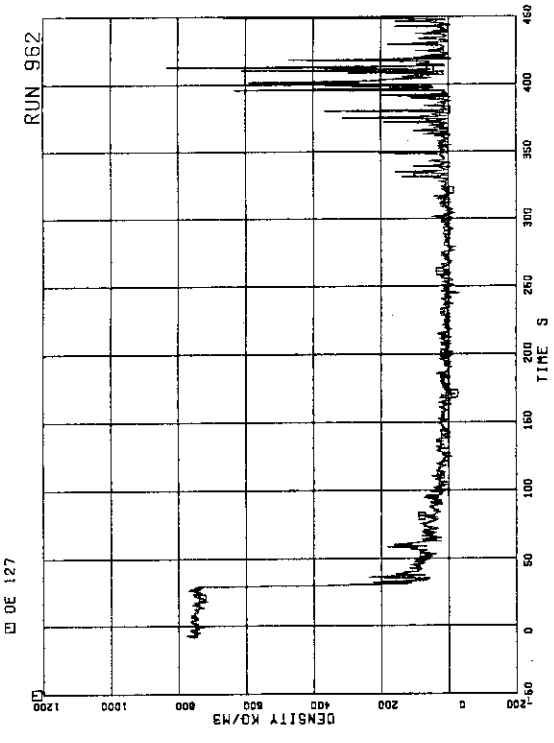

FIG.5. 57 FLUID DENSITY AT JP SIDE OF BREAK, BEAM B

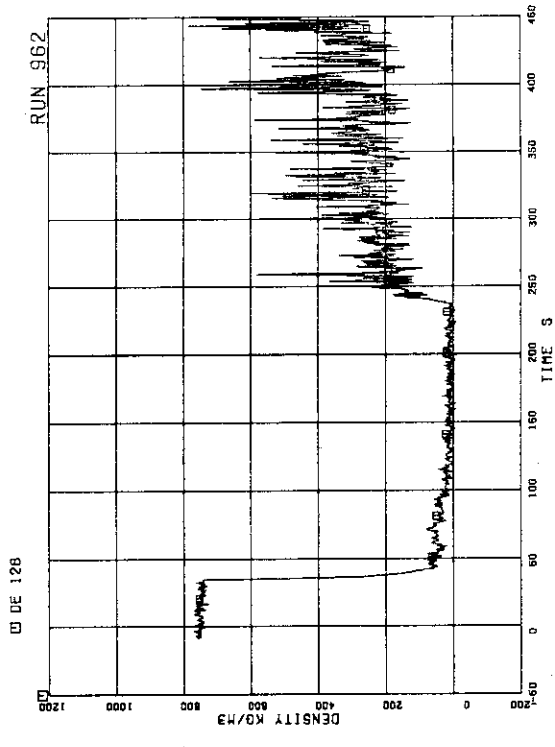

FIG.5. 58 FLUID DENSITY AT MRP SIDE OF BREAK, BEAM A

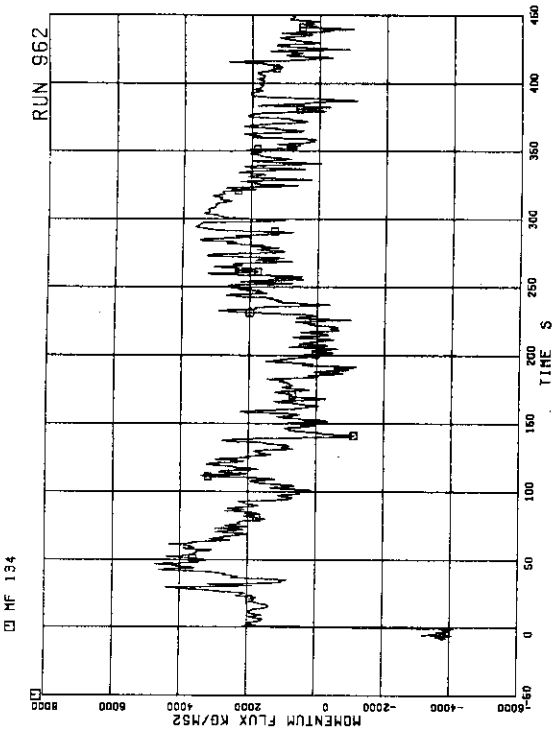

FIG.5. 63 MOMENTUM FLUX AT BREAK A SPOOL PIECE (HIGH RANGE)

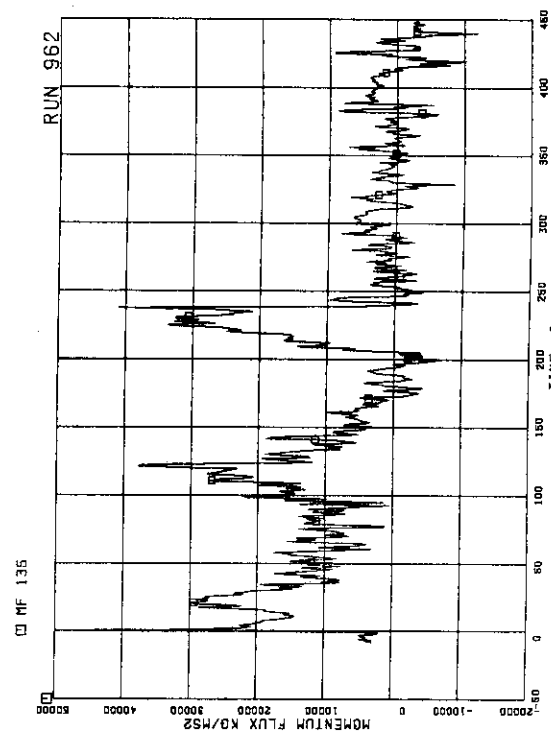

FIG.5. 64 MOMENTUM FLUX AT BREAK B SPOOL PIECE (HIGH RANGE)

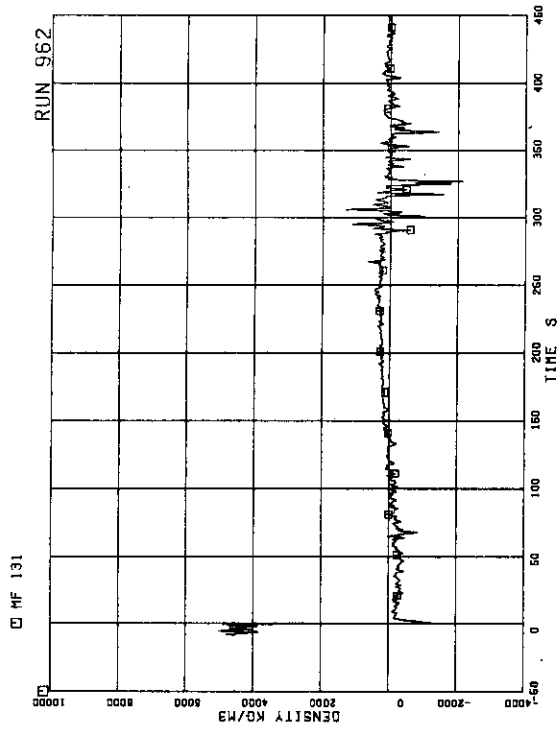

FIG.5. 61 MOMENTUM FLUX AT JP-3,4 OUTLET SPOOL

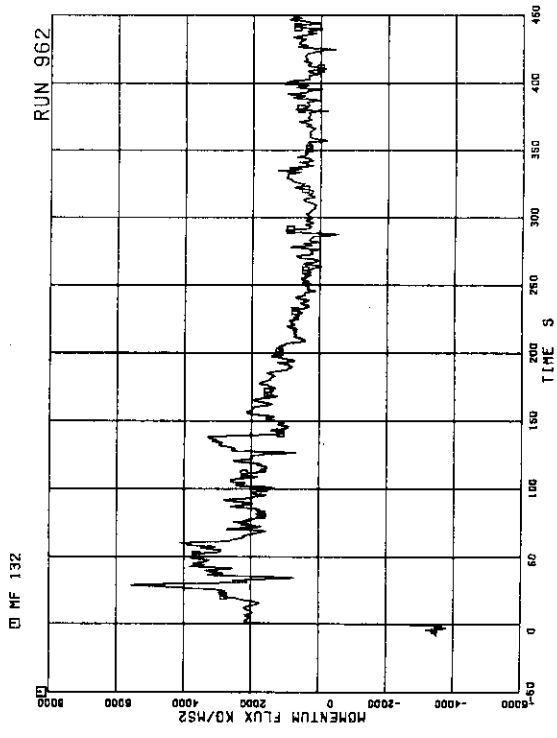

FIG.5. 62 MOMENTUM FLUX AT BREAK A SPOOL PIECE (LOW RANGE)

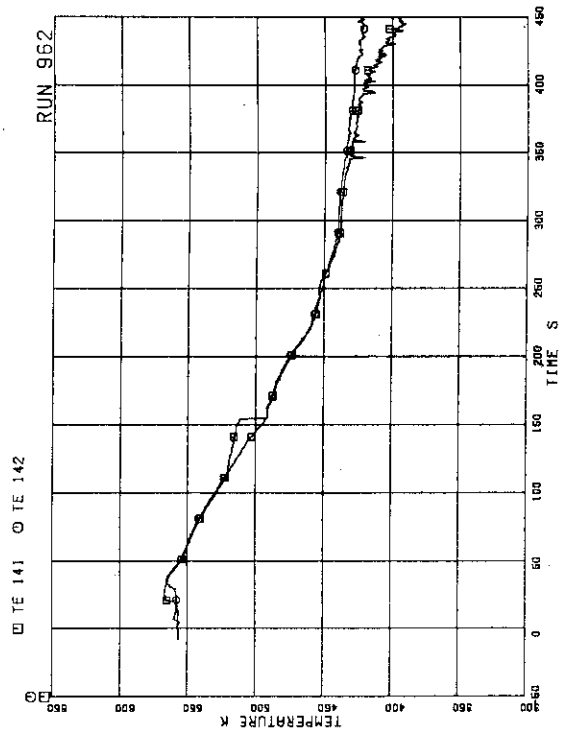

FIG.5. 67 FLUID TEMPERATURES IN DOWNCOMER

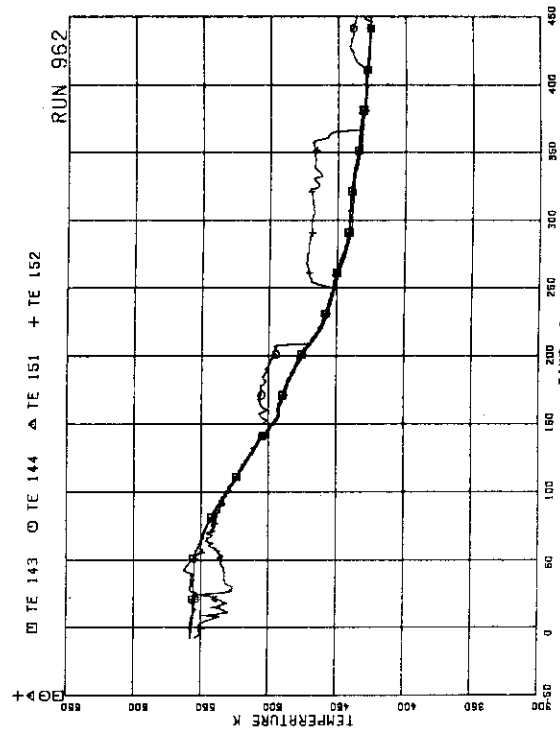

FIG.5. 68 FLUID TEMPERATURES IN INTACT RECIRCULATION LOOP

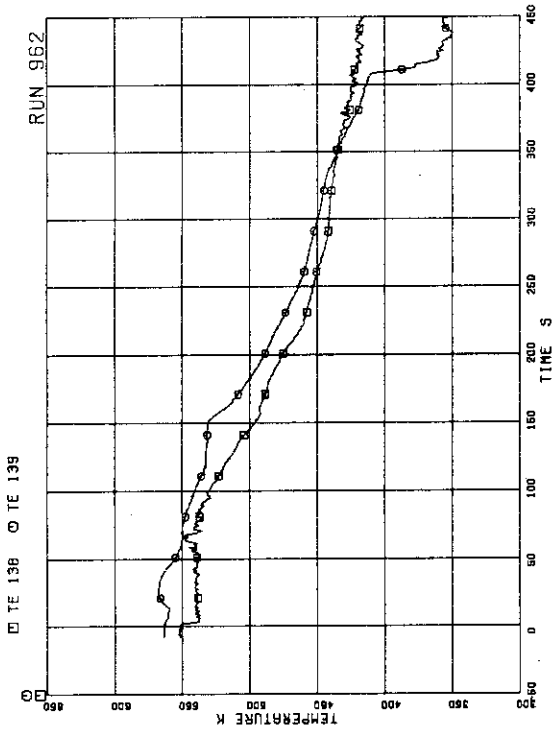

FIG.5. 65 FLUID TEMPERATURES IN LOWER PLENUM AND UPPER PLENUM

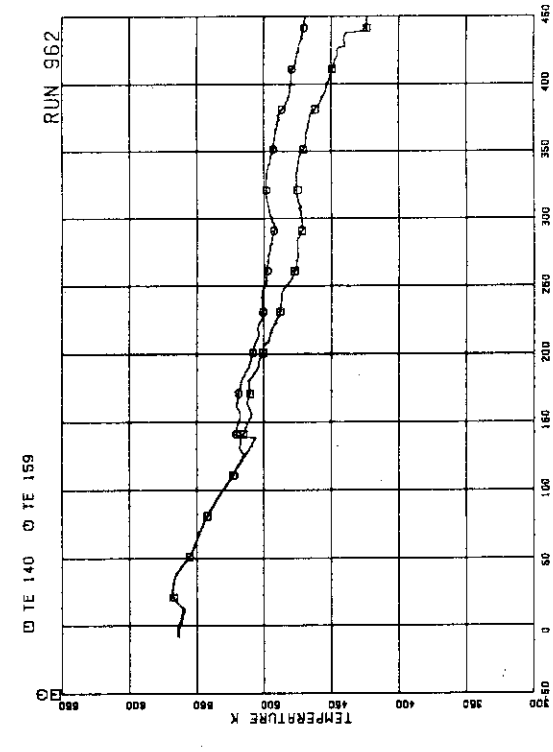

FIG.5. 66 FLUID TEMPERATURES IN STEAM DOME AND MSL

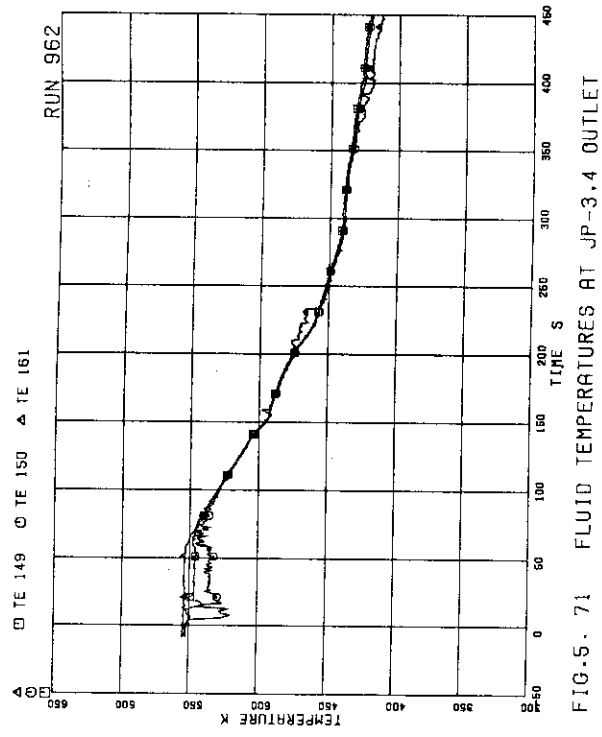

FIG.5. 71 FLUID TEMPERATURES AT JP-3.4 OUTLET

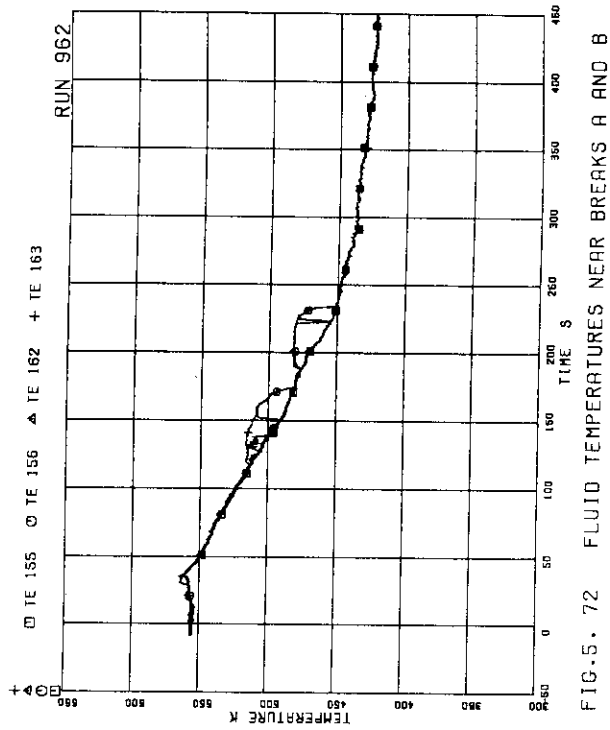

FIG.5. 72 FLUID TEMPERATURES NEAR BREAKS A AND B

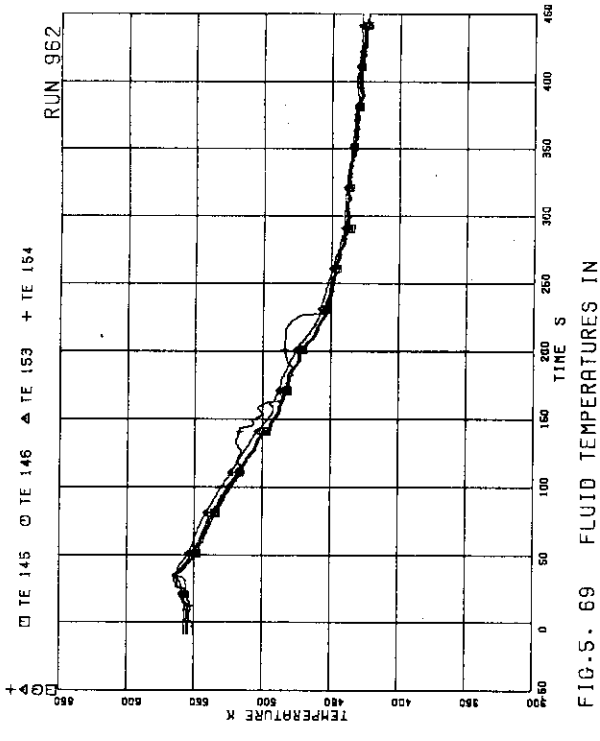

FIG.5. 69 FLUID TEMPERATURES IN BROKEN RECIRCULATION LOOP

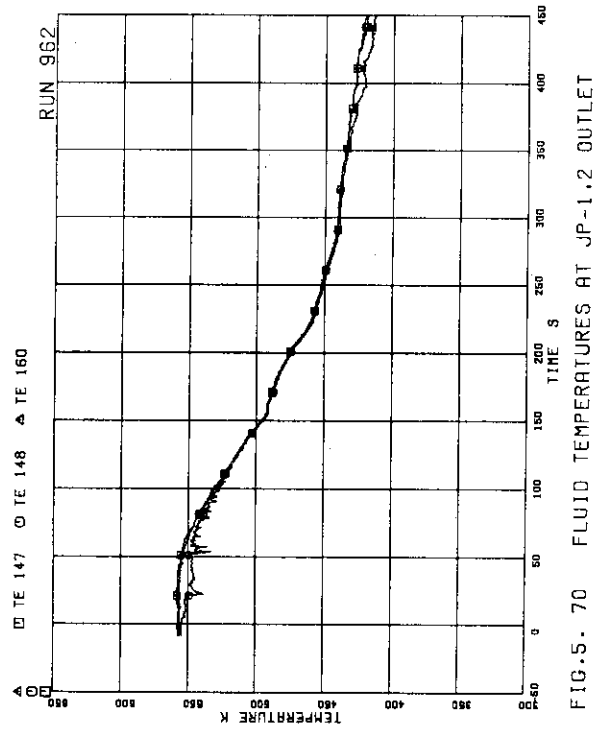

FIG.5. 70 FLUID TEMPERATURES AT JP-1.2 OUTLET

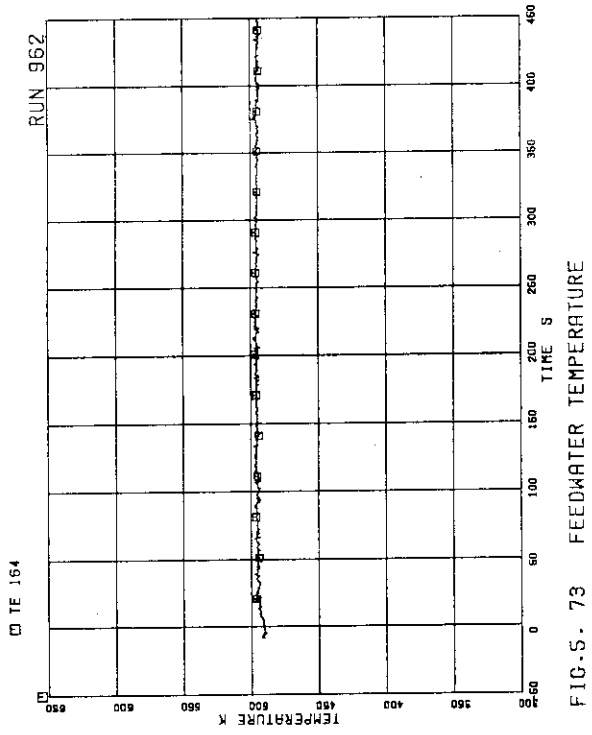

FIG.5. 73 FEEDWATER TEMPERATURE

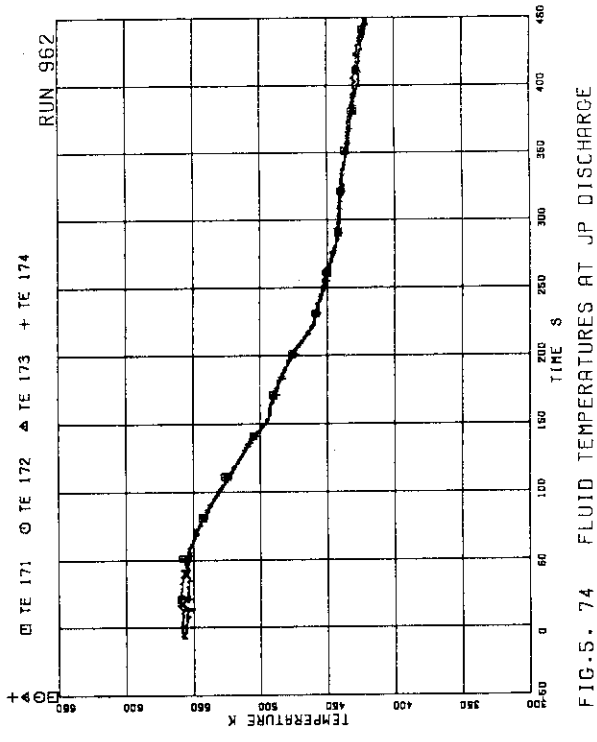

FIG.5. 74 FLUID TEMPERATURES AT JP DISCHARGE

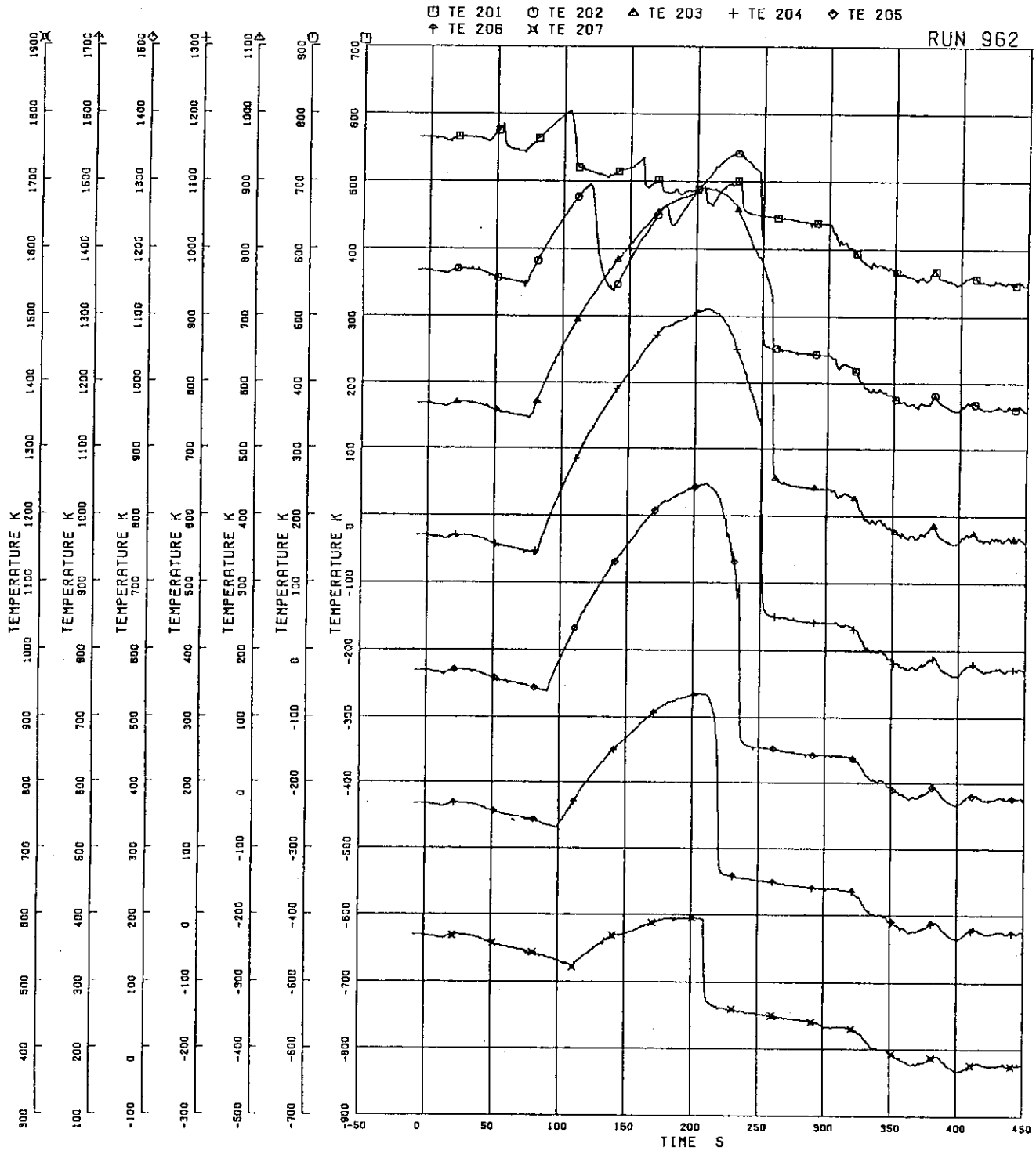

FIG.5. 75 SURFACE TEMPERATURES OF FUEL ROD A11

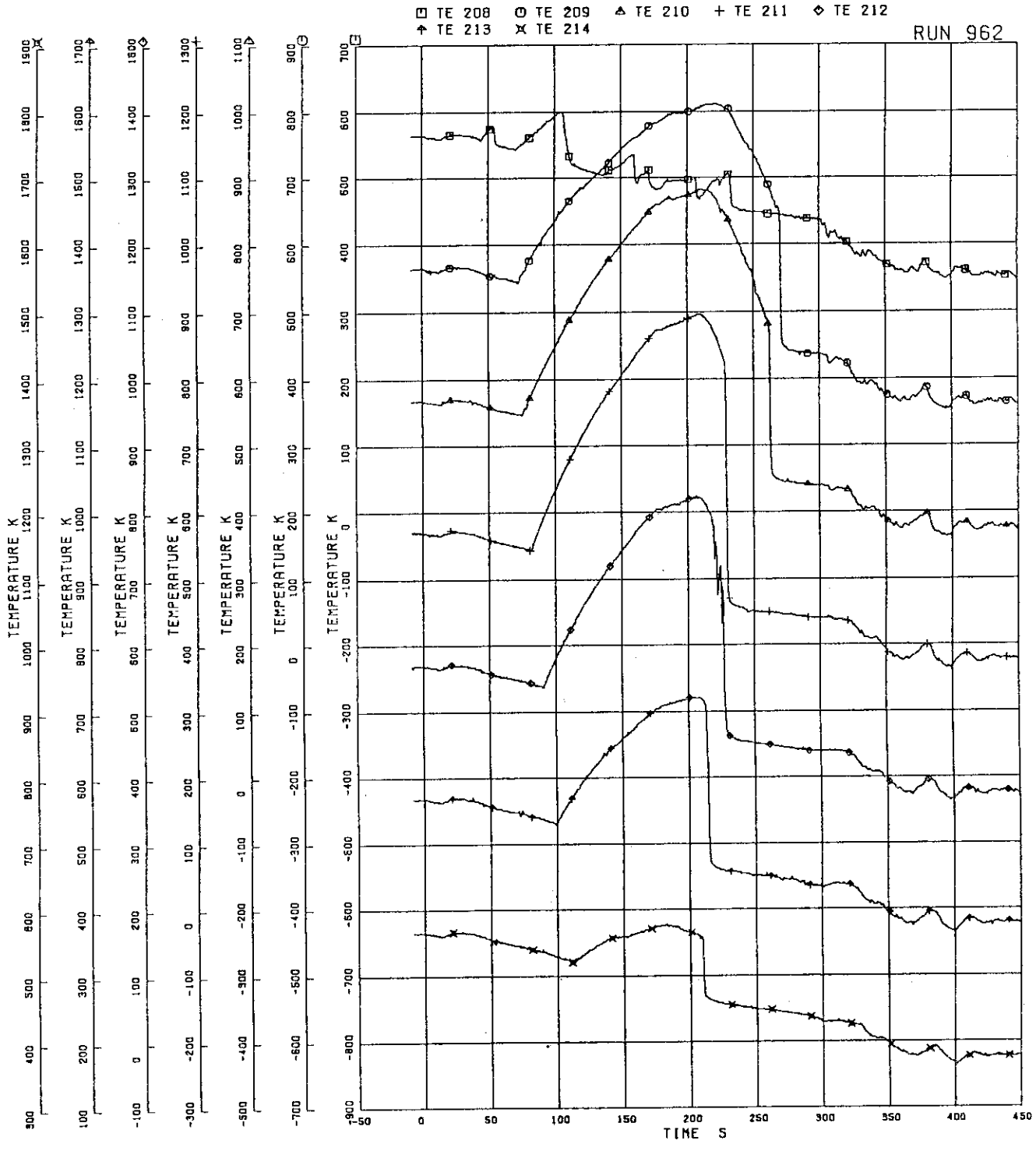

FIG.5. 76 SURFACE TEMPERATURES OF FUEL ROD A12

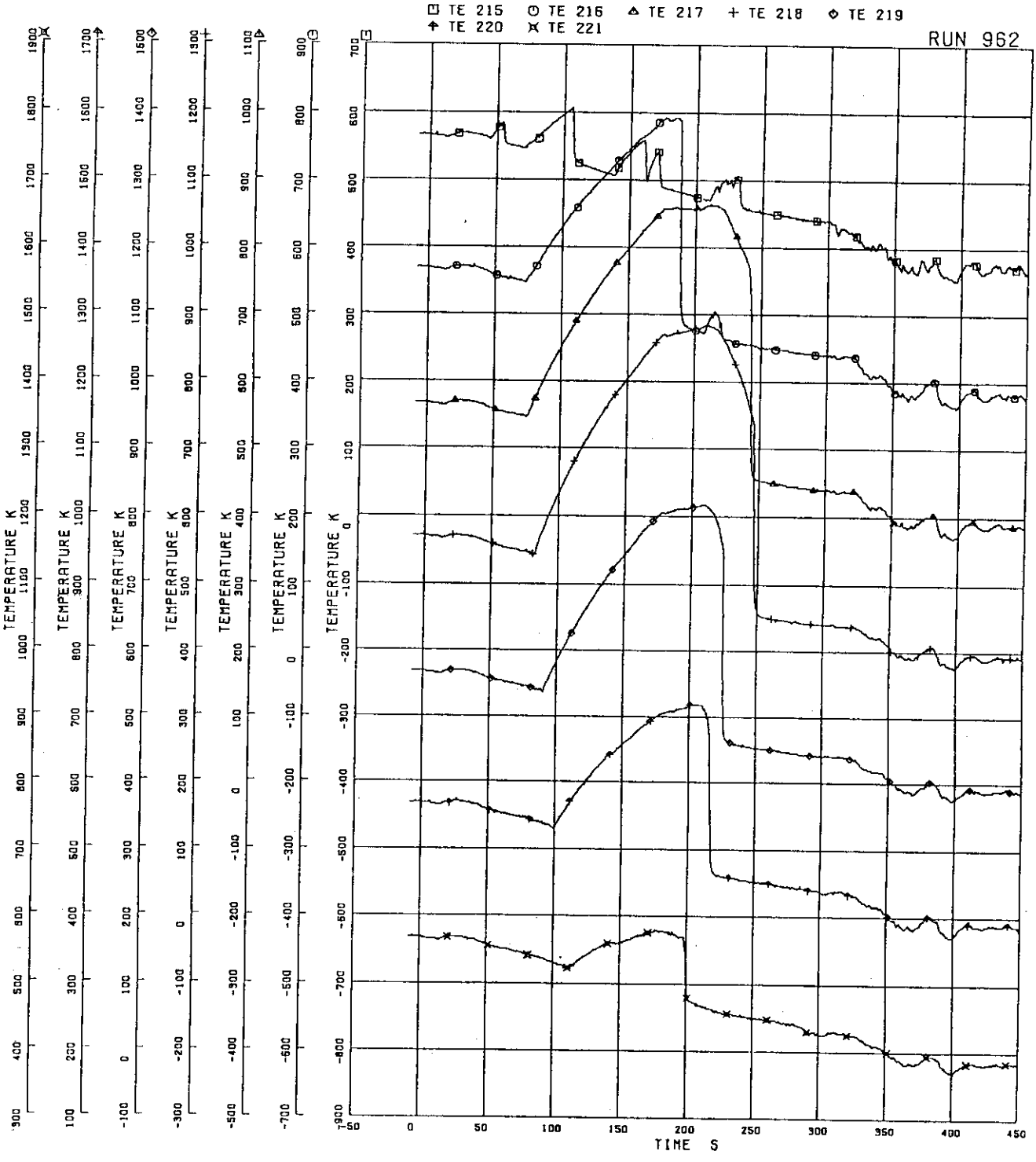

FIG.5. 77 SURFACE TEMPERATURES OF FUEL ROD A13

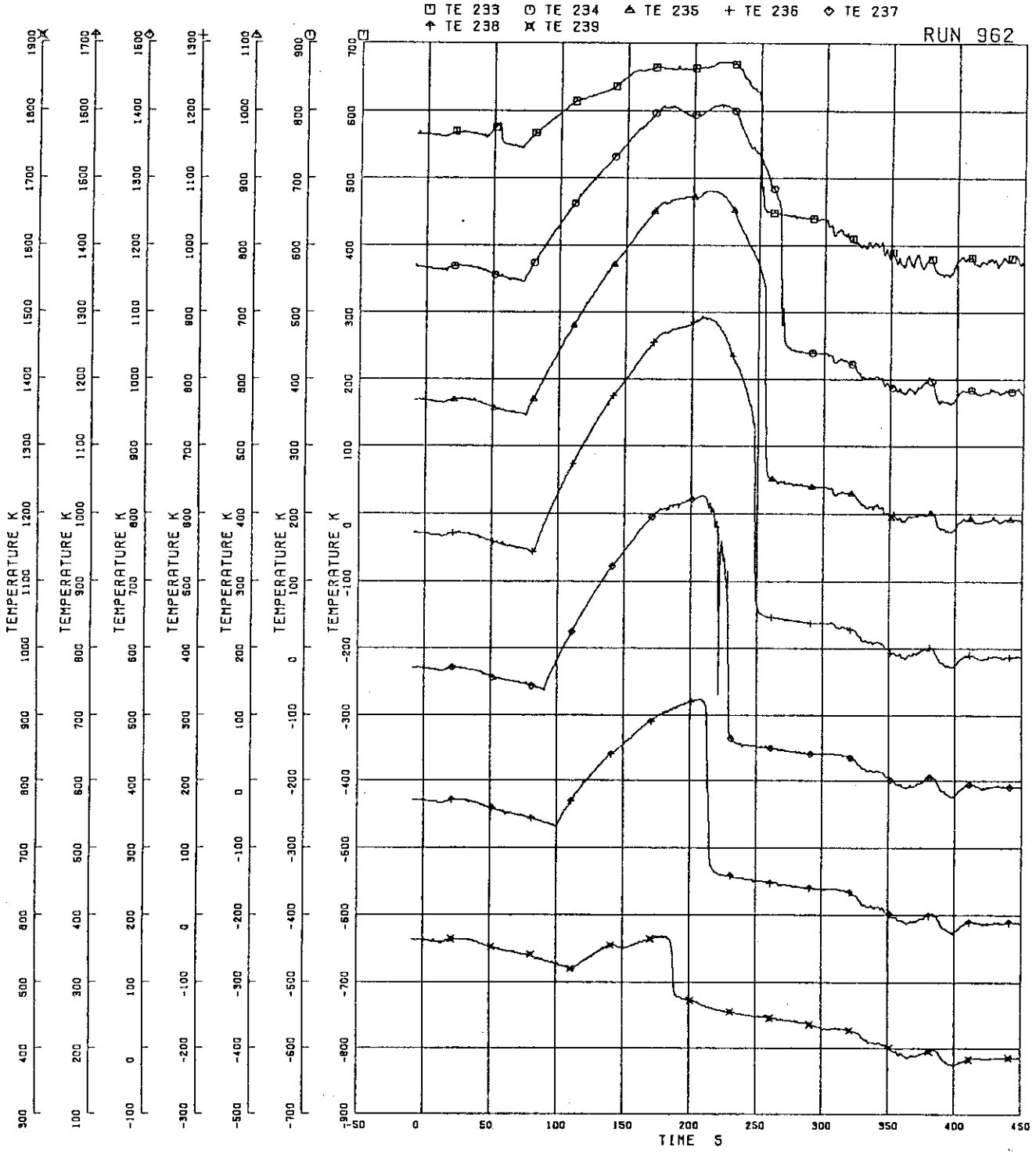

FIG.5. 78 SURFACE TEMPERATURES OF FUEL ROD A22

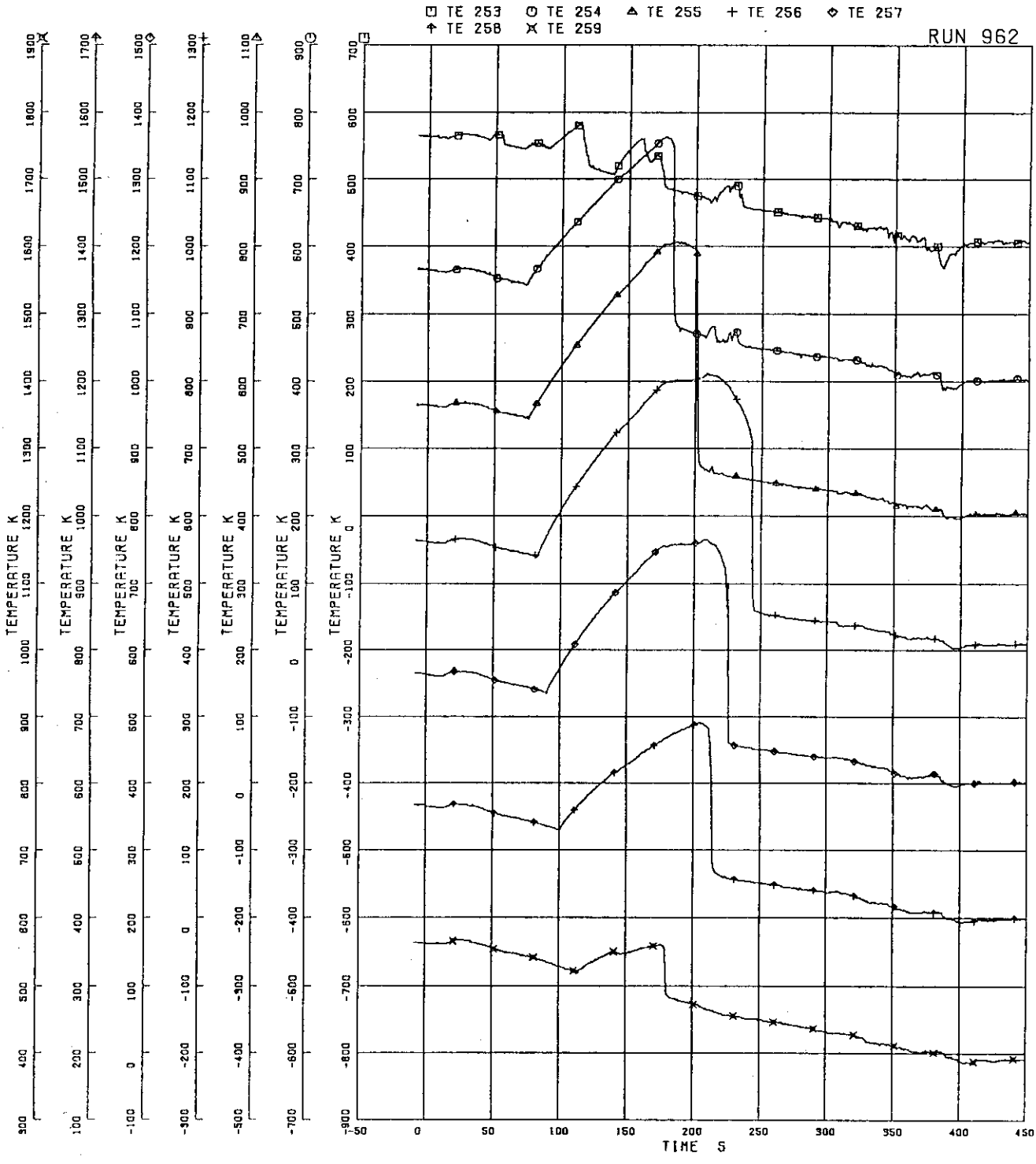

FIG.5. 79 SURFACE TEMPERATURES OF FUEL ROD A33

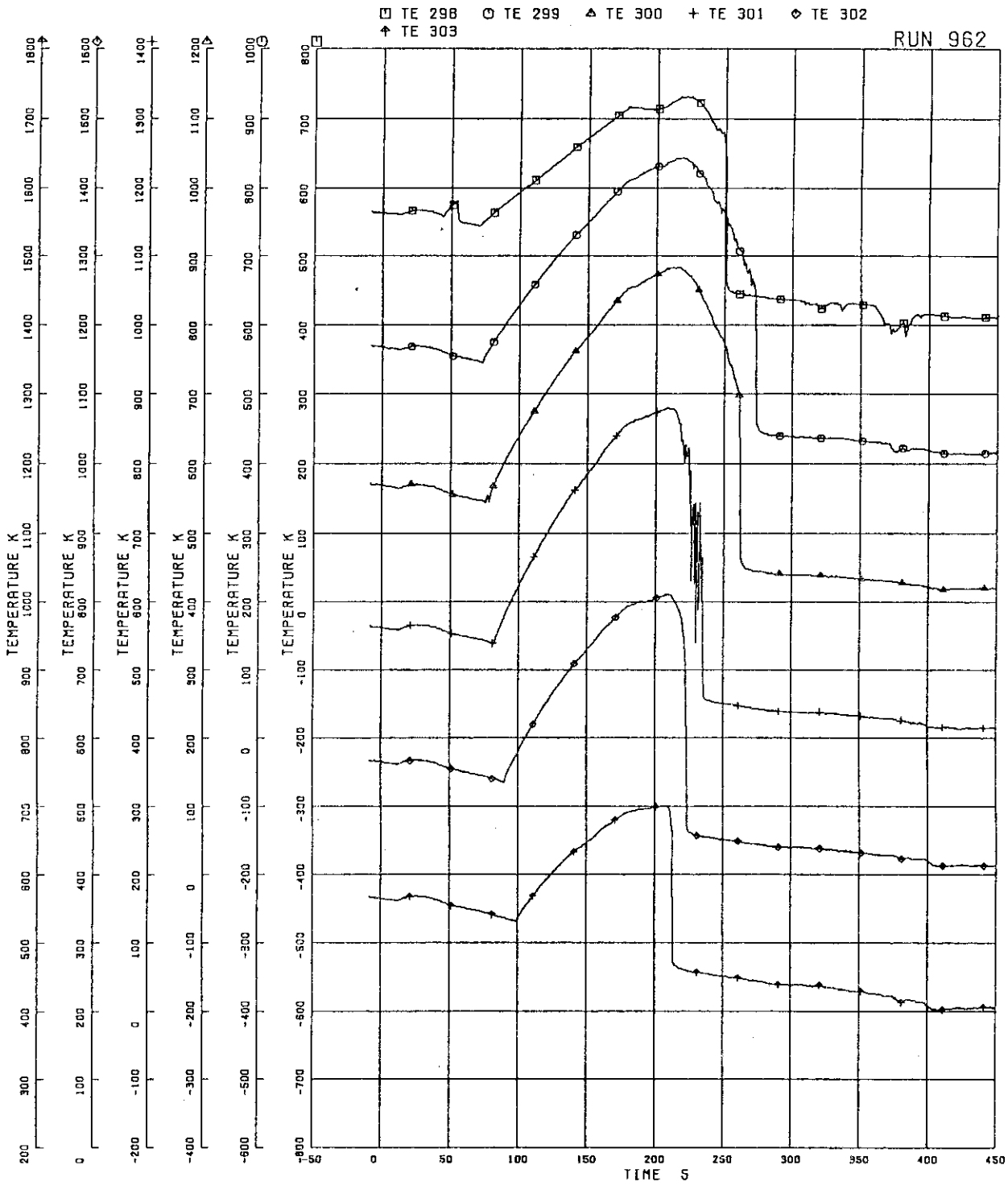

FIG.5. 80 SURFACE TEMPERATURES OF FUEL ROD A77

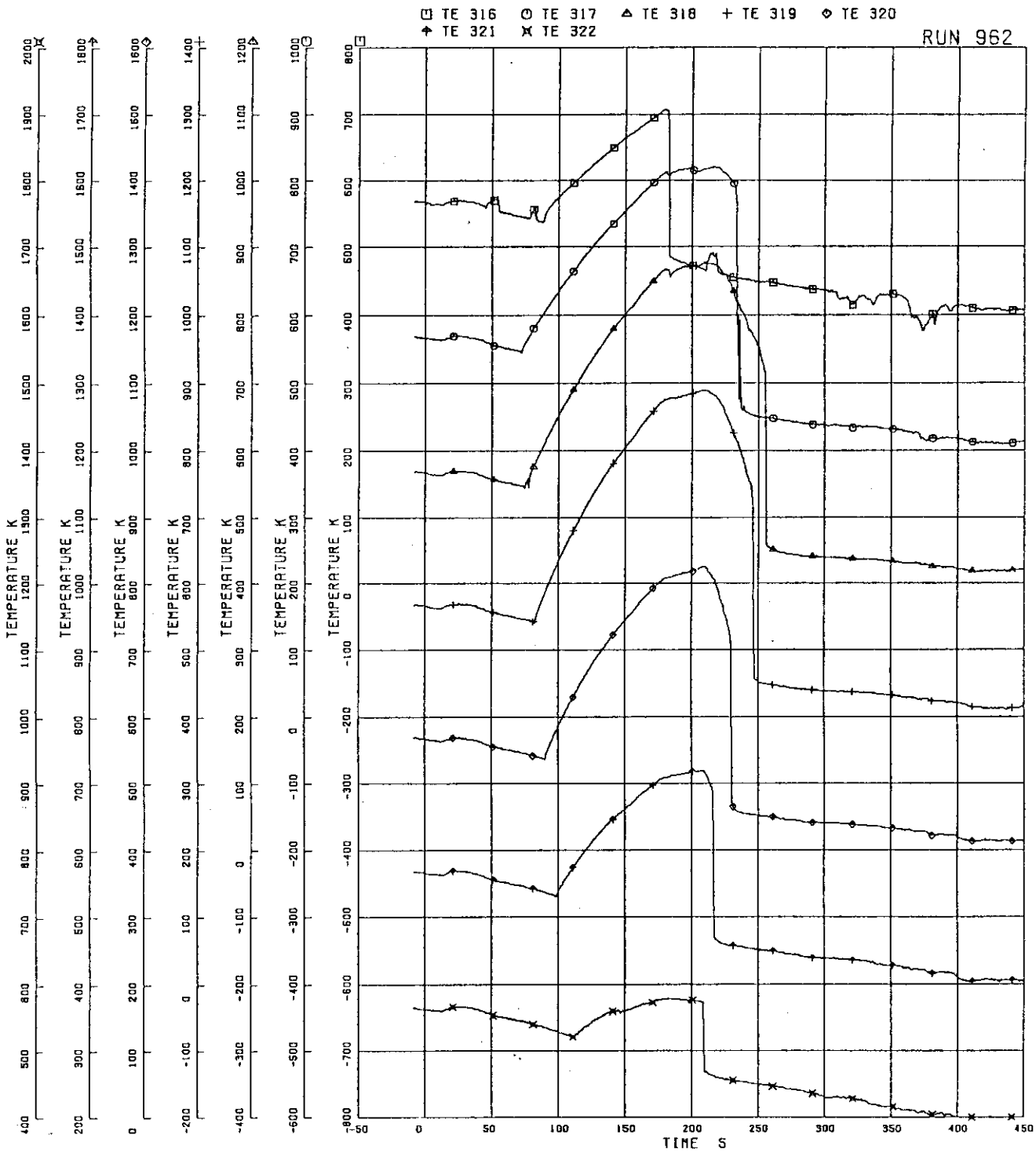

FIG.5. 81 SURFACE TEMPERATURES OF FUEL ROD A87

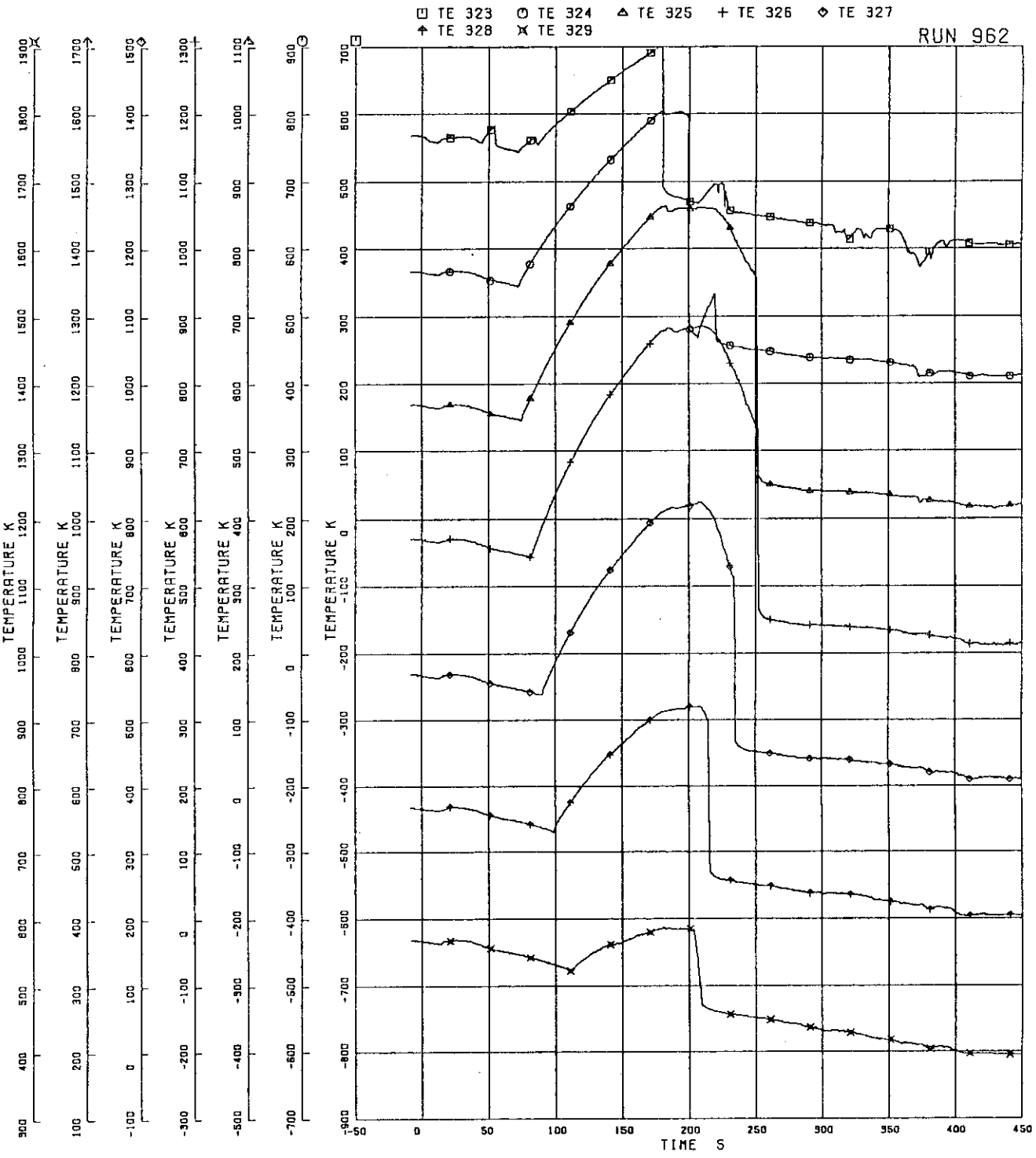

FIG.5. 82 SURFACE TEMPERATURES OF FUEL ROD A88

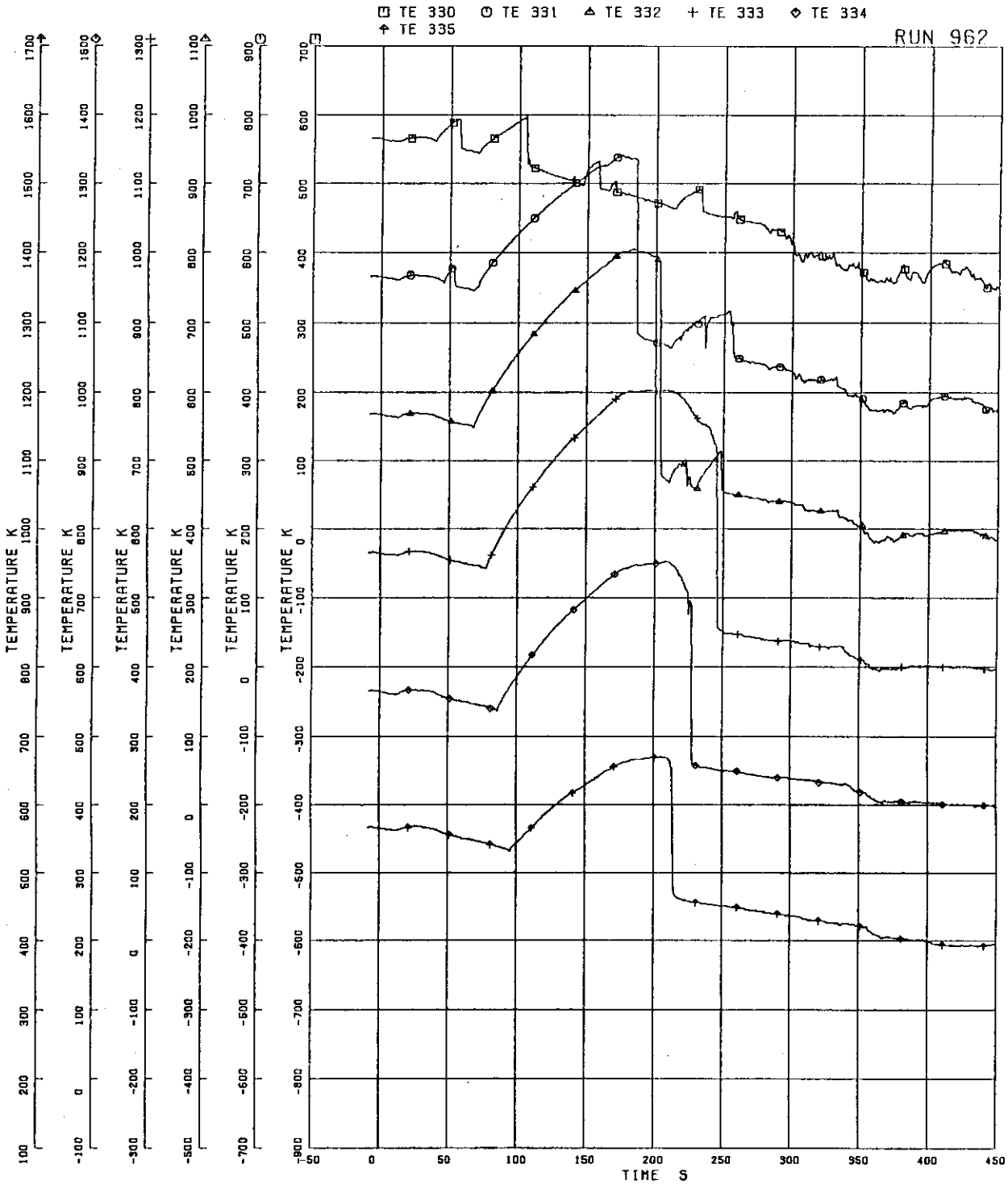

FIG.5. 83 SURFACE TEMPERATURES OF FUEL ROD B11

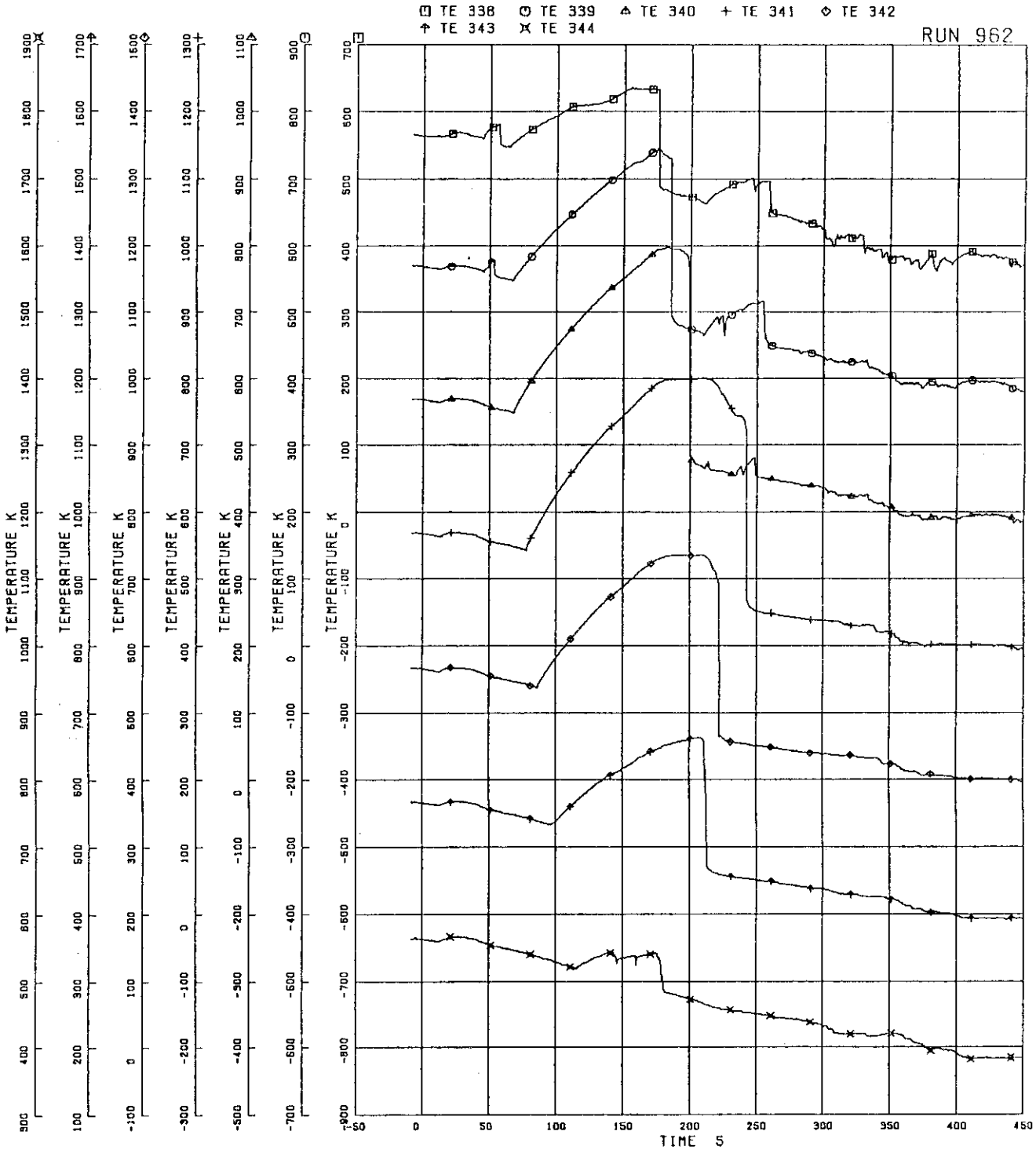

FIG.5. 84 SURFACE TEMPERATURES OF FUEL ROD B22

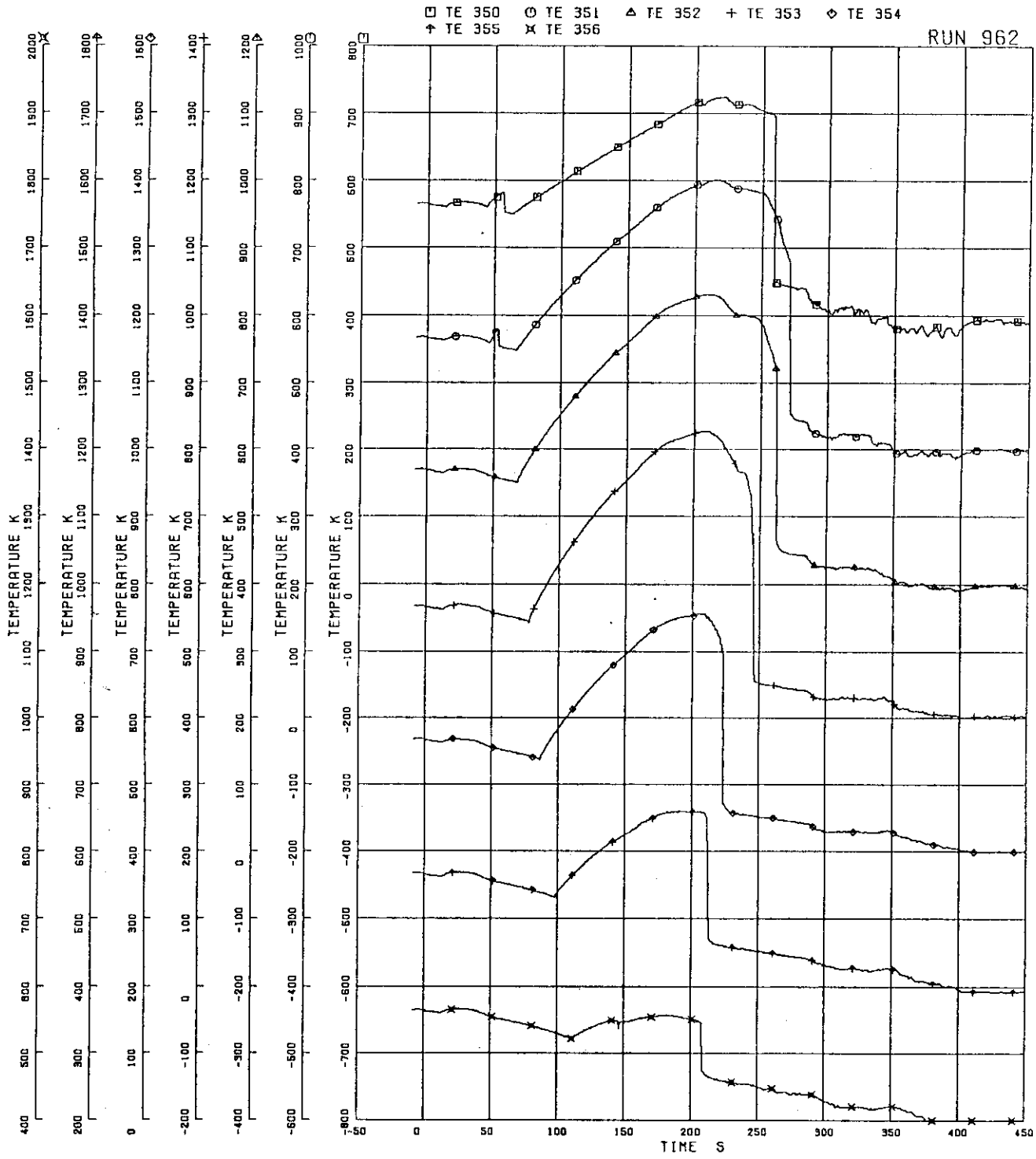

FIG.5. 85 SURFACE TEMPERATURES OF FUEL ROD B77

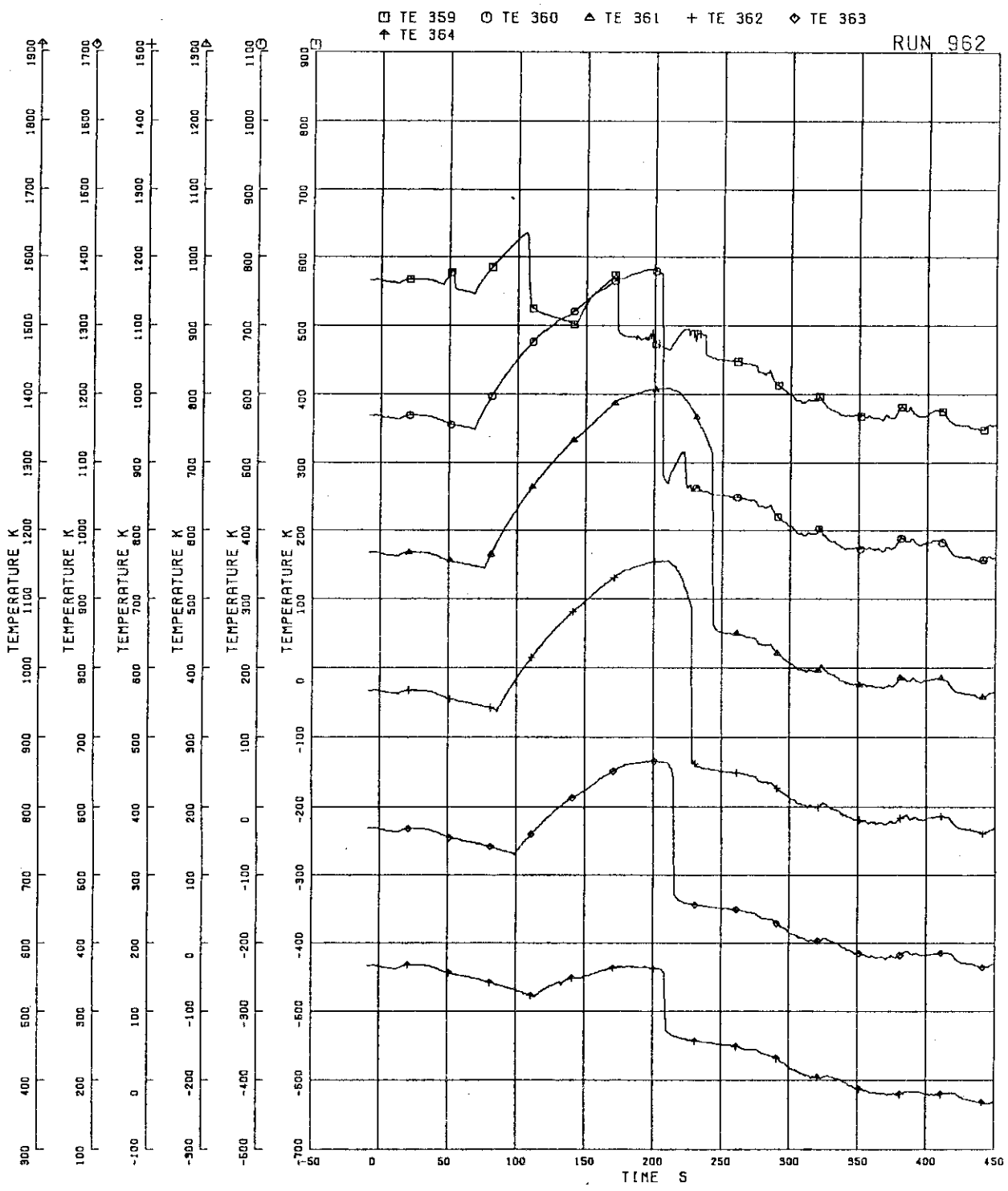

FIG.5. 86 SURFACE TEMPERATURES OF FUEL ROD C11

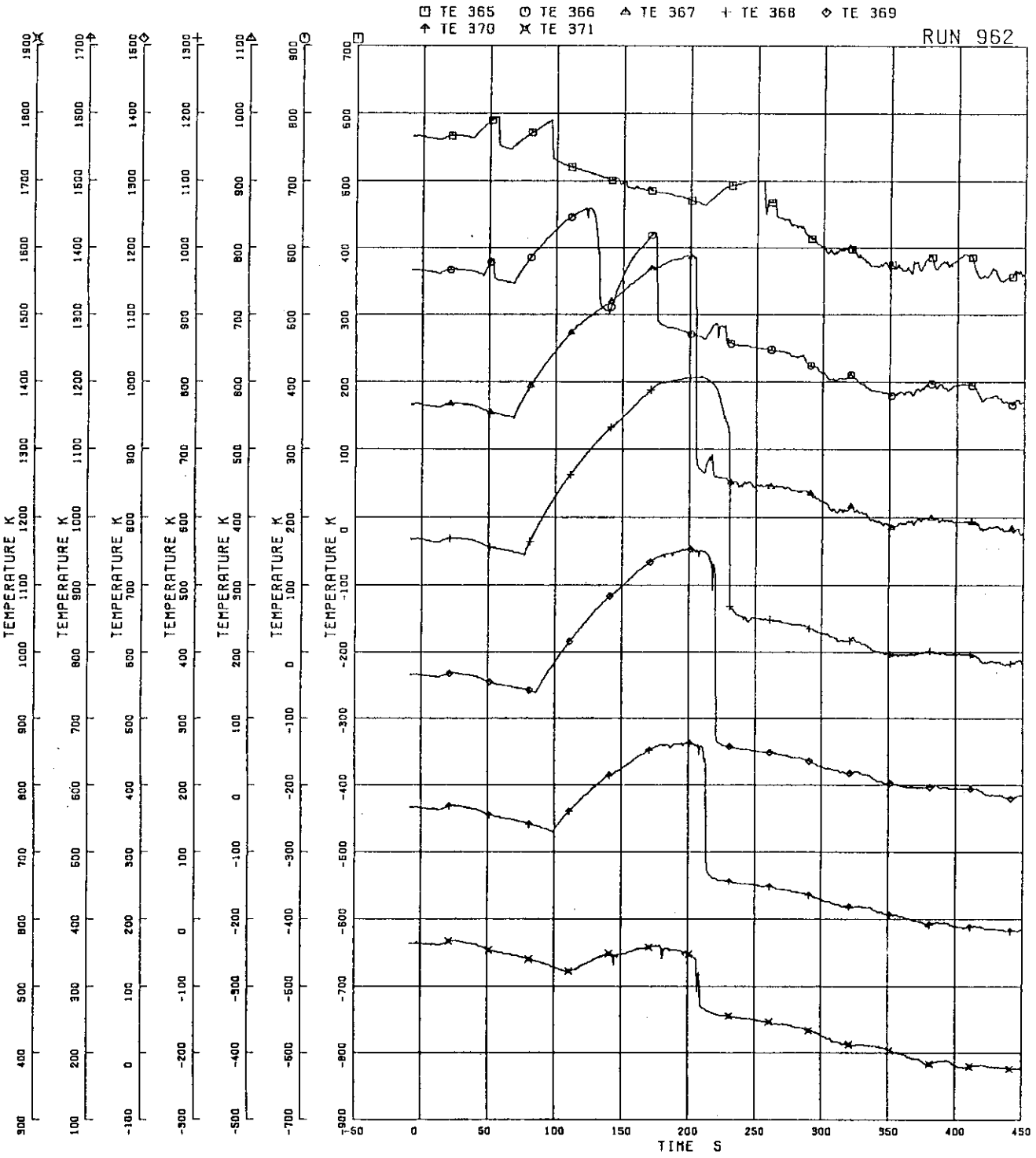

FIG.5. 87 SURFACE TEMPERATURES OF FUEL ROD C13

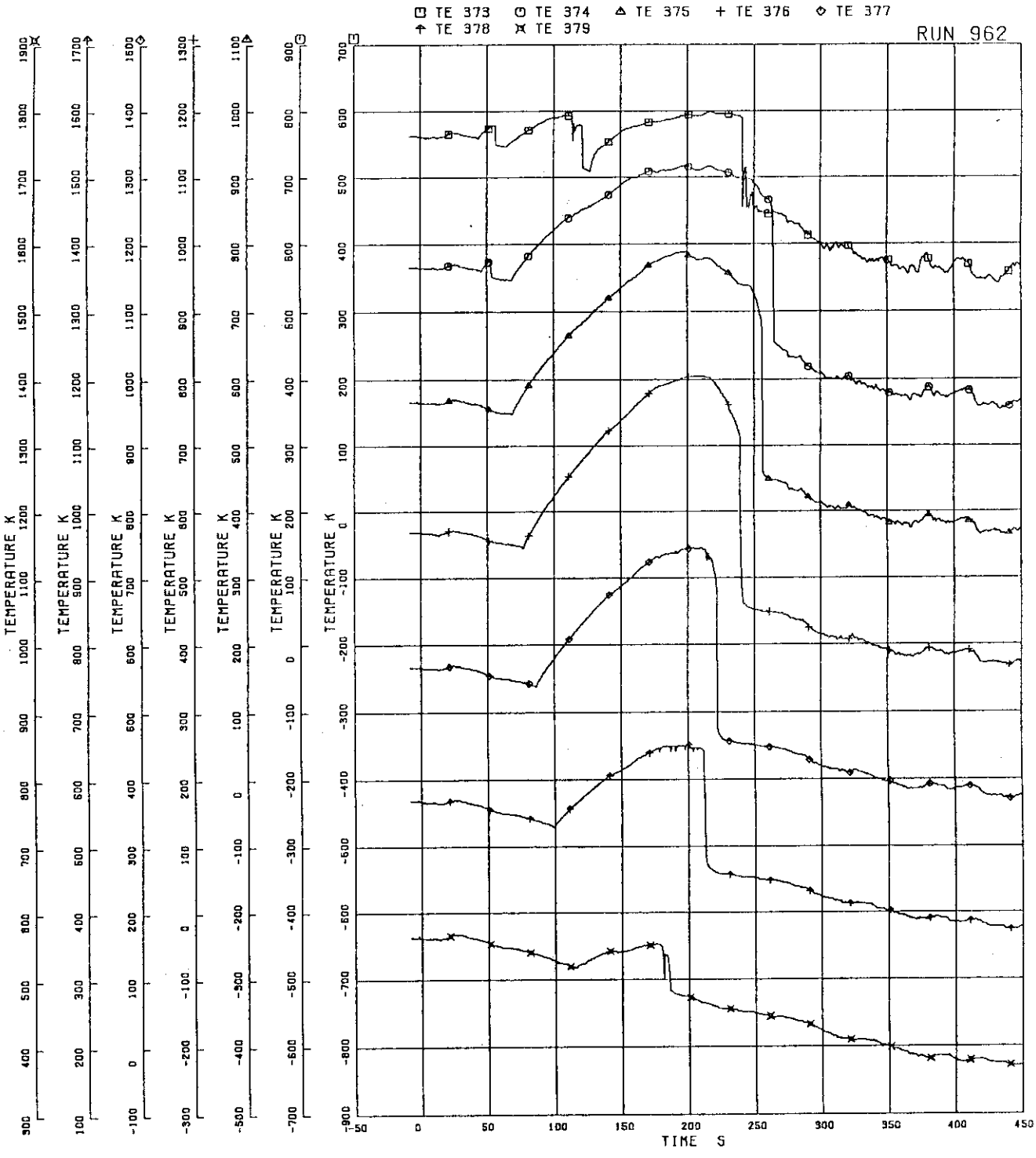

FIG.5. 88 SURFACE TEMPERATURES OF FUEL ROD C22

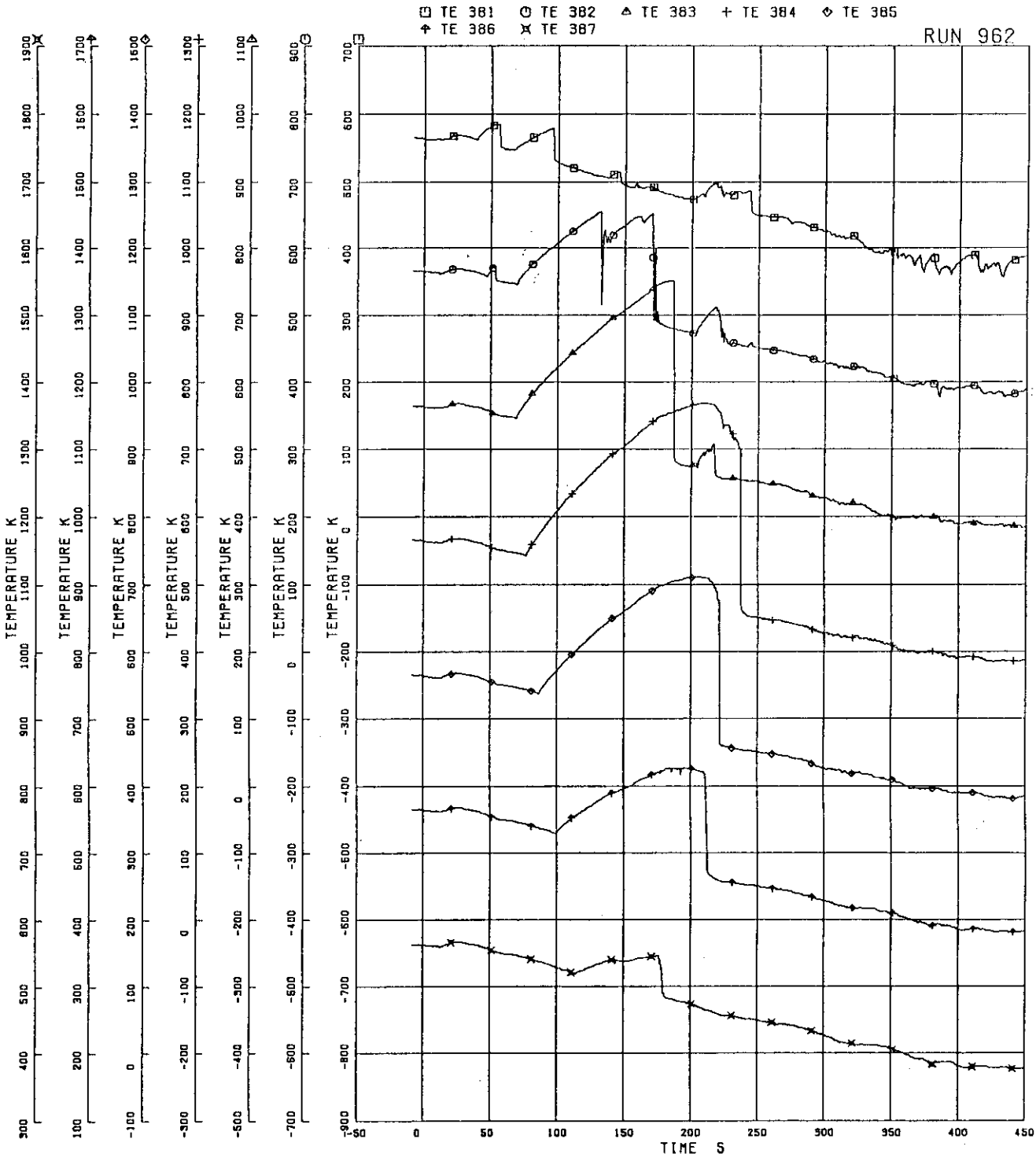

FIG.5. 89 SURFACE TEMPERATURES OF FUEL ROD C33

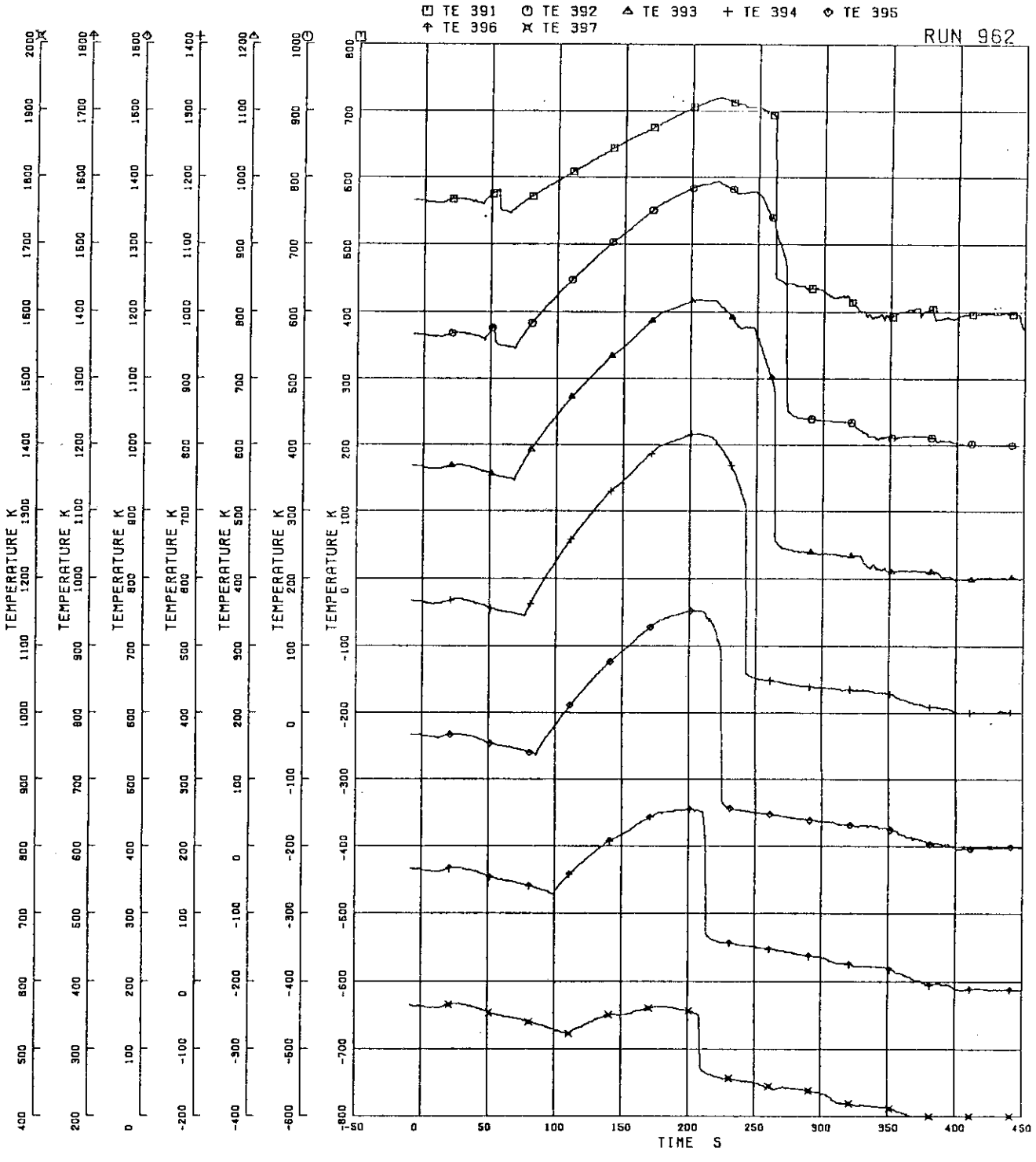

FIG.5. 90 SURFACE TEMPERATURES OF FUEL ROD C77

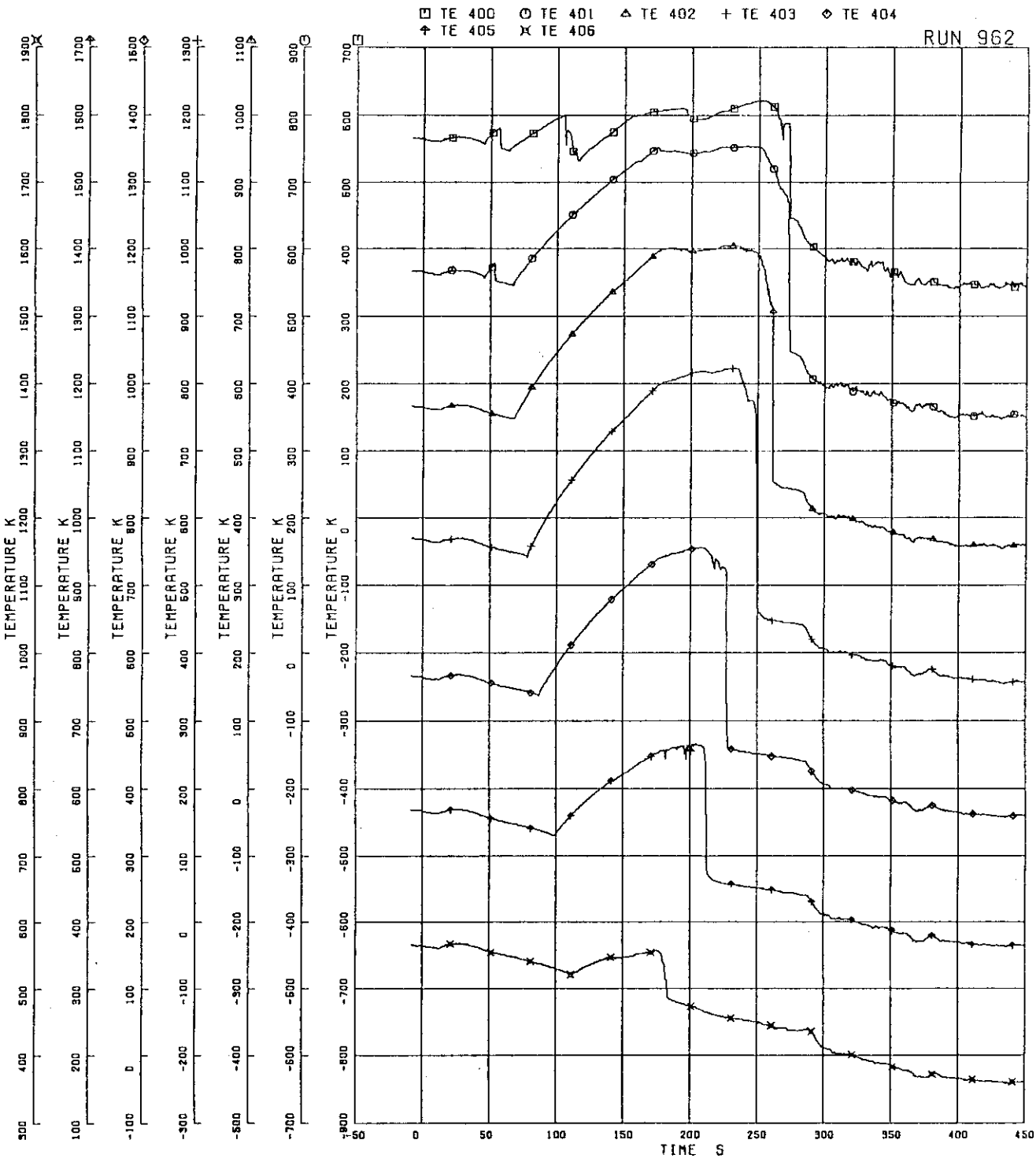

FIG.5. 91 SURFACE TEMPERATURES OF FUEL ROD D22

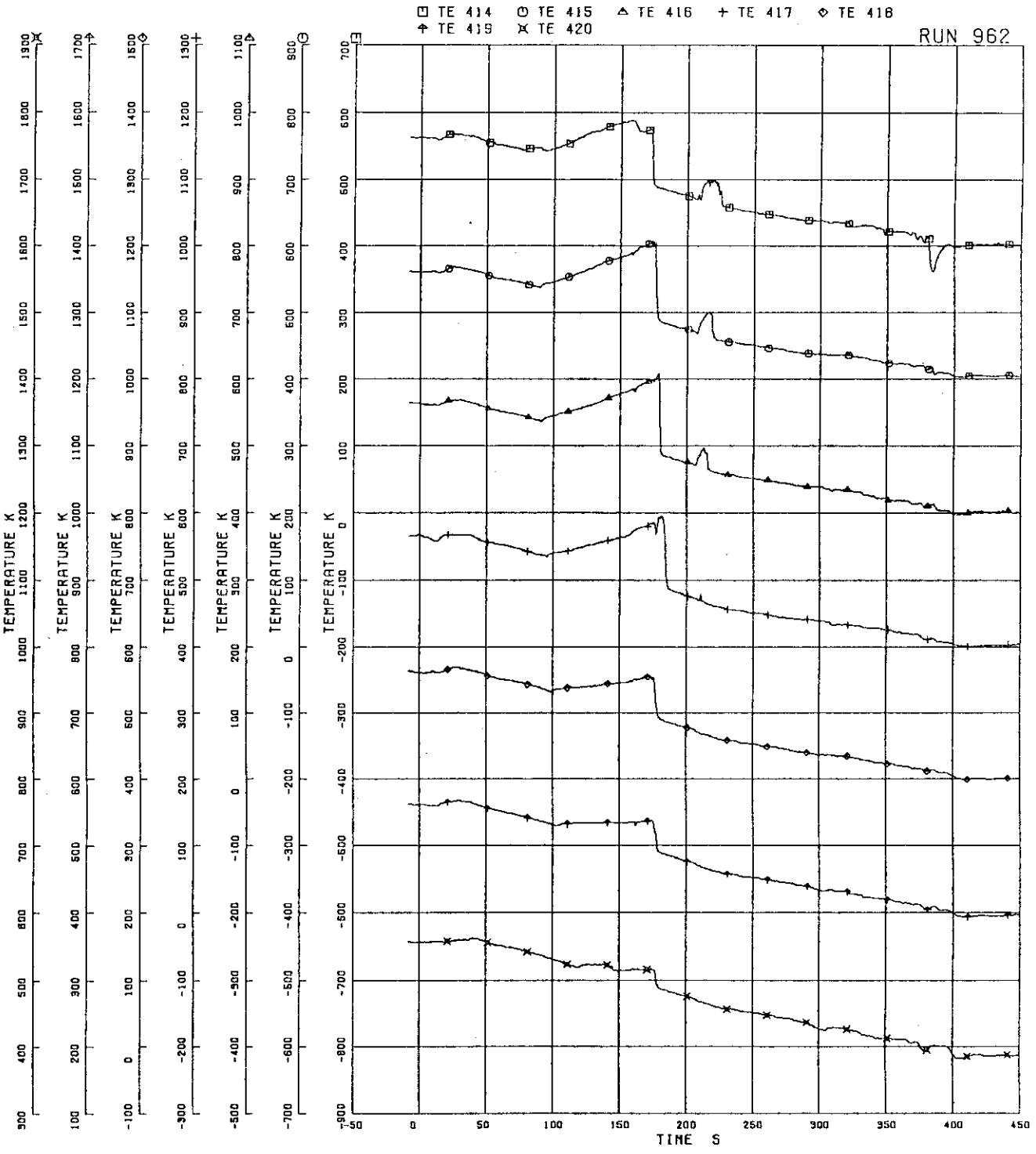

FIG.5. 92 SURFACE TEMPERATURES OF WATER ROD SIMULATOR A45

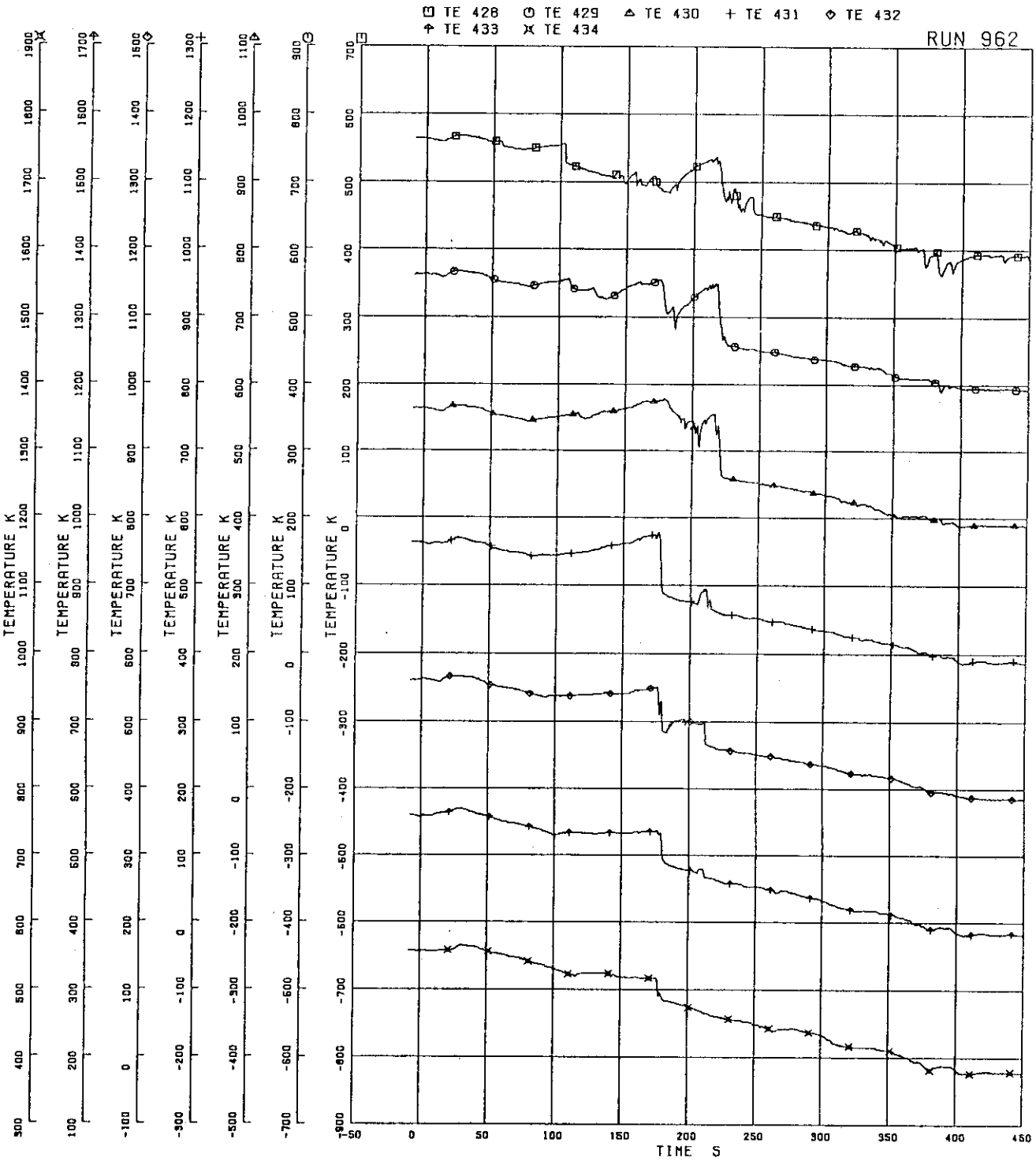

FIG.5. 93 SURFACE TEMPERATURES OF WATER ROD SIMULATOR C45

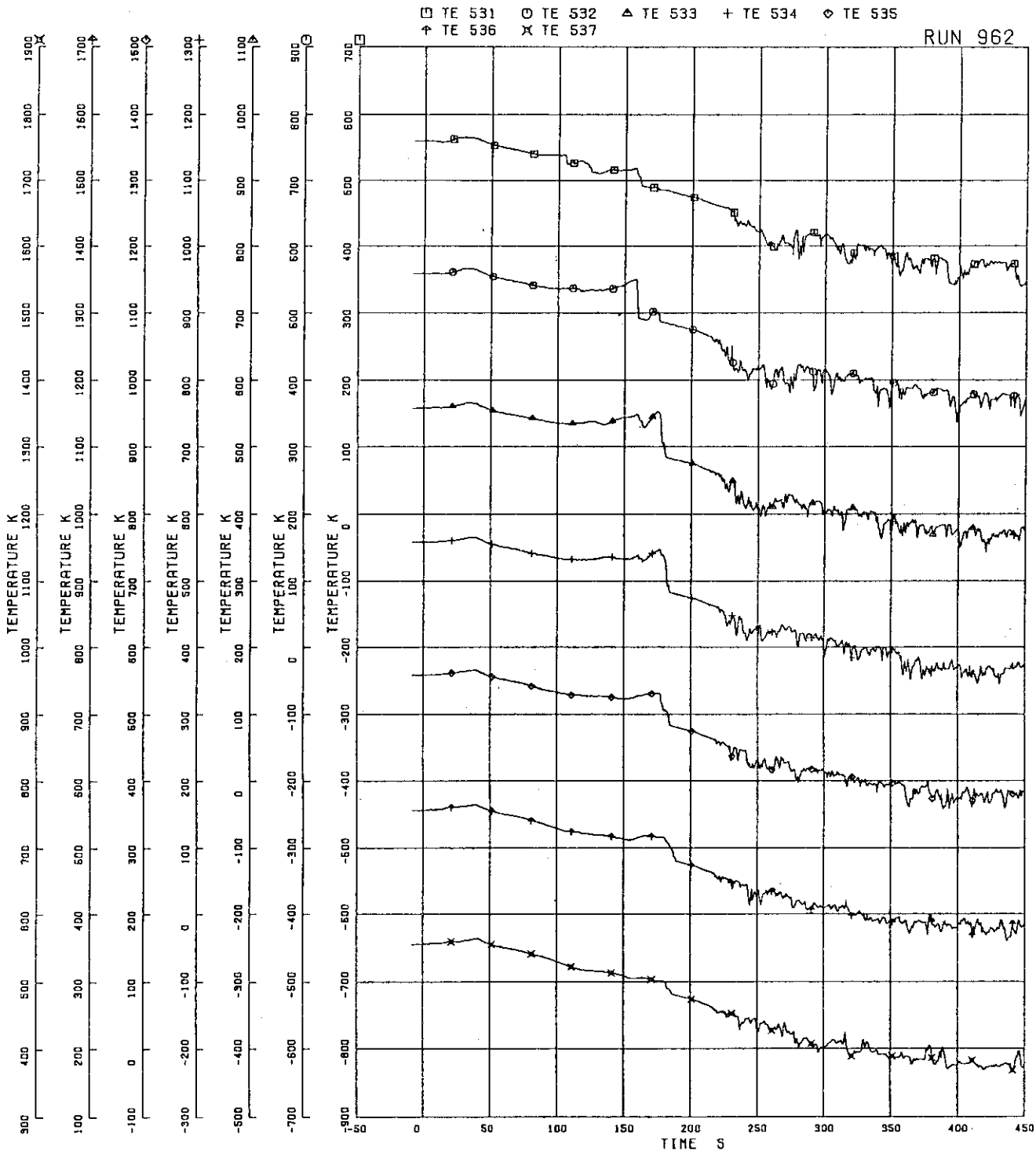

FIG.5. 94 OUTER SURFACE TEMPERATURES OF CHANNEL BOX A

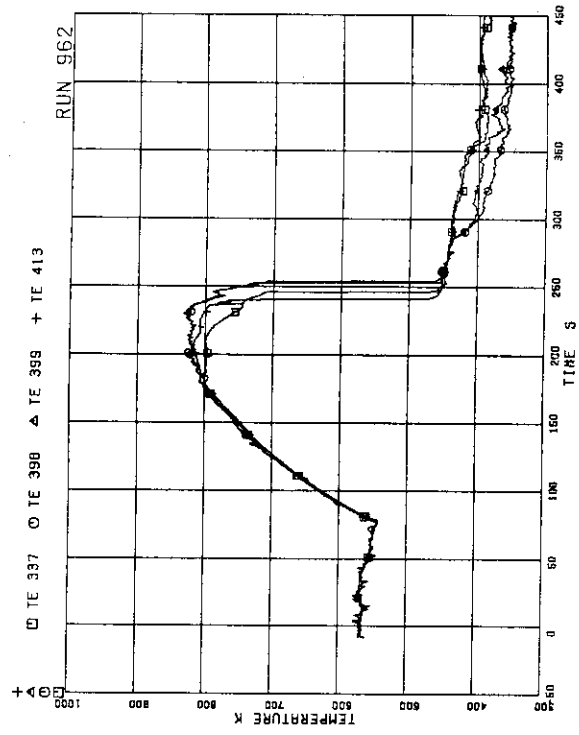

FIG.5. 97 SURFACE TEMPERATURES OF B13,D11, D13 AND D86,POSITION 4

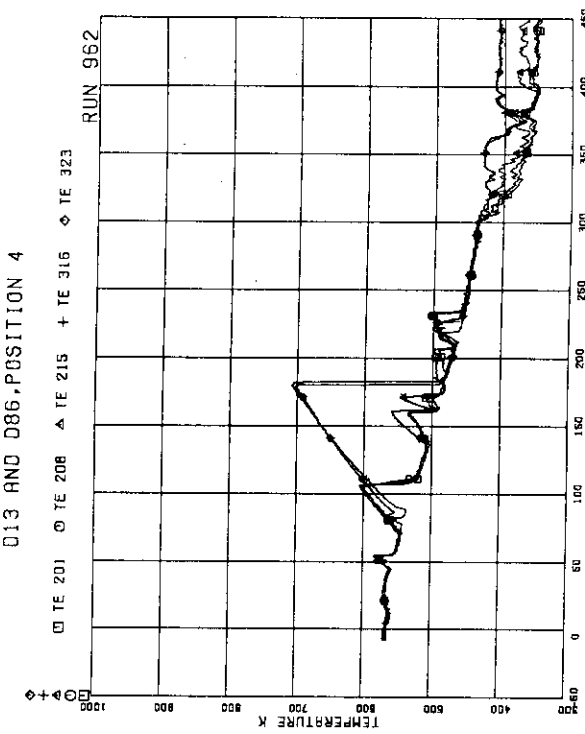

FIG.5. 98 SURFACE TEMPERATURES OF FUEL RODS A11,A12,A13,A87,A88 AT POSITION 1

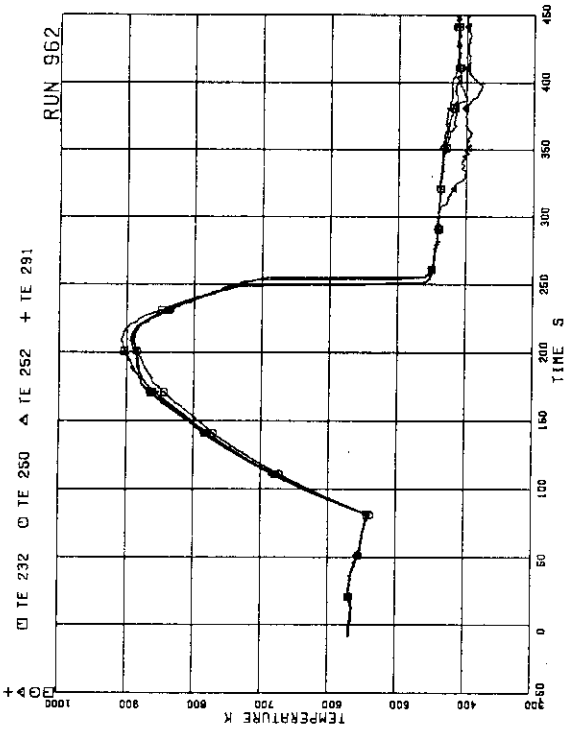

FIG.5. 95 SURFACE TEMPERATURES OF PERIPHERAL RODS A17,A28,A31 AND A68,POSITION 4

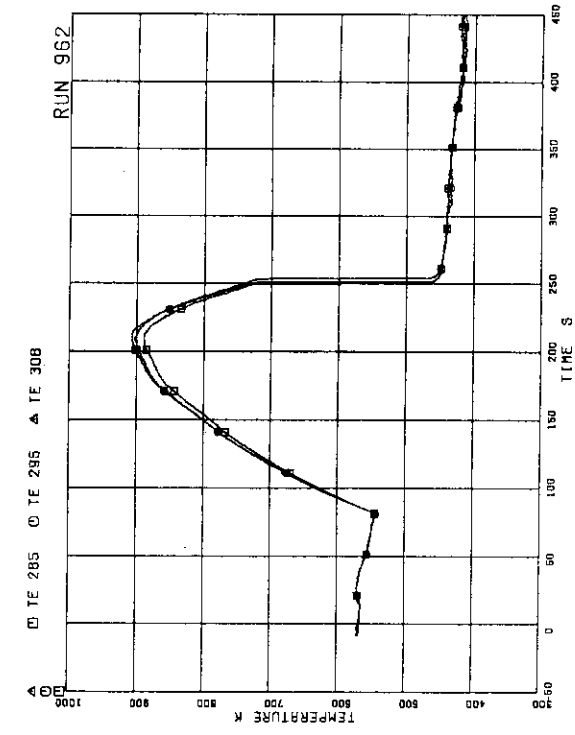

FIG.5. 96 SURFACE TEMPERATURES OF A57,A73 AND A84,POSITION 4

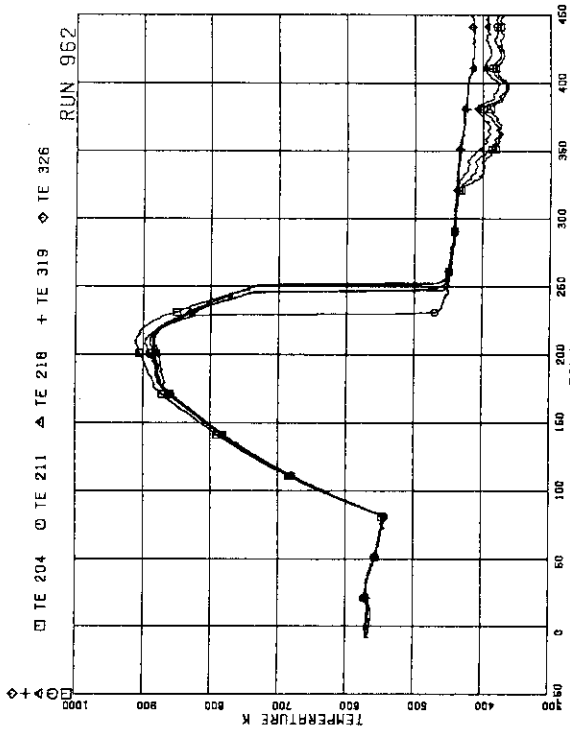

FIG.5.101 SURFACE TEMPERATURES OF FUEL RODS A11,A12,A13,A87,A88 AT POSITION 4

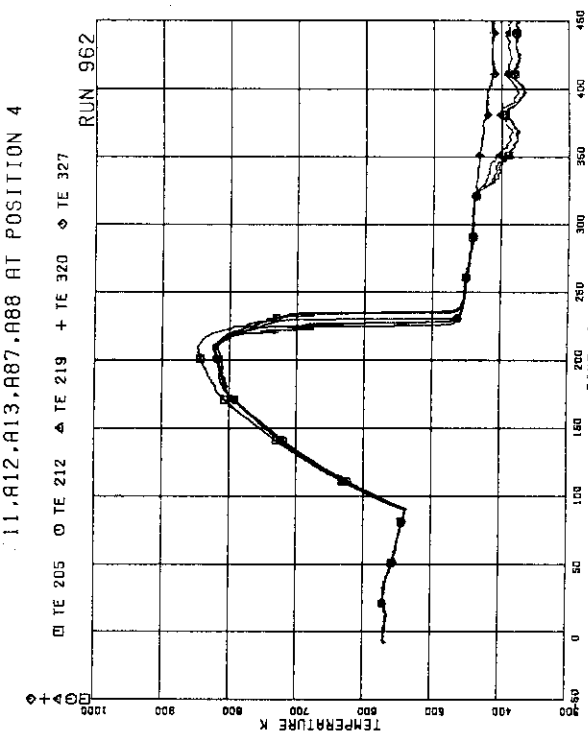

FIG.5.102 SURFACE TEMPERATURES OF FUEL RODS A11,A12,A13,A87,A88 AT POSITION 5

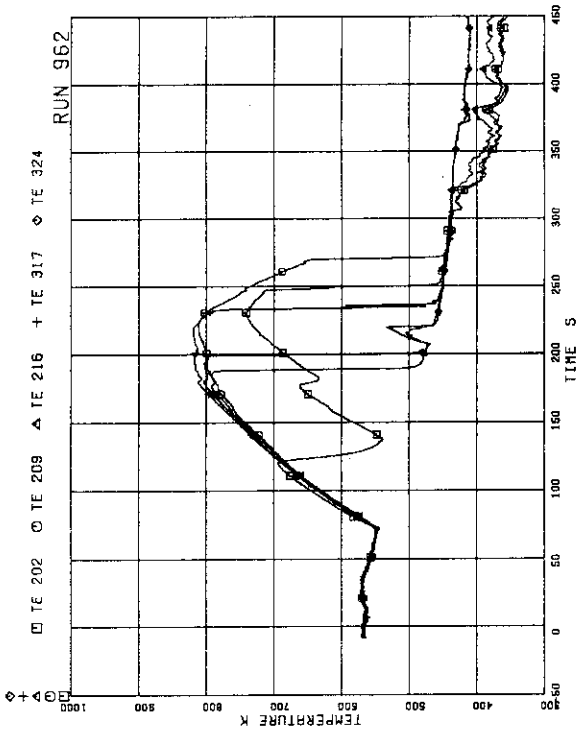

FIG.5.99 SURFACE TEMPERATURES OF FUEL RODS A11,A12,A13,A88 AT POSITION 2

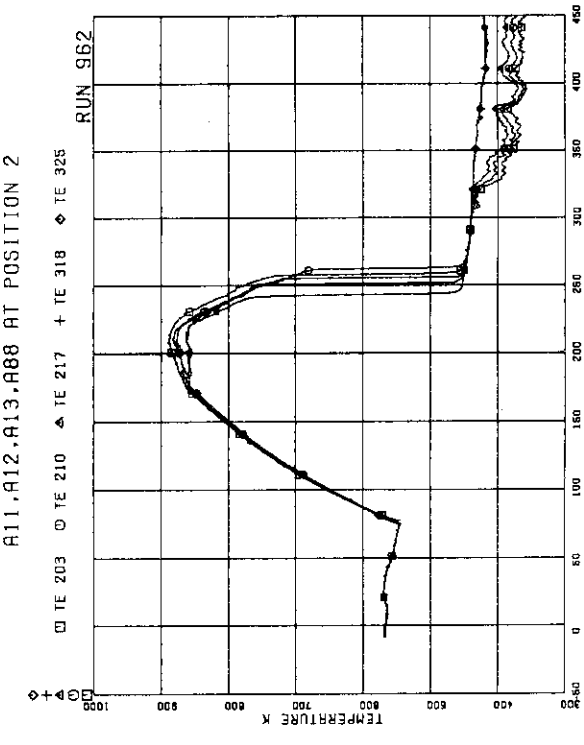

FIG.5.100 SURFACE TEMPERATURES OF FUEL RODS A11,A12,A13,A87,A88 AT POSITION 3

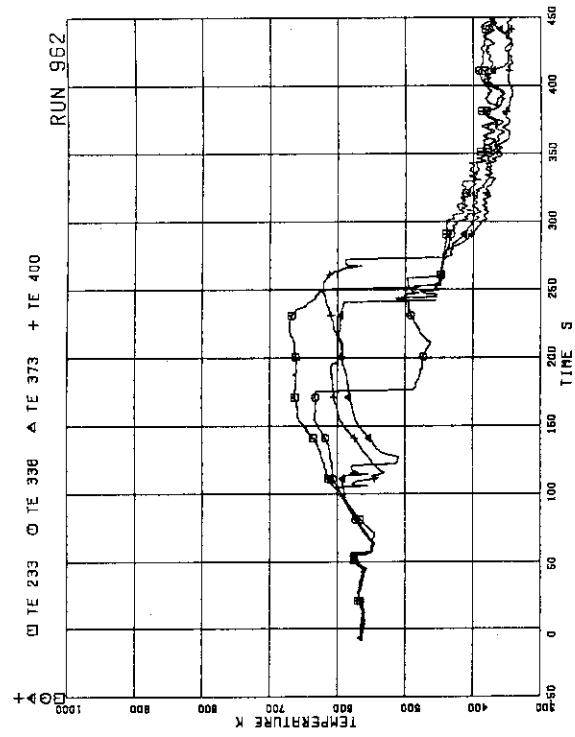

FIG.5.105 SURFACE TEMPERATURES OF FUEL RODS A22,B22,C22,D22 AT POSITION 1

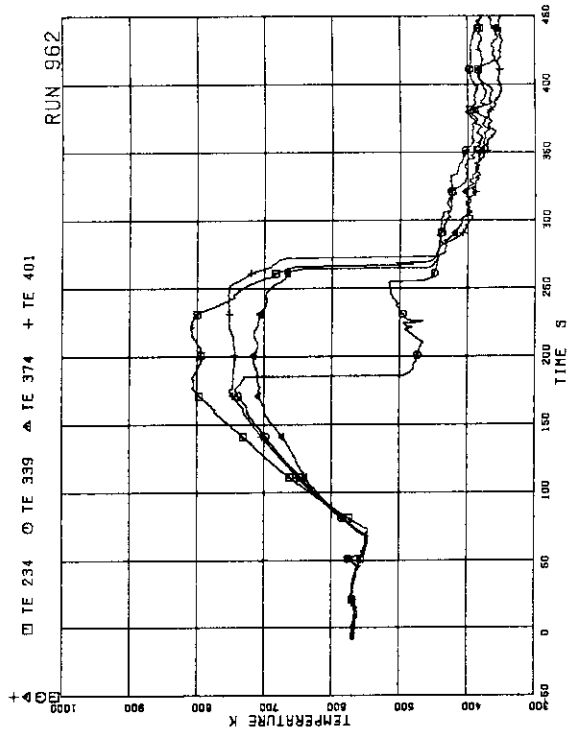

FIG.5.106 SURFACE TEMPERATURES OF FUEL RODS A22,B22,C22,D22 AT POSITION 2

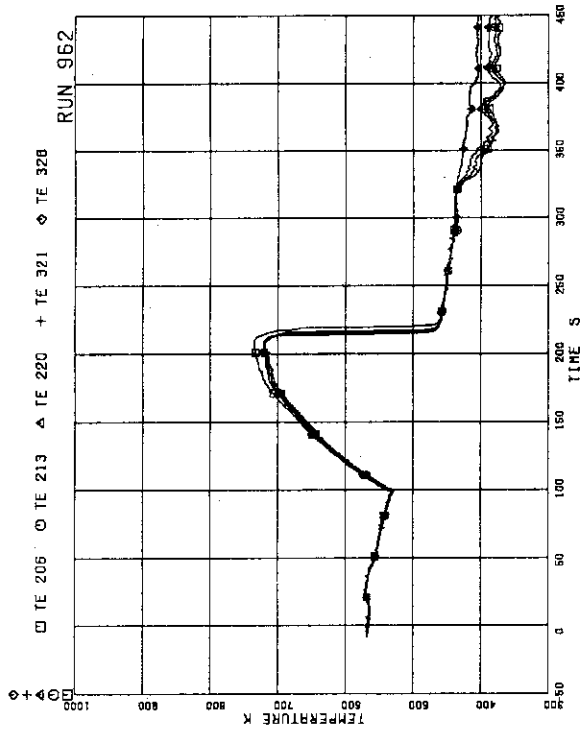

FIG.5.103 SURFACE TEMPERATURES OF FUEL RODS A11,A12,A13,A87,A88 AT POSITION 6

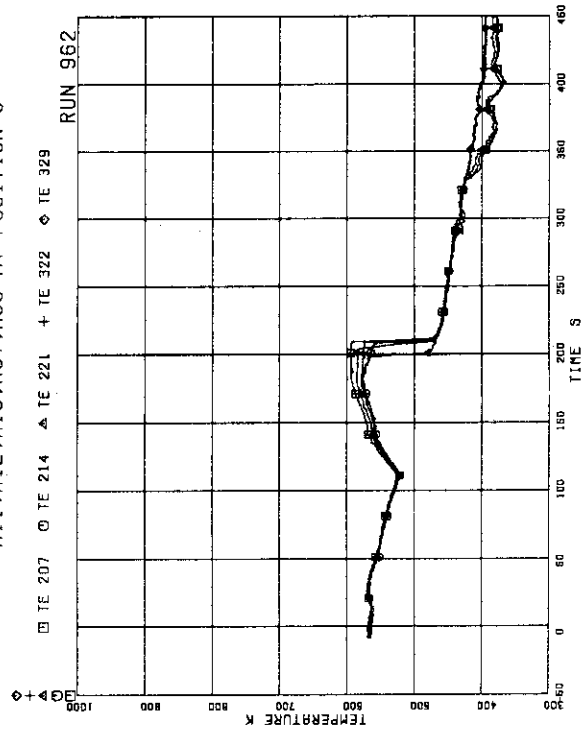

FIG.5.104 SURFACE TEMPERATURES OF FUEL RODS A11,A12,A13,A87,A88 AT POSITION 7

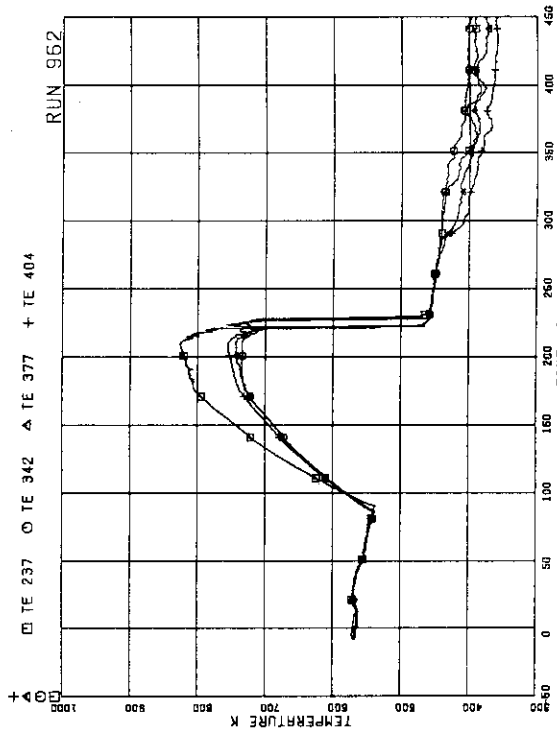

FIG.5.109 SURFACE TEMPERATURES OF FUEL RODS A22,B22,C22,D22 AT POSITION 5

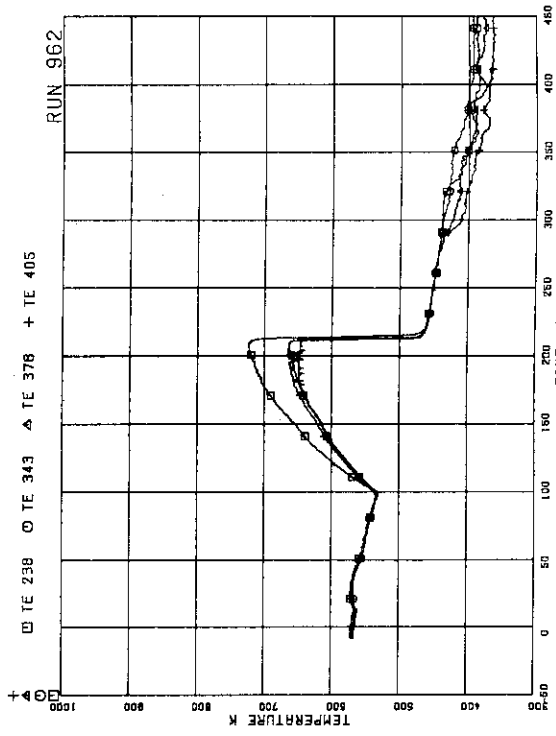

FIG.5.110 SURFACE TEMPERATURES OF FUEL RODS A22,B22,C22,D22 AT POSITION 6

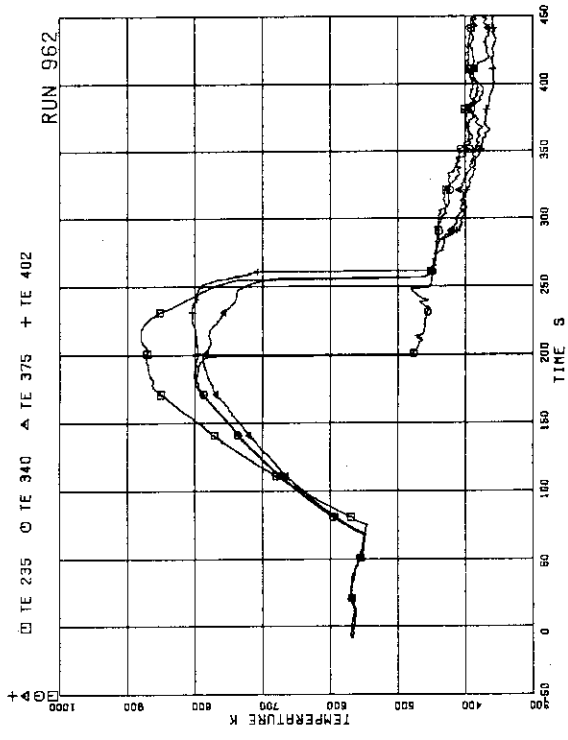

FIG.5.107 SURFACE TEMPERATURES OF FUEL RODS A22,B22,C22,D22 AT POSITION 3

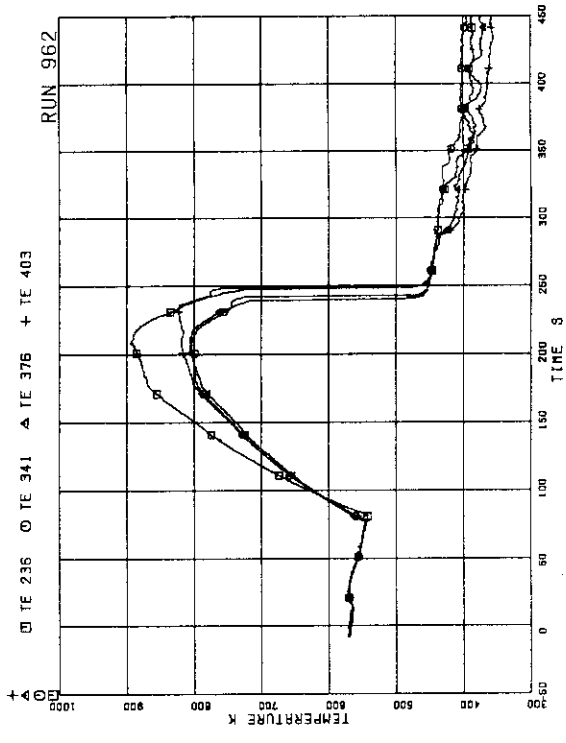

FIG.5.108 SURFACE TEMPERATURES OF FUEL RODS A22,B22,C22,D22 AT POSITION 4

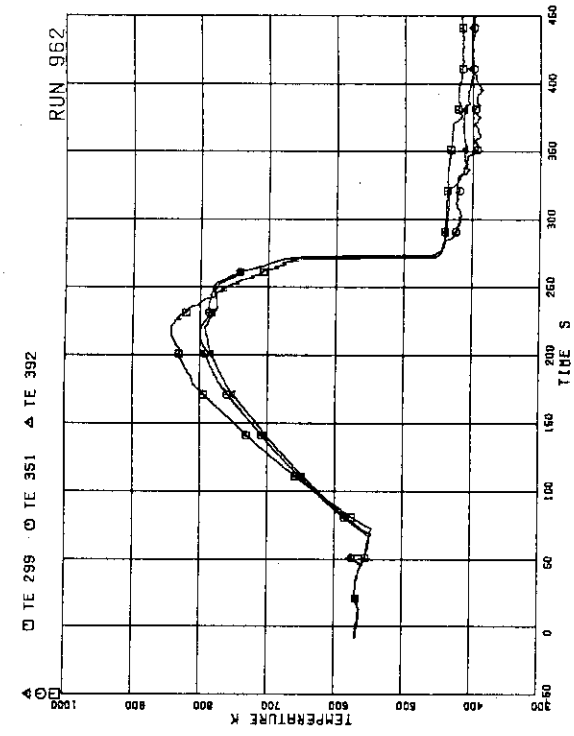

FIG.5.113 SURFACE TEMPERATURES OF FUEL RODS A77,B77,C77 AT POSITION 2

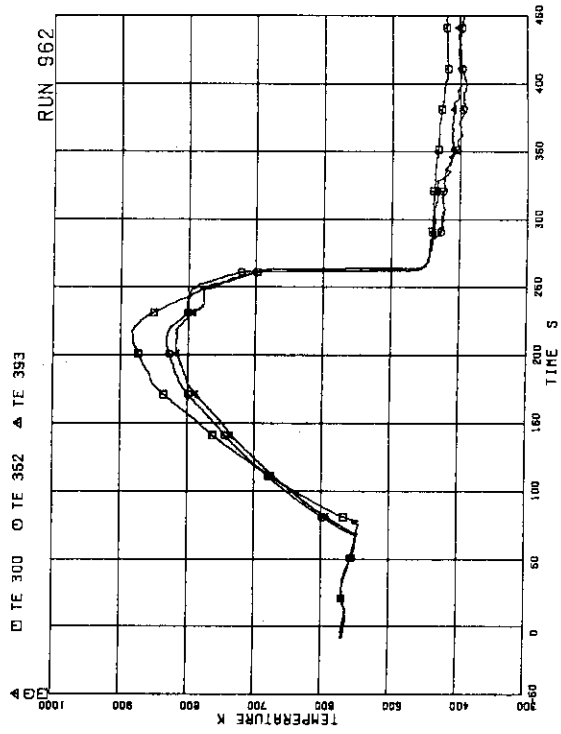

FIG.5.114 SURFACE TEMPERATURES OF FUEL RODS A77,B77,C77 AT POSITION 3

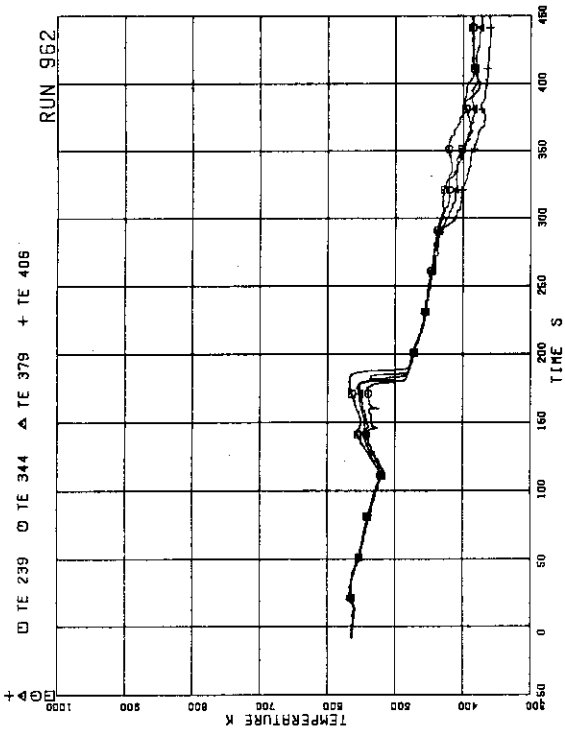

FIG.5.111 SURFACE TEMPERATURES OF FUEL RODS A22,B22,C22,D22 AT POSITION 7

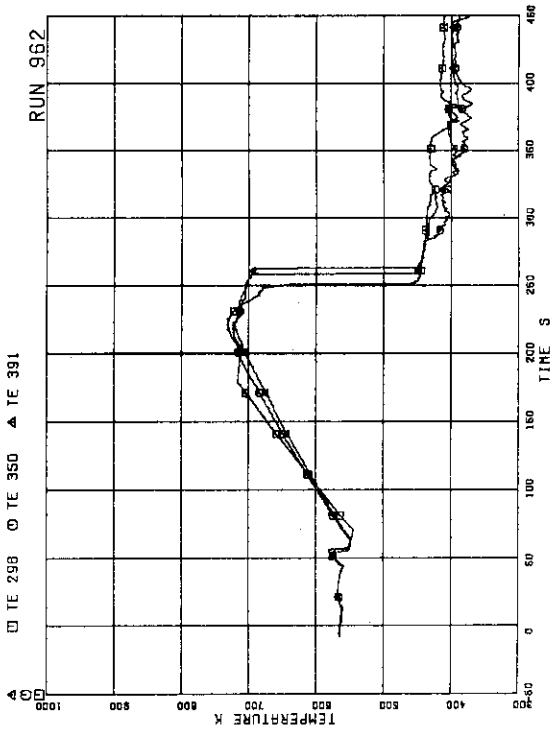

FIG.5.112 SURFACE TEMPERATURES OF FUEL RODS A77,B77,C77 AT POSITION 1

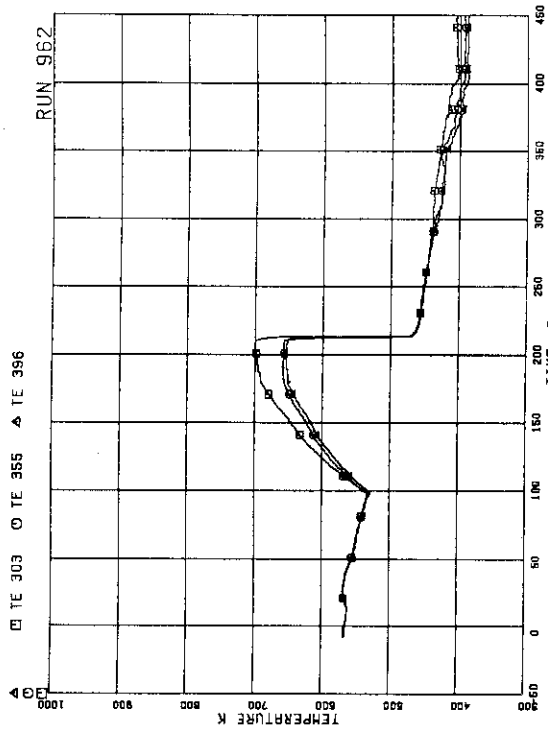

FIG.5.117 SURFACE TEMPERATURES OF FUEL RODS A77,B77,C77 AT POSITION 6

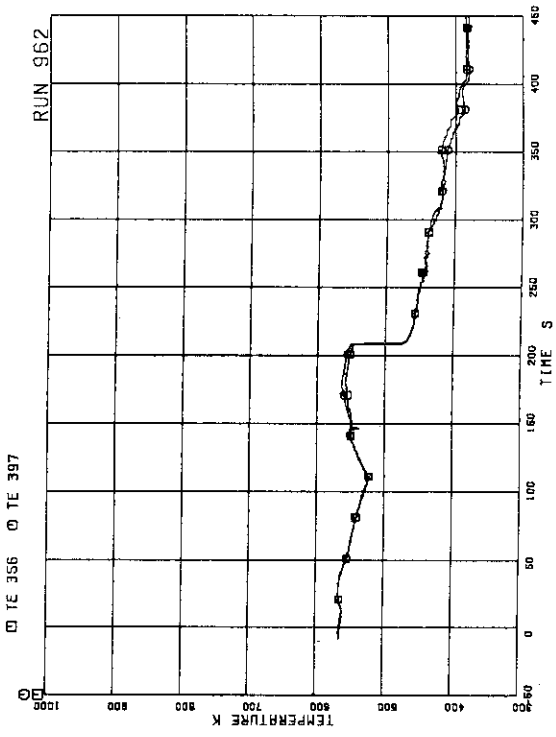

FIG.5.118 SURFACE TEMPERATURES OF FUEL RODS B77,C77 RODS AT POSITION 7

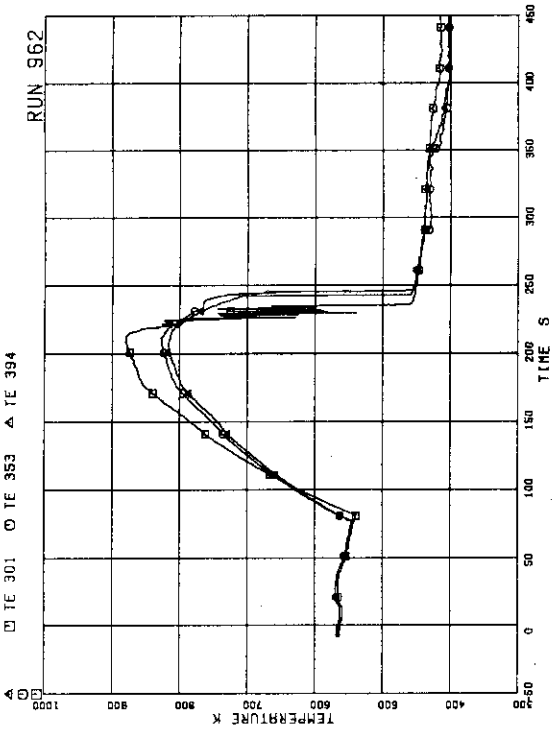

FIG.5.115 SURFACE TEMPERATURES OF FUEL RODS A77,B77,C77 AT POSITION 4

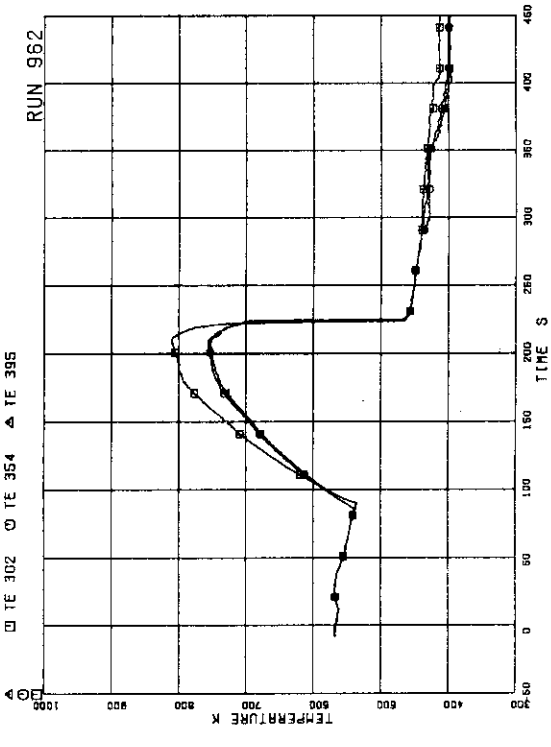

FIG.5.116 SURFACE TEMPERATURES OF FUEL RODS A77,B77,C77 AT POSITION 5

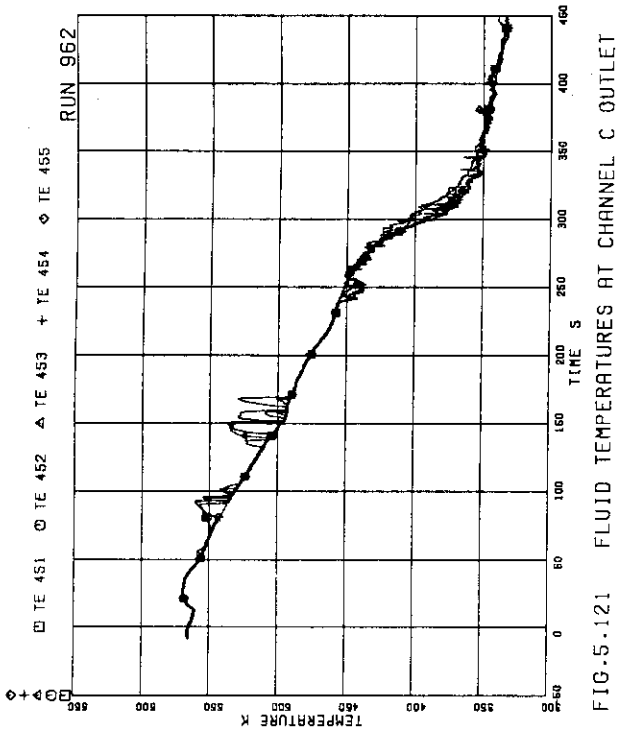

FIG.5.121 FLUID TEMPERATURES AT CHANNEL C OUTLET

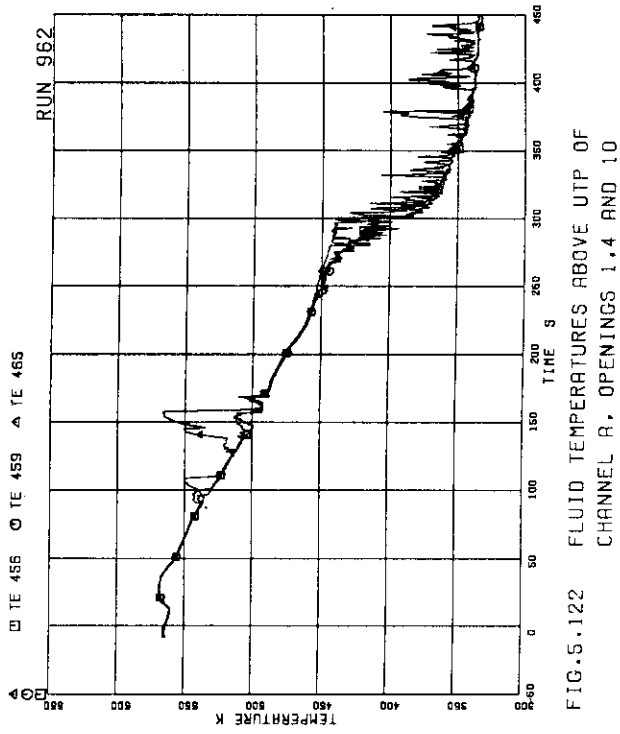

FIG.5.122 FLUID TEMPERATURES ABOVE UTP OF CHANNEL A, OPENINGS 1,4 AND 10

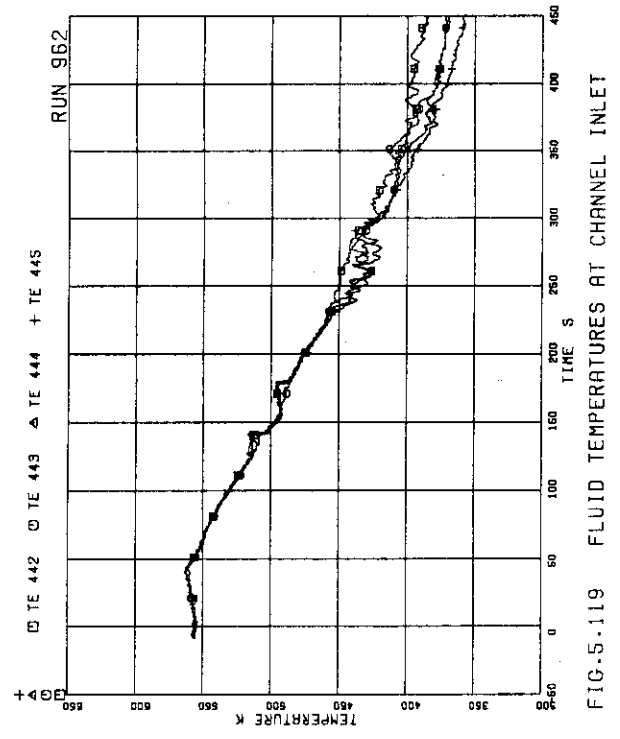

FIG.5.119 FLUID TEMPERATURES AT CHANNEL INLET

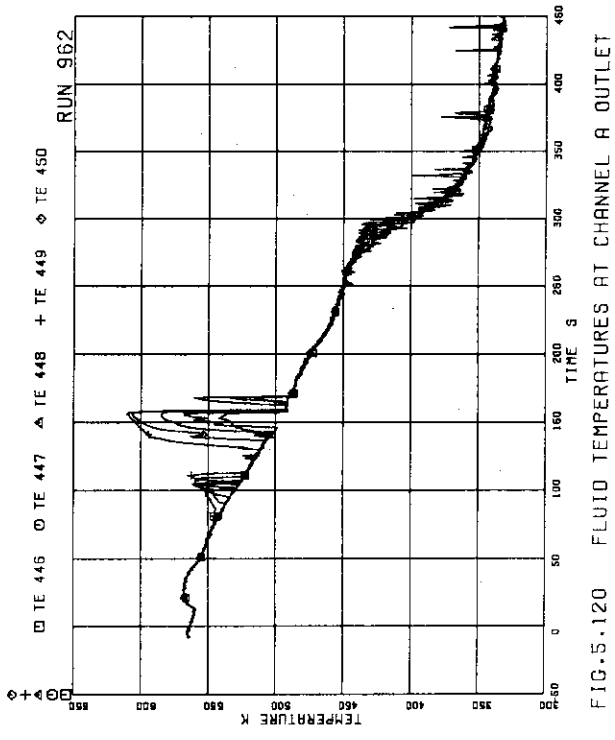

FIG.5.120 FLUID TEMPERATURES AT CHANNEL A OUTLET

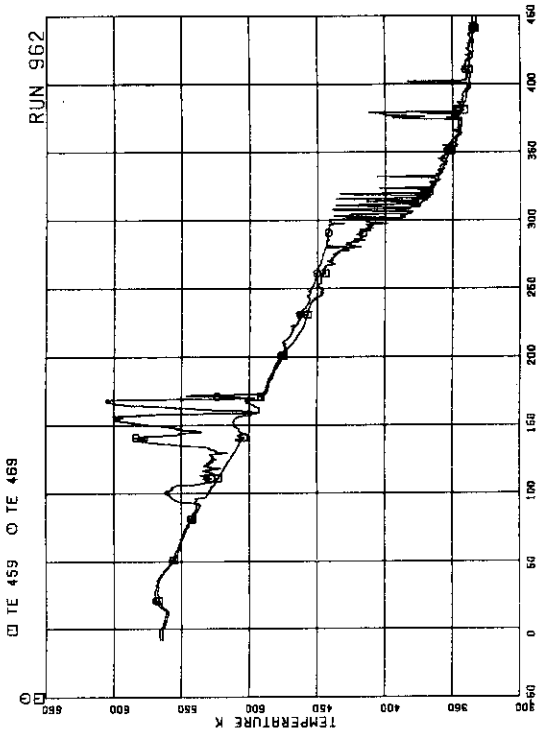

FIG.5.125 FLUID TEMPERATURES AT UTP IN CHANNEL A, OPENING 4

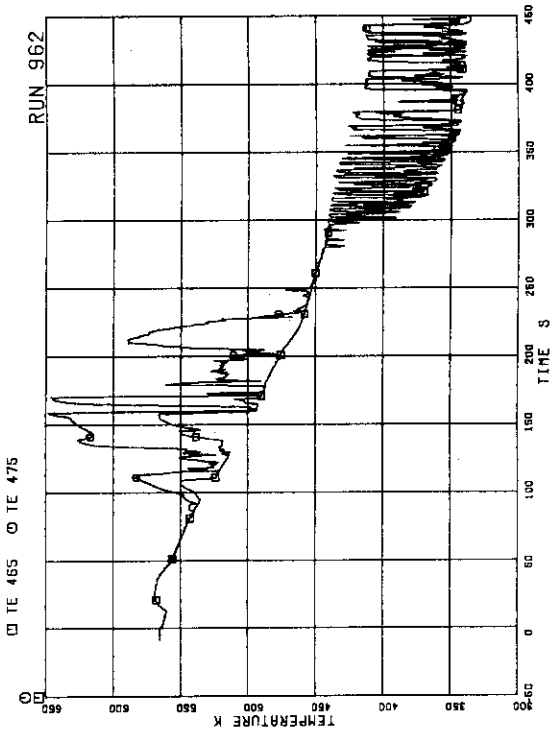

FIG.5.126 FLUID TEMPERATURES AT UTP IN CHANNEL A, OPENING 10

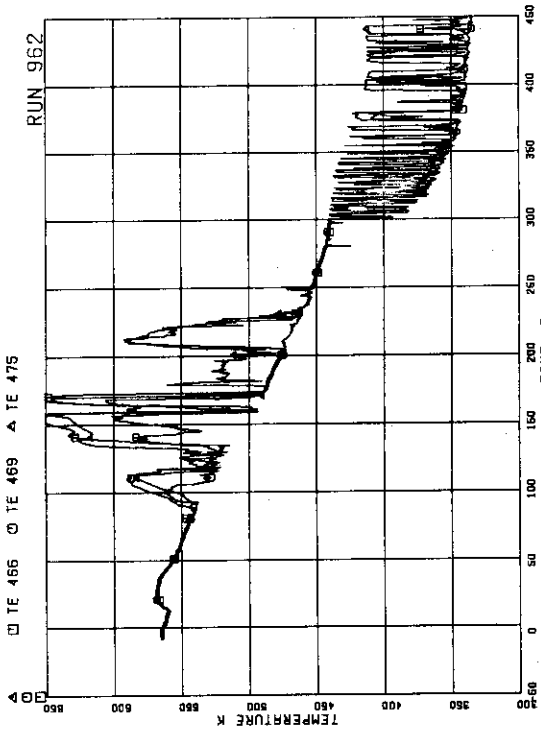

FIG.5.123 FLUID TEMPERATURES BELOW UTP OF CHANNEL A, OPENINGS 1,4 AND 10

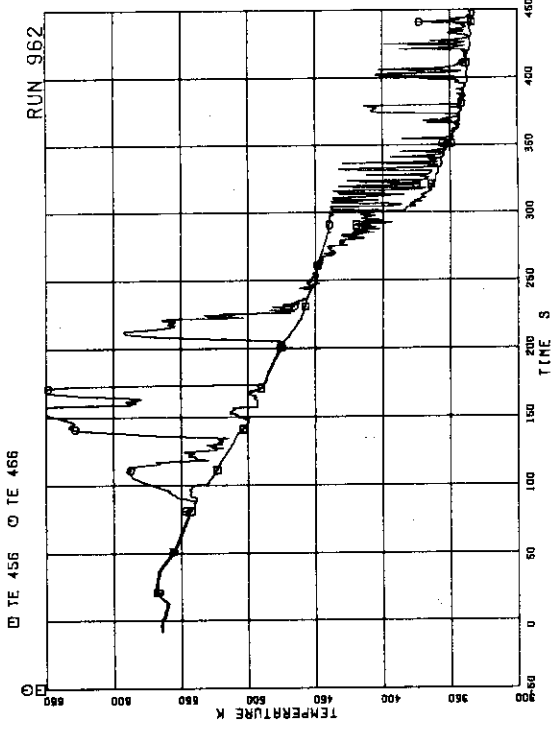

FIG.5.124 FLUID TEMPERATURES AT UTP IN CHANNEL A, OPENING 1

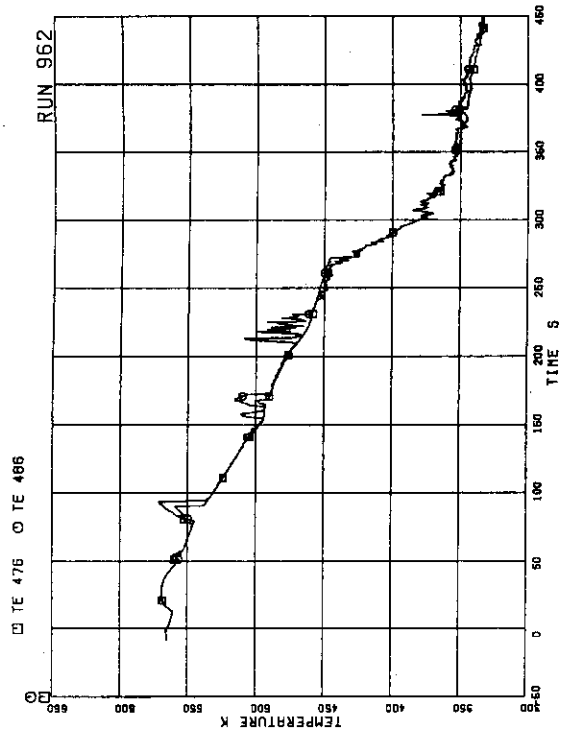

FIG.5.129 FLUID TEMPERATURES AT UTP IN CHANNEL C. OPENINGS 1

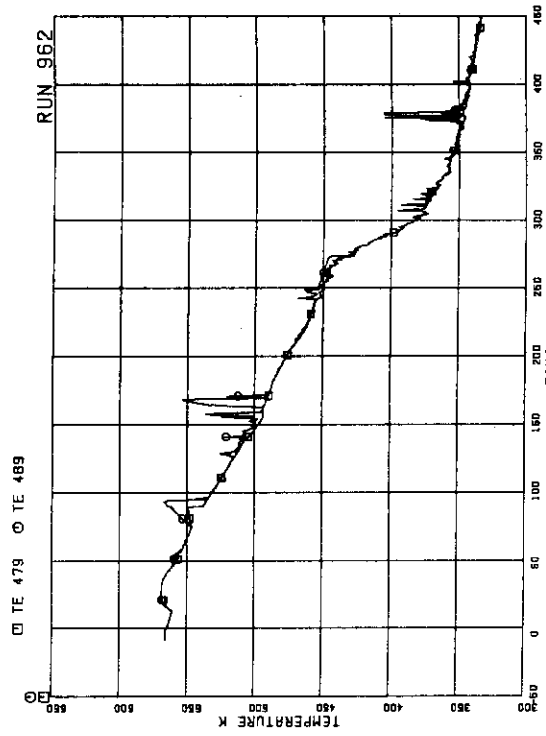

FIG.5.130 FLUID TEMPERATURES AT UTP IN CHANNEL C. OPENING 4

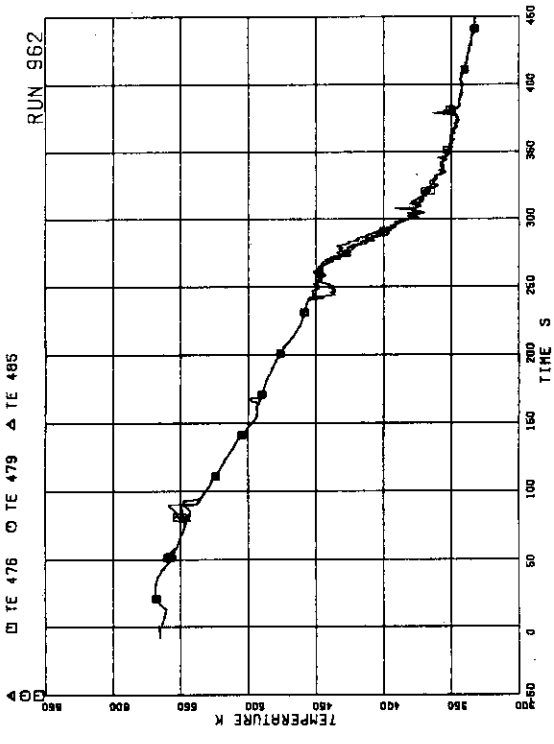

FIG.5.127 FLUID TEMPERATURES ABOVE UTP OF CHANNEL C. OPENINGS 1.4 AND 10

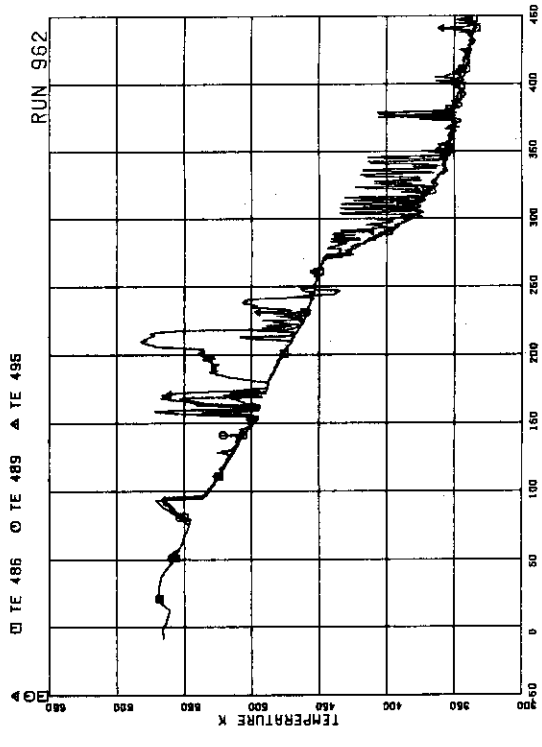

FIG.5.128 FLUID TEMPERATURES BELOW UTP OF CHANNEL C. OPENINGS 1.4 AND 10

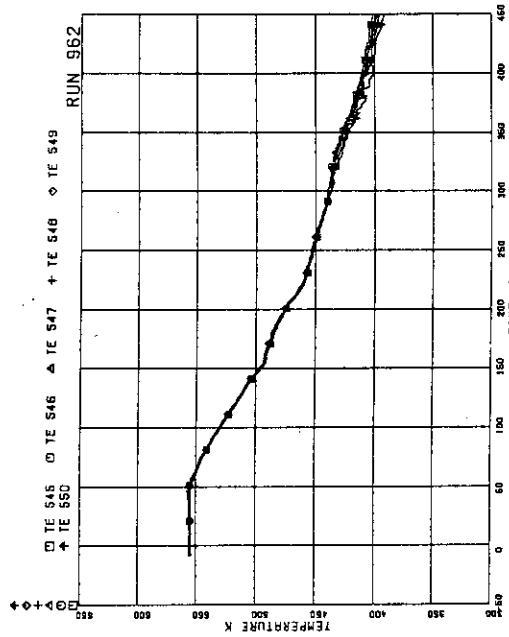

FIG.5.133 FLUID TEMPERATURES IN LOWER PLENUM, CENTER

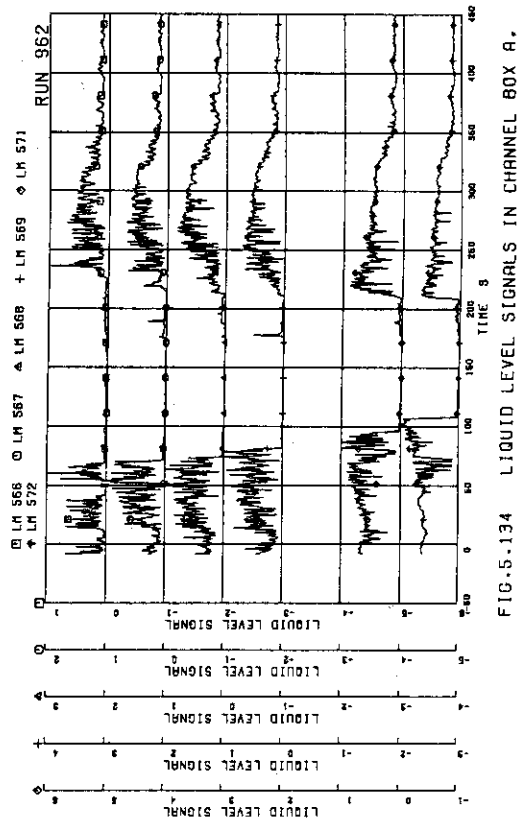

FIG.5.134 LIQUID LEVEL SIGNALS IN CHANNEL BOX A, LOCATION A2

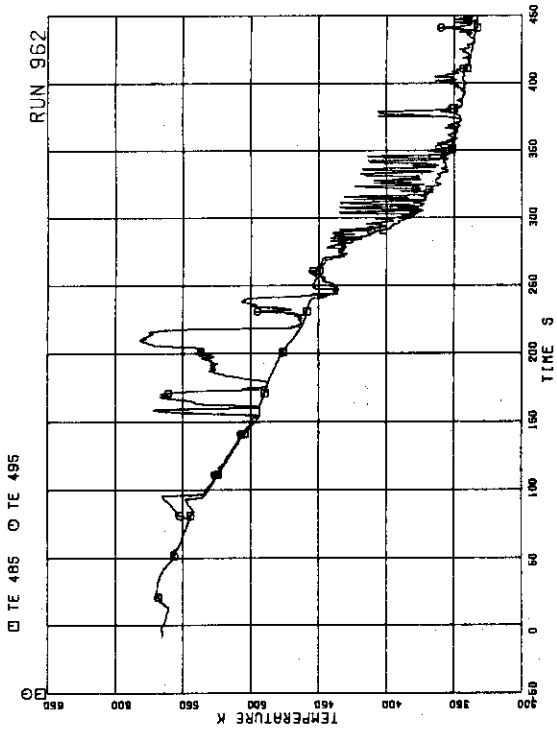

FIG.5.131 FLUID TEMPERATURES AT UTP IN CHANNEL C, OPENING 10

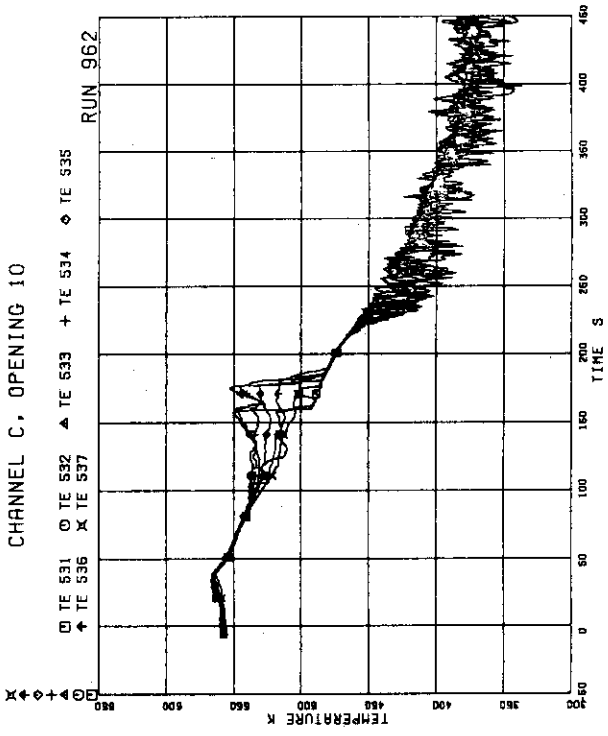

FIG.5.132 OUTER SURFACE TEMPERATURES OF CHANNEL BOX AT POS.1 THROUGH 7

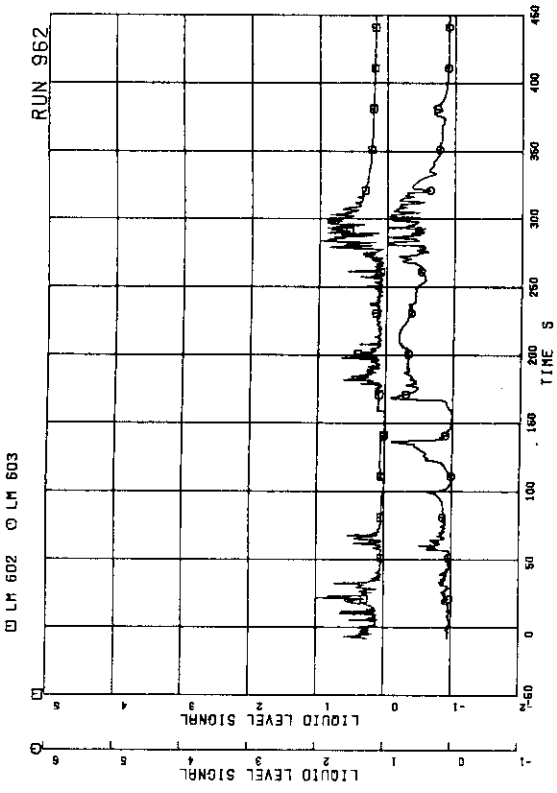

FIG.5.137 LIQUID LEVEL SIGNALS IN CHANNEL A OUTLET CENTER

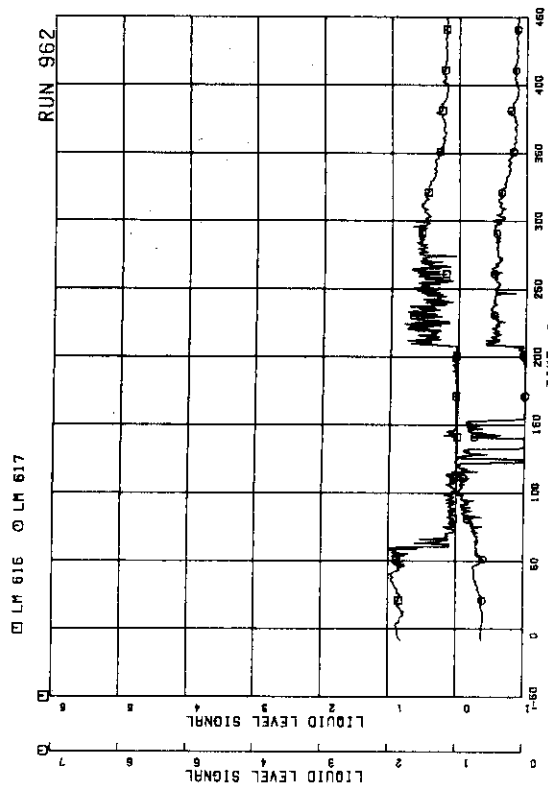

FIG.5.138 LIQUID LEVEL SIGNALS IN CHANNEL A INLET

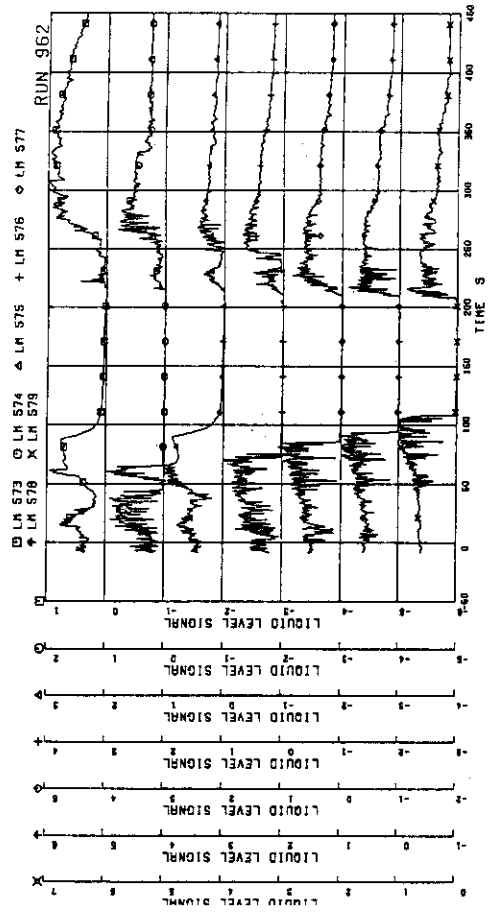

FIG.5.135 LIQUID LEVEL SIGNALS IN CHANNEL BOX B

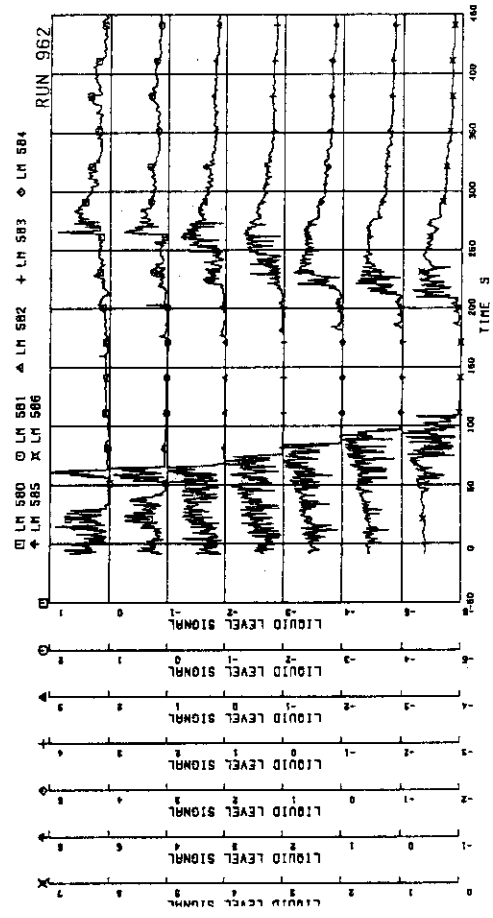

FIG.5.136 LIQUID LEVEL SIGNALS IN CHANNEL BOX C

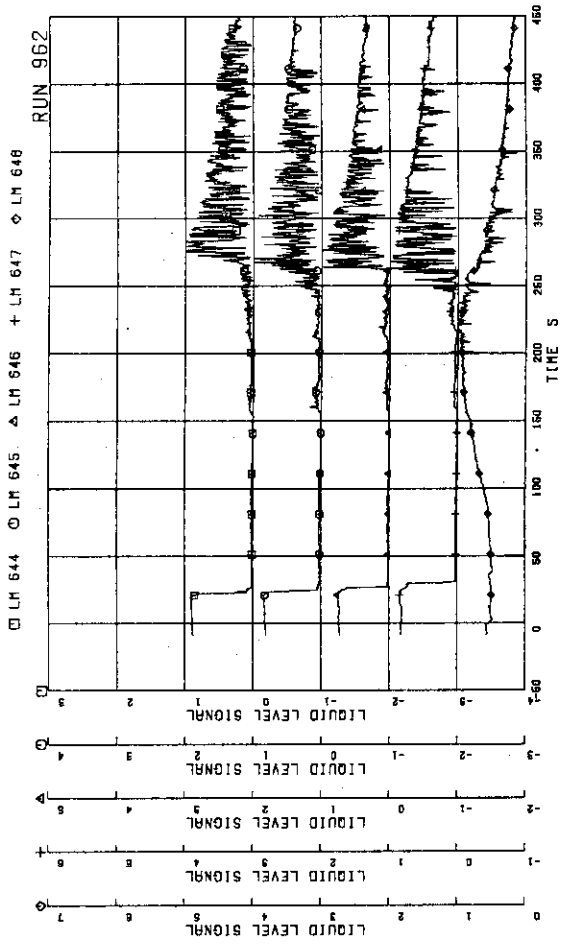

FIG.5.141 LIQUID LEVEL SIGNALS IN DOWNCOMER, D SIDE

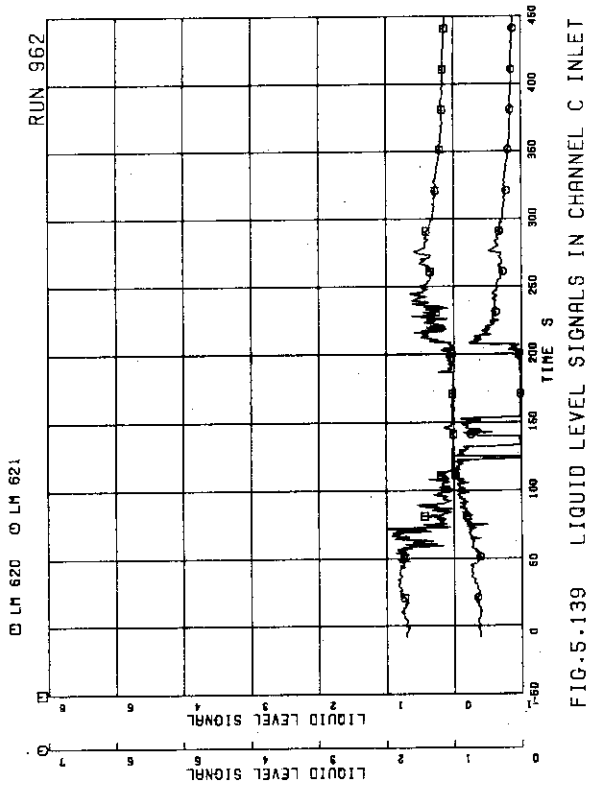

FIG.5.139 LIQUID LEVEL SIGNALS IN CHANNEL C INLET

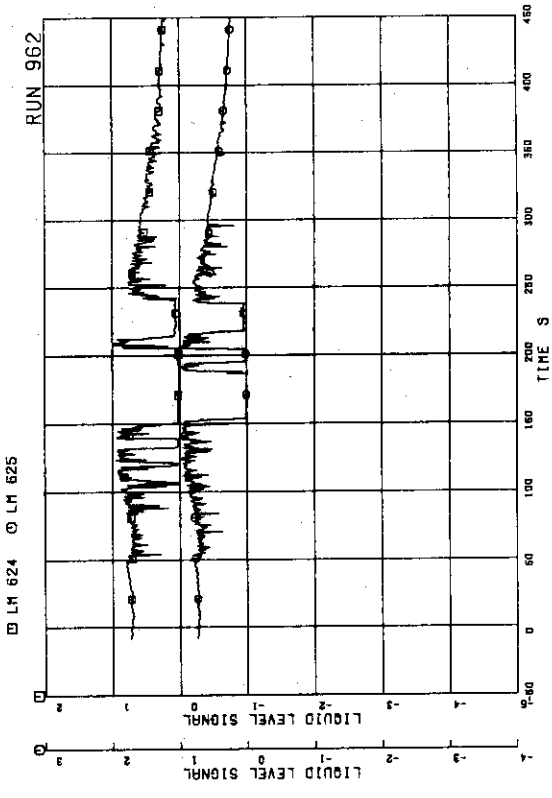

FIG.5.140 LIQUID LEVEL SIGNALS IN LOWER PLENUM, NORTH

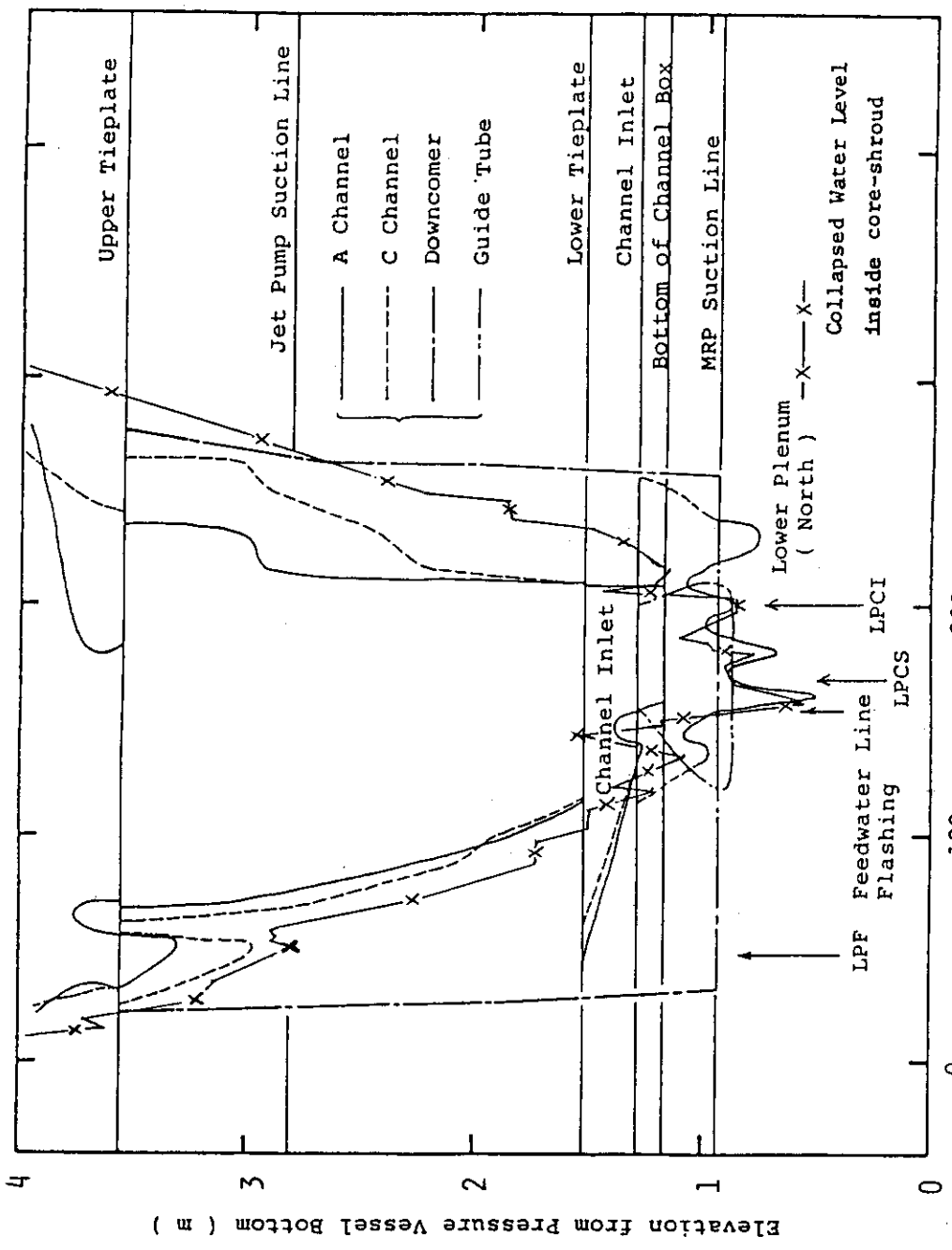

Fig. 5.142 Estimated liquid levels in pressure vessel

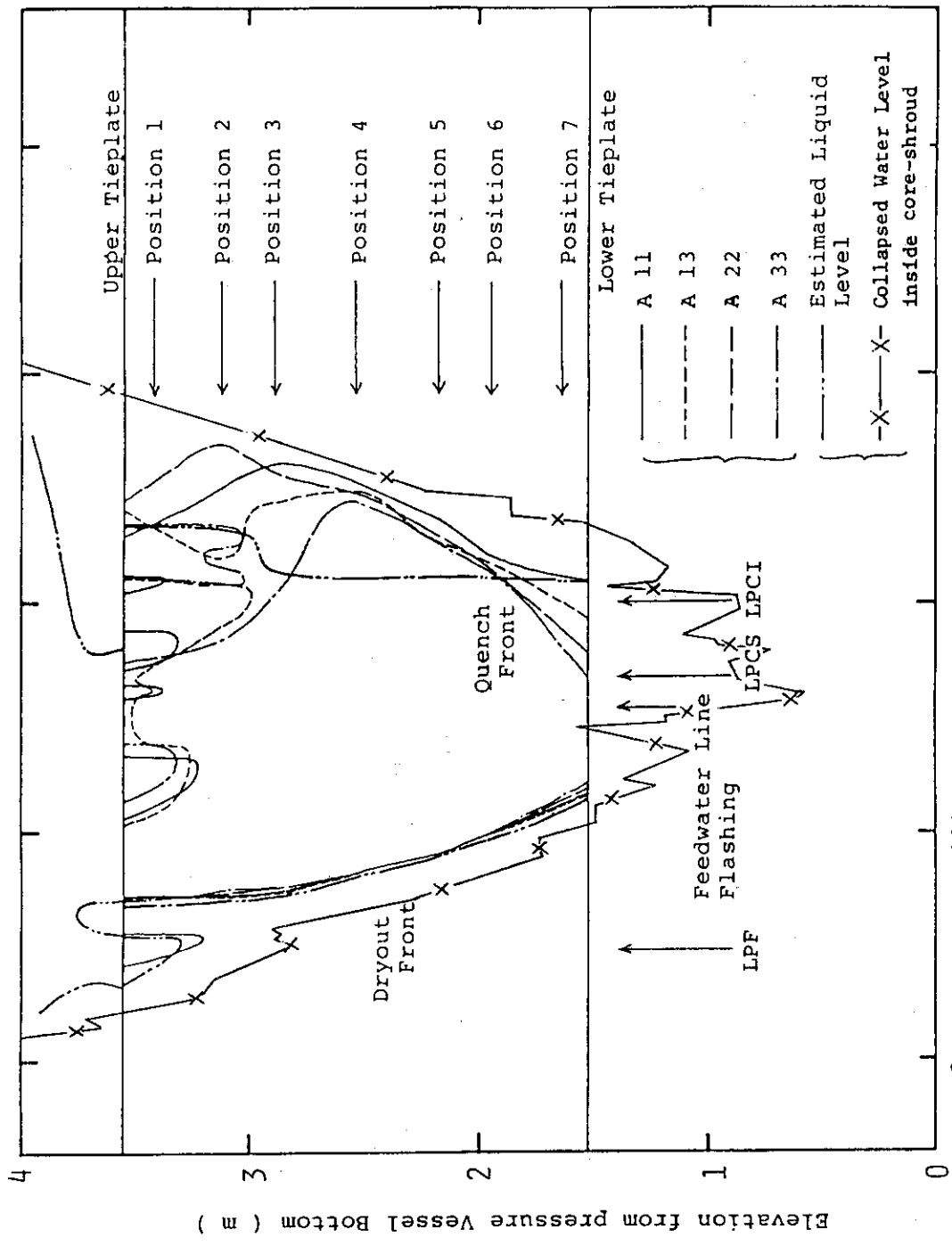

Fig. 5.143 Dryout and quench times of fuel rods in bundle A

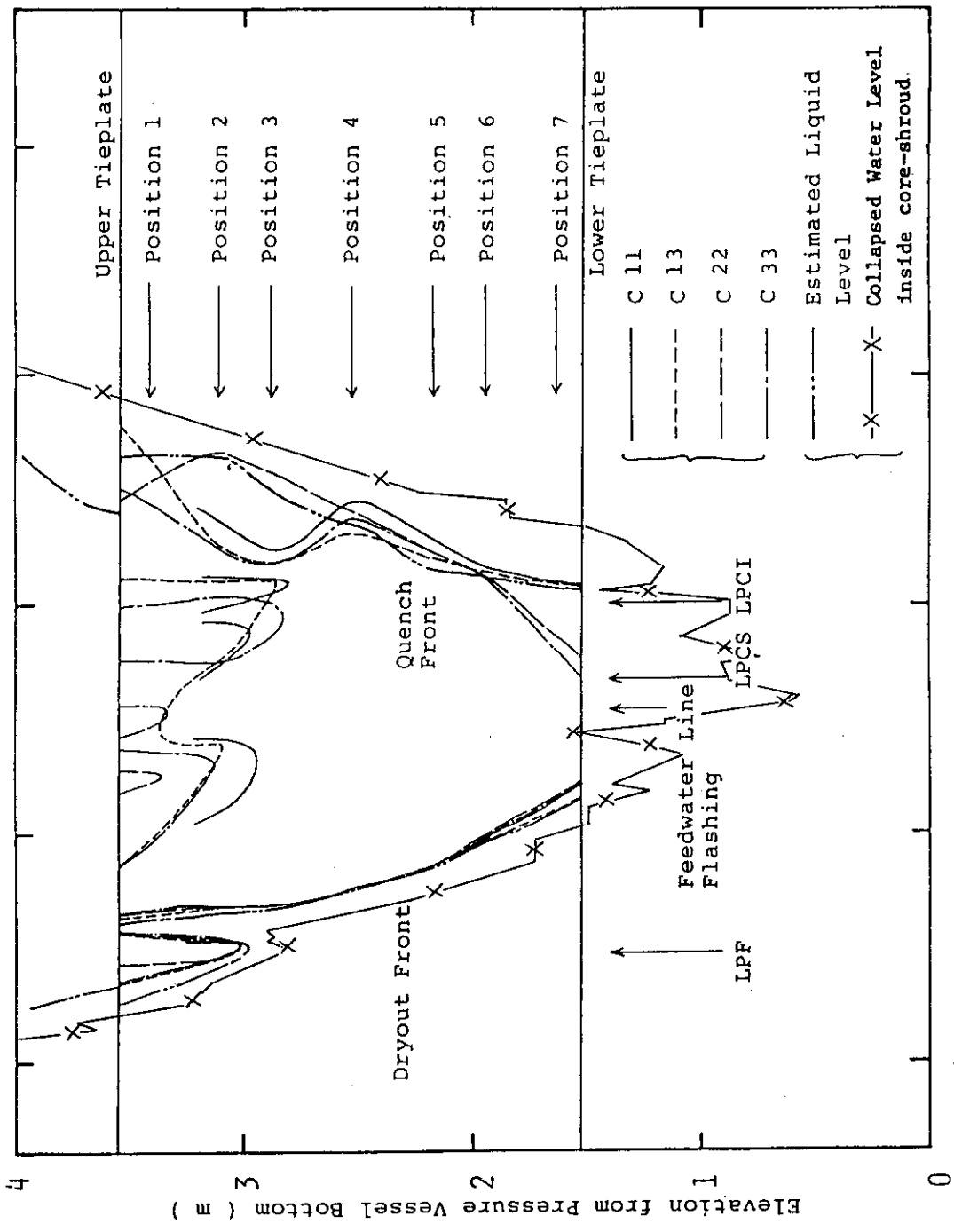

Fig. 5.144 Dryout and quench times of fuel rods in bundle C

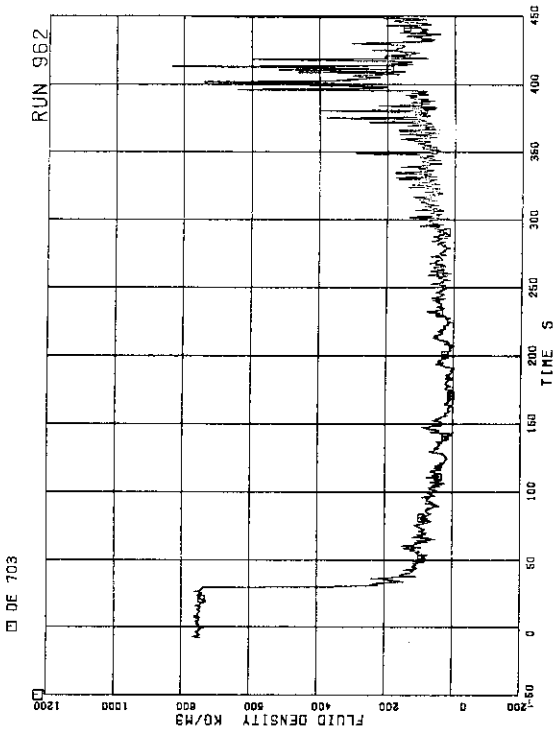

FIG.5.147 AVERAGE DENSITY AT JP SIDE OF BREAK

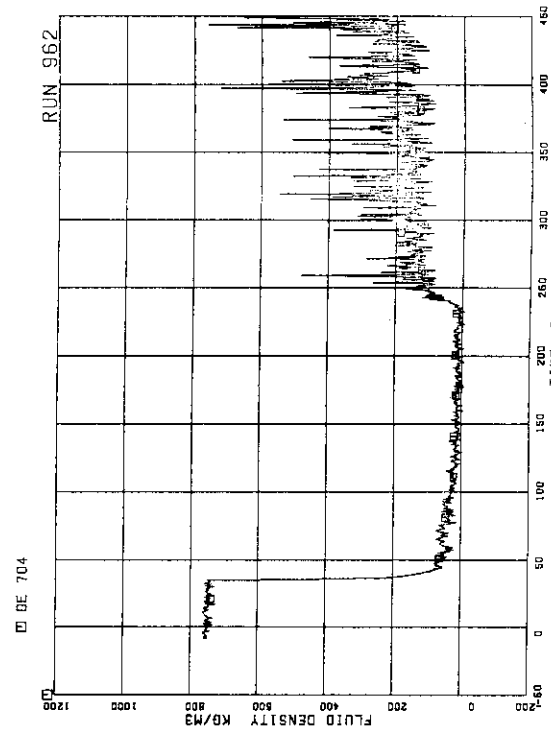

FIG.5.148 AVERAGE DENSITY AT MRP SIDE OF BREAK

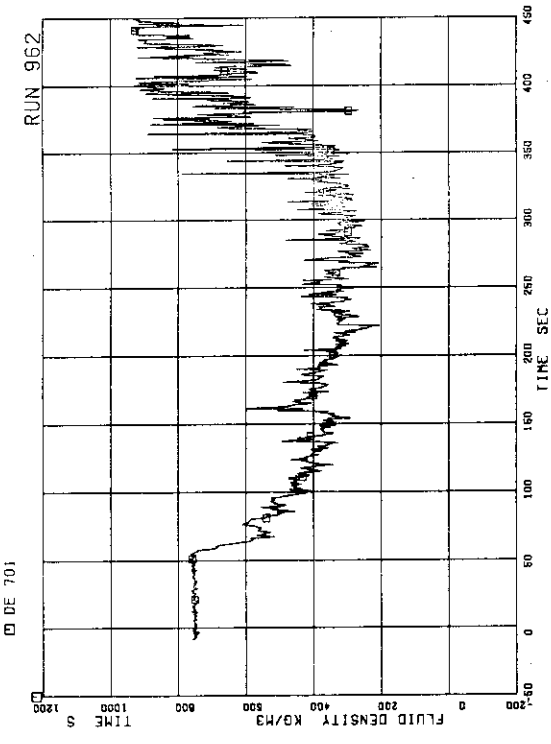

FIG.5.145 AVERAGE DENSITY AT JP-1,2 OUTLET

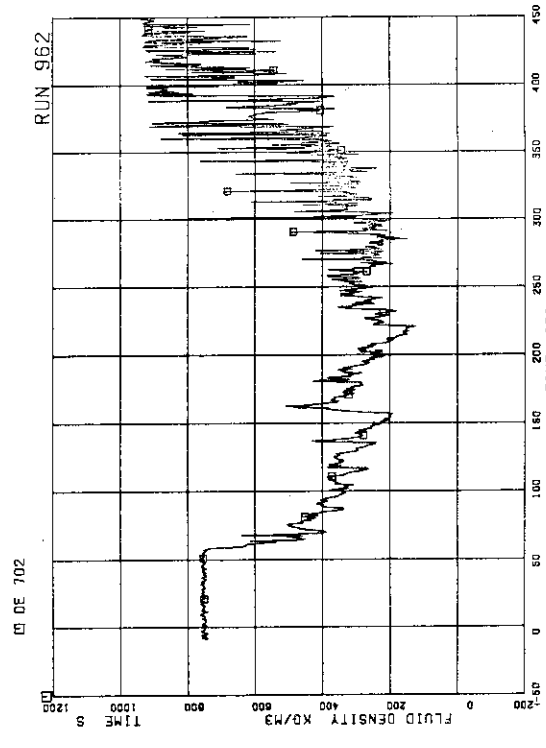

FIG.5.146 AVERAGE DENSITY AT JP-3,4 OUTLET

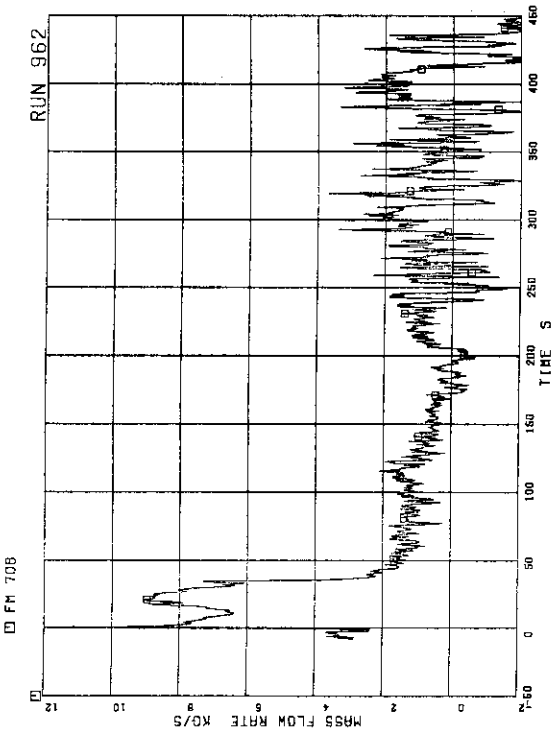

FIG.5.151 FLOW RATE AT MRP SIDE OF BREAK
(BASED ON HIGH RANGE DRAG DISK DATA)

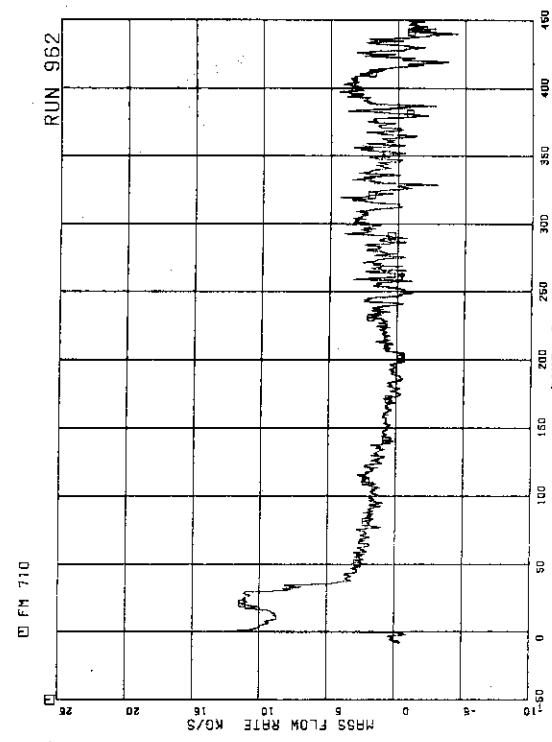

FIG.5.152 TOTAL DISCHARGE FLOW RATE FROM BREAK
(BASED ON HIGH RANGE DRAG DISK DATA)

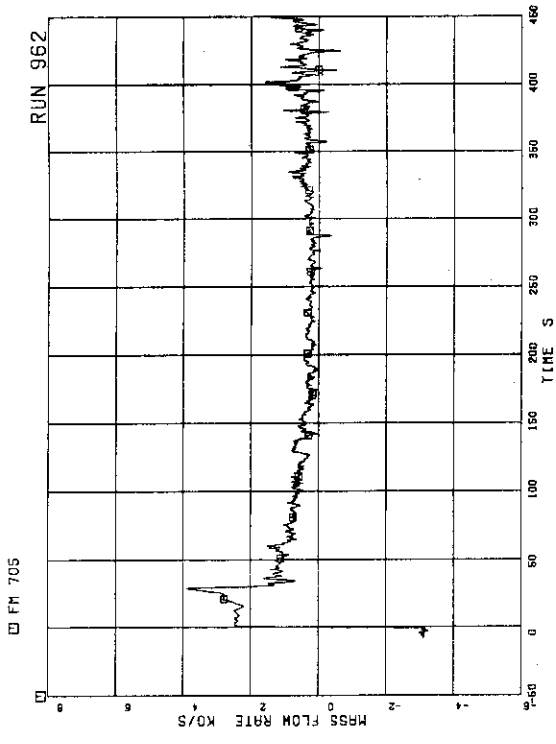

FIG.5.149 FLOW RATE AT JP SIDE OF BREAK
(BASED ON LOW RANGE DRAG DISK DATA)

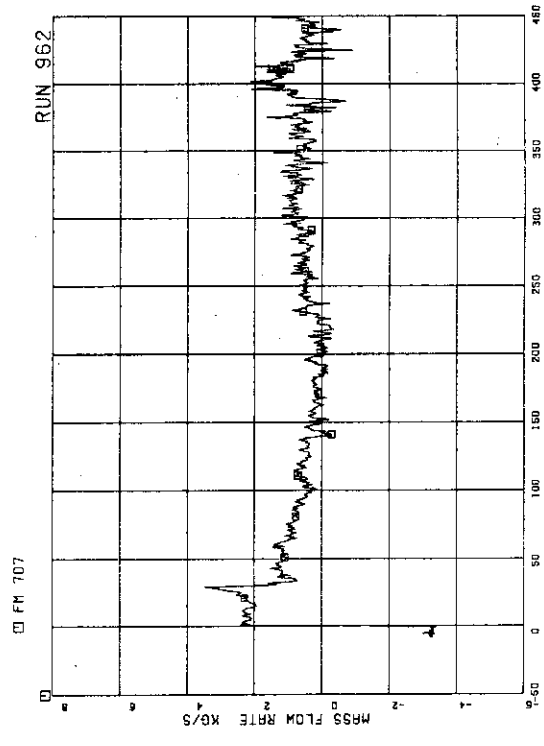

FIG.5.150 FLOW RATE AT JP SIDE OF BREAK
(BASED ON HIGH RANGE DRAG DISK DATA)

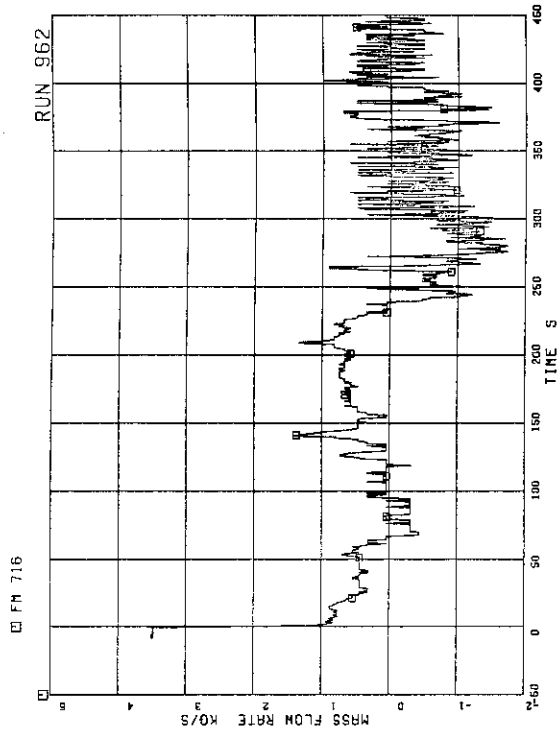

FIG.5.155 MASS FLOW RATE AT CHANNEL C INLET

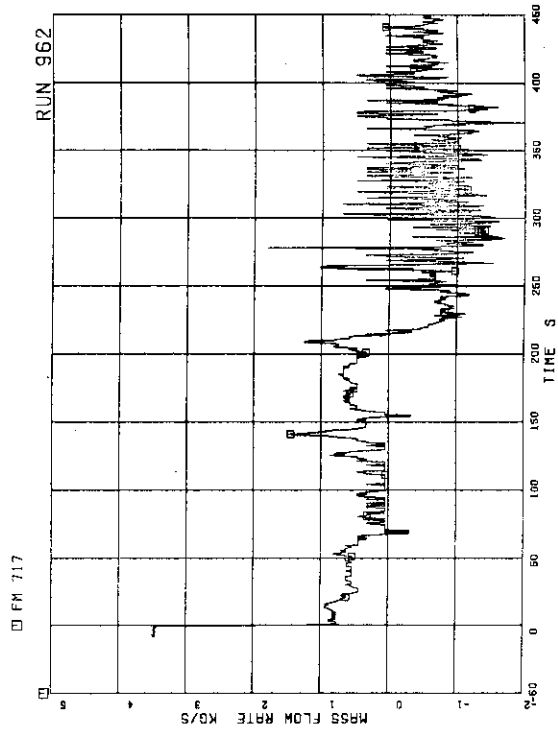

FIG.5.156 MASS FLOW RATE AT CHANNEL D INLET

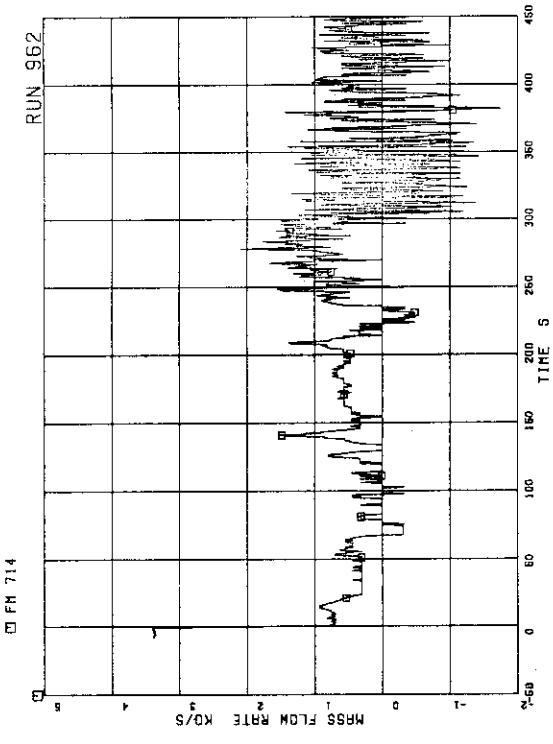

FIG.5.153 MASS FLOW RATE AT CHANNEL A INLET

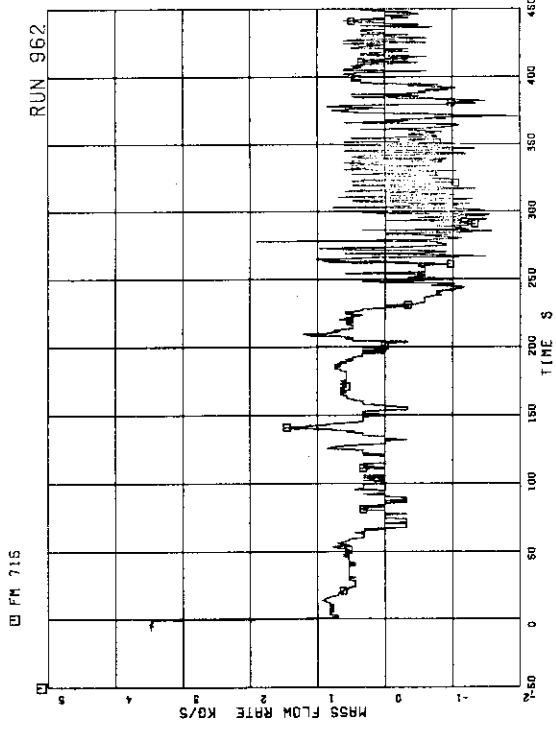

FIG.5.154 MASS FLOW RATE AT CHANNEL B INLET

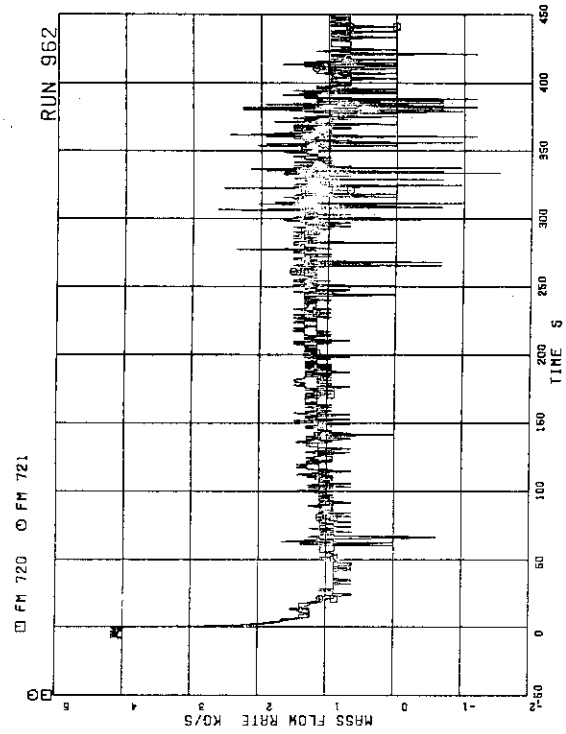

FIG.5.159 MASS FLOW RATE AT JP-1,2 OUTLET (POS.FLOW)

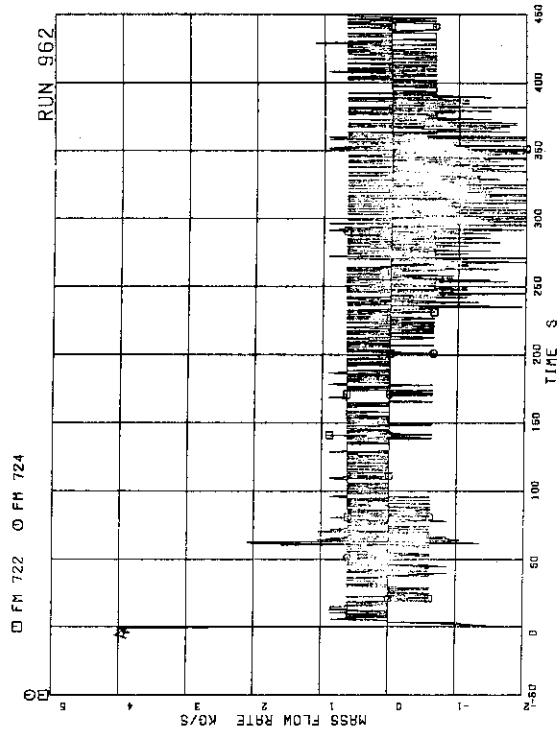

FIG.5.160 MASS FLOW RATE AT JP-3,4 OUTLET (POS.FLOW)

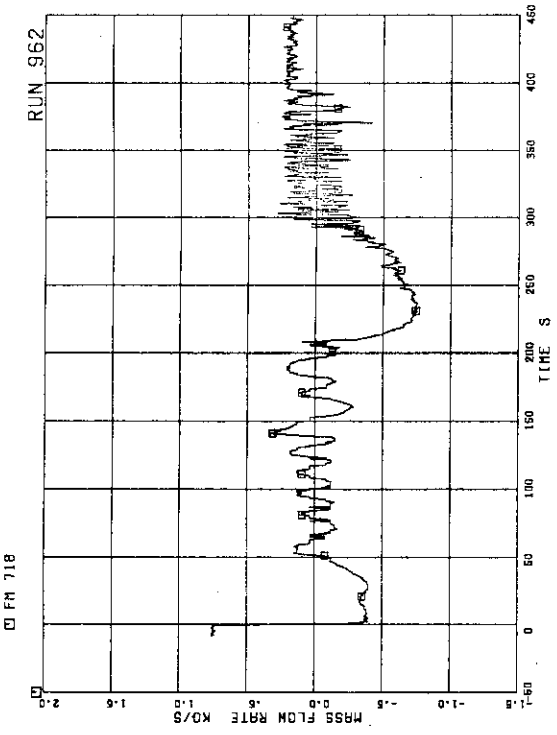

FIG.5.157 MASS FLOW RATE AT BYPASS HOLE

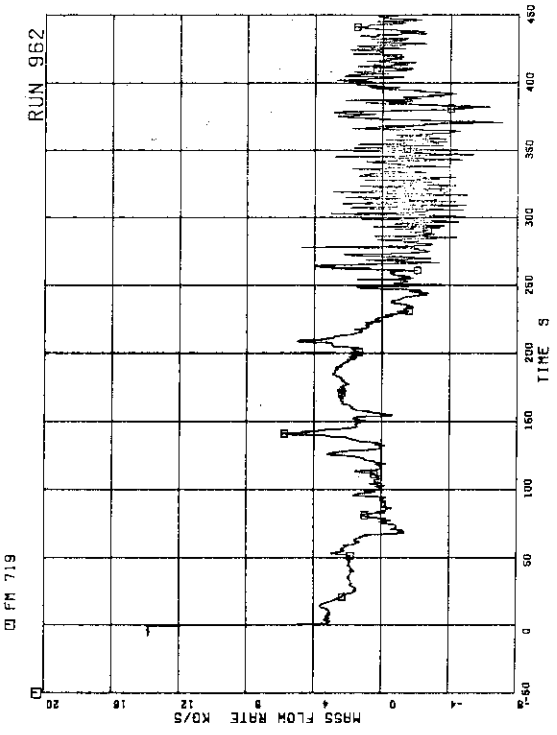

FIG.5.158 TOTAL CHANNEL INLET FLOW RATE

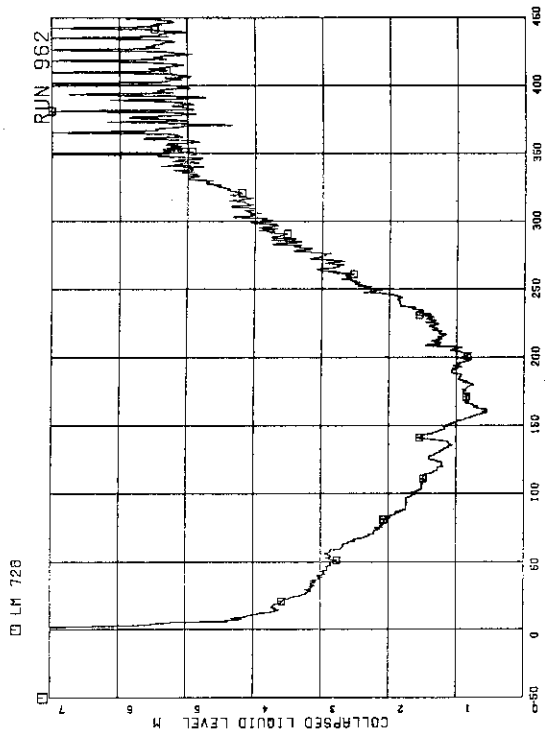

FIG.5.163 COLLAPSED LIQUID LEVEL INSIDE CORE SHROUD

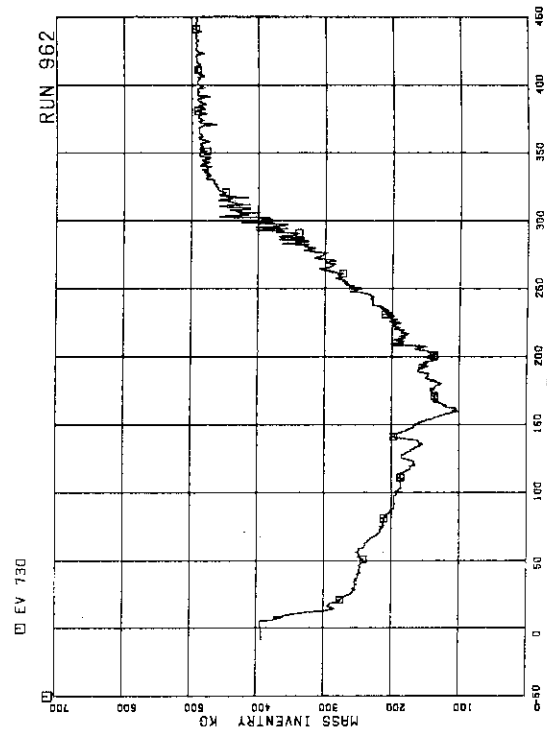

FIG.5.164 FLUID INVENTORY INSIDE CORE SHROUD

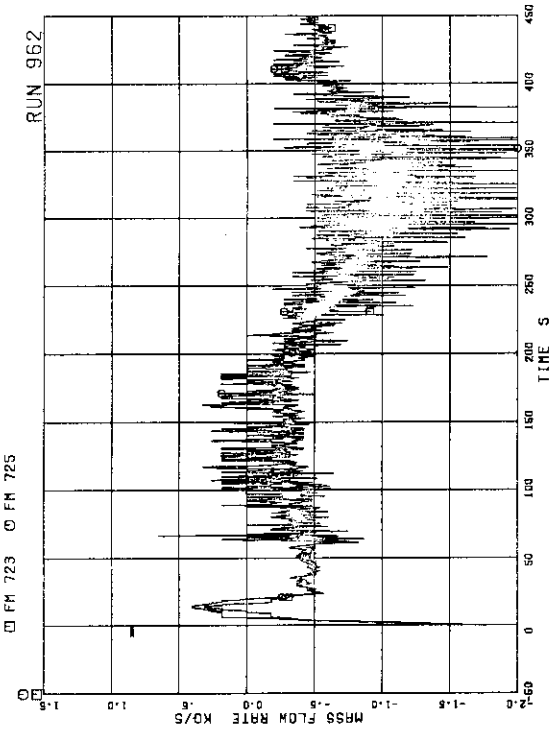

FIG.5.161 MASS FLOW RATE AT JP-3.4 OUTLET (NEG.FLOW)

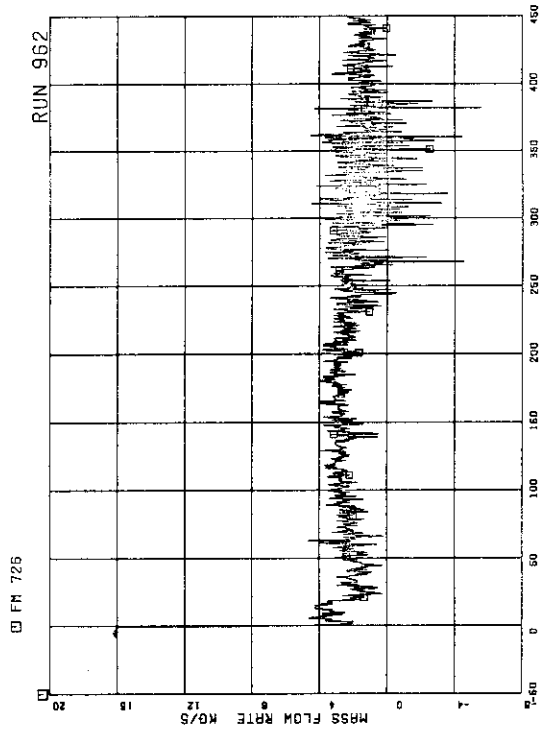

FIG.5.162 TOTAL JP OUTLET FLOW RATE (POS.FLOW)

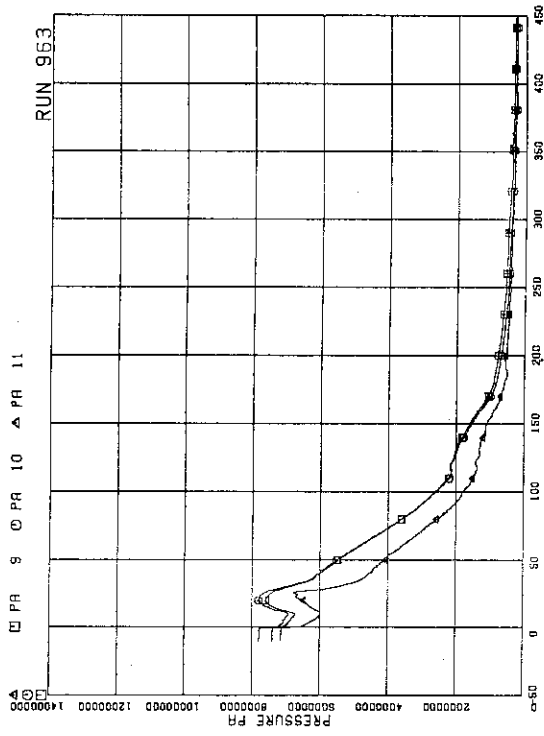

FIG.5.167 PRESSURE NEAR MRP (MAIN RECIRCULATION PUMP)

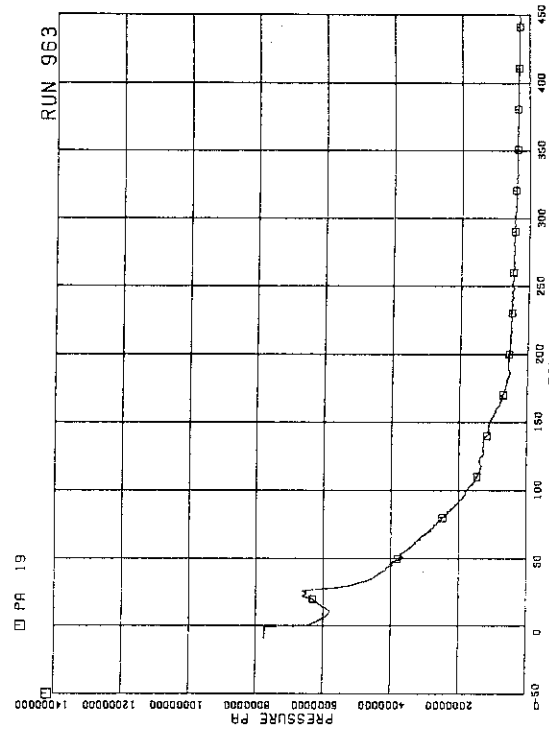

FIG.5.168 PRESSURE AT BREAK A SPOOL

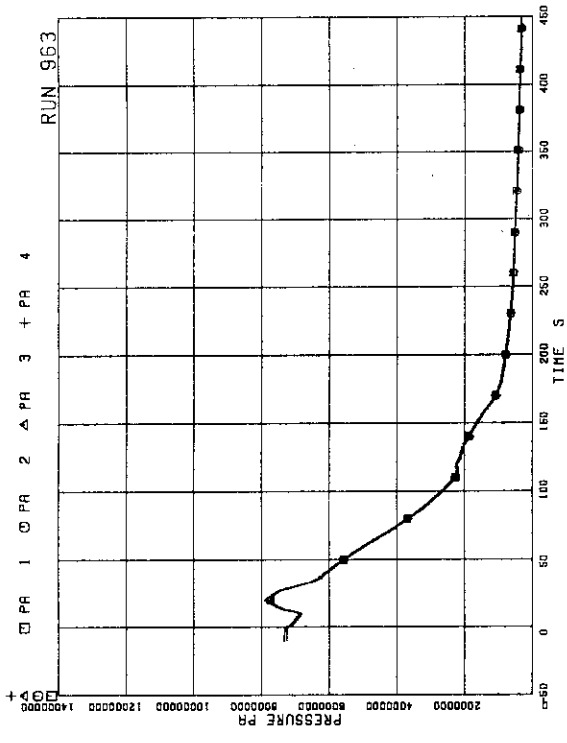

FIG.5.165 PRESSURE IN PV (PRESSURE VESSEL)

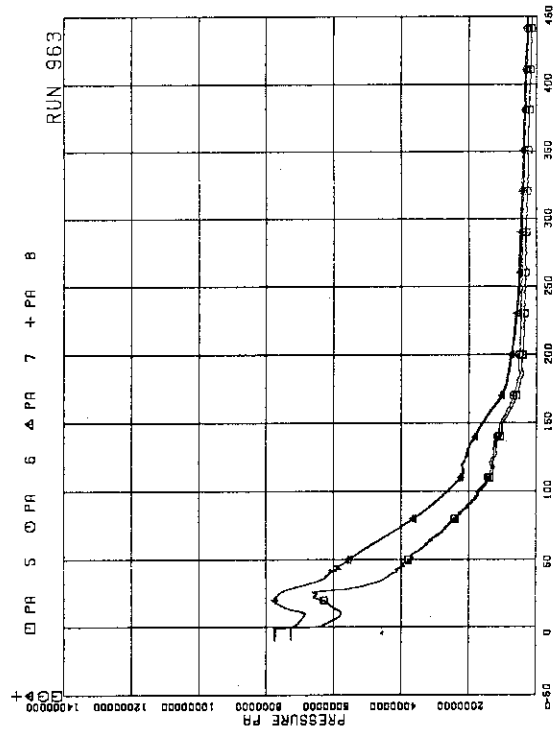

FIG.5.166 PRESSURE IN BROKEN LOOP JP (JET PUMP)

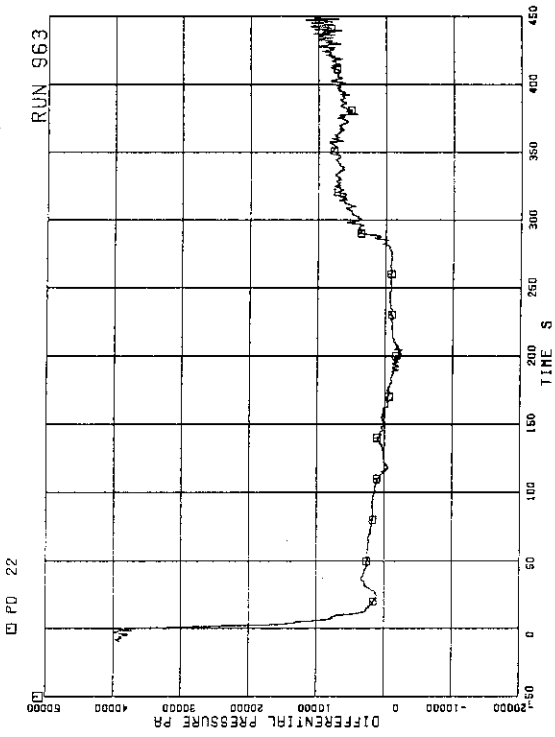

FIG.5.171 DIFFERENTIAL PRESSURE BETWEEN UPPER PLENUM AND STEAM DOME

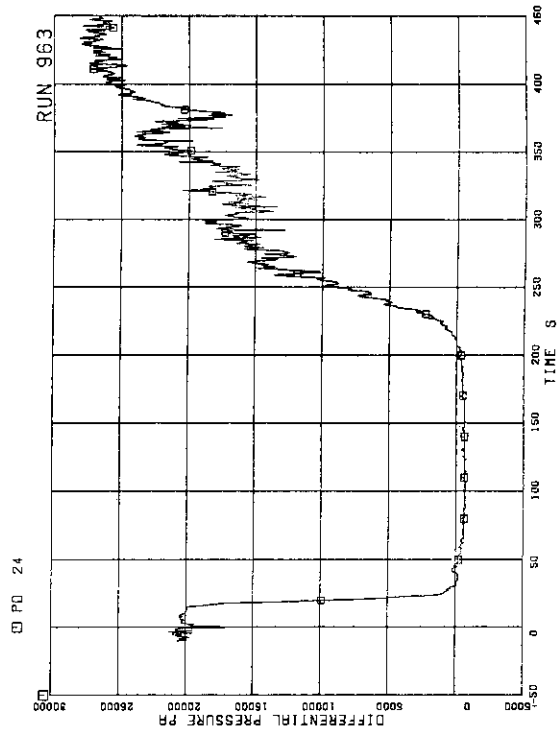

FIG.5.172 DC (DOWNCOMER) HEAD

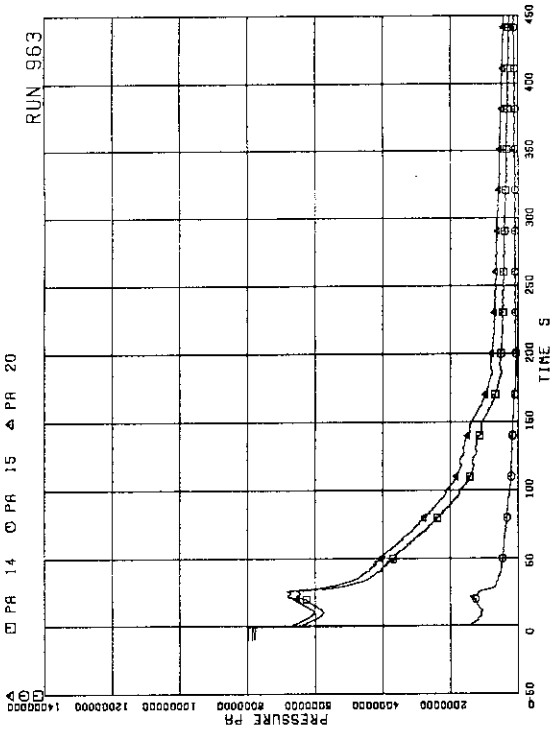

FIG.5.169 PRESSURE AT PV SIDE OF BREAK

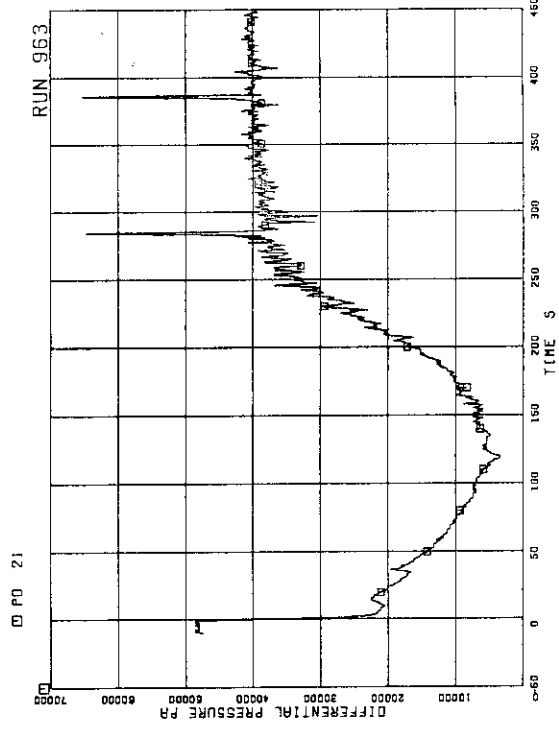

FIG.5.170 DIFFERENTIAL PRESSURE BETWEEN LOWER PLENUM AND UPPER PLENUM

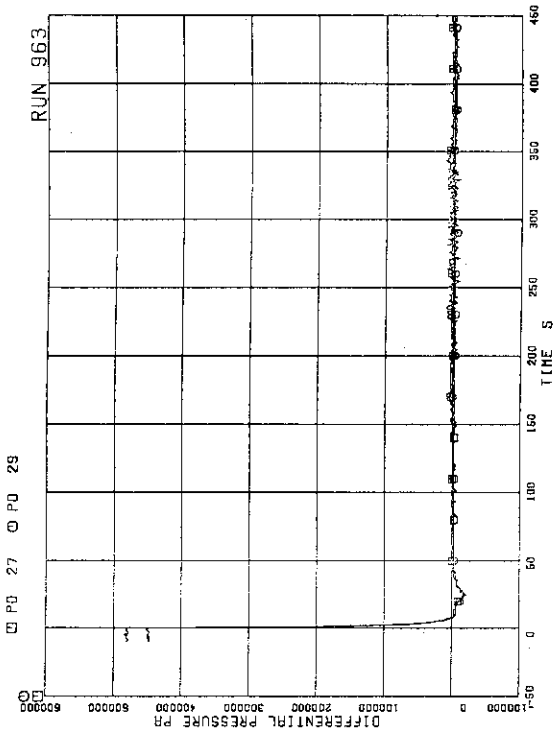

FIG.5.175 DIFFERENTIAL PRESSURE BETWEEN JP-1,2 DRIVE AND SUCTION

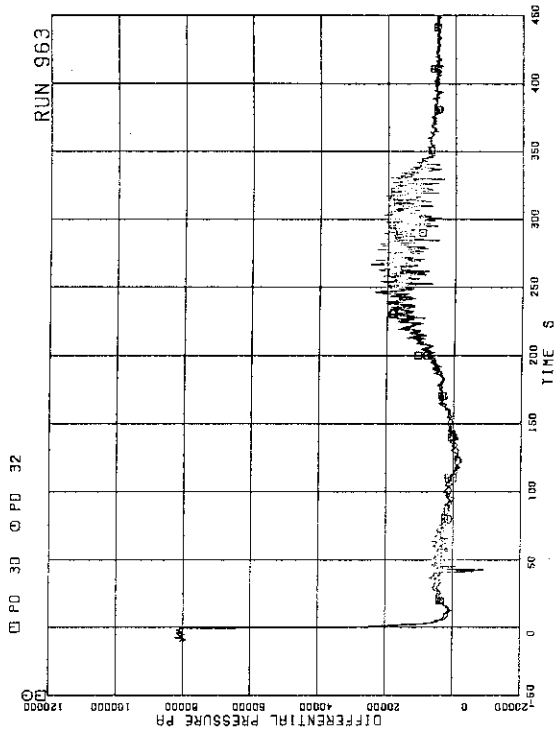

FIG.5.176 DIFFERENTIAL PRESSURE BETWEEN JP-3,4 DISCHARGE AND SUCTION

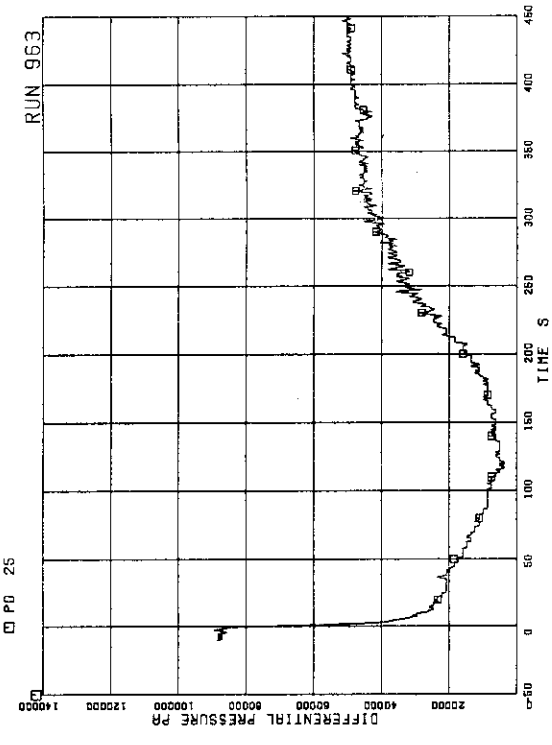

FIG.5.173 DIFFERENTIAL PRESSURE BETWEEN PV BOTTOM AND TOP

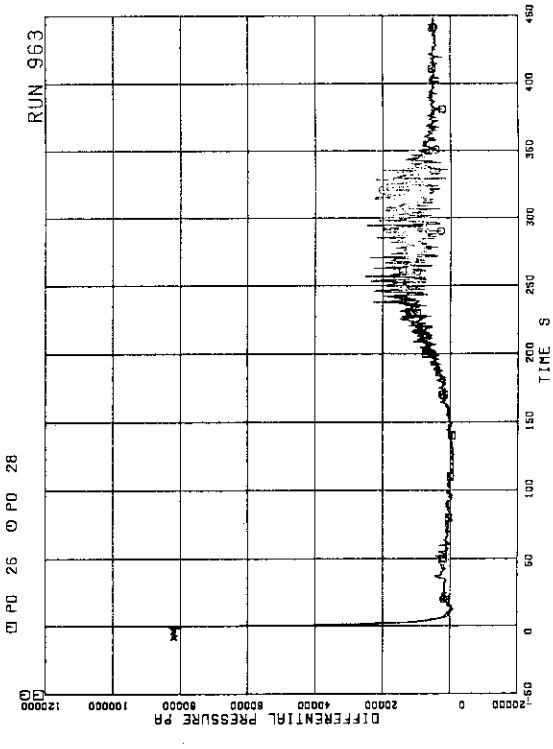

FIG.5.174 DIFFERENTIAL PRESSURE BETWEEN JP-1,2 DISCHARGE AND SUCTION

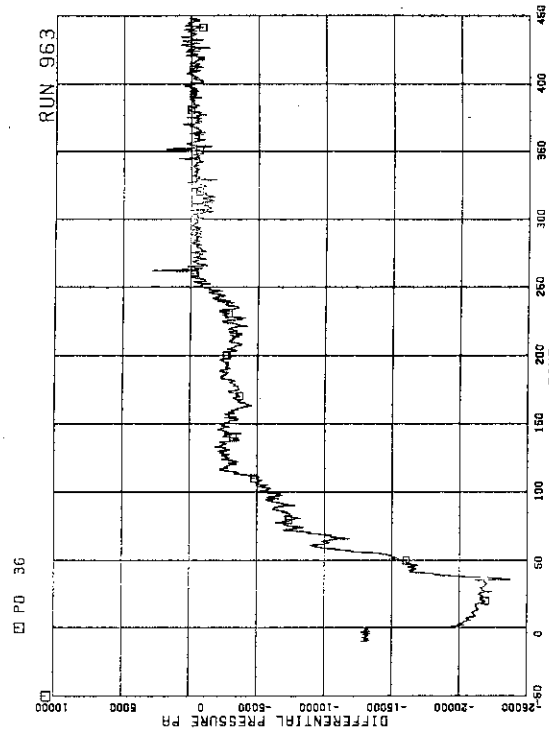

FIG.5.179 DIFFERENTIAL PRESSURE BETWEEN DOWNCOMER BOTTOM AND MRP1 SUCTION

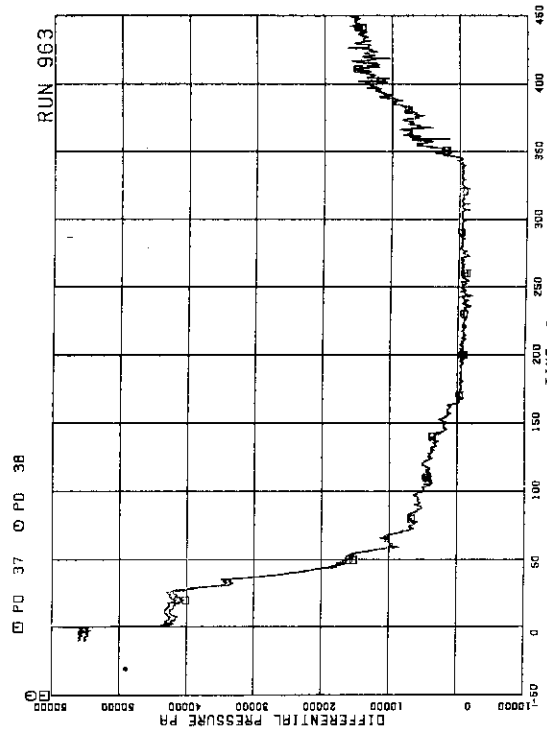

FIG.5.180 DIFFERENTIAL PRESSURE BETWEEN MRP DELIVERY AND JP-1.2 DRIVE

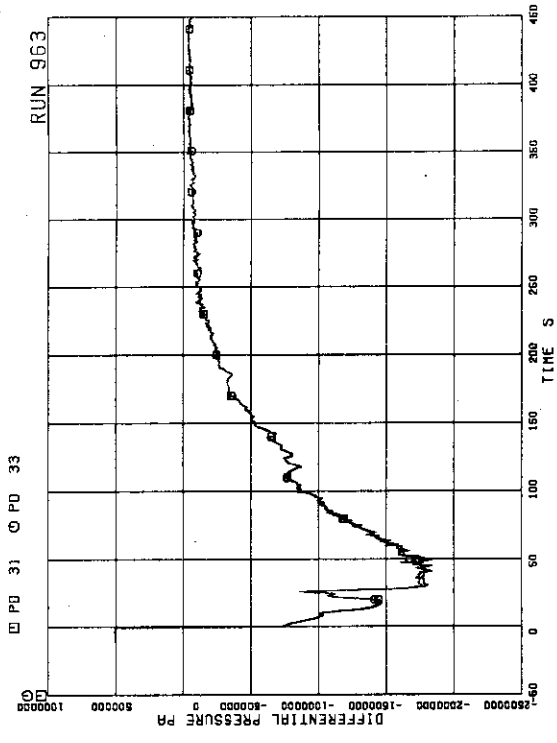

FIG.5.177 DIFFERENTIAL PRESSURE BETWEEN JP-3.4 DRIVE AND SUCTION

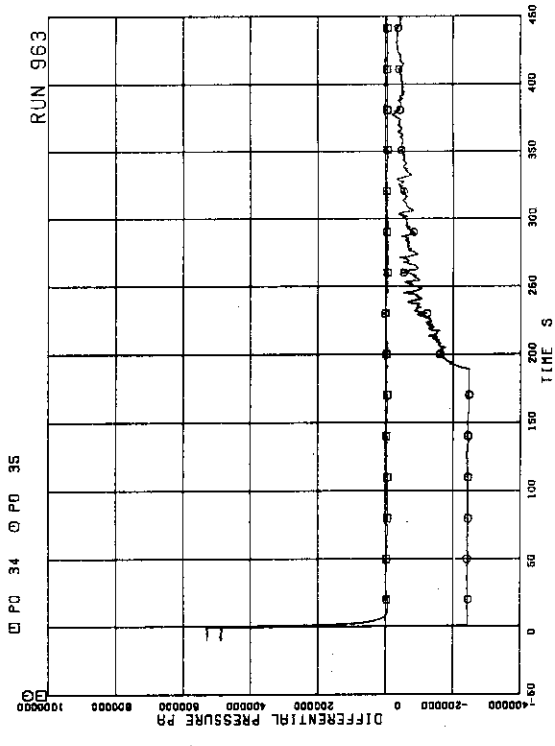

FIG.5.178 DIFFERENTIAL PRESSURE BETWEEN MRP DELIVERY AND SUCTION

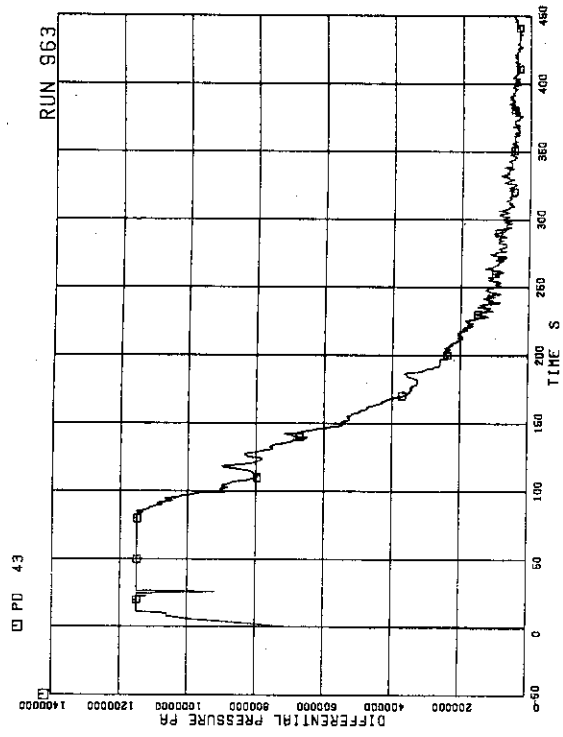

FIG.5.183 DIFFERENTIAL PRESSURE BETWEEN DOWNCOMER BOTTOM AND BREAK B

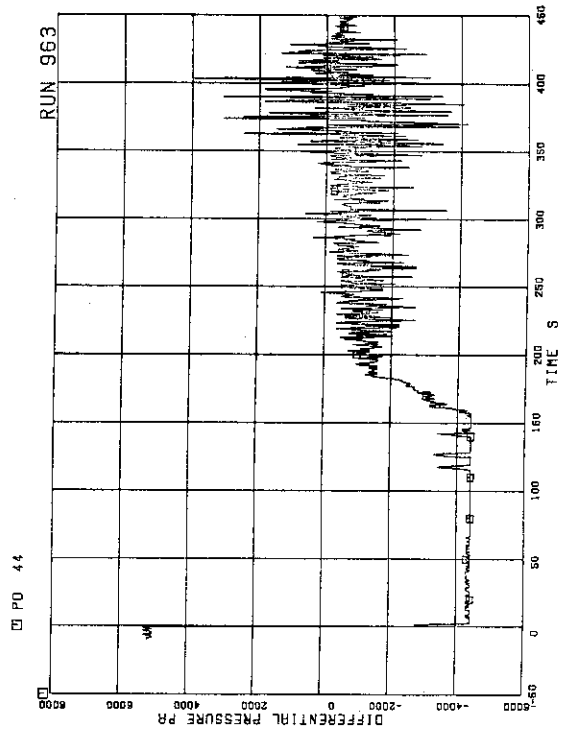

FIG.5.184 DIFFERENTIAL PRESSURE BETWEEN BREAKS A AND B

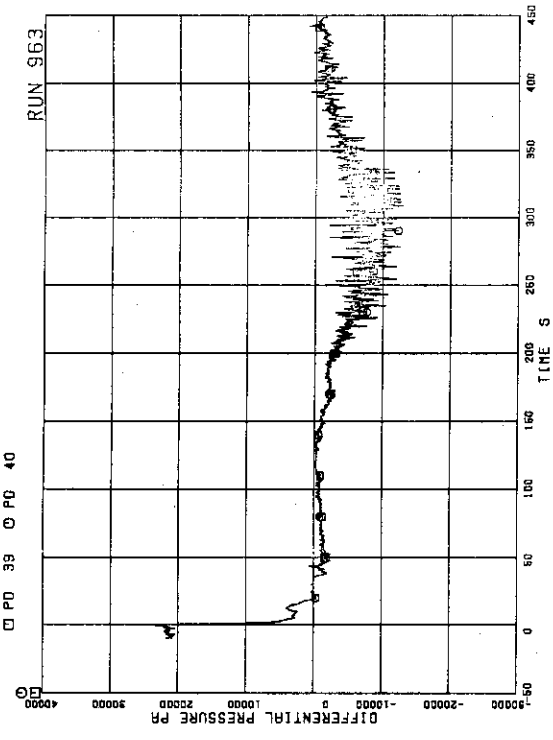

FIG.5.181 DIFFERENTIAL PRESSURE BETWEEN DOWNCOMER MIDDLE AND JP-1.2 SUCTION

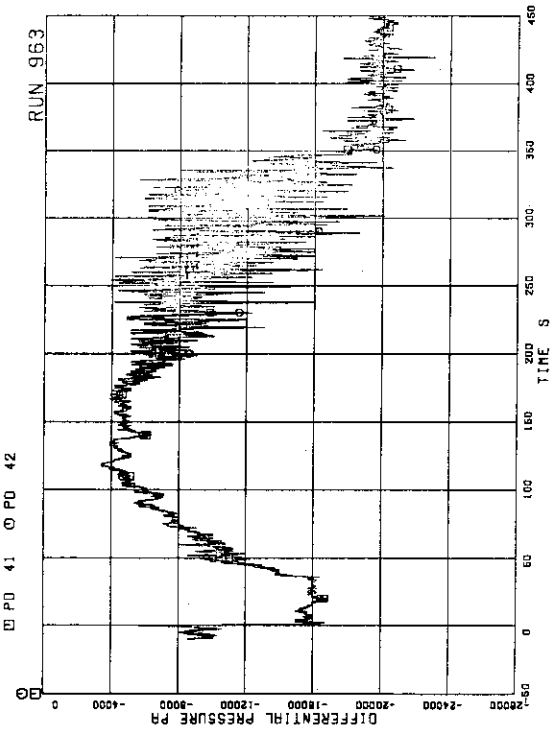

FIG.5.182 DIFFERENTIAL PRESSURE BETWEEN JP-1.2 DISCHARGE AND LOWER PLENUM

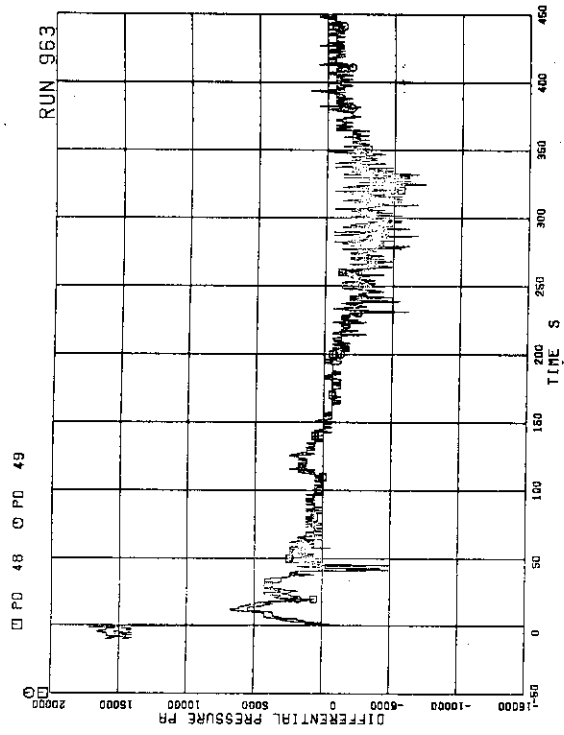

FIG.5.187 DIFFERENTIAL PRESSURE BETWEEN DOWNCOMER MIDDLE AND JP-3.4 SUCTION

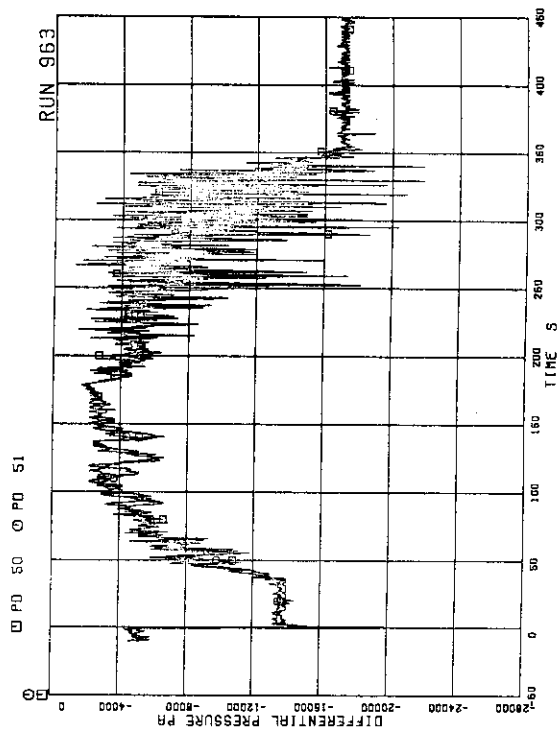

FIG.5.188 DIFFERENTIAL PRESSURE BETWEEN JP-3.4 DISCHARGE AND CONFLURNCE

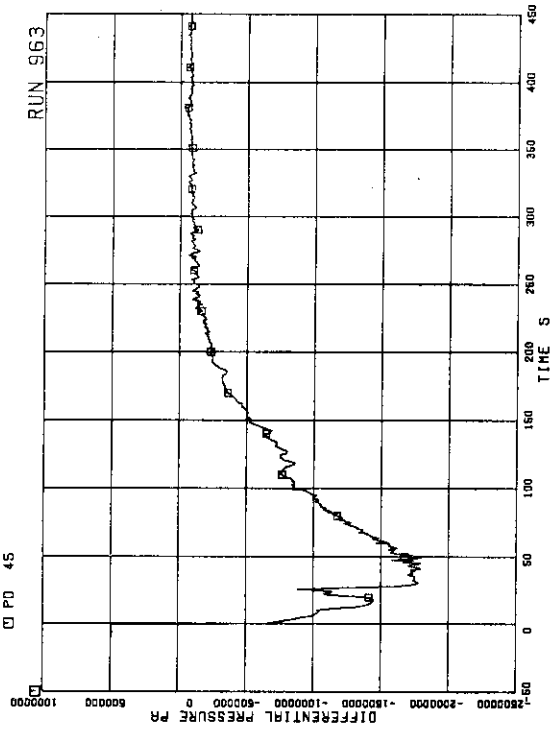

FIG.5.185 DIFFERENTIAL PRESSURE BETWEEN BREAK A AND MRP2 SUCTION

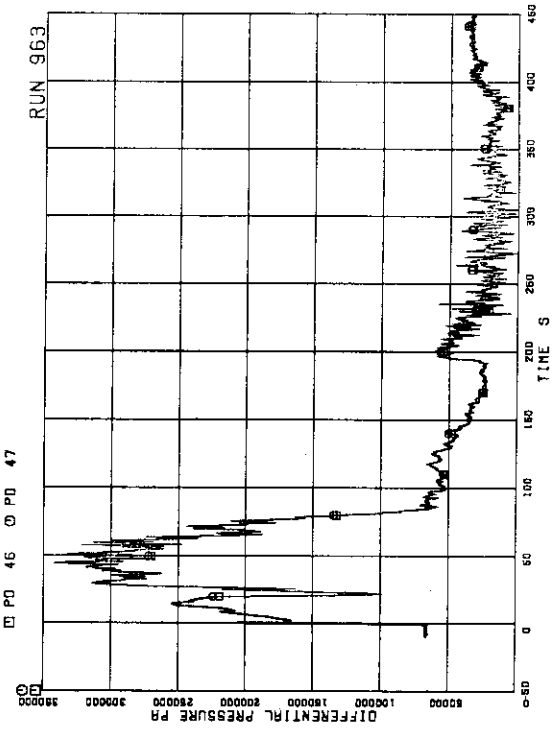

FIG.5.186 DIFFERENTIAL PRESSURE BETWEEN MRP DELIVERY AND JP-3.4 DRIVE

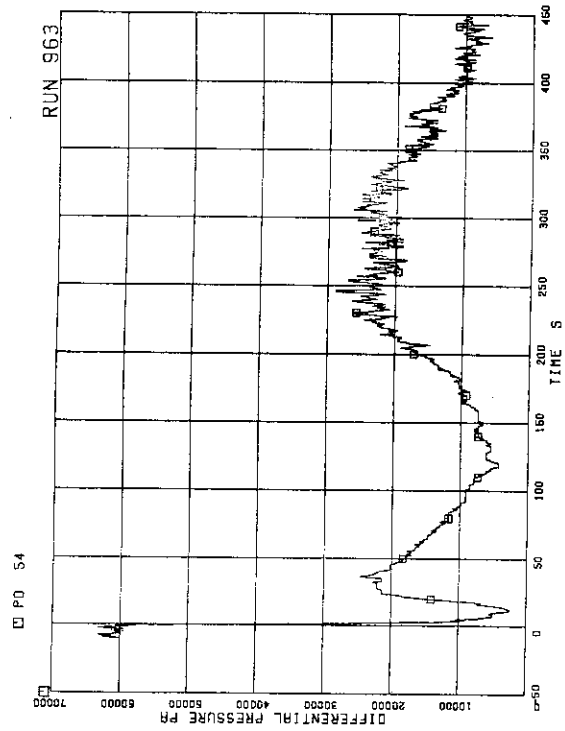

FIG.5.191 DIFFERENTIAL PRESSURE BETWEEN LOWER PLENUM AND DOWNCOMER BOTTOM

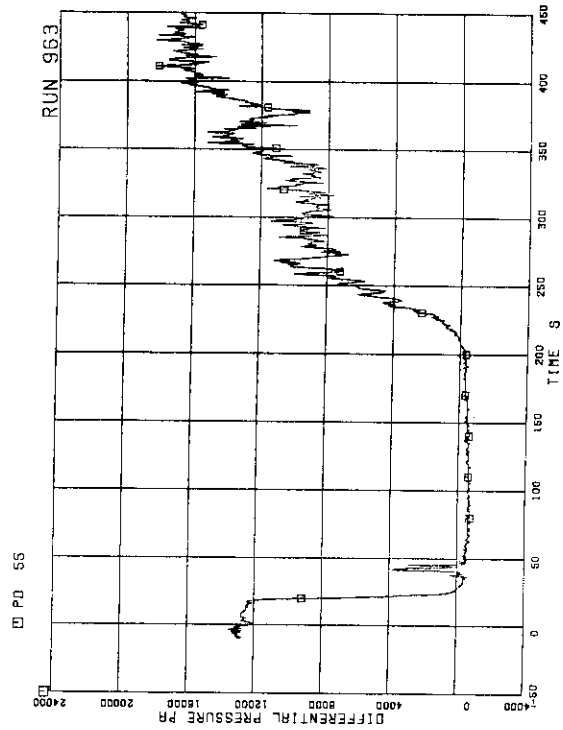

FIG.5.192 DIFFERENTIAL PRESSURE BETWEEN DOWNCOMER BOTTOM AND DOWNCOMER MIDDLE

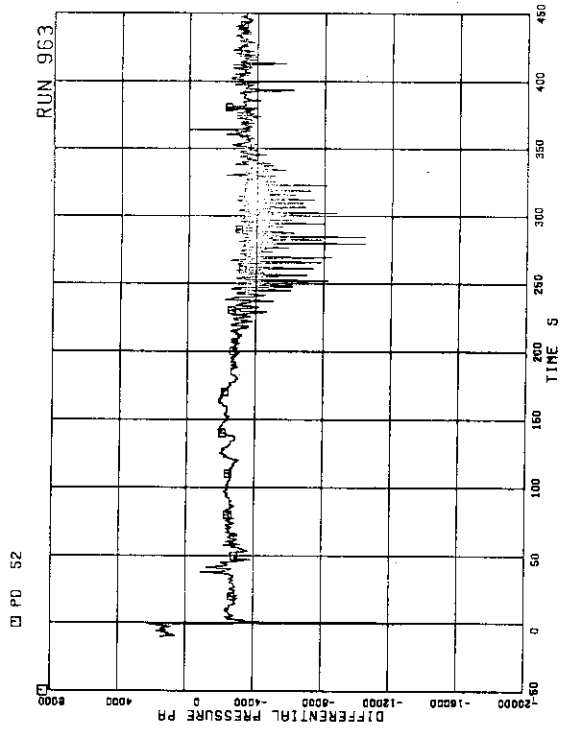

FIG.5.189 DIFFERENTIAL PRESSURE BETWEEN JP-3.4 CONFLUENCE IN BROKEN LOOP AND LP

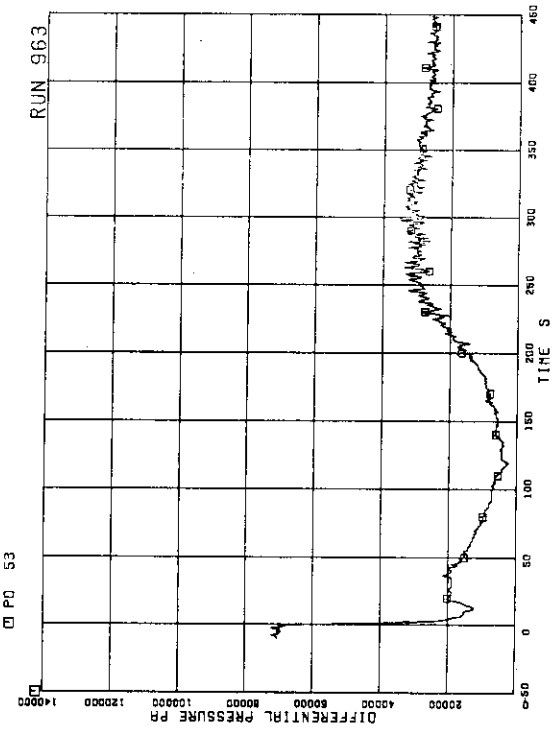

FIG.5.190 DIFFERENTIAL PRESSURE BETWEEN LOWER PLENUM AND DOWNCOMER MIDDLE

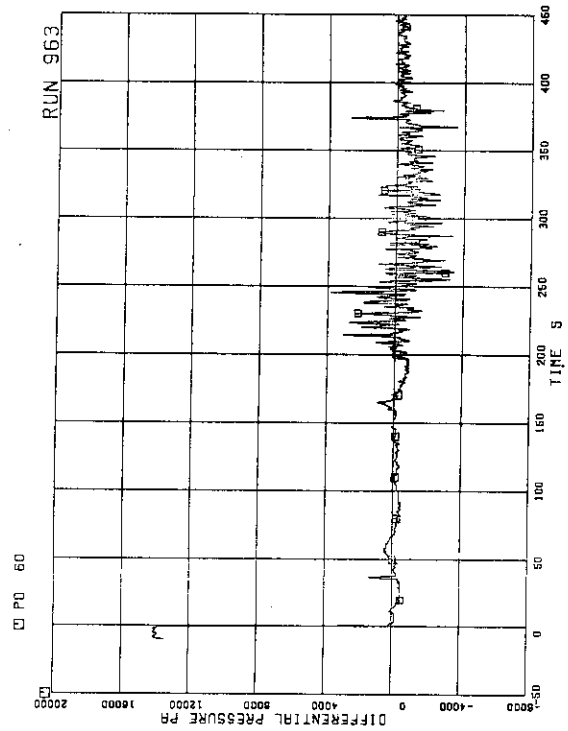

FIG.5.195 DIFFERENTIAL PRESSURE ACROSS CHANNEL INLET ORIFICE A

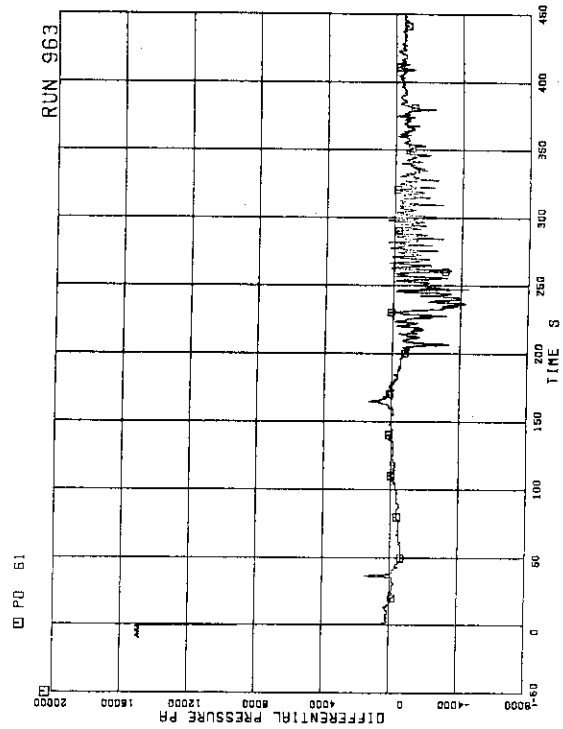

FIG.5.196 DIFFERENTIAL PRESSURE ACROSS CHANNEL INLET ORIFICE B

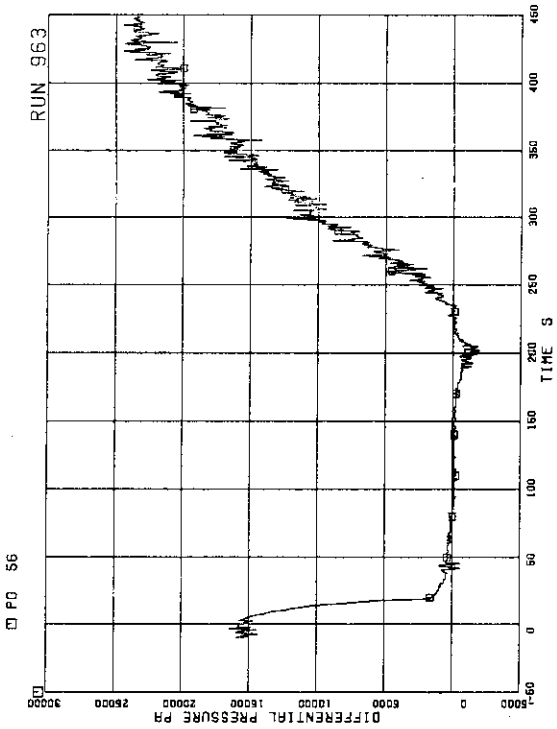

FIG.5.193 DIFFERENTIAL PRESSURE BETWEEN DOWNCOMER MIDDLE AND STEAM DOME

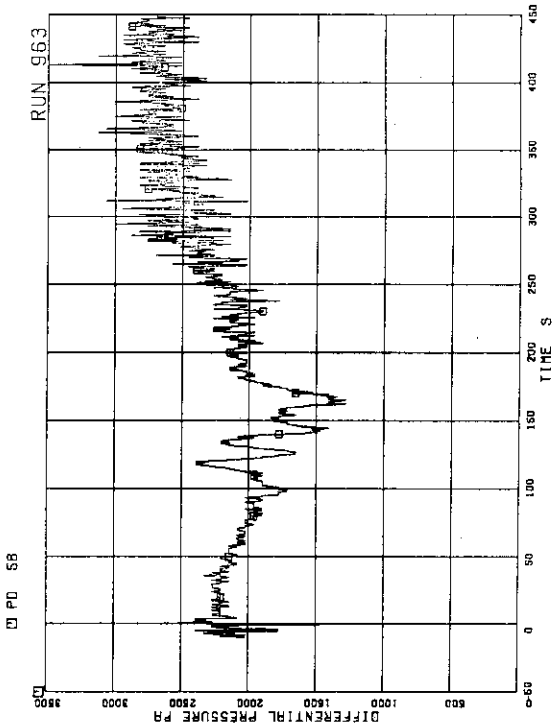

FIG.5.194 DIFFERENTIAL PRESSURE BETWEEN LP BOTTOM AND LP MIDDLE

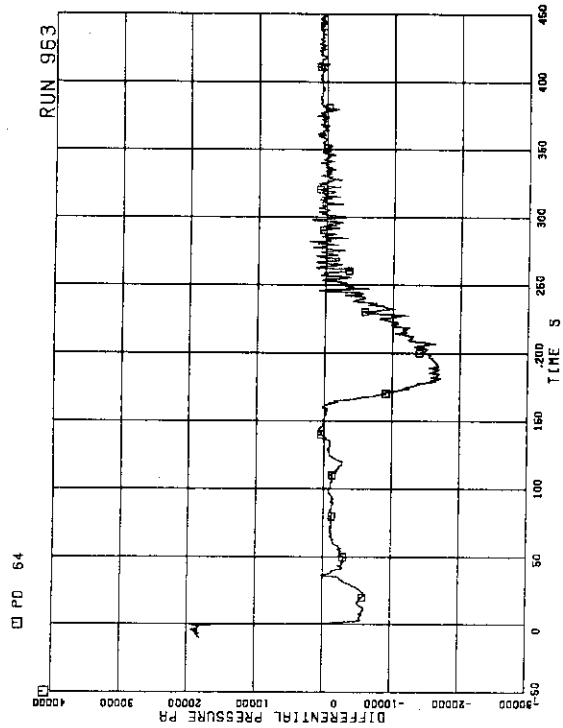

FIG.5.199 DIFFERENTIAL PRESSURE ACROSS BYPASS HOLE

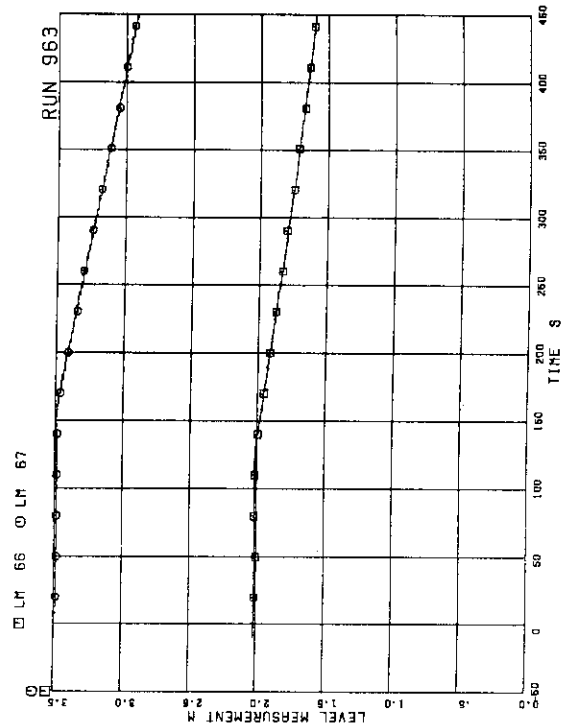

FIG.5.200 LIQUID LEVELS IN ECCS TANKS

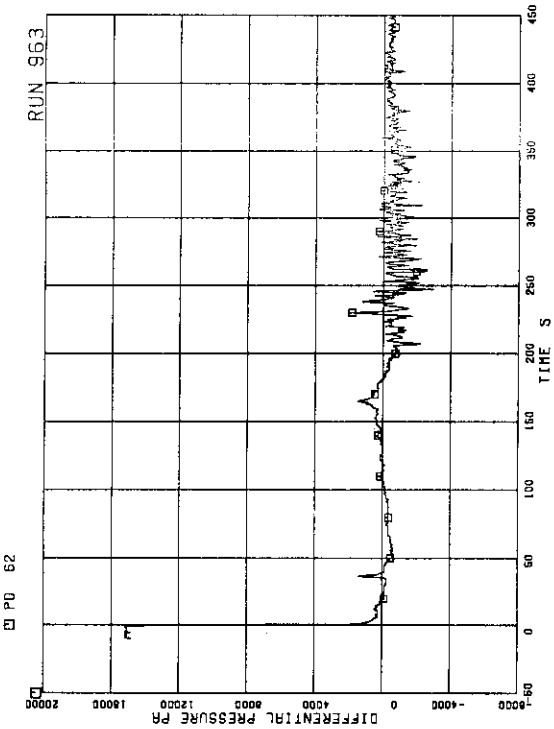

FIG.5.197 DIFFERENTIAL PRESSURE ACROSS CHANNEL INLET ORIFICE C

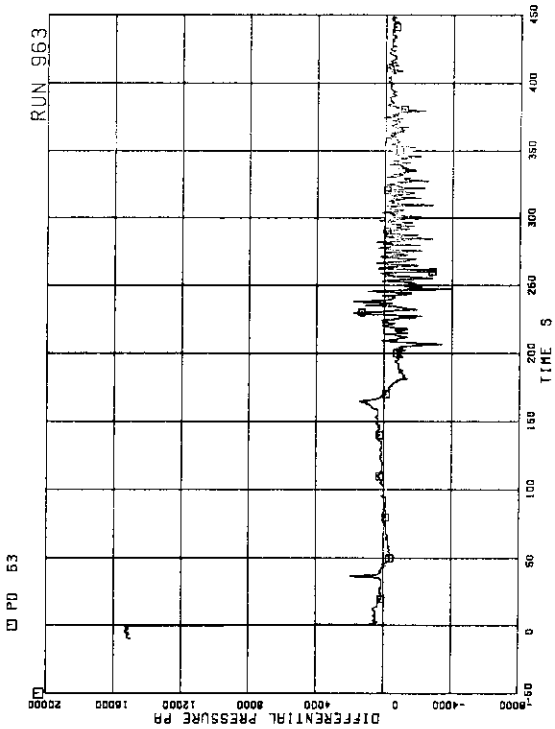

FIG.5.198 DIFFERENTIAL PRESSURE ACROSS CHANNEL INLET ORIFICE D

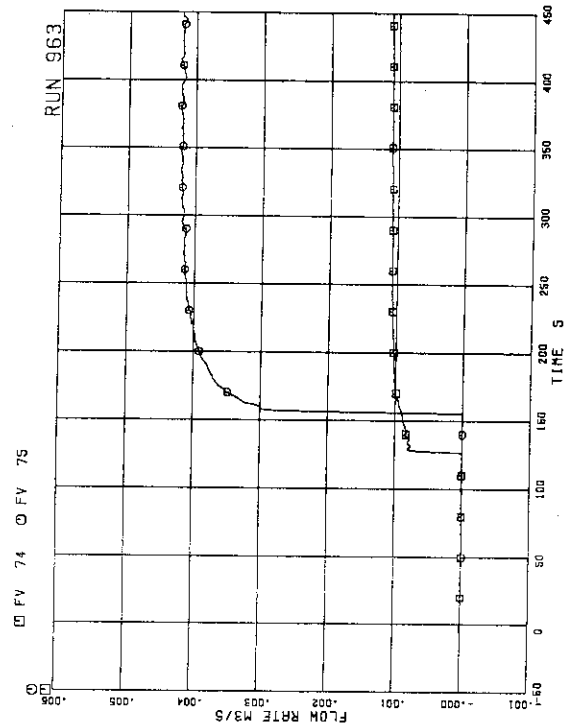

FIG.5.203 ECC INJECTION FLOW RATES

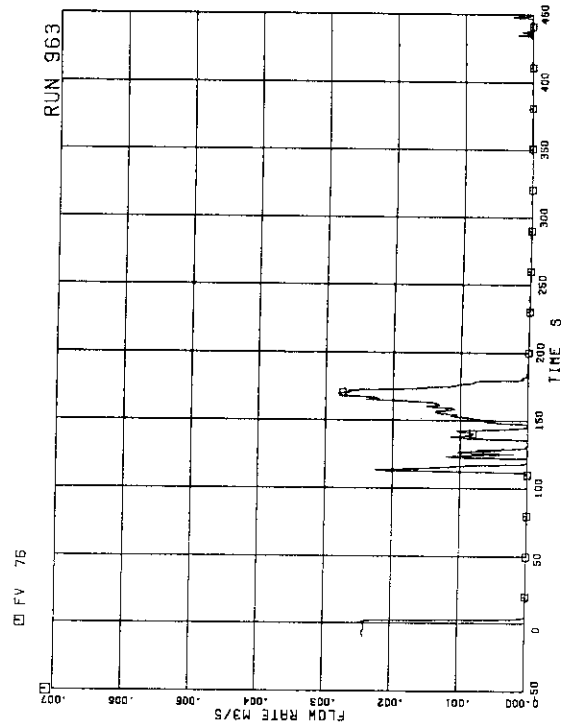

FIG.5.204 FEEDWATER FLOW RATE

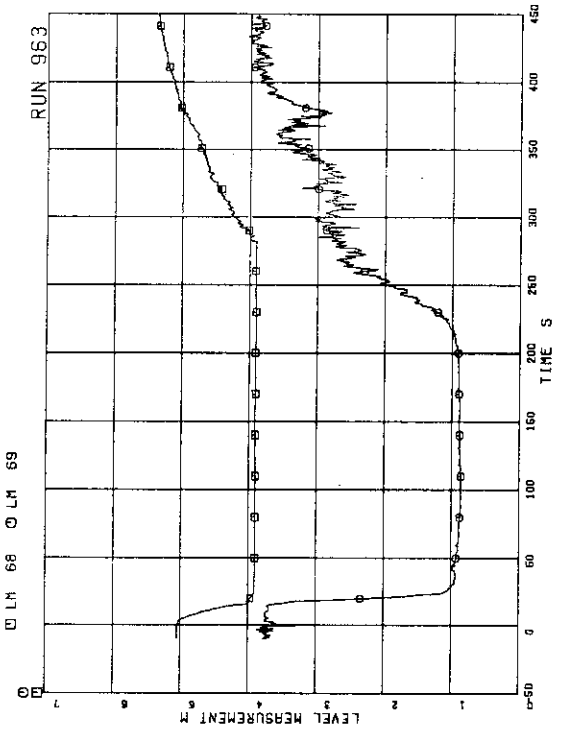

FIG.5.201 LIQUID LEVELS IN DOWNCOMER

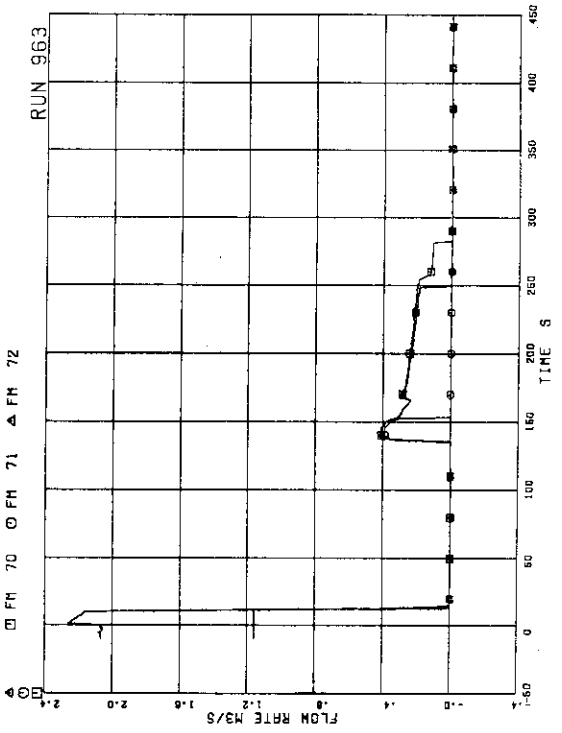

FIG.5.202 MASS FLOW RATE IN MSL

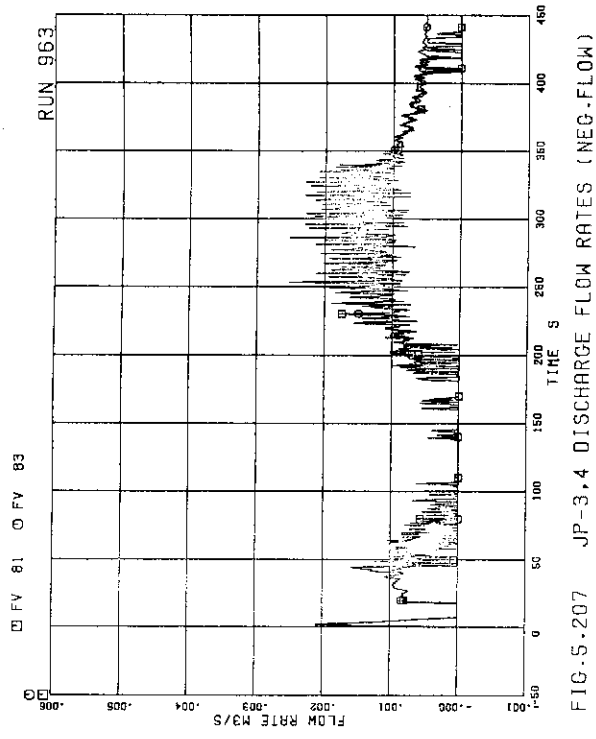

FIG.5.207 JP-3,4 DISCHARGE FLOW RATES (NEG.FLOW)

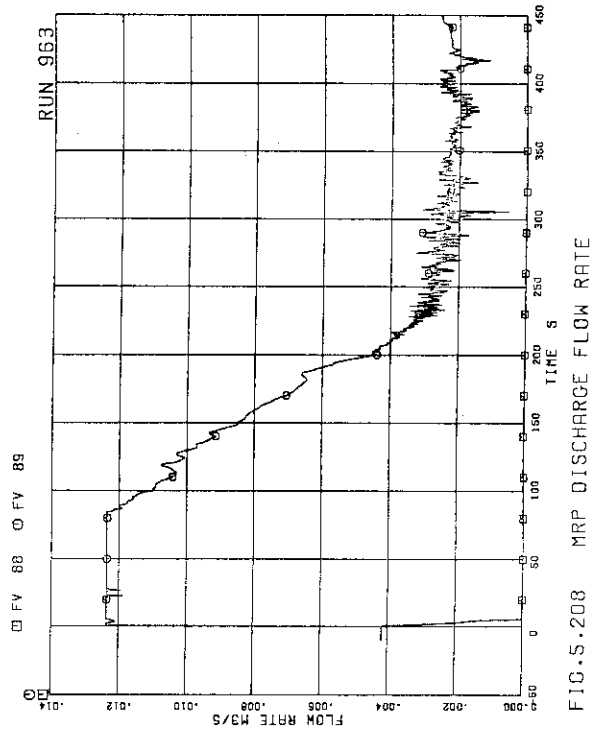

FIG.5.208 MRP DISCHARGE FLOW RATE

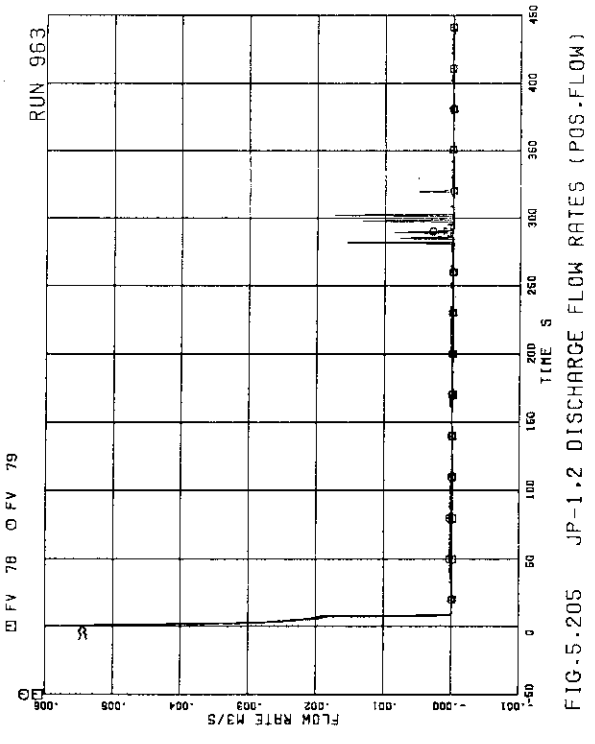

FIG.5.205 JP-1,2 DISCHARGE FLOW RATES (POS.FLOW)

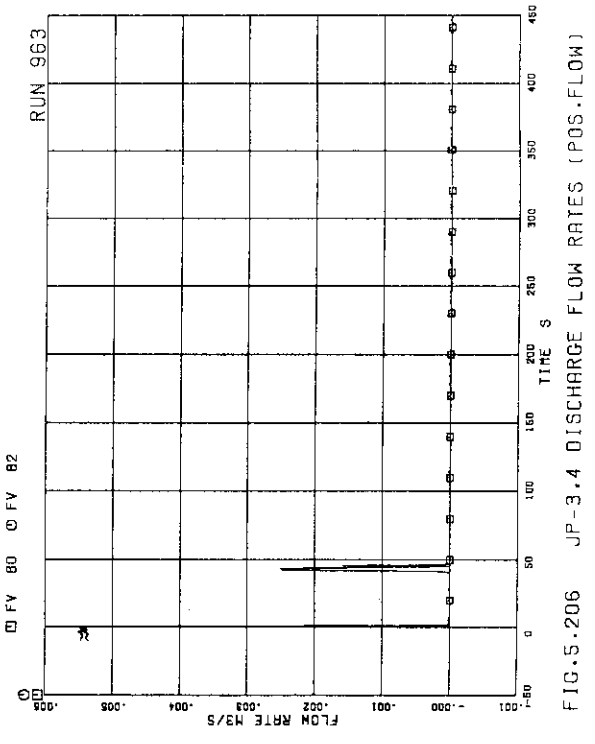

FIG.5.206 JP-3,4 DISCHARGE FLOW RATES (POS.FLOW)

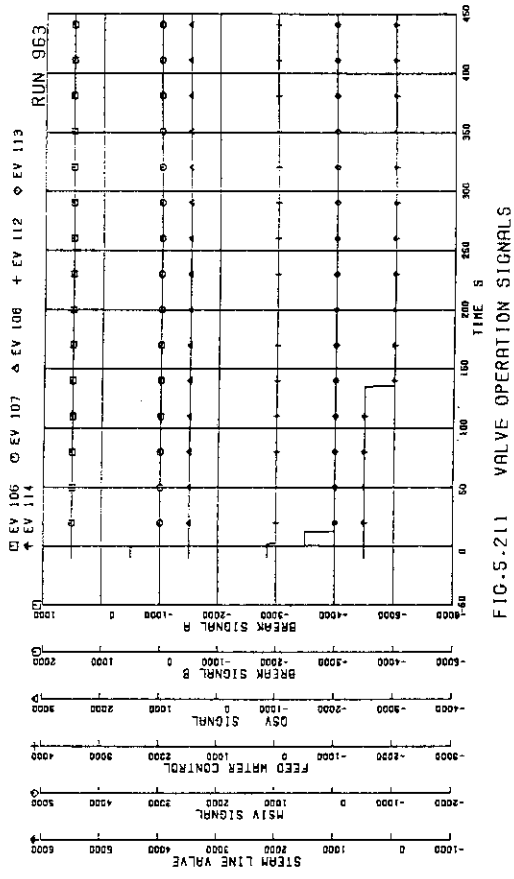

FIG.5.211 VALVE OPERATION SIGNALS

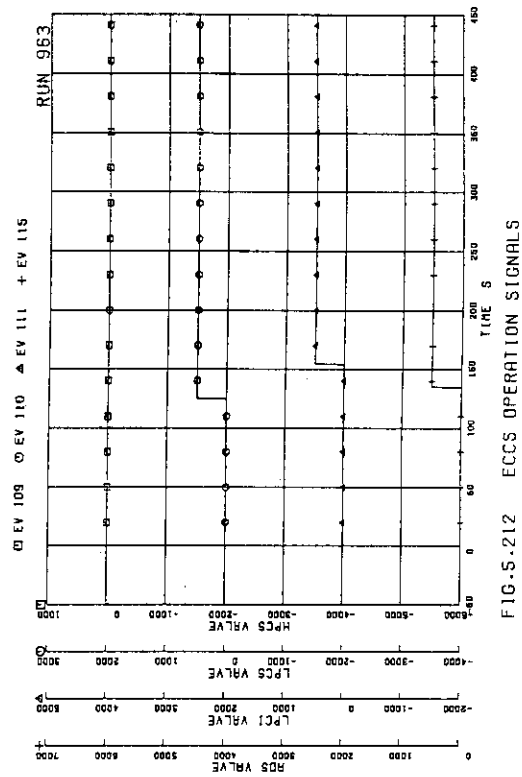

FIG.5.212 ECCS OPERATION SIGNALS

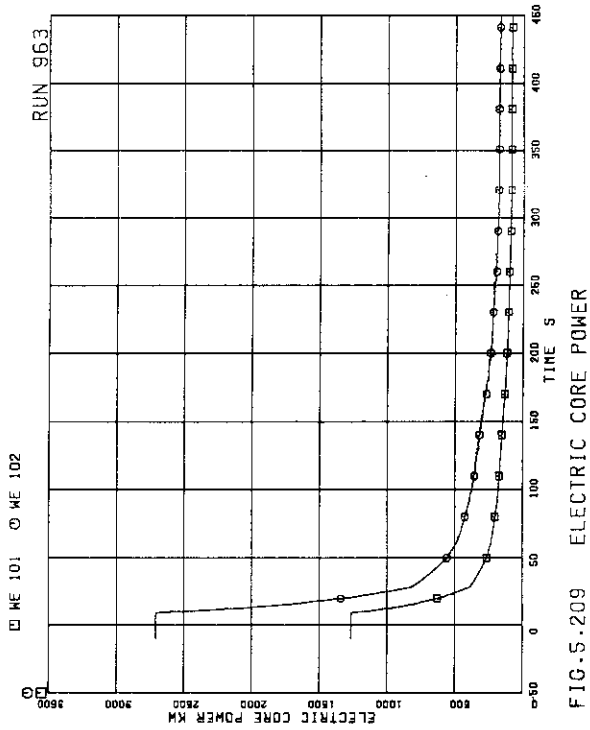

FIG.5.209 ELECTRIC CORE POWER

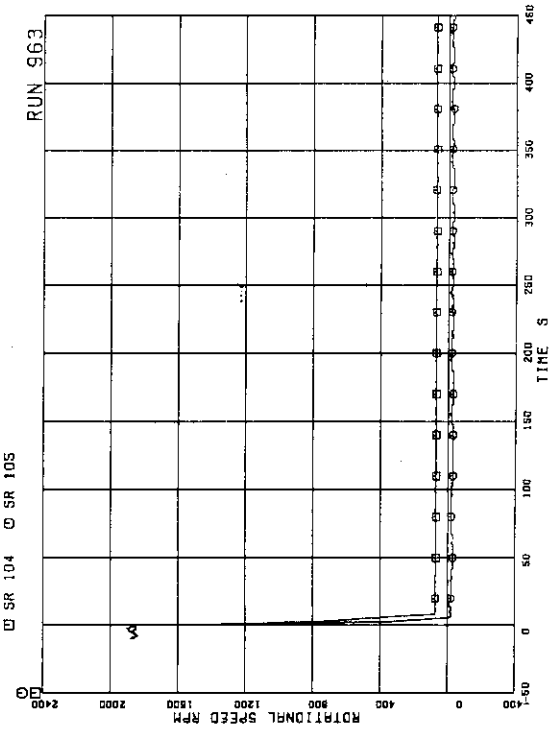

FIG.5.210 MRP PUMP SPEEDS

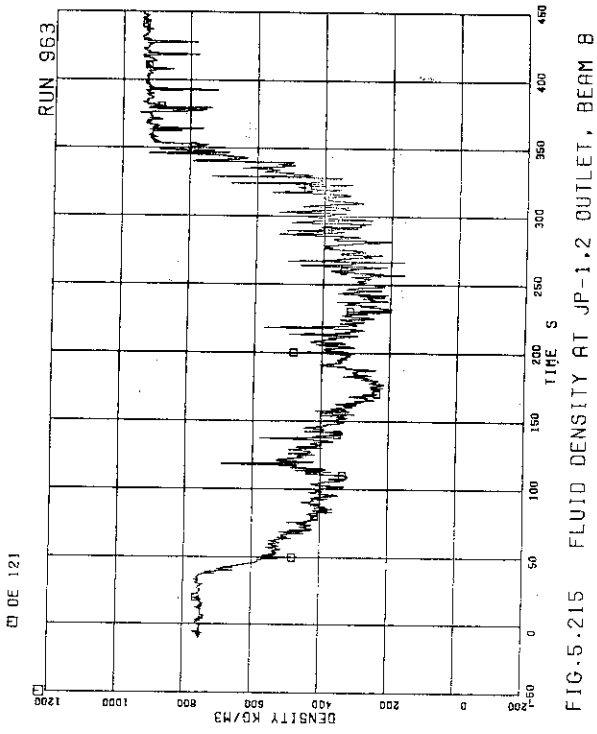

FIG.5.215 FLUID DENSITY AT JP-1,2 OUTLET, BEAM B

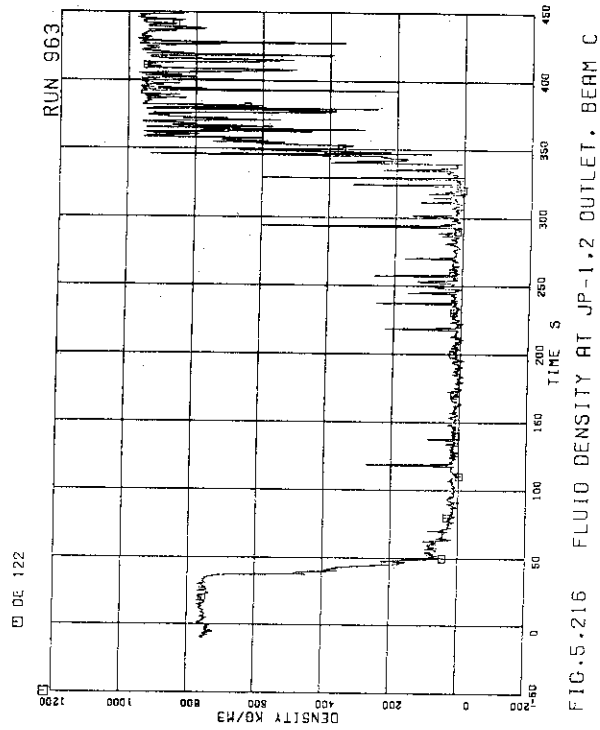

FIG.5.216 FLUID DENSITY AT JP-1,2 OUTLET, BEAM C

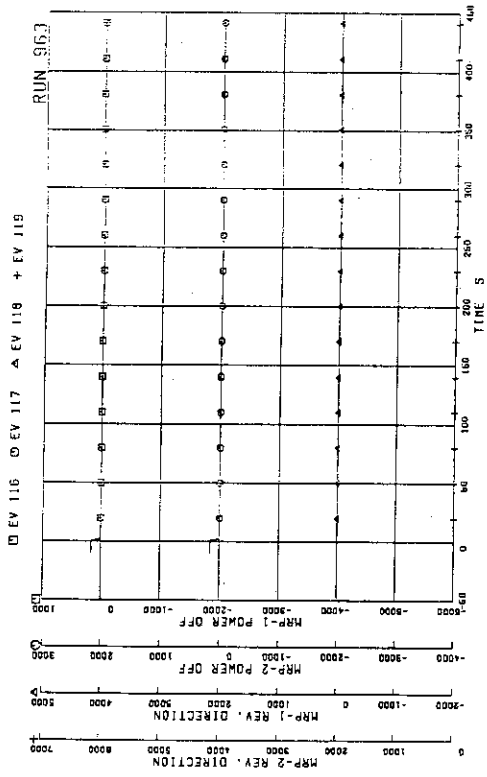

FIG.5.213 MRP OPERATION SIGNALS

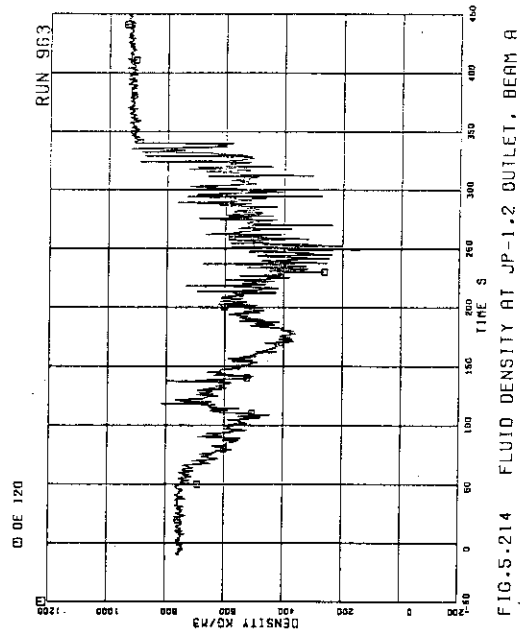

FIG.5.214 FLUID DENSITY AT JP-1,2 OUTLET, BEAM A

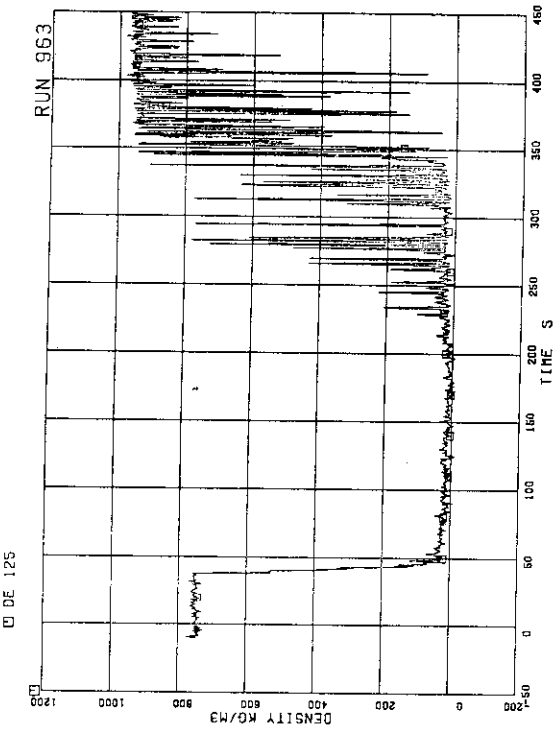

FIG.5.219 FLUID DENSITY AT JP-3,4 OUTLET, BEAM C

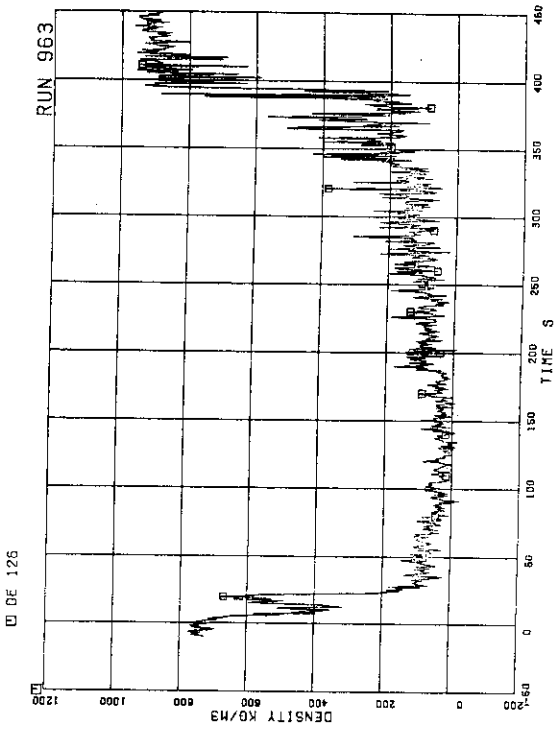

FIG.5.220 FLUID DENSITY AT JP SIDE OF BREAK, BEAM A

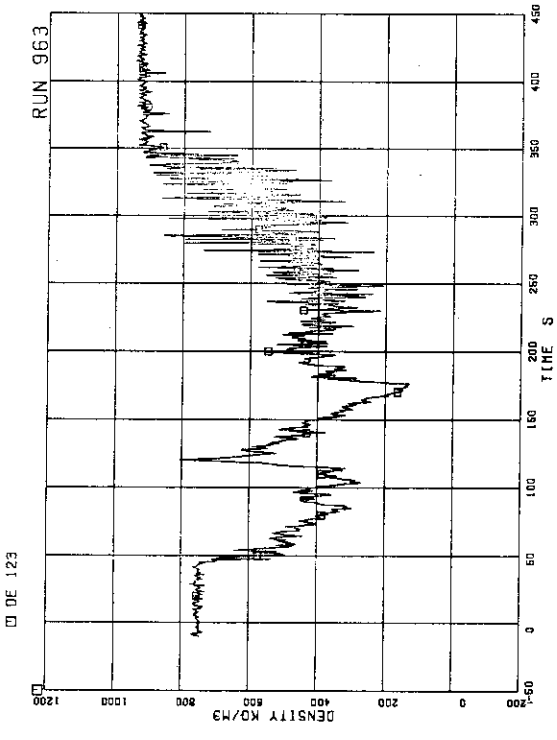

FIG.5.217 FLUID DENSITY AT JP-3,4 OUTLET, BEAM A

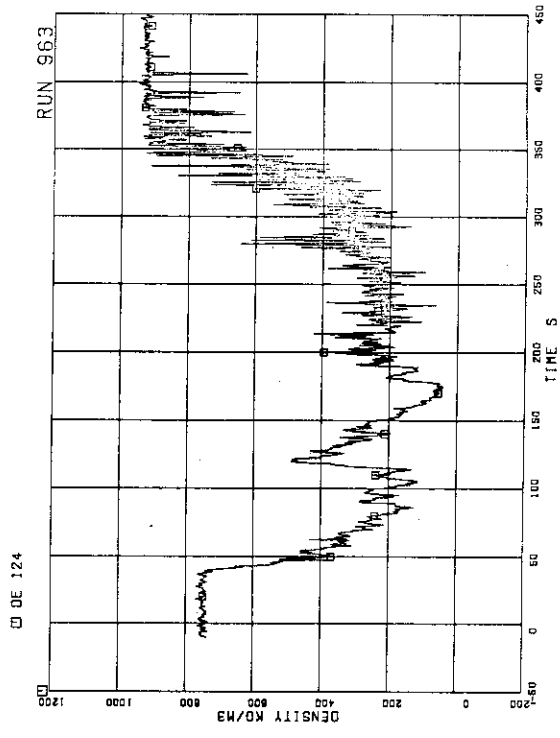

FIG.5.218 FLUID DENSITY AT JP-3,4 OUTLET, BEAM B

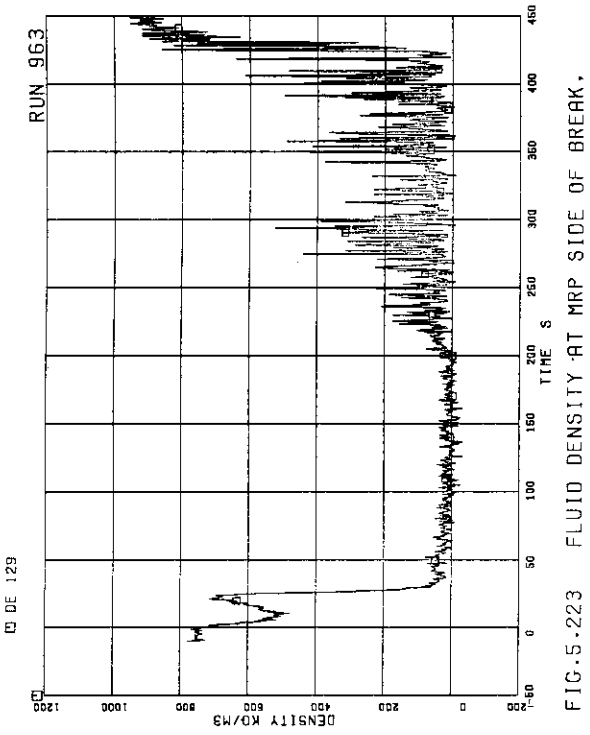

FIG.5.223 FLUID DENSITY AT MRP SIDE OF BREAK, BEAM B

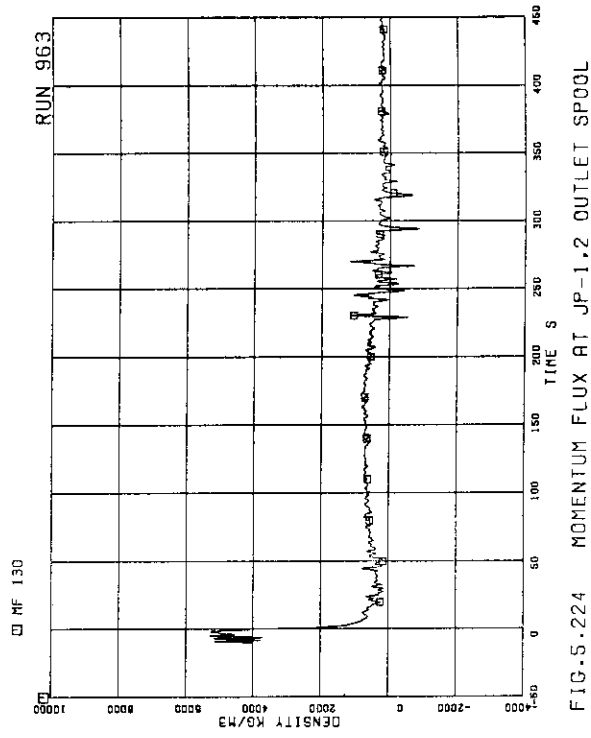

FIG.5.224 MOMENTUM FLUX AT JP-1,2 OUTLET SPOOL

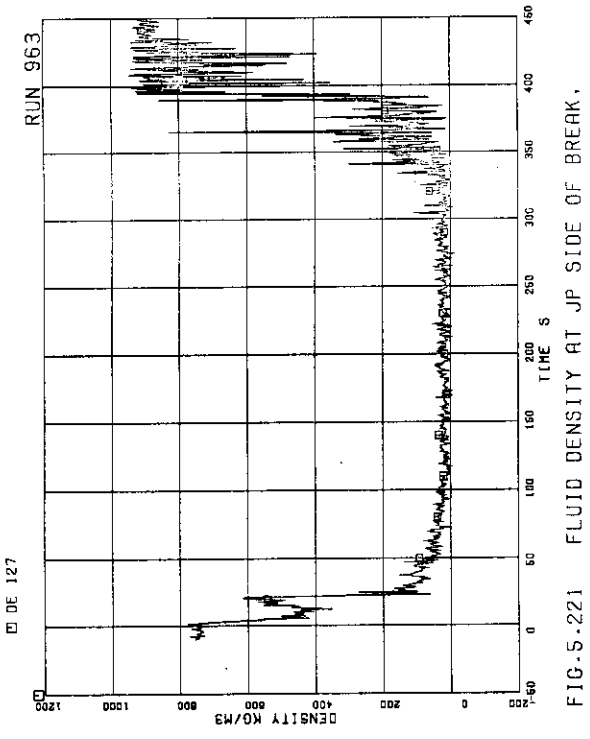

FIG.5.221 FLUID DENSITY AT JP SIDE OF BREAK, BEAM B

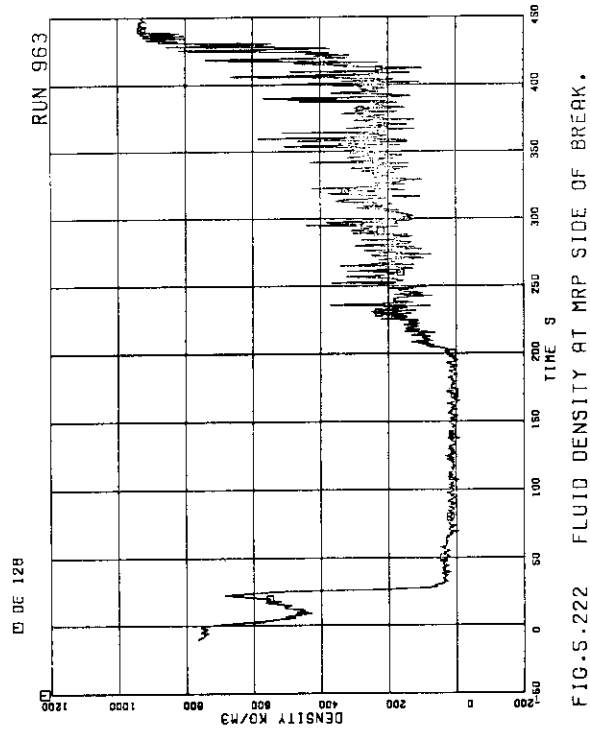

FIG.5.222 FLUID DENSITY AT MRP SIDE OF BREAK, BEAM A

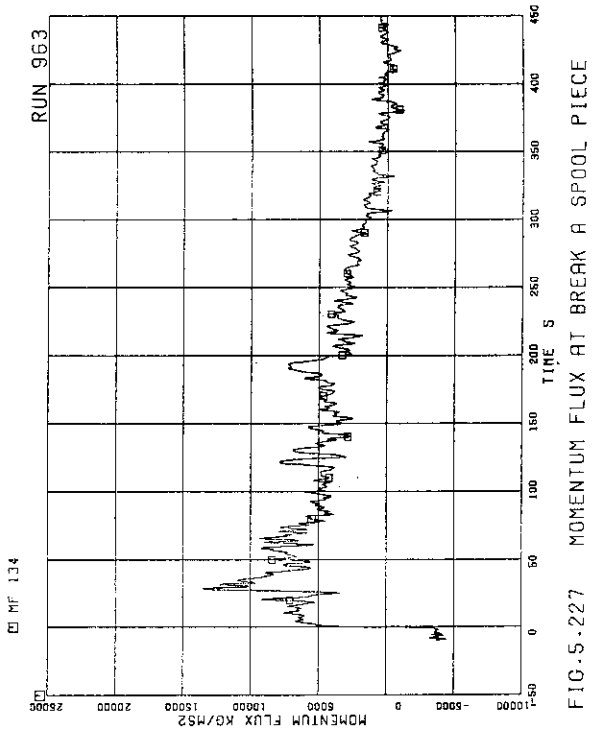

FIG.5.227 MOMENTUM FLUX AT BREAK A SPOOL PIECE (HIGH RANGE)

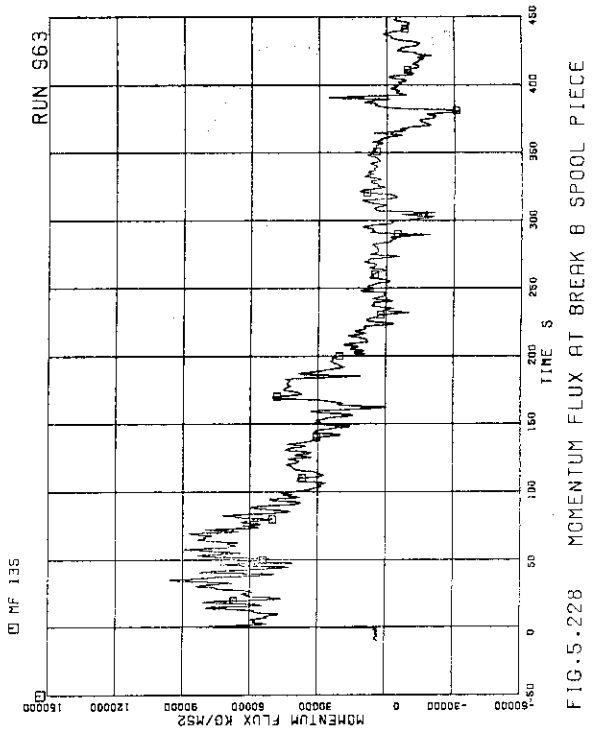

FIG.5.228 MOMENTUM FLUX AT BREAK B SPOOL PIECE (HIGH RANGE)

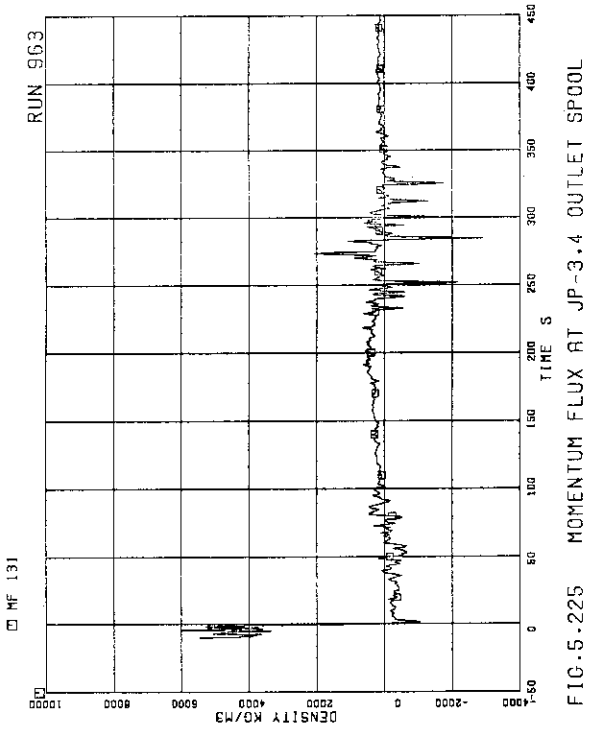

FIG.5.225 MOMENTUM FLUX AT JP-3.4 OUTLET SPOOL

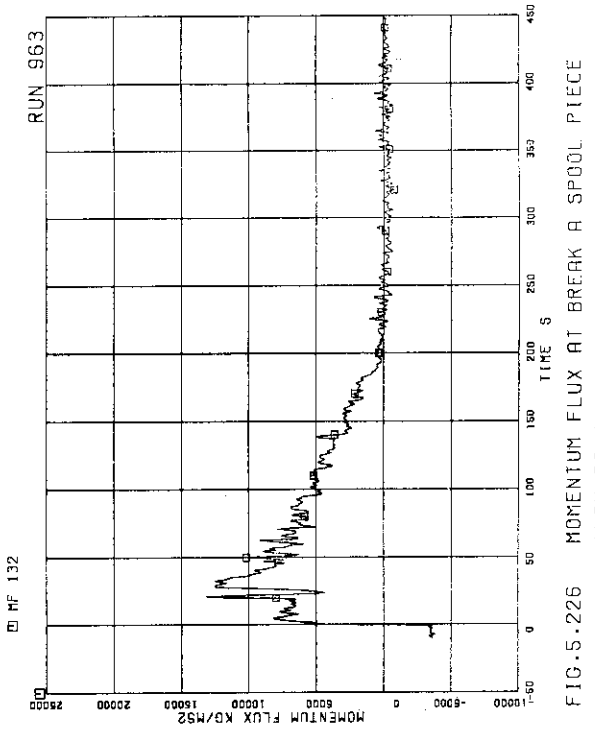

FIG.5.226 MOMENTUM FLUX AT BREAK A SPOOL PIECE (LOW RANGE)

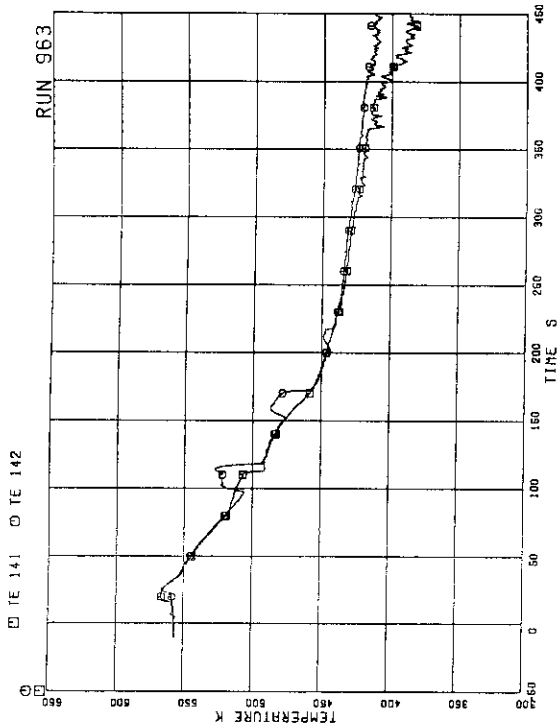

FIG.5.231 FLUID TEMPERATURES IN DOWNCOMER

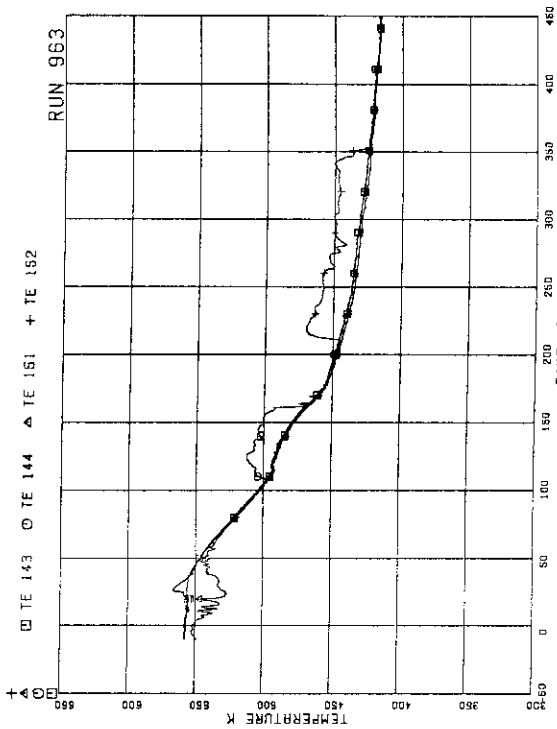

FIG.5.232 FLUID TEMPERATURES IN INTACT RECIRCULATION LOOP

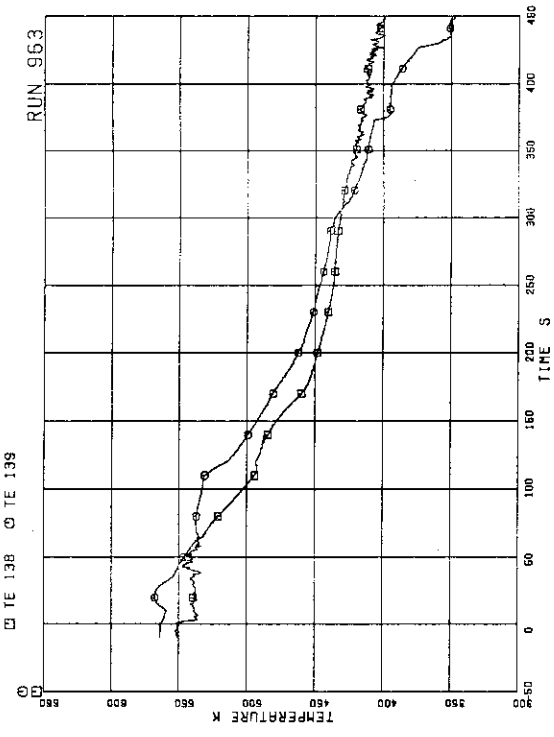

FIG.5.229 FLUID TEMPERATURES IN LOWER PLENUM AND UPPER PLENUM

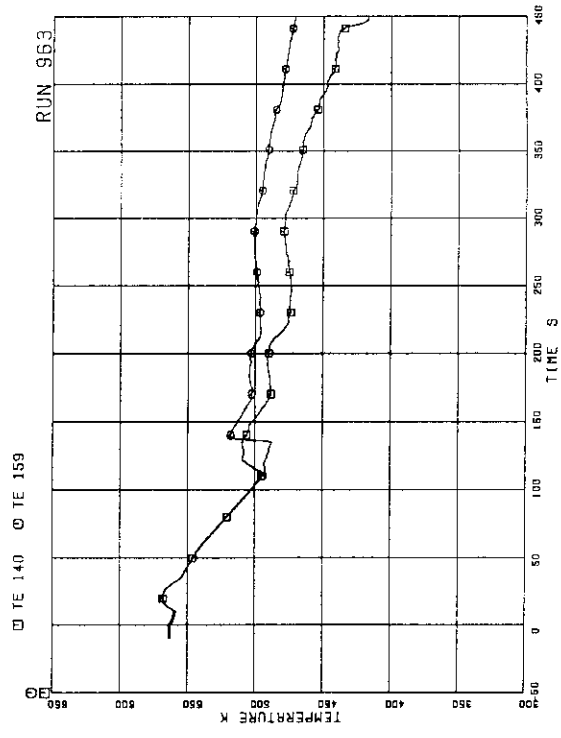

FIG.5.230 FLUID TEMPERATURES IN STEAM DOME AND MSL

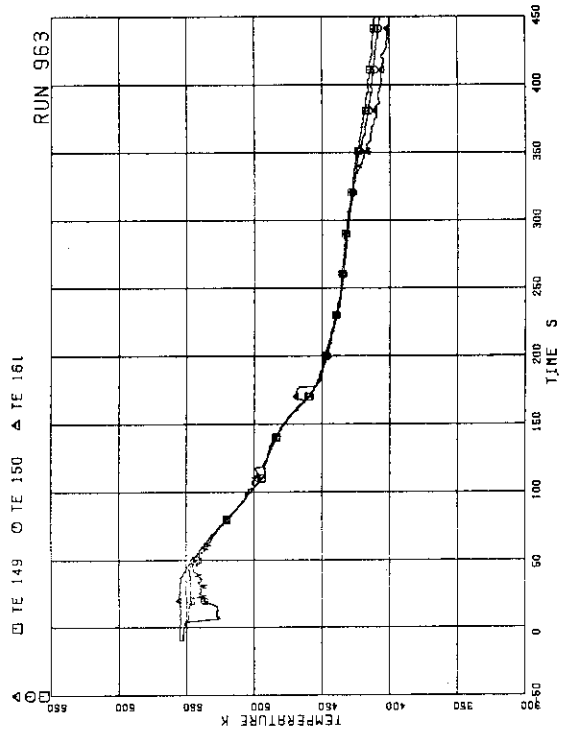

FIG.5.235 FLUID TEMPERATURES AT JP-3,4 OUTLET

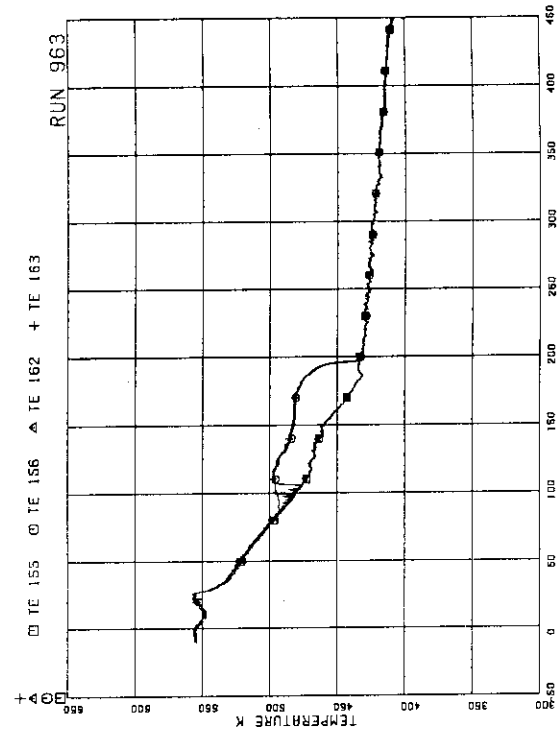

FIG.5.236 FLUID TEMPERATURES NEAR BREAKS A AND B

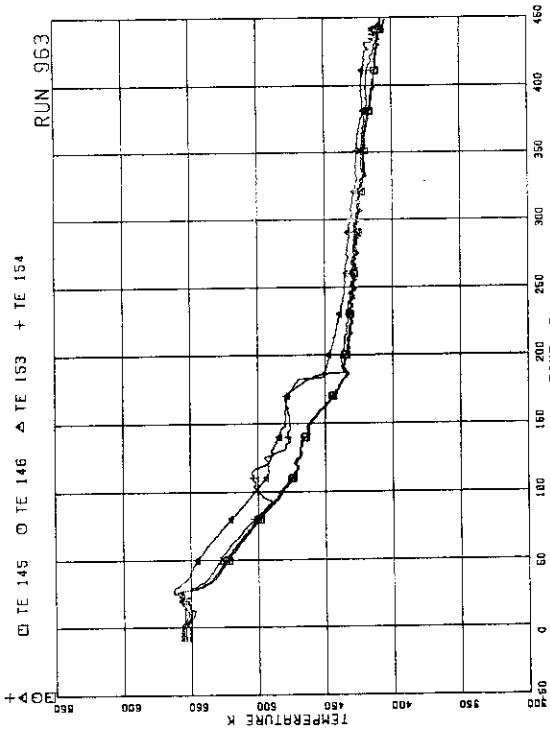

FIG.5.233 FLUID TEMPERATURES IN BROKEN RECIRCULATION LOOP

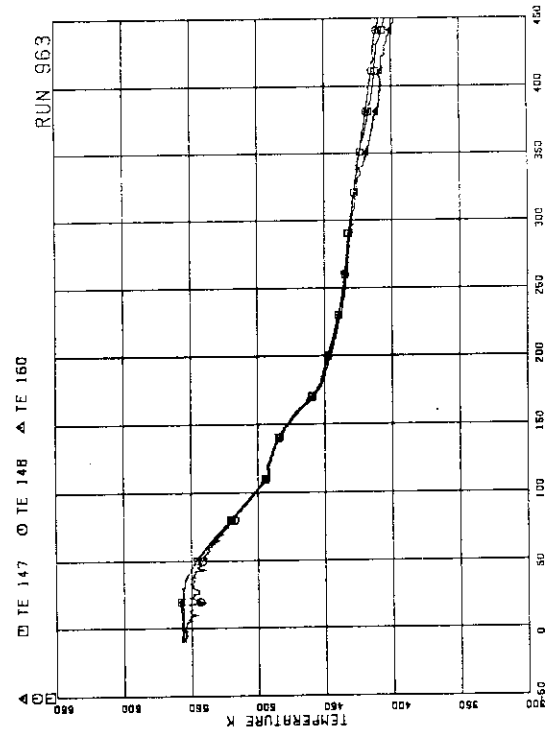

FIG.5.234 FLUID TEMPERATURES AT JP-1,2 OUTLET

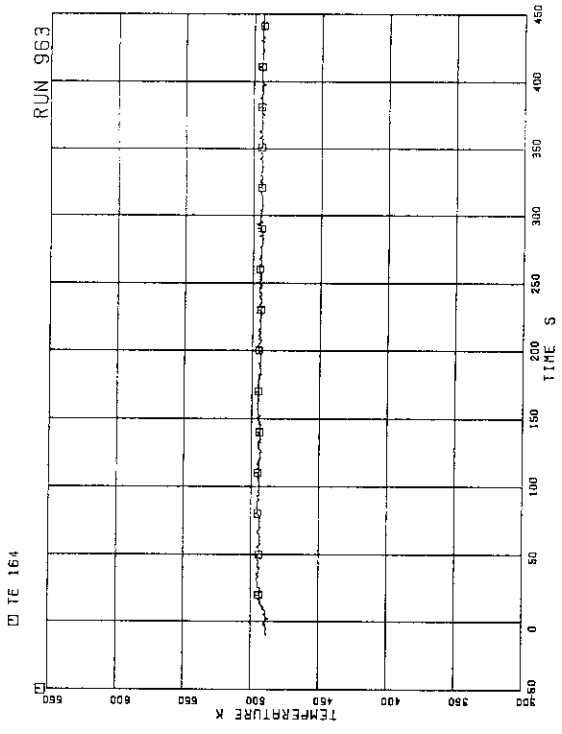

FIG.5.237 FEEDWATER TEMPERATURE

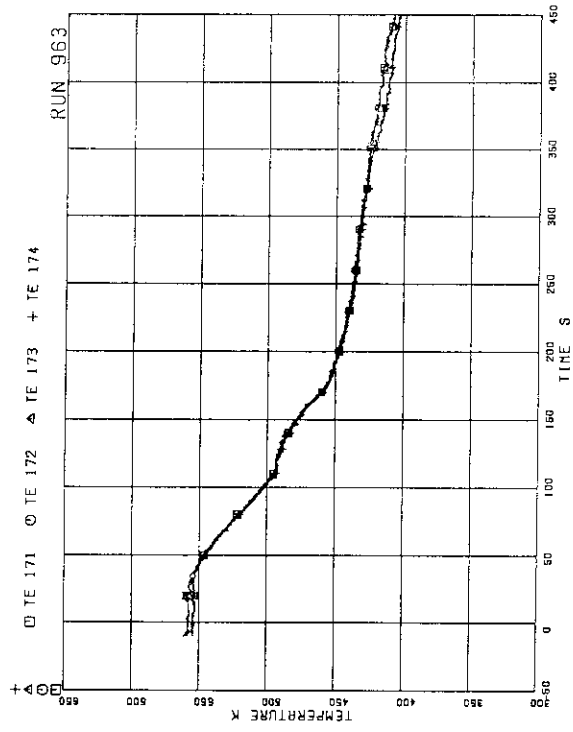

FIG.5.238 FLUID TEMPERATURES AT JP DISCHARGE

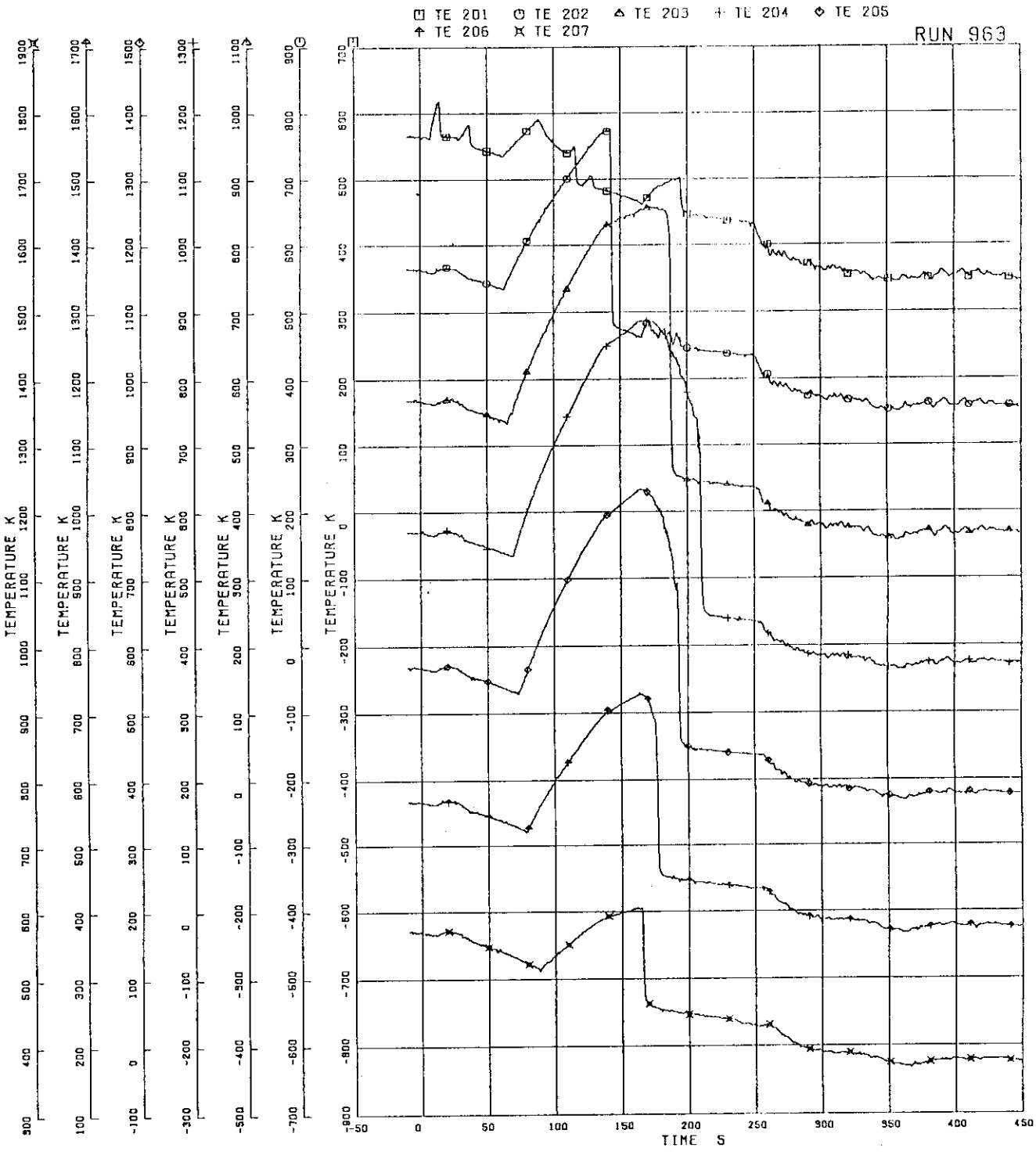

FIG.5-239 SURFACE TEMPERATURES OF FUEL ROD A11

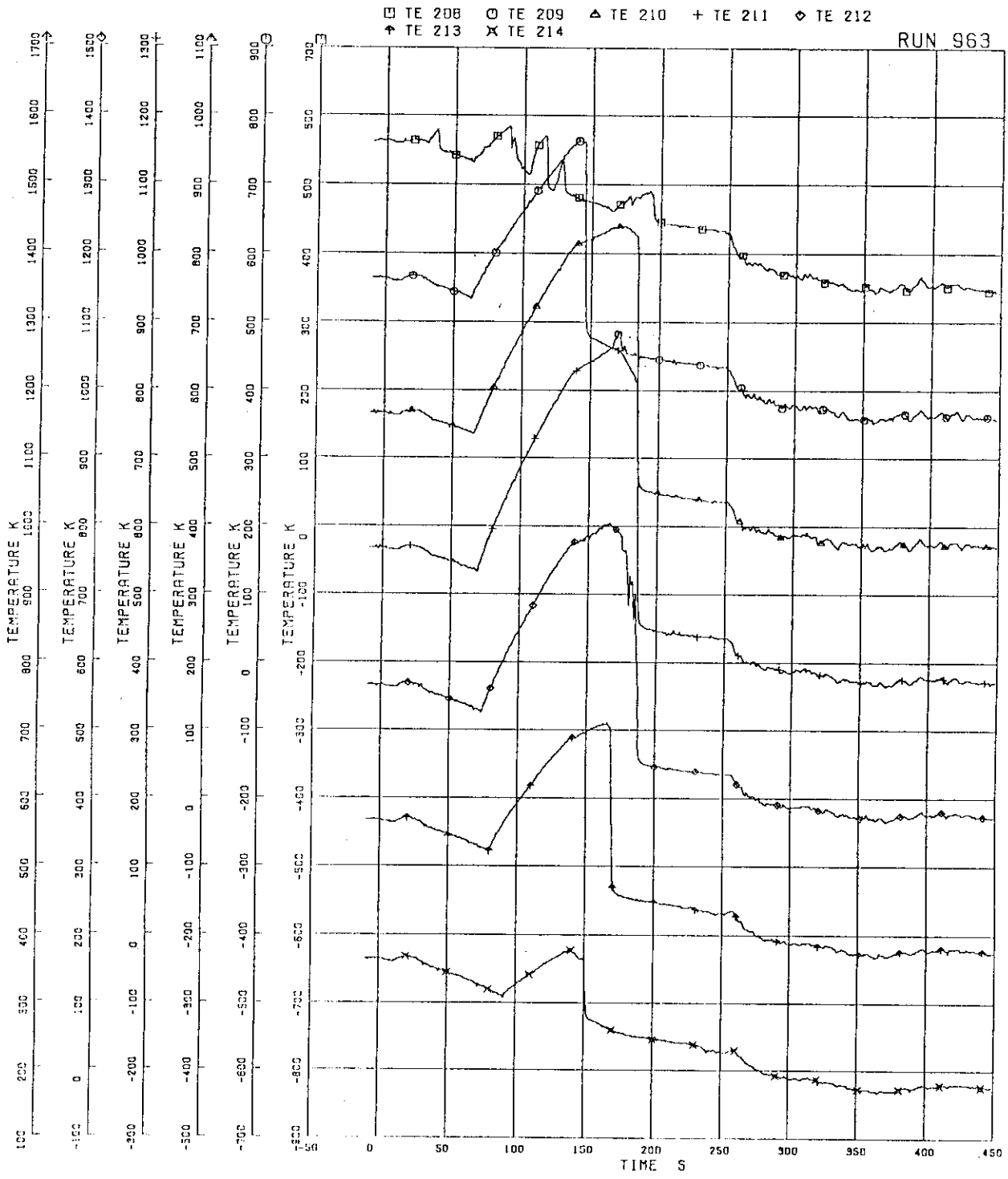

FIG.5.240 SURFACE TEMPERATURES OF FUEL ROD A12

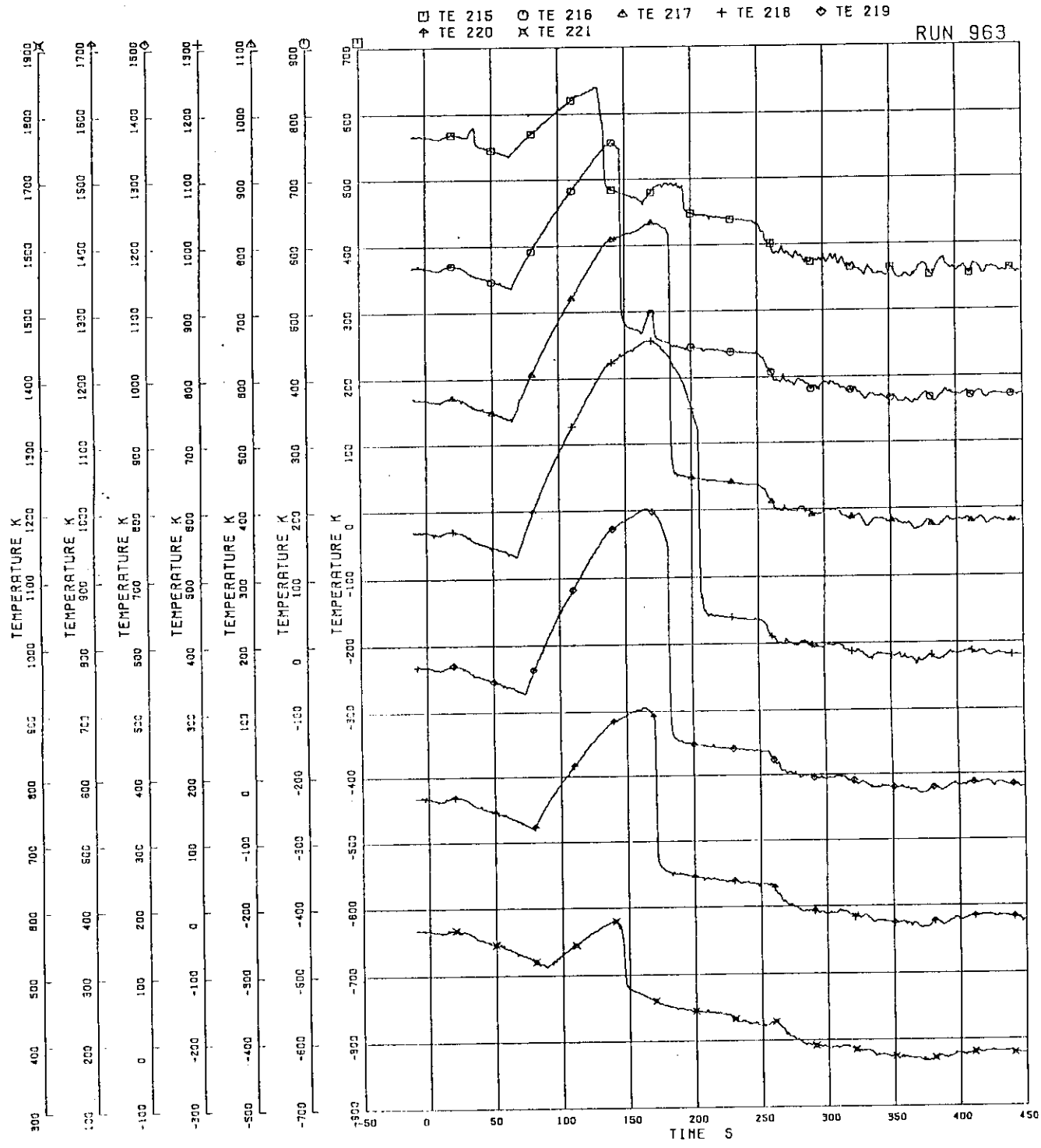

FIG.5.241 SURFACE TEMPERATURES OF FUEL ROD A13

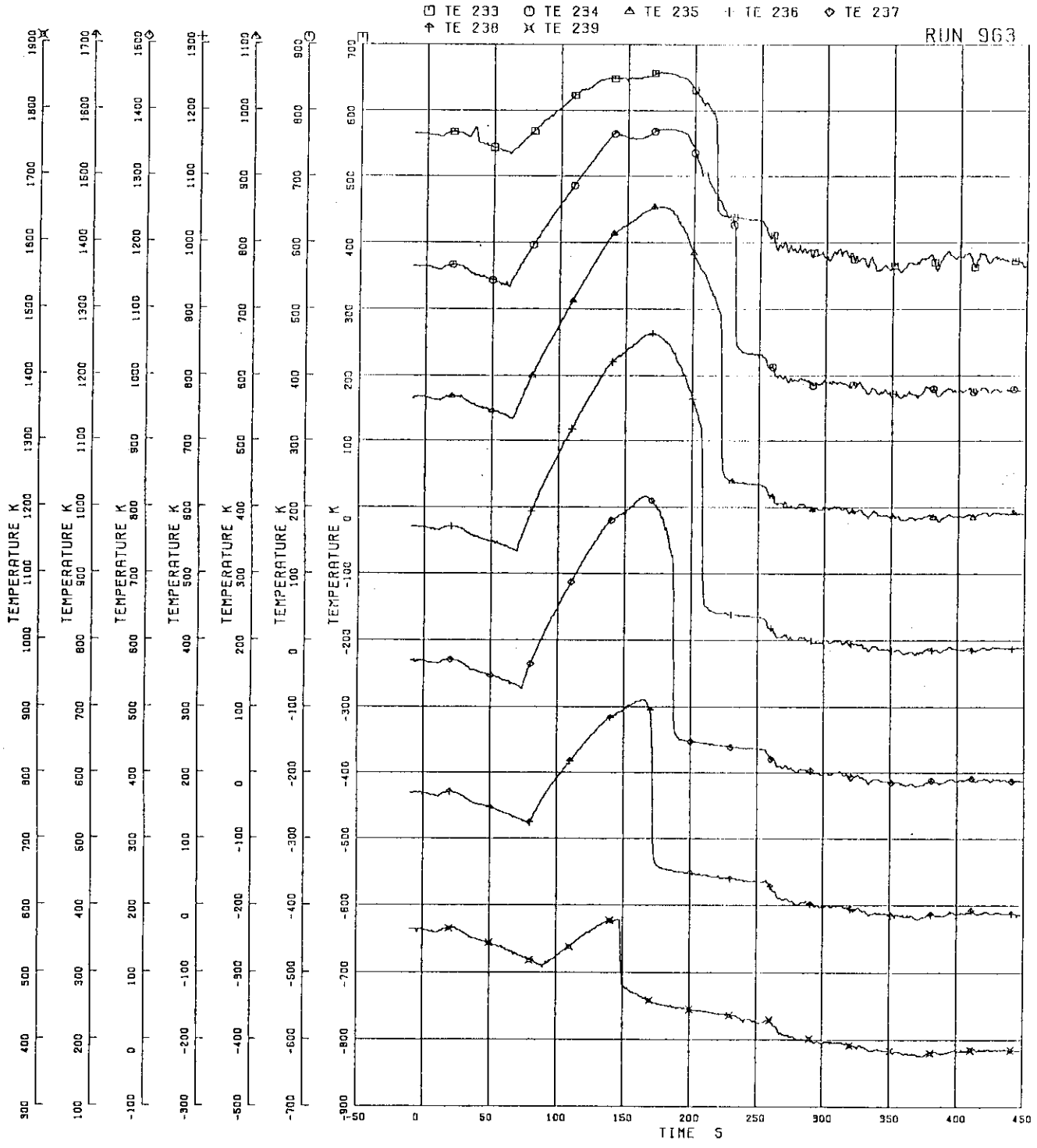

FIG.5.242 SURFACE TEMPERATURES OF FUEL ROD A22

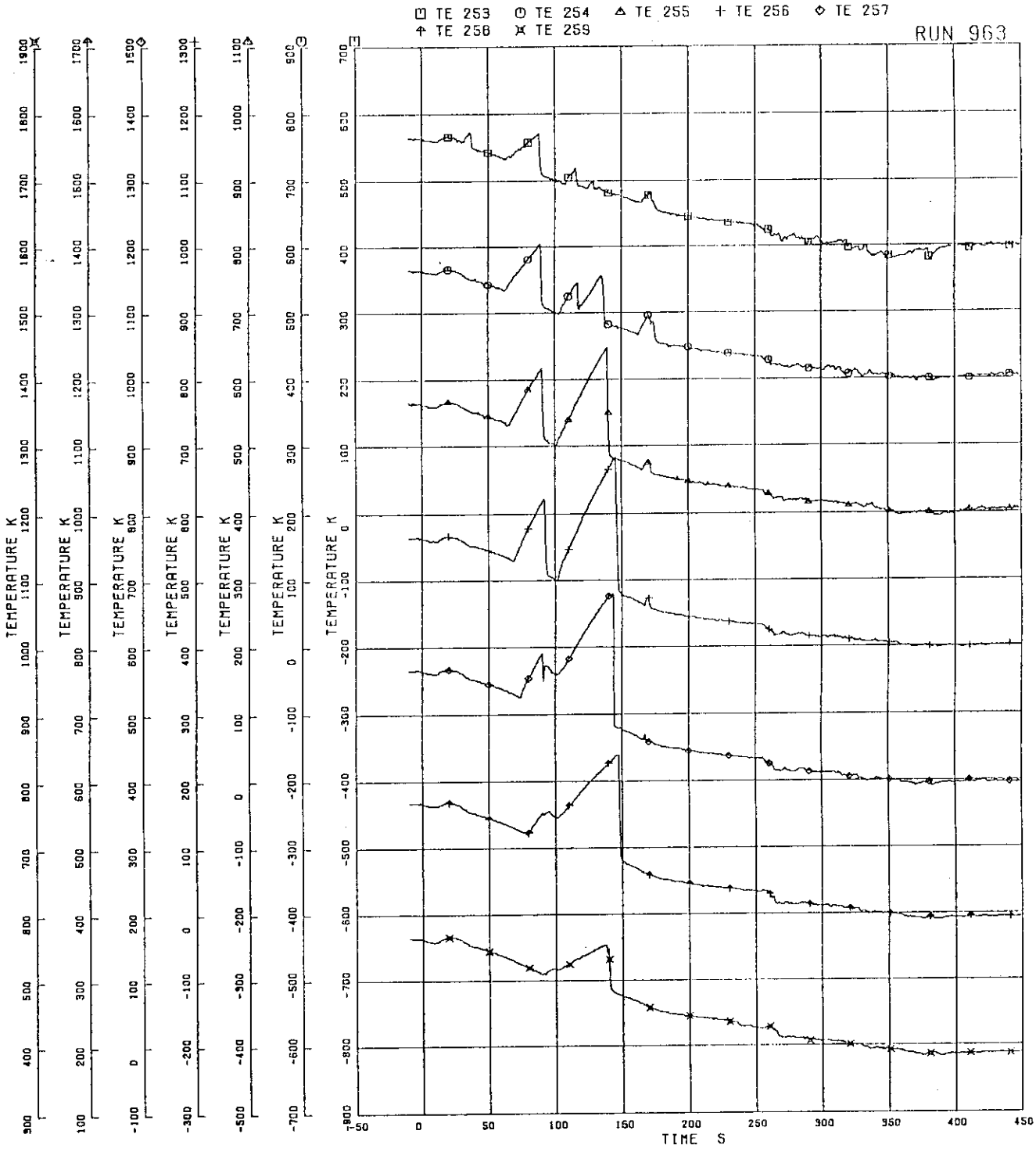

FIG.5.243 SURFACE TEMPERATURES OF FUEL ROD A33

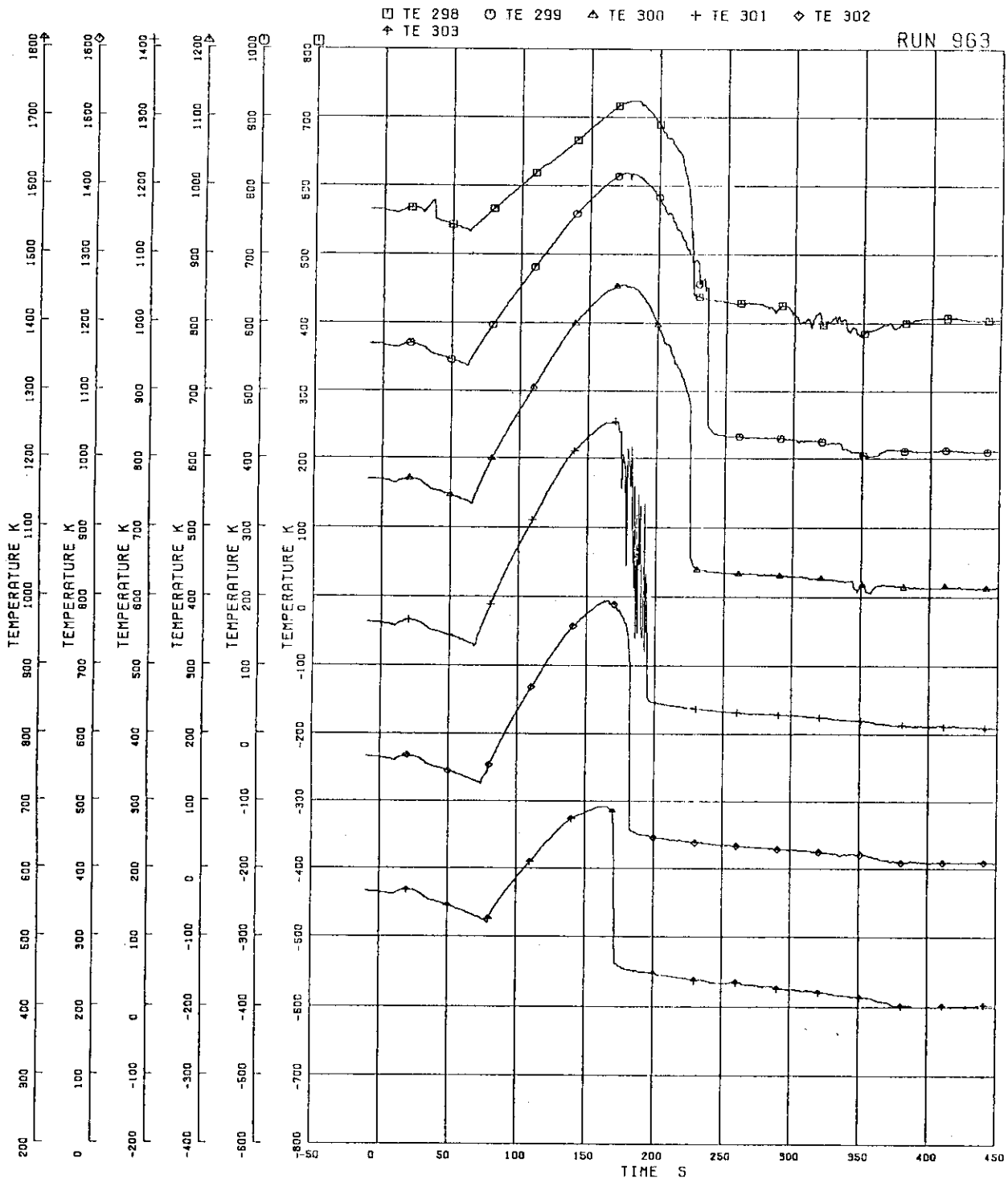

FIG.5.244 SURFACE TEMPERATURES OF FUEL ROD A77

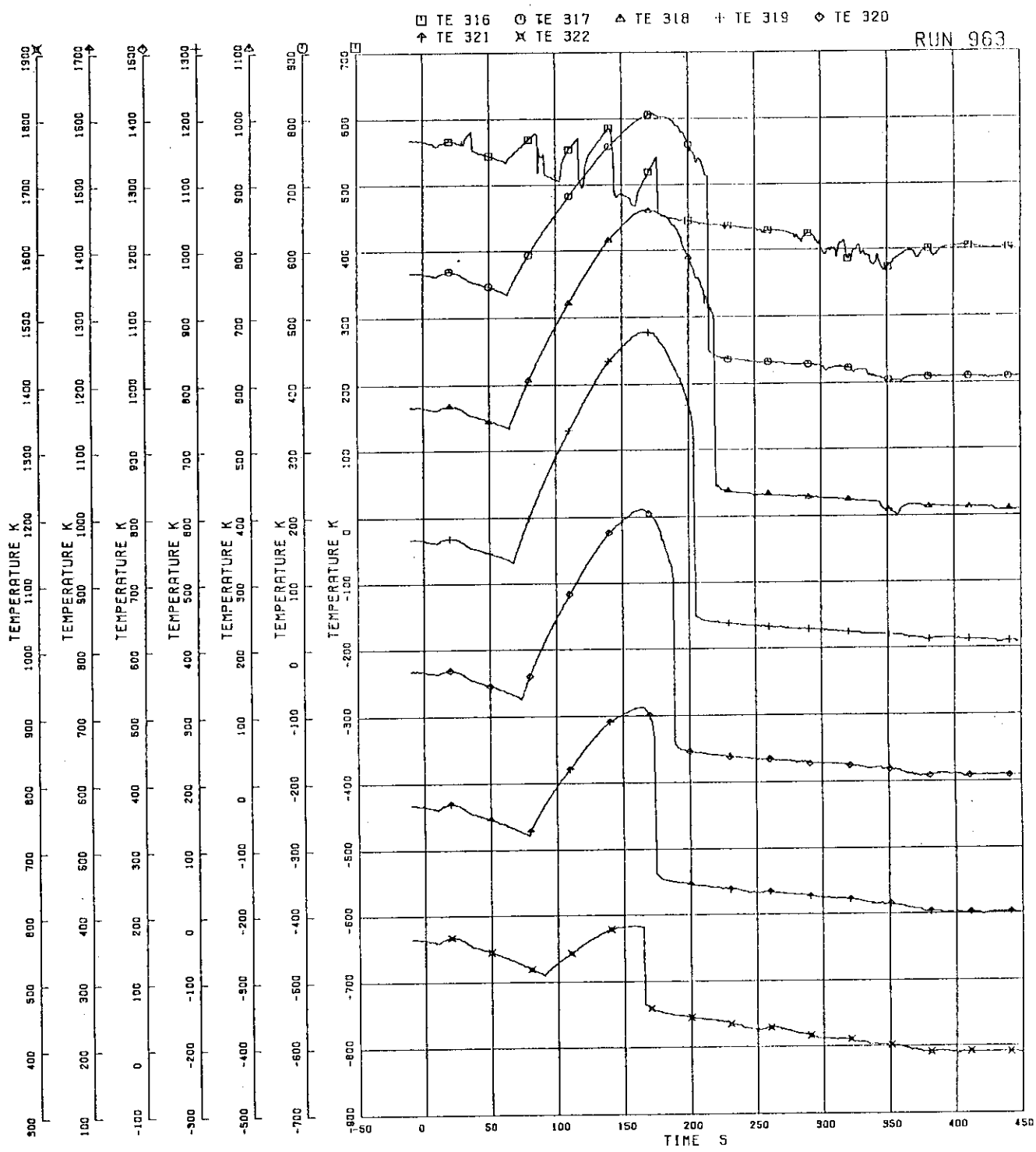

FIG.5.245 SURFACE TEMPERATURES OF FUEL ROD A87

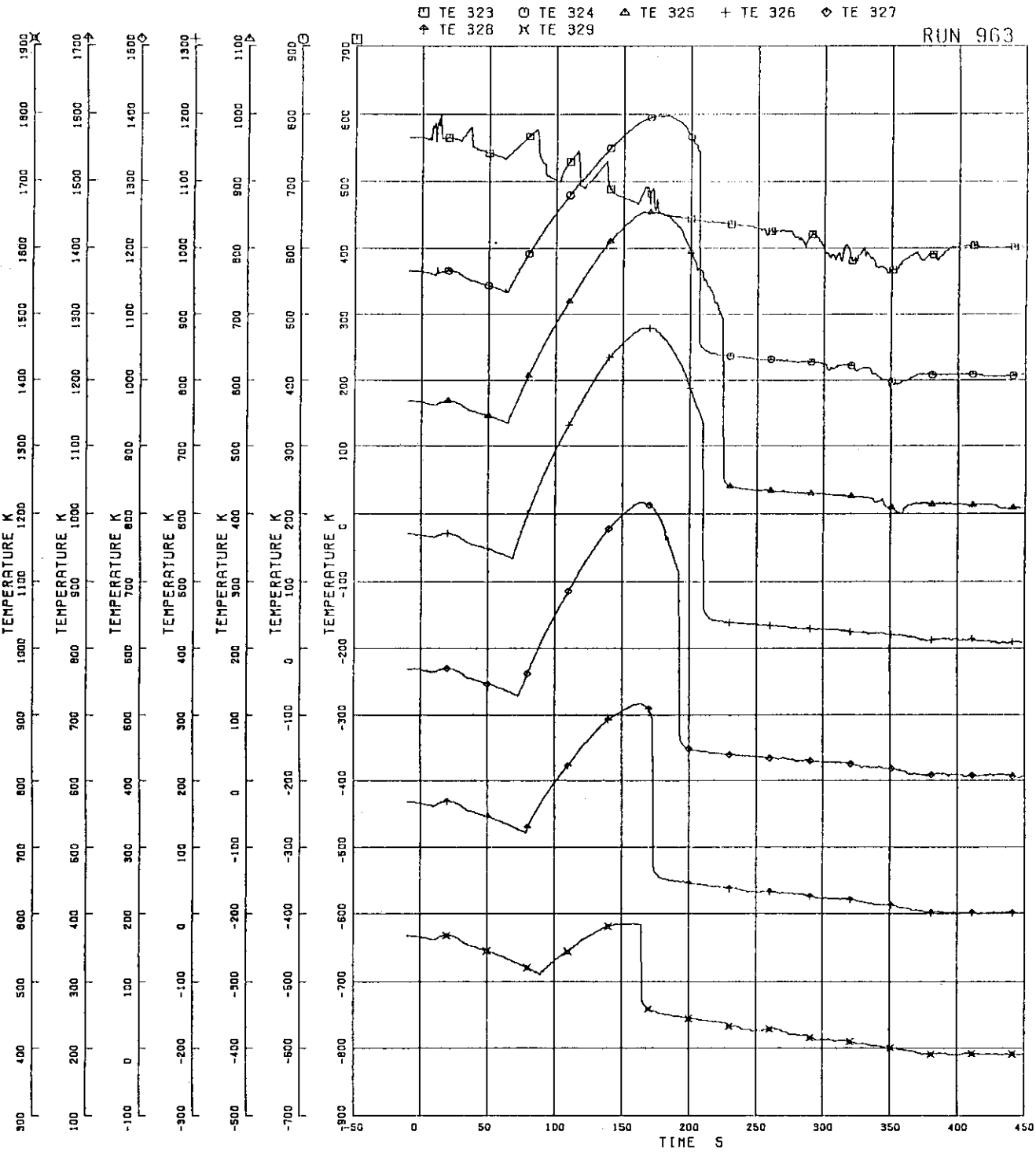

FIG.5.246 SURFACE TEMPERATURES OF FUEL ROD A88

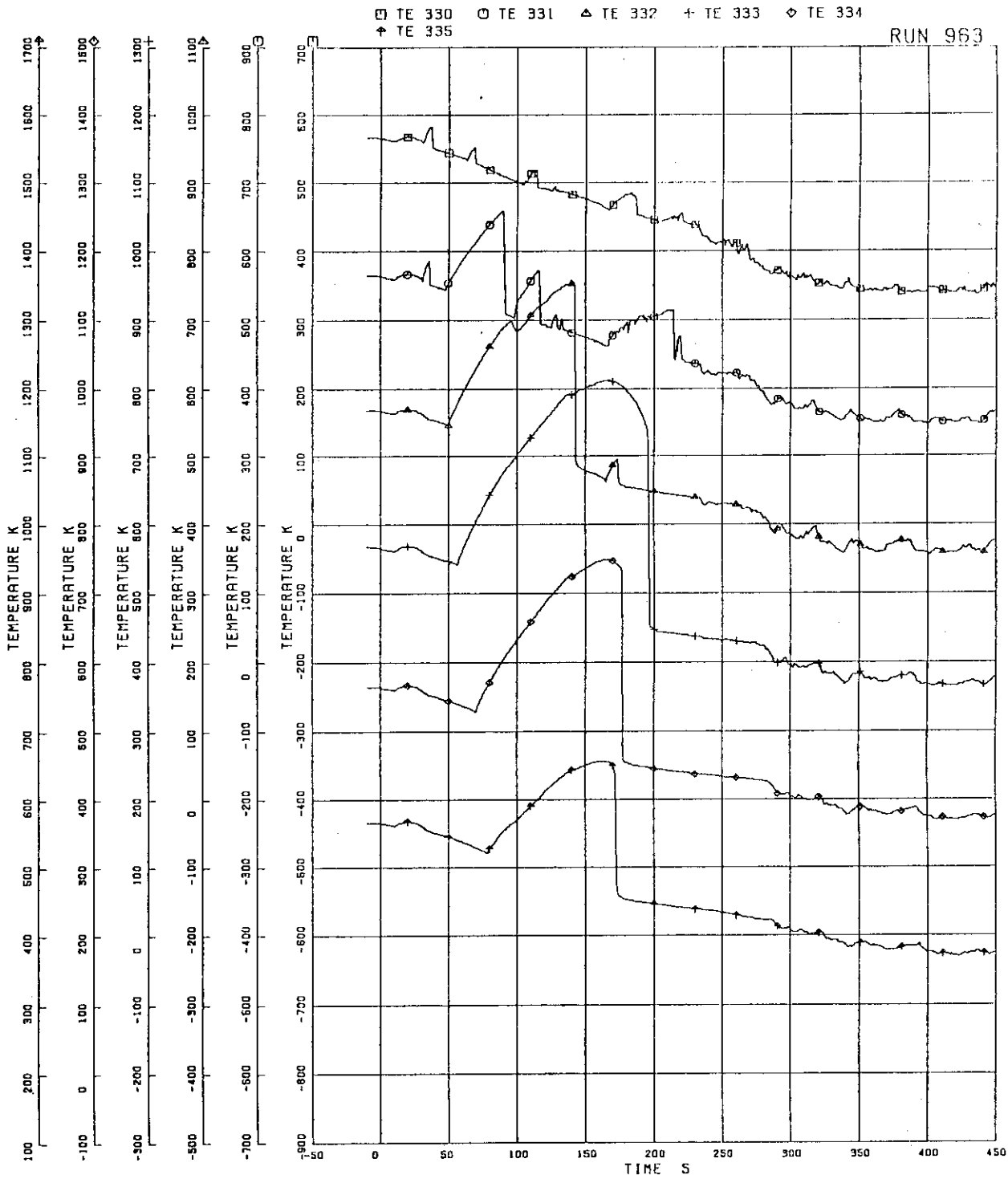

FIG.5-247 SURFACE TEMPERATURES OF FUEL ROD B11

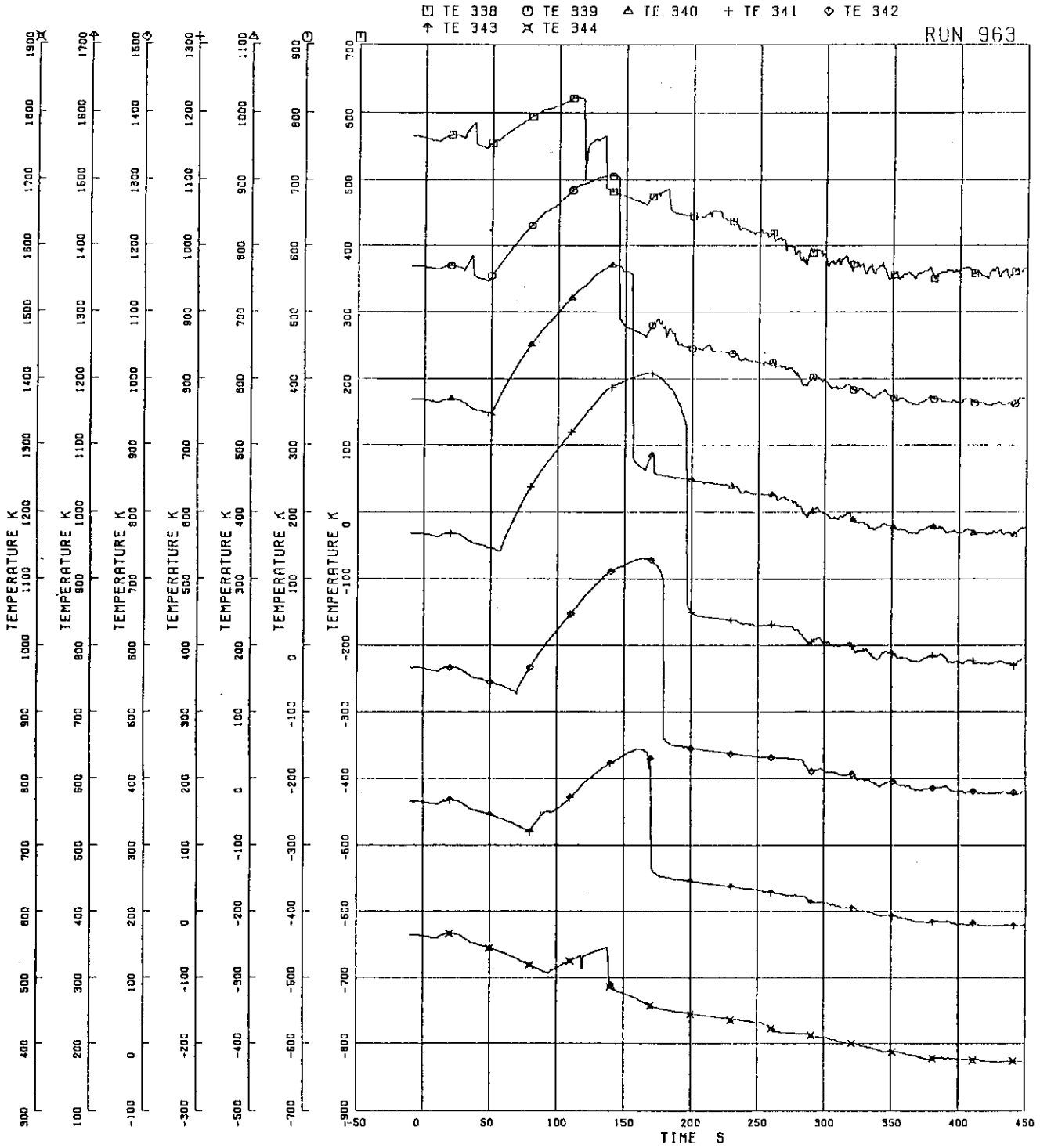

FIG.5.248 SURFACE TEMPERATURES OF FUEL ROD B22

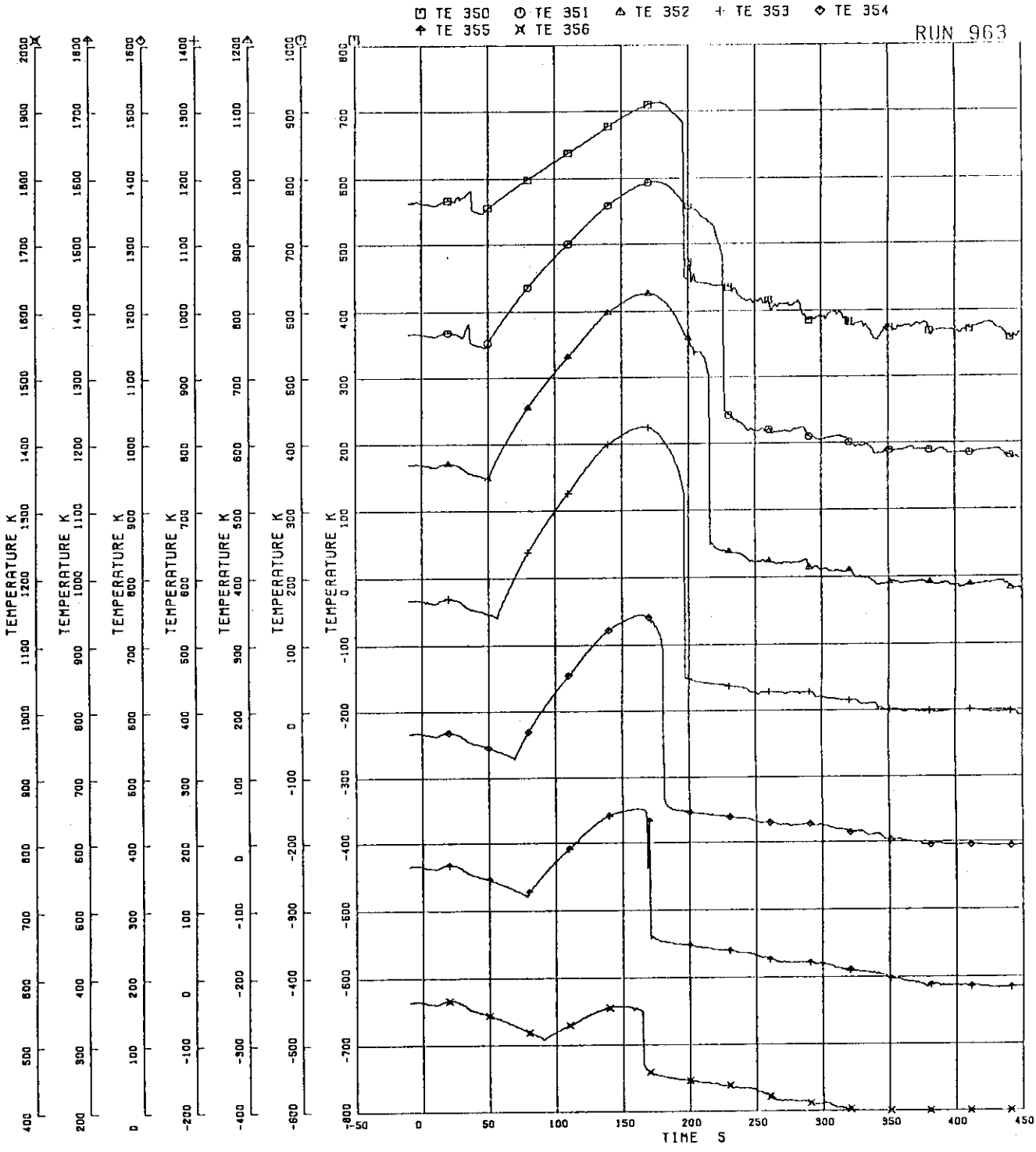

FIG.5.249 SURFACE TEMPERATURES OF FUEL ROD B77

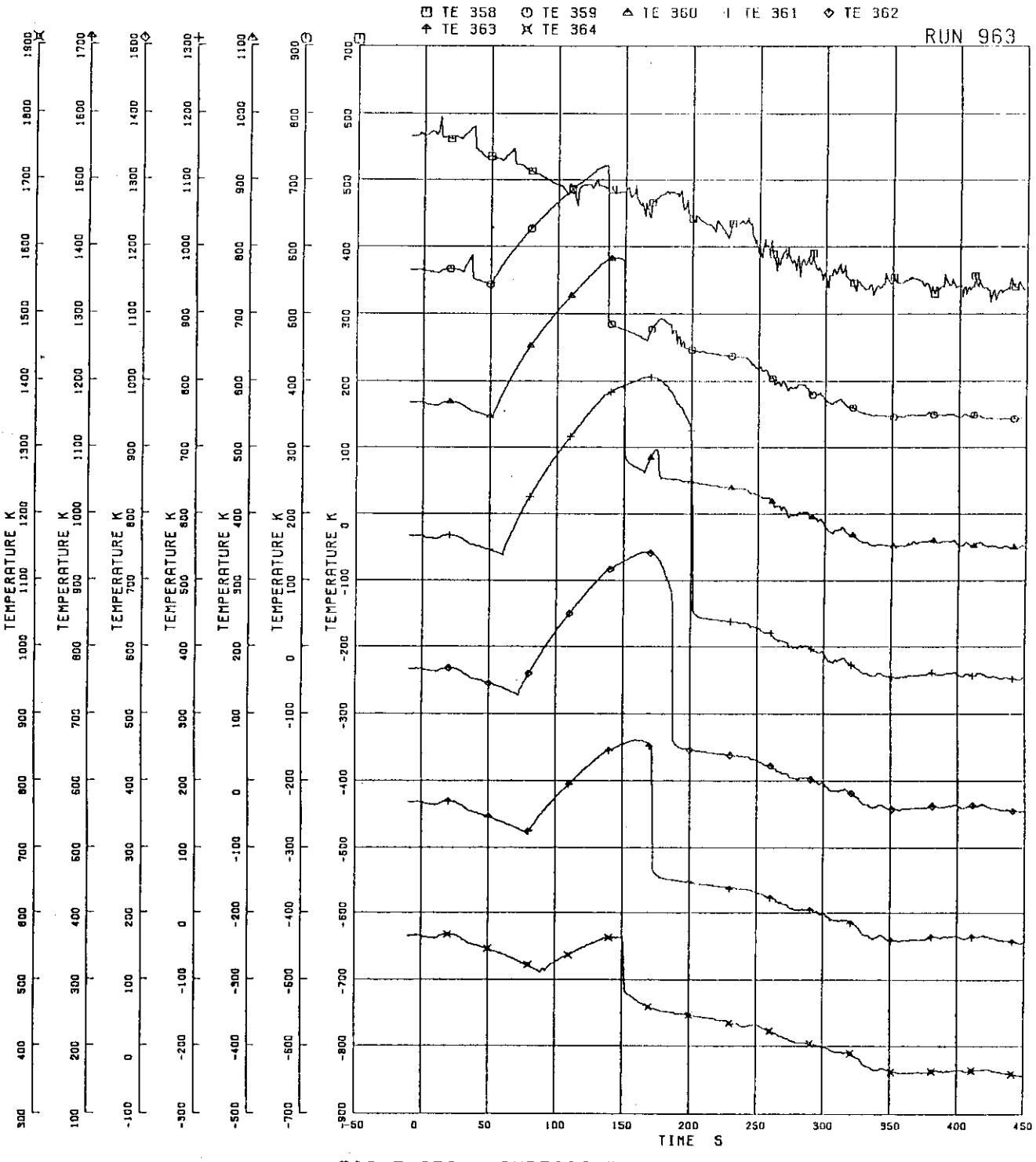

FIG.5.250 SURFACE TEMPERATURES OF FUEL ROD C11

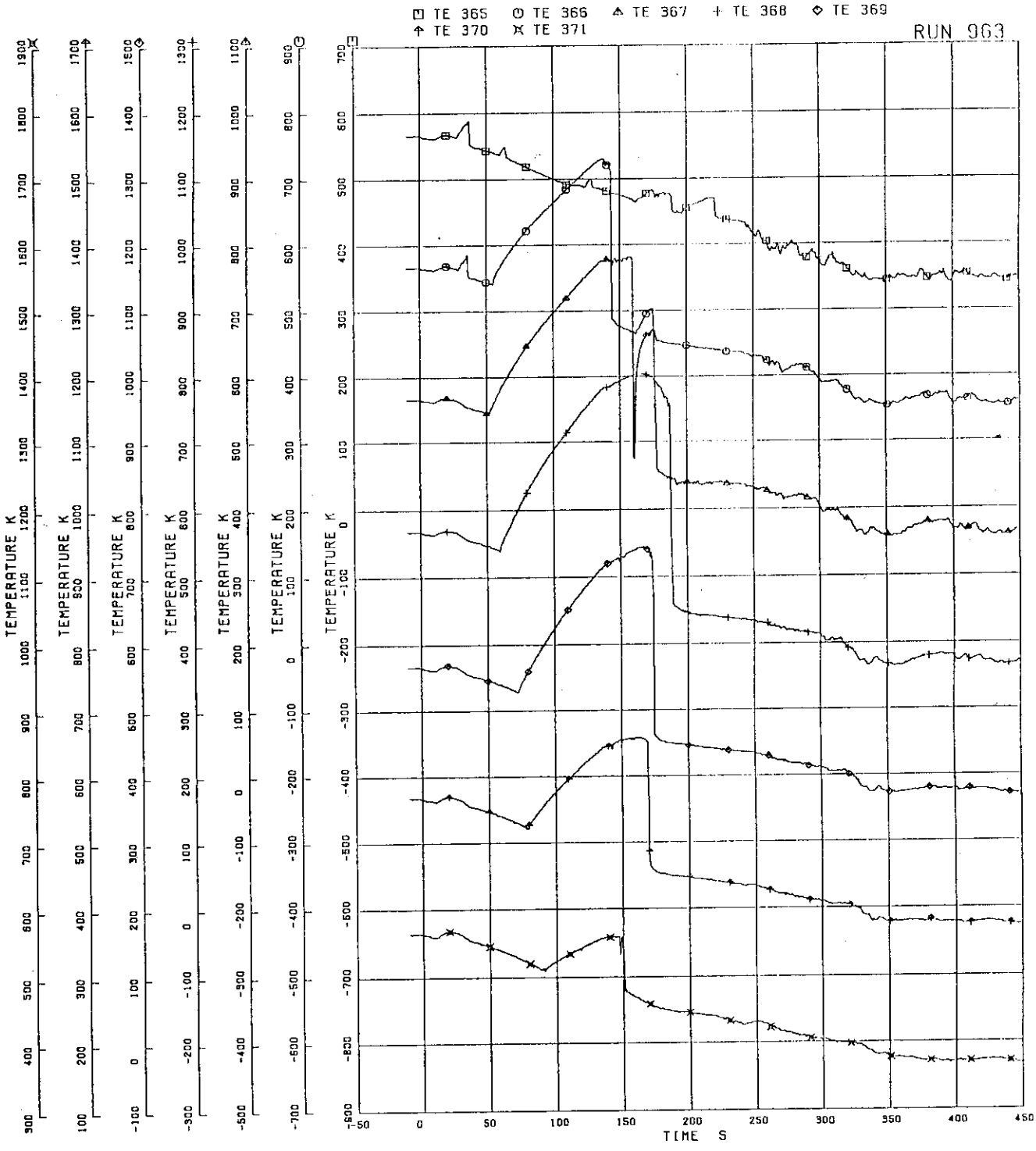

FIG.5.251 SURFACE TEMPERATURES OF FUEL ROD C13

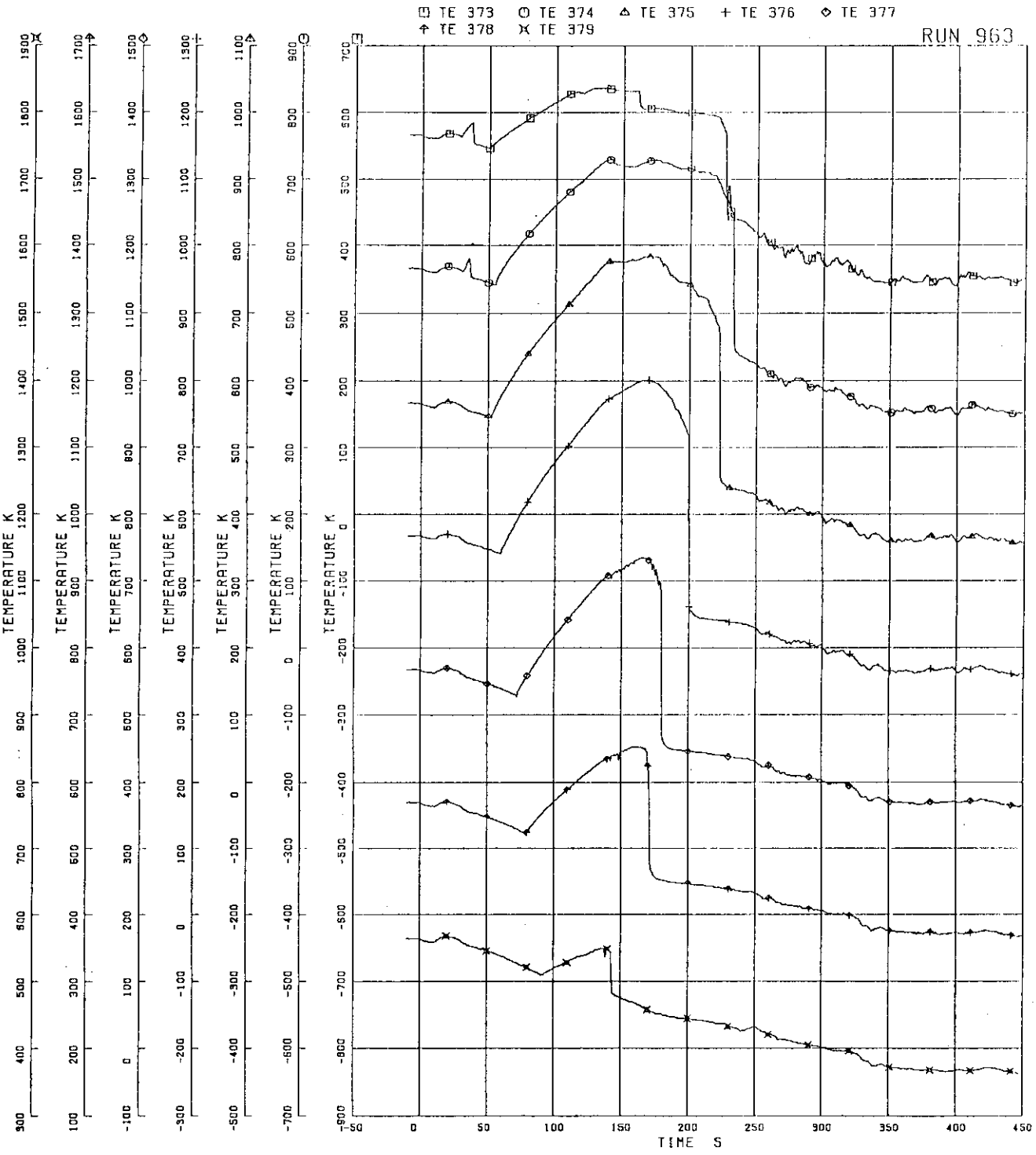

FIG.5.252 SURFACE TEMPERATURES OF FUEL ROD C22

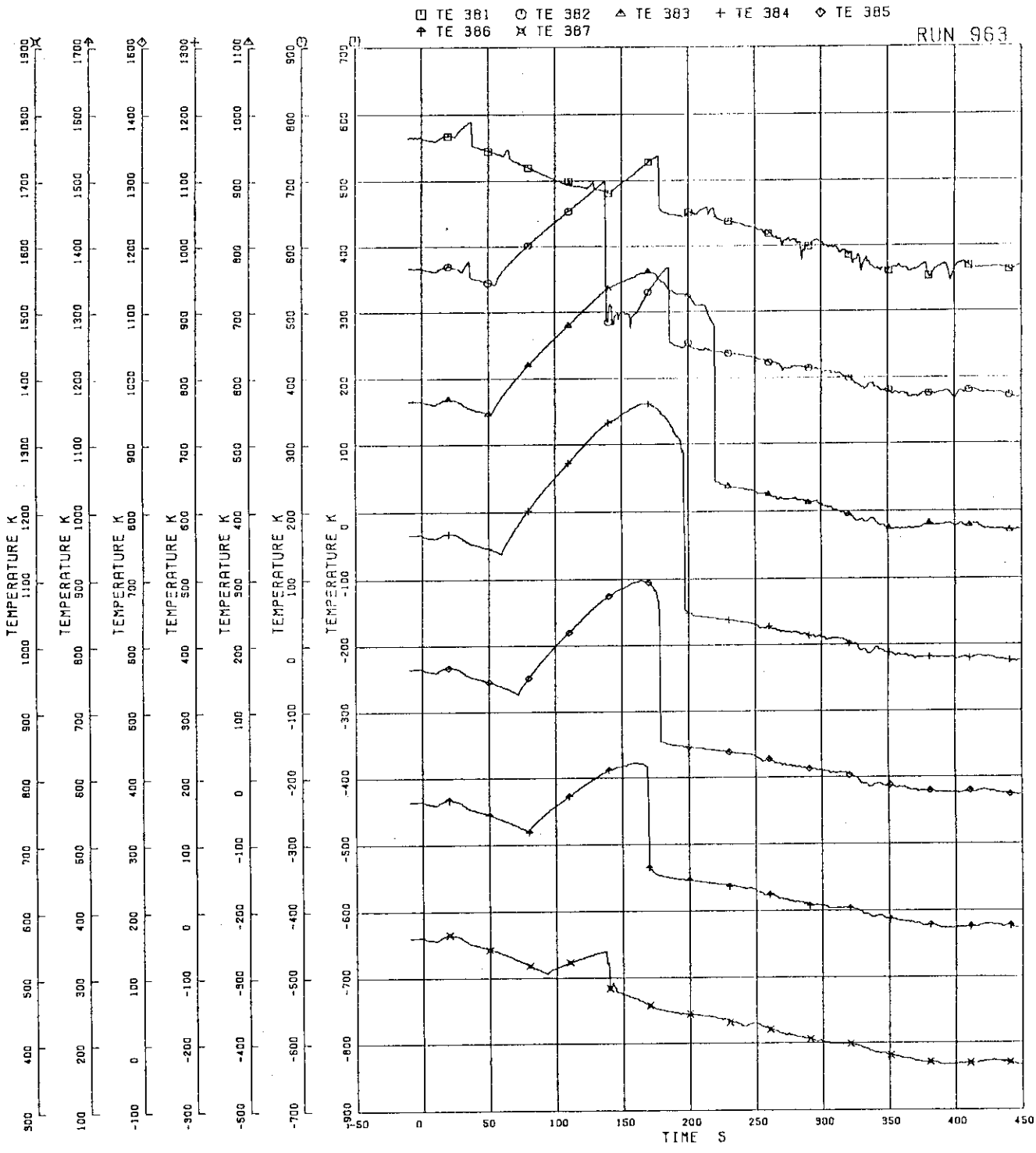

FIG.5.253 SURFACE TEMPERATURES OF FUEL ROD C33

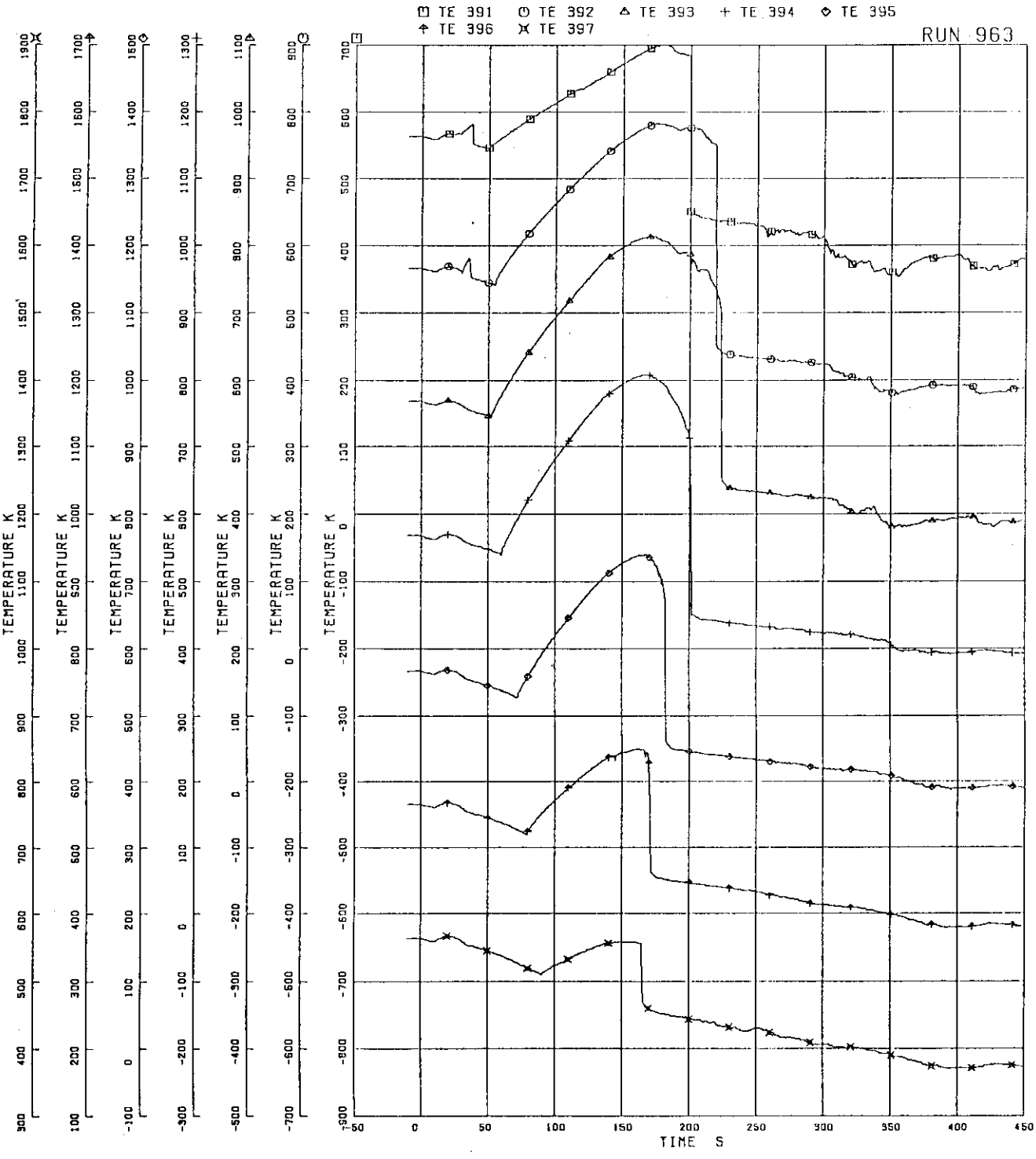

FIG.5-254 SURFACE TEMPERATURES OF FUEL ROD C77

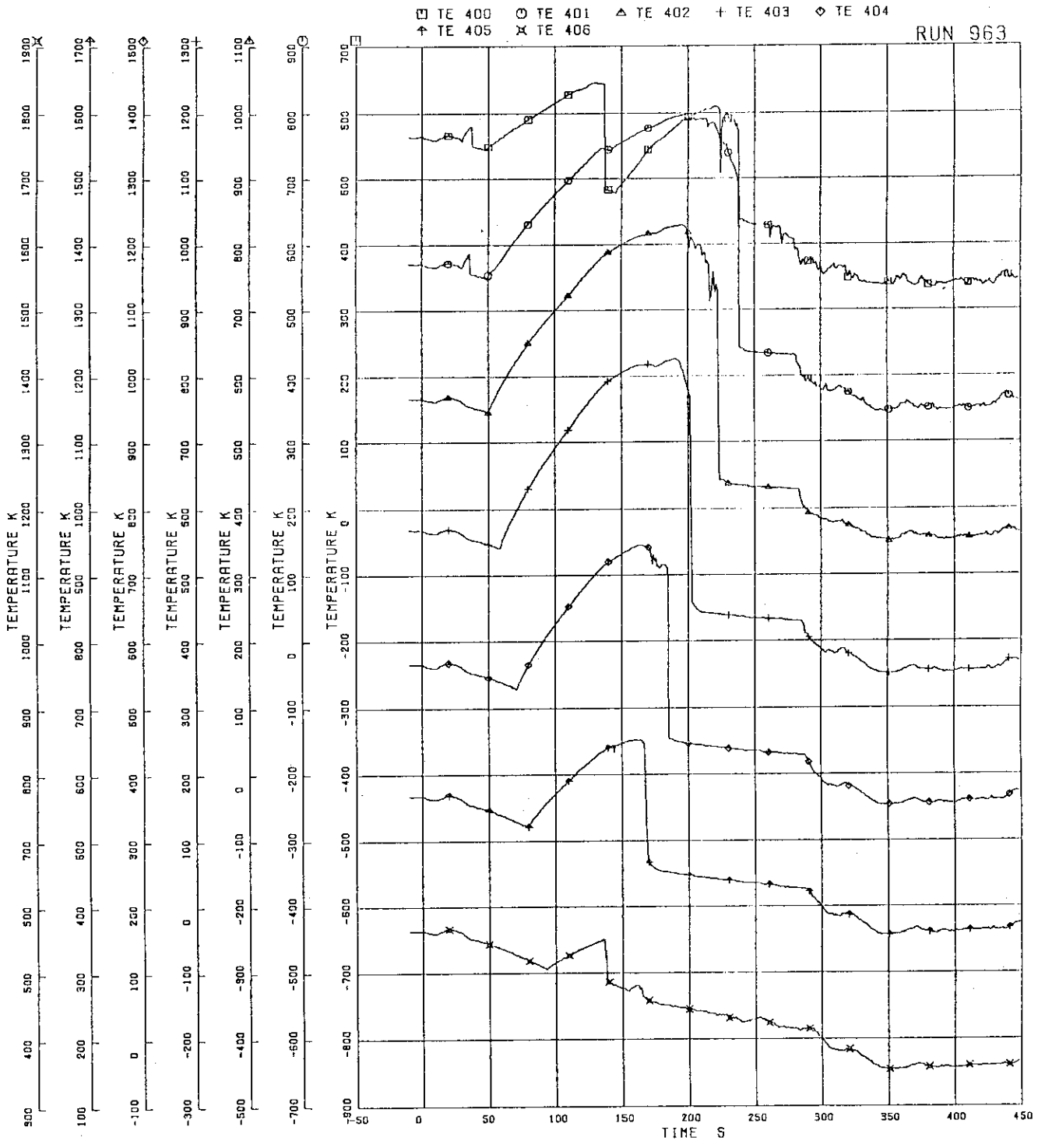

FIG.5.255 SURFACE TEMPERATURES OF FUEL ROD D22

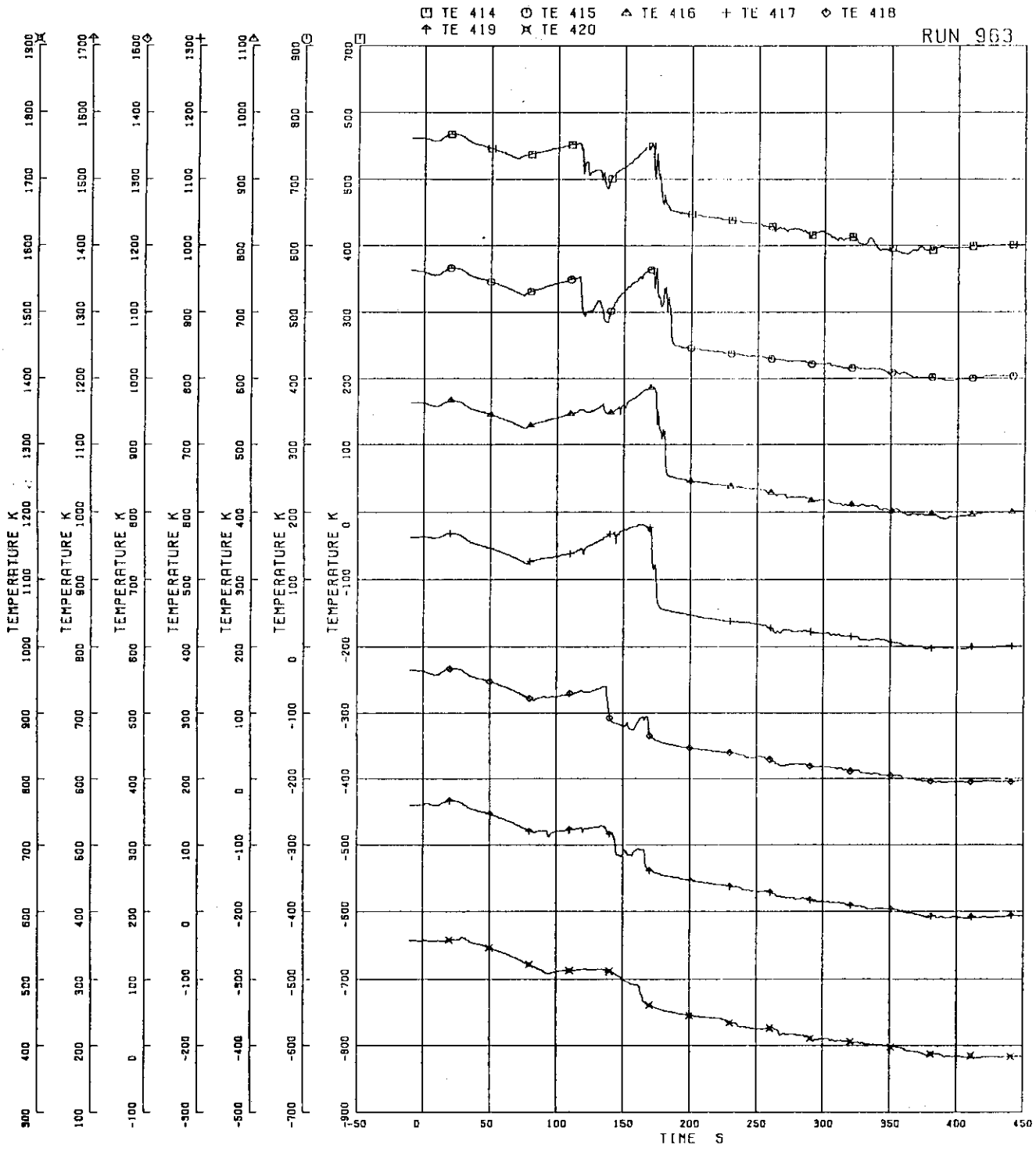

FIG.5.256 SURFACE TEMPERATURES OF WATER ROD SIMULATOR A45

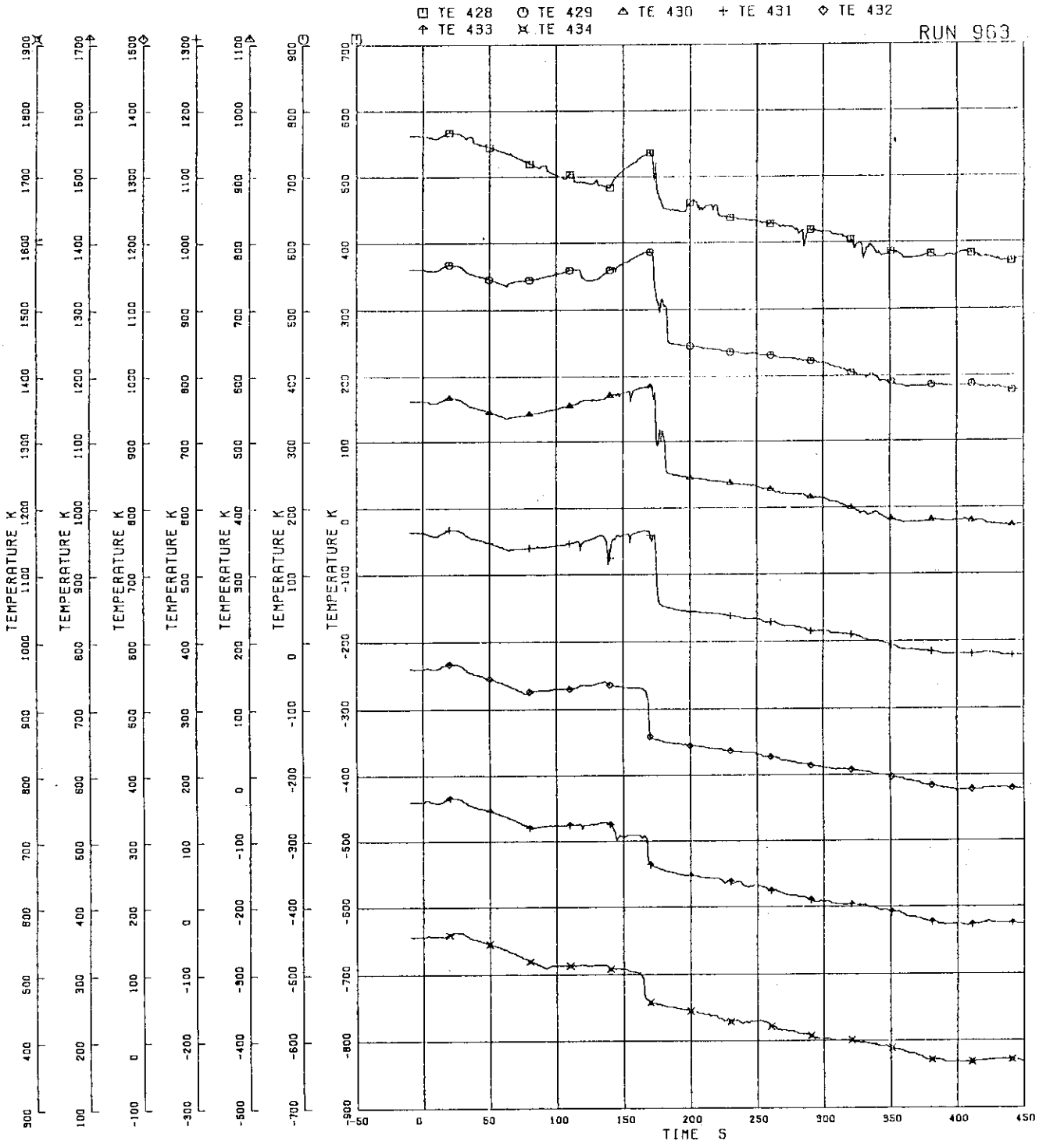

FIG.5.257 SURFACE TEMPERATURES OF WATER ROD SIMULATOR C45

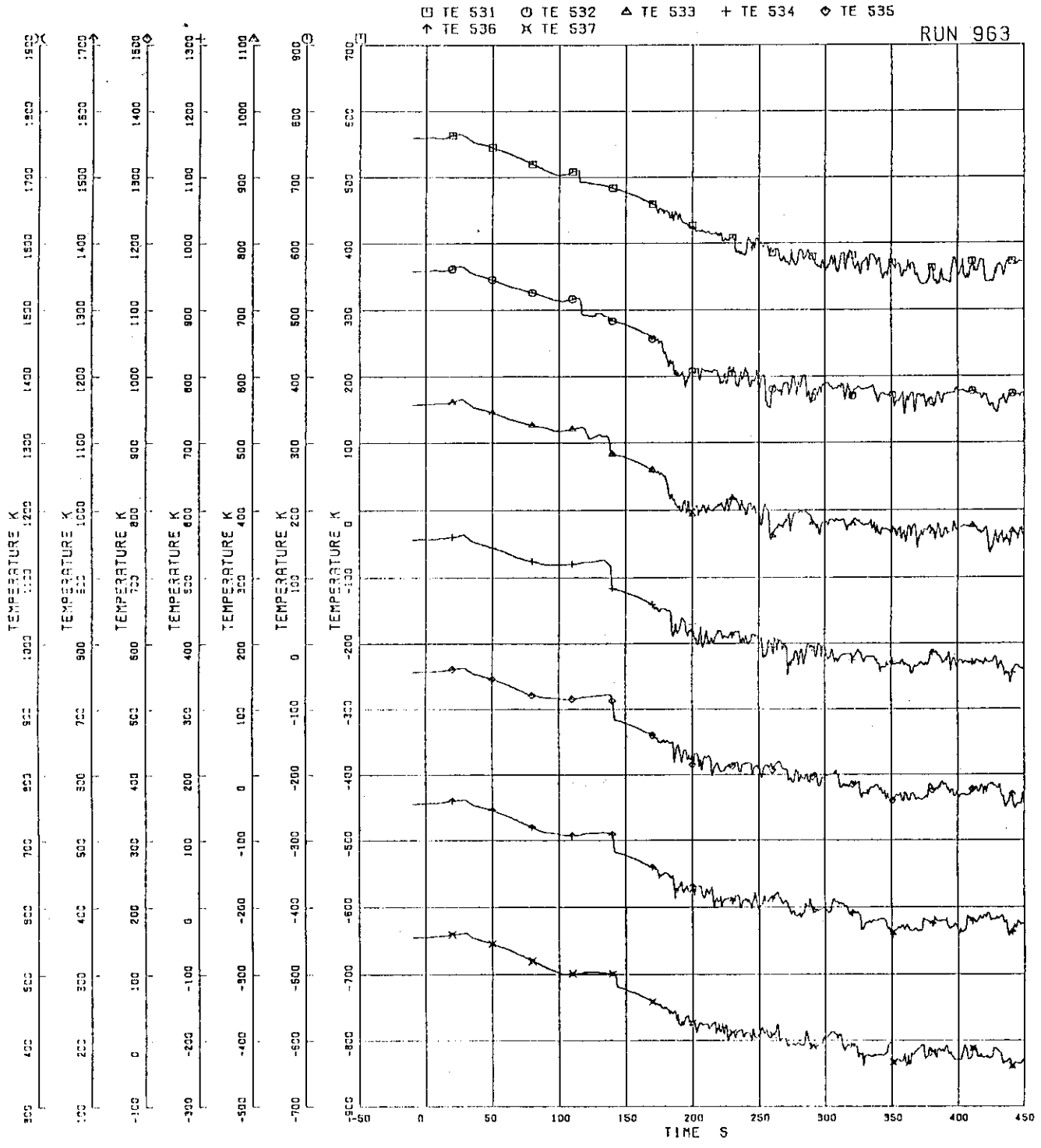

FIG.5.258 OUTER SURFACE TEMPERATURES OF CHANNEL BOX A

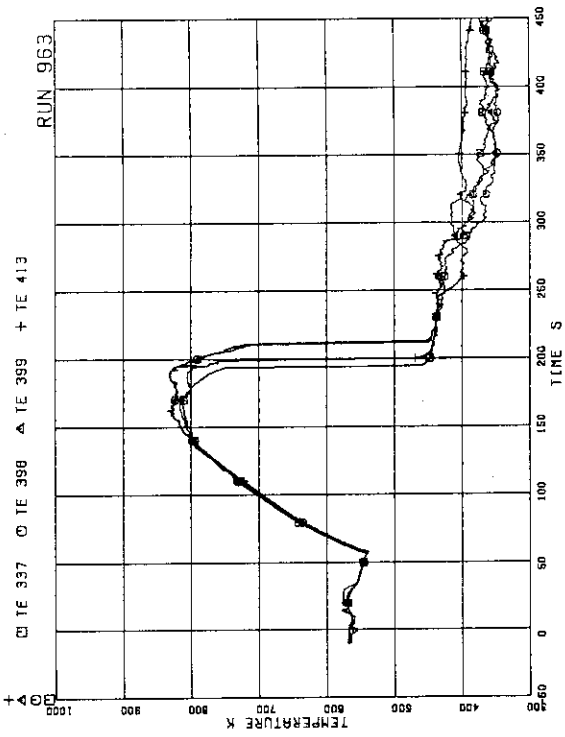

FIG.5.261 SURFACE TEMPERATURES OF B13,D11, D13 AND D86,POSITION 4

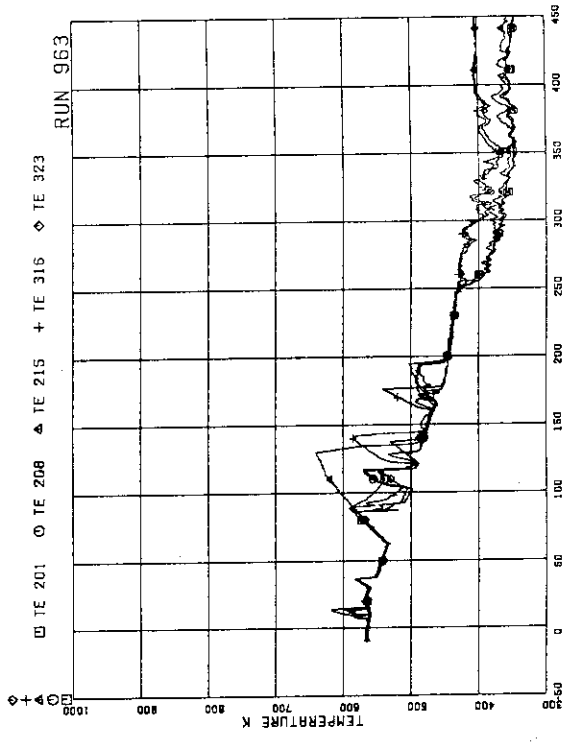

FIG.5.262 SURFACE TEMPERATURES OF FUEL RODS A11,A12,A13,A87,A88 AT POSITION 1

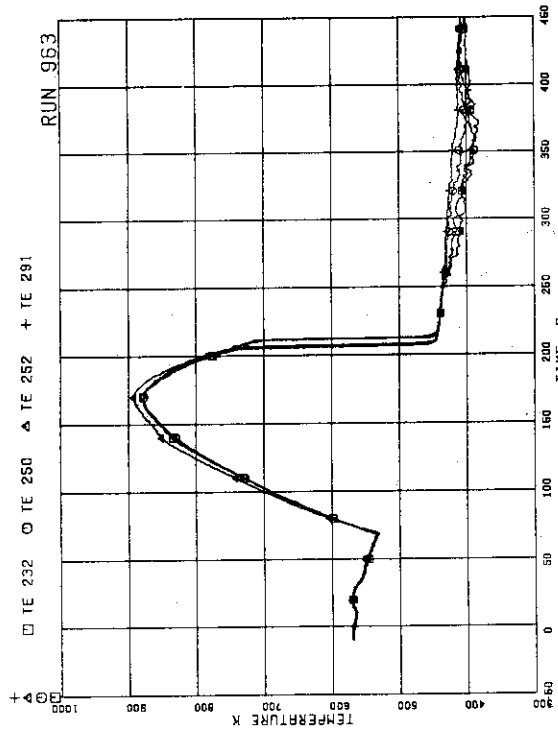

FIG.5.259 SURFACE TEMPERATURES OF PERIPHERAL RODS A17,A28,A31 AND A68,POSITION 4

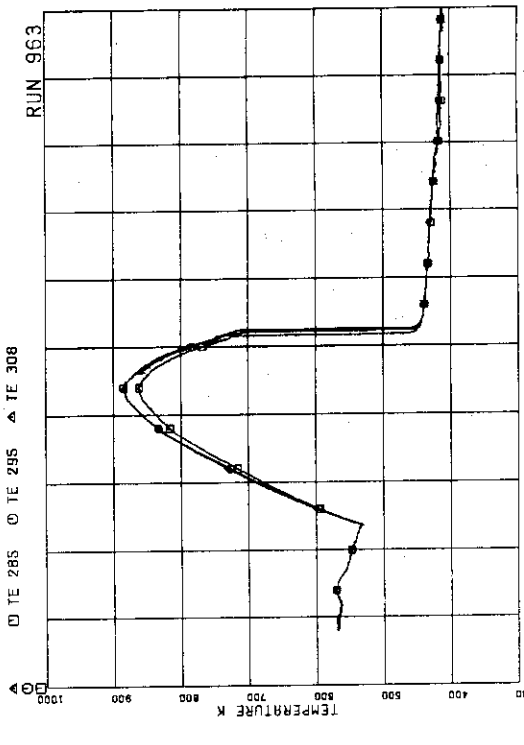

FIG.5.260 SURFACE TEMPERATURES OF A57,A73 AND A84,POSITION 4

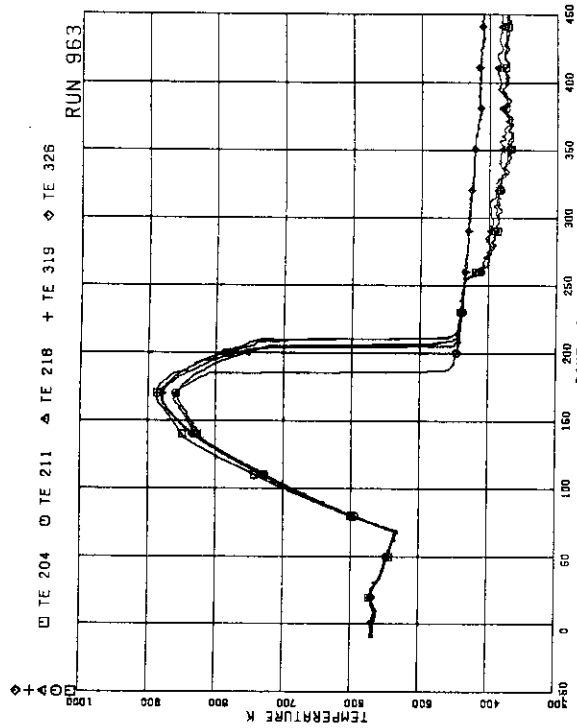

FIG.5.265 SURFACE TEMPERATURES OF FUEL RODS A11,A12,A13,A87,A88 AT POSITION 4

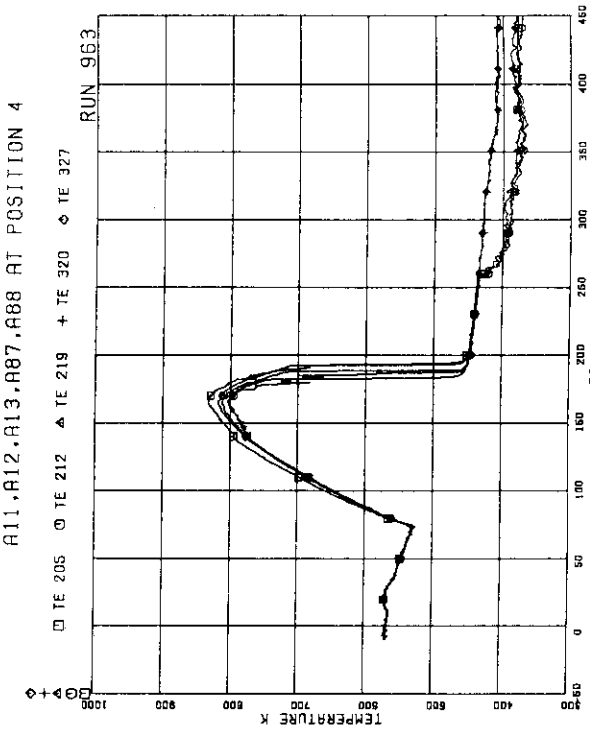

FIG.5.266 SURFACE TEMPERATURES OF FUEL RODS A11,A12,A13,A87,A88 AT POSITION 5

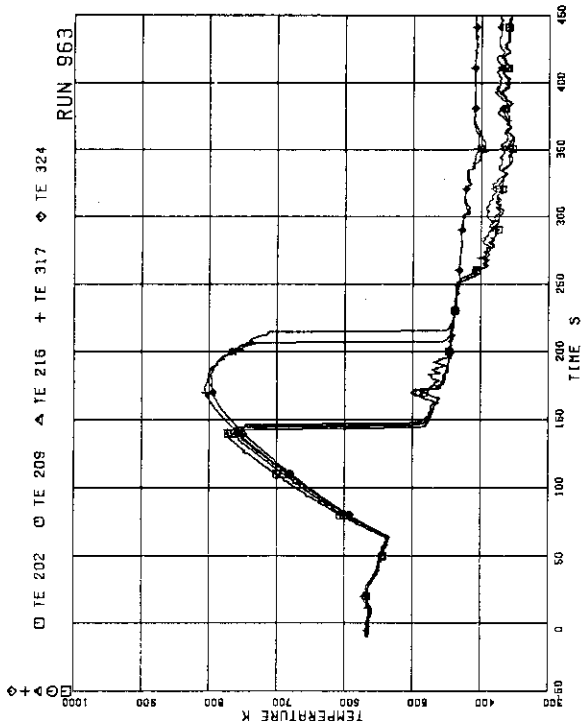

FIG.5.263 SURFACE TEMPERATURES OF FUEL RODS A11,A12,A13,A87,A88 AT POSITION 2

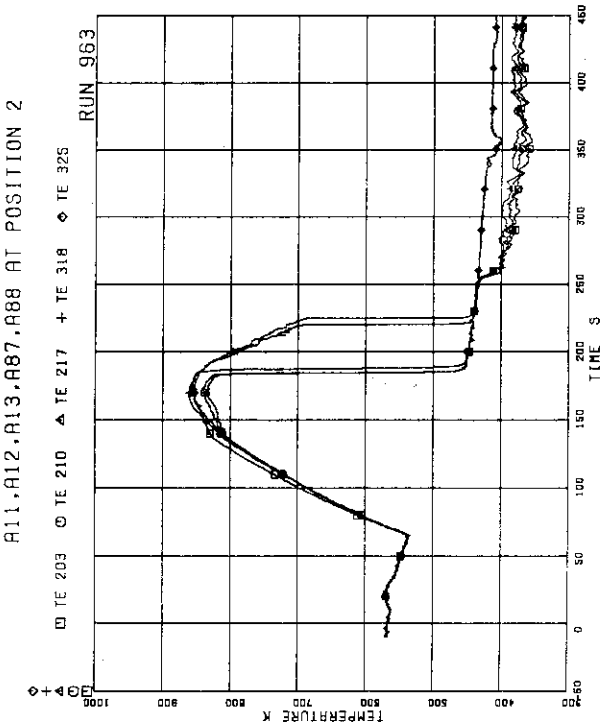

FIG.5.264 SURFACE TEMPERATURES OF FUEL RODS A11,A12,A13,A87,A88 AT POSITION 3

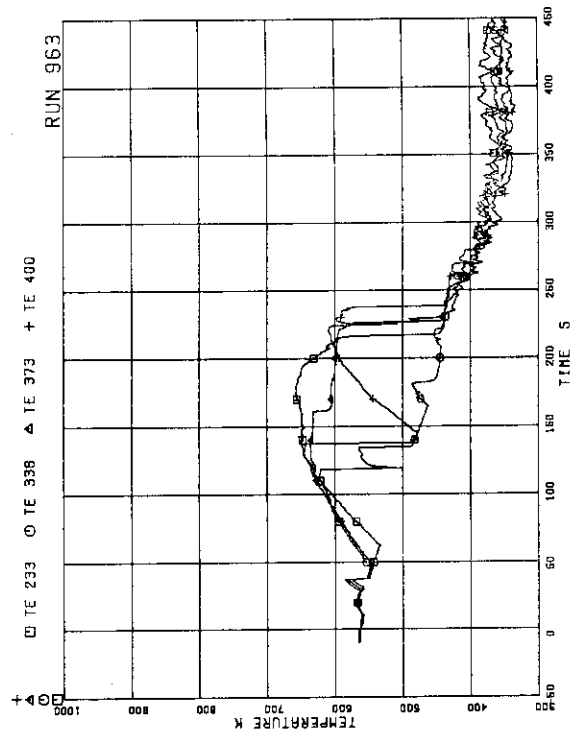

FIG.5.269 SURFACE TEMPERATURES OF FUEL RODS A22,B22,C22,D22 AT POSITION 1

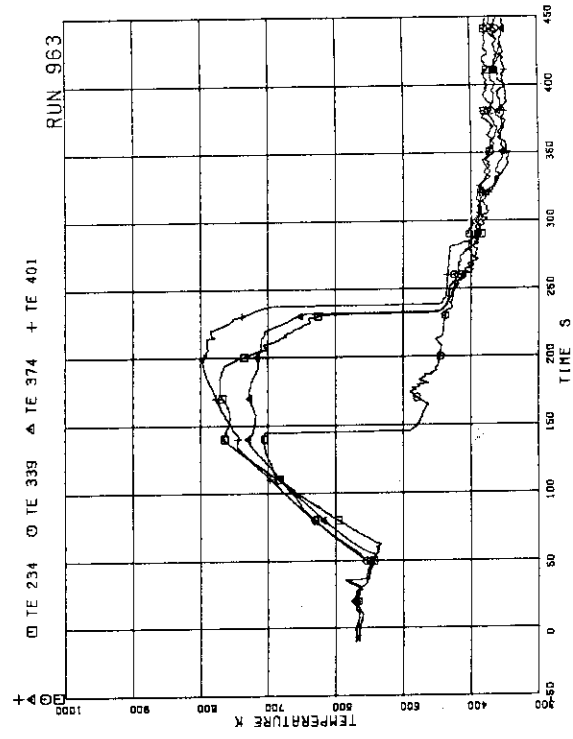

FIG.5.270 SURFACE TEMPERATURES OF FUEL RODS A22,B22,C22,D22 AT POSITION 2

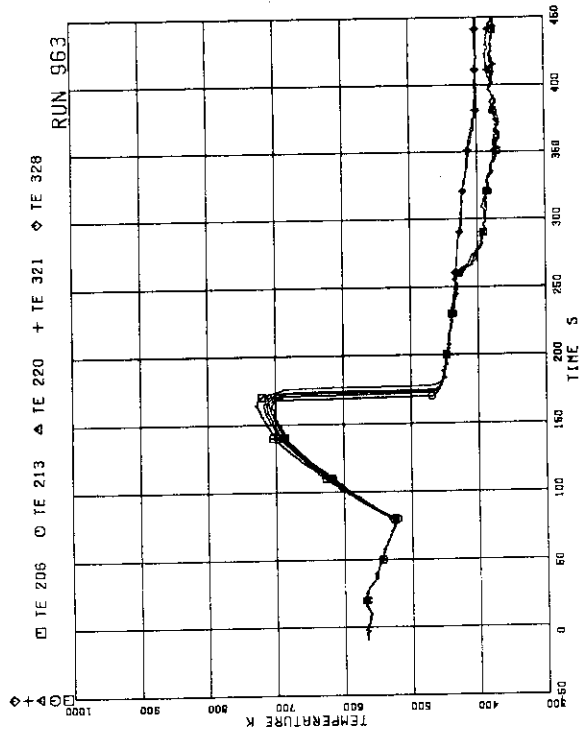

FIG.5.267 SURFACE TEMPERATURES OF FUEL RODS A11,A12,A13,A87,A88 AT POSITION 6

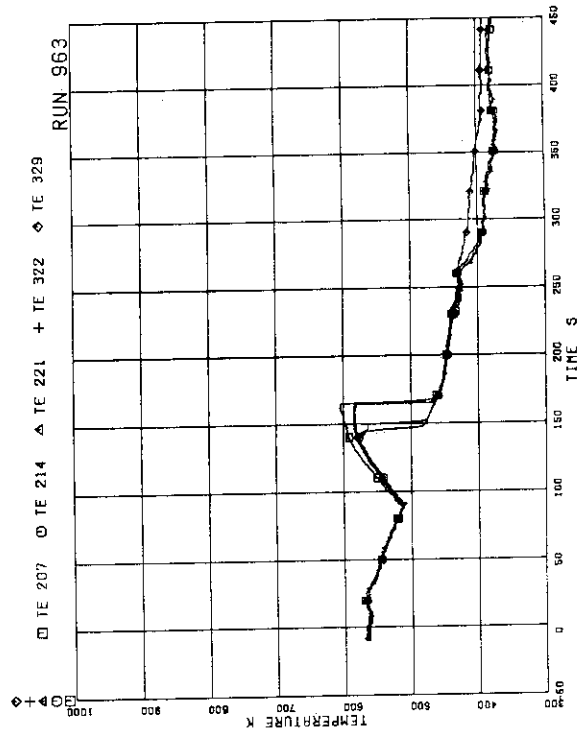

FIG.5.268 SURFACE TEMPERATURES OF FUEL RODS A11,A12,A13,A87,A88 AT POSITION 7

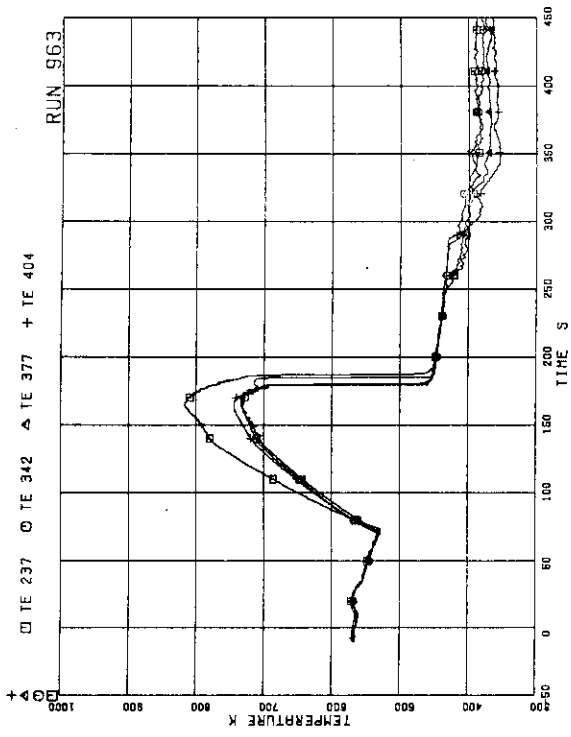

FIG.5.273 SURFACE TEMPERATURES OF FUEL RODS A22,B22,C22,D22 AT POSITION 5

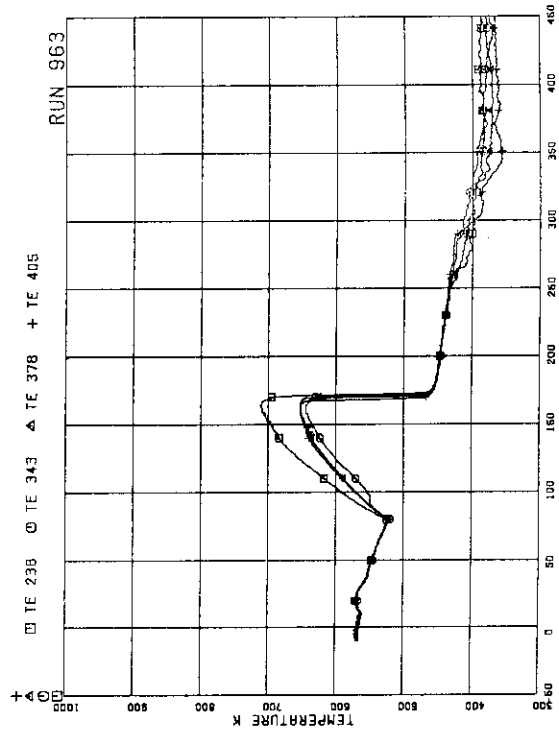

FIG.5.274 SURFACE TEMPERATURES OF FUEL RODS A22,B22,C22,D22 AT POSITION 6

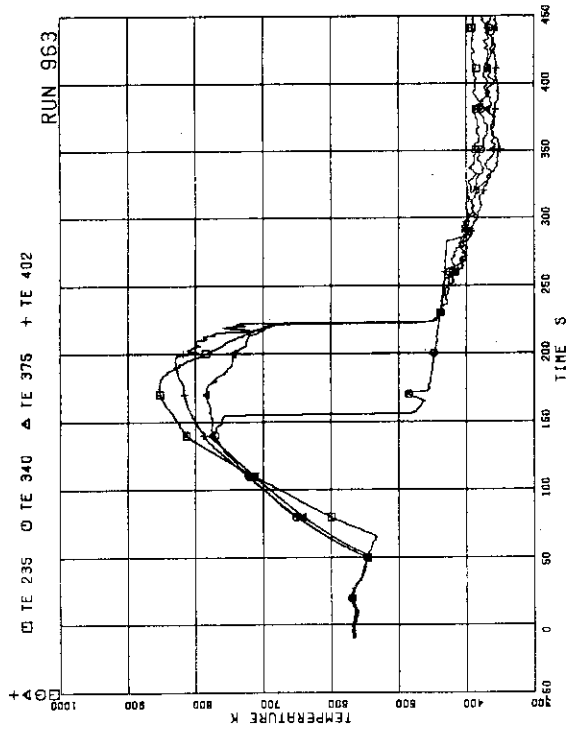

FIG.5.271 SURFACE TEMPERATURES OF FUEL RODS A22,B22,C22,D22 AT POSITION 3

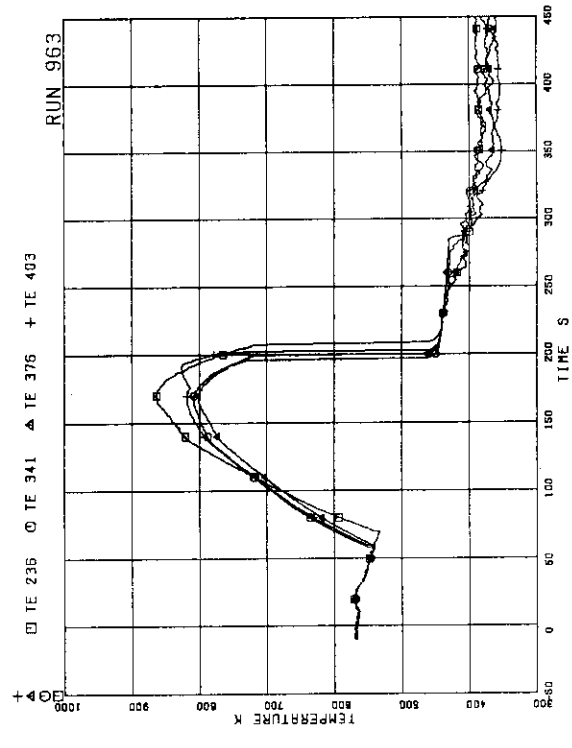

FIG.5.272 SURFACE TEMPERATURES OF FUEL RODS A22,B22,C22,D22 AT POSITION 4

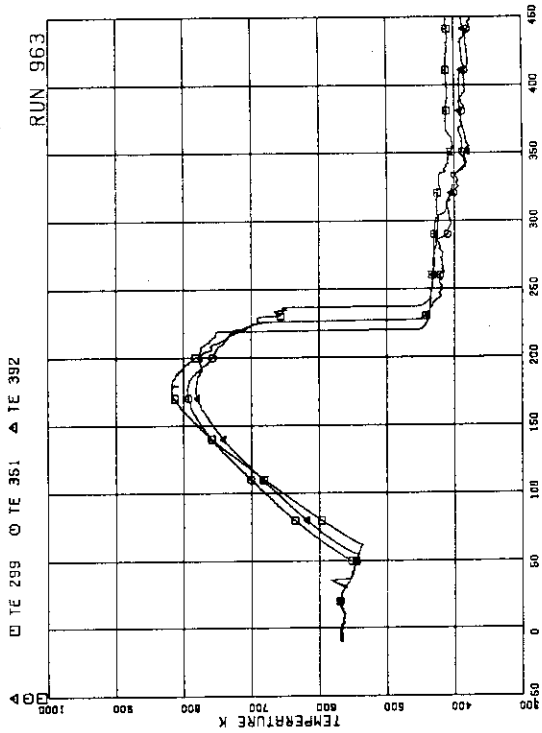

FIG.5.277 SURFACE TEMPERATURES OF FUEL RODS A77,B77,C77 AT POSITION 2

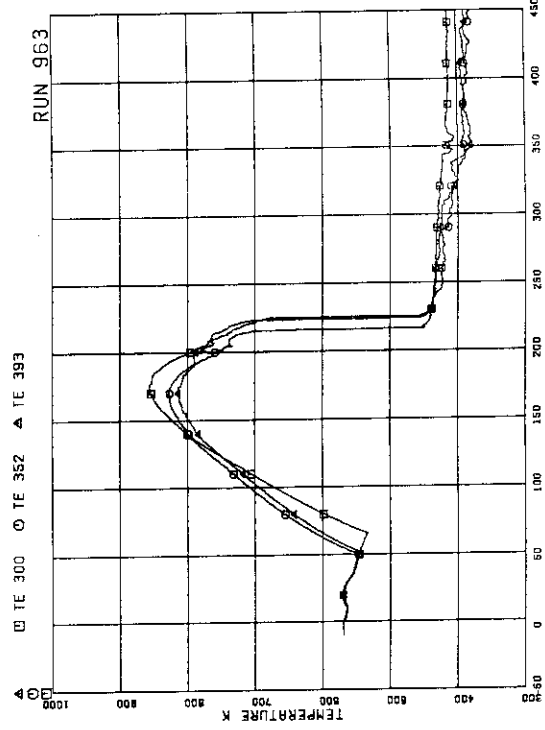

FIG.5.278 SURFACE TEMPERATURES OF FUEL RODS A77,B77,C77 AT POSITION 3

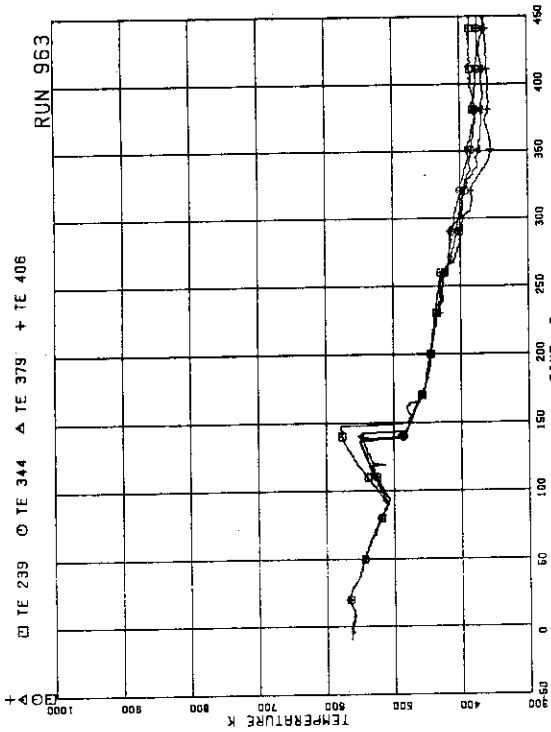

FIG.5.275 SURFACE TEMPERATURES OF FUEL RODS A22,B22,C22,D22 AT POSITION 7

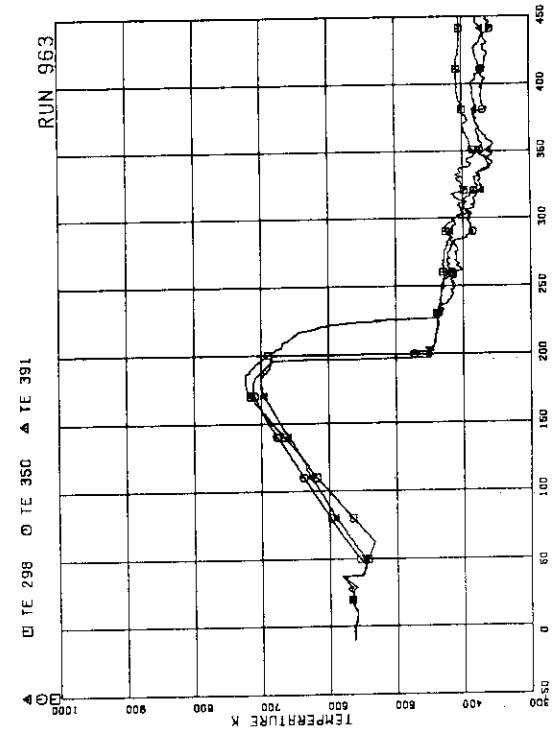

FIG.5.276 SURFACE TEMPERATURES OF FUEL RODS A77,B77,C77 AT POSITION 1

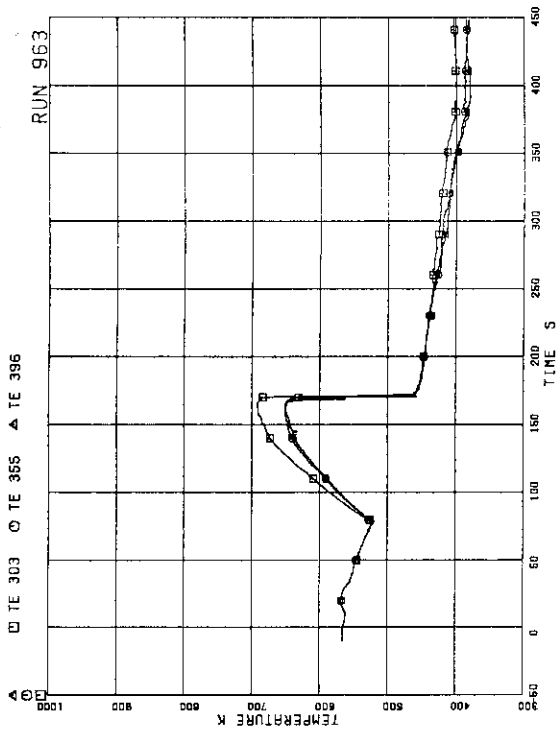

FIG.5.281 SURFACE TEMPERATURES OF FUEL RODS A77,B77,C77 AT POSITION 6

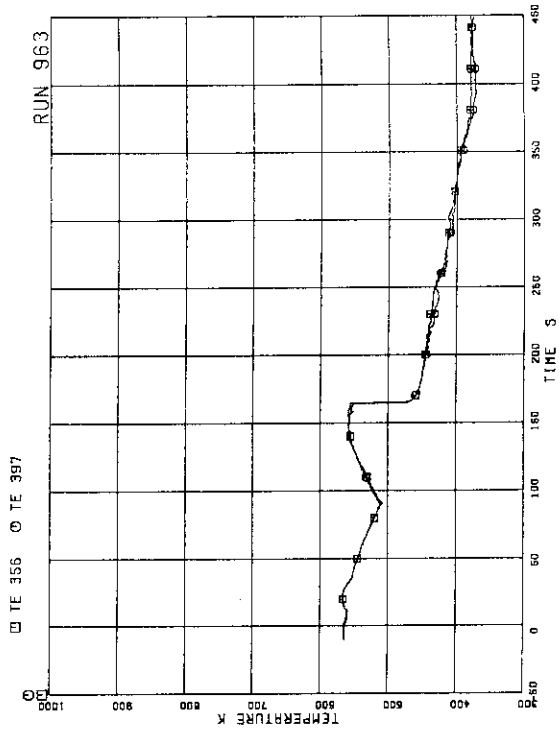

FIG.5.282 SURFACE TEMPERATURES OF FUEL RODS B77,C77 RODS AT POSITION 7

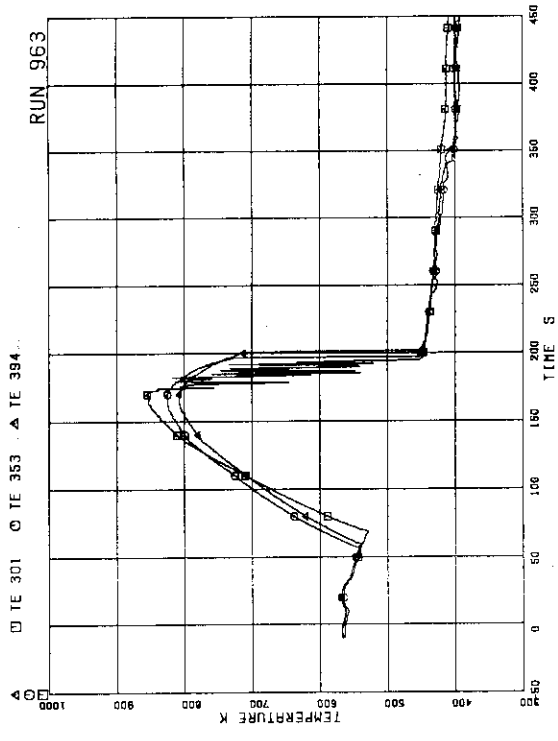

FIG.5.279 SURFACE TEMPERATURES OF FUEL RODS A77,B77,C77 AT POSITION 4

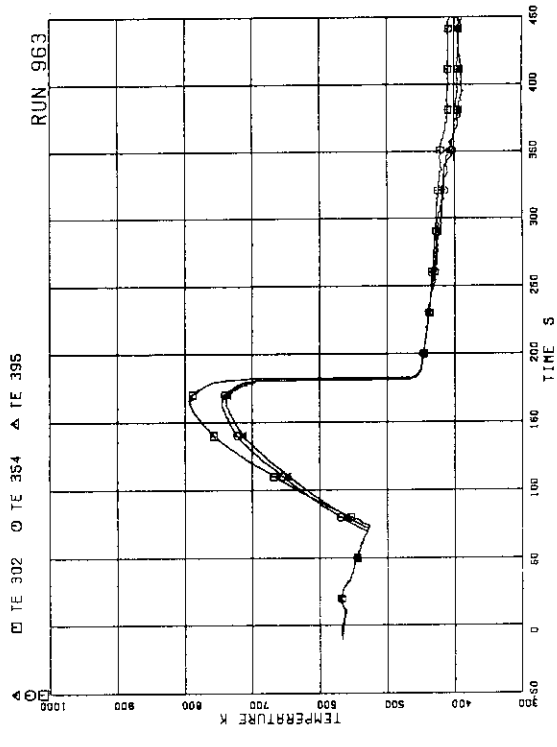

FIG.5.280 SURFACE TEMPERATURES OF FUEL RODS A77,B77,C77 AT POSITION 5

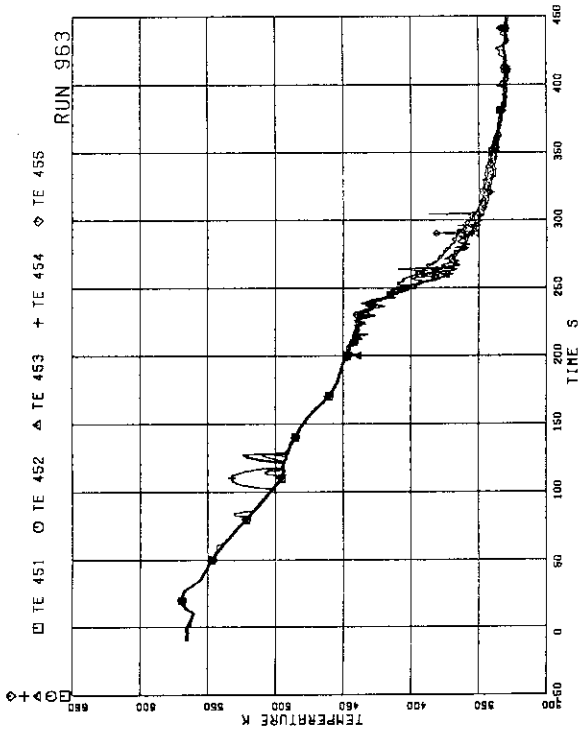

FIG.5.285 FLUID TEMPERATURES AT CHANNEL C OUTLET

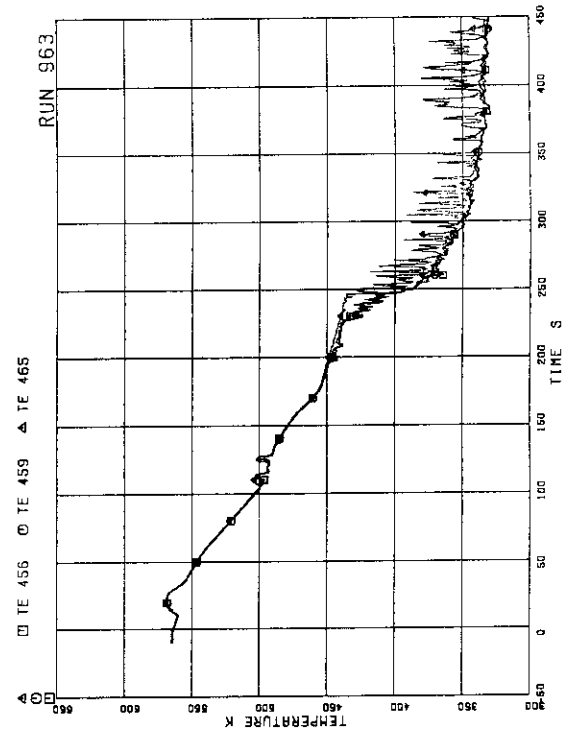

FIG.5.286 FLUID TEMPERATURES ABOVE UTP OF CHANNEL A, OPENINGS 1,4 AND 10

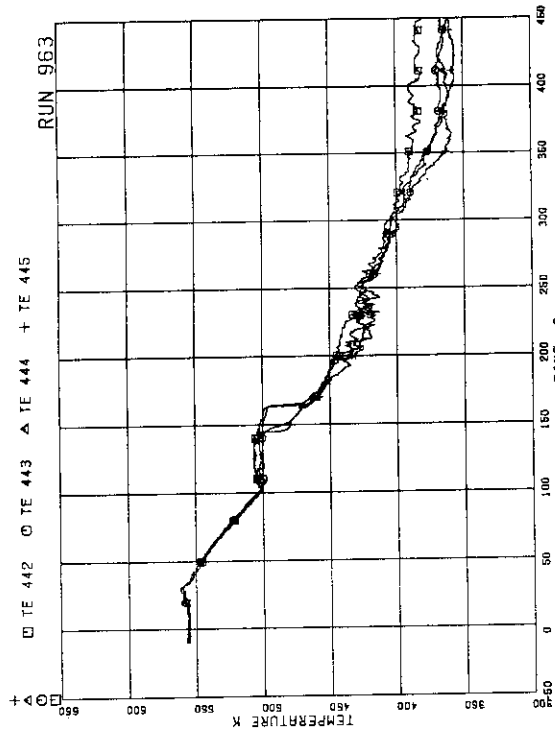

FIG.5.283 FLUID TEMPERATURES AT CHANNEL INLET

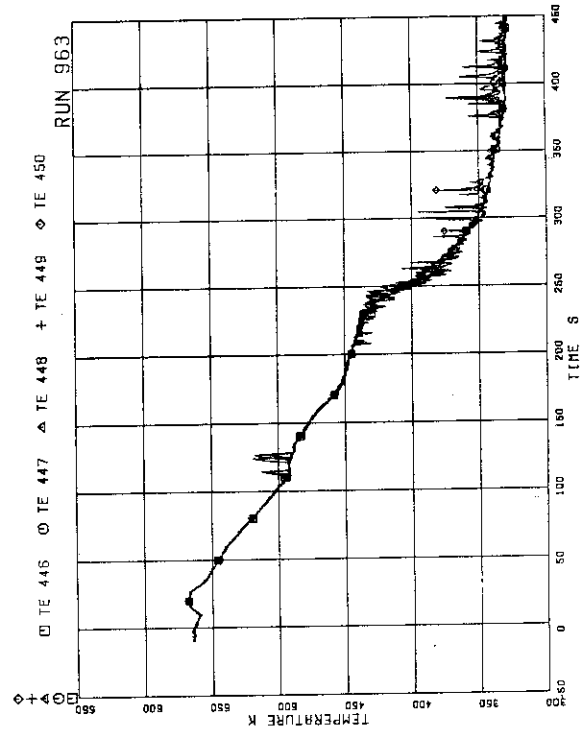

FIG.5.284 FLUID TEMPERATURES AT CHANNEL A OUTLET

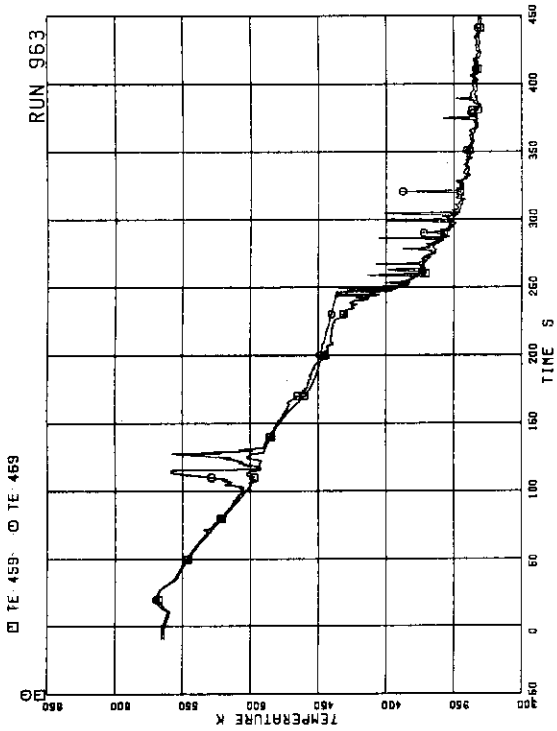

FIG.5.289 FLUID TEMPERATURES AT UTP IN CHANNEL A, OPENING 4

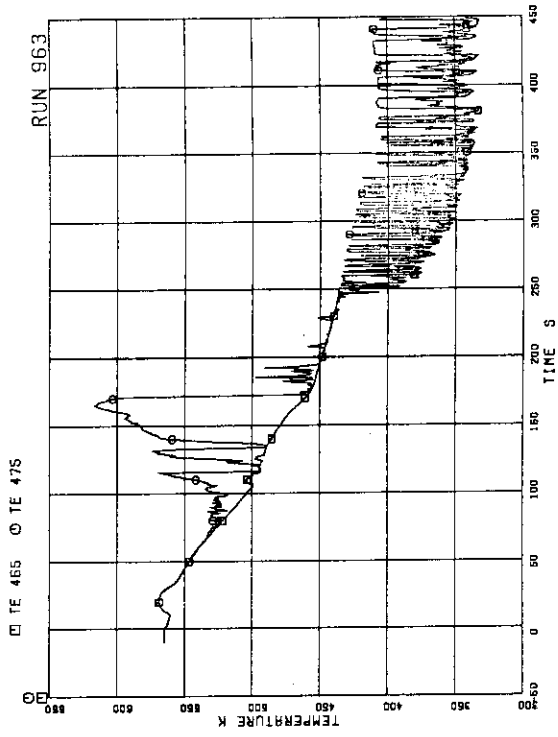

FIG.5.290 FLUID TEMPERATURES AT UTP IN CHANNEL A, OPENING 10

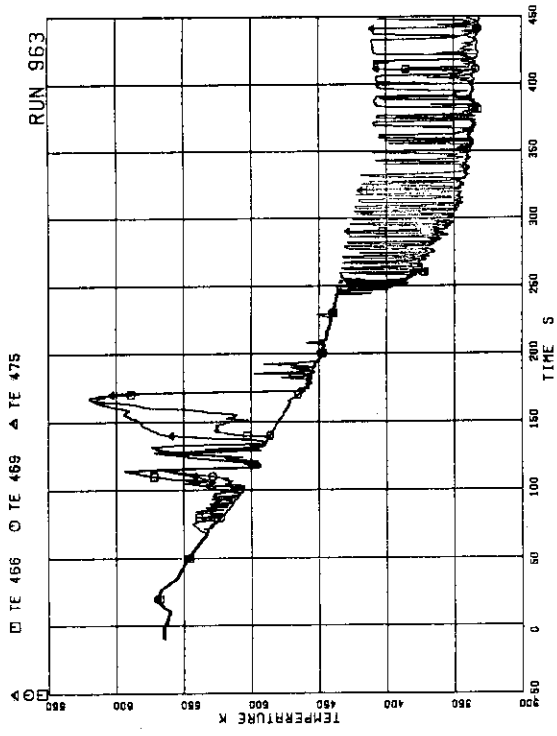

FIG.5.287 FLUID TEMPERATURES BELOW UTP OF CHANNEL A, OPENINGS 1,4 AND 10

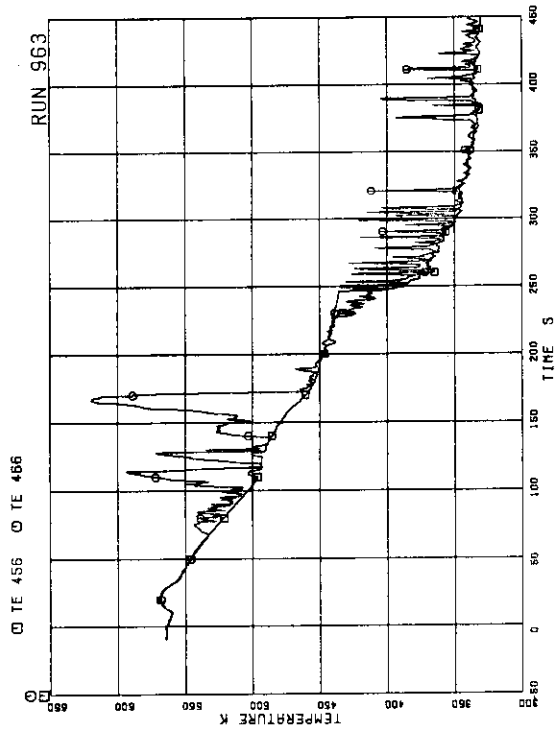

FIG.5.288 FLUID TEMPERATURES AT UTP IN CHANNEL A, OPENING 1

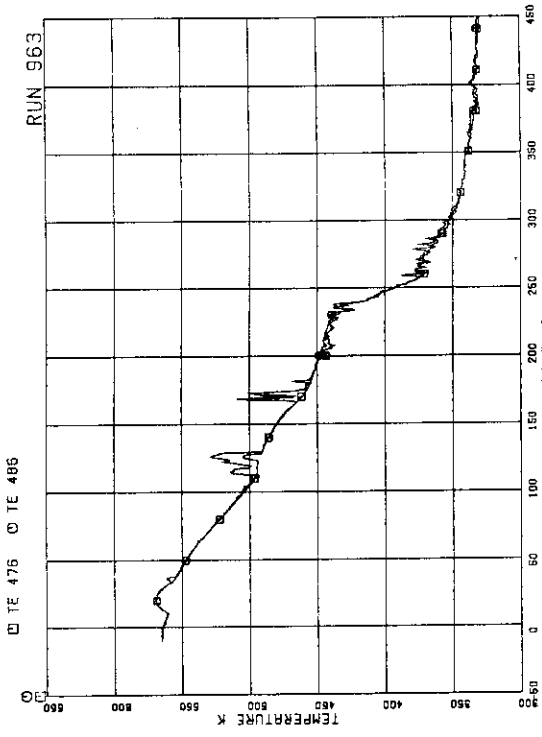

FIG.5.293 FLUID TEMPERATURES AT UTP IN CHANNEL C, OPENINGS 1

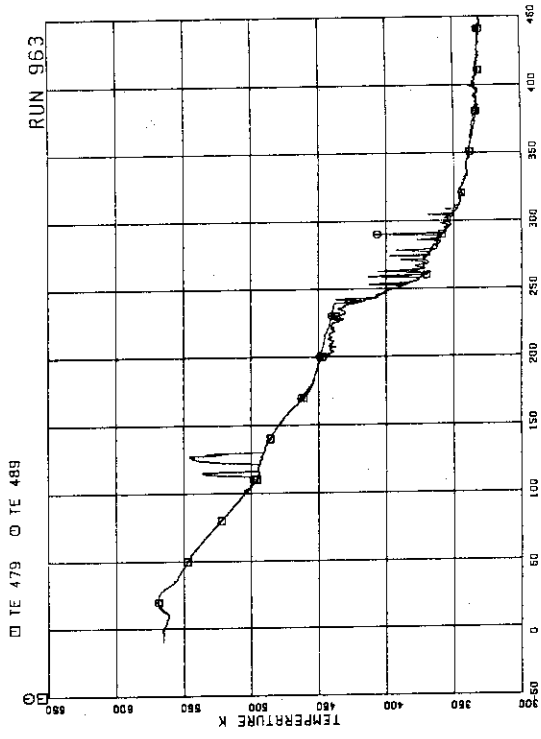

FIG.5.294 FLUID TEMPERATURES AT UTP IN CHANNEL C, OPENING 4

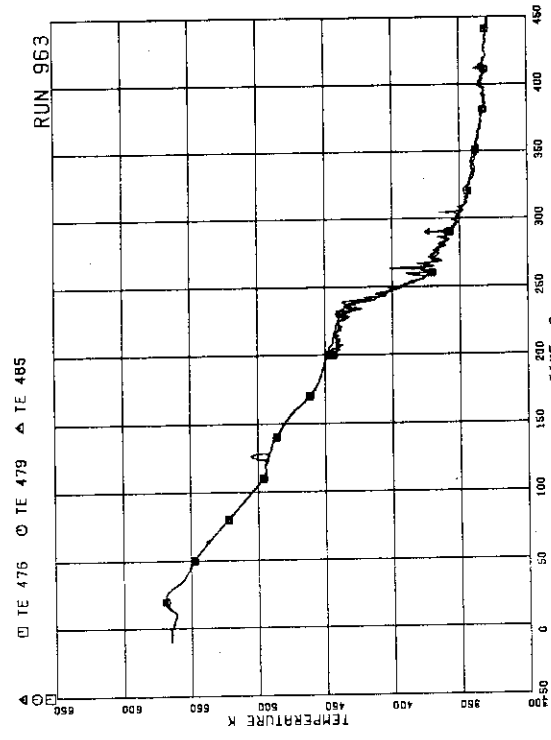

FIG.5.291 FLUID TEMPERATURES ABOVE UTP OF CHANNEL C, OPENINGS 1,4 AND 10

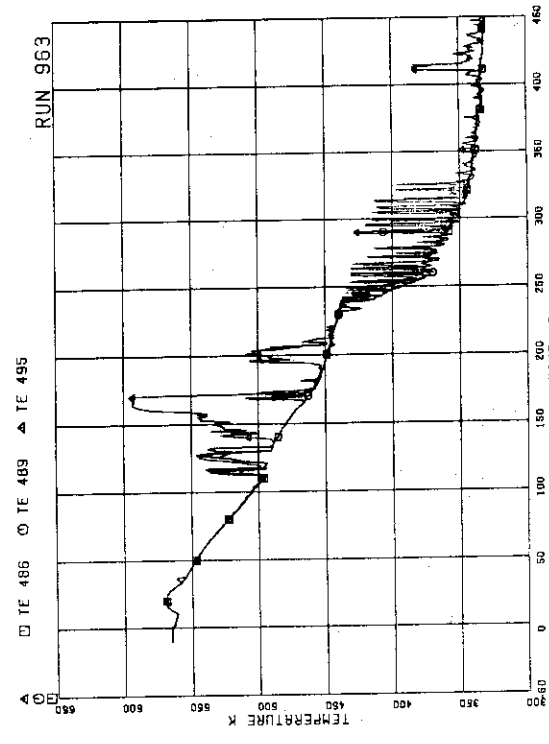

FIG.5.292 FLUID TEMPERATURES BELOW UTP OF CHANNEL C, OPENINGS 1.4 AND 10

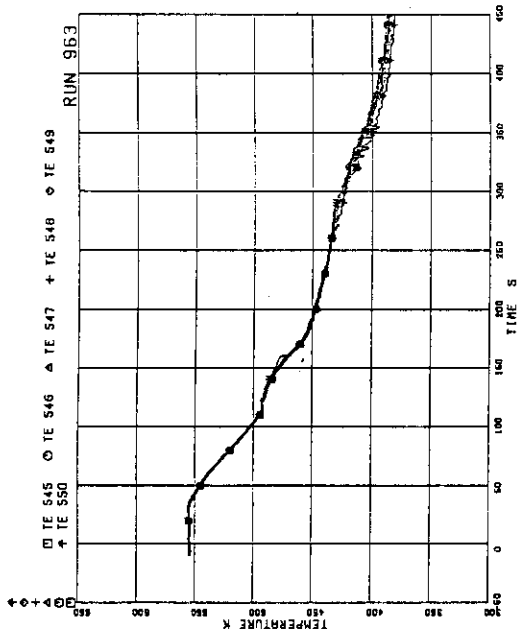

FIG.5.297 FLUID TEMPERATURES IN LOWER PLENUM, CENTER

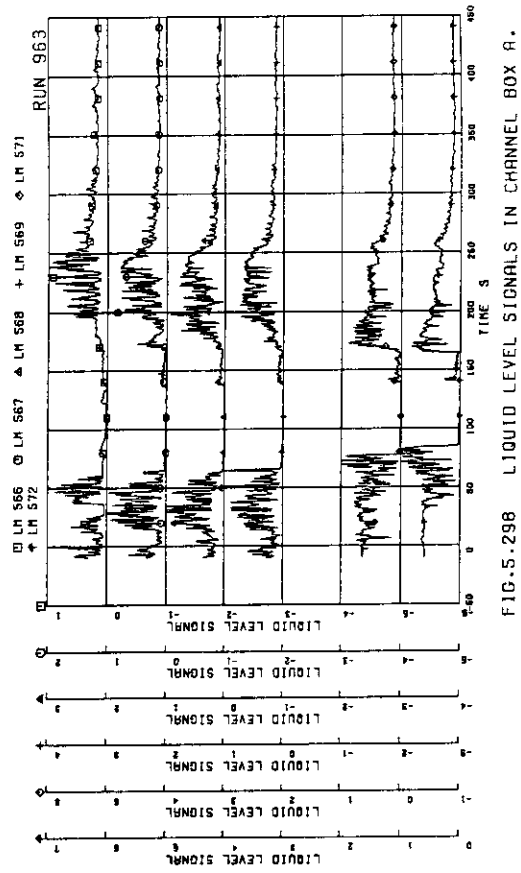

FIG.5.298 LIQUID LEVEL SIGNALS IN CHANNEL BOX A, LOCATION A2

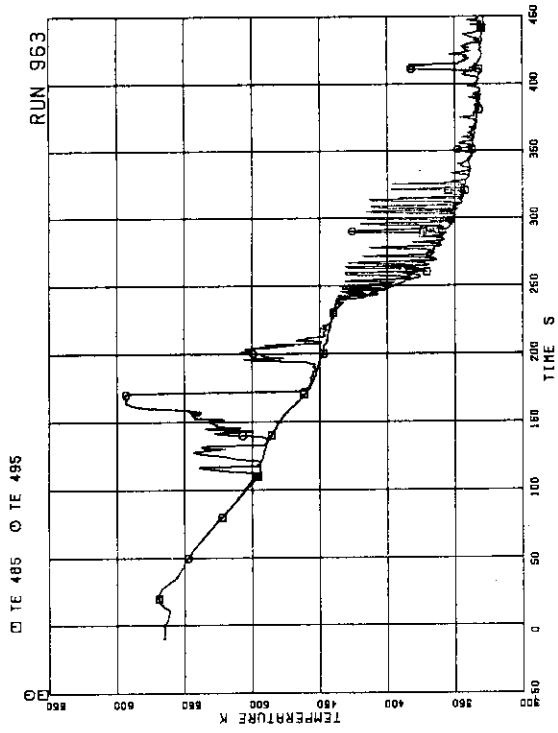

FIG.5.295 FLUID TEMPERATURES AT UTP IN CHANNEL C, OPENING 10

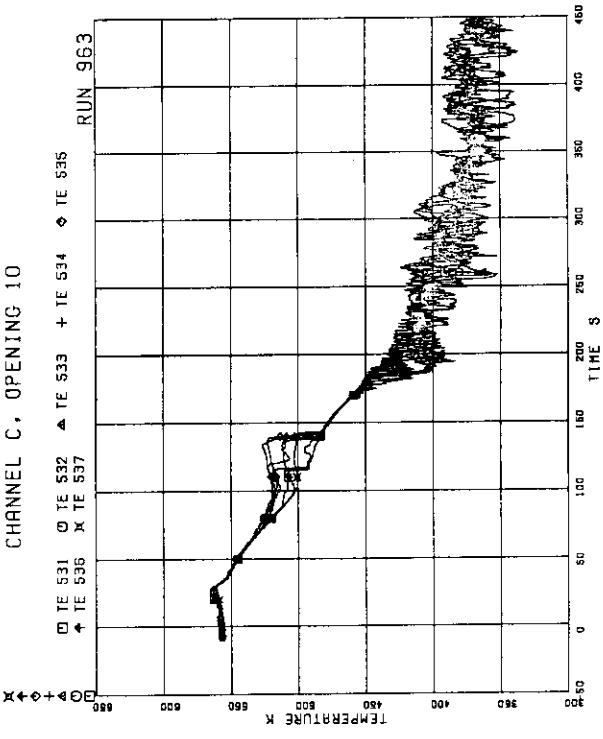

FIG.5.296 OUTER SURFACE TEMPERATURES OF CHANNEL BOX AT POS.1 THROUGH 7

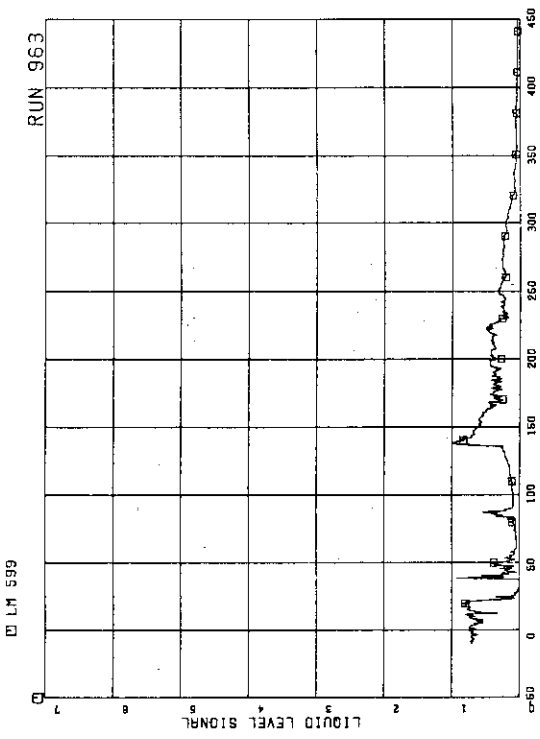

FIG.5.301 LIQUID LEVEL SIGNAL IN CHANNEL A OUTLET LOCATION A2

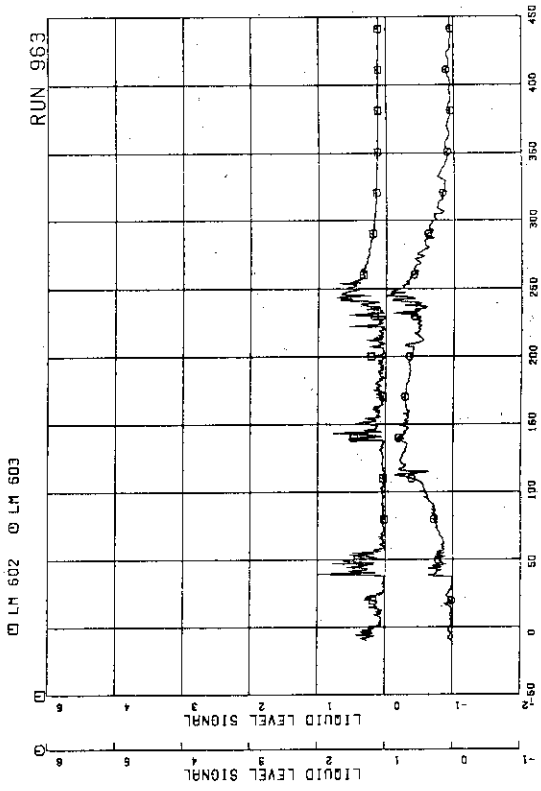

FIG.5.302 LIQUID LEVEL SIGNALS IN CHANNEL A OUTLET CENTER

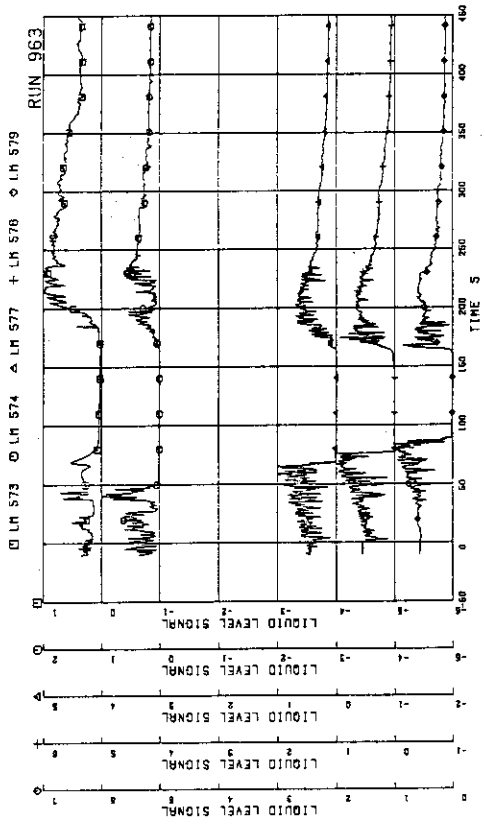

FIG.5.299 LIQUID LEVEL SIGNALS IN CHANNEL BOX B

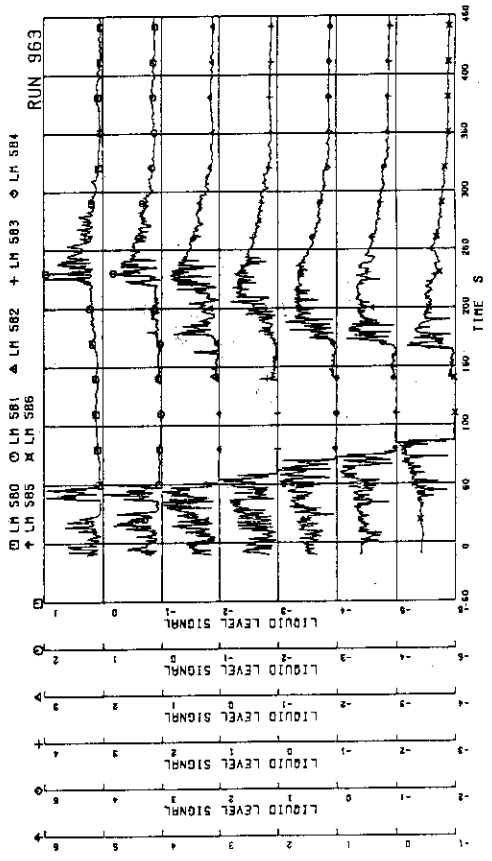

FIG.5.300 LIQUID LEVEL SIGNALS IN CHANNEL BOX C

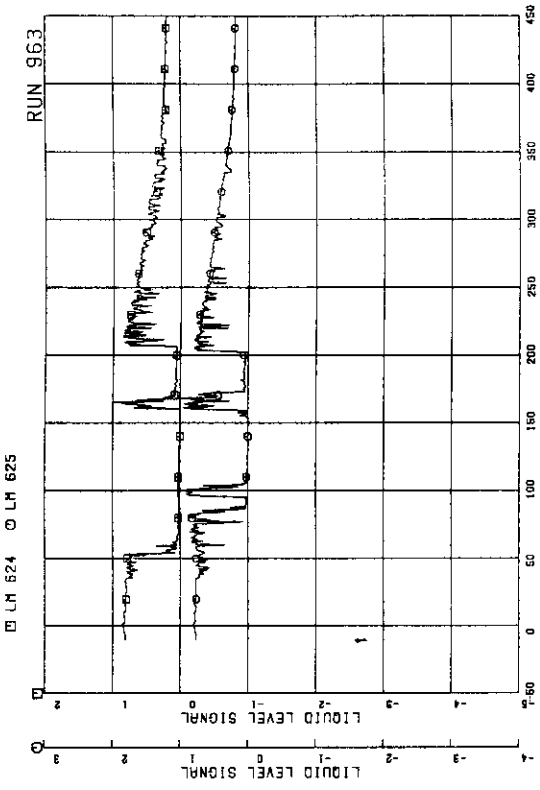

FIG.5.305 LIQUID LEVEL SIGNALS IN LOWER PLENUM, NORTH

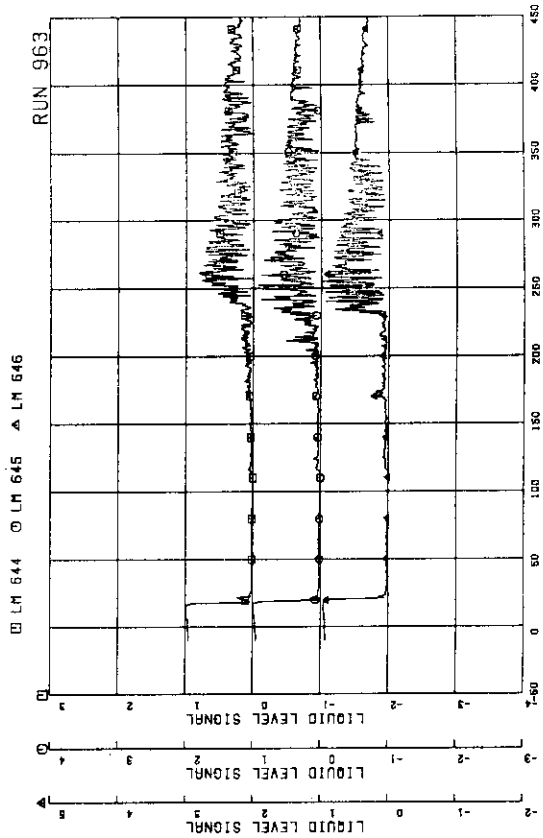

FIG.5.306 LIQUID LEVEL SIGNALS IN DOWNCOMER, D SIDE

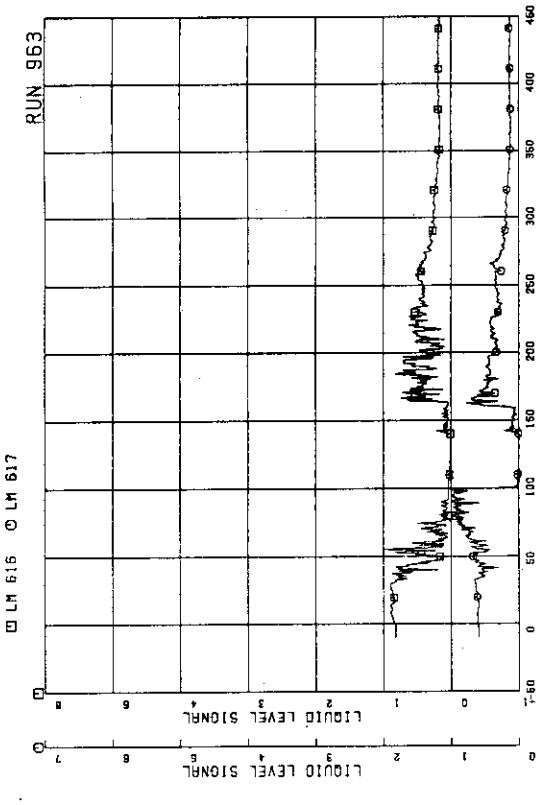

FIG.5.303 LIQUID LEVEL SIGNALS IN CHANNEL A INLET

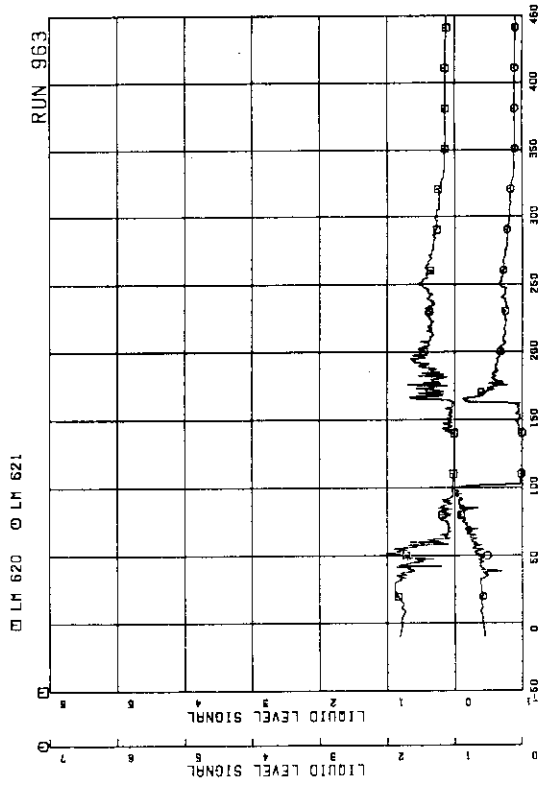

FIG.5.304 LIQUID LEVEL SIGNALS IN CHANNEL C INLET

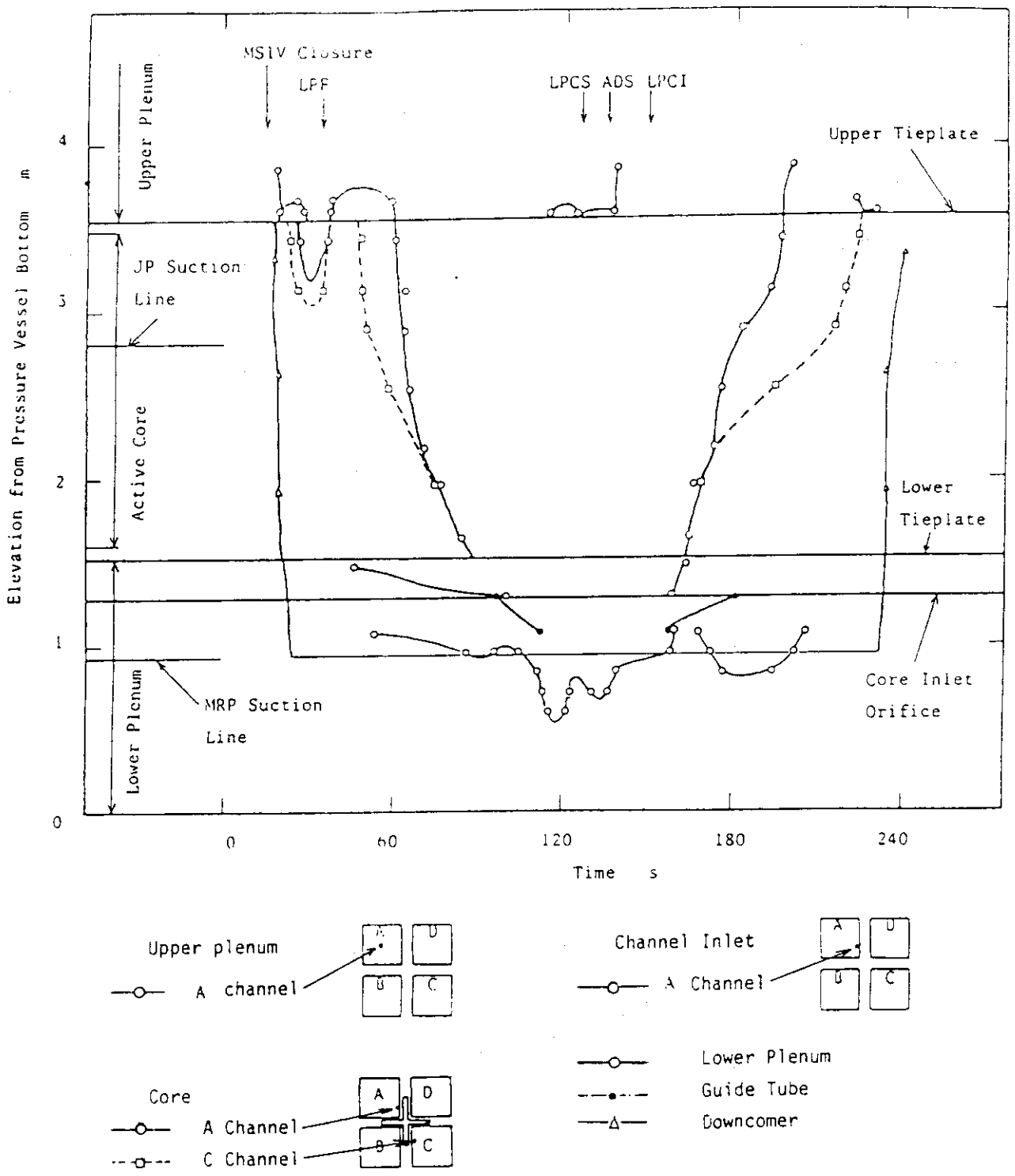

Fig. 5.307 Estimated liquid levels in pressure vessel

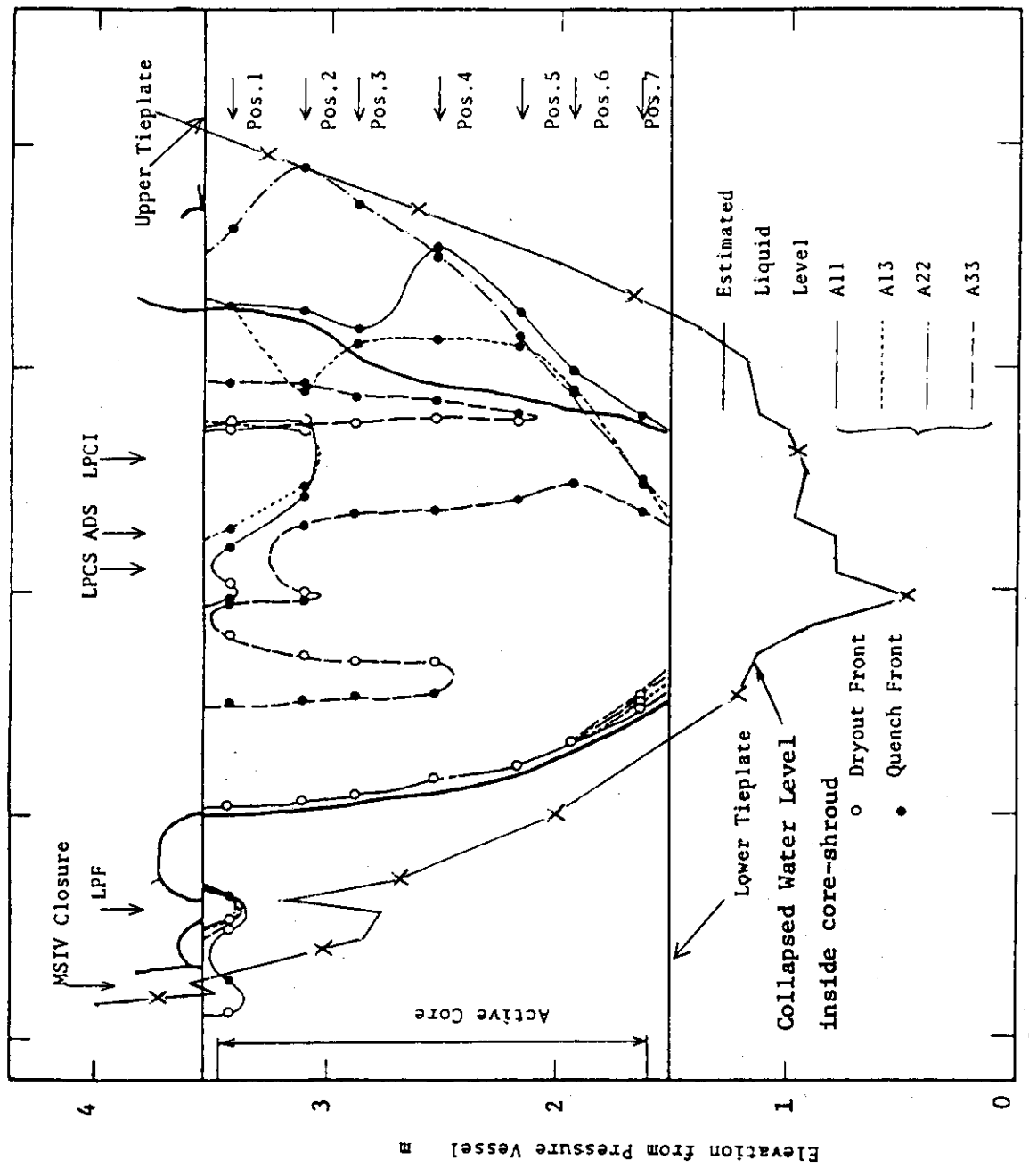

Fig. 5.308 Dryout and quench times of fuel rods in bundle A

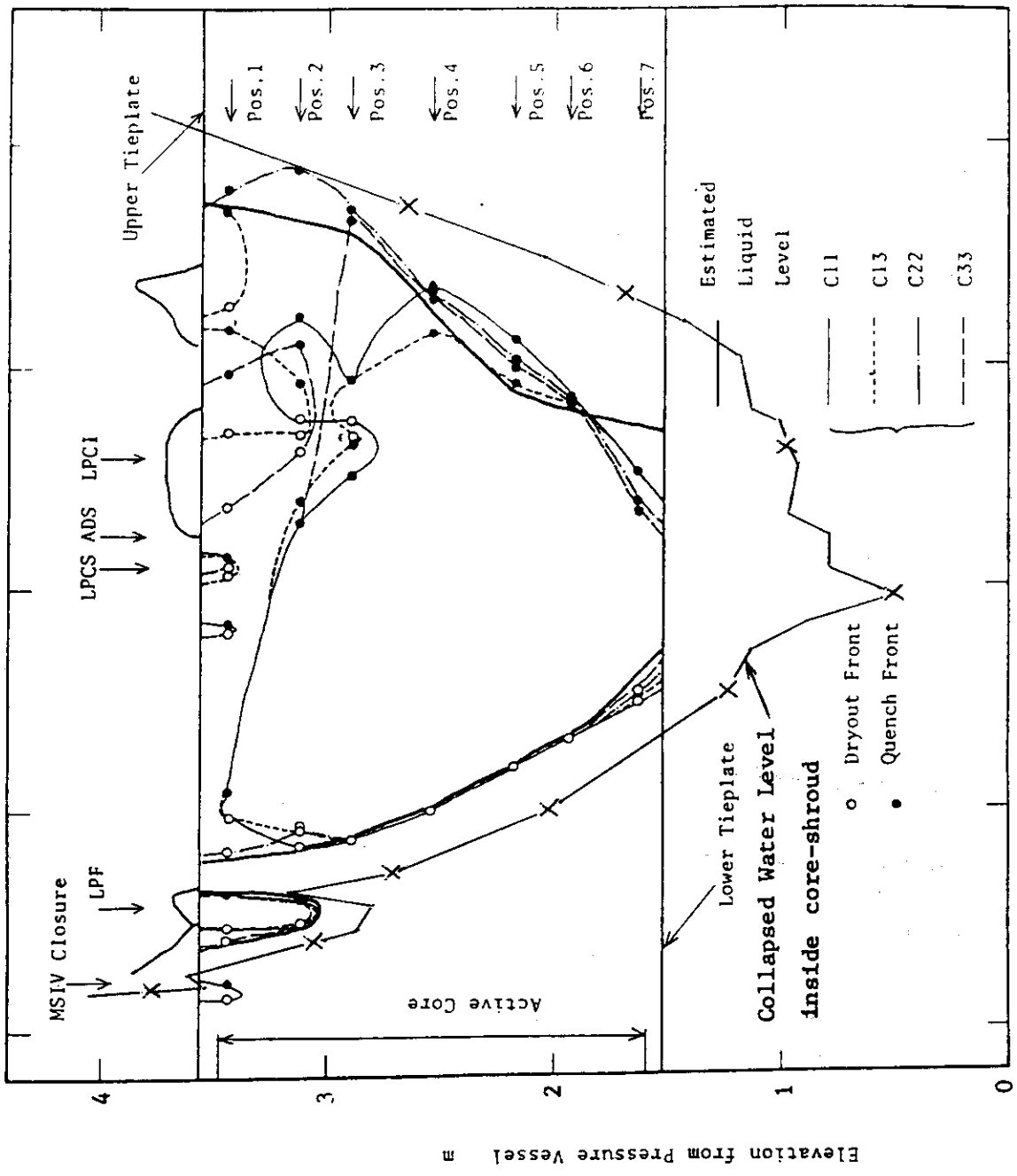

Fig. 5.309 Dryout and quench times of fuel rods in bundle C

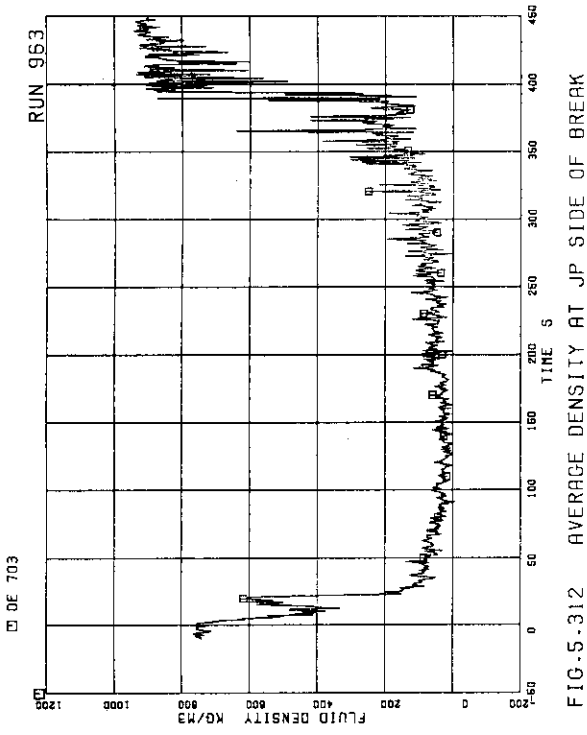

FIG.5.312 AVERAGE DENSITY AT JP SIDE OF BREAK

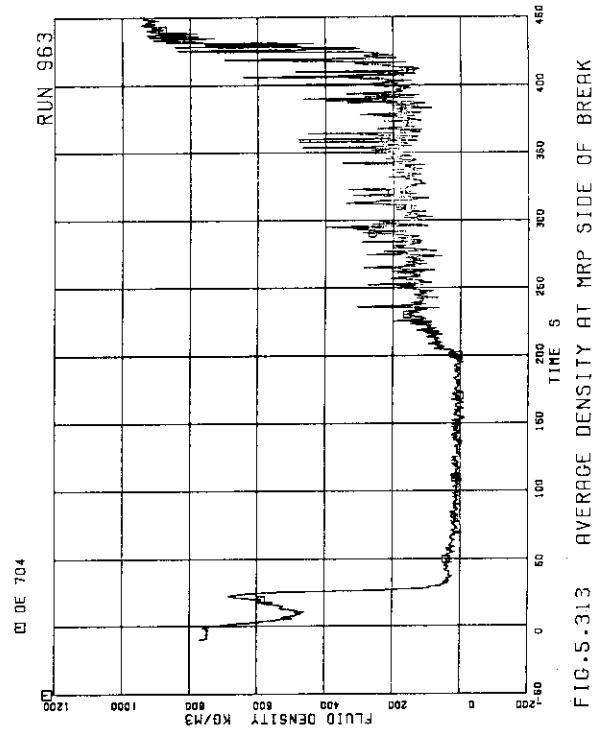

FIG.5.313 AVERAGE DENSITY AT MRP SIDE OF BREAK

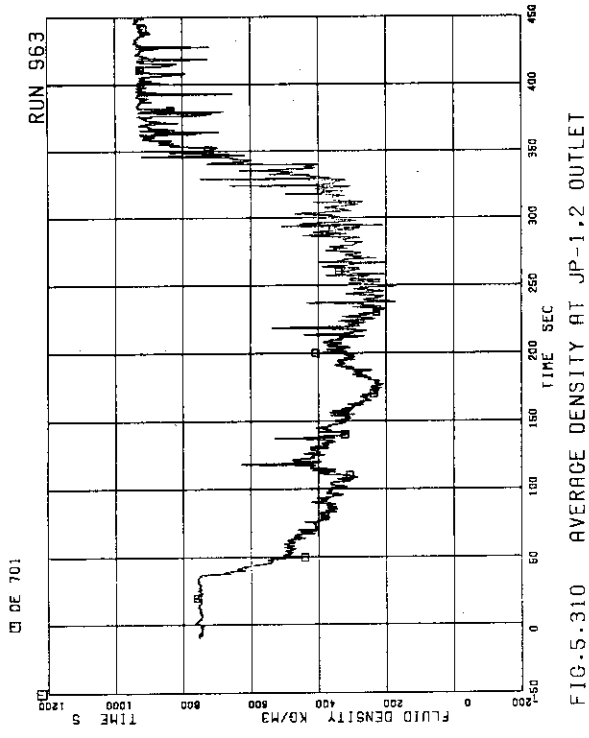

FIG.5.310 AVERAGE DENSITY AT JP-1,2 OUTLET

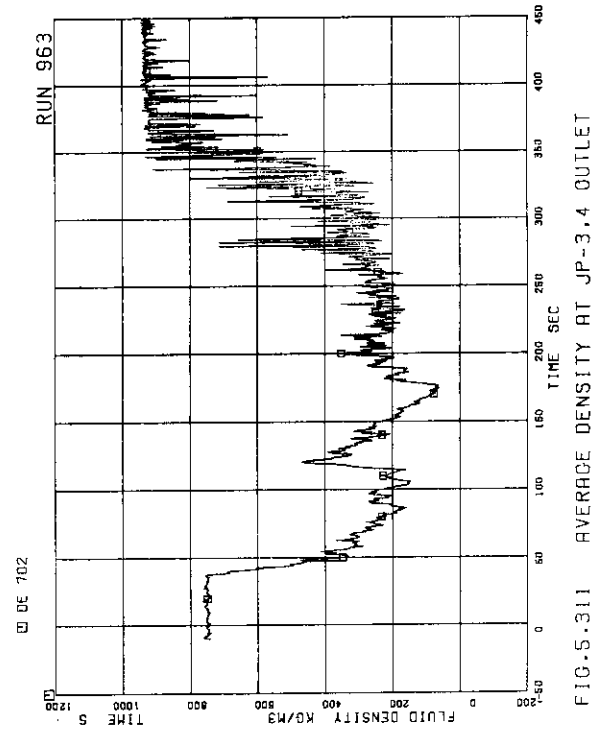

FIG.5.311 AVERAGE DENSITY AT JP-3,4 OUTLET

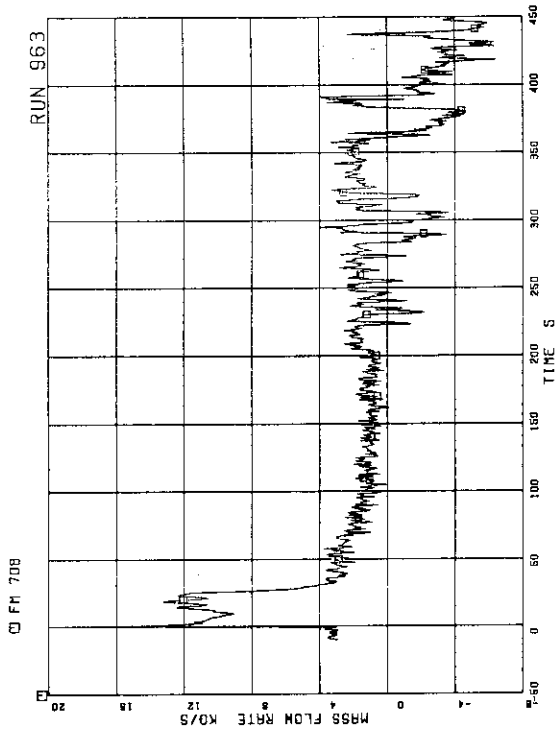

FIG.5.316 FLOW RATE AT MRP SIDE OF BREAK
(BASED ON HIGH RANGE DRAG DISK DATA)

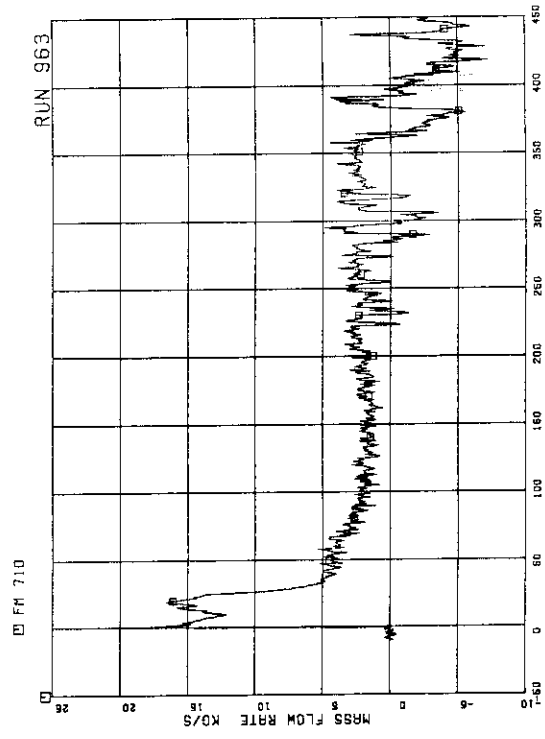

FIG.5.317 TOTAL DISCHARGE FLOW RATE FROM BREAK
(BASED ON HIGH RANGE DRAG DISK DATA)

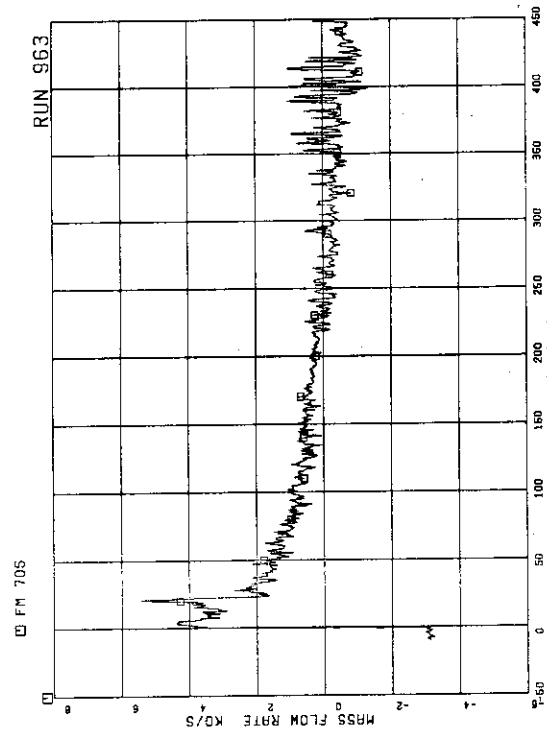

FIG.5.314 FLOW RATE AT JP SIDE OF BREAK
(BASED ON LOW RANGE DRAG DISK DATA)

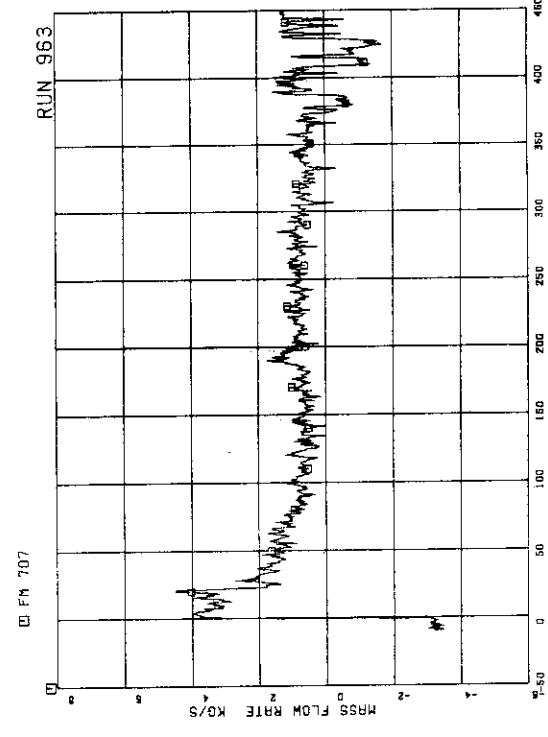

FIG.5.315 FLOW RATE AT JP SIDE OF BREAK
(BASED ON HIGH RANGE DRAG DISK DATA)

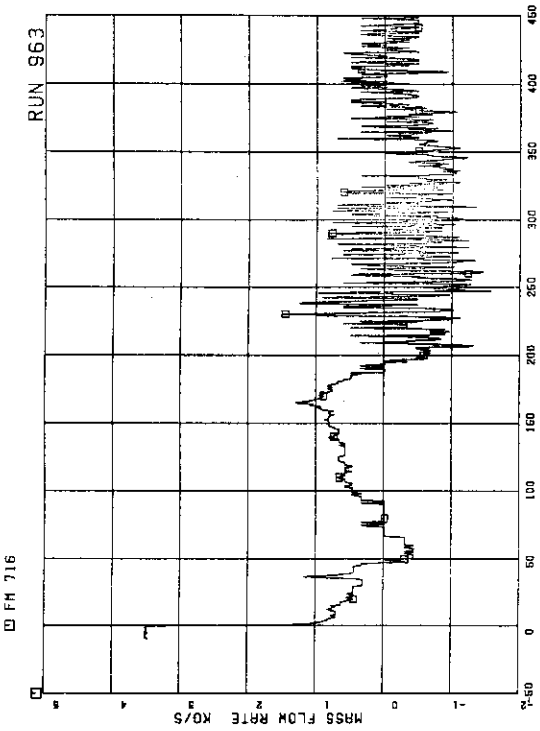

FIG.5.320 MASS FLOW RATE AT CHANNEL C INLET

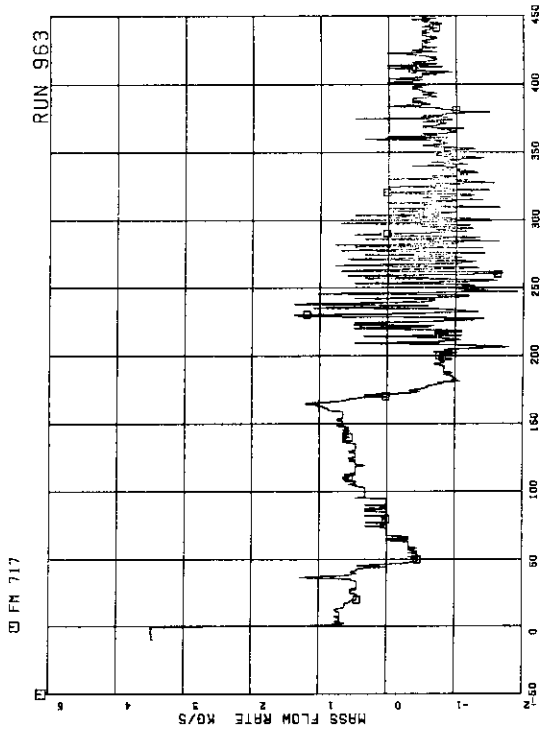

FIG.5.321 MASS FLOW RATE AT CHANNEL D INLET

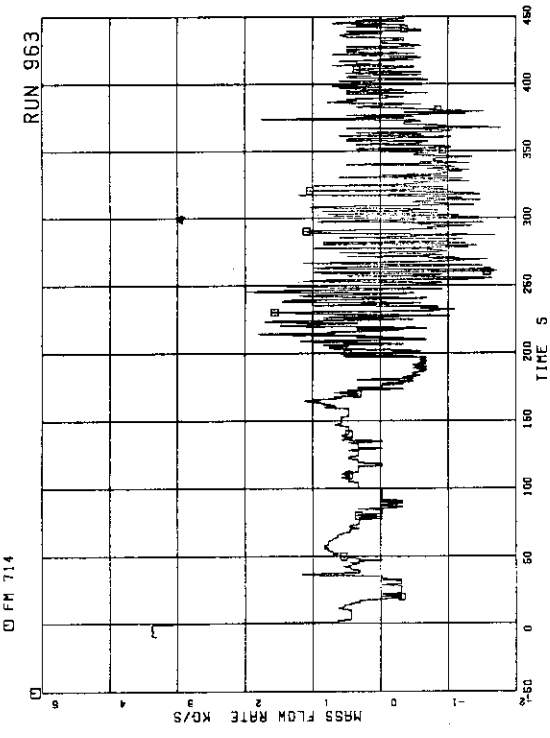

FIG.5.318 MASS FLOW RATE AT CHANNEL A INLET

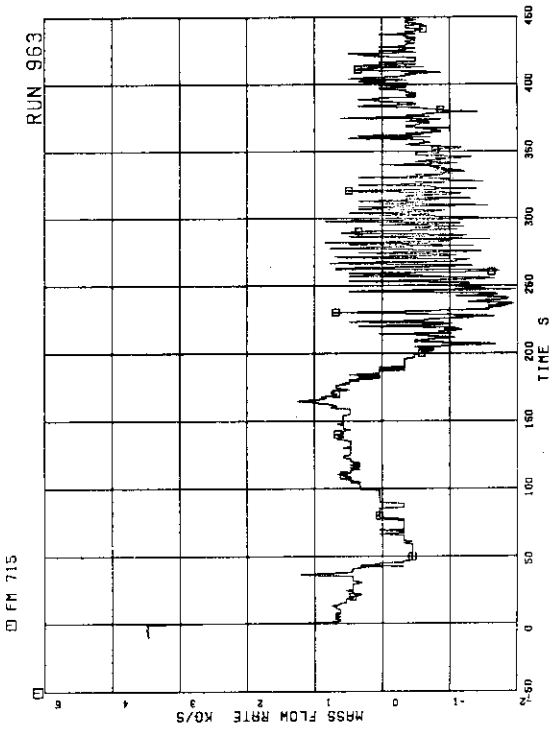

FIG.5.319 MASS FLOW RATE AT CHANNEL B INLET

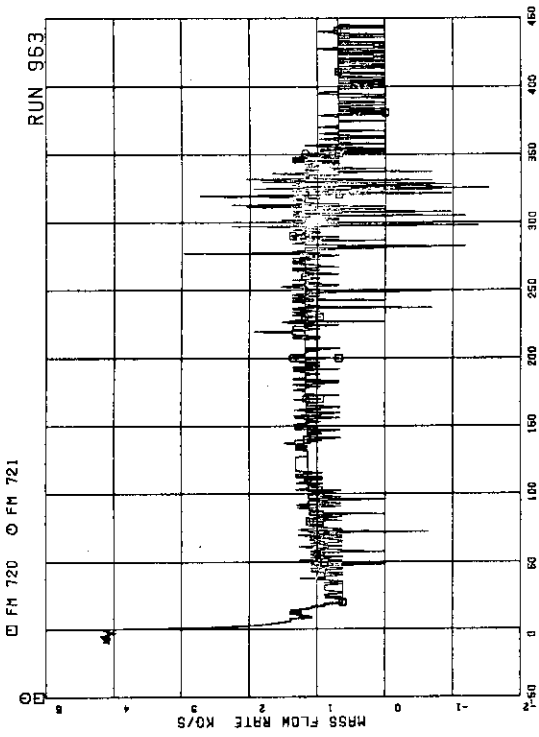

FIG.5.324 MASS FLOW RATE AT JP-1,2 OUTLET (POS.FLOW)

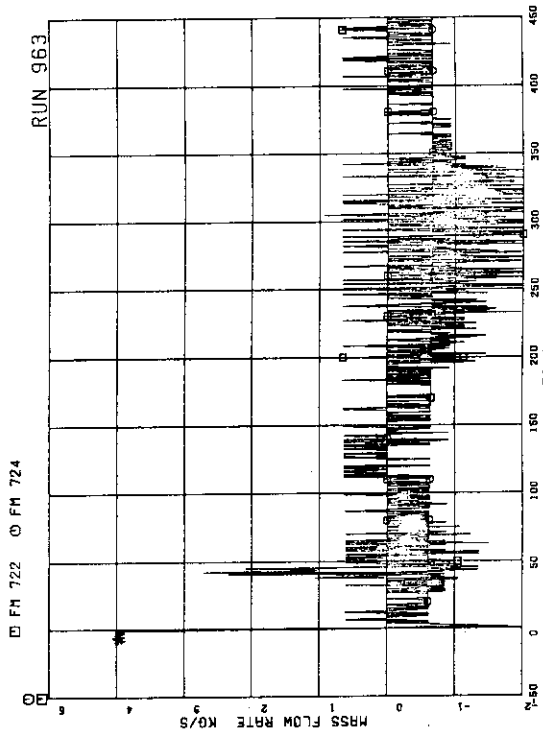

FIG.5.325 MASS FLOW RATE AT JP-3,4 OUTLET (POS.FLOW)

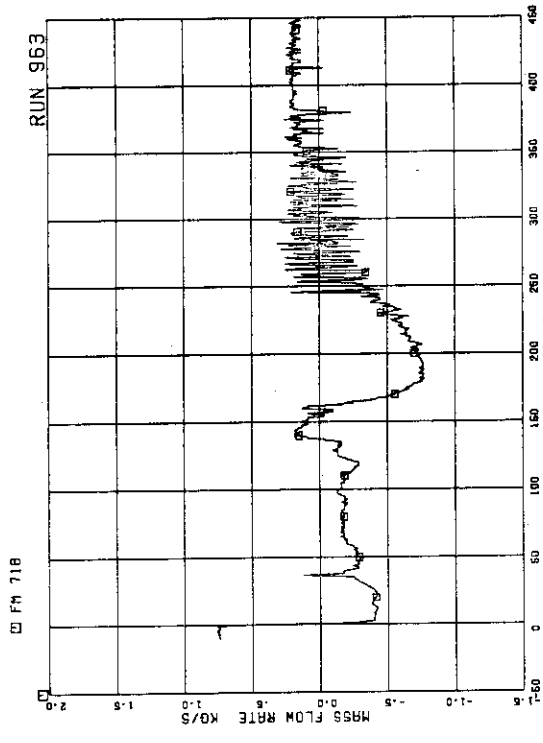

FIG.5.322 MASS FLOW RATE AT BYPASS HOLE

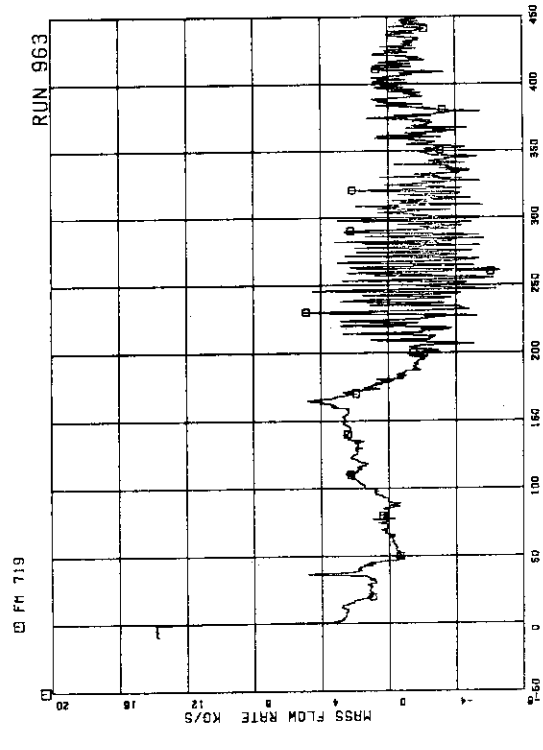

FIG.5.323 TOTAL CHANNEL INLET FLOW RATE

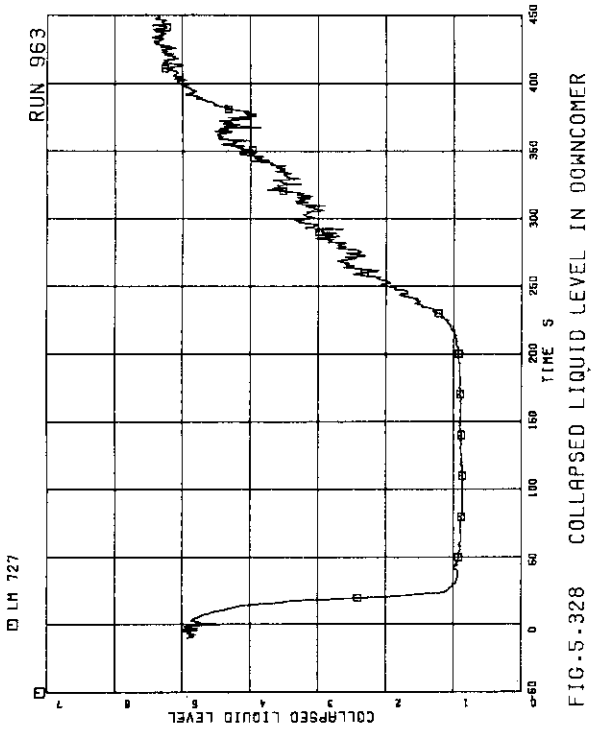

FIG.5.328 COLLAPSED LIQUID LEVEL IN DOWNCOMER

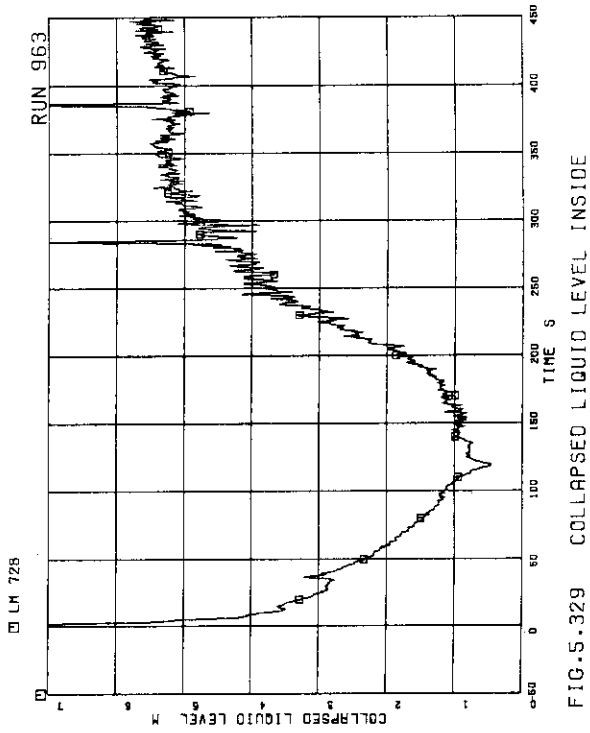

FIG.5.329 COLLAPSED LIQUID LEVEL INSIDE CORE SHROUD

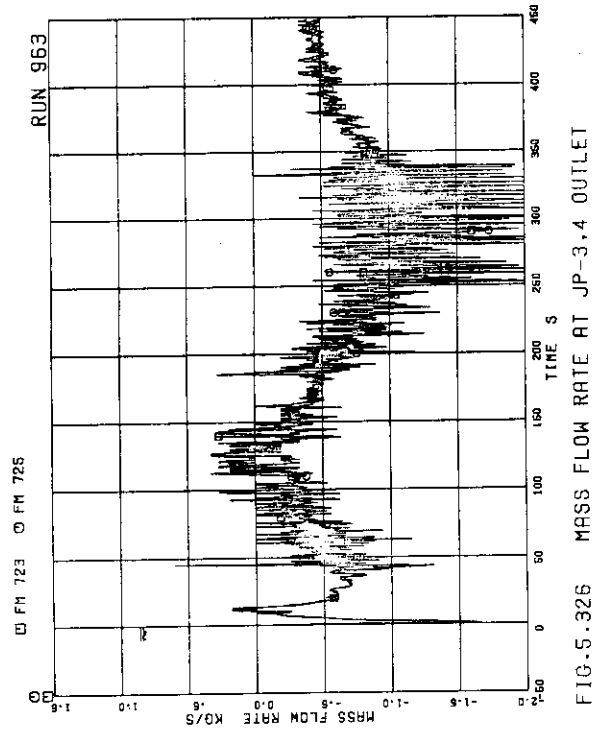

FIG.5.326 MASS FLOW RATE AT JP-3,4 OUTLET (NEG.FLOW)

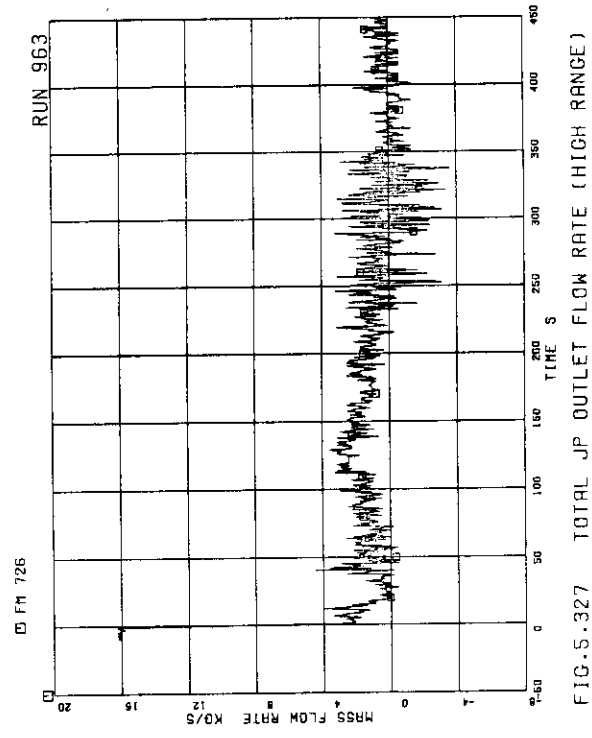

FIG.5.327 TOTAL JP OUTLET FLOW RATE (HIGH RANGE)

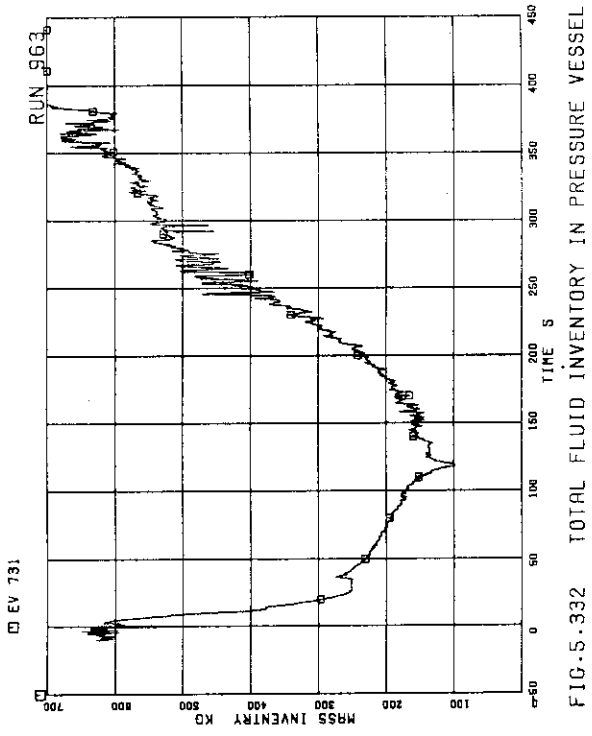

FIG.5.332 TOTAL FLUID INVENTORY IN PRESSURE VESSEL

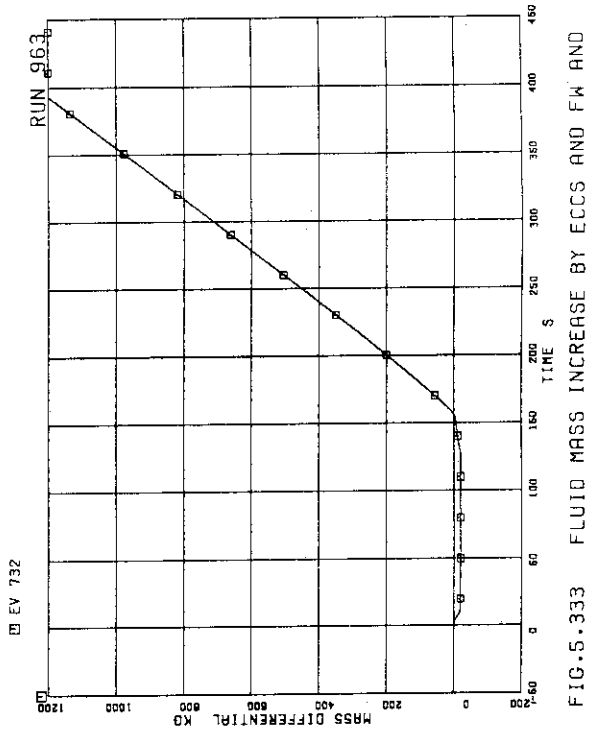

FIG.5.333 FLUID MASS INCREASE BY ECCS AND FW AND DECREASE BY STEAM DISCHARGE FLOW

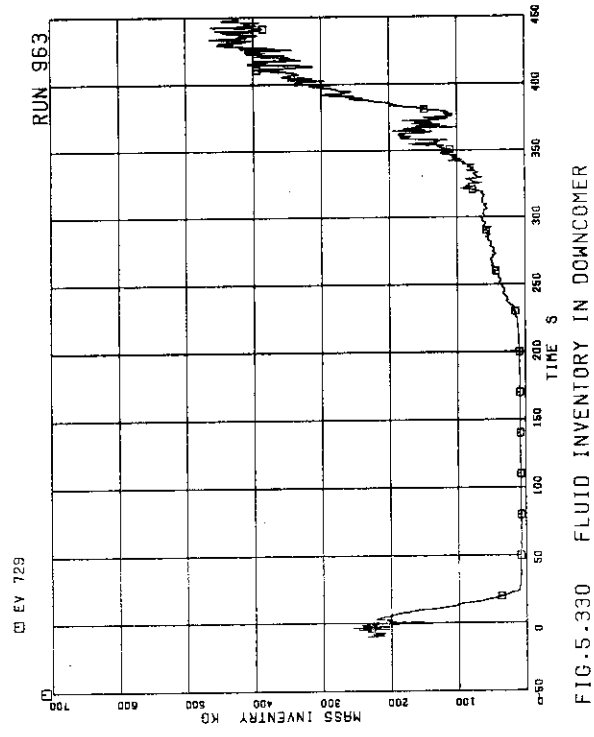

FIG.5.330 FLUID INVENTORY IN DOWNCOMER

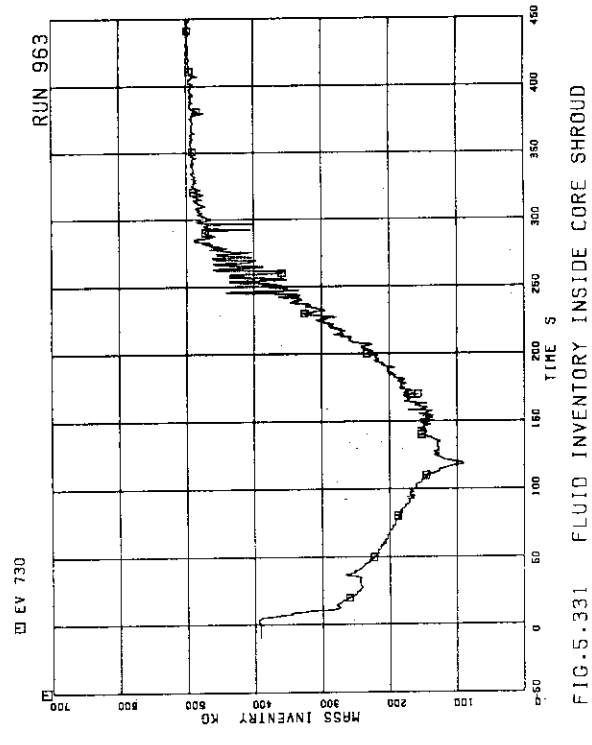

FIG.5.331 FLUID INVENTORY INSIDE CORE SHROUD

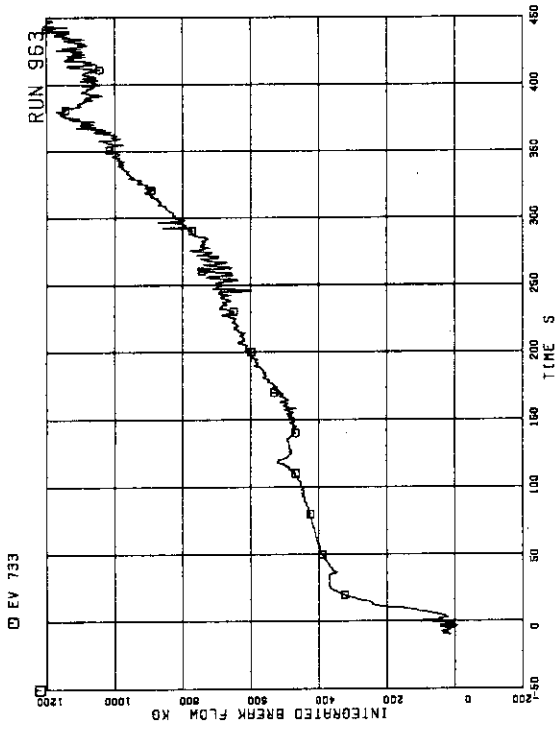

FIG.5.334 DISCHARGED FLUID MASS FROM BREAK

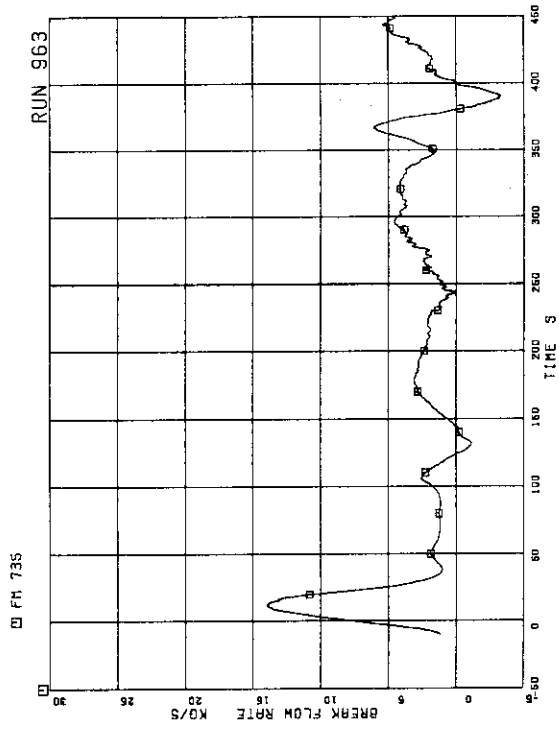

FIG.5.335 DISCHARGED FLOW RATE FROM BREAK

Table 6.1 Comparison of test conditions and major events in RUNs 961, 962 and 963

(a) Test conditions

Items	Unit	RUN961	RUN963	RUN962
Break Area Ratio	%	200	100	50
Break Type		D.E.B.	Split B.	Split B.
Initial Pressure	MPa	7.35	7.35	7.35
Initial Core Power	MW	3.983	3.971	3.972
Core Inlet Subcooling	K	11.0	10.4	10.9
Initial UP Quality	%	13.0	13.1	13.2
Initial Water Level	m	5.0	5.0	5.0
MSIV Closure Logic	s	L2 + 3	L2 + 3	L2 + 3
LPCS Actuation Logic	s	L1+40,	L1+40,	L1+40,
"	MPa	& P 2.2	& P 2.2	& P 2.2
3LPCI Actuation Logic	s	L1 + 40	L1 + 40	L1 + 40
"	MPa	& P 1.6	P 1.6	P 1.6
ADS Actuation Logic	s	L1 + 120	L1 + 120	L1 + 120
L2 Level	m	4.76	4.76	4.76
L1 Level	m	4.25	4.25	4.25

(b) Times of major events

Events (s)	RUN961	RUN963	RUN962
Break Initiation	0.0	0.0	0.0
FWL Closure	1.7	2.1	1.7
L2 Level	6.7	8.2	9.0
MSIV Closure	8.5	9.5	12
L1 Level	12	14	19
JP Suction Uncovery	17	19	24
MRP Suction Uncovery	22	25	32
LP Flashing	30	35	50
Dryout at Top of Core	46	50	62
Bryout at Bottom of Core	81	89	116
LPCS Actuation	105	126	167
ADS Actuation	134	135	139
LPCI Actuation	144	155	200
PCT Detection	155	167	208
Completion of Quench	215	233	272

Table 6.2 Comparison of break flow rates in RUNs 961, 962 and 963

Items	Unit	RUN961	RUN963	RUN962
A. Break Area Ratio	%	200	100	59
B. Steam Discharge (JP-side)	s	17	22	29
C. Steam Dischar-e (MRP-side)	s	21	25	35
D. JP-side Break Flow until Steam Discharge	kg/s	4.3	3.5	2.4
E. MRP-side Break Flow until Steam Discharge	kg/s	12.2	11.2	7.6
F. Total Break Flow until Steam Discharge	kg/s	16.2	14.4	9.8
G. Discharged Mass until Steam Discharge	kg	340	360	2.8
H. D / F	%	26	24	24
I. E / F	%	74	76	76

Table 6.3 Comparison of effective choking flow areas in RUNs 961, 962 and 963

Items	Unit	RUN961	RUN963	RUN962
A. Break Area Ratio	%	200	100	59
B. Break Diameter	mm	2 × 26.2	26.2	18.5
C. JP-3.4 Nozzle Area Ratio	%	21	21	21
D. JP-3.4 Nozzle Diameter	mm	2 × 8.4	2 × 8.4	2 × 8.4
E. MRP Nozzle Ar-a Ratio	%	51	51	51
F. MRP Nozzle Diameter	mm	18.7	18.7	18.7
G. Effective Choking Area Ratio	%	72	72	50
H. Ratio	-	1.0	1.0	0.69
I. Depressurization Rate between 6.4 and 2.2 MPa	MPa/s	0.056	0.055	0.040
J. Ratio	-	1.0	0.98	0.71

Table 6.4 Peak cladding temperatures in RUNs 961, 962 and 963

Items	Unit	Discharge Line Breaks			Suction Line Breaks			
		RUN961	RUN963	RUN962	RUN926	RUN914	RUN949	RUN928
Break Area Ratio		200	100	50	200	100	75	50
Effective Cheking A. Ratio	%	72	72	50	121	100	75	50
PCT Time	s	155	167	208	119	133	154	201
PCT Location	-	A71,P.4	A82,P.4	A82,P.4	A71,P.4	A.11,P.4	A71,P.4	A71,P.4
PCT Calue	K	894	915	933	784	832	885	893
Dryout Time of PCT Rod	s	61	68	81	56	60	65	82
Quench Time of PCT Rod	s	191	215	253	132	170	195	235
Dryout Period	s	130	147	172	76	110	130	153
LPCI Actuation Time	s	144	155	200	96	118	145	188

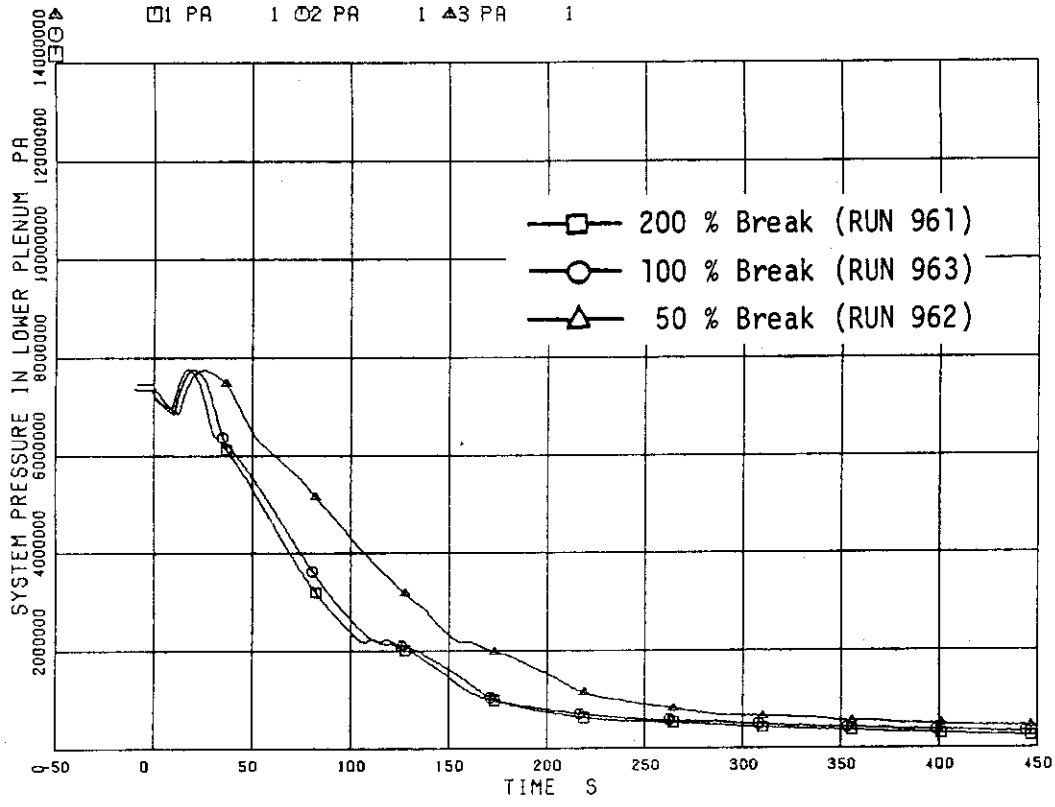

Fig. 6.1 Effects of break area on pressure transients of three tests

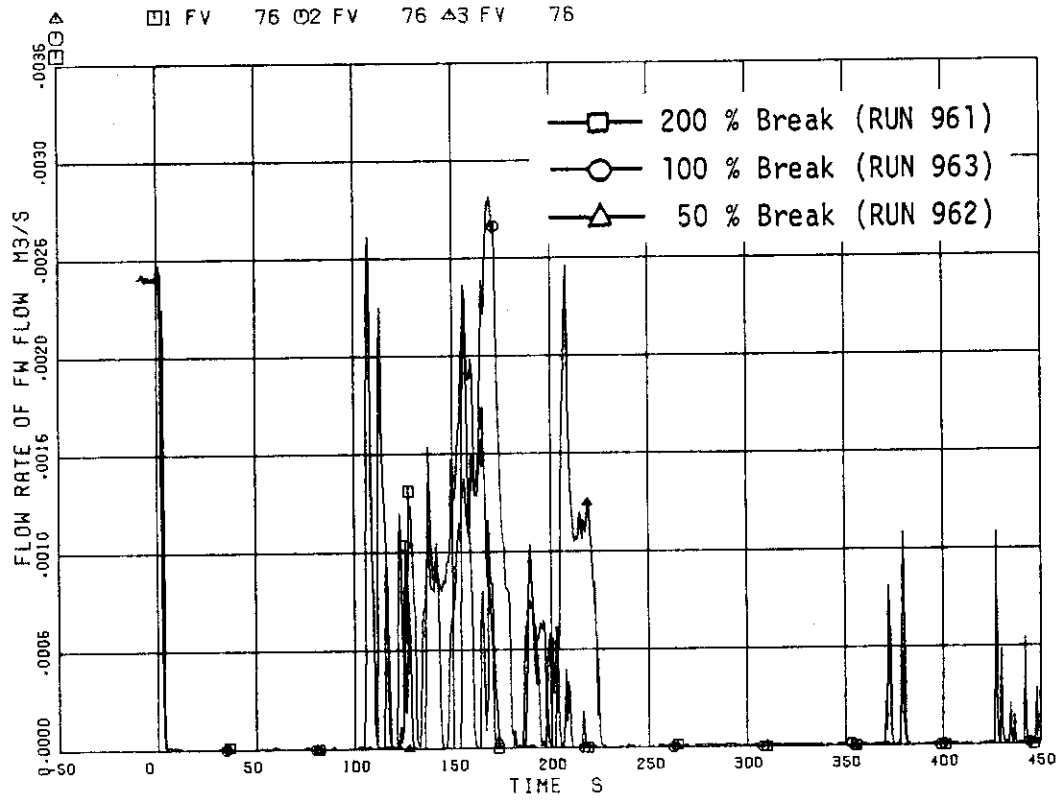

Fig. 6.2 Comparison of feedwater flow rates of three tests

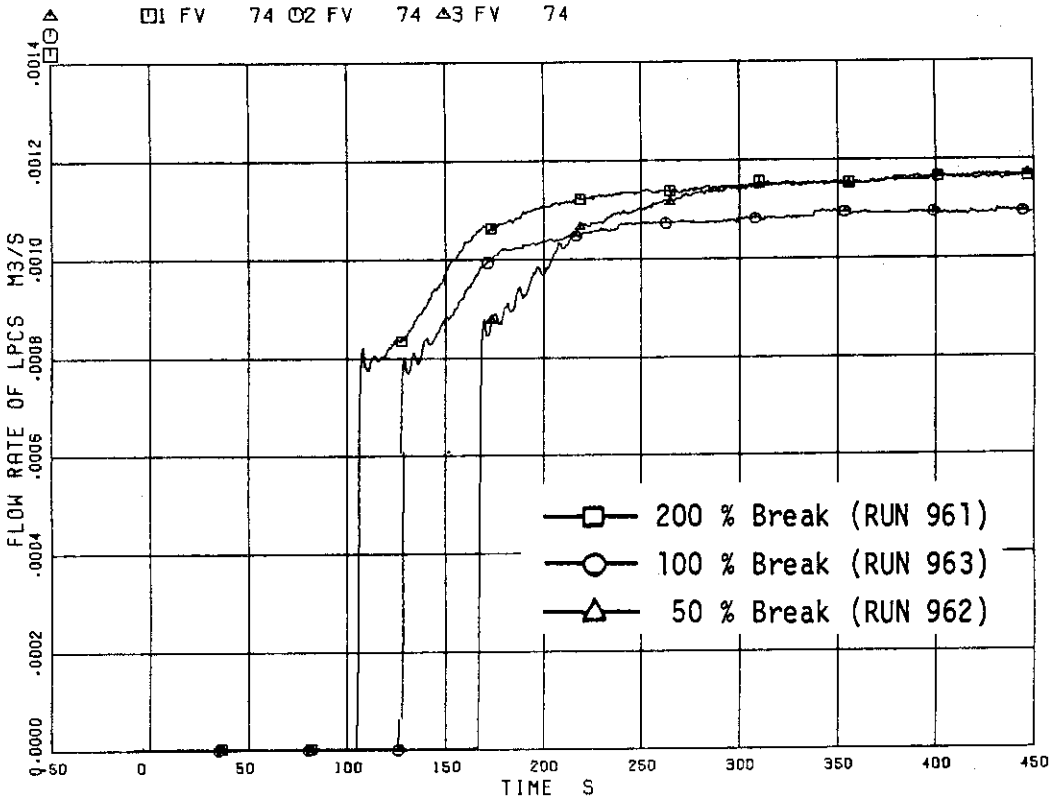

Fig. 6.3 Comparison of LPCS flow rates of three tests

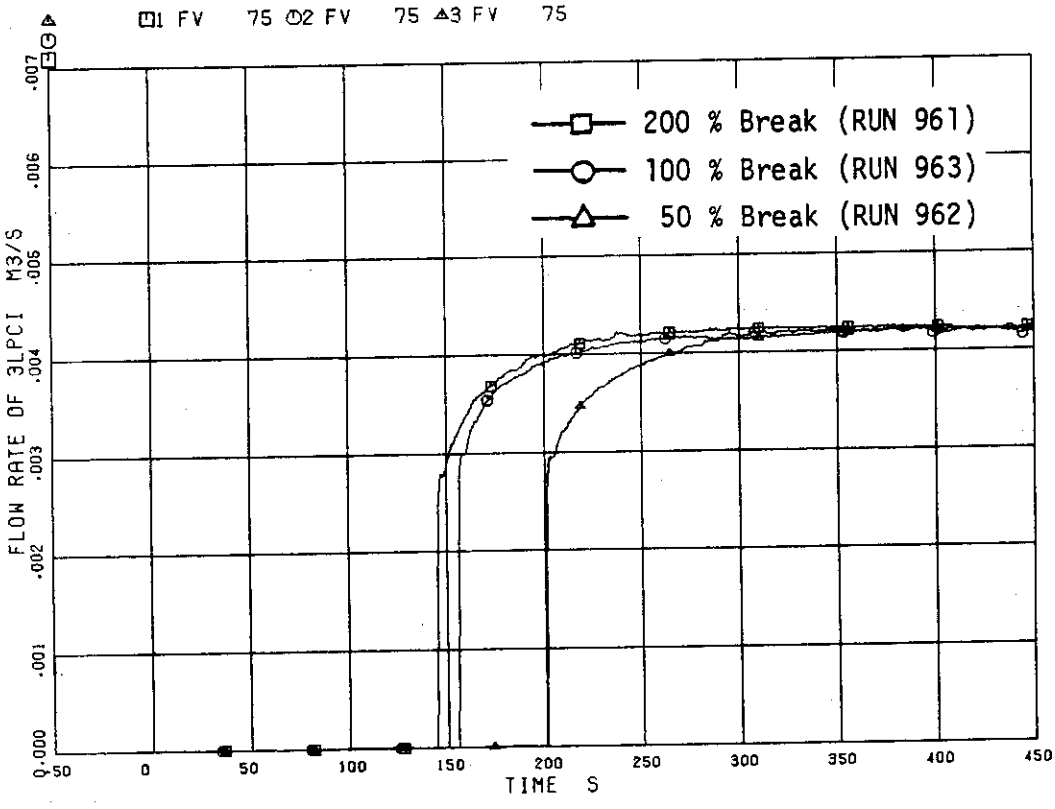

Fig. 6.4 Comparison of 3 LPCI flow rates of three tests

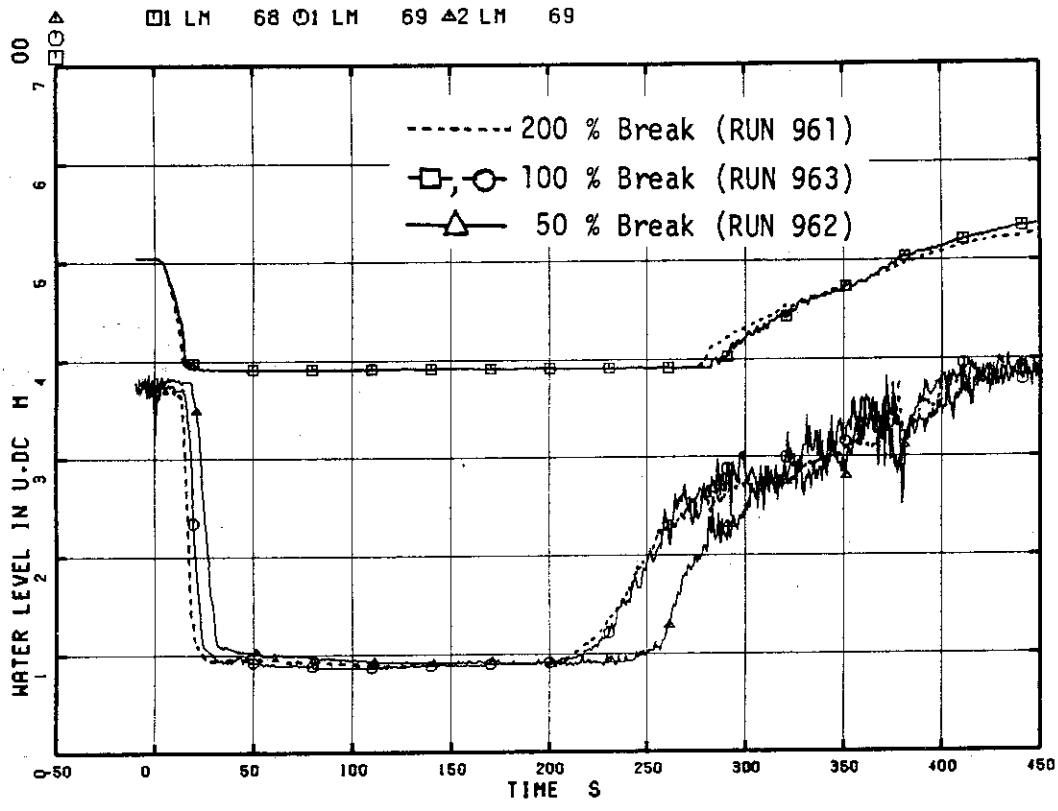

Fig. 6.5 Comparison of water level in downcomer of three tests

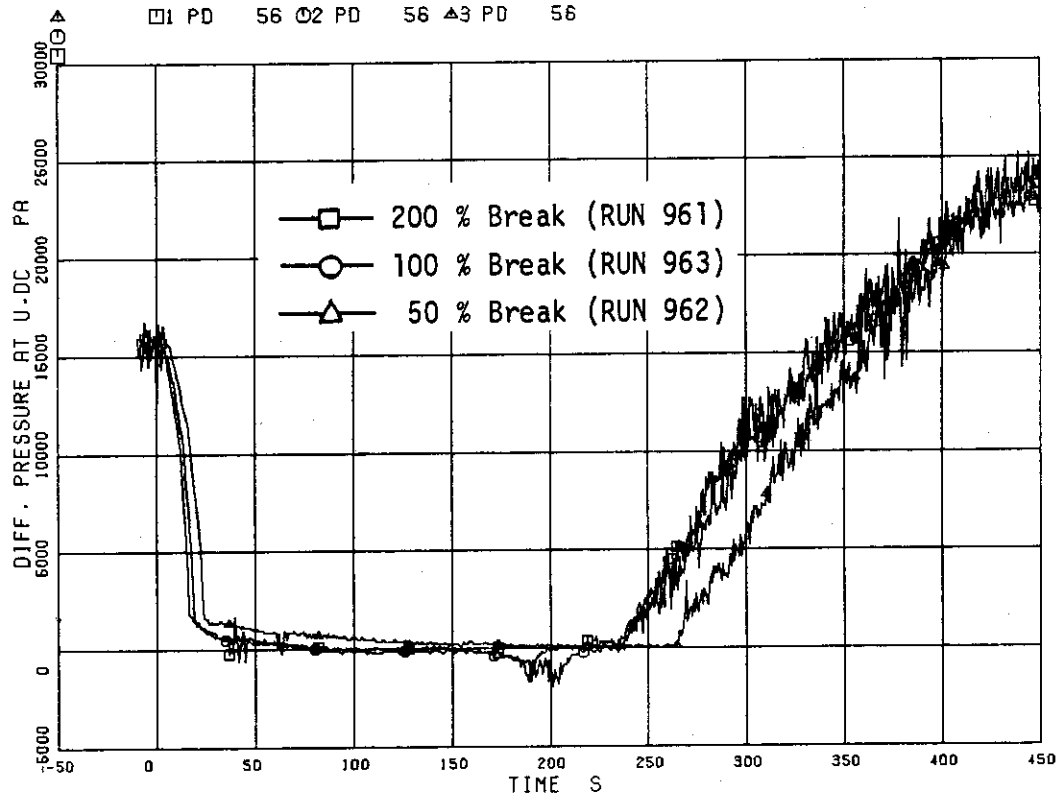

Fig. 6.6 Comparison of diff. pressures in upper downcomer

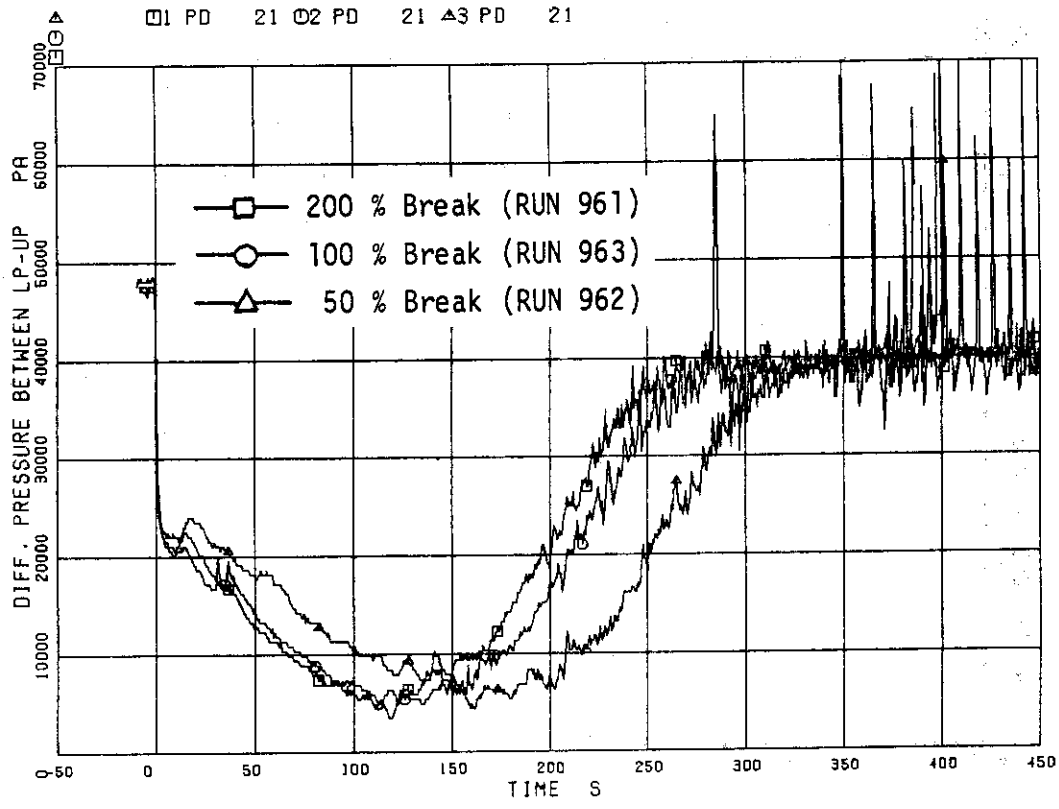

Fig. 6.7 Comparison of diff. pressures across the core

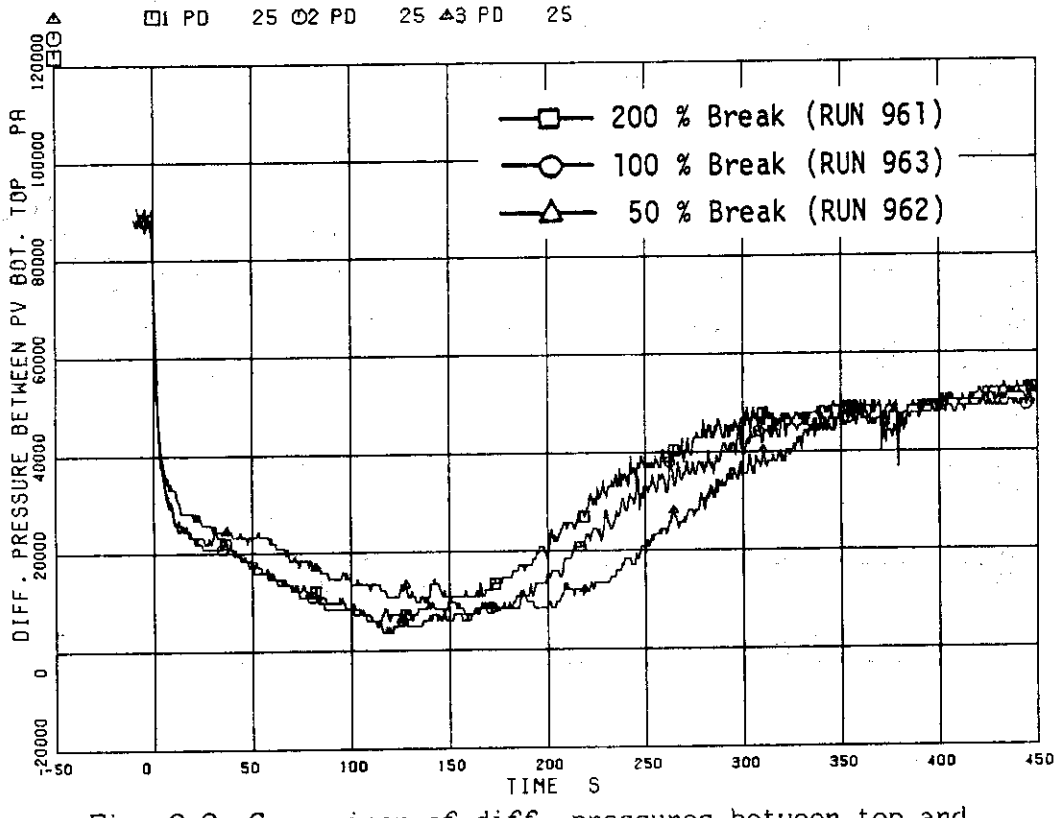

Fig. 6.8 Comparison of diff. pressures between top and bottom of PV

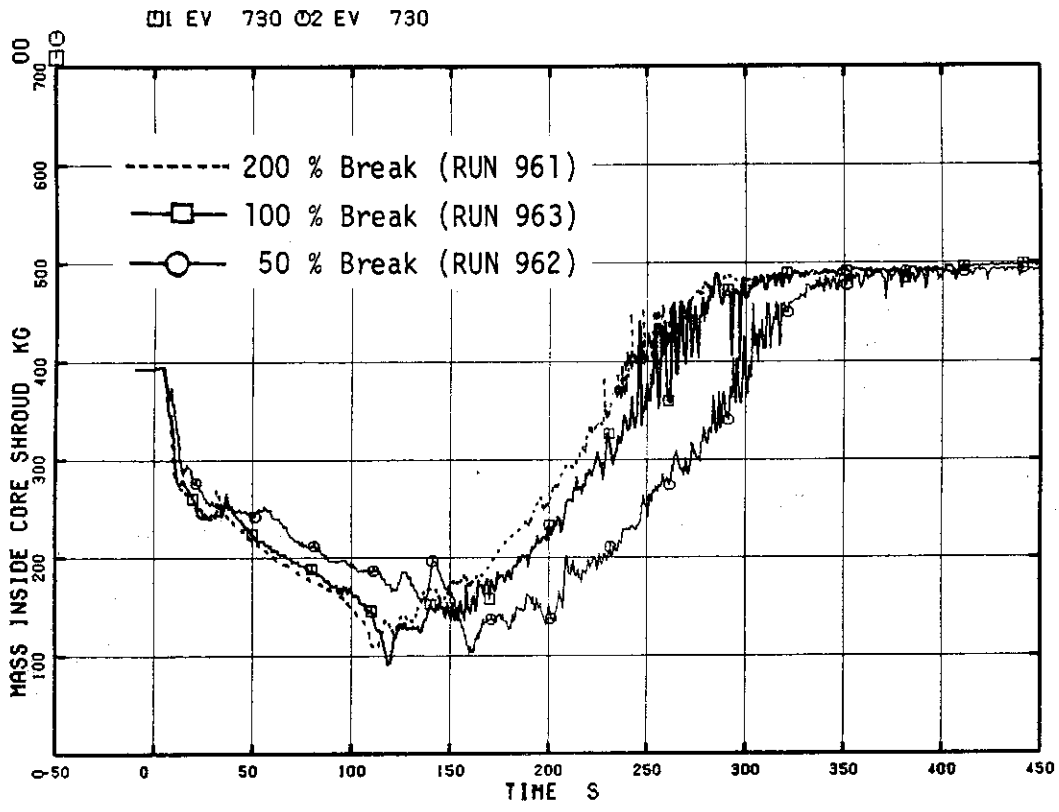

Fig. 6.9 Effects of break area on mass inventory inside core shroud

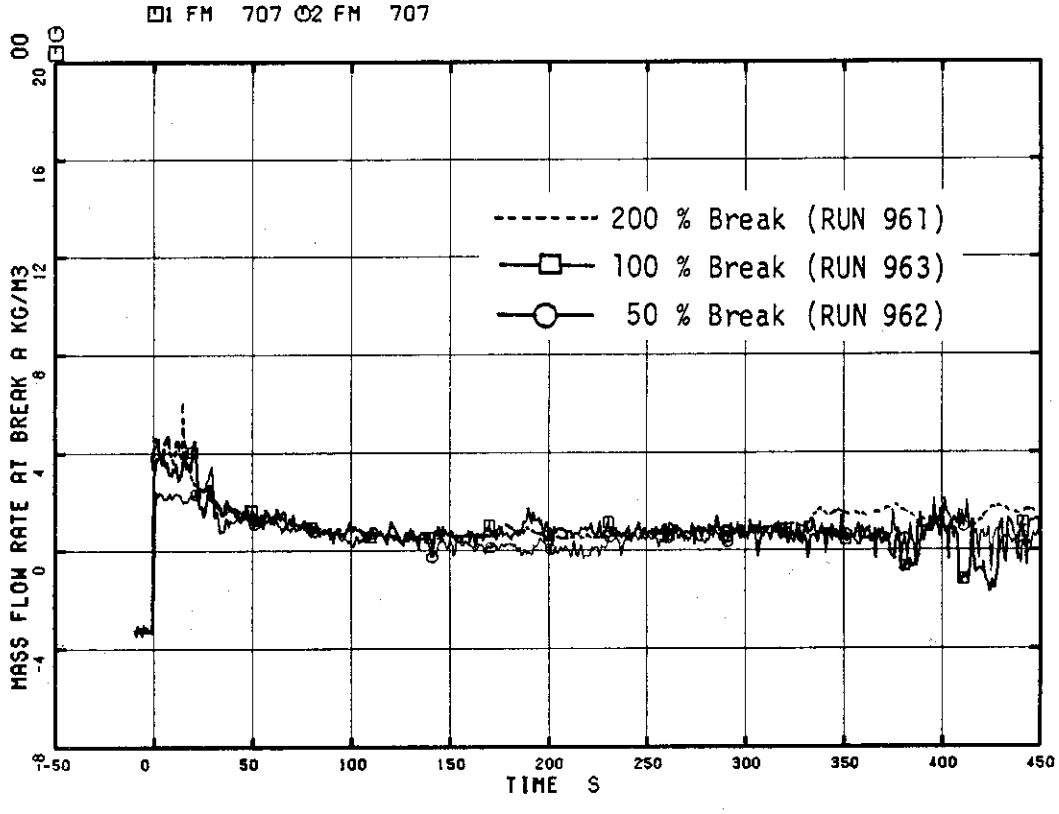

Fig. 6.10 Effects of break area on JP-side break flow

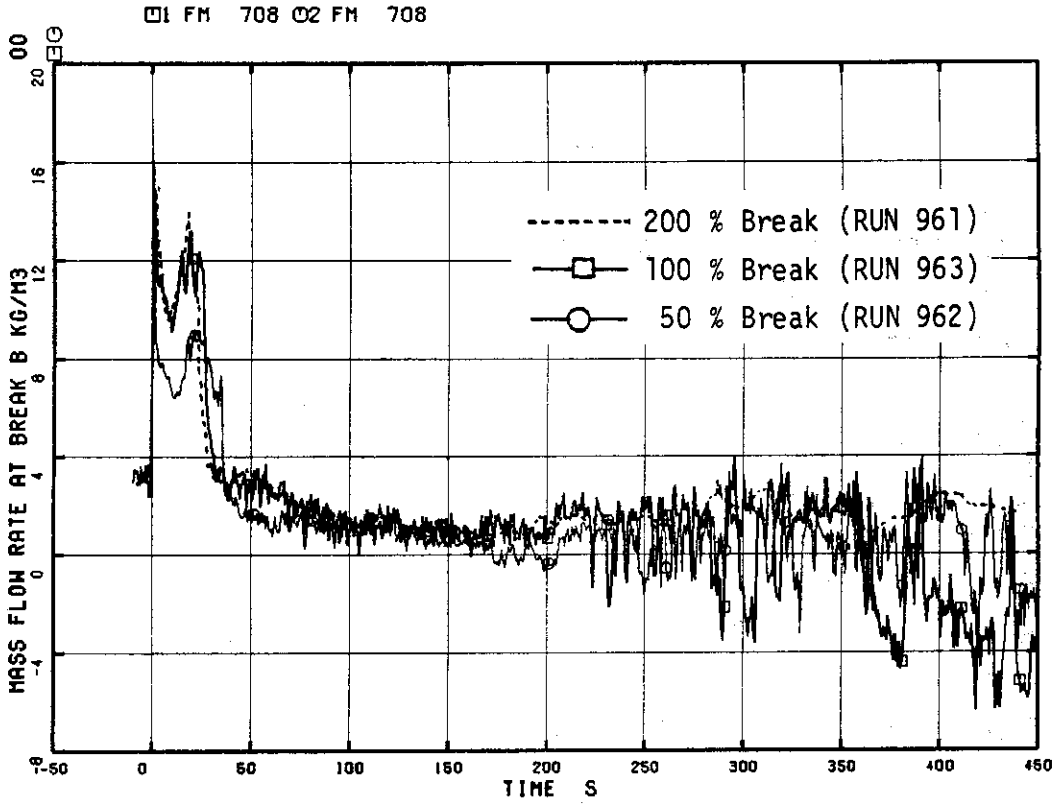

Fig. 6.11 Effects of break area on MRP-side break flow

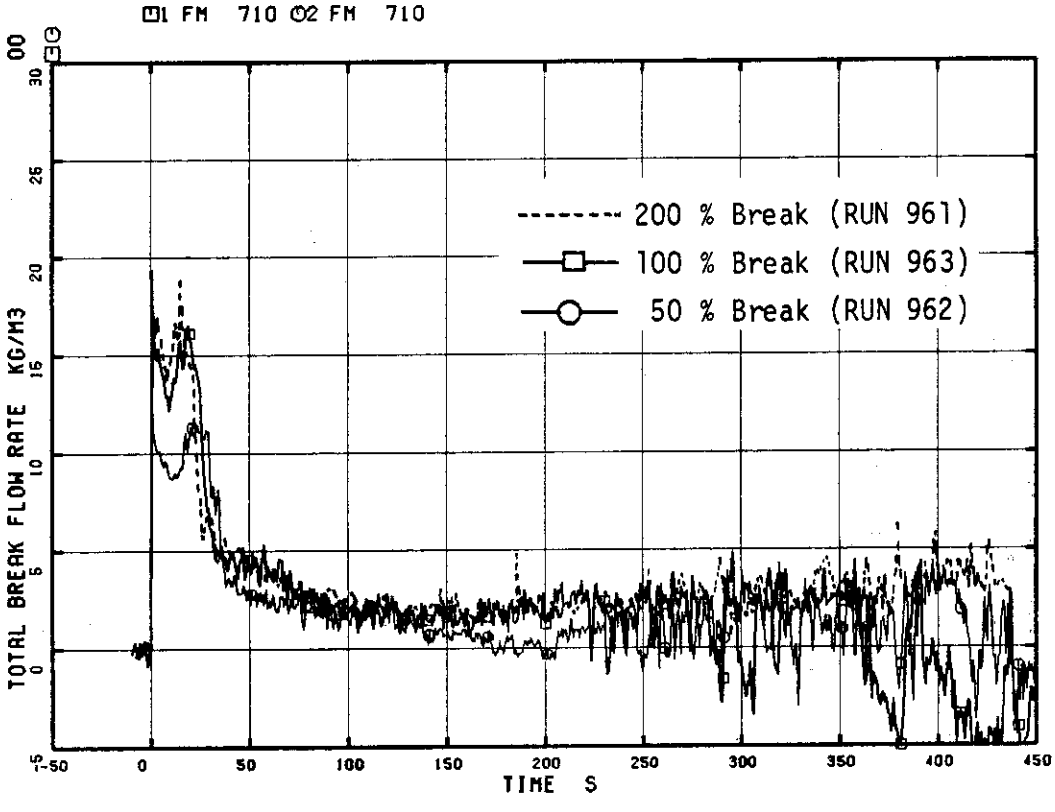

Fig. 6.12 Effects of break area on total break flow

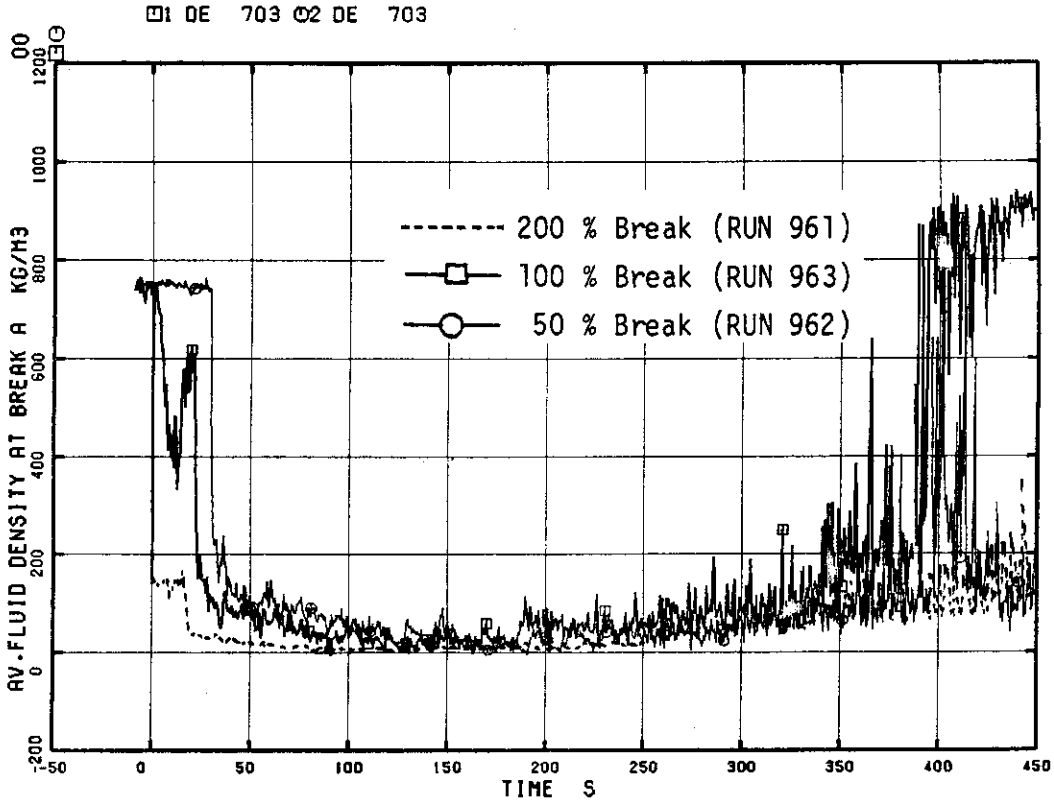

Fig. 6.13 Effects of break area on JP-side break fluid density

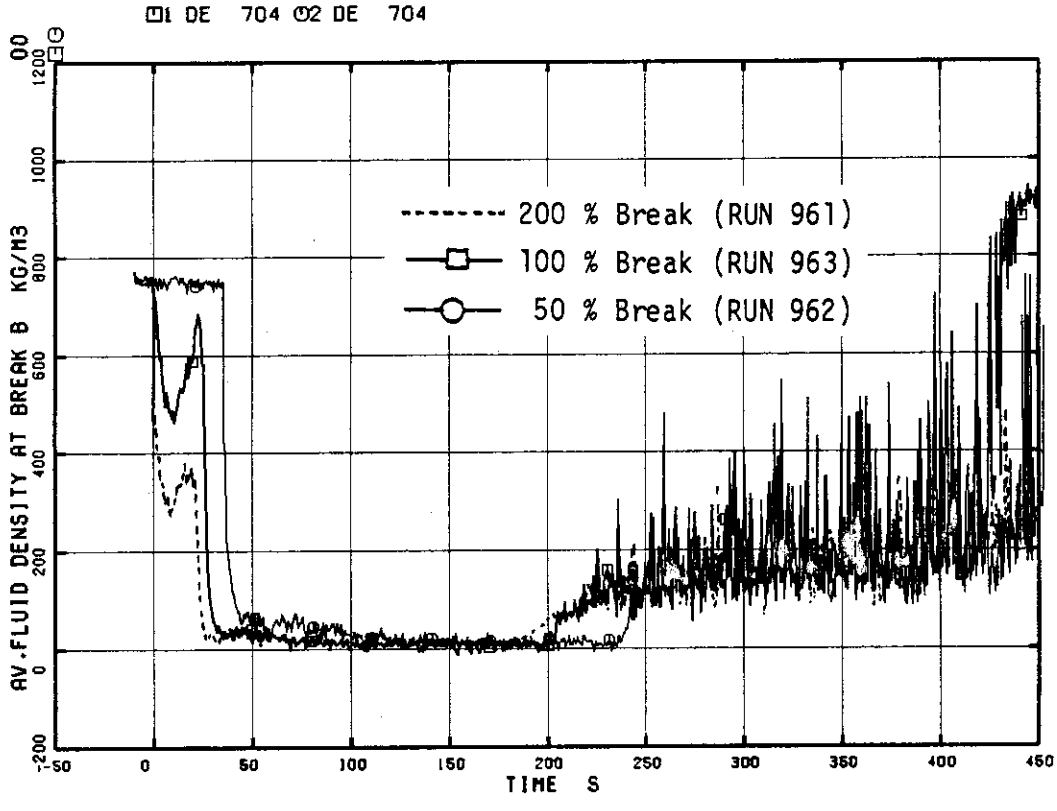

Fig. 6.14 Effects of break area on MRP-side break fluid density

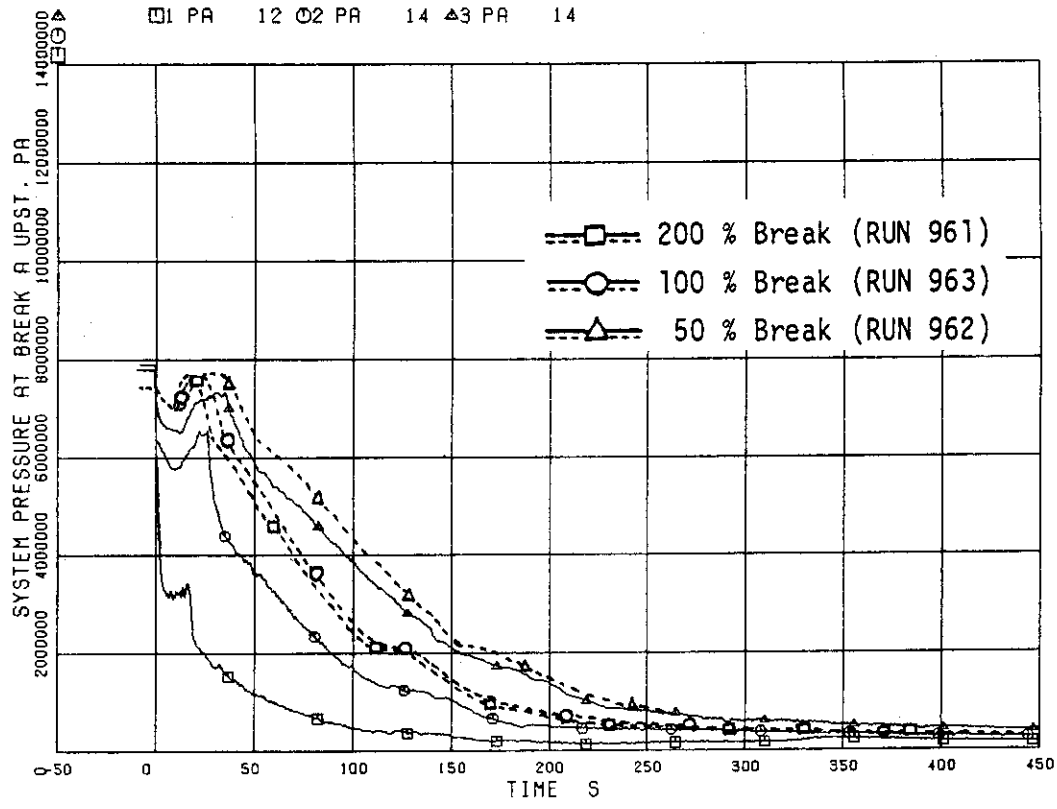

Fig. 6.15 Effects of break area on pressure distribution along JP-side break flow path

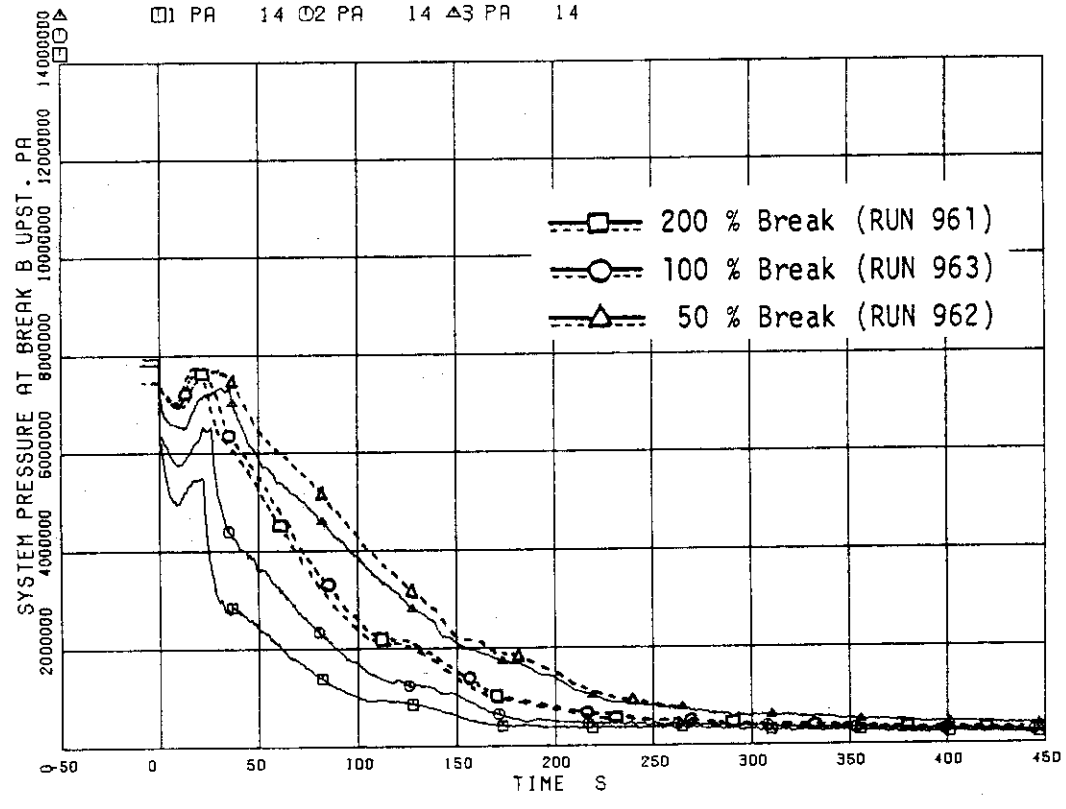

Fig. 6.16 Effects of break area on pressure distribution along MRP-side break flow path

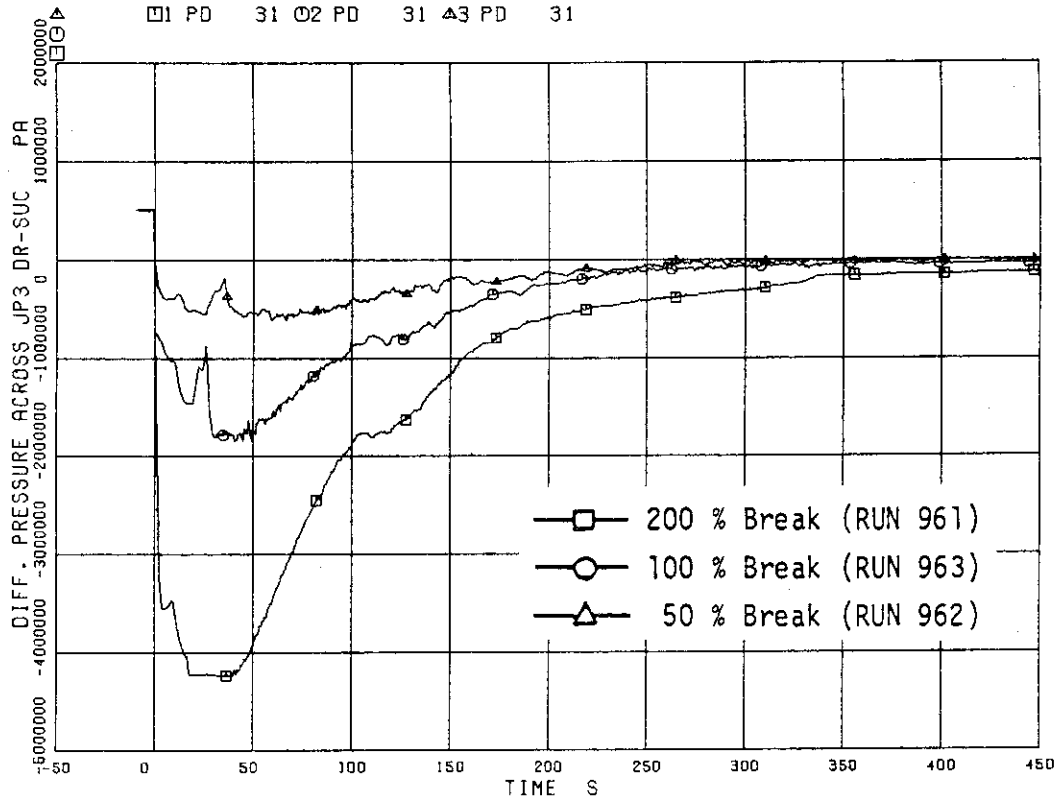

Fig. 6.17 Effects of break area on diff. pressures across the JP-3 drive nozzles

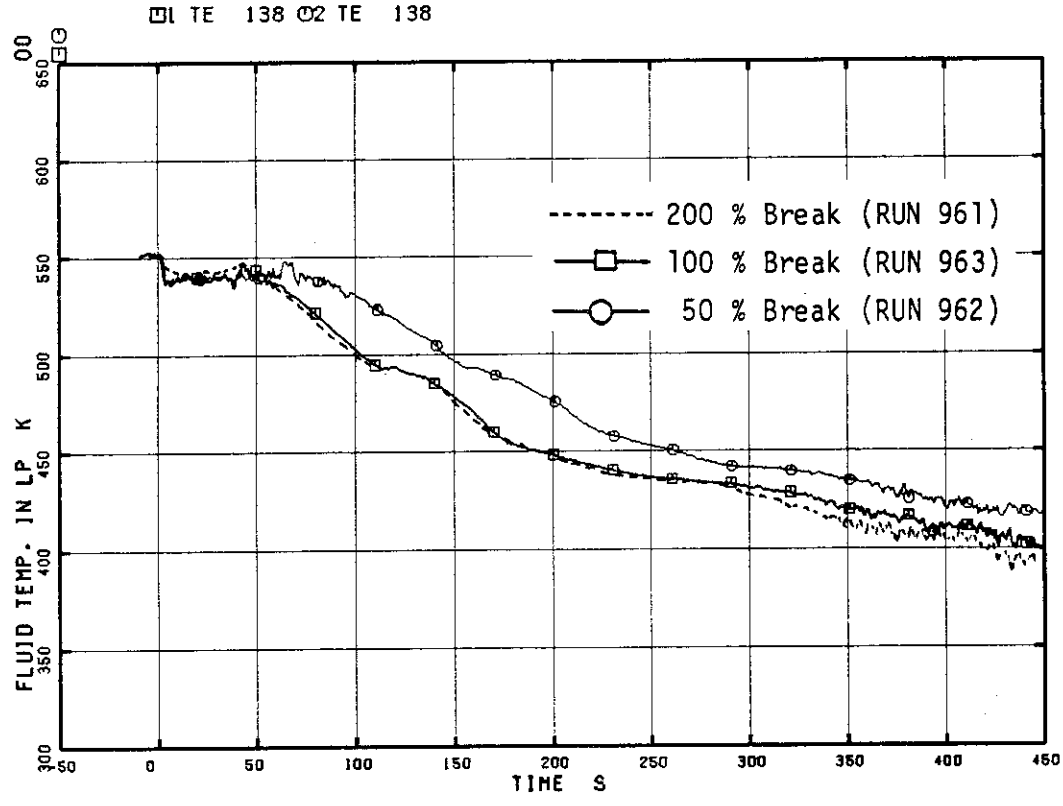

Fig. 6.18 Comparison of fluid temperature in lower plenum

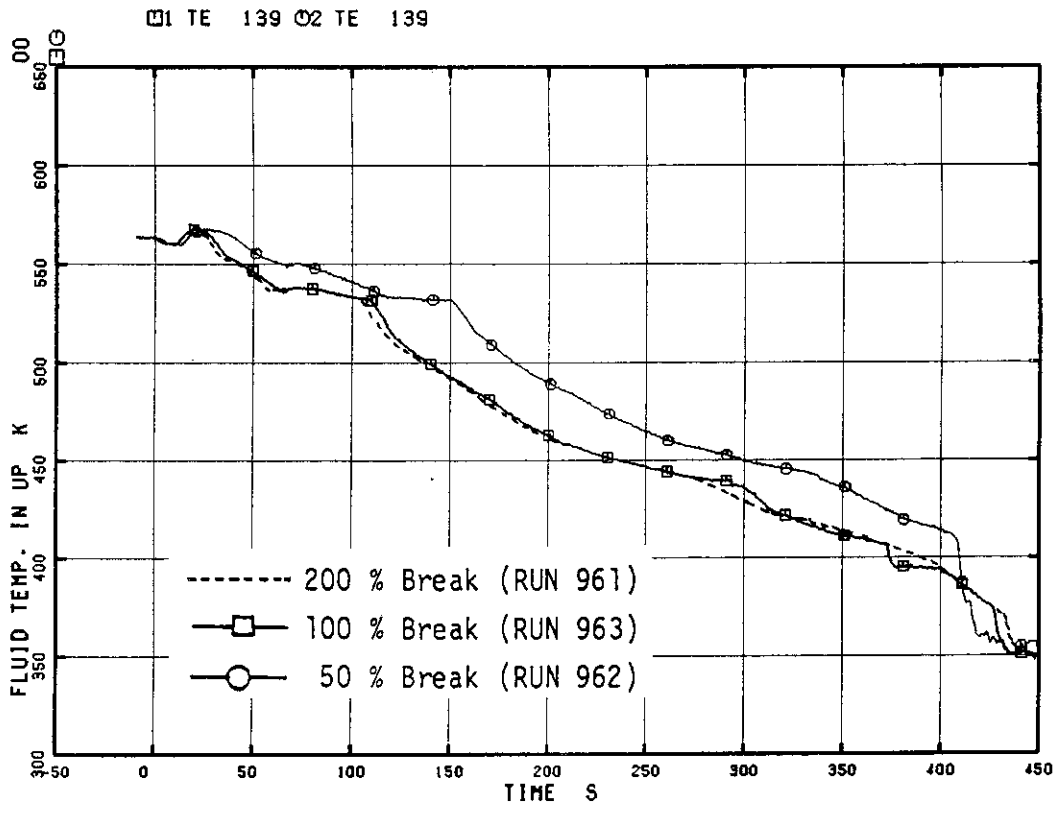

Fig. 6.19 Comparison of fluid temperature in upper plenum

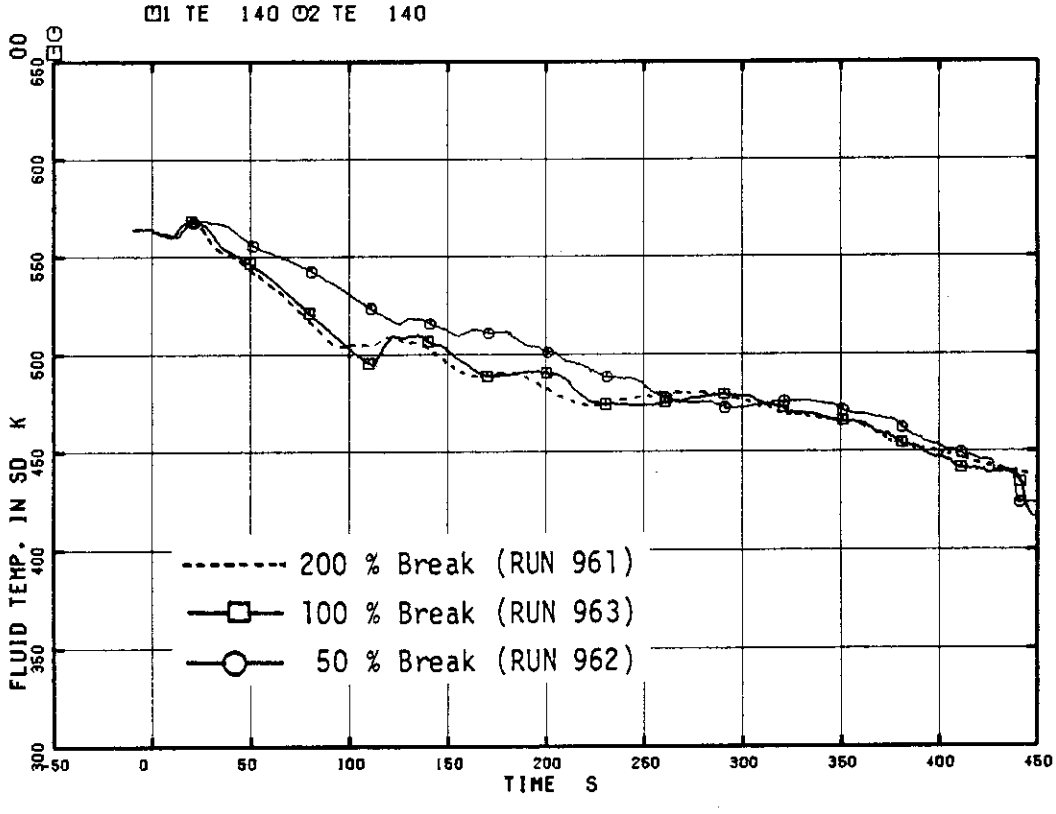

Fig. 6.20 Comparison of fluid temperature in steam dome

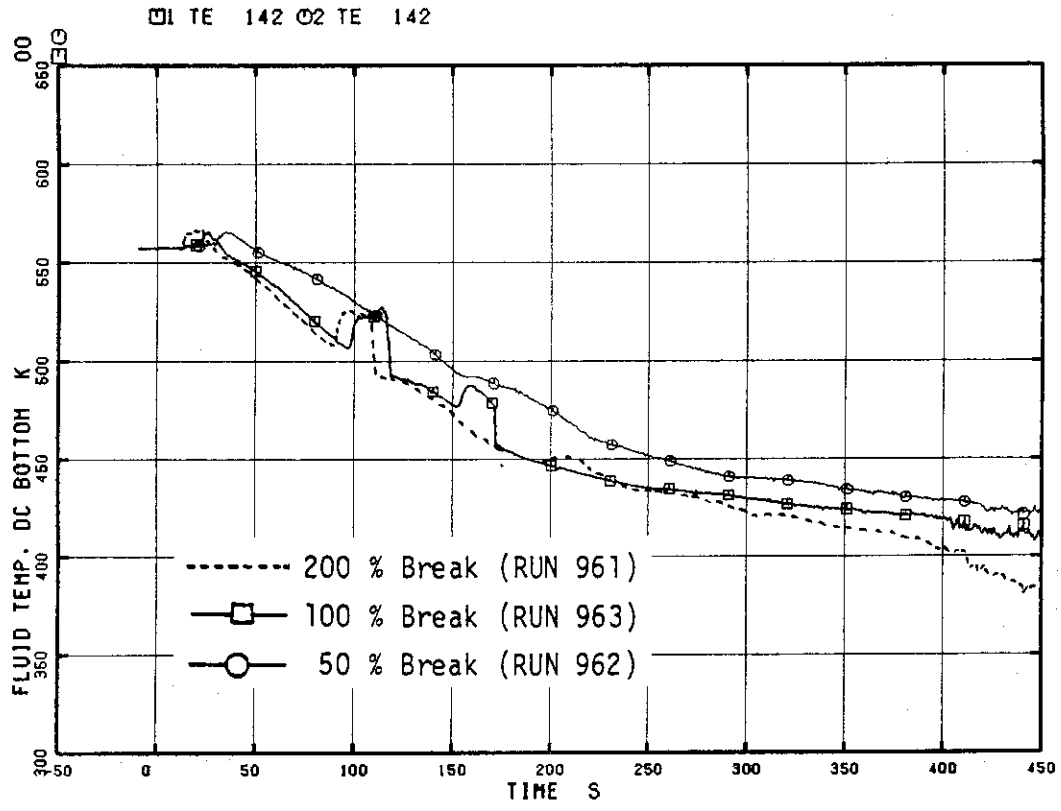

Fig. 6.21 Comparison of fluid temperature in downcomer bottom

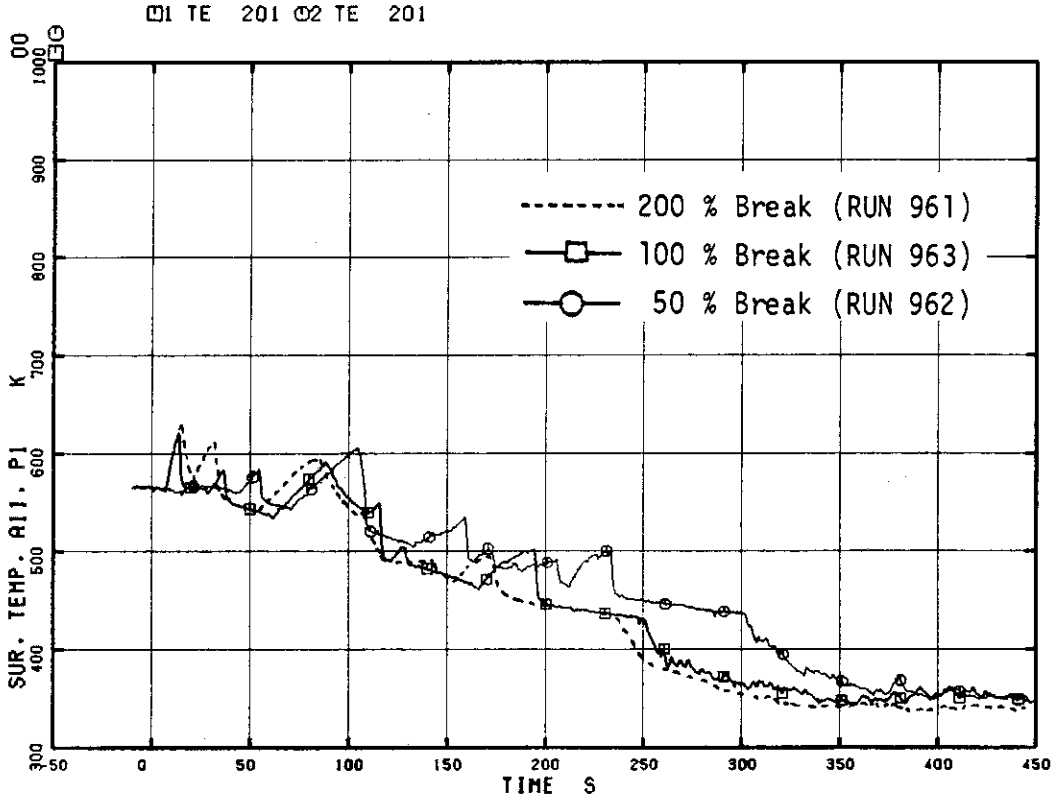

Fig. 6.22 Comparison of rod surface temperatures at the top of A11 rod in three tests

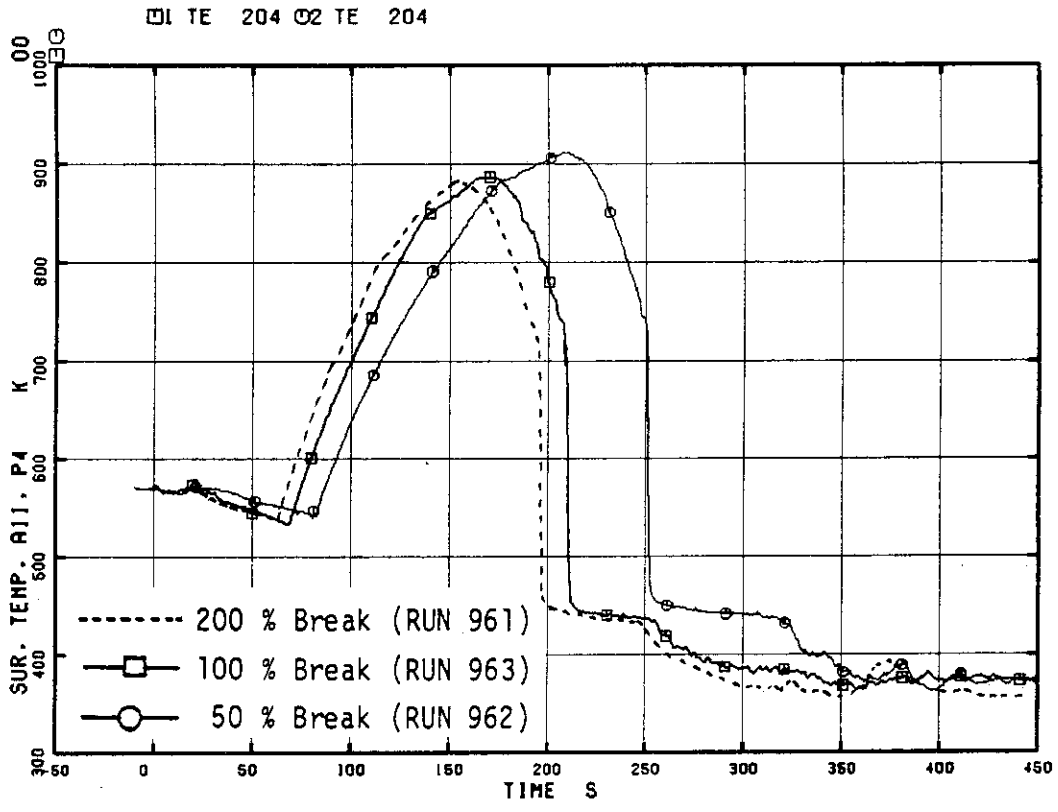

Fig. 6.23 Comparison of rod surface temperatures at the middle of A11 rod in three tests

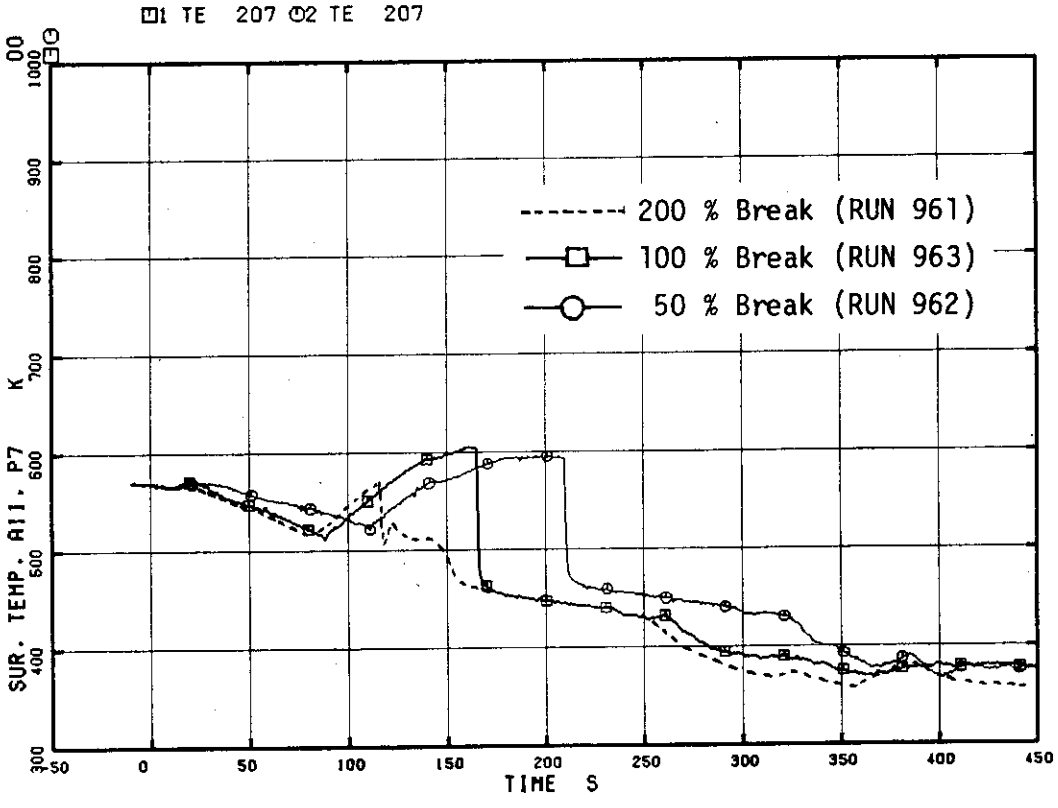

Fig. 6.24 Comparison of rod surface temperatures at the bottom of A11 rod in three tests

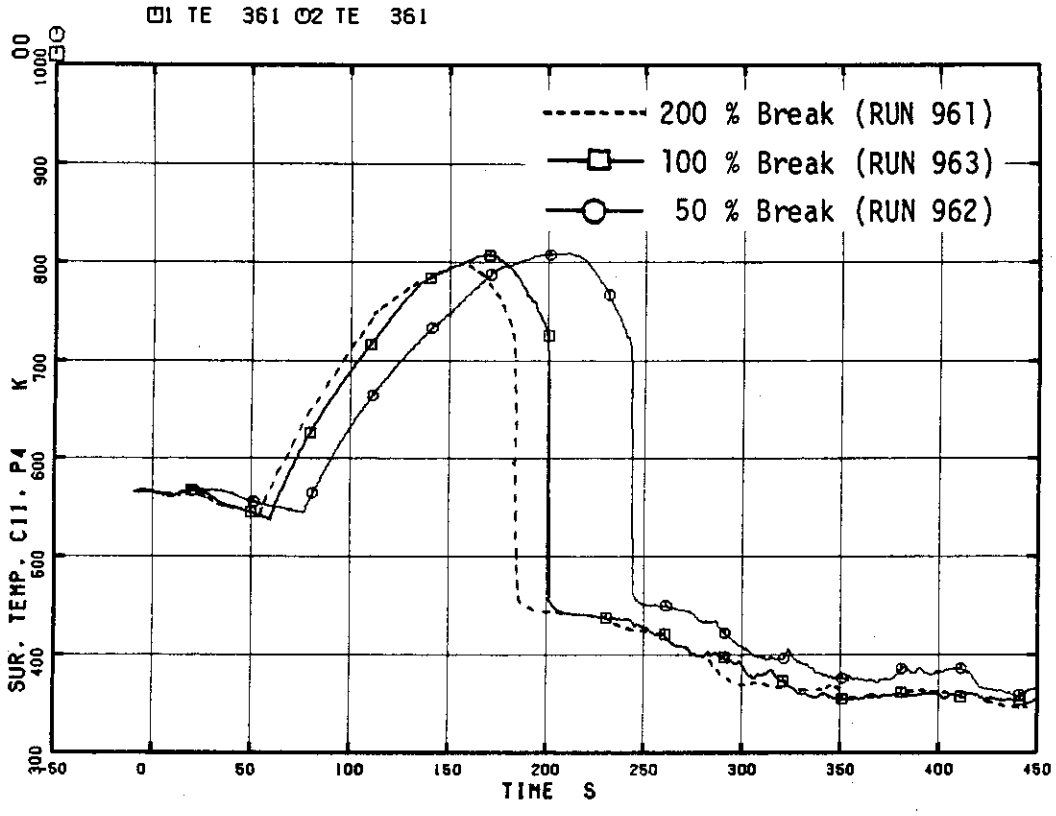

Fig. 6.25 Comparison of rod surface temperatures at the middle of C11 rod in three tests

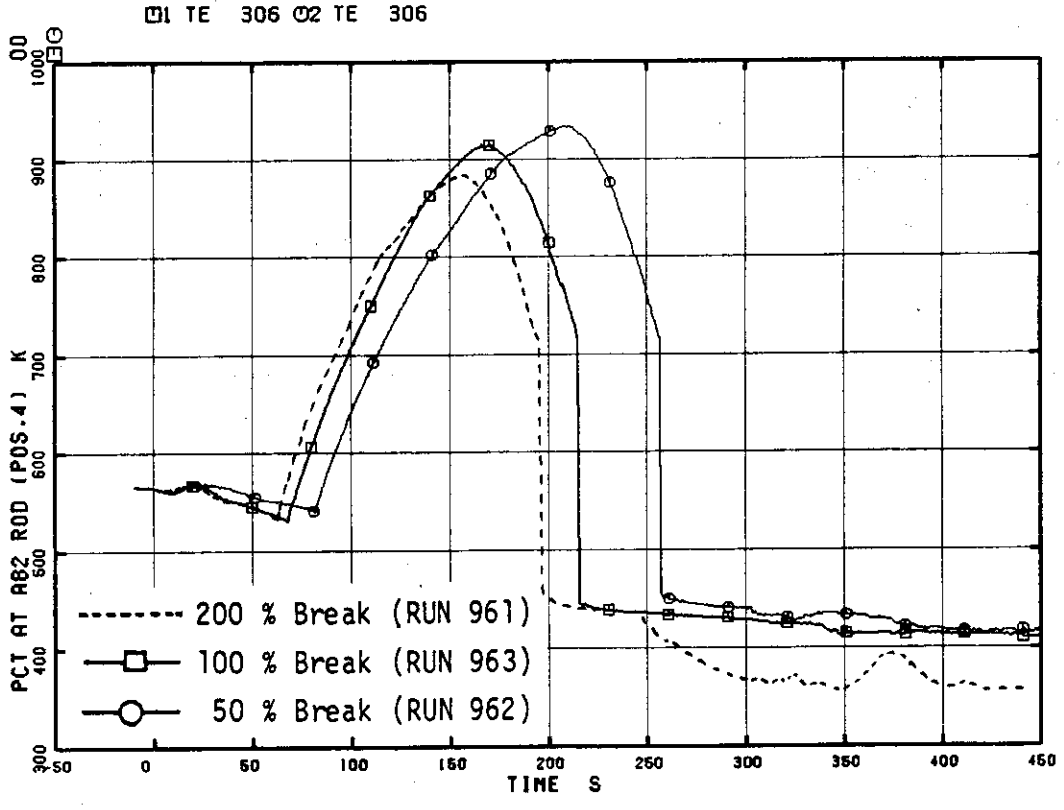

Fig. 6.26 Comparison of PCTs of three tests

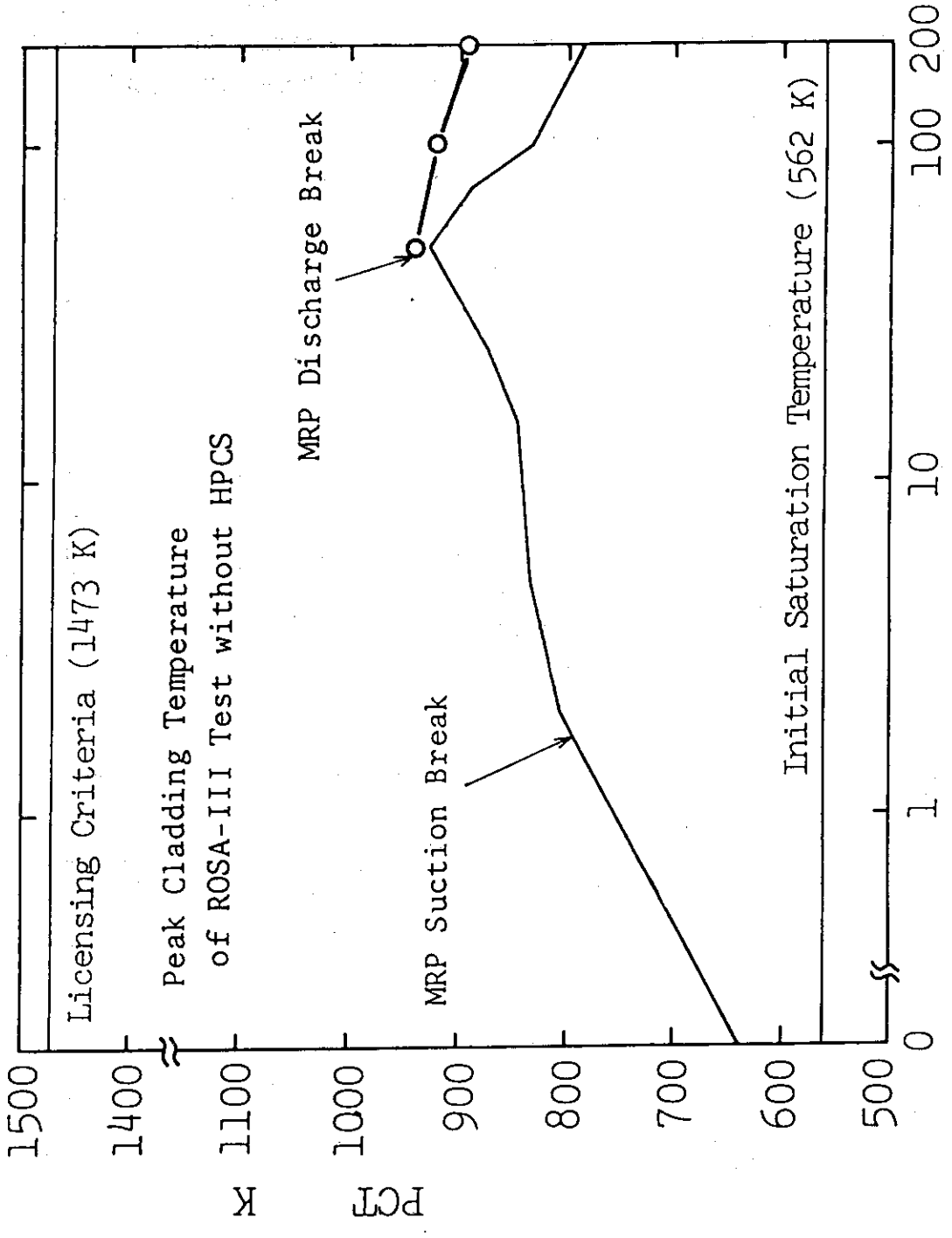

Fig. 6.27 PCT related with break area in ROSA-III recirculation line breaks without HPCS